Vladimir A. Basiuk · Elena V. Basiuk
Editors

Green Processes for Nanotechnology

From Inorganic to Bioinspired Nanomaterials

Springer

Green Processes for Nanotechnology

Vladimir A. Basiuk • Elena V. Basiuk
Editors

Green Processes for Nanotechnology

From Inorganic to Bioinspired Nanomaterials

Springer

Editors
Vladimir A. Basiuk
Universidad Nacional Autónoma de México
México, DF, Mexico

Elena V. Basiuk
Universidad Nacional Autónoma de México
México, DF, Mexico

ISBN 978-3-319-15460-2 ISBN 978-3-319-15461-9 (eBook)
DOI 10.1007/978-3-319-15461-9

Library of Congress Control Number: 2015933381

Springer Cham Heidelberg New York Dordrecht London

Printed on acid-free paper

Springer International Publishing AG Switzerland is part of Springer Science+Business Media (www.springer.com)

Preface

Nanotechnology is an integral part of our reality. One can hardly imagine modern life without nanomaterials, which can be found in diverse spheres of human activities ranging from food production and conservation, medicine and biotechnology, to computers, telecommunications, transport, and space exploration.

Unfortunately, all this comes at a cost. As any other chemical process, the production of nanomaterials inevitably contributes to environmental contamination. Given the constantly growing rate of nanomaterial production, the related environmental issues become more and more obvious and pressing and thus urge for radical solutions. The present book represents a joint effort of a number of authors to summarize recent advances in the green chemistry of nanomaterials and related areas. In particular, the chapters touch upon such aspects as environmentally friendly chemical synthesis and functionalization of different types of nanoparticles, from simple inorganic (e.g., metal, metal oxides, carbon nanotubes, and nanodiamond) to organic dendrimers and biomimetic nanomaterials; the use of biological synthesis as an alternative to traditional chemical synthesis of nanoparticles; properties (including catalytical, toxicity, and antibacterial) and applications of nanomaterials obtained via green routes in catalysis, solar energy conversion, medicine, etc.; the use of theoretical approaches to generate important guidelines for designing and improving photovoltaic and photocatalytic devices for nanotechnologies; life cycle assessment of nanomaterials; and, finally, the economic contributions of nanotechnology to green and sustainable growth.

We are deeply grateful to all our contributors for their outstanding chapters, who not only accepted to contribute and to share their valuable experience in spite of their infinite routine with numerous commitments (projects, reports, students, presentations, other chapters and papers, etc.), but, *most importantly*, fulfilled their promise and thus helped us to complete this book project in a timely manner.

We would also like to thank Merry Stuber, editorial assistant at Springer, who encouraged us to undertake editing of the present book; Prasad Gurunadham, the book project coordinator; Sharmila Kirouchenadassou, the project manager; and the entire Springer team involved into its publication, for their hard work, skillful handling of related technical issues, support, and patience.

Finally, we thank the reader, who noticed this book, read, and found it interesting and useful. We welcome any comments regarding its content and form of presentation.

Mexico-City, Mexico

Vladimir A. Basiuk
Elena V. Basiuk

Contents

Chapter 1
Sustainable and Very-Low-Temperature Wet-Chemistry Routes for the Synthesis of Crystalline Inorganic Nanostructures

Silvia Gross

Abstract In this chapter, selected low (T < 200 °C)-temperature wet-chemistry routes for the synthesis of crystalline inorganic compounds are described and reviewed, outlining their main features and application fields. In particular, the chosen approaches are hydro/solvothermal synthesis, template-assisted approaches, nucleation and growth in solution/suspension, microemulsion and miniemulsion. The described synthetic strategies have been selected since all of them, once optimized the experimental set-up and conditions, comply with the paradigms of green chemistry, being based on low (or even room) temperature of processing, on low chemical consumption (they are all bottom-up approach), in many cases having water as solvent or dispersing medium. In this regard, environmentally friendly methodologies for the controlled synthesis of inorganic nanostructures represent a stimulating research playground, since the use of environmentally friendly, green, cost-effective and technically sound approaches to inorganic crystalline nanostructures does not necessarily imply to sacrifice the sample crystallinity, purity, and monodispersity.

Keywords Wet-chemistry • Colloids • Crystalline • Inorganic compounds • Low temperature • Room temperature • Colloidal routes

1.1 Introduction

The concepts of green chemistry are currently entailing all the fields of chemistry and particularly inorganic chemistry represents an exciting playground for the design and optimisation of green chemistry-inspired routes. Green chemistry, defined as "the utilization of a set of principles that reduces or eliminates the use or generation of hazardous substances in the design, manufacture, and application of

S. Gross (✉)
Istituto per l'Energetica e le Interfasi, IENI-CNR, Dipartimento di Scienze Chimiche, Consiglio Nationale delle Richerche (CNR), Università degli Studi di Padova and INSTM, via Francesco Marzolo, 1, Padova I-35131, Italy
e-mail: silvia.gross@unipd.it

V.A. Basiuk, E.V. Basiuk (eds.), *Green Processes for Nanotechnology*,
DOI 10.1007/978-3-319-15461-9_1

chemical products" [1] is an already established and widened concept in the field of preparative chemistry, its extension to inorganic chemistry being one of the most bewitching developments. Environmentally friendly methodologies for the controlled synthesis of inorganic nanostructures are a noticeably stimulating research field since this encompasses not only the control of the final composition but also, and more importantly, a fine-tuning of the obtained materials in terms of crystallinity (crystalline phase, crystallite size), shape, morphology.

The control over size, shape, and morphology, combined with mild conditions of processing parameters (mainly in terms of temperature and pressure), are important conditions to be fulfilled for sustainable and cost-efficient production of functional inorganic materials. Further requirements to be met in order to chemically design and implement from the environmental, technical, and economical points of view sustainable synthesis routes are (1) reproducibility, (2) ease of processing, (3) use of safe, cost-effective, earth-abundant and common chemicals and solvents, (4) easy purification steps, and (5) high yields.

As pointed out by Wong, Mao et al. [2] in one excellent review on the topic, the use of environmentally friendly, green, cost-effective and technically sound approaches to inorganic crystalline nanostructures does not necessarily imply to sacrifice the sample crystallinity, purity, and monodispersity. Furthermore, the huge application potential of functional inorganic nanomaterials in many fields can be realized only provided that large quantities of materials can be prepared with high reproducibility in terms of composition, size, shape, morphology by applying sustainable and green procedures, involving (1) the lowest amount of toxic chemical and/or solvents, (2) low temperature and, last but not least, (3) easy-to-be-implemented and to-be-scaled-up safe procedures.

Several synthetic approaches to crystalline inorganic nanostructures, either metallic or binary (oxides, chalcogenides, halides) compounds, have been extensively described in some books and excellent reviews [3–7]. In particular, the books of Caruso [8] and Schmid [9] provide a comprehensive collection of the main synthetic approaches to colloids, colloids assemblies, and nanostructures, together with a thorough overview on their properties and applications. One of the mentioned reviews, the one by Dahl et al. [4] is particularly focused on "green approaches" to engineered nanomaterials, outlining the possibility to produce, in an environmentally friendly approach, ligand-functionalized inorganic nanoparticles. In this regard, the use of novel dispersing phases such as ionic liquid and supercritical fluids has also been reported.

In a further comprehensive review by Cushing et al. [3], the main advances in the liquid-based processing of inorganic materials, ranging from coprecipitation, to sol–gel process and Pechini method, to microemulsion to hydrothermal/solvothermal and from template synthesis to biomimetic-based routes have been extensively reviewed. Some of the above-mentioned approaches such as sol–gel or the Pechini method will, however, not be further discussed in this review, since they involve a final annealing step at high temperatures.

The present review chapter is instead devoted to provide a general overview, with no aim to be extensive and comprehensive, on the most important, technically relevant, and sustainable wet-chemistry routes to inorganic materials.

Wet-chemical routes are preferred to solid-state ones for preparing inorganic crystalline materials since the liquid phase is more versatile with respect to the variation of structural, compositional, and morphological features of the resulting compound materials. Furthermore, the molecular homogeneity of the starting solution or the microscopic homogeneity of the suspensions typically used in colloidal-based methods is generally retained in the final materials. At variance to that, an inherent limit of solid-state reactions is that there is no medium in which the reactants are dissolved, therefore severely limiting the interaction between components. The reaction can only take place either at the interface between the two solid precursors, or through migration of the reactants through a third phase; such processes are therefore usually relatively slow, can lead to nonhomogeneous final products and/or require high energies and/or intermediate milling steps. Also from the environmental point of view, solid-state syntheses present several drawbacks, such as long processing times and high energy consumption, determined by the high processing temperatures. The main advantage of these techniques is that they are relatively simple to implement and, once the protocol has been optimized, they proceed without significant intervention on part of the operator. Also, scaling-up of the protocols is generally quite straightforward [10].

In conclusion, within the framework of nanostructures synthesis, liquid-phase synthetic routes are instead generally considered a more promising alternative to the ceramic method and ball milling [11–13] (mechanosynthesis) method, as these latter are rather crude and energy-consuming approaches, whereas liquid-phase synthesis allow a finer and more direct control over the reaction pathways on a molecular level during the synthetic process itself. In this context, a first distinction among wet-chemistry approaches can be performed between surfactant-assisted and surfactant-free approaches, the latter being characterized in some cases by the presence of coordinating organic solvents [14], which may play also the role of stabilizing agents.

In this chapter, the underlying idea is to focus on low temperature-based routes, being in this particular context "low" intended as lower than 200 °C, since this further constraint not only fulfills one of the paradigms of green chemistry but also enables unusual crystallization pathways to be explored. The other focal point of this chapter is the obtainment of "crystalline" inorganic nanomaterials since, as already outlined in a previous work by Muñoz-Espí et al. [15], crystallinity is in many case *conditio sine qua non* for the achievement of particular functional properties. It is worth to mention, *inter alia*, luminescence as well as catalytic, electronic, and magnetic properties. Also Liz-Marzan with coauthors has extensively pointed out the role played by nanostructures shape, morphology, and possible anisotropy in dictating some relevant functional properties, typically optical ones [16–19].

To accomplish an ordered growth of the targeted nanostructures, which is a mandatory requirement to control also their structure and morphology at the upper (up to micrometers) length scales, is a fascinating and even challenging playground for the preparative inorganic chemist. In fact, the mastery of nanocrystal nucleation and growth represents a primary challenge in inorganic materials chemistry and the formation of an ordered array of atoms or molecules (i.e., the obtainment of a crystalline structure) is, as already outlined, in many cases a necessary requirement to afford enhanced functional properties [17]. Although the temperature can be set by the operator, to dictate the structural evolution of an inorganic systems toward the 3D long-range periodical order characterizing crystalline materials is not straightforward. To better understand the pathways leading to crystallization in order to properly orientate the structurally controlled formation of the materials, in situ as well as temperature- and time resolved studies are always required [20–22].

In this regard, the basic concept of achieving a fine control on the evolution of the resulting material over several length scales, up to final crystalline phase, is the *file rouge* of many recently implemented low-temperature routes to inorganic colloids. Several authors have thorough investigated the effect of the different experimental parameters in directing and ruling the growth of the obtained nanostructures [23].

This review chapter is aimed at providing a broad overview on the main features as well as on the *pros* and *cons* of the some selected routes for the low or even room temperature obtainment of targeted crystalline inorganic materials.

The chapter begins with the description of more classical wet-chemistry approaches to crystalline inorganic nanostructures, such as the hydrothermal one, and then review some of the most relevant colloidal-based approaches, with a special focus on those affording crystallization of the desired nanostructures in confined space, such as miniemulsion and microemulsion. The template-assisted synthesis of nanostructures is also concisely reviewed, as well as the classical colloidal methods based on the nucleation and growth of nanostructures from solutions/suspensions, typically in presence of stabilizing ligands [3]. Although some examples are provided, the detailed discussion of the application of the described routes to the synthesis of different types of inorganic materials is out of the scope of the present contributions, aimed instead at providing a comprehensive, though general, perspective. Nevertheless several bibliographic references are provided for interested readers.

As mentioned at the very beginning, being the topic of the chapter the low-temperature synthesis of inorganic nanosized materials, only those examples and routes involving the low-temperature solution- or suspension-based processing of materials will be reviewed and discussed. Moreover, due to the broadness of the topic, several references to tutorial textbooks are also provided thorough. Due to space constraints, some methods will only be shortly mentioned, and interested readers are referred to pertinent references. In particular, some less common, though very elegant, routes such as biomimetic approaches [24–28], sonochemical synthesis [4, 29–31] and the use of supercritical fluids [10, 32–34], though low temperature, are not discussed further.

1.2 Wet-Chemistry Approaches to Crystalline Inorganic Nanostructures

1.2.1 Hydrothermal and Solvothermal Synthesis

The term *hydrothermal synthesis* typically refers to synthesis based on an aqueous medium which are carried out at relatively high pressures and temperatures [2, 10, 21, 33–50], either above or under critical conditions. The analogous term "solvothermal" refers instead to the same typology of reactions carried out in solvents other than water. Being, however, the focus of this chapter on sustainable wet-chemistry routes, the former will be discussed in more detail.

Whereas the first hydrothermal synthesis protocols were developed to mimic the conditions in which crystals grow within the Earth crust [38, 44], more recently, this method has been applied to the synthesis of more complex systems, such as binary or ternary metal compounds, in nanosized crystalline form. As it can be appreciated by the figures below (Fig. 1.1), the interest towards hydrothermal synthesis for the production of inorganic nanostructures has exponentially and steadily increased in the last 20 years.

This general and versatile strategy has been widely implemented to the preparation of different classes of inorganic compounds, encompassing binary and ternary oxides, sulfides, nitrides, etc., as extensively reported elsewhere [21, 51]. In their review, Mao, Park et al. [2] describe the application of these methods to the synthesis of titania and titanate nanostructures.

Several works have been published on many different compounds such as zinc oxide [52, 53], titania [54, 55], ceria [56], metal sulfides [57–60] as well as several more complex ternary oxide compounds [21] such as titanates [2], phosphates [61] and ferrites [11, 34, 43, 62–67]. As far as interesting class of ternary oxides, e.g., ferrites, are concerned, the literature reports several examples of hydro/solvothermal approaches to these functional inorganic materials. Most commonly synthe-

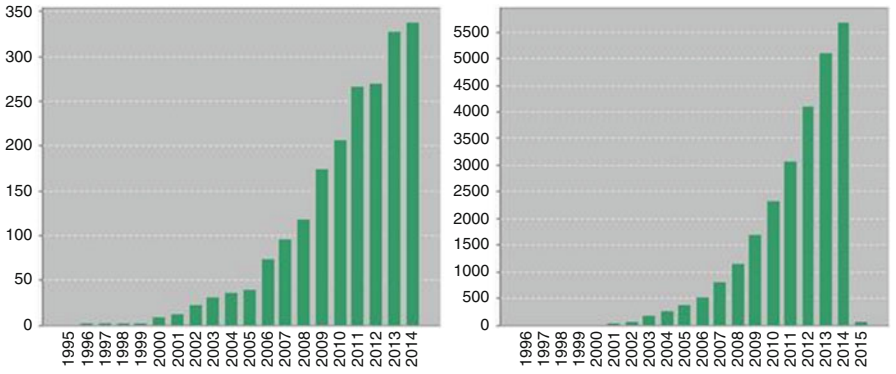

Fig. 1.1 Published items in each year (*left*) and citations in each year (*right*) on the "hydrothermal synthesis of nanostructures" (used keywords: "hydrothermal synthesis" and "nanostructures"). Source Web of Science December 2014

sized ferrites are perovskite ferrites, with general formula $MFeO_3$, and spinel ferrites with general formula MFe_2O_4. When the hydrothermal method is taken into consideration, the bismuth ferrite $BiFeO_3$ is the most commonly synthesized perovskite. Low temperature hydrothermal routes (60–250 °C) have also been used for the synthesis of spinel ferrites (e.g., $CoFe_2O_4$, $NiFe_2O_4$, and $ZnFe_2O_4$) [65, 68–70]. Recently we have applied hydrothermal synthesis to the preparation of nanostructured crystalline spinel ferrites and manganites [67]. The synthesis is based on the successful combination of coprecipitation of metal oxalates from an aqueous solution with hydrothermal treatment of the resulting suspension at mild temperatures (i.e., < 180 °C). In this protocol, hydrothermal conditions, though sub-critical, were achieved through autogenous pressure (by heating the reaction mixture in a closed vessel); additionally the possible decomposition of oxalate species to carbon dioxide could also determine a further increase in pressure. This approach has been proven to be very attractive due to several factors: (1) excellent reproducibility, (2) ease of procedure and implementation (possibly scale-up), (3) nontoxic precursors, (4) mild temperatures, (5) the use of water as greenest solvent, (6) easy and quick purification of products (without the need for other solvents), (7) high yields, (8) high product purity, (9) and high versatility (numerous different compounds were synthesized through this method, since oxalates of many metals can be easily prepared). Hydrothermal synthesis of transition metal oxides such as W, Mo, V, Mn, Ti, Fe oxides under milder conditions (i.e., temperature < 200 °C) has been the topic of a contribution by Whittingham [40, 41], whereas more recently a paper focused on hydrothermal synthesis strategies for inorganic semiconductor nanostructures has appeared [51] In this latter review, the authors describe the most representative hydrothermal synthetic strategies of inorganic semiconducting nanostructures in particular evidencing four types of approaches: (1) organic additive- and template-free hydrothermal synthesis, (2) organic additive-assisted hydrothermal synthesis, (3) template-assisted hydrothermal synthesis, and (4) substrate-assisted hydrothermal synthesis. In addition, the two strategies based on exterior reaction environment adjustments, including microwave-assisted and magnetic field-assisted hydrothermal synthesis, are also reviewed.

All these hydrothermal-related synthetic protocols take advantage of the particular physical conditions involved whenever the starting solution or suspension is subjected to an increase of pressure and temperature, both parameters being either separately changed or interdependent. In fact, hydrothermal (and solvothermal) synthesis can be actually carried out by using special devices such as autoclaves, ensuring a separate control of temperature and pressure, or rather by using hermetically closed reactors in which the increase in the pressure (autogeneous pressure) is determined by the fact that the reaction suspension/solution is heated in a closed vessel. The temperature can be either under or at the critical point of the chosen solvents, both conditions, however, affording remarkable variations in the main physicochemical properties of the solvent. In fact, in general, ionic product of the solvent tends to increase with rising temperature and pressure, whereas viscosity decreases. In the case of water, the dielectric constant depends on both pressure and temperature as it is directly proportional with the former, but inversely proportional

with the latter [10, 44]. All these variations strongly affect the kinetics of dissolution of the inorganic precursors and also of the nucleation and growth phenomena of the resulting materials, also disclosing unusual pathways for the crystallization of the targeted compounds.

In this regard, being the present chapter focussed on crystalline inorganic compounds, it is worth to devote some attention to the pathways leading to crystallization under (even subcritical) hydrothermal conditions. In this context, whenever nanocrystals form from an aqueous supersaturated solution, the precipitation process should occur slowly [71], in order to avoid the uncontrolled formation of amorphous solids. The nonstandard conditions in which hydrothermal synthesis takes place [2, 34–39, 43–45, 72–76], enables the solubilization of generally less soluble compounds which can, in these particular solvent-dependent conditions, be solvated more efficiently and therefore react more fastly and easily [37, 44]. Many different process mechanisms can be hypothesized, also depending on the specific synthetic protocol adopted. As outlined in one of our recent publication on the topic [67], in the most widely accepted theory [36, 37, 54, 66], the process involves two steps: (1) in situ transformation followed by (2) precipitation and growth. During the former phase the inorganic precursors are dissolved: therefore tiny amounts of the target oxide form as solvated species (owing to the conditions in which the process occurs); during the second phase, the low solubility of the aforementioned products causes them to nucleate and form crystals. Depending on the conditions involved (temperature, pressure, precursors, etc.) different products and/or crystalline polymorphs can nucleate and grow.

In general, hydrothermal synthesis is attractive, compared to more traditional synthesis protocols, due to the fact that crystalline products with high purity and compositional uniformity, as well as appreciable crystallinity, may be obtained under relatively mild conditions. Furthermore, since, as mentioned, changing the temperature and pressure of the reaction mixture induces relevant variations in the properties of the solvent [10, 36, 79], nonclassical crystallization pathways may be explored [80]. The environmental significant aspect of this class of synthesis is that hydrothermal and solvothermal routes allow inorganic materials to be prepared at substantially lower temperatures than those typically employed in solid-state reactions or also in many wet-chemistry routes such as the Pechini method or the sol–gel process, both involving a final annealing step at high temperature.

As reported in the cited as well as in further books and reviews [2, 10, 33–37, 39, 42–45, 47, 48, 50, 79–84] on the topic, solvo- and hydrothermal routes have been extensively applied to prepare a wide array of different inorganic compounds, many with also technological relevance such as ternary oxides. Recently, Walton [21] reviewed the mild solvothermal synthesis of metal perovskites and pyrochlores, by wisely outlining as solvothermal route is not a "processing step," but rather a "genuine synthesis method," allowing in most cases a one-pot and one-step formation of a highly crystalline form of the desired inorganic compounds. Furthermore, this approach enables, by using easy set-ups and recovery/purification steps, the synthesis of a wide plethora of inorganic materials in high yield and with reasonably short processing times.

Nevertheless, a challenging aspect of solvo/hydrothermal syntheses is that they occur in closed vessel, thus in many cases hindering the evolution of the system to be followed by spectroscopic, diffraction, or microscopy-related methods. Also the monitoring of the complex relationships among temperature, pressure, and the solvent chemicophysical properties (e.g., viscosity, dielectric constant), which have been extensively studied only for water [48, 85, 86] and which are relevant for the solubilization and recrystallization of the precursors, is in many cases prevented, or at least dramatically limited, by the reaction occurring in the "black-box" represented by the autoclave or by the reactor. In this context many efforts have been devoted to time- and temperature-resolved studies, always carried out at synchrotron facilities, thus exploiting the high spectral resolution and the shorter acquisition times (critical to follow the different steps of the reaction) enabled by the use of synchrotron light.

Recent and future developments in this field are to be mainly envisioned in the application of continuous flow reactors [87–92] as well as in the combination of hydrothermal synthesis with microwave heating [4, 43, 46, 62, 87, 93–96], affording formation of the targeted structures at relatively low temperatures.

1.2.2 Template-Assisted Synthesis Approaches

In the wide realm of low-temperature green synthesis approaches towards inorganic nanostructures, the use of structure directing agents such as templating agents and membranes, scaffolds, surfactants micelles, and ligands represents a powerful tool to direct the structural evolution of the targeted nanostructures [2, 27, 28, 97–116]. The resulting nanostructures display typically, depending on the morphology of the template, either 3D, 1D, or hollow morphologies. As outlined by Cushing et al. in their comprehensive review on the topic [3], a sharp distinction and classification can be hardly performed, since the general definition "template synthesis" encompasses a wide range of synthetic routes and methods which can be better described as hybrid approaches among further already discussed strategies (e.g., seeded growth in the presence of a ligand and colloidal-related methods).

The template-assisted synthesis is conceptually simple: the nucleation/growth of the targeted materials is let to occur either *on* or *inside/within* a suitable chosen or designed templating scaffold (typically displaying a completely different chemical nature and composition) dictating both the shape as well as the size of the forming material. In other words, the replication of one structure into another is accomplished under structural inversion. The scaffold can be either an assembly of monodispersed and shape-controlled nanostructures, a porous materials (the porosity being tuneable from the micro- (pore diameter $d<2$ nm) to the mesoporous ($2<d<50$) scale, according to IUPAC definition [117]), or a membrane (for instance in the case nanotubes or nanorods are the targeted morphology).

The most acknowledged definition of a template is as "a structure-directing agent." As reported by Thomas [100], in case of direct or "true" templating, the templated material is a 1:1 (but inverse) copy of the template structure, and no

changes in order or length scale of the template structure occur. Templating can therefore be seen as an effective approach to the formation of nanostructured or porous materials, as size and shape of the resulting pore structures can be easily tuned by choosing the appropriate template structures.

A further rough distinction can be performed between soft templating and hard templating [100]. The former are typically soft materials, such as micelles, gels, nature-derived scaffolds (e.g., chitin), affording the formation of globular or spherical systems which serve as templates, which then yield 3D, typically spherical. On the contrary, in the case of hard templating, hard inorganic materials such as silica and alumina are employed as negative replica of the targeted materials. In both cases, the removal of the templating agent (in the former case by typically using thermal treatment to trigger the oxidative degradation of the organic material or by an extraction with suitable solvents, in the latter one by selectively dissolving the inorganic template with etching agents such as HF) affords the formation of a material displaying a morphology which is the replica of the templating scaffold. The material can be either grown *on* the template or *within* the template. The use of reactive templates, acting both as structure directing agents as well as precursors have been also reviewed in the literature [104].

As far as the use of hard templates for the shaping of soft materials is concerned, a relevant contribution in this field is the paper by Thomas, Goettmann, and Antonietti [100], reviewing the use of hard templates for soft materials, also outlining the related critical issues. This review describes the possibilities of using hard templates to create nanostructured "soft" materials, for example, polymer networks, or carbonaceous materials. The authors give first of all a classification based on the distinction between endo- (e.g., silica and colloidal crystals) and exotemplating (e.g., zeolites, periodic mesoporous silica, and alumina membranes) inorganic materials (see Scheme 1.1), and for each class of approaches they provide extensive examples concerning the whole range of hard templates described in the literature, such as silica nanoparticles, zeolites, periodic mesoporous silicas, aluminum oxide membranes, and colloidal crystals. These approaches are, however, mostly devoted to the synthesis of soft materials, though the review of Thomas reports also the use of porous materials and membrane as scaffold for the synthesis of inorganic materials.

In the last years, an increasing interest has been devoted to the use of well defined and shape-controlled, ideally monodisperse polymer particles (latex) to be used as soft templates for the synthesis of metal or metal oxide nanoparticles. The template can be either sacrificial, being removed (through calcination or etching agents) in the final step of the synthesis (and yielding in this case hollow spheres), or rather be the core of a core-shell nanostructure. Alternatively, also inorganic hard templates can be used for the controlled formation of inorganic hollow spheres, although these latter approaches typically require the etching of valuable inorganic cores such as Au or Ag. Very spread is also the use of porous structures [3] to afford the spatially controlled growth on nanostructures. Zeolites [72, 73, 118–123], mesoporous materials [120, 124–135] as well as metalorganic framework [136–144] can be conveniently used as 3D scaffolds and/or nanoreactors for the formation of metal, metal oxides, and further inorganic binary or even ternary compounds. The main application for this kind of inorganic nanocomposites (typically metal or metal oxide

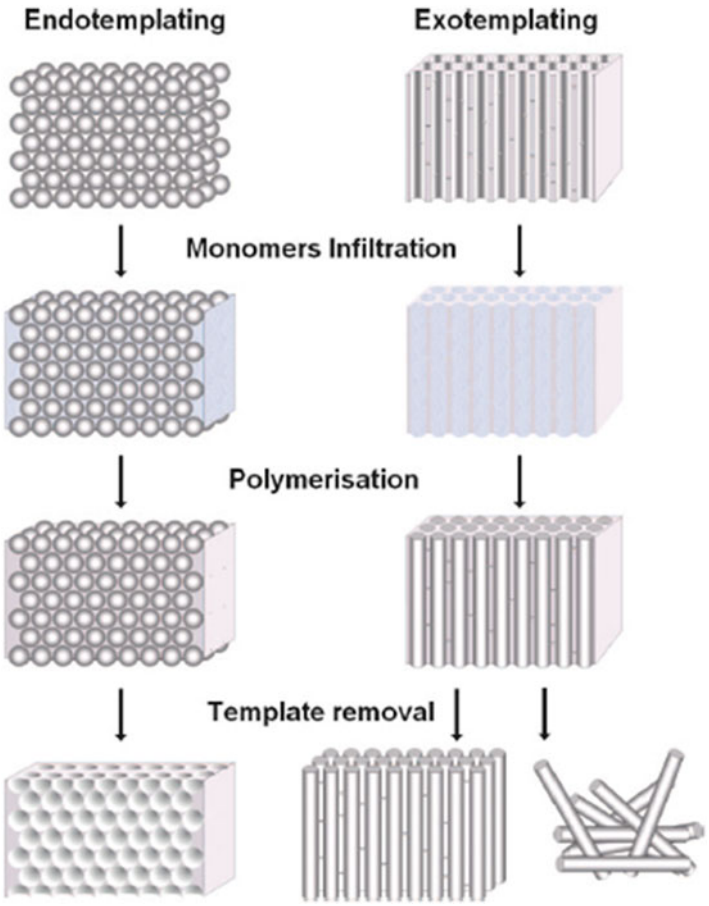

Scheme 1.1 Schematic presentation of templating approaches toward nanostructured soft materials using endo and exotemplates. Reprinted with permission from ref. [100]. Copyright 2008 American Chemical Society

nanoparticles inside metal oxides templating matrices) is as supported catalysts [145, 146] in the field of heterogeneous catalysis, although some authors have envisioned also further fascinating potential uses of these nanocomposites, for instance as luminescent materials [147–150]. A further implementation is represented by inorganic scaffolds serving as templates for the growth of further inorganic hard materials. As it can be appreciated from the figure below (Fig. 1.2), the degree of control on the final structures and morphology is very high.

In this case, which could be also envisioned as a particular case of growth in confined spaces, the wall of the porous material acts as "seed" for the formation of the targeted structure. For instance, mesoporous alumina has proven to display suitable surface chemistry to promote the adsorption of ions from aqueous solution [151], whereas a further and related approach is the impregnation of these porous

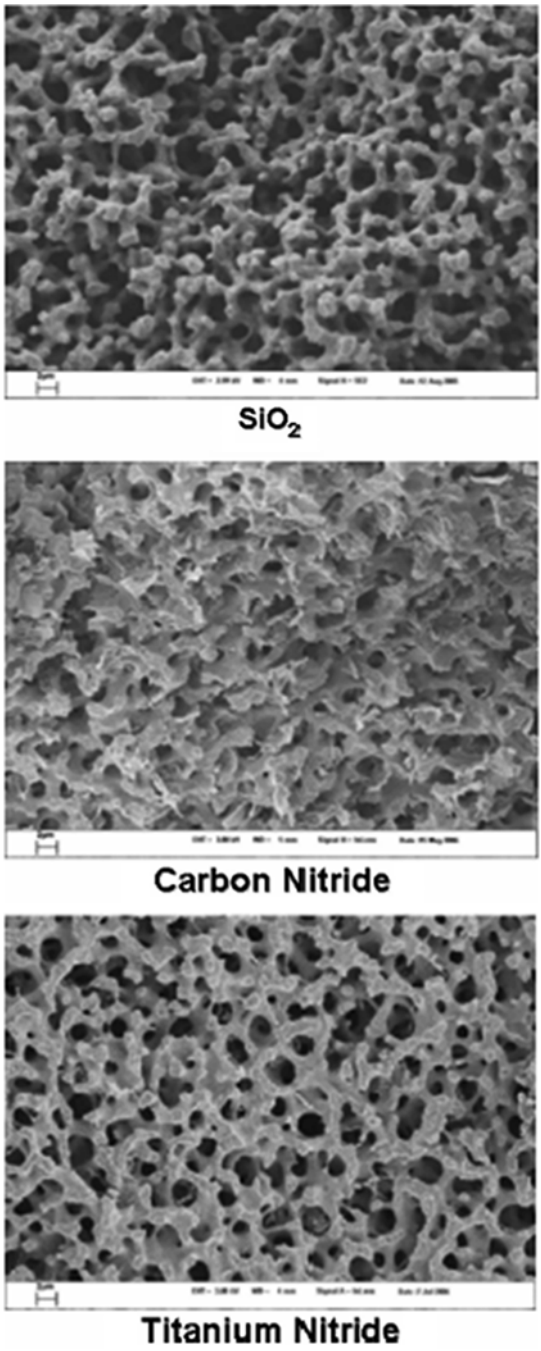

Fig. 1.2 SEM images of a macro-/mesoporous silica template, its carbon nitride replica, and a titanium nitride replica derived therefrom. Reprinted with permission from ref. [100]. Copyright 2008 American Chemical Society

materials in solution of a salt of the targeted compound and subsequent chemical reduction to the metal species. By this route, several examples on M-SiO_2 (M = Pt, Pd, Au) have been reported in the literature. As outlined in the review of Cushing et al., the aqueous nature of the reactions in which these processes occur somehow limits the number of metals (i.e., metals with negative standard electron potential are excluded) which can be produced by this approach [3].

As far as 1D nanostructures are concerned [100, 104], their ordered growth typically requires the presence of a tubular channel-based template. In this regard, a very widely used approach is based on the resort to inorganic membranes to template and direct the growth of anisotropic inorganic nanostructures. As reported in the review by Wong et al. [2], by using the cylindrical channels of membranes, different inorganic nanorods, nanowires, nanofibers, also displaying impressively ordered vertical assembly, have been prepared. From the sustainability point of view, as outlined by Wong, these template-assisted approaches are typically high-throughput, relatively simple, cost-effective, and requiring a low amount of reagents, the reactions typically occurring in aqueous media, and at low temperatures. The final step, implying the transformation of the precursors into the targeted compound is typically chemically triggered (i.e. a chemical reduction). Therefore, they can be generally considered environmentally friendly approaches. The use of the template method for the controlled synthesis of ordered array of inorganic functional materials, among which several ternary oxides ($BiFeO_3$, $Bi_2Ti_2O_7$, $BaCrO_4$, $BaWO_4$) as well as of metal fluorides such as CaF_2, SrF_2, BaF_2 have been reviewed by several authors [2, 104]. In particular, an exhaustive overview of different kinds of inorganic 1D nanostructures, also chiral ones, grown inside the channels of inorganic oxides is reported by Qi [104], discussing also the complex topological and structural relationships existing among the templating matrix and the resulting materials, as well as the obtainment of complex architectures and superstructures.

Hollow particles [8, 98, 102, 152–158] have gained an increasing attention, also in the field of drug delivery and biomedicine, for their unique ability to serve as confined reaction cavities as well as delivery systems able to release encapsulated substances upon certain stimuli. As far as hollow structures are instead concerned, their formation is typically based on the oriented growth of the final material on a sacrificial templating scaffold. In this framework, different authors have reported the successful synthesis of hollow spheres by typically using soft templates, which are then eventually removed.

1.3 Colloidal and Colloid Assemblies for the Synthesis of Inorganic Nanostructures

By exploiting the bewitching and fascinating potentials of the colloidal state [160–173], it can be realized how colloidal methods are among the most appealing routes for the low temperature preparation of inorganic colloids, since the complex interplay among the different experimental parameters involved (chemical nature

and chemico-physical properties of the surfactants, cosurfactants, dispersing media, and of dispersed phase) represents a versatile playground for the tailored growth of nanocrystals, enabling, in the above-mentioned mild conditions, a fine control on the very early stages of nanostructure formation (i.e., nucleation and growth).

As a matter of fact, the interplay among the different parameters involved (nature of dispersing and dispersed phase, chemical nature and structure of the surfactant(s), temperature, pH, power and time of sonication concentration of the reactants, the possible presence of electrolytes, water content, etc.) strongly affects the stability of the resulting colloidal dispersion, as well as size and polydispersity of the obtained nanostructures, and their role has been the topic of different reports and investigations [8, 15, 159–173]. The use of colloidal systems for crystallization processes in liquid phase has been recently reviewed by Rafael Muñoz-Espí et al. [15], but in the following section, we focus on the approaches involving a controlled nucleation and growth of crystalline colloidal nanostructures from solution/suspension and on the synthesis in confined space by exploiting the confinement dictated by the boundaries of droplets in suspension. Also, the crystallization of colloidal systems have been the focus of several investigations [15, 161, 166, 174–191].

1.3.1 Nucleation and Growth of Crystalline Colloidal Nanostructures from Solution/Suspension

This very wide class of approaches encompasses not only the experimentally optimized (1) nucleation and growth of inorganic nanocrystals in suspension (typically in the presence of stabilizing ligands) [192, 193], (2) the chemical reduction of metal salts to give different kinds of metal featuring very different morphologies (nanoparticles, nanoprisms, nanostars, etc.), and combination thereof, but also (3) the seeded growth in which small (<5 nm) nanoparticles act as seed for the epitaxial attachment of metal ions to give bigger nanostructures, thus turning a suspension of small nanoparticles into larger colloids.

Several further low temperature synthetic approaches are reported in the literature, which are based on colloids, colloid assemblies. A comprehensive overview is reported in some dedicated books [8, 9].

The nucleation of crystals from solution has been the topic of extensive investigations, from both the experimental and theoretical point of view. In this regard, classical and two-step models have been recently reviewed [80, 194]. In this paper by Erdemir it is pointed out as, in solution crystallization, the first event of nucleation plays a decisive role in determining the crystal structure and size distribution. The account further discusses the shortcomings and limitations of classical nucleation theory and review studies contributing to the development of the modern two-step model. This latter is based on the assumption that a sufficient-sized cluster of solute molecules forms first, followed by reorganization of that cluster into an ordered structure (Fig. 1.3).

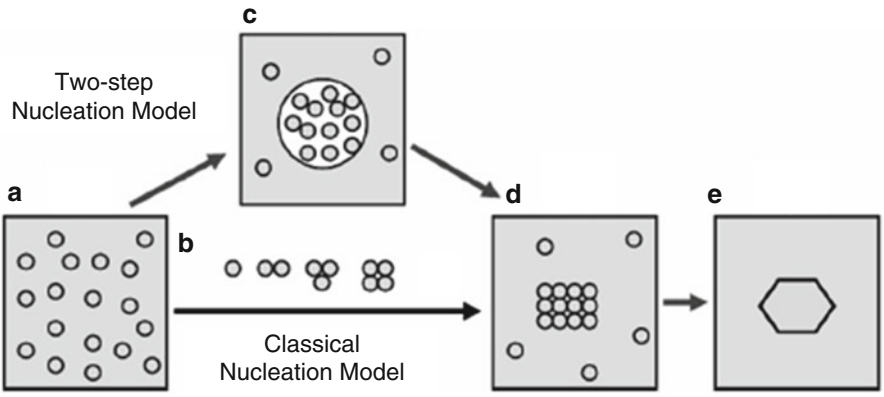

Fig. 1.3 Alternative pathways leading from solution to solid crystal: (**a**) supersaturated solution; (**b**) ordered subcritical cluster of solute molecules, proposed by classical nucleation theory; (**c**) liquid like cluster of solute molecules, dense precursor proposed by two-step nucleation theory; (**d**) ordered crystalline nuclei; (**e**) solid crystal. Reprinted with permission from Ref. [194]. Copyright 2008 American Chemical Society

The molecular mechanism of nucleation, the evolution from nuclei to seeds, and from seeds to nanocrystals, and the influence on it of thermodynamic and kinetic control, have been described also by Xia and other authors in a recent review [195] devoted to shape-controlled synthesis of metal nanocrystals, highlighting also the pivotal role played by structure, shape, and exposed facets of an inorganic nanocrystal in catalysis and optics. In a comprehensive and excellent paper, Polarz [196] discusses the morphology energy landscape leading to anisotropy of inorganic colloidal particles and points out the strong effects that shape and morphology have not only on the catalytic properties but also on the optical, electronic, mechanical, and self-assembly properties. Therefore, the tailoring of particle shape, size, morphology, and crystallinity becomes a condition to get the desired functionality and properties [104, 187, 189, 197–201].

As far as the nucleation and growth of metal colloidal nanostructures is concerned, some comprehensive reviews have been published dealing with the synthesis of nanosized metal and alloys nanoparticles from solution. Starting from the pioneering work of Faraday, dated back to 1857, the chemical reduction of transition metal salts in the presence of stabilizing agents to generate zerovalent metal colloids in aqueous or organic media is one of the most applied approach to the wet-chemistry low-temperature synthesis of these materials (S. Bradley, in: [202]). The first reproducible standard protocols for the preparation of metal colloids (e.g., gold by reduction of $HAuCl_4$ with sodium citrate) were established by Turkevich [174, 203], but afterwards several further paramount contributions were reported [204]. Solution synthesis of metal nanoparticles and their applications have been reviewed by several authors [4, 8, 16, 49, 182, 205–213].

As far as this approach is concerned, reducing metal salts to the zerovalent metallic form is a widely used, effective, one-step and one-pot strategy to produce a wide

plethora of metal nanostructure. This real bottom-up approach ensures limited use of reactants and thus complies with the atom economy paradigm of green chemistry. Typically used ligands are, according to the nature of the metal to be stabilized, thiol, amines, phosphines. For instance, gold nanoparticles are effectively stabilized by thiol ligands. Different thiol-stabilized noble metal nanoparticles (e.g., Au, Ag, Pt, Pd) have been extensively reviewed elsewhere [4, 17, 23, 207, 214–217]. The synthesis of metals through reduction from both aqueous and not aqueous solutions has been extensively reviewed by Cushing et al., also reporting a survey of metals (Fe, Co, Ni, Ru, Ag, Au) and metal alloys (Co_xNi_y, Fe_xNi_{1-x}) reduced from both typologies of solutions. The review by Cushing also reports a very detailed (though not updated, dating the review 2004) survey of several coordinating polymers and capping ligands for the stabilization of nucleated colloids, based on O-, C-, N-, P-, S- donor atoms [3].

In regard to the synthesis of inorganic oxidic nanostructures, the surfactants-free nucleation/growth of transparent suspensions of colloidal nanocrystals from a precursors solution is typically relying on the sol–gel reaction of suitable precursors (e.g., metal acetates and acetylacetonates) in the presence of a base. Among metal oxides, one of the most investigated ones is zinc oxide. ZnO is a very intensively studied material: and its properties, applications [218–220] and synthesis route have been extensively reviewed by several authors [52, 53, 182, 218–237], to which interested readers are referred. The classical route to ZnO nanocrystals explored by Bahnemann is based on the reaction of zinc acetate with NaOH in 2-propanol [192]. In this paper, Bahnemann and coworkers observed as the changes in the solvent nature could affect also the spectral features of the obtained colloids. In an analogous fashion, we have recently performed a thorough study and pointed out also the role that the chemicophysical properties of the dispersing medium, mainly its viscosity and dielectric constant, have on the structural and morphological evolution of the forming inorganic colloids, in our case nanosized zinc oxide [238]. In our case, by modifying and optimizing the well-known procedure reported by Spanhel et al. and Bahmemann et al. [192, 193, 221, 229, 239], we developed an easy and highly reproducible route to nanostructured colloidal ZnO nanoparticles based on the controlled hydrolysis and condensation of zinc acetylacetonate (acac) in alkaline conditions. It turned out that the four different tested dispersing media (water, glycol, 2-propanol, ethanol) proven to exert a strong influence not on the crystalline phase (in all cases wurtzite) but on the growth direction of the nanostructures and on their final shape and morphology (spherical or needle-like). In the case of metal oxides, effective moieties to strong bind the ligand to the hydroxylated surface of the oxides are carboxylates, cathecolates, phosphates [240–247].

Many further example of the application of these straightforward syntheses to other inorganic crystalline materials are reported in the literature. The same approach, based on a controlled precipitation, can be implemented to the synthesis of metal sulfides and further oxide colloids. A further approach relies on the reaction of suitably tailored molecular precursors, which spontaneously or under application of stimuli (e.g., heat) decomposes to give the targeted M_xS_y compounds.

As far as the seeded growth is instead concerned, it turns out that the use of structurally well defined seeds is critical to afford nanostructures with controlled morphologies and narrow size distribution. The co-presence, in the precursor suspension, of further structure directing agents such as surfactants can further contribute to achieve, for instance, anisotropic structures. By suitably optimizing the experimental conditions, the controlled, low or even room temperature crystallization of inorganic nanomaterials can be accomplished. In this regard, the review of Dahl also discusses in detail the role that seeds, reducing agent, additives and ligands (if present) have on the final morphology, structure, size, and size distribution of the resulting inorganic materials. The use of etching agents and methods enable in this context to access also exotic anisotropic nanostructures (such as nanoprisms), whose achievement is justified by enhanced functional properties, typically optical ones, anisotropic nanostructures are endowed with [248]. In fact, just to cite the most relevant ones, the optical properties of nanostructures are shown to be mainly influenced by the surface plasmon resonance of conduction electrons, the frequency of which is determined not only by the nature of the metal but also by a number of other parameters, such as particle size and shape, the presence of a capping shell on the particle surface, or the dielectric properties of the surrounding medium [16]. In this framework, Mulvaney, Alivisatos, Marzan, Pileni [16, 23, 179, 183, 201, 249–256] and further authors have also investigated the role that surfactants as well as ligands can play in orienting the anisotropic growth by, for instance, directing the epitaxial growth of one crystallographic phase at the same time hindering the growth of others. As far as the use of etching agents is concerned, their use allows modifying the growth mechanism within typical reduction-based approaches, affording the crystallization of colloids featuring unusual and exotic geometries. A very simple example in this regard is the adaptation of the classical reduction synthesis method for silver nanoparticles, typically obtained by reduction of silver nitrate in the presence of either citrate or sodium borohydride. If hydrogen peroxide and potassium bromide are added in tiny amounts to the starting solution, before the reducing agent is added, instead of the classical spherical shaped nanoparticles, the formation of silver nanoprims [210, 249] can be observed. In this case, the careful choice of suitable shape modifying agents affords the growth of the nanostructures in the desired morphology. Analogously, Murphy et al. successfully prepared silver nanowires by etching the metallic nanostructures with sodium hydroxide [257].

As far as other binary metal compounds are concerned, metal sulfides [5, 182, 258–262] are surely those attracting most interest, due to their exciting functional properties. One example of interesting colloidal approach to metal sulfides by exploiting the different experimental parameters of colloidal suspensions is the one we developed some years ago, addressing the synthesis of colloidal CuS nanostructures by taking advantage of the peculiar features, i.e. inherent viscosity and low dielectric constant, of the dispersing media, in this case carboxylic acids [263]. The crystalline hexagonal phase (covellite) of CuS is often described as a p-type semiconductor (*energy gap* 1.2–2.0 eV) [264–268] which shows superconductivity at 1.6 K. In our case, we design an original synthesis route base on promoting the controlled nucleation and growth on the CuS nanoparticles in a carboxylic acid.

In detail, the optimized methodology was based on the fast nucleation of the sulfide triggered by the reaction of thioacetic acid (acting as a slowly releasing sulfide source) with water and copper carboxylates (acetate, propionate) in the corresponding carboxylic acid (acetic, propionic) as a solvent.

1.3.2 Miniemulsion and Microemulsion: Chemistry in Nanoreactors

This section is not intended to be comprehensive and cover the whole array of available colloidal emulsion-based methods, but rather to focus on selected methods allowing the spatially controlled formation and growth of colloidal nanostructures. Among these colloidal methods, those of microemulsion and the related miniemulsion approaches represent a very appealing option. Although the reviewed methods have been initially developed for polymer and hybrid systems, our attention will be exclusively focused on their implementation in the field of inorganic preparative chemistry. At the beginning the definition of microemulsion was quite contested [269], but presently a general accepted definition describes microemulsion as a dispersion made of water, oil, and surfactant(s), which is an isotropic and thermodynamically stable system with dispersed structure having a diameter typically ranging in the 1–100 nm range [167, 168, 270–272]. In this context, the role of the surfactant is to reduce the interfacial tension and stabilize the whole dispersion: its chemical nature, in particular in terms of hydrophilic-lipophilic balance (HLB) is one of the most important parameters in ruling the dispersion stability. HLB is an empirical value which numerically depends on the amount and nature of the hydrophilic/lipophilic chemical moieties present in the given surfactant chemical structure [273].

Though the many similarities and common features, at variance to that, miniemulsions are kinetically stabilized heterophase system with an average droplet size is in the range of 30–500 nm [15, 152, 169, 274–282]. This metastable state is represented by a critically stabilized system for which droplets collision and diffusional degradation processes are hindered. This means that, whereas upon mixing two microemulsions there is an immediate reagents exchange, when mixing two miniemulsions the droplets do not spontaneously exchange reactants, but rather require an external stimulus (i.e., ultrasound).

Both systems can be classified according to the nature of the prevailing phase as direct or inverse micro- or miniemulsion, the former being characterized by oil droplets dispersed in water as dispersing medium (oil-in-water (O/W) micro- or miniemulsions) the latter being instead characterized by water droplets in dispersed in the continuous organic phase (water-in-oil, W/O).

In miniemulsion, the diffusional degradation processes, leading to the Ostwald ripening phenomenon (larger droplets growing at the expense of smaller ones), is counteracted by adding a “co-stabilizer” or “osmotic pressure agent.” This additive is insoluble in the continuous phase and therefore generates an osmotic pressure between the droplets, which counterbalances the Laplace pressure (due to the

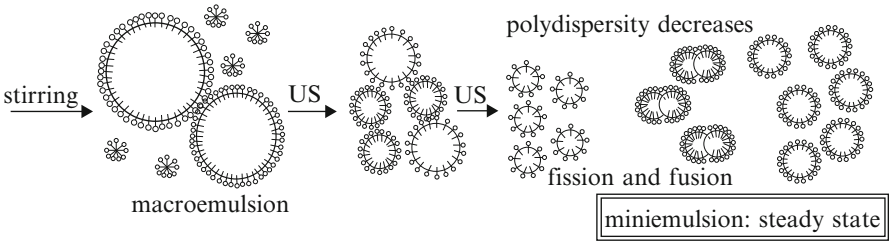

Fig. 1.4 Scheme for the formation of miniemulsion by ultrasounds. Reprinted with permission from ref. [276]. Copyright 2002 Elsevier

curved interfaces and causing the diffusional degradation) and restricts the mass transfer. This co-stabilizer is usually a long-chain hydrocarbon (most commonly hexadecane) in the case of direct miniemulsions, whereas in the case of inverse miniemulsion is either a salt or a sugar.

Whereas microemulsions are typically spontaneously formed by mechanical stirring, miniemulsion does instead require high shear forces produced by high energy ultrasounds (on a lab scale) or high-pressure devices (for upscaled applications). These high shear forces induce constant fission and fusion processes between the droplets, leading to a strong decrease in droplets size and polydispersity, until a "steady state" is eventually reached (see Fig. 1.4) [152, 169, 275–278, 283].

Although, as previously mentioned, they have been mostly used for the preparation of polymer or hybrid systems [274–276, 284–289], the fascinating concept underlying the extension of these two approaches to the inorganic synthesis is the use of the formed droplets to let the desired reaction to occur within the confined space dictated by the droplets boundaries. This "chemistry in a nanoreactor" has been successfully applied by several authors to accomplish the formation of crystalline inorganic nanostructures at low or even room temperatures [15, 152, 169, 173, 277, 278, 281, 282, 290]. In particular, if the inorganic nanoparticles and nanostructures are targeted, inverse W/O microemulsions are the most convenient systems to be used, since the involved reactions are typically occurring in aqueous medium and also because the solubility of inorganic precursors in water is typically higher than in organic solvents.

For both methods, the nanoreactor approach is a two steps one: two different micro- or miniemulsion are prepared: one containing a metal salt aqueous solution, the other one an aqueous solution containing a precipitating (e.g., a base and a sulfide source) or a reducing agent (e.g., sodium borohydride and a citrate). Upon miniemulsification, the shear forces imparted on the individual droplets of both precursors force them to undergo fission and fusion processes, leading to an immediate reaction between the precursors, typically a precipitation or a chemical reduction.

The described two-microemulsions/miniemulsions-based approach can be conveniently used to prepare binary metal compounds such as metal halogenides,

sulfide and oxide. These latter represents the main class of compounds prepared through microemulsion systems, being the reaction of choice typically a precipitation of the targeted oxide by adding to the micro- or miniemulsion containing the metal oxide

Mini- and microemulsion can be also conveniently used for the preparation of hollow structures [154, 291], as well as of core-shell nanostructures [173, 292], either fully inorganic or hybrid organic–inorganic. The most common strategy to prepare hollow particles relies on the use of a sacrificial template, removed afterwards by thermolysis or dissolution [98, 153, 293]. An even more elegant approach to these inorganic nanocapsules is to promote the sol–gel processes at the liquid–liquid interface. This is possible through the so-called "soft-template" routes, involving the presence of surface-active agents [15].

Whereas for silica several examples are reported [291], for metal compounds such as metal oxides and chalcogenides, reports on the formation of hollow particles by soft-template methods are much more limited. Recently, Muñoz-Espí et al. successfully addressed the synthesis of transition metal oxides and hydroxides of group 4 (i.e., TiO_2, ZrO_2, and HfO_2) by exploiting the sol–gel precipitation of zirconium and hafnium hydroxides ($ZrO(OH)_2 \cdot H_2O$ and $HfO(OH)_2 \cdot H_2O$) at the droplet interface by creating interfacial species through the addition of triethylamine to water in- oil miniemulsions containing the inorganic precursor (zirconium or hafnium oxychloride). In this case, a mild thermal treatment of the samples was required to yield the corresponding metal oxide, ZrO_2 or HfO_2, being the method suitable also to prepare mixed metal oxides of defined composition, $Hf_xZr_{1-x}O_2$ [294]

The careful optimization of the surfactant self-assembly and concentration enables also a fine control over particle shape, which can be also tailored through the addition of different salts to the emulsion [295]. As outlined in Sect. 1.3.1, the most straightforward approach to metallic nanoparticles is the chemical reduction of corresponding metal salts. Such method can be easily implemented to micro- and miniemulsion systems, letting the reduction reaction to occur in the confined space of the droplets. As far as microemulsions are concerned, Pileni and coworkers have pioneered an interesting approach in which an anionic surfactant (typically Aerosol OT (AOT)), is used, whose counter ion is the metal of interest [296, 297]. They reported the successful synthesis of metallic copper [298, 299] and silver [300–302].

An alternative route relies on the incorporation and subsequent decomposition of single-source precursors such as metal complexes with 2-ethylhexanoates, acetylacetonates, or 1,5-cyclooctadienes into o/w microemulsion to promote the synthesis of metallic nanoparticles [303]. Microemulsions were also exploited for the preparation of substitutional alloys, such as Fe_xPt_y alloys [304].

As far as the resort to inverse miniemulsion for the synthesis of metal or metal alloys is concerned, Landfester et al. [274, 290] used, as polar phase, low melting point metals (gallium, mp = 29 °C or sodium, mp = 98 °C) or alloys (Wood's metal, mp = 70 °C or Rose's metal, mp = 110 °C), which were heated above their melting temperature and miniemulsified in hydrophobic continuous phase by using amphi-

philic block copolymers. By lowering again the temperature, solidification of the metal and formation of stable nanoparticles were accomplished.

For oxidic nanostructures, the sol–gel process is particularly convenient for the preparation of oxide materials, especially when aiming at porous materials, due to the high flexibility and tunability they allow (good control on stoichiometry of the final products). At the same time, micro- and miniemulsion ensure a finer and more controllable grain size [305, 306].

By the two miniemulsions-based route, different inorganic crystalline compounds were produced by precipitation in confined space, such as pure and doped ZnO [307, 308], $M(OH)_2$ (M = Ca, Mg) [309], lanthanide-based phosphors [310], ZrO_2/HfO_2, CeO_2 [311], TiO_2 [312, 313]. The nanoreactor concept can be also conveniently exploited to afford the controlled decomposition of tailored single–source to yield crystalline nanocomposites, for instance through decomposition processes triggered by light. An example in this framework is reported by our group [314]. The gold-containing titanium peroxo-complex $AuCl_4(NH_4)_7[T_{i2}(O_2)_2(Hcit)(cit)]_2 \cdot 12H_2O$ is a crystalline molecular single-source precursor of the composite Au/TiO_2 [315]. Upon thermal treatment at 700 °C it decomposes to generate the crystalline composite; the decomposition can also be induced by UV irradiation. In the mentioned work, the single-source precursor was suspended in an inverse miniemulsion and subjected to photodecomposition. As expected by this pathway, a fine dispersion of crystalline gold nanoparticles dispersed on amorphous titania was obtained. The products were used as catalyst in the gaseous phase oxidation of 2-propanol, also comparing them with similar products obtained in bulk suspension. Interestingly, samples prepared in miniemulsion showed a strong increase in both conversion and selectivity.

All these examples have shown as, in the confined space produced inside the droplets, unconventional crystallization pathways can occur, leading to the crystallization already at room temperature. For instance, in the case of miniemulsion, Landfester and coworkers [15, 152, 169, 275, 277, 278, 283] have already pointed out interesting effects of the confined space on the fate and structural evolution of the contained inorganic systems. It was pointed out as physical properties of liquids in nanodroplets can be substantially different from those of the bulk phase and therefore the morphosynthetical control of the crystalline *habitus* of the formed structures was highlighted.

Also, the confined space can alter the fate of the chemical systems. As a working example, in the case of ZnO synthesis in inverse miniemulsion [307], the confinement of the precursor formulation in a the droplet was proven to be a key issue in determining the formation of wurtzite instead of the expected (in the adopted pH range) zinc hydroxide. In fact, in basic media (in our case the pH of the final miniemulsion was determined to be 13.4), Zn^{II} ions form the amphoteric hydroxide species, $ZnO_x(OH)_g(H_2O)_z$ in a colloidal state, which forms as amorphous or crystalline species. This species spontaneously evolves to crystalline wurtzite ZnO not only under the action of heating or irradiation, through a dehydration process, but also upon prolonged storing and aging in its mother liquor, which in this case was pursued by their confinement.

1.4 Conclusions

In this chapter, four of the most employed wet-chemistry and colloid-based routes affording the controlled crystallization of different inorganic nanostructures at low or even room temperature, have been reviewed and discussed. In particular, the focus of the contribution was on synthetic approaches based on mild conditions and/or low temperatures. In most of the presented examples, the crystallization of the inorganic nanostructures was pursued at low ($T < 200$ °C) or room temperature. Though not comprehensive, the chapter aimed at providing a broad overview on the potential and advantages of these low temperature approaches to controlled shaped inorganic nanostructures.

Acknowledgements The Italian National Research Council (CNR), the University of Padua, Italy, and the SABIC company are acknowledged for equipment and financial support. S. G. would like to warmly thank her present and former master and PhD students, in particular Dr. Stefano Diodati and Dr. Paolo Dolcet (Dipartimento di Scienze Chimiche, Università di Padova) for their valuable and reliable support in the everyday chemist life and for their precious scientific contribution.

References

1. Anastas PT, Warner JC (2000) Green chemistry theory and practice. Oxford University Press, New York
2. Mao Y, Park T-J et al (2007) Environmentally friendly methodologies of nanostructure synthesis. Small 3(7):1122–1139
3. Cushing BL, Kolesnichenko VL et al (2004) Recent advances in the liquid-phase syntheses of inorganic nanoparticles. Chem Rev 104(9):3893–3946
4. Dahl JA, Maddux BLS et al (2007) Toward greener nanosynthesis. Chem Rev 107:2228–2269
5. Mitzi DB (2004) Solution-processed inorganic semiconductors. J Mater Chem 14(15):2355–2365
6. Mitzi DB (2009) Solution processing of inorganic materials. Wiley, Hoboken
7. Schubert U, Hüsing N et al (2008) Materials syntheses. Springer, Vienna
8. Caruso F (ed) (2004) Colloids and colloid assemblies—synthesis, modification, organization and utilization of colloid particles, 1st edn. Wiley-VCH, Weinheim
9. Schmid G (ed) (2004) Nanoparticles: from theory to application. Wiley-VCH Verlag GmbH & Co. KGaA, Weinheim
10. Schubert U, Hüsing N (2005) Synthesis of inorganic materials, 2nd edn. Wiley-VCH, Weinheim
11. Glaister RM, Allen NA et al (1965) Comparison of methods for preparing fine ferrite powders. Proc Brit Ceram Soc No 3:67–80
12. Sritharan T, Boey FYC et al (2007) Synthesis of complex ceramics by mechanochemical activation. J Mater Process Technol 192–193:255–258
13. Lazarevic ZZ, Jovalekic C et al (2012) Preparation and characterization of nano ferrites. Acta Phys Pol 121:682–686
14. Niederberger M, Pinna N (2009) Metal oxide nanoparticles in organic solvents—synthesis, formation assembly and applications. Springer, New York
15. Muñoz-Espí R, Mastai Y et al (2013) Colloidal systems for crystallization processes from liquid phase (invited highlight). CrystEngComm 15(12):2175–2191

16. Liz-Marzan LM (2006) Tailoring surface plasmons through the morphology and assembly of metal nanoparticles. Langmuir 22(1):32–41
17. Grzelczak M, Perez-Juste J et al (2008) Shape control in gold nanoparticle synthesis. Chem Soc Rev 37(9):1783–1791
18. Abalde-Cela S, Aldeanueva-Potel P et al (2010) Surface-enhanced Raman scattering biomedical applications of plasmonic colloidal particles. J R Soc Interface 7:S435–S450
19. Alvarez-Puebla RA, Liz-Marzan LM (2010) Environmental applications of plasmon assisted Raman scattering. Energy Environ Sci 3(8):1011–1017
20. Wang YX, Yun WB et al (2003) Achromatic Fresnel optics for wideband extreme-ultraviolet and X-ray imaging. Nature 424(6944):50–53
21. Modeshia DR, Walton RI (2010) Solvothermal synthesis of perovskites and pyrochlores: crystallisation of functional oxides under mild conditions. Chem Soc Rev 39(11):4303–4325
22. Sakdinawat A, Attwood D (2010) Nanoscale X-ray imaging. Nat Photon 4(12):840–848
23. Romo-Herrera JM, Alvarez-Puebla RA et al (2011) Controlled assembly of plasmonic colloidal nanoparticle clusters. Nanoscale 3(4):1304–1315
24. Calvert P, Rieke P (1996) Biomimetic mineralization in and on polymers. Chem Mater 8(8):1715–1727
25. Livage J, Sanchez C (2005) Towards a soft and biomimetic nanochemistry. Actual Chim 290–291:72–76
26. Sanchez C, Arribart H et al (2005) Biomimetism and bioinspiration as tools for the design of innovative materials and systems. Nat Mater 4:277–288
27. Andre R, Tahir MN et al (2012) Bioinspired synthesis of multifunctional inorganic and bioorganic hybrid materials. FEBS J 279:1737–1749
28. Ma T-Y, Yuan Z-Y (2012) Bioinspired approach to synthesizing hierarchical porous materials. Wiley-VCH Verlag GmbH & Co. KGaA, Weinheim
29. Lepoint T, Lepoint-Mullie F et al (1999) Single bubble sonochemistry. In: Crum LA, Mason TJ, Reisse JL, Suslick KS (eds) Sonochemistry and sonoluminescence. Kluwer, Dordrecht, Netherlands, pp 285–290
30. Kumar RV, Palchik O et al (2002) Sonochemical synthesis and characterization of Ag2S/PVA and CuS/PVA nanocomposite. Ultrason Sonochem 9(2):65–70
31. Wang H, Zhang J-R et al (2002) Preparation of copper monosulfide and nickel monosulfide nanoparticles by sonochemical method. Mater Lett 55(4):253–258
32. Cansell F, Chevalier B et al (1999) Supercritical fluid processing: a new route for materials synthesis. J Mater Chem 9:67–75
33. Aimable A, Muhr H et al (2009) Continuous hydrothermal synthesis of inorganic nanopowders in supercritical water: towards a better control of the process. Powder Technol 190:99–106
34. Hayashi H, Hakuta Y (2010) Hydrothermal synthesis of metal oxide nanoparticles in supercritical water. Materials 3:3794–3817
35. Kuznestov VA (1973) Hydrothermal method for the growth of crystals. Sov Phys Crystallogr 17(4):775–804
36. Labachev AN (1973) Crystallization processes under hydrothermal conditions. Consultants Bureau, New York
37. Francis RJ, O'Hare D (1998) The kinetics and mechanisms of the crystallisation of microporous materials J Chem Soc Dalton Trans 19:3133–3148
38. Rickard DT, Wickman FE (1981) Chemistry and geochemistry of solutions at high temperature and pressure. Pergamon, New York
39. Laudise RA (1987) Hydrothermal crystal growth—some recent results. In: Dryburgh PM, Cockayne B, Barraclough KG (eds) Advanced crystal growth. Prentice Hall, New York, pp 267–286
40. Whittingham MS, Guo J-D et al (1995) The hydrothermal synthesis of new oxide materials. Solid State Ion 75:257–268
41. Whittingham MS (1996) Hydrothermal synthesis of transition metal oxides under mild conditions. Curr Opin Solid State Mater Sci 1(2):227–232

42. Segal D (1997) Chemical synthesis of ceramic materials. J Mater Chem 7:1297–1305
43. Somiya S, Roy R (2000) Hydrothermal synthesis of fine oxide powders. Bull Mater Sci 23:453–460
44. Byrappa K, Yoshimura M (2001) Handbook of hydrothermal technology—a technology for crystal growth and materials processing. Noyes, Park Ridge
45. Feng S, Xu R (2001) New materials in hydrothermal synthesis. Acc Chem Res 34(3):239–247
46. Yu S-H (2001) Hydrothermal/solvothermal processing of advanced ceramic materials. J Ceram Soc Jpn 109:S65–S75 (Copyright (C) 2013 American Chemical Society (ACS). All Rights Reserved.)
47. Cundy CS, Cox PA (2005) The hydrothermal synthesis of zeolites: precursors, intermediates and reaction mechanism. Microporous Mesoporous Mater 82(1–2):1–78
48. Sheets WC, Mugnier E et al (2006) Hydrothermal synthesis of delafossite-type oxides. Chem Mater 18(1):7–20
49. Tavakoli A, Sohrabi M et al (2007) A review of methods for synthesis of nanostructured metals with emphasis on iron compounds. Chem Pap 61(3):151–170
50. Querejeta A, Varela A et al (2009) Hydrothermal synthesis: a suitable route to elaborate nanomanganites. Chem Mater 21(9):1898–1905
51. Shi W, Song S et al (2013) Hydrothermal synthetic strategies of inorganic semiconducting nanostructures. Chem Soc Rev 42(13):5714–5743
52. Ehrentraut D, Sato H et al (2006) Solvothermal growth of ZnO. Prog Cryst Growth Ch 52(4):280–335
53. Baruah S, Dutta J (2009) Hydrothermal growth of ZnO nanostructures. Sci Technol Adv Mater 10(1):013001
54. Chen X, Fan H et al (2005) Synthesis and crystallization behavior of lead titanate from oxide precursors by a hydrothermal route. J Cryst Growth 284:434–439
55. Liu N, Chen X et al (2014) A review on TiO_2-based nanotubes synthesized via hydrothermal method: formation mechanism, structure modification, and photocatalytic applications. Catal Today 225:34–51
56. Mai H-X, Sun L-D et al (2005) Shape-selective synthesis and oxygen storage behavior of ceria nanopolyhedra, nanorods, and nanocubes. J Phys Chem B 109(51):24380–24385
57. Zhang J, Liu S et al (2011) A simple cation exchange approach to Bi-doped ZnS hollow spheres with enhanced UV and visible-light photocatalytic H_2-production activity. J Mater Chem 21(38):14655–14662
58. Liu S, Lu X et al (2013) Preferential c-axis orientation of ultrathin SnS_2 nanoplates on graphene as high-performance anode for Li-Ion batteries. ACS Appl Mater Interfaces 5(5):1588–1595
59. Zhang H, Wei B et al (2013) Cation exchange synthesis of ZnS-Ag_2S microspheric composites with enhanced photocatalytic activity. Appl Surf Sci 270:133–138
60. Zhang Y-P, Liu W et al (2014) Morphology–structure diversity of ZnS nanostructures and their optical properties. Rare Metals 33(1):1–15
61. Weiß Ö, Ihlein G et al (2000) Synthesis of millimeter-sized perfect $AlPO_4$-5 crystals. Micropor Mesopor Mater 35–36:617–620
62. Baruwati B, Nadagouda MN et al (2008) Bulk synthesis of monodisperse ferrite nanoparticles at water-organic interfaces under conventional and microwave hydrothermal treatment and their surface functionalization. J Phys Chem C 112:18399–18404
63. Lorentzou S, Zygogianni A et al (2009) Advanced synthesis of nanostructured materials for environmental applications. J Alloys Compd 483(1–2):302–305
64. Makovec D, Kodre A et al (2009) Structure of manganese zinc ferrite spinel nanoparticles prepared with co-precipitation in reversed microemulsions. J Nanopart Res 11:1145–1158
65. Goh SC, Chia CH et al (2010) Hydrothermal preparation of high saturation magnetization and coercivity cobalt ferrite nanocrystals without subsequent calcination. Mater Chem Phys 120(1):31–35

66. Diodati S (2013) Sintesi e caratterizzazione di ferriti nanostrutturate (Synthesis and characterisation of nanostructured ferrites). Ph.D. thesis, Scuola di Dottorato in Scienze Molecolari [Scienze Chimiche], University of Padova, Italy
67. Diodati S, Pandolfo L et al (2014) Green and low temperature synthesis of nanocrystalline transition metal ferrites by simple wet chemistry routes. Nano Res 7(7):1027–1042
68. Chen L, Shen Y et al (2009) Large-scale synthesis of uniform spinel ferrite nanoparticles from hydrothermal decomposition of trinuclear heterometallic oxo-centered acetate clusters. Mater Lett 63:1099–1101
69. Ma Z, Zhou B et al (2013) Crystalline mesoporous transition metal oxides: hard-templating synthesis and application in environmental catalysis. Front Environ Sci Eng 7(3):341–355
70. Gyergyek S, Drofenik M et al (2012) Oleic-acid-coated $CoFe_2O_4$ nanoparticles synthesized by co-precipitation and hydrothermal synthesis. Mater Chem Phys 133(1):515–522
71. Holden A, Singer P (1971) Crystals and crystal growing. Anchor Books Doubleday & Company Inc., Garden City, New York
72. Ferey G (2000) Building units design and scale chemistry. J Solid State Chem 152:37–48 (Copyright (C) 2013 American Chemical Society (ACS). All Rights Reserved.)
73. Ferey G (2000) The zeolites. Recherche: 72
74. Altmaier S, Behrens P (2003) Modification of ordered mesostructured materials during synthesis. Wiley-VCH Verlag GmbH & Co. KGaA, Weinheim
75. Lide DR (2004) Handbook of chemistry and physics, 84th edn. CRC Press, Boca Raton
76. Dolejš D, Manning CE (2010) Thermodynamic model for mineral solubility in aqueous fluids: theory, calibration and application to model fluid-flow systems. Geofluids 10(1–2):20–40
77. MacLaren I, Ponton CB (2000) A TEM and HREM study of particle formation during barium titanate synthesis in aqueous solution. J Eur Ceram Soc 20:1267–1275
78. Bacha E, Deniard P et al (2011) An inexpensive and efficient method for the synthesis of BTO and STO at temperatures lower than 200 °C. Thin Solid Films 519(17):5816–5819
79. Labachev AN (1971) Hydrodrothermal synthesis of crystals. Nauka, Moscow
80. Cölfen H, Antonietti M et al (2008) Mesocrystals and nonclassical crystallization. Wiley, New York
81. Cheng H, Ma J et al (1995) Hydrothermal preparation of uniform nanosize rutile and anatase particles. Chem Mater 7(4):663–671
82. Gopalakrishnan J (1995) Chimie Douce approaches to the synthesis of metastable oxide materials. Chem Mater 7(7):1265–1275
83. Mao Y, Banerjee S et al (2003) Hydrothermal synthesis of perovskite nanotubes. Chem Commun 3:408–409
84. Burda C, Chen X et al (2005) Chemistry and properties of nanocrystals of different shapes. Chem Rev 105(4):1025–1102
85. Antoine C (1888) Tensions des vapeurs; vouvelle relation entre les tensions et les températures. C R Acad Sci 107:681–684
86. Lide DR (2009) CRC handbook of chemistry and physics (Internet version), 89th edn. CRC Press/Taylor and Francis, Boca Raton
87. Rajamathi M, Seshadri R (2002) Oxide and chalcogenide nanoparticles from hydrothermal/solvothermal reactions. Curr Opin Solid State Mater Sci 6:337–345
88. Tighe CJ, Gruar RI et al (2012) Investigation of counter-current mixing in a continuous hydrothermal flow reactor. J Supercrit Fluids 62:165–172
89. Gimeno-Fabra M, Dunne P et al (2013) Continuous flow synthesis of tungsten oxide (WO3) nanoplates from tungsten (VI) ethoxide. Chem Eng J 226:22–29
90. Wang Q, Tang SVY et al (2013) Synthesis of ultrafine layered double hydroxide (LDHs) nanoplates using a continuous-flow hydrothermal reactor. Nanoscale 5(1):114–117
91. Makgwane PR, Ray SS (2014) Synthesis of nanomaterials by continuous-flow microfluidics: a review. J Nanosci Nanotechnol 14(2):1338–1363
92. Middelkoop V, Tighe CJ et al (2014) Imaging the continuous hydrothermal flow synthesis of nanoparticulate CeO_2 at different supercritical water temperatures using in situ angle-dispersive diffraction. J Supercrit Fluids 87:118–128

93. Moreira ML, Mambrini GP et al (2008) Hydrothermal microwave: a new route to obtain photoluminescent crystalline $BaTiO_3$ nanoparticles. Chem Mater 20(16):5381–5387
94. Bilecka I, Niederberger M (2010) Microwave chemistry for inorganic nanomaterials synthesis. Nanoscale 2:1358–1374
95. Pang J, Luan Y et al (2010) Microwave-assistant synthesis of inorganic particles from ionic liquid precursors. Colloids Surf A 360:6–12
96. Majcher A, Wiejak J et al (2013) A novel reactor for microwave hydrothermal scale-up nanopowder synthesis. Int J Chem Reactor Eng 11:361–368
97. Zhou Y (2005) Recent advances in ionic liquids for synthesis of inorganic nanomaterials. Curr Nanosci 1:35–42
98. Lou XW, Archer LA et al (2008) Hollow micro-/nanostructures: synthesis and applications. Adv Mater 20(21):3987–4019
99. Tanaka D, Kitagawa S (2008) Template effects in porous coordination polymers. Chem Mater 20(3):922–931
100. Thomas A, Goettmann F et al (2008) Hard templates for soft materials: creating nanostructured organic materials. Chem Mater 20(3):738–755
101. Yamauchi Y, Kuroda K (2008) Rational design of mesoporous metals and related nanomaterials by a soft-template approach. Chem Asian J 3(4):664–676
102. Zhang Q, Wang WS et al (2009) Self-templated synthesis of hollow nanostructures. Nano Today 4(6):494–507
103. Ethirajan A, Landfester K (2010) Functional hybrid materials with polymer nanoparticles as templates. Chem 16:9398–9412 (Copyright (C) 2014 American Chemical Society (ACS). All Rights Reserved.)
104. Qi L (2010) Colloidal chemical approaches to inorganic micro- and nanostructures with controlled morphologies and patterns. Coord Chem Rev 254:1054–1071
105. Ariga K, Ji QM et al (2012) Soft capsules, hard capsules, and hybrid capsules. Soft Mater 10(4):387–412
106. Deleuze H, Backov R (2012) Integrative chemistry routes toward advanced functional hierarchical foams. Wiley-VCH Verlag GmbH & Co. KGaA, Weinheim
107. Kimling MC, Caruso RA (2012) Templating of macroporous or swollen macrostructured polymers. Wiley-VCH Verlag GmbH & Co. KGaA, Weinheim
108. Petkovich ND, Stein A (2012) Colloidal crystal templating approaches to materials with hierarchical porosity. Wiley-VCH Verlag GmbH & Co. KGaA, Weinheim
109. Su B-L, Sanchez C et al (2012) Insights into hierarchically structured porous materials: from nanoscience to catalysis, separation, optics, energy, and life science. Wiley-VCH Verlag GmbH & Co. KGaA, Weinheim
110. Yan Q, Yu J et al (2012) Colloidal photonic crystals: fabrication and applications. Wiley-VCH Verlag GmbH & Co. KGaA, Weinheim
111. Zhang H (2012) Porous materials by templating of small liquid drops. Wiley-VCH Verlag GmbH & Co. KGaA, Weinheim
112. Liu YD, Goebl J et al (2013) Templated synthesis of nanostructured materials. Chem Soc Rev 42(7):2610–2653
113. Pal N, Bhaumik A (2013) Soft templating strategies for the synthesis of mesoporous materials: inorganic, organic-inorganic hybrid and purely organic solids. Adv Colloid Interface Sci 189–190:21–41
114. Petkovich ND, Stein A (2013) Controlling macro- and mesostructures with hierarchical porosity through combined hard and soft templating. Chem Soc Rev 42(9):3721–3739
115. Sanchez C, Boissiere C, Grosso D, Laberty C, Nicole L (2008) Design, synthesis, and properties of inorganic and hybrid thin films having periodically organized nanoporosity Chem Mater 20:682–737
116. Soler-Illia GJ, Sanchez C et al (2002) Chemical strategies to design textured materials: from microporous and mesoporous oxides to nanonetworks and hierarchical structures. Chem Rev 102:4093–4138
117. Rouquerol J, Avnir D et al (1994) Recommendations for the characterization of porous solids. Pure Appl Chem 66(8):1739–1758

118. Seo J, Sakamoto H et al (2010) Chemistry of porous coordination polymers having multimodal nanospace and their multimodal functionality. J Nanosci Nanotechnol 10(1):3–20
119. Xiao F-S, Meng X (2012) Zeolites with hierarchically porous structure: mesoporous zeolites. Wiley-VCH Verlag GmbH & Co. KGaA, Weinheim
120. Yokoi T, Tatsumi T (2012) Hierarchically porous materials in catalysis. Wiley-VCH Verlag GmbH & Co. KGaA, Weinheim
121. Zhang Y-H, Chen L-H et al (2012) Micro-macroporous structured zeolite. Wiley-VCH Verlag GmbH & Co. KGaA, Weinheim
122. Janiak C, Henninger SK (2013) Porous coordination polymers as novel sorption materials for heat transformation processes. Chimia 67:419–424
123. Moeller K, Bein T (2013) Mesoporosity—a new dimension for zeolites. Chem Soc Rev 42(9):3689–3707
124. Crepaldi EL, Soler-Illia GJAA et al (2002) Design of transition metal oxide mesoporous thin films. Stud Surf Sci Catal 141:235–242
125. Grosso D, Cagnol F et al (2003) Amorphous and crystalline mesoporous materials prepared via evaporation. Self-assembled nanostructured materials. Mat Res Soc Symp Proc 775:91–99, Lu Y, Brinker CJ, Antonietti M, Bai C (eds)
126. Soler-Illia GJAA, Crepaldi EL et al (2003) Block copolymer-templated mesoporous oxides. Curr Opin Colloid Interface Sci 8:109–126
127. Hüsing N, Schubert U (2004) Porous inorganic-organic hybrid materials. Wiley-VCH Verlag GmbH & Co. KGaA, Weinheim
128. Kickelbick G (2004) Hybrid inorganic-organic mesoporous materials. Angew Chem Int Ed 43:3102–3104
129. Grosso D, Boissiere C et al (2006) Preparation, treatment and characterisation of nanocrystalline mesoporous ordered layers. J Sol Gel Sci Technol 40:141–154
130. Eder F, Hüsing N (2009) Mesoporous silica layers with controllable porosity and pore size. Appl Surf Sci 256:S18–S21
131. Hoffmann F, Fröba M (2010) Silica-based mesoporous organic-inorganic hybrid materials. Wiley, New York
132. Keppeler M, Holzbock J et al (2011) Inorganic-organic hybrid materials through post-synthesis modification: impact of the treatment with azides on the mesopore structure. Beilstein J Nanotechnol 2:486–498
133. Shi YF, Wan Y et al (2011) Ordered mesoporous non-oxide materials. Chem Soc Rev 40(7):3854–3878
134. Nakanishi K (2012) Hierarchically structured porous materials: application to separation sciences. Wiley-VCH Verlag GmbH & Co. KGaA, Weinheim
135. Walcarius A (2013) Mesoporous materials and electrochemistry. Chem Soc Rev 42:4098–4140
136. Ferey G, Haouas M et al (2014) Nanoporous solids: how do they form? An in situ approach. Chem Mater 26(1):299–309
137. Ferey G (2007) Hybrid porous solids. Stud Surf Sci Catal 168:327–374
138. Ferey G (2007) Metal-organic frameworks. The young child of the porous solids family. Stud Surf Sci Catal 170A:66–86
139. Mu CZ, Xu F et al (2007) Application of functional metal-organic framework materials. Progr Chem 19(9):1345–1356
140. O'Keeffe M, Peskov MA et al (2008) The reticular chemistry structure resource (RCSR) database of, and symbols for, crystal nets. Acc Chem Res 41(12):1782–1789
141. Czaja AU, Trukhan N et al (2009) Industrial applications of metal-organic frameworks. Chem Soc Rev 38(5):1284–1293
142. Ferey G, Sanchez, C et al. (2010) Solid inorganic-organic polycarboxylate hybrid material based on titanium, its method of preparation and uses, Mater thesis, Université Pierre et Marie CURIE, Paris Vi, FR, pp. 42
143. McKinlay AC, Morris RE et al (2010) BioMOFs: metal-organic frameworks for biological and medical applications. Angew Chem Int Ed 49(36):6260–6266

144. Betard A, Fischer RA (2012) Metal-organic framework thin films: from fundamentals to applications. Chem Rev 112:1055–1083 (Washington, DC, U.S.)
145. Morey MS, O'Brien S et al (2000) Hydrothermal and postsynthesis surface modification of cubic, MCM-48, and ultralarge pore SBA-15 mesoporous silica with titanium. Chem Mater 12(4):898–911
146. Moeller K, Yilmaz B et al (2011) One-step synthesis of hierarchical zeolite beta via network formation of uniform nanocrystals. J Am Chem Soc 133(14):5284–5295
147. Calzaferri G, Bruhwiler D et al (2001) Quantum-sized silver, silver chloride and silver sulfide clusters. J Imag Sci Tech 45(4):331–339
148. Bruhwiler D, Leiggener C et al (2002) Luminescent silver sulfide clusters. J Phys Chem B 106(15):3770–3777
149. Leiggener C, Bruhwiler D et al (2003) Luminescence properties of Ag_2S and Ag_4S_2 in zeolite A. J Mater Chem 13(8):1969–1977
150. Leiggener C, Calzaferri G (2005) Synthesis and luminescence properties of Ag_2S and PbS clusters in zeolite A. Chemistry 11(24):7191–7198
151. Wang YF, Bryan C et al (2002) Interface chemistry of nanostructured materials: ion adsorption on mesoporous alumina. J Colloid Interface Sci 254(1):23–30
152. Landfester K (2001) The generation of nanoparticles in miniemulsions. Adv Mater 13(10):765–768
153. Liu J, Liu F et al (2009) Recent developments in the chemical synthesis of inorganic porous capsules. J Mater Chem 19(34):6073–6084
154. Groger H, Kind C et al (2010) Nanoscale hollow spheres: microemulsion-based synthesis, structural characterization and container-type functionality. Materials 3(8):4355–4386
155. Hu J, Chen M et al (2011) Fabrication and application of inorganic hollow spheres. Chem Soc Rev 40(11):5472–5491
156. Amstad E, Reimhult E (2012) Nanoparticle actuated hollow drug delivery vehicles. Nanomedicine 7(1):145–164
157. Bao Y, Yang YQ et al (2013) Research progress of hollow structural materials prepared via templating method. J Inorg Mater 28(5):459–468
158. Zhang BH, Fan H et al (2013) Synthesis of mesoporous hollow inorganic micro-/nanostructures via self-templating methods. Chem J Chinese U Chinese 34(1):1–14
159. Sarquis J (1980) Colloidal systems. J Chem Educ 57:602–605
160. Everett DH (1989) Basic principles of colloid science [fotocopie]. Royal Society of Chemistry, London
161. Hiemenz PC, Rajagopalan R (1997) Principles of colloid and surface chemistry, 3rd edn. CRC Press, Boca Raton
162. Fennell D, Wennerstroem H (1999) The colloidal domain. Wiley-VCH, New York
163. Hunter RJ (2001) Foundations of colloid science, 2nd edn. Oxford University Press, New York
164. Bucak S, Rende D (2014) Colloid and surface chemistry, CRC Press, Boca Raton
165. Schramm L (2001) Dictionary of colloid and interface science. Wiley, New York
166. Weller H (2003) Synthesis and self-assembly of colloidal nanoparticles. Philos Trans R Soc London, Ser A 361:229–240
167. Goodwin J (2004) Colloids and interfaces with surfactants and polymers. Wiley, New York
168. Eastoe J, Hollamby MJ et al (2006) Recent advances in nanoparticle synthesis with reversed micelles. Adv Colloid Interface Sci 128–130:5–15
169. Landfester K (2006) Synthesis of colloidal particles in miniemulsions. Annu Rev Mater Res 36(1):231–279
170. Shaw D (1992) Introduction to Colloid and Surface Chemistry (Fourth Edition). Elsevier Ltd
171. Hamley IW (2007) Soft matter. Wiley, New York
172. Cosgrove T (2010) Colloid science: principles, methods and applications. Wiley, New York
173. Crespy D, Staff RH et al (2012) Chemical routes toward multicompartment colloids. Macromol Chem Phys 213:1183–1189

174. Turkevich J, Stevenson PC et al (1951) A study of the nucleation and growth processes in the synthesis of colloidal gold. Disc Faraday Soc 11:55–75
175. Ramsay JDF (1992) Characteristics of inorganic colloids. Pure Appl Chem 64:1709–1713
176. Palberg T (1997) Colloidal crystallization dynamics. Curr Opin Colloid Interface Sci 2(6):607–614
177. Peng X, Wickham J et al (1998) Kinetics of II-VI and III-V colloidal semiconductor nanocrystal growth: "focusing" of size distributions. J Am Chem Soc 120:5343–5344
178. Ruckenstein E, Djikaev YS (2005) Recent developments in the kinetic theory of nucleation. Adv Colloid Interface Sci 118(1–3):51–72
179. Alekseeva AV, Bogatyrev VA et al (2006) Gold nanorods: synthesis and optical properties. Colloid J 68(6):661–678
180. Roh K-H, Martin DC et al (2006) Triphasic nanocolloids. J Am Chem Soc 128:6796–6797
181. Finney EE, Finke RG (2008) Nanocluster nucleation and growth kinetic and mechanistic studies: a review emphasizing transition-metal nanoclusters. J Colloid Interface Sci 317(2):351–374
182. Kwon SG, Hyeon T (2008) Colloidal chemical synthesis and formation kinetics of uniformly sized nanocrystals of metals, oxides, and chalcogenides. Acc Chem Res 41(12):1696–1709
183. Tao AR, Habas S et al (2008) Shape control of colloidal metal nanocrystals. Small 4(3):310–325
184. Gasser U (2009) Crystallization in three- and two-dimensional colloidal suspensions. J Phys Condens Matter 21(20)
185. Aerts A, Haouas M et al (2010) Investigation of the mechanism of colloidal silicalite-1 crystallization by using DLS, SAXS, and Si-29 NMR spectroscopy. Chemistry 16(9):2764–2774
186. Herlach DM, Klassen I et al (2010) Colloids as model systems for metals and alloys: a case study of crystallization. J Phys Condens Matter 22(15)
187. Pileni MP (2011) Supra- and nanocrystallinities: a new scientific adventure. J Phys Condens Matter 23(50)
188. Richter K, Birkner A et al (2011) Stability and growth behavior of transition metal nanoparticles in ionic liquids prepared by thermal evaporation: how stable are they really? Phys Chem Chem Phys 13:7136–7141
189. Pileni MP (2012) Self organization of inorganic nanocrystals: unexpected chemical and physical properties. J Colloid Interface Sci 388:1–8
190. Pileni MP (2012) Supra- and nanocrystallinity: specific properties related to crystal growth mechanisms and nanocrystallinity. Acc Chem Res 45(11):1965–1972
191. Palberg T (2014) Crystallization kinetics of colloidal model suspensions: recent achievements and new perspectives. J Phys Condens Matter 26(33)
192. Bahnemann DW, Kormann C et al (1987) Preparation and characterization of quantum size zinc oxide: a detailed spectroscopic study. J Phys Chem 91(14):3789–3798
193. Bahnemann DW (1993) Ultrasmall metal oxide particles: preparation, photophysical characterisation and photocatalytic properties. Isr J Chem 33(1):115–136
194. Erdemir D, Lee AY et al (2009) Nucleation of crystals from solution: classical and two-step models. Acc Chem Res 42(5):621–629
195. Xia Y, Xiong Y et al (2009) Shape-controlled synthesis of metal nanocrystals: simple chemistry meets complex physics? Angew Chem Int Ed 48:60–103
196. Bronstein LM, Polarz S et al (2001) Sub-nanometer noble-metal particle host synthesis in porous silica monoliths. Adv Mater 13(17):1333–1336
197. Pileni MP, Lalatonne Y et al (2004) Self assemblies of nanocrystals: preparation, collective properties and uses. Faraday Discuss 125:251–264
198. Pileni MP (2007) Control of the size and shape of inorganic nanocrystals at various scales from nano to macrodomains. J Phys Chem C 111(26):9019–9038
199. Pileni MP (2008) Self-assembly of inorganic magnetic nanocrystals: a new physics emerges. J Phys D Appl Phys 41(13)

200. Pileni MP (2009) Self assembly of inorganic nanocrystals in 3D supra crystals: intrinsic properties. Surf Sci 603(10–12):1498–1505
201. Pileni MP (2010) Inorganic nanocrystals self ordered in 2D superlattices: how versatile are the physical and chemical properties? Phys Chem Chem Phys 12(38):11821–11835
202. Schmid G (2006) Nanoparticles: from theory to application. Wiley VCH, Weinheim
203. Enustun BV, Turkevich J (1963) Coagulation of colloidal gold. J Am Chem Soc 85:3317–3328
204. Hutchings GJ, Brust M et al (2008) Gold—an introductory perspective. Chem Soc Rev 37(9):1759–1765
205. Jolivet JP, Tronc E et al (2000) Synthesis of iron oxide- and metal-based nanomaterials. Eur Phys J Appl Phys 10:167–172
206. Liz-Marzan LM (2004) Nanometals formation and color. Mater Today 7(2):26–31
207. Perez-Juste J, Pastoriza-Santos I et al (2005) Gold nanorods: synthesis, characterization and applications. Coord Chem Rev 249(17–18):1870–1901
208. Wang X, Zhuang J et al (2005) A general strategy for nanocrystal synthesis. Nature 437:121–124
209. Liao H, Nehl CL et al (2006) Biomedical applications of plasmon resonant metal nanoparticles. Nanomedicine 1(2):201–208
210. Jain PK, Huang X et al (2008) Noble metals on the nanoscale: optical and photothermal properties and some applications in imaging, sensing, biology, and medicine. Acc Chem Res 41:1578–1586
211. Mudring A-V, Alammar T et al (2009) Nanoparticle synthesis in ionic liquids. ACS Symp Ser 1030:177–188
212. Pastoriza-Santos I, Alvarez-Puebla RA et al (2010) Synthetic routes and plasmonic properties of noble metal nanoplates. Eur J Inorg Chem 27:4288–4297
213. Zeng H, Du X-W et al (2012) Nanomaterials via laser ablation/irradiation in liquid: a review. Adv Funct Mater 22:1333–1353
214. Daniel M-C, Astruc D (2004) Gold nanoparticles: assembly, supramolecular chemistry, quantum-size-related properties, and applications toward biology, catalysis, and nanotechnology. Chem Rev 104:293–346
215. Pasquato L, Pengo P et al (2004) Functional gold nanoparticles for recognition and catalysis. J Mater Chem 14(24):3481–3487
216. Guarise C, Pasquato L et al (2005) Reversible aggregation/deaggregation of gold nanoparticles induced by a cleavable dithiol linker. Langmuir 21(12):5537–5541
217. Cao-Milan R, Liz-Marzan LM (2014) Gold nanoparticle conjugates: recent advances toward clinical applications. Expert Opin Drug Deliv 11(5):741–752
218. Özgür Ü, Alivov YI et al (2005) A comprehensive review of ZnO materials and devices. J Appl Phys 98(4):1–103
219. Morkoç H, Özgür Ü (2008) Zinc oxide: materials preparation, properties, and devices. Wiley-VCH Verlag GmbH & Co. KGaA, Weinheim
220. Morkoç H, Özgür Ü (2009) Zinc oxide: fundamentals materials and device technology. Wiley-VCH Verlag GmbH & Co. KGaA, Weinheim
221. Hilgendorff M, Spanhel L et al (1998) From ZnO colloids to nanocrystalline highly conductive films. J Electrochem Soc 145(10):3632–3637
222. Look DC (2001) Recent advances in ZnO materials and devices. Mater Sci Eng B Solid 80(1–3):383–387
223. Cozzoli PD, Kornowski A et al (2005) Colloidal synthesis of organic-capped ZnO nanocrystals via a sequential reduction-oxidation reaction. J Phys Chem B 109(7):2638–2644
224. Fan Z, Lu JG (2005) Zinc oxide nanostructures: synthesis and properties. J Nanosci Nanotechnol 5(10):1561–1573
225. Klingshirn C, Hauschild R et al (2005) ZnO rediscovered—once again!? Superlattices Microstruct 38(4–6):209–222

226. Buha J, Djerdj I et al (2006) Nonaqueous synthesis of nanocrystalline indium oxide and zinc oxide in the oxygen-free solvent acetonitrile. Cryst Growth Des 7(1):113–116
227. Dem'yanets L, Li L et al (2006) Zinc oxide: hydrothermal growth of nano- and bulk crystals and their luminescent properties. J Mater Sci 41(5):1439–1444
228. Djurisic AB, Leung YH (2006) Optical properties of ZnO nanostructures. Small 2(8–9):944–961
229. Spanhel L (2006) Colloidal ZnO nanostructures and functional coatings: a survey. J Sol Gel Sci Technol 39(1):7–24
230. Klingshirn C (2007) ZnO: from basics towards applications. Phys Status Solidi B 244(9):3027–3073
231. Klingshirn C (2007) ZnO: material, physics and applications. ChemPhysChem 8(6):782–803
232. Ellmer K, Klein A (2008) ZnO and its applications. In: Ellmer K, Klein A, Rech B (eds) Transparent conductive zinc oxide, vol 104. Springer, Berlin/Heidelberg, pp 1–33
233. Anderson J, Chris GVW (2009) Fundamentals of zinc oxide as a semiconductor. Rep Prog Phys 72(12):126501
234. Ahmad M, Zhu J (2011) ZnO based advanced functional nanostructures: synthesis, properties and applications. J Mater Chem 21(3):599–614
235. Gomez J, Tigli O (2013) Zinc oxide nanostructures: from growth to application. J Mater Sci 48(2):612–624
236. Ludi B, Niederberger M (2013) Zinc oxide nanoparticles: chemical mechanisms and classical and non-classical crystallization. Dalton Trans 42(35):12554–12568
237. Wahab R, Khan F et al (2013) Hydrogen adsorption properties of nano- and microstructures of ZnO. J Nanomater 542753
238. Famengo A, Anantharaman S et al (2009) Facile and reproducible synthesis of nanostructured colloidal ZnO nanoparticles from zinc acetylacetonate: effect of experimental parameters and mechanistic investigations. Eur J Inorg Chem 33:5017–5028
239. Spanhel L, Anderson MA (1991) Semiconductor clusters in the sol-gel process: quantized aggregation, gelation, and crystal growth in concentrated zinc oxide colloids. J Am Chem Soc 113(8):2826–2833
240. Niederberger M, Garnweitner G et al (2006) Non-aqueous routes to crystalline metal oxide nanoparticles: formation mechanisms and applications. Prog Solid State Chem 33:59–70
241. Pinna N, Niederberger M (2008) Surfactant-free nonaqueous synthesis of metal oxide nanostructures. Angew Chem Int Ed 47:5292–5304
242. Franzmann E, Khalil F et al (2011) A biomimetic principle for the chemical modification of metal surfaces: synthesis of tripodal catecholates as analogues of siderophores and mussel adhesion proteins. Chemistry Eur. J (Chemistry- A European Journal) 17(31):8596–8603
243. Khalil F, Franzmann E et al (2014) Biomimetic PEG-catecholates for stabile antifouling coatings on metal surfaces: applications on TiO_2 and stainless steel. Colloids Surf B Biointerfaces 117:185–192
244. Maison W, Khalil F et al. Synthesis of tripodal bisphosphonate derivatives with an adamantyl base for functionalising surfaces Patent number: EP 2428517 B1 20131106 (DE) Univ Giessen, Justus-Liebig, Germany
245. Maison W, Khalil F et al. Synthesis of tripodal catechol derivatives with a flexible base for functionalising surfaces Patent number: EP 2428503 B1 20141210 (DE) Univ Giessen, Justus-Liebig, Germany
246. Xu C, Xu K, Gu H, Zheng R, Liu H, Zhang X, Guo Z, Xu B (2004) Dopamine as A Robust Anchor to Immobilize Functional Molecules on the Iron Oxide Shell of Magnetic Nanoparticles J Am Chem Soc 126:9938–9939
247. Ye Q, Zhou F et al (2011) Bioinspired catecholic chemistry for surface modification Chem Soc Rev 7:4244–4258
248. Sau TK, Murphy CJ (2004) Room temperature, high-yield synthesis of multiple shapes of gold nanoparticles in aqueous solution. J Am Chem Soc 126(28):8648–8649
249. Pastoriza-Santos I, Liz-Marzan LM (2002) Synthesis of silver nanoprisms in DMF. Nano Lett 2(8):903–905

250. Murphy CJ, Sau TK et al (2005) Surfactant-directed synthesis and optical properties of one-dimensional plasmonic metallic nanostructures. MRS Bull 30(5):349–355
251. Yin Y, Alivisatos AP (2005) Colloidal nanocrystal synthesis and the organic-inorganic interface. Nature 437:664–670 (London, U. K.)
252. Jiang XC, Pileni MP (2007) Gold nanorods: influence of various parameters as seeds, solvent, surfactant on shape control. Colloids Surf 295(1–3):228–232
253. Nelayah J, Kociak M et al (2007) Mapping surface plasmons on a single metallic nanoparticle. Nat Phys 3(5):348–353
254. Lu X, Rycenga M et al (2009) Chemical synthesis of novel plasmonic nanoparticles. Annu Rev Phys Chem 60:167–192
255. Llevot A, Astruc D (2012) Applications of vectorized gold nanoparticles to the diagnosis and therapy of cancer. Chem Soc Rev 41(1):242–257
256. Klinkova A, Choueiri RM et al (2014) Self-assembled plasmonic nanostructures. Chem Soc Rev 43(11):3976–3991
257. Caswell KK, Bender CM et al (2003) Seedless, surfactantless wet chemical synthesis of silver nanowires. Nano Lett 3(5):667–669
258. Li J, Chen Z et al (1999) Low temperature route towards new materials: solvothermal synthesis of metal chalcogenides in ethylenediamine. Coord Chem Rev 190–192:707–735 (Copyright (C) 2013 American Chemical Society (ACS). All Rights Reserved.)
259. Gautam UK, Ghosh M et al (2002) Solvothermal routes to capped oxide and chalcogenide nanoparticles. Pure Appl Chem 74:1643–1649 (Copyright (C) 2013 American Chemical Society (ACS). All Rights Reserved.)
260. Lewis AE (2010) Review of metal sulphide precipitation. Hydrometallurgy 104(2):222–234
261. Sokolov MN, Abramov PA (2012) Chalcogenide clusters of groups 8-10 noble metals. Coord Chem Rev 256(17–18):1972–1991
262. Tolia J, Chakraborty M et al (2012) Synthesis and characterization of semiconductor metal sulfide nanocrystals using microemulsion technique. Cryst Res Technol 47(8):909–916
263. Armelao L, Camozzo D et al (2006) Synthesis of copper sulphide nanoparticles in carboxylic acids as solvent. J Nanosci Nanotechnol 6(2):401–408
264. Grozdanov I, Najdoski M (1995) Optical and electrical properties of copper sulfide films of variable composition. J Solid State Chem 114(2):469–475
265. Grijalva H, Inoue M et al (1996) Amorphous and crystalline copper sulfides, CuS. J Mater Chem 6(7):1157–1160
266. Raevskaya AE, Stroyuk AL et al (2004) Catalytic activity of CuS nanoparticles in hydrosulfide ions air oxidation. J Mol Catal A Chem 212(1–2):259–265
267. Basu M, Sinha AK et al (2010) Evolution of hierarchical hexagonal stacked plates of CuS from liquid–liquid interface and its photocatalytic application for oxidative degradation of different dyes under indoor lighting. Environ Sci Technol 44(16):6313–6318
268. Goel S, Chen F et al (2014) Synthesis and biomedical applications of copper sulfide nanoparticles: from sensors to theranostics. Small 10(4):631–645
269. Prince LM (1977) Microemulsions: theory and practice. Academic, New York
270. Landfester K, Bechthold N et al (1999) Formulation and stability mechanisms of polymerizable miniemulsions. Macromolecules 32(16):5222–5228
271. Aserin A (2008) Multiple emulsion: technology and applications. Wiley, New York
272. Tovstun SA, Razumov VF (2011) Preparation of nanoparticles in reverse microemulsions. Russ Chem Rev 80(10):953–969
273. Tadros TF (2014) An introduction to surfactants. Walter de Gruyter, Berlin
274. Bechthold N, Tiarks F et al (2000) Miniemulsion polymerization: applications and new materials. Macromol Symp 151:549–555
275. Landfester K (2000) Recent developments in miniemulsions—formation and stability mechanisms. Macromol Symp 150:171–178
276. Antonietti M, Landfester K (2002) Polyreactions in miniemulsions. Prog Polym Sci 27(4):689–757
277. Landfester K (2003) Miniemulsions for nanoparticle synthesis. In: Antonietti M (ed) Colloid chemistry II. Springer, Berlin/Heidelberg, pp 75–123

278. Landfester K (2003) Miniemulsions for nanoparticle synthesis. Top Curr Chem 227:75–123
279. Landfester K (2005) Designing particles: miniemulsion technology and its application in functional coating systems. Eur Coating J 20–22:24–25
280. Muñoz-Espí R, Weiss CK et al (2012) Inorganic nanoparticles prepared in miniemulsion. Curr Opin Colloid Interface Sci 17(4):212–224
281. Muñoz-Espí R, Weiss CK et al (2012) Inorganic nanoparticles prepared in miniemulsion. Curr Opin Colloid Interface Sci 17(4):212–224
282. Cao Z, Ziener U (2013) Synthesis of nanostructured materials in inverse miniemulsions and their applications. Nanoscale 5(21):10093–10107
283. Landfester K, Antonietti M 2004 Miniemulsions for the convenient synthesis of organic and inorganic nanoparticles and "single molecule" applications in materials chemistry. F. Caruso (ed.). Wiley-VCH Verlag GmbH & Co. KGaA, Weinheim, FRG
284. Landfester K, Tiarks F et al (2000) Polyaddition in miniemulsions. A new route to polymer dispersions. Macromol Chem Phys 201:1–5
285. Landfester K, Willert M et al (2000) Preparation of polymer particles in nonaqueous direct and inverse miniemulsions. Macromolecules 33(7):2370–2376
286. Weiss CK, Ziener U et al (2007) A route to nonfunctionalized and functionalized poly(n-butylcyanoacrylate) nanoparticles: preparation in miniemulsion. Macromolecules 40(4):928–938
287. Landfester K (2009) Miniemulsion polymerization and the structure of polymer and hybrid nanoparticles. Angew Chem Int Ed 48(25):4488–4507
288. Crespy D, Landfester K (2010) Miniemulsion polymerization as a versatile tool for the synthesis of functionalized polymers. Beilstein J Org Chem 6:1132–1148
289. Landfester K, Weiss CK (2010) Encapsulation by miniemulsion polymerization. Adv Polym Sci 229:1–49
290. Willert M, Rothe R et al (2001) Synthesis of inorganic and metallic nanoparticles by miniemulsification of molten salts and metals. Chem Mater 13(12):4681–4685
291. Peng B, Chen M et al (2008) Fabrication of hollow silica spheres using droplet templates derived from a miniemulsion technique. J Colloid Interface Sci 321(1):67–73
292. Musyanovych A, Landfester K (2007) Core-shell particles. Wiley-VCH Verlag GmbH & Co. KGaA, Weinheim
293. Caruso F, Spasova M et al (2001) Multilayer assemblies of silica-encapsulated gold nanoparticles on decomposable colloid templates. Adv Mater 13(14):1090–1095
294. Hajir M, Dolcet P et al (2012) Sol-gel processes at the droplet interface: hydrous zirconia and hafnia nanocapsules by interfacial inorganic polycondensation. J Mater Chem 22(12):5622–5628
295. Pinna N, Weiss K et al (2001) Triangular CdS nanocrystals: synthesis, characterization, and stability. Langmuir 17(26):7982–7987
296. Pileni MP (1993) Reverse micelles as microreactors. J Phys Chem 97(27):6961–6973
297. Pileni MP (2003) The role of soft colloidal templates in controlling the size and shape of inorganic nanocrystals. Nat Mater 2(3):145–150
298. Lisiecki I, Pileni MP (1993) Synthesis of copper metallic clusters using reverse micelles as microreactors. J Am Chem Soc 115(10):3887–3896
299. Lisiecki I, Pileni MP (1995) Copper metallic particles synthesized in-situ in reverse micelles—influence of various parameters on the size of the particles. J Physa Chem 99(14):5077–5082
300. Maillard M, Giorgio S et al (2002) Silver nanodisks. Adv Mater 14(15):1084–1086
301. Pinna N, Maillard M et al (2002) Optical properties of silver nanocrystals self-organized in a two-dimensional superlattice: Substrate effect. Phys Rev B 66(4)
302. Maillard M, Giorgio S et al (2003) Tuning the size of silver nanodisks with similar aspect ratios: synthesis and optical properties. J Phys Chem B 107(11):2466–2470
303. Mishra S, Daniele S et al (2007) Metal 2-ethylhexanoates and related compounds as useful precursors in materials science. Chem Soc Rev 36:1770–1787 (Copyright (C) 2014 American Chemical Society (ACS). All Rights Reserved.)

304. Carpenter EE, Sims JA et al (2000) Magnetic properties of iron and iron platinum alloys synthesized via microemulsion techniques. J Appl Phys 87(9):5615–5617
305. Lopez-Quintela MA (2003) Synthesis of nanomaterials in microemulsions: formation mechanisms and growth control. Curr Opin Colloid Interface Sci 8(2):137–144
306. Lopez-Quintela MA, Tojo C et al (2004) Microemulsion dynamics and reactions in microemulsions. Curr Opin Colloid Interface Sci 9(3–4):264–278
307. Dolcet P, Casarin M et al (2012) Miniemulsions as chemical nanoreactors for the room temperature synthesis of inorganic crystalline nanostructures: ZnO colloids. J Mater Chem 22:1620–1626 (Copyright (C) 2013 American Chemical Society (ACS). All Rights Reserved.)
308. Dolcet P, Latini F et al (2013) Inorganic chemistry in a nanoreactor: doped ZnO nanostructures by miniemulsion. Eur J Inorg Chem 2013(13):2291–2300
309. Butturini E, Dolcet P et al (2014) Simple, common but functional: biocompatible and luminescent rare-earth doped magnesium and calcium hydroxides from miniemulsion. J Mater Chem 2:6639–6651
310. Taden A, Antonietti M et al (2004) Inorganic films from three different phosphors via a liquid coating route from inverse miniemulsions. Chem Mater 16(24):5081–5087
311. Nabih N, Schiller R et al (2011) Mesoporous CeO_2 nanoparticles synthesized by an inverse miniemulsion technique and their catalytic properties in methane oxidation. Nanotechnology 22(13):135606
312. Rossmanith R, Weiss CK et al (2008) Porous anatase nanoparticles with high specific surface area prepared by miniemulsion technique. Chem Mater 20:5768–5780
313. Kubiak P, Froeschl T et al (2011) TiO_2 anatase nanoparticle networks: synthesis, structure, and electrochemical performance. Small 7:1690–1696
314. Heutz NA, Dolcet P et al (2013) Inorganic chemistry in a nanoreactor: Au/TiO2 nanocomposites by photolysis of a single-source precursor in miniemulsion. Nanoscale 5:10534–10541
315. Rohe M, Löffler E et al (2008) A gold-containing TiO complex: a crystalline molecular precursor as an alternative route to Au/TiO_2 composites. Dalton Trans 864(44):6106–6109

Chapter 2
Green Techniques for Biomedical Metallic Materials with Nanotechnology

Kelvii Wei Guo and Hon Yuen Tam

Abstract From a clinic or medical viewpoint, it is important that the surgical implant retains a combination of high strength (including surface wear resistance), good biocompatibility, and chemical stability. To enable safe interactions between the surgical implants and tissues, surface modification and functionalization are commonly employed.

Biological coatings such as TiN and titanium oxides are widely adopted and functionalized with various biological properties such as corrosion resistance, bioactivity, cytocompatibility, and bioconductivity. However, failure of the biological coatings due to the long term corrosion and wear or fretting is the main problem and debris from the materials is the main cause of joint replacement failure. Since the surgical implants are implanted into the human body for a long time, cyclic motions between the surgical implants and human tissues may disrupt the protective biological coatings accelerating corrosion and increasing the risks of immunological response by the leached metallic ions.

Therefore, improved metallic biomaterials and the relevant manufacturing techniques are being introduced to meet this demand. Apart from the biocompatibility requirement, metallic biomedical materials also have to meet high standards regarding its performance (functionality, reliability) and selection criteria (cost, manufacturing ability). Up to now, the most often used metallic biomedical materials include stainless steel, cobalt-based alloys, and commercially pure titanium or titanium-based alloys. However, the implant metallic biomaterials, like all mechanical components, are subjected to degradation and have limited lifetime. Damaged implant requires successive operation to replace worn components and so intensive efforts are made to increase durability of implants metallic biomaterials.

For enhancing the mechanical retention, engineered nanostructures on the surface are normally taken to increase effective surface area on implant surfaces (such as both dental and orthopedic applications) to exhibit biological, mechanical, and morphological compatibilities to receiving vital hard/soft tissue, resulting in promoting osseointegration.

K.W. Guo (✉) • H.Y. Tam
Department of Mechanical and Biomedical Engineering, City University of Hong Kong, Kowloon Tong, Kowloon 999077, Hong Kong
e-mail: guoweichinese@yahoo.com

V.A. Basiuk, E.V. Basiuk (eds.), *Green Processes for Nanotechnology*,
DOI 10.1007/978-3-319-15461-9_2

The surface engineered nanostructures play a crucial role in biomedical metallic materials because (1) the surface of a biomaterials is the only part contacting with the bioenvironment, (2) the surface region of a biomaterial is almost always different in morphology and composition from the bulk, (3) for biomaterials that do not release or leak biologically active or toxic substance, the characteristics of the surface governs the biological response (foreign material vs. host tissue), and (4) surface properties such as topography affect the mechanical stability of the implant-tissue interface.

Therefore, aim to provide vital information about the growing field of engineered nanostructures on the surface of metallic biomedical materials, the relevant green technologies such as equal channel angular extrusion (ECAE), high pressure torsion (HPT), cold rolling, heat rolling, high energy ball milling, sandblasting, and shot peening are reviewed.

At the same time, implant industry is experiencing rapid growth mainly due to age-related degenerative diseases. with the increase of the need to diagnose diseases at an early stage in accordance with the saying: prevention is better than cure, the future prospects related to the significantly feasible surface nanostructured technology for the foreseeable future are also pointed out. It indicates that new surface bioengineering technologies should be explored to help the scientists and clinicians in the initiation of targeted treatments and in the follow-up of treatment responses.

Keywords Nanostructure • Green technique • Equal channel angular extrusion (ECAE) • High pressure torsion (HPT) • Cold rolling • Heat rolling • Ball milling • Sandblasting • Shot peening

2.1 Introduction

An increasing demand for reliable metallic biomedical materials is being observed as a result of an aging population with higher quality of life expectations. Improved metallic biomaterials and the relevant manufacturing techniques are being introduced to meet this demand. Apart from the biocompatibility requirement, metallic biomedical materials also have to meet high standards regarding its performance (functionality, reliability) and selection criteria (cost, manufacturing ability).

Up to now, the most often used metallic biomedical materials include stainless steel, cobalt-based alloys, and commercially pure titanium or titanium-based alloys. However, the implant metallic biomaterials, like all mechanical components, are subjected to degradation and have limited lifetime. Damaged implant requires successive operation to replace worn components and so intensive efforts are made to increase durability of implants metallic biomaterials.

For instance, Titanium alloy such as Ti6Al4V has been widely used in implantable devices for several decades, because of its attractive mechanical and corrosion characteristics [1]. However, failure often occurs, due to wear in the contact areas [2, 3]. Release of metallic ions and wear fragments due to wear corrosion lead to

allergy and to tissues inflammation. Cytotoxicity concerns are mainly related to the presence of vanadium, but also high concentrations of titanium and aluminum ions can be dangerous [4–6].

Many titanium alloys have been studied under co-joint action of corrosion and sliding wear [3]. Under these conditions, Ti6Al4V is found to undergo the strongest degradation, among all the alloys tested, but according to different tests it results the best combination of both corrosion and wear resistance [1]. The wear corrosion mechanism consists in the removal of the surface passive film in the sliding contact and its subsequent regeneration [7]. It should be stressed that the two mechanisms of degradation, that is, wear and corrosion, do not proceed separately but depend on each other in a complex way. Normally corrosion is accelerated by wear, and, similarly, wear may be affected by corrosion phenomena [1, 3, 8, 9]. Corrosion was found to be stimulated by wear, because of galvanic coupling between the anodic wear track and the cathodic region outside [6]. The effect of wear on the electrochemical behavior is marked and depends on frictional load, applied potential and pH of the solution [10]. Duisabeau et al. [11] studied the tribocorrosion behavior of a Ti6Al4V/316L stainless steel pairs in a Ringer's solution, under gross slip conditions and concluded that the dissipated mechanical energy and fretting regimes are strongly affected by the presence of a corrosive lubricant, because of the electrochemical phenomena caused by the electrolyte. Many investigations on titanium and its alloys are carried out under fretting corrosion. Degradation is accompanied by depassivation and repassivation phenomena which can be investigated by electrochemical noise technique [12]. At anodic potentials, it is found that the electrochemical response of the alloy to tribocorrosion is critically affected by the prevailing fretting regime (stick, mixed, or slip regime) and significant wear and enhancement of the anodic current occurred only in the presence of slip [13]. The applied potential markedly stimulates the wear process, owing to continuous oxidation of the surface layer formed by mechanical mixing of plastically deformed metal and oxide debris [14].

Biological survival, particularly longevity of biological adhesive joints, is often dependent on thin surface films. Surfaces and interfaces behave completely different from bulk properties. The characteristics of a biomaterial surface govern the processes involved in biological response. Surface properties such as surface chemistry, surface energy, and surface morphology play a crucial role in biological interactions for four reasons: (1) the surface of a biomaterials is the only part contacting with the bioenvironment, (2) the surface region of a biomaterial is almost always different in morphology and composition from the bulk, (3) for biomaterials that do not release or leak biologically active or toxic substance, the characteristics of the surface governs the biological response (foreign material vs. host tissue), and (4) some surface properties such as topography affect the mechanical stability of the implant-tissue interface. Like the interface, the surface has a certain characteristic thickness, (1) for the case when the interatomic reaction is dominant, such as wetting or adhesion, atoms within a depth of 100 nm (1,000 Å) will be important, (2) for the case of the mechanical interaction, such as tribology and surface hardening, since the elasticity due to the surface contact and the plastically deformed layer will be a

governing area, the thickness of about 0.1–10 μm will be important, and (3) for the case when mass transfer or corrosion is involved, the effective layer for preventing the diffusion will be within 1–100 μm.

Current implants materials such as stainless steels and Co–Cr alloys have Young's module varying from 100 to 200 GPa and the values are quite different from that of human bones (1–30 GPa) [15]. An implant with a high Young's module absorbs most of the loading causing "stress shielding effects" to loosen human bones [16]. Nowadays, the commonly used materials for surgical implantation are titanium alloys, stainless steels, and Co–Cr alloys, and Table 2.1 lists the mechanical properties of commonly used surgical materials.

Although surfaces of biomaterials have been modified by various techniques (laser melting [18], sol–gel method [19, 20], multi-arc ion plating [21], O implantation [22, 23], ion implantation [24–27], thermal oxidation [28, 29], electrochemical treatment [30–32]) to improve the specific surface properties and functions, all the problems cannot be overcome and further surface modification is often needed. One of the problems is associated with Ni which is known to have some toxicity and causes allergic reactions in some people. Recent study shows that the amount of Ni released from commercial orthodontic wires varied in a wide range from 0.2 to 7 $\mu g/cm^2$ [33]. It has also been reported that Ni release can increase significantly with time and the high concentration will be maintained up to a few months [34].

Another problem is the disruption of the surface coatings due to the mechanical abrasion. Cyclic motions between the implants and human tissues not only disrupt the protective surface coatings but also generate wear debris, further increasing the risks of immunological response. The failure of biological coatings due to the long term corrosion, wear, and fretting is a serious concern and it has been reported that wear debris mainly causes the failure of joint replacements [35].

However, the TiN or TiO film fabricated on biomaterials is usually less than 200 nm thick and any disruption of the film due to mechanical abrasion can easily reduce its biocompatibility. Although a thicker titanium oxide layer can be produced on biomaterials by thermal oxidation, the phase transformation behavior is usually occurred during the processing. Hence, in order to obtain a high-quality biological coating on biomaterials for long term biomedical application, the treatment temperature, bonding strength between the coating and substrate, and thickness of the coatings should be considered.

Nowadays, nanotechnology has been defined as "the creation of functional materials, devices and systems through control of matter on the nanometer length scale (1–100 nm), and exploitation of novel phenomena and properties (physical, chemical, and biological) at that length scale" [36]. Nanotechnology involves materials that have the nanosized topography or are composed of nanosized materials. These materials have a size range between 1 and 100 nm (10^{-9} m). Nanostructured materials also have enormous surface areas per unit weight or volume, so that vastly more surface area is available for interactions with other materials around them. That is useful because many important chemical and electrical reactions occur only at surfaces and are sensitive to the shape and texture of a surface as well as its chemical composition.

Table 2.1 Mechanical property of common biomedical materials [15, 17]

Materials	Young's module (GPa)	Tensile strength (MPa)	Recoverable strain (%)	Elongation (%)	Pressure resistance (MPa)	Fatigue limit	Hardness
NiTi	70–110	800–1,500	2	—	—	100–800	65–68 (HRA)
NiTi (processed)	21–69	103–1,100	8	>60	–	50–300	–
Annealed 316L	176–196	552	0.8	50	550	343	170–200 (HV)
Ti6Al4V	110	900	–	12	900	170–240	–
CoCr	213–248	650–690	–	8	–	240–280	300 (HV)
Tooth enamel	50	70	–	0	265	–	–
Dentin	14	40	–	0	145	–	–
Cortical bone	18	140	–	1	130	–	–

The novel properties of nanomaterials offer great promise to provide new technological breakthroughs. Nanotechnology has been explored for creating lighter and stronger materials, for cleaning contaminated groundwater, for replacing toxic chemicals in various applications, for enhancing solar cell efficiency, and for targeted cancer treatment. Nanotechnology is already used in hundreds of products across various industries such as electronics, healthcare, chemicals, cosmetics, materials, and energy [36–42].

Nanotechnology has become a powerful tool in modern materials science. It is able to incorporate biomimicry on the nanoscale into materials engineering. Research on nanotechnology/nanostructured biomaterials is also one of the hottest topics in the biomaterials field and in fact, "nanotechnology/nanostructured biomaterials" are also very important keywords in WBC (World Biomaterial Congress) 2008. Nanoscale materials are thought to interact with some proteins more effectively than conventional materials. For instance, osteoblast functions are mediated due to their similar size and altered energetics. Balasundaram et al. [43] suggested that nanophase materials may be alternative orthopedic implant materials because of their ability to mimic the dimensions of the constituents and components in natural bone-like proteins and hydroxyapatite. Nanofibers with shape resembling hydroxyapatite crystals in bones can influence the conformation of typical adhesive proteins such as fibronectin and vitronectin as well as osteoblast behavior [44, 45]. Some other nanostructures that spur enhanced response from osteoblasts and subsequently more efficient deposition of calcium-containing minerals include nanometals, carbon nanofibers and nanotubes, nanopolymers, and nanocomposites of ceramics and polymers. A number of studies have been conducted to evaluate the nanomaterials chemistry and preliminary results suggest that increased bone cell functions may be independent of the bulk materials chemistry but rather rely on the degree of the nanostructured surface roughness [46–49].

Many nanostructures can be found in nature [50]. For example, the surface of lotus leaves is composed of microscale and nanoscale hierarchical structures composed of fine-branched nanostructures (ca. 120 nm) on top of micropapillae (5–9 mm). Scanning electron microscopy (SEM) reveals that on the lotus leave surface, every epidermal cell forms a micrometer-scale papilla and has a dense layer of epicuticular waxes superimposed on it. Each of the papillae consists of branch-like nanostructures. The synergistic effects between these special double-scale surface structures and hydrophobic cuticular waxes are thought to be the reason for the super-hydrophobicity as indicated by a high water contact angle and low sliding angle. As another example, butterflies [51] and cicadae [52] can keep themselves uncontaminated by removing dust particles, dew, or water droplets easily from their wings spontaneously. Such properties also originate from the special structures on their wings. The cicada wing is composed of aligned nanocolumns with diameters of about 70 nm and a column-to-column distance of about 90 nm. These surface microstructures bestow the wing with its self-cleaning property. The relevant references cited are listed in Table 2.2.

Nanostructures also exist in the human body. For example, the size of ions, DNA, proteins, and virus in the human body ranges from several nanometers to submicrometers. Human bones are composed of nanosized organic and mineral phases

Table 2.2 Focus of the cited references

Authors	Focus	Reference
Ganesan Balasundaram and Thomas J. Webster	Nanophase materials for orthopedic implant applications	[43]
Molly M. Stevens and Julian H. George	Approaches to control cell behavior through the nanoscale engineering of materials surfaces	[44]
Cameron J. Wilson, Richard E. Clegg et al.	Mediation of cell responses to biomaterials coated with adsorbed proteins	[45]
Thomas J. Webster and Jeremiah U. Ejiofor	Synthesization, characteristics, and evaluation of osteoblast adhesion on nanophase metals (specifically, Ti, Ti6Al4V, and CoCrMo alloys)	[46]
Rachel L. Price, Michael C. Waid et al.	Determine effects of select properties of novel carbon nanofibers and polycarbonate urethane/carbon nanofiber (PCU/CNF) composites (specifically, dimension, surface energy, and chemistry) on osteoblast, fibroblast, chondrocyte, and smooth muscle cell adhesion	[47]
Thomas J. Webster and Tyler A. Smith	Efficacy of nanophase materials as implants—the first evidence of greater functions of osteoblasts on PLGA scaffolds containing nanophase compared to conventional titania	[48]
I. Manjubala, S. Scheler et al.	Nucleate the hydroxyapatite crystals onto three-dimensional porous polymeric scaffolds with nano-apatite formation	[49]
Joanna Aizenberg	Bio-inspired approach to controlled crystallization at the nanoscale	[50]
Thomas Wagner, Christoph Neinhuis, Wilhelm Barthlott	Wettability and contaminability of insect wings as a function of their surface sculptures	[51]
Woo Lee, Mi-Kyoung Jin et al.	Simple and highly reproducible method for fabricating well-defined nanostructured polymeric surfaces with aligned nanoembosses or nanofibers of controllable aspect ratios similarity with interesting natural biostructures such as the wing surface of *Cicada orni* and the leaf surface of *Lotus*	[52]

agglomerating to form a large macrostructure. Proteins present in the extracellular matrix of bones are nanostructured comparable to collagen fibrils. Furthermore, tiny mineral particles composed of calcium phosphate, an important constituent of the bone matrix, is compositionally and structurally nanostructured.

It is well known that nanotechnology has been applied to metallic biomedical materials in order to improve its mechanical, chemical, and physical properties such as anti-abrasion, corrosion resistance, biocompatibility, surface energy, etc. and understand the long term impact on human health.

For enhancing the mechanical retention, engineered nanostructures on the surface are normally taken to increase effective surface area on implant surfaces (such as both dental and orthopedic applications) to exhibit biological, mechanical, and morphological compatibilities to receiving vital hard/soft tissue, resulting in promoting osseointegration.

The surface engineered nanostructures play a crucial role in biomedical applications because (1) the surface of a biomaterials is the only part contacting with the bioenvironment, (2) the surface region of a biomaterial is almost always different in morphology and composition from the bulk, (3) for biomaterials that do not release or leak biologically active or toxic substance, the characteristics of the surface governs the biological response (foreign material vs. host tissue), and (4) surface properties such as topography affect the mechanical stability of the implant-tissue interface.

Nanostructured surfaces can be produced on conventional biomaterials by surface modification. Depending on the ways surfaces are modified, nano-functionalization techniques can be categorized into two groups, namely nano coating and film deposition as well as in situ surface nano-functionalization. These two types of techniques are often combined to produce surfaces with hybrid nanostructures such as a coating/film and a nanostructured zone.

In the past 10 years, much work has been performed on surface nanofunctionalization of titanium. Coatings and films with nanostructures such as nanograins, nanopores, nanotubes, nanoparticles, nanowires, and nanorods have been synthesized on titanium and its alloys.

Moreover, such important surfaces can be fabricated in a favorable fashion to accommodate, facilitate, or promote more biofunctionality and bioactivity in mechanical, chemical, electrochemical, thermal, or any combination of these technologies.

However, to date, a new generation of green technologies is expected to arrive, as pressures on resources grow and investors see healthy profit in a wide range of innovative products. Moreover, in an attempt to alleviate fossil fuel usage and CO_2 emissions, fuels, heat, or electricity must be produced from biological sources in a way that is economic (and therefore efficient at a local scale), energetically (and greenhouse gas) efficient, environmentally friendly, and not competitive with food production. Aims to advance the development of clean technologies using nanotechnology, to minimize potential environmental and human health risks associated with the manufacture and use of nanotechnology products in general, to apply nano to solve legacy environmental problems, and to encourage replacement of existing products with new nanoproducts, bionanotechnology, a new crosscutting technology platform, should build an environmentally sustainable society in the twenty-first century.

2.2 Fabrication of Nanocrystalline Metals

Generally, two complementary approaches are commonly employed to synthesize nanostructured solids. One is the "bottom-up" approach in which the nanostructured materials are assembled from individual atoms or from nanoscale building blocks such as nanoparticles. The second one is the "top-down" approach in which existing coarse-grained materials are processed to produce substantial grain refinement and nanostructure. The most successful top-down approaches which are eco to environments, mainly involved the application of large plastic deformation in which materials are subjected to plastic strain typically larger than 4–6.

Nanocrystalline metals and alloys are usually produced by severe plastic deformation (SPD). There are several variations of SPD based techniques such as high pressure torsion (HPT) [53–55], equal channel angular pressing (ECAP)/equal channel angular extrusion (ECAE) [56–60], cold rolling [61–65], hot rolling [66–68], high energy milling (ball milling) [69–73], sandblasting [74–90], and shot peening [91–93].

2.2.1 High Pressure Torsion (HPT)

One of the major tools to produce bulk nanocrystalline metals is high pressure torsion (HPT) which can produce extremely high pressure and strain consequently leading to exceptional grain refinement. Generally, HPT produces nano-grains with size ranging from 50 to 100 nm. The schematic setup of HPT is depicted in Fig. 2.1.

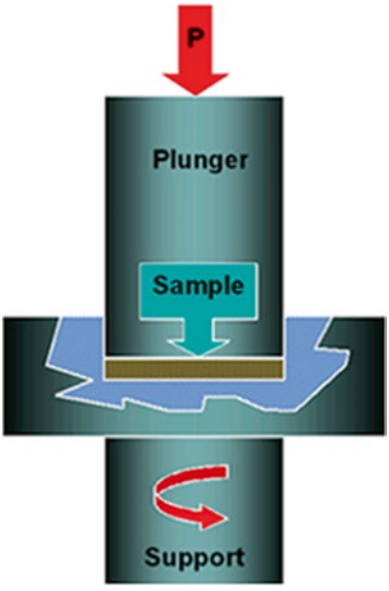

Fig. 2.1 Setup of high pressure torsion (HPT). In a high pressure torsion device, a metallic disk is constrained by high pressure between two anvils as one keeps steady and the other one rotates, leading to a very strain onto the sample [55]. Reprinted with permission from Elsevier

The HPT treated sample is usually in the form of a thin disk with a thickness of 0.8 mm. This disk is placed between two massive anvils and held in place within a depression machined into the face of each anvil. During operation, the sample is subjected to a high applied pressure, *P*, and concurrent torsional straining through rotation of the lower anvil. This process is designated quasi-constrained HPT because there is some limited outward flow of the materials around the periphery of the disk during operation [53].

In order to assess the advantages of HPT-processed titanium over the conventional and coated titanium implants, as both mechanical properties and cellular response, Faghihi et al. [54] investigated the nature and mechanism of cell–substrate interaction, in particular, the molecular machinery controlling cell response to the surface of the nanostructured titanium based material produced by the high pressure torsion (HPT) process. Titanium disks with diameters of ~12 mm and thicknesses of ~0.3 mm were chosen for processing by HPT. Each disk was placed between anvils and compressed and deformed under an applied pressure (*P*) of 6 GPa at room temperature to a total of five complete revolutions, equivalent to a true logarithmic strain of ~6.

Annealed titanium substrates were prepared by heating the titanium disks in a tube furnace for 12 h at 800 °C in an atmosphere of ultrapure argon and then cooling to room temperature. The untreated, nanostructured, and annealed disks of the titanium substrates with a diameter of one centimeter were placed in 24-well culture plates and incubated in alpha minimum essential medium (α-MEM, Invitrogen Corporation, USA) and Dulbecco's modified Eagle's medium supplemented with 10 % fetal bovine serum, 100 U/ml penicillin containing 100 mg/ml streptomycin at 37 °C in a humidified atmosphere of 5 % CO_2 and 95 % air using mouse pre-osteoblast MC3T3-E1 subclone 14 and rat fibroblast Rat1 cell lines. Fluorescent labeling of nucleic acids was performed to assess the number of attached pre-osteoblasts and fibroblasts on the surface of the titanium substrates with different microstructures. Results show that the microstructure of the untreated titanium substrate had a mean grain size of ~9 mm (Fig. 2.2a) as determined by orientation image microscopy (OIM). After 12 h annealing at 800 °C under an argon atmosphere, its mean grain size increased to ~50 μm (Fig. 2.2b). The microstructure of the HPT processed titanium substrate was below the resolution limit of the OIM and its nanostructure was investigated in ultrathin section obtained by the FIB system. The FETEM showed the substrates to have a highly disordered, very fine-grained, polycrystalline structure that ranged in size between 10 and 50 nm (Fig. 2.2c). The grain boundaries of the individual grains were, however, difficult to recognize. Lattice-fringe images showed that coherent regions of the crystal structure within individual grains are even smaller and ranged in size between 5 and 10 nm.

The results of immunofluorescence microscopy (IM) suggest that the expression level of fibronectin (FN) varied among samples with different microstructure where higher concentration was observed in the cells grown on the HPT processed substrate (Fig. 2.3). There was a reduction in FN expression in cells grown on the untreated and annealed substrates. To further understand the nature of the interactions of pre-osteoblasts with different substrates, the expression level of vinculin

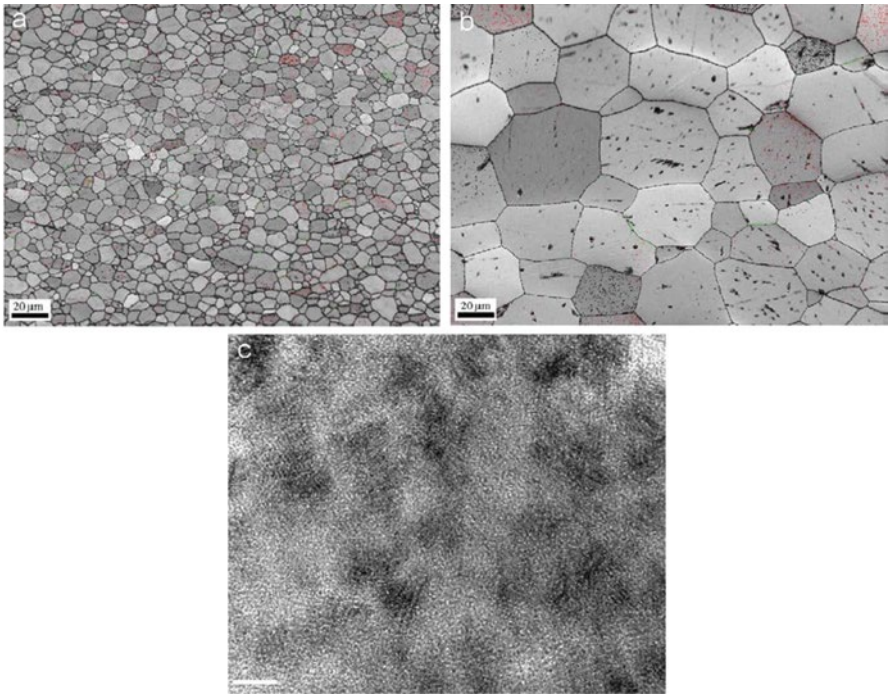

Fig. 2.2 Structure of untreated, annealed, and HPT processed titanium substrates. (**a**, **b**) Gray scale map type of orientation image microscope (OIM) images of untreated, and annealed titanium substrates showing the grain size and statistics of individual grain boundaries. (**c**) TEM images of ultrathin section obtained from the focused ion beam (FIB) system of HPT processed titanium substrates showing highly disordered, polycrystalline nanoparticles which is ranged in size between 10 and 50 nm. High resolution TEM image representing lattice-fringe image suggests the coherent regions of the crystal structure within individual grains is ranged in size between 5 and 10 nm (bar shows 5 nm) [54]. Reprinted with permission from Elsevier

and the organization of actin filaments were determined by immunofluorescence technique (Fig. 2.4). Immunofluorescence microscopy of pre-osteoblasts grown on HPT-processed substrates showed strong vinculin signals associated with the actin stress fibers in peripheral regions of the cells as well as throughout the cellular extensions (Fig. 2.5). Vinculin was also present along the extended actin microfilaments with the highest concentration at their leading edges which resulted in focal adhesion on the surface of these substrates (Fig. 2.4a). On the untreated substrates, the vinculin signal was less intense (Fig. 2.4b). On the surface of annealed substrates, the vinculin signal was not visible at the contact sites, but was present along the actin stress fibers (Fig. 2.4c). Immunofluorescence of the actin labeling showed a different organization of the microfilaments on all three fabricated substrates. Pre-osteoblasts grown on HPT-processed and untreated substrates developed a strong network of more well-defined and elongated fibers (Fig. 2.4d–e), whereas cells on annealed substrates had fewer prominent stress fibers crossing the cells (Fig. 2.4f).

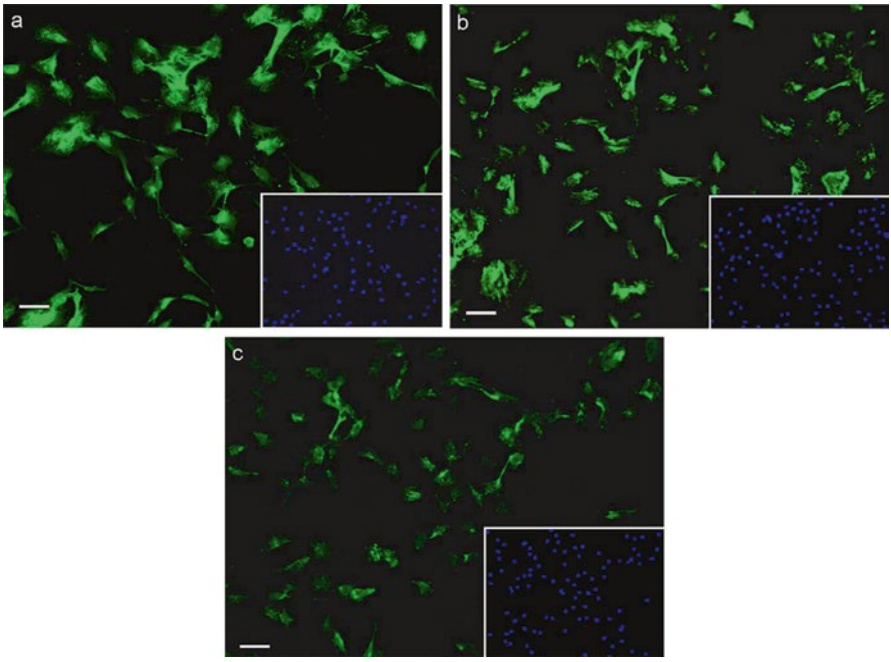

Fig. 2.3 Immunocytochemistry of fibronectin expressed by pre-osteoblast cells after 2 days of incubation. (**a**) HPT-processed, (**b**) untreated and (**c**) annealed titanium substrates. Pre-osteoblast cells cultured on HPT processed substrates show an increased fluorescent intensity with distinct network pattern. DAPI staining of the cell nuclei demonstrated that the cellular density was comparable for the selected area in all the samples (*insets*). Bars show 50 μm [54]. Reprinted with permission from Elsevier

Western blot analysis from pre-osteoblast cells were also in agreement with the immunofluorescence results and showed elevated expression levels of fibronectin and vinculin in cells cultured on the HPT processed substrates compared to the annealed untreated substrates and the control (Fig. 2.6).

Cell culture experiments on microstructured and nanostructured solid substrates fabricated through heat treatment and HPT of commercially available pure titanium show that pre-osteoblast cell responses are strongly influenced by the surface structural features of the titanium substrates. Pre-osteoblast attachment and growth rate is improved on the surface of ultrafine grained titanium substrates produced by the HPT process. These nanostructured titanium substrates had superior properties in terms of their interaction with pre-osteoblast cells compared to other analyzed substrates. These substrates preferentially supported the attachment and spreading of pre-osteoblasts over fibroblasts as well as increased cytoskeletal and extracellular matrix activity.

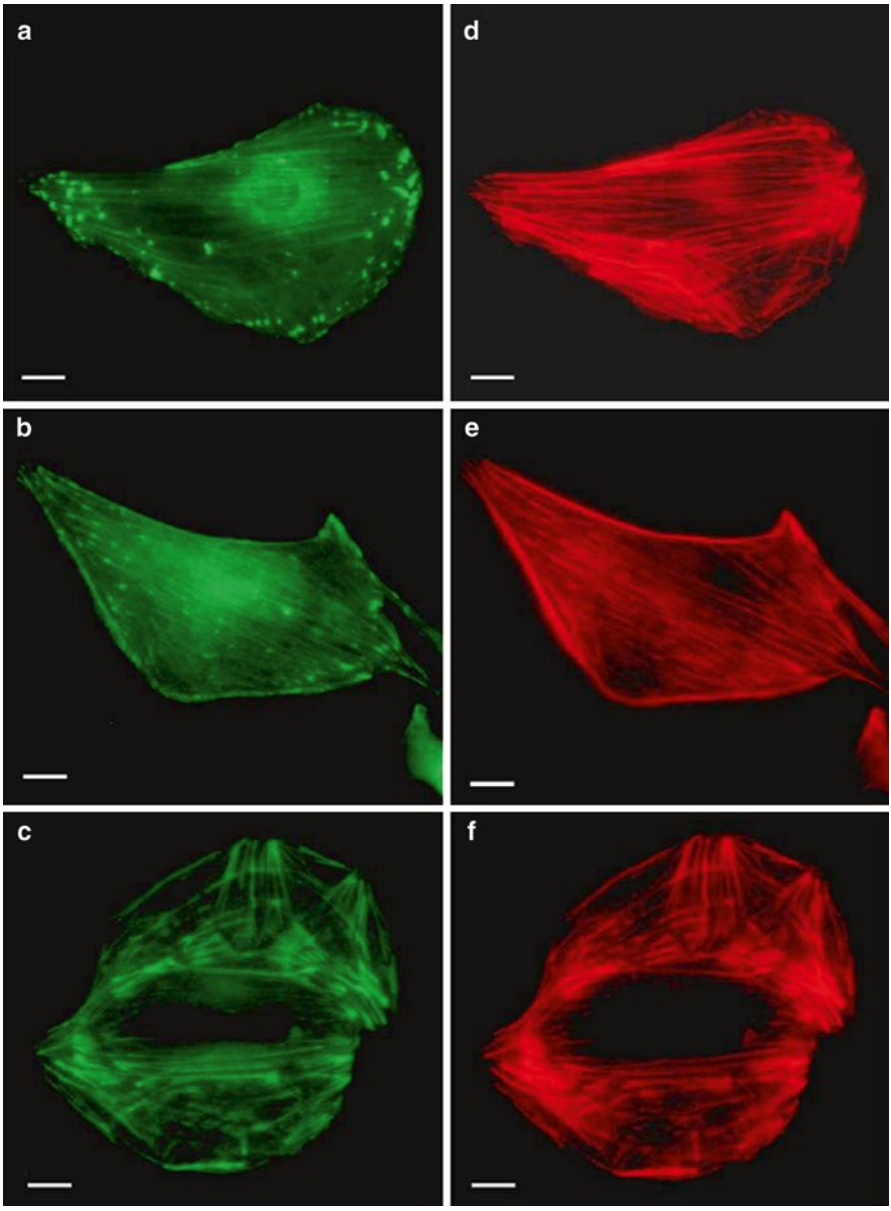

Fig. 2.4 Visualization of focal contacts and stress fibers in pre-osteoblast cells and level of vinculin expression on the surface of titanium substrates after 2 days of incubation. (**a**) Vinculin was more expressed and detected at the focal contact site in the cells grown on HPT-processed substrates than in the cells cultured on (**b**) untreated and (**c**) annealed titanium substrates. Pre-osteoblasts grown on (**d**) HPT-processed and (**e**) untreated titanium substrates exhibited well-defined stress fibers whereas cells cultured on (**f**) annealed substrates, formed poor bundles of stress fibers. Bars show 5 μm [54]. Reprinted with permission from Elsevier

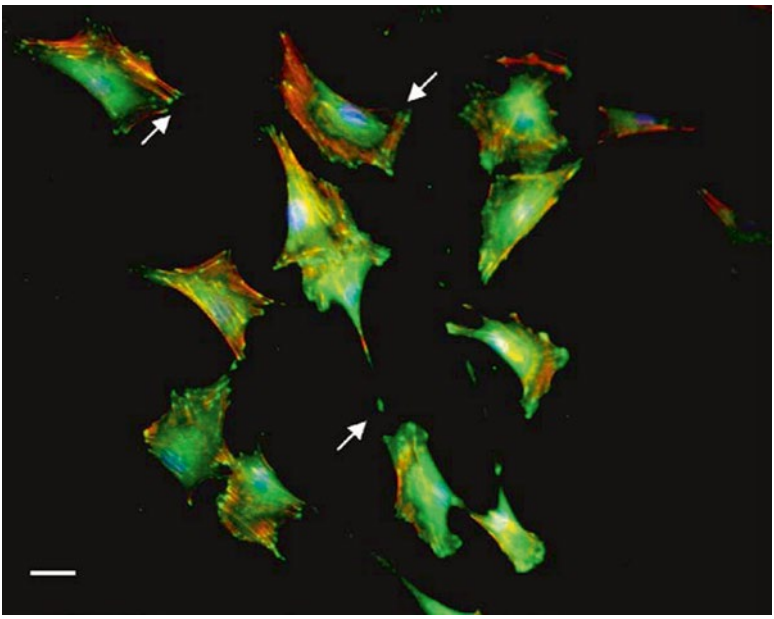

Fig. 2.5 Merged fluorescence images of nucleus (*blue*), actin filaments (*red*), and vinculin (*green*) in pre-osteoblast cells grown on HPT-processed titanium substrates after 2 days incubation. The *arrows* show the focal contact sites where vinculin is visible at the actin leading edges that connect cells to the titanium substrate. Bar shows 25 μm [54]. Reprinted with permission from Elsevier

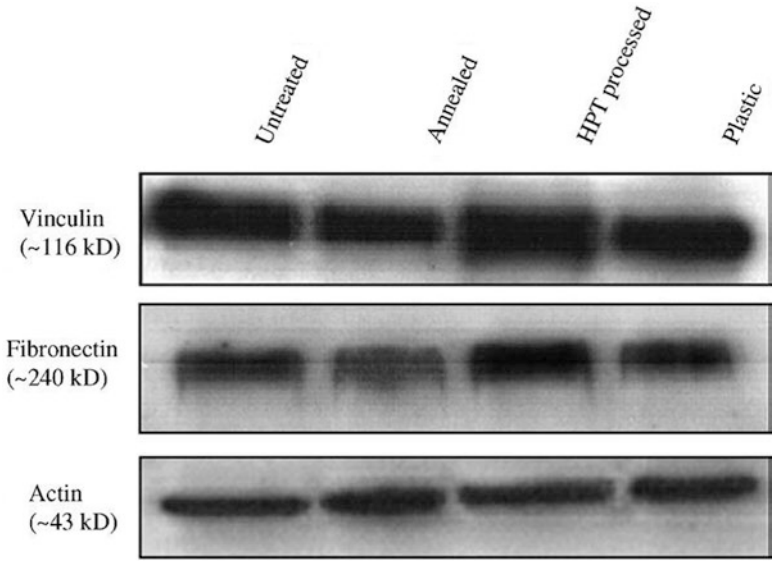

Fig. 2.6 Immunoblot of cell lysates prepared from mouse monoclonal antivinculin (*upper*) indicate that there is a reduction of vinculin expression on annealed substrates, compared to HPT-processed titanium substrates. Immunoblots of cell lysates prepared from mouse monoclonal antifibronectin (*middle*) indicating the highest expression of fibronectin in pre-osteoblast cells cultured on HPT-processed substrates. Lower bands show expression of actin as loading control [54]. Reprinted with permission from Elsevier

2.2.2 *Equal Channel Angular Pressing (ECAP)/Equal Channel Angular Extrusion (ECAE)*

Equal channel angular pressing (ECAP)/Equal channel angular extrusion (ECAE) is a more recent technique to produce ultrafine grained metals or alloys. The schematic setup of ECAE is illustrated in Fig. 2.7. In a typical ECAE process, intense shear is concentrated on the shear plane and each pass imposes an equivalent strain ε of about 1. Usually, the sample is subjected to several passes to attain exceptionally high strain covering the whole cross-sectional area. In the case of hard-to-deform materials, ECAP/ECAE is conducted at elevated temperature. The technique can produce ultrafine grained metals or alloys, bulk nanostructured materials with submicrometer-sized grains, subgrain structures, nanoparticles, or other nano-sized structural features. Grain refinement during ECAP/ECAE is associated with some dislocation characteristics, e.g., cells, subgrains, microbands, that are established during the first one or two passes and their transformation to ultrafine grains during further straining [59]. At present, ECAP/ECAE is the most popular severe plastic deformation technique and has been used in grain refinement in various metals and alloys including commercial ones. However, the final grain size, grain phase, and fraction of high angle grain boundaries depend strongly on the processing methods and parameters as well as material properties.

Shin et al. [57] studied the microstructure development during equal-channel angular pressing of titanium. The experimental material was 18 mm diameter× 130 mm length machined from commercial-purity titanium (grade 2) bars with an

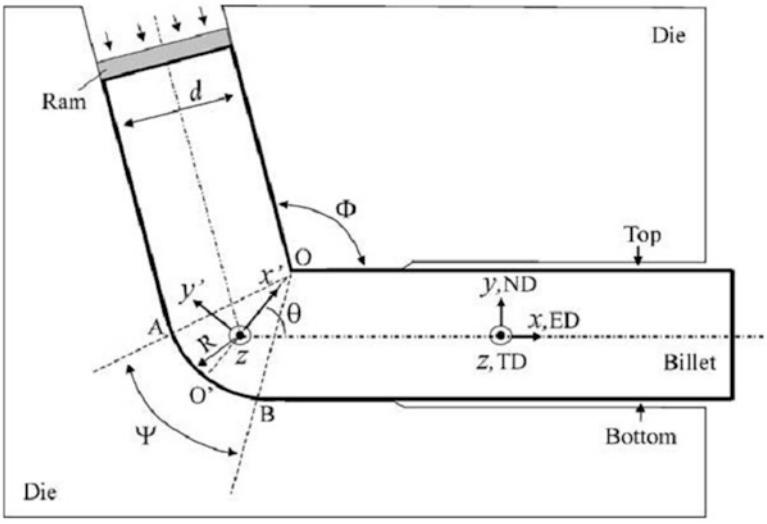

Fig. 2.7 Illustration of the ECAE process. During the treatment, material is forced through a channel that contains a sharp bend, resulting in large deformations at the shearing plane. Repeating the process creates very large strains [59]. Reprinted with permission from Elsevier

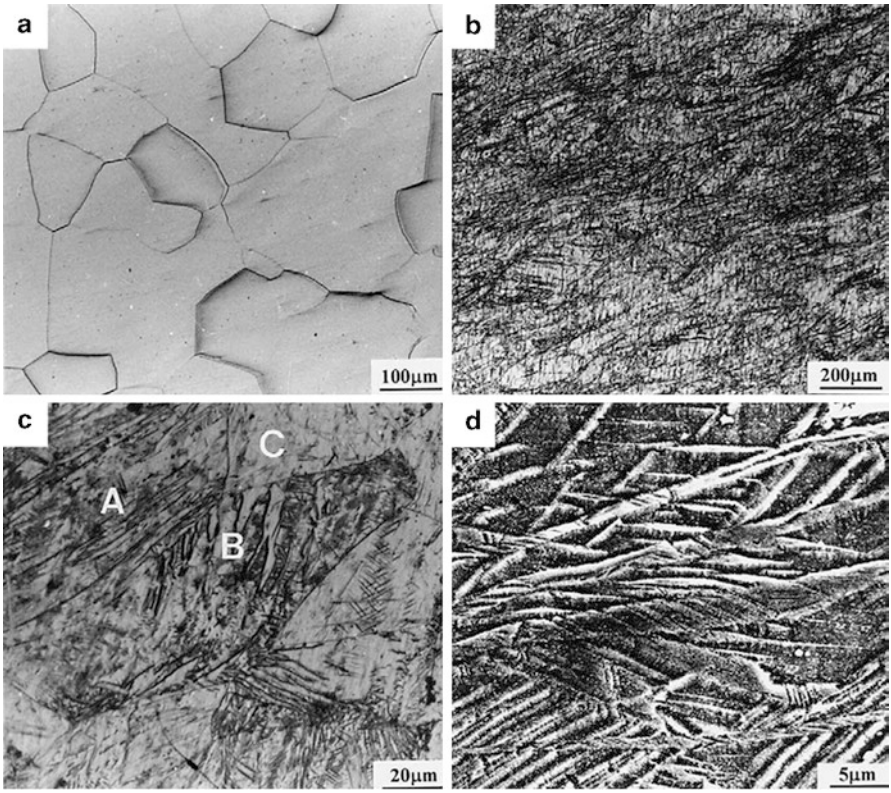

Fig. 2.8 Optical and SEM micrographs of as-annealed and as-pressed (single pass) Ti: (**a**) as-annealed and (**b–d**) as-pressed. Etched with a solution of 4 % HF, 20 % perchloric acid, and 76 % distilled water [57]. Reprinted with permission from Elsevier

average grain size of 30 μm. Before ECAP, the samples were annealed at 1,073 K for 1 h under an argon atmosphere in order to remove any residual hot work. ECAP die was designed to yield a shear strain of ~1.83 during each pass. It contained an inner contact angle (Φ) and arc of curvature at the outer point of contact between the channels (Ψ) of 90 and 20°, respectively. Pressing through a single pass or two passes was conducted at 623 K at a constant pressing speed of 2 mm/s. The pressing temperature was chosen to avoid shear localization that characterizes ECAP of commercial-purity titanium at temperatures between 298 and 598 K.

Figure 2.8a shows an optical micrograph of the as annealed titanium used as the starting material. The grain structure was equiaxed with an average size of ~100 μm. During the first ECAP pass, fine microstructural features inclined ~30° to the longitudinal direction were developed (Fig. 2.8b). (The micrograph in Fig. 2.8b was taken from the *Y* plane as shown in Fig. 2.9.) Observation of the fine features in titanium at a higher magnification, however, revealed that they consisted of deformation twins (Fig. 2.8c). In particular, grains with three distinct microstructures,

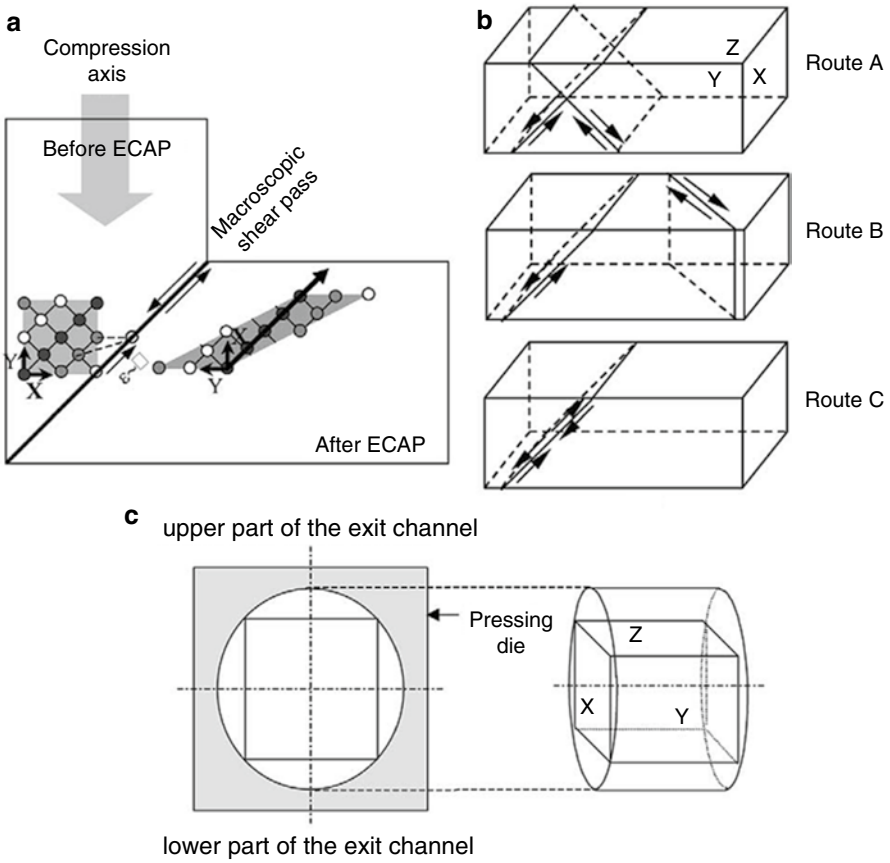

Fig. 2.9 (**a**) Macroscopic shearing path associated with a single passage. (**b**) Macroscopic shearing patterns associated with different processing routes. (**c**) Schematic diagram of the sectioning of pressed samples for microstructural observation [57]. Reprinted with permission from Elsevier

marked A, B, and C, were observed. In A, twins spanning the entire grain were formed parallel to the flow lines. On the other hand, the twins in B were inclined approximately 40° to the orientation of the deformation zone of the pressing, and were observed to include microtwins inside. Inasmuch as the optical microstructure of C was not as evident as those of A and B, SEM observation of this region was required for a detailed analysis (Fig. 2.8d). As shown in the figure, the grain contained microtwins whose width was less than 1 μm. Thus, all of the observations after the first ECAP pass revealed deformation twins either on a macroscale or a microscale.

A TEM micrograph of the structure developed during the first ECAP pass is shown in Fig. 2.10. Elongated parallel bands with a width of ~0.07 μm were observed. These bands were similar in appearance to slip bands formed in cubic metals, but were much finer. A SAD pattern from a region containing two adjacent

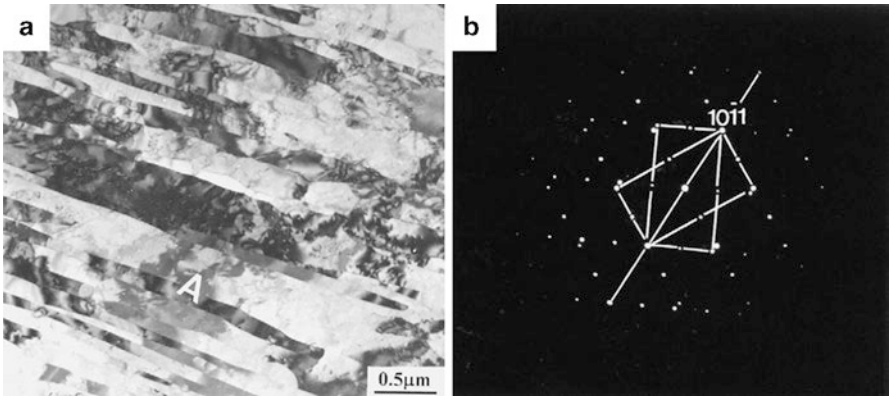

Fig. 2.10 (**a**) TEM micrograph of Ti after a single ECAP pass and (**b**) the corresponding SAD pattern [57]. Reprinted with permission from Elsevier

bands (marked "A" in Fig. 2.10a) was taken using a $\left[\bar{1}2\bar{1}0\right]$ zone axis (Fig. 2.10b). The mirror spots of the $\left[\bar{1}2\bar{1}0\right]$ diffraction pattern appeared with respect to the $\left(10\bar{1}1\right)$ plane, indicating that the two adjacent bands constituted a $\left\{10\bar{1}1\right\}$ twin structure. The same twin system was consistently observed for more than 50 different regions, even from twins aligned differently in the same grain. In addition, the dislocation density within the bands was approximately $10^{13}/m^2$, a value much lower than that typically developed in heavily deformed cubic metals, i.e., ~$10^{15}/m^2$.

Results show that during the first ECAP pass, titanium was observed to deform by deformation twinning. TEM analysis revealed that twinning occurred on $\left\{10\bar{1}1\right\}$ planes. During the second ECAP pass, however, strain was accommodated primarily by dislocation-glide processes. The specific slip system was strongly dependent on the processing route, i.e., route A, B, or C as shown in Fig. 2.9. Also, the texture formed during the first pass and the resolved shear stress for each slip system determine the deformation mechanism during the second ECAP pass and thus must be carefully considered in understanding microstructure development during equal-channel angular pressing.

2.2.3 Cold Rolling

Cold rolling is one kind of severe plastic deformation (SPD) techniques. González et al. [65] investigated the properties of the new Ti25Nb16Hf alloy (wt.%, vacuum arc-melted, treated at 1,100 °C for 1.5 h and quenched in a mixture of ethanol/water at 0 °C) for biomedical application before and after 95 % cold rolling (95 % C.R.). Rectangular samples of the alloy were cold rolled at room temperature to a 95 % reduction in thickness in a laboratory rolling mill with tool steel work rolls

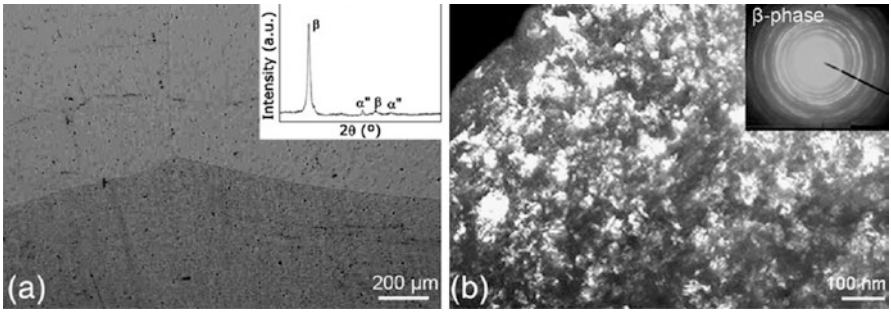

Fig. 2.11 Optical microscopy image of Ti25Nb16Hf (0 % C.R.) alloy with an X-ray diffraction pattern (**a**) and a bright-field TEM image of the 95 % C.R. alloy with an electron diffraction pattern of the selected area (**b**) [65]. Reprinted with permission from Elsevier

measuring 92 mm in diameter. Unidirectional multipass rolling was carried out using 5 % reduction per pass using a fixed rolling speed of 35 rpm and silicone grease as lubricant.

The microstructure of the Ti25Nb16Hf (0 % C.R.) alloy is shown in Fig. 2.11a. X-ray diffraction analysis confirms the presence of β-phase, together with a low fraction of α″ phase (inset in Fig. 2.11a). Figure 2.11b shows a bright field image obtained by TEM from the 95 % C.R. alloy. The picture shows the formation of a nanocrystalline structure with grain size less than 50 nm. Inset in Fig. 2.11b shows the corresponding selected area electron diffraction pattern with continual diffraction rings, which confirms the presence of many crystalline grains. The indexation of the rings corresponds to the reticular parameters of β-phase.

Moreover, Ti25Nb16Hf (95 % C.R.) alloy was selected for the cell adhesion test due to its low elastic modulus and to its high corrosion resistance. In the cell adhesion studies, 3×104 MG63 cells were seeded on triplicate specimens and incubated for 4 h in a 48-well culture plate. After 4 h the cells were fixed with 4 % paraformaldehyde/PBS for 15 min at room temperature, permeabilized with 0.05 % Triton X-100/PBS for 10 min and blocked with 1 % BSA/PBS for 30 min for nonspecific binding. After that the cells were stained using the double indirect immunofluorescence technique. Primary monoclonal antivinculin V9131 antibodies from mice (Sigma-Aldrich) were used during 30 min to stain the focal points. The designated antibodies were conjugated with Alexa Fluor 488 anti-mouse IgG (Molecular Probes). Then the cells were incubated for 30 min with rhodamine-phalloidin and secondary Hoechst antibodies (Invitrogen), for the actin filaments and cell nuclei, respectively. Between each step, cells were washed with PBS for three times. Coverslips were mounted on glass slides in Mowiol (Calbiochem) mounting medium.

Immunofluorescence images (Fig. 2.12) show the cells adhering to the new alloy and to the control materials after 4 h of culture. MG63 cells were stained to visualize focal contacts (green), cytoskeletal structures of actin filaments (red) and nuclei (blue). The observation of the cell morphology shows a good polygon-like adherent

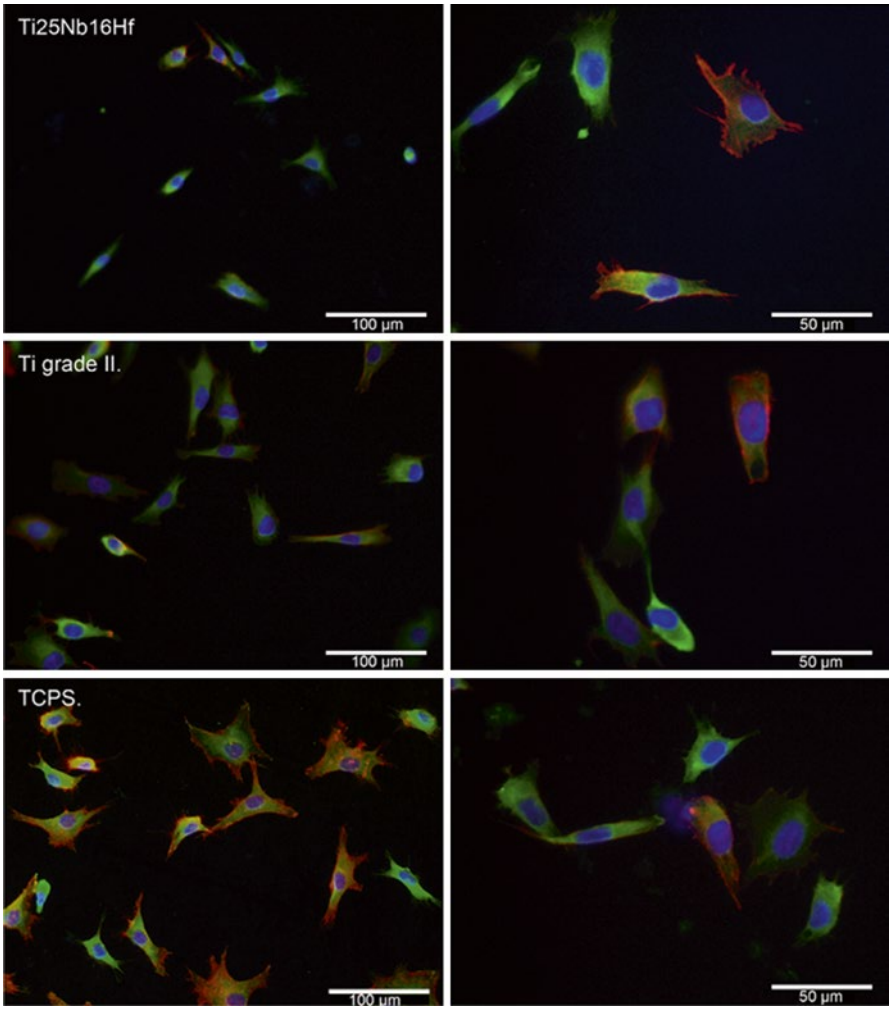

Fig. 2.12 Double immunofluorescence staining (*blue*—nucleus, *red*—actin filaments and *green*—focal points) of MG63 adhered cells after 4 h of culture corresponding to the Ti25Nb16Hf alloy, Ti grade II and TCPS substrates [65]. Reprinted with permission from Elsevier

growth and good cell spreading with well-defined clusters of focal adhesion points in the different surfaces studied. The figure shows a lower number of adhering cells on the Ti25Nb16Hf specimen, compared to the control materials. The higher cell recruitment corresponds to the TCPS surface.

It demonstrates that the potentialities of the cold rolled novel Ti alloy are similar to those of cortical bone and with a good osteoblast cell response. This material could be considered a good candidate to be used in implant devices for replacing failed hard tissue.

2.2.4 *Hot Rolling*

As for hot rolling, Li et al. [67] studied the contribution of twinning and slip to the evolution of texture and microstructure during large strain hot rolling of magnesium alloy ME20 (Mg-2.0Mn-0.3Ce) using X-ray and EBSD analysis. The rolling specimens with a dimension of 60 mm × 40 mm × 4 mm were machined out in such a way that the crystallographic *c*-axis was parallel to the normal direction (ND), parallel to the transverse direction (TD) and 30° inclined from the transverse direction (TD) towards the rolling direction (RD) in the RD-TD plane (Fig. 2.13). Solution heat treatment at 400 °C for 30 min was applied in order to obtain a homogeneous microstructure prior to processing. Large strain hot rolling (LSHR) experiments at 400 °C up to 90 % reductions were carried out. The materials were hot rolled using a laboratory rolling mill with diameter 250 mm and rolling speed of 23 m/min. After LSHR, the samples were quickly quenched in water.

The microstructure and second phase distribution images of the initial ME20 hot rolled plate after 400 °C for 30 min annealing are presented in Fig. 2.14. Figure 2.14a shows equiaxed grains with an average grain size of about 9.5 μm; the range of grain size is from 3 to 20 μm. After annealing, the microstructure is composed of fully recrystallized grains without any twinning left. Figure 2.14b shows the most prominent second phase particles observed in the initial ME20 rolled plate. The second phase particles containing Mg and Ce with a stoichiometry of $Mg_{12}Ce$ were identified by energy dispersive X-ray spectroscopy (EDS) in the form of rod and plate morphology (Fig. 2.14c). The $Mg_{12}Ce$ particles were homogeneously distributed throughout the matrix with a size of 1–4 μm (Fig. 2.14b). Additionally, very fine ellipsoidal particles (<20 nm) were detected by TEM-EDS as pure Mn in

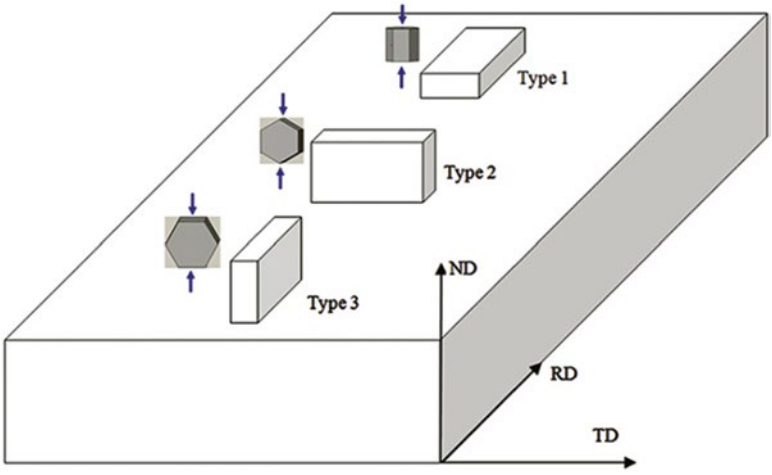

Fig. 2.13 Schematic diagram of sample types and their reference system for the large strain hot rolling (LSHR) experiments [67]. Reprinted with permission from Elsevier

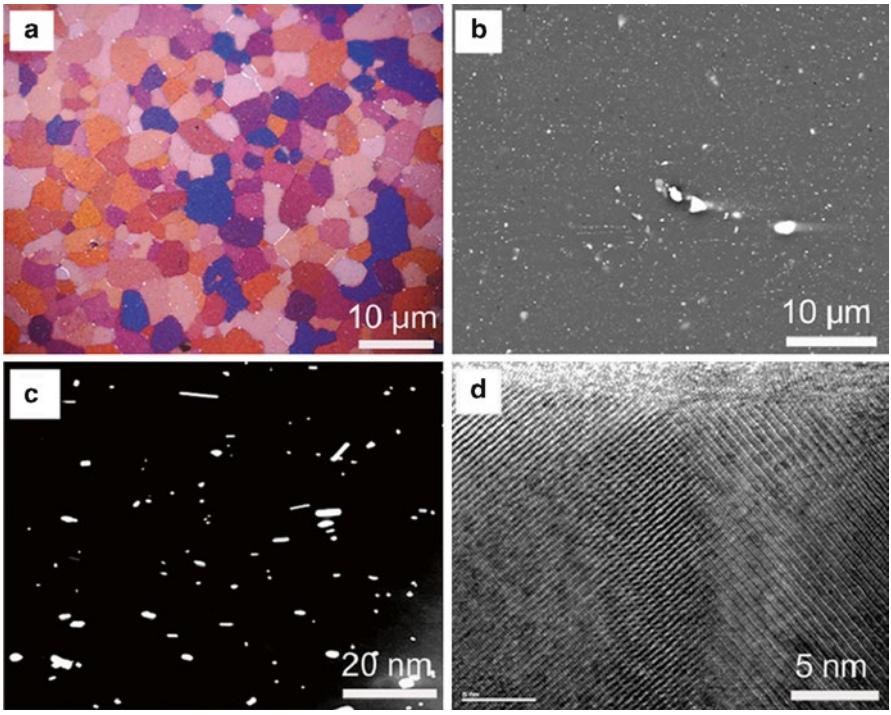

Fig. 2.14 The microstructures of the ME20 alloy prior to hot rolling after annealing at 400 °C for 30 min: (**a**) optical micrograph revealing equiaxed grains without twinning observation, (**b**) SEM, (**c**) STEM and (**d**) HRTEM images showing second phase particles sizes and distributions [67]. Reprinted with permission from Elsevier

Fig. 2.14c. The structure of the fine particles was further investigated by HRTEM techniques, as shown in Fig. 2.14d. It is clear that the interface between the particles and matrix is semi-coherent.

Figures 2.15a, c EBSD maps illustrate the different types of twins that are produced in ME20 during lower strain hot rolling. As can be seen, in type 3 the main twins are $\{10\bar{1}2\}$ extension twins with a misorientation angle 86°; $\{10\bar{1}1\}-\{10\bar{1}2\}$ double twins with a misorientation angle 38° were also present but were fewer in number. Only a few $\{10\bar{1}1\}$ contraction twins were formed and most of these are located near the double twins. However, in type 1, only a few extension twins are formed during the hot rolling deformation. The volume fraction of extension twins is 3.97 and 20.52 % in type 1 and type 3, respectively.

Figure 2.16 shows microstructure and orientation distributions of the parent grains and selective twins in type 3 at 400 °C after 5 % thickness reduction. The matrix grains are nearly consumed by the growth of new tension twins in excess of 40 % indicated by naked eye. In Fig. 2.16a, twin seems across the grain boundary; theoretically speaking, grain boundary is a barrier to impede the dislocation motion.

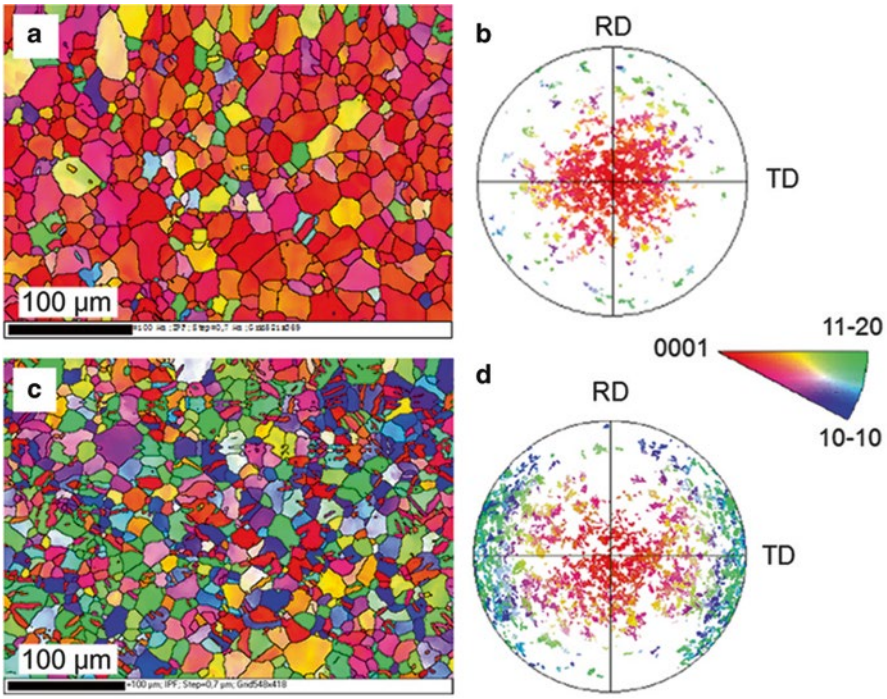

Fig. 2.15 EBSD images of ME20 samples after hot rolled at 400 °C for 5 % thickness reductions: (**a**) type 1 and (**c**) type 3; raw data of (0002) pole figure was shown in corresponding EBSD images, (**b**) type 1 and (**d**) type 3 [67]. Reprinted with permission from Elsevier

It is found that some twins can be intersected near the grain boundary. The matrix and twin orientations of all determined twins are displayed in pole figure in Fig. 2.15b. It is also visible that the matrix grains in pole figure are oriented such that the *c*-axis is tilted 45–90° away from the normal direction.

It elucidates that in type 1, a strong basal texture was found to be retained during all stage deformations of ME20. The texture intensity increases with growing thickness reductions. The main deformation modes were basal and prismatic <*a*> slips. In type 2 and type 3, at low strains, the texture was made up of two components: initial prismatic orientation and newly off-basal orientation. The main deformation modes were $\{10\bar{1}2\}$ -twinning, basal, and prismatic <*a*> slips. When the thickness reduction exceeds 30 %, a stable basal fiber texture was observed. The basal, prismatic <*a*>, and pyramidal <*c*+*a*> slip systems are also active. At 90 % reductions, apart from the dislocation glide, shear bands became another contributor to accommodate the strain and significantly alter the final textures. There is no obvious recrystallization behavior observed in type 1; on the contrary, to a certain extent recrystallization took place in type 3. The addition of cerium to magnesium in relatively small amount (0.3 wt%) probably promotes activation of the prismatic <*a*> glide.

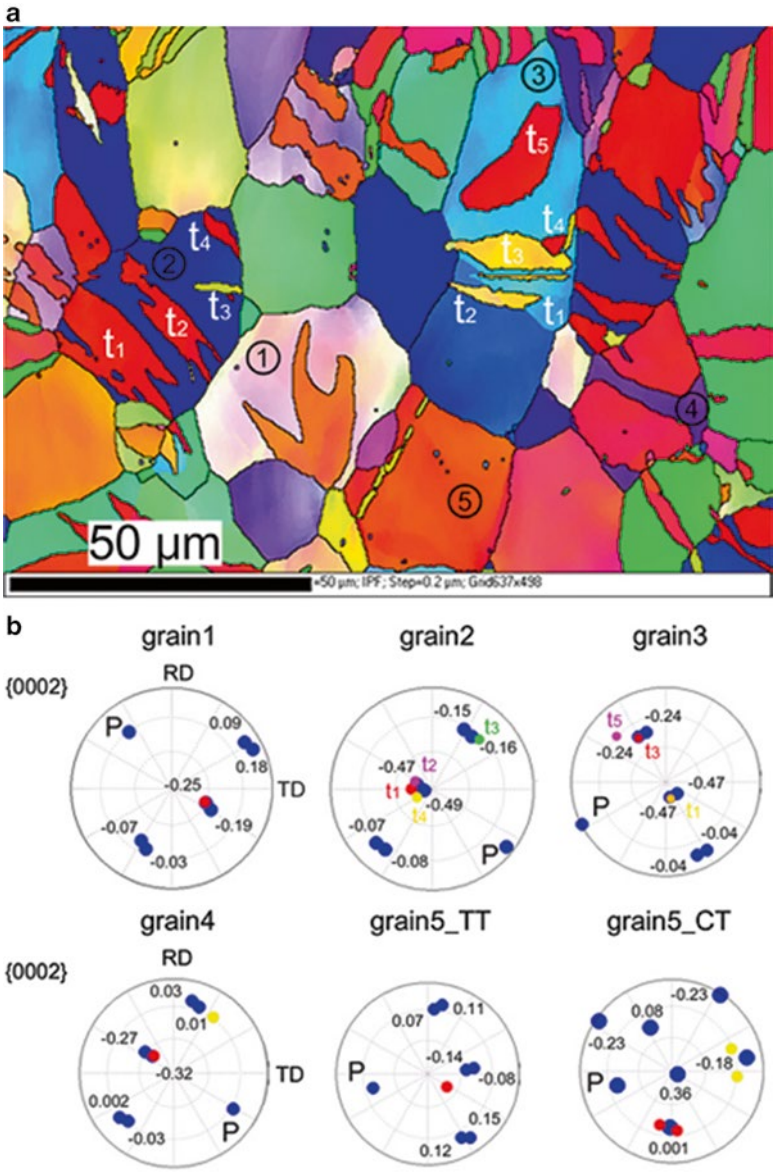

Fig. 2.16 (**a**) Crystallographic orientation map of sample type 3 obtained by hot rolling at 400 °C for 5 % thickness reduction along the RD and grains from 1 to 5 indicated in the image, (**b**) crystallographic orientation of parent grains and twin bands *TT* tension twin, *CT* contraction twin [67]. Reprinted with permission from Elsevier

2.2.5 High Energy Ball Milling/Mechanical Alloying

The earliest plastic deformation technique for synthesizing nanostructured materials was ball milling, and it is still used to fabricate nanostructured materials. The ball milled powders need to be consolidated to form the bulk nanostructured materials. This technique has been successfully used to form a nanostructured surface layer on alloys. Ortiz et al. [69] reported that nano-grains and grain size gradient were introduced into the surface of nickel-based C-2000 alloy after high energy ball milling.

Over the past few years, mechanical alloying (MA) has shown great potential in synthesizing a wide variety of nanocrystalline, supersaturated solid solutions and amorphous phase with unique characteristics [71]. Nasiri-Tabrizi et al. [72] studied the influence of milling parameters (time and atmosphere) on the mechanochemical synthesis of nanocrystalline hydroxyapatite (n-HAp) using different raw materials. Starting materials including calcium hydroxide ($Ca(OH)_2$), anhydrous dicalcium phosphate ($CaHPO_4$) and calcium carbonate ($CaCO_3$) with given stoichiometric proportionality within the reagents were milled using a high energy planetary ball mill under air or in a purified argon (99.998 vol.%) atmosphere. Mechanical activation was performed in polyamide-6 vials (volume of 125 ml) using Zirconia balls (20 mm in diameter) for 15, 40, and 80 h. The weight ratio of ball-to-powder and rotational speed were 20:1 and 600 rpm, respectively. To control temperature and prevent excessive heat, the millings were completed in 45 min milling steps with 15 min interval pauses. Two distinct chemical reactions were utilized as follows to investigate the effect of chemical composition of raw materials on the mechanosynthesis and purity of final products:

$$6CaHPO_4 + 4Ca(OH)_2 \rightarrow Ca_{10}(PO_4)_6(OH)_2 + 6H_2O \tag{2.1}$$

$$4CaCO_3 + 6CaHPO_4 \rightarrow Ca_{10}(PO_4)_6(OH)_2 + 4CO_2 + 2H_2O \tag{2.2}$$

Subsequently, the mechanically activated powder was filled in a quartz boat, and then annealed for 1 h under atmospheric pressure at 800 °C. The heating rate from room temperature up to the desired temperature was fixed at 10 °C min^{-1}.

The morphological characteristics of the n-HAp out of reaction (1) after 80 h milling under both milling atmospheres are shown in Fig. 2.17. TEM observations showed that the HAp particles had rod-like morphology with an average length of about 20 and 25 nm under air and argon atmospheres, respectively. However, in outcomes from reaction (1), there are some particles with ellipse-like morphology, and it is because of the axis orientation of nanorods with respect to the image plane. In fact, if the rod axis is perpendicular or oblique to the image plane, the rod may be seen as a full circle or ellipse shape, subsequently. It has been found that the n-HAp with ellipse- or rod-like morphology inhibit the proliferation of malignant melanoma cells. Therefore, these nanostructures may be helpful to remedy cancer. Furthermore, since the synthetic HAp nanorods have an excellent sinterability, using this structure

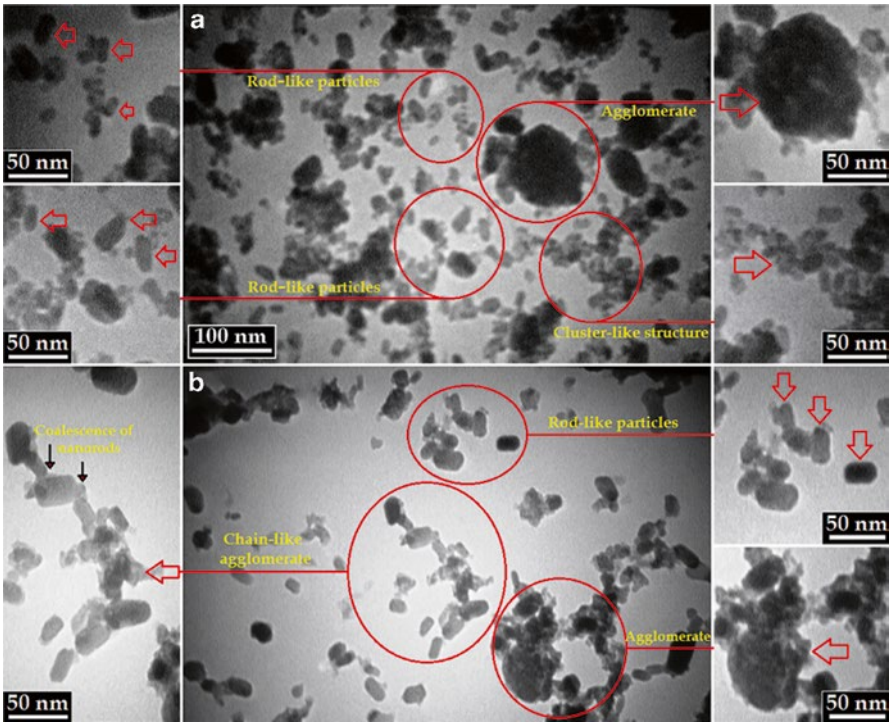

Fig. 2.17 TEM images of n-HAp powders produced through reaction (1) after 80 h milling under (**a**) air and (**b**) argon atmospheres [72]. Reprinted with permission from Elsevier

is an effective route to obtain dense bioceramics with high mechanical properties. As a result, the gained HAp nanorods may be utilized as strength enhancing additives for the preparation of the bionanocomposites with improved mechanical properties.

Figure 2.18 shows the TEM images of n-HAp out of reaction (2) after 80 h milling under both milling atmospheres. According to this figure, the HAp particles had spheroidal morphology with an average size of about 23 and 25 nm under air and argon atmospheres, respectively. It has been found that spherical particles are better than other irregular shapes due to the well space fillings and the low percentage of voids in the final product. Besides, granules with a smooth spherical geometry are useful in growth and attachment of bone tissue that improve osseointegration.

The synthesized powders exhibited average sizes about 32 and 27 nm under air atmosphere, and about 32 and 34 nm under argon atmosphere. The results of morphological evaluation confirmed the formation of n-HAp with different morphologies each of which can be used for particular purpose.

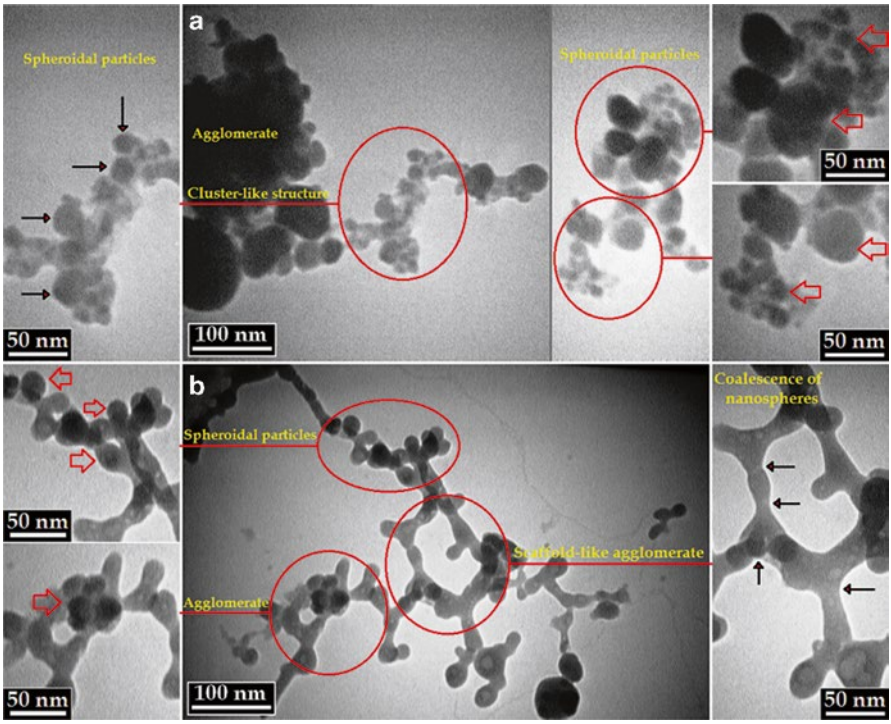

Fig. 2.18 TEM images of n-HAp powders produced through reaction (2) after 80 h milling under (**a**) air and (**b**) argon atmospheres [72]. Reprinted with permission from Elsevier

2.2.6 Sandblasting

Usually blasting is explained as the use of abrasive particles such as hard ceramics against another material under high pressure in order to make it smoother, remove surface contaminants or to roughen the surface [74–76]. The dynamic contact between the forced particles and the surface leads to higher roughness values, increasing metal surface reactivity [77]. The desired roughness can be set up by the particle size. Thus, for the blasting of biomedical materials the particles should be chemically stable and biocompatible. Usually alumina, titania, or hydroxyapatite particles are applied for blasting treatments.

Sandblasting possesses three purposes: (1) cleaning surface contaminants, (2) roughening surfaces to increase effective surface area, and (3) producing beneficial surface compressive residual stress. As a result, such treated surfaces exhibit higher surface energy, indicating higher surface chemical and physical activities, and enhancing fatigue strength as well as fatigue life.

In order to obtain satisfactory fixation and biofunctionality of biotolerated and bioinert materials, some of the mechanical surface alternation such as threaded surface, grooved surface, pored surface, and rough surface have been produced that promote tissue and bone ingrowth. But so far, there is no report on suitable roughness to specific metallic biomaterials. In general, on the macroscopic level (>10 μm), roughness will influence the mechanical properties of the interface, the way stresses are distributed and transmitted, the mechanical interlocking of the interface, and the biocompatibility of biomaterials. On a smaller scale, surface roughness in the range from 10 nm to 10 μm may influence the interface biology, since it is of the same order in size as cells and large biomolecules. Topographic variations of the order of 10 nm and less may become important because micro-roughness on this scale length consists of material defects such as grain boundaries, steps, and vacancies, which are known to be active sites for adsorption, and thus may influence the bonding of biomolecules to the implant surface. There is evidence that surface roughness on a micron scale allows cellular adhesion that alters the overall tissue response to biomaterials. Micro-rough surfaces allow early better adhesion of mineral ions or atoms, biomolecules, and cells, form stronger fixation of bone or connective tissue, result in a thinner tissue-reaction layer with inflammatory cells decreased or absent, and prevent microorganism adhesion and plaque accumulation, when compared with the smooth surfaces [78].

Although alumina (Al_2O_3) or silica (SiO_2) particles are most frequently used as a blasting media, there are several different types of powder particles utilized as media. This process may cause the release of cytotoxic silicon or aluminum ions in the periimplant tissue. To generate a biocompatible roughened titanium surface, an innovative grid-blasting process using biphasic calcium phosphate (BCP) particles was developed. Ti6Al4V disks were either polished, BCP grid-blasted, or left as-machined. BCP grid-blasting created an average surface roughness of 1.57 μm compared to the original machined surface of 0.58 μm. X-ray photoelectron spectroscopy indicated traces of calcium and phosphorus and relatively less aluminum on the BCP grid-blasted surface than on the initial titanium specimen [79].

Figure 2.19 shows a clear discrepancy between each of the three groups. Polished titanium samples (Fig. 2.19a) display a mirror polished surface. On the contrary, both Tipassiv (Fig. 2.19b) and Tiblast (Fig. 2.19c) samples exhibited a highly rugged and irregular surface.

SEM images of cell morphology are illustrated in Fig. 2.20a–f. On Tipolish (mirror-polished titanium disks) samples (Fig. 2.20a, b) cells exhibited large spreading with numerous dorsal microvilli and numerous specula-like lamelipodes. On Tipassiv (as-machined and passivated titanium disks) samples (Fig. 2.20c, d) MC3T3-E1 had an almost spread-out aspect, with multiple peripheral filopodia, dorsal microvilli, and cytoplasmic extensions. On Tiblast (BCP grid-blasted titanium disks) samples, MC3T3-E1 cells had a round shape, displayed dorsal microvilli but exhibited few cytoplasmic extensions (Fig. 2.20e, f). Cellular interconnections were frequently observed whatever the surface treatment (Fig. 2.20b, d, f). Cellular distribution appears to be obvious only on the polished surface (Fig. 2.20a) with the appearance of multicellular spindles. Cells showed particular distribution neither on the surface of Tipassiv (Fig. 2.20c) nor Tiblast samples (Fig. 2.20e).

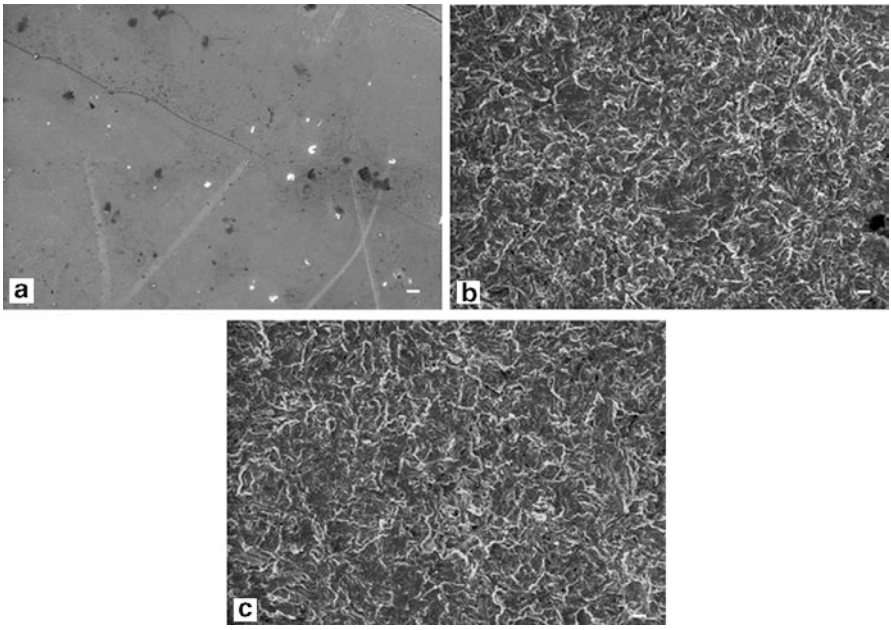

Fig. 2.19 SEM micrographs showing the surface roughness of the various tested titanium disks. (**a**) mirror-polished titanium disks (Tipolish); (**b**) as-machined and passivated titanium disks (Tipassiv); (**c**) BCP grid-blasted titanium disks (Tiblast). Original magnification 1,000×; Bar = 10 mm [79]. Reprinted with permission from Elsevier

It was reported that (1) according to scanning electronic microscopy observations and measurement of mitochondrial activity (MTS assay), it showed that osteoblastic MC3T3-E1 cells were viable in contact with the BCP grid-blasted titanium surface, (2) MC3T3-E1 cells expressed alkaline phosphate (ALP) activity and conserved their responsiveness to bone morphogenetic protein BMP-2, and (3) the calcium phosphate grid-blasting technique increased the roughness of titanium implants and provided a non-cytotoxic surface with regard to mouse osteoblasts [79]. Tribo-chemical treatment has been proposed to enhance the bond strength between titanium crown and resin base [80]. Using silica-coated alumina as a blasting media under relatively low pressure, silica layer is expected to remain on the blasted surface so that retention force is enhanced by silan coupling treatment.

Although blasting shows several advantages, there is evidence of adverse effects: (1) surface contamination, depending on type of blasting media, and (2) distortion of blasted workpiece, depending on blasting manner and intensity. Miyakawa et al. [81] studied the surface contamination of abraded titanium. Despite low grinding speeds and water cooling, the abraded surfaces were found to be contaminated by abrasive constituent elements. Element analysis and chemical bond state analysis of the contaminants were performed using an electron probe microanalyzer. X-ray diffraction of the abraded surface was performed to identify the contaminants.

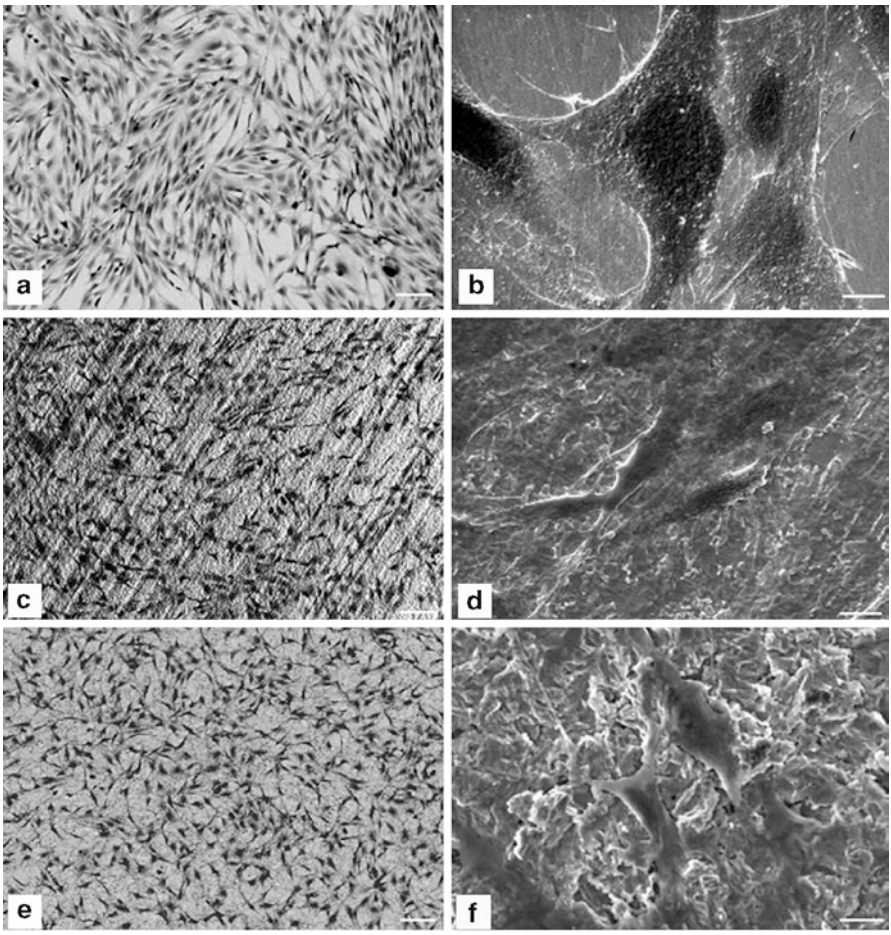

Fig. 2.20 SEM observation of MC3T3-E1 morphology after a 2 days culture in direct contact on titanium disks with different surface roughness. (**a**, **b**) Group Tipolish, (**c**) and (**d**) Group Tipassiv, (**e**, **f**) Group Tiblast. (**a**, **c**, **e**) Samples were observed using back-scattered electrons. Original magnification 250×, bar = 100 mm. (**b**, **d**, **f**) Samples were observed using secondary electrons. Original magnification 3,000×; bar = 10 mm [79]. Reprinted with permission from Elsevier

It was reported that (1) the contamination of titanium was related to its reactivity as well as its hardness, (2) in spite of water cooling and slow-speed abrading, titanium surfaces were obviously contaminated, (3) contaminant deposits with dimensions ranging from about 10 to 30 μm occurred throughout the surfaces, and (4) the contaminant of titanium, although related also to the hardness, resulted primarily from a reaction with abrasive materials, and such contamination could negatively influence titanium's resistance to corrosion and its biocompatibility [81].

Normally, fine alumina particles (50 μm Al_2O_3) are recycled within the sandblasting machine. Ceramics such as alumina are brittle in nature, and therefore,

some portions of recycled alumina might be brittle-fractured. If fractured sandblasting particles are involved in the recycling media, it might result in irregular surfaces, as well as potential contamination. Using fractal dimension analysis [82–85], a sample plate surface was weekly analyzed in terms of topographic changes, as well as chemical analysis of sampled recycled Al_2O_3 particles. It was found that after accumulated use time exceeded 30 min, the fractal dimension (DF) [82] remained a constant value of about 1.4, prior to which it continuously increased from 1.25 to 1.4. By the electron probe microanalysis on collected blasting particles, unused Al_2O_3 contains 100 % Al, whereas used (accumulated usage time was about 2,400 s) particles contained Al (83.32 wt%), Ti (5.48), Ca (1.68), Ni (1.36), Mo (1.31), S (1.02), Si (0.65), P (0.55), Mn (0.49), K (0.29), Cl (0.26), and V (0.08), strongly indicating that used alumina powder was heavily contaminated, and a high risk for the next material surface to be contaminated. Such contaminants were from previously blasted materials having various chemical compositions, and investing materials as well [85].

There are several evidences of surface contamination due to mechanical abrasive actions. As a metallographic preparation, the surface needs to be mechanically polished with a metallographic paper (which is normally SiC-adhered paper) under running water [86, 87]. It is worth mentioning here that polishing paper should be changed between different types of materials, and particularly when a dissimilar metal-couple is used for galvanic corrosion tests, such couple should not be polished prior to corrosion testing because both materials could become cross-contaminated [87]. Hence, there are attempts to use TiO_2 powder for blasting onto titanium material surfaces. It was reported that titanium surfaces were sandblasted using TiO_2 powder (particle size ranging from 45, 45–63, and 63–90 μm) to produce the different surface textures prior to fibroblast cell attachment [88].

Recently, it has been reported that sandblasting using alumina as a media caused a remarkable distortion on a Co–Cr alloy and a noble alloy [89, 90]. It was estimated that the stress causing the deflection exceeded the yield strength of tested materials. It was also suggested that the sandblasting should be done using the lowest air pressure, duration of blasting period, and particle size alumina in order to minimize distortion of crowns and frameworks. To measure distortion, Co–Cr alloy plates (25 mm long, 5 mm wide, and 0.7 mm thick) were sandblasted with Al_2O_3 of 125 μm. Distortion was determined as the deflection of the plates as a distance of 20 mm from the surface. It was reported that (1) the mean deflections varied between 0.37 and 1.72 mm, and (2) deflection increased by an increase in duration of the blasting, pressure, particle size, and by a decrease in plate thickness [89].

2.2.7 Shot Peening and Laser Shock Peening

Shot peening (which is a similar process to sandblasting, but has more controlled peening power, intensity, and direction) is a cold working process in which the surface of a part is bombarded with small spherical media called shot. Each piece of

shot striking the material acts as a tiny hammer, imparting to the surface small indentations or dimples. In order for the dimple to be created, the surface fibers of the material must be yielded in tension. Below the surface, the fibers try to restore the surface to its original shape, thereby producing below the dimple a hemisphere of cold-worked material highly stressed in compression. Overlapping dimples (which are sometimes called forged dimples) develop an even layer of metal in residual compressive stress. It is well known that cracks will not initiate or propagate in a compressively stressed zone due to a tendency of crack-closure. Since nearly all fatigue and stress corrosion cracking failures originate at the surface of a part, compressive stresses induced by shot peening provide considerable increases in part life, since advancing crack-opening is suppressed by preexisting compressive residual stress. The maximum compressive residual stress produced at or under the surface of a part by shot peening is at least as great as half the yield strength of the material being peened. Many materials will also increase in surface hardness due to the cold working effect of shot peening. Both compressive stresses and cold working effects are used in the application of shot peening in forming metal parts, called "shot forming" [91].

Hashemi et al. [92] investigated the wear resistance of shot peened–nitrided 316 L austenitic stainless steel. The shot peening treatment was performed on some of the 316 L stainless steel sheet samples (3 mm in thickness) for 15 min using an SBRT-ISO shot peening machine containing steel balls with mean hardness of 40–45 RC, diameter of 1–2 mm, and shooting angle of 45°. Wear tests were carried out using a rotating pin-on-disk wear testing machine with a speed of 2 cm/s. The diameter of wearing circumferential trajectory was adjusted to be 7 mm. These tests were performed against a 5 mm diameter SAE 52100 pin (ball) and repeated at least three times per specimen. The sliding distance was 250 m with normal loads of 5 and 10 N. The weight loss value of the specimens and the traversed distance were the criterion for comparison of the wear resistance.

Figure 2.21 shows the cross-section microstructure of different specimens. A gray layer or nitrided layer was seen at the surface of nitride specimen (Fig. 2.21c, d). The nitrided layer of shot peened–nitrided specimen was thicker than the nitrided specimen without shot peening. The increase of dislocations density and grain refinement at the surface layers of specimen after shot peening was shown in Fig. 2.21b.

Results show that severe plastic deformations due to shot peening caused strain-induced martensite transformation in the surface layers, and the amounts of grain boundaries and other defects increased in the shot peened specimens. The wear rate due to motion of pin on specimen's surface at a constant load, for the shot peened–nitrided specimen was less than this quantity for the nitride specimen, which was itself less than that of the untreated specimen. When 5 N load was exerted, the wear rate of specimens was eligible; however, exerting the 10 N load made the wear rate of untreated specimens to increase intensely. While, the wear rate for the other specimens did not show a significant increase. Therefore, surface treatments played an important role in increasing the hardness and wear resistance of 316 L stainless steel, and according to surface hardness of specimens, shot peening–nitriding treatment had the highest effect in decreasing wear. Signs of a mixture of adhesive

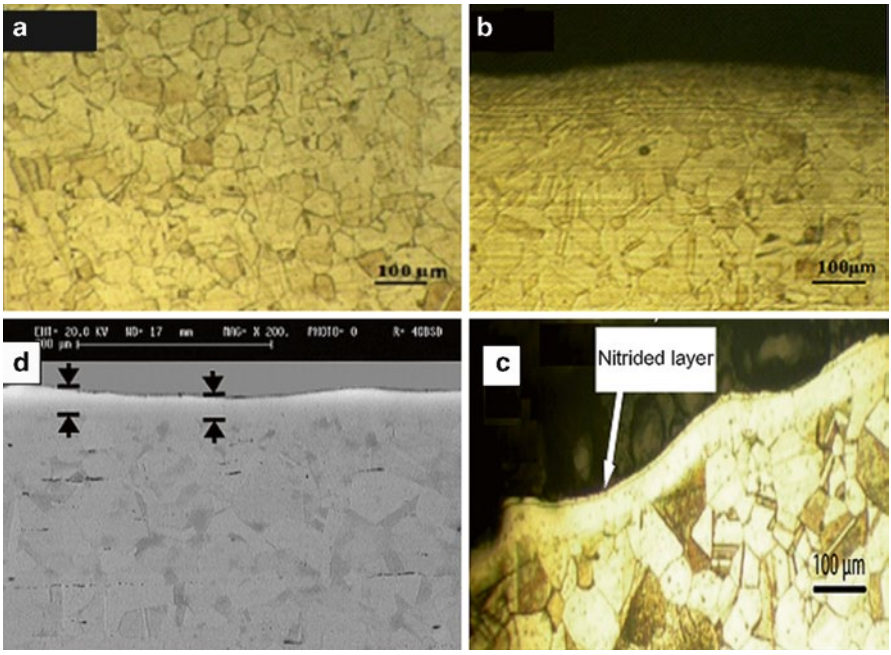

Fig. 2.21 (**a**) Cross-section microstructure of untreated specimen, (**b**) shot peened specimen, (**c**) nitrided specimen and (**d**) SEM micrograph of nitrided specimen [92]. Reprinted with permission from Elsevier

(which was usually the predominant mechanism in wear of austenitic stainless steel) and abrasive wear mechanisms were observed on the surface of the untreated specimen. The crushed particles due to the high pressure of the pin were probably the reason of abrasive wear between the ball and the specimen.

It seems that how much the surface hardness increases, the abrasive mechanism becomes more controlling. The controlling mechanism for the untreated specimen is adhesive–abrasive, according to its low hardness value. While, investigating shot peened specimens showed that the controlling mechanism goes more and more to abrasive mechanism, because of the considerable increase in the surface hardness.

The laser peening (laser shock peening) technology has been recently developed, claiming non-contact, no-media, and contamination-free peening method. Before treatment, the workpiece was covered with a protective ablative layer (paint or tape) and a thin layer of water. High-intensity (5–15 GW/cm^2) nanosecond pulses (10–30 ns) of laser light beam (3–5 mm width) striking the ablative layer generated a short-lived plasma which caused a shock wave to travel into the workpiece. The shock wave induced compressive residual stress that penetrated beneath the surface and strengthened the workpiece, resulting in improvements in fatigue life and retarding in stress corrosion cracking occurrence.

Sealy et al. [93] researched surface integrity and process mechanics of laser shock peening of novel biodegradable magnesium–calcium (Mg–Ca) alloy.

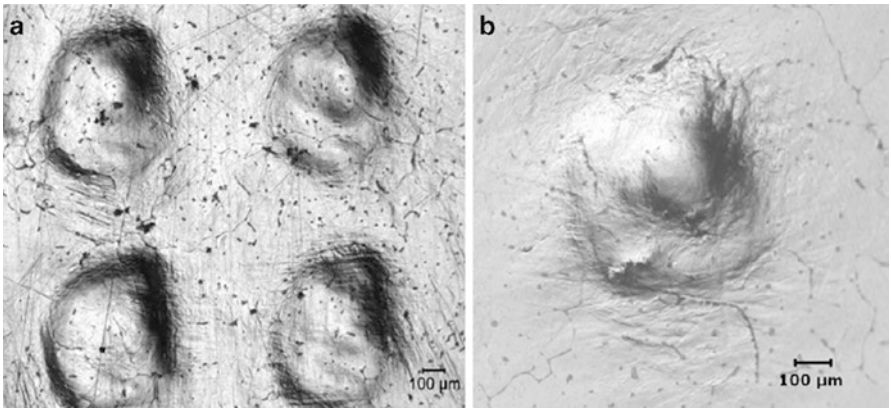

Fig. 2.22 Dent topography [93]. (**a**) Sequential LSP. (**b**) Single LSP. Reprinted with permission from Elsevier

An Nd:YAG laser (wavelength D 1,064 nm, pulse width (τ) = 5–7 ns, frequency (f) = 30 Hz) with power range 0.1–10 W was used in the experiments. The estimated spot diameter was approximately 250 μm using a 100 mm focal length lens where the cross-sectional area was 0:0491 mm^2. The sample was oriented vertically so particulate could not accumulate in the laser's path. Each experiment was performed in water confined regime at a depth of 1–2 mm. Black tape with a thickness of 0.05 mm was used as the ablative medium. The average power measured 8 W.

Figure 2.22 shows the optical images of dents by sequential and single laser shock peening (LSP). As material behavior is characterized by stress/strain graphs along the peening or depth direction and radial directions, tensile pile up is critical to tribological applications in implants. Results showed that due to the radial expansion of neighboring peens, the magnitude of the pile up increased approximately 50 %, which drastically affected the wear and fatigue performance of a surface.

2.3 Future Prospects

Green technologies or hybrid eco-friendly techniques should be developed for nanostructured metallic biomaterials with/without masking the unwanted area. Through the choice of processing parameters, the width and depth of the nanotextured features can be controlled over a wide range resulted in higher quality in the bio environment. Nanotexturing such prosthetic items as hip implants; textures could be sized and shaped to favor the ingrowth of adjacent bone to anchor the implants with the suitable properties of tribology in the practical applications.

Proposing an ideal implant structure with nano modification or nanostructure should be integrated by bioengineering, nanotechnology, and biomaterials science. The four important factors and requirements for successful and biofunctional implant

systems should be satisfied: (1) biological compatibility (or, biocompatibility); (2) mechanical compatibility (or mechanocompatibility); (3) morphological compatibility, and (4) crystallographic compatibility (or micromorphological compatibility).

Up to now there is no absolute knowledge on the influence of nanostructure features on the biological environment, because of the absence of standardized surfaces with repetitive topography at the nanoscale level with highly controllable lateral resolution. The increasing availability of well understood and standardized surface structures in the sub-100 nm scale will strongly help to understand the interactions between specific proteins and cells.

Acknowledgement The work was fully supported by a grant from City University of Hong Kong (Project No. 7004246).

References

1. Khan MA, Williams RL, Williams DF (1996) In vitro corrosion and wear of titanium alloys in the biological environment. Biomaterials 17:2117–2126
2. Okazaki Y, Gotoh E (2005) Comparison of metal release from various metallic biomaterials in vitro. Biomaterials 26:11–21
3. Khan MA, Williams RL, Williams DF (1999) Conjoint corrosion and wear in titanium alloys. Biomaterials 20:765–772
4. McKay GC, Macnair R, MacDonald C, Grant MH (1996) Interactions of orthopaedic metals with an immortalized rat osteoblast cell line. Biomaterials 17:1339–1344
5. Eisenbarth E, Velten D, Schenk-Meuser K, Linez P, Biehl V, Duschner H, Breme J, Hildebrand H (2002) Interactions between cells and titanium surfaces. Biomol Eng 19:243–249
6. Hanawa T (2002) Evaluation techniques of metallic biomaterials in vitro. Sci Tech Adv Mater 3:289–295
7. Dearnley PA, Dahm KL, Çimenoğlu H (2004) The corrosion-wear behaviour of thermally oxidised CP–Ti and Ti–6Al–4V. Wear 256:469–479
8. Barril S, Debaud S, Mischler S, Landolt D (2002) A tribo-electrochemical apparatus for in vitro investigation of fretting-corrosion of metallic implant materials. Wear 252:744–754
9. Ponthiaux P, Wenger F, Drees D, Celis JP (2004) Electrochemical techniques for studying tribocorrosion processes. Wear 256:459–468
10. Okazaki Y (2002) Effect of friction on anodic polarization properties of metallic biomaterials. Biomaterials 23:2071–2077
11. Duisabeau L, Combrade P, Forest B (2004) Environmental effect on fretting of metallic materials for orthopaedic implants. Wear 256:805–816
12. Vieira AC, Ribeiro AR, Rocha LA, Celis JP (2006) Influence of pH and corrosion inhibitors on the tribocorrosion of titanium in artificial saliva. Wear 261:994–1001
13. Barril S, Mischler S, Landolt D (2004) Influence of fretting regimes on the tribocorrosion behaviour of Ti6Al4V in 0.9 wt% sodium chloride solution. Wear 256:963–972
14. Barril S, Mischler S, Landolt D (2005) Electrochemical effects on the fretting corrosion behaviour of Ti6Al4V in 0.9 % sodium chloride solution. Wear 259:282–291
15. Duerig T, Pelton A, Stockel D (1999) An overview of nitinol medical applications. Mater Sci Eng A 149:273–275
16. Narayan R (2009) Biomedical materials. Springer, New York
17. Otsuka K, Wayman CM (1998) Shape memory materials. Cambridge University Press, Cambridge

18. Abboud JH, Fidel AF, Benyounis KY (2008) Surface nitriding of Ti–6Al–4V alloy with a high power CO_2 laser. Optic Laser Tech 40(2):405–414
19. Advincula MC, Rahemtulla FG, Advincula RC, Ada ET, Lemons JE, Bellis SL (2006) Osteoblast adhesion and matrix mineralization on sol–gel-derived titanium oxide. Biomaterials 27(10):2201–2212
20. Tredwin CJ, Georgiou G, Kim HW, Knowles JC (2013) Hydroxyapatite, fluor-hydroxyapatite and fluorapatite produced via the sol–gel method: bonding to titanium and scanning electron microscopy. Dent Mater 29(5):521–529
21. Lin NM, Huang XB, Zhang XY, Fan AL, Qin L, Tang B (2012) In vitro assessments on bacterial adhesion and corrosion performance of TiN coating on Ti6Al4V titanium alloy synthesized by multi-arc ion plating. Appl Surf Sci 258(18):7047–7051
22. Tan L, Crone WC (2002) Surface characterization of nitinol modified by plasma source ion implantation. Acta Materialia 50:4449–4460
23. Tan L, Dodd RA, Crone WC (2003) Corrosion and wear-corrosion behavior of NiTi modified by plasma source ion implantation. Biomaterials 24(22):3931–3939
24. Bilek MMM (2014) Biofunctionalization of surfaces by energetic ion implantation: review of progress on applications in implantable biomedical devices and antibody microarrays. Appl Surf Sci 310:3–10
25. McGrory BJ, Ruterbories JM, Pawar VD, Thomas RK, Salehi AB (2012) Comparison of surface characteristics of retrieved cobalt-chromium femoral heads with and without ion implantation. J Arthroplasty 27(1):109–115
26. Campoccia D, Montanaro L, Arciola CR (2013) A review of the biomaterials technologies for infection-resistant surfaces. Biomaterials 34(34):8533–8554
27. Rautray TR, Narayanan R, Kim KH (2011) Ion implantation of titanium based biomaterials. Progr Mater Sci 56(8):1137–1177
28. Kumar S, Narayanan TSNS, Raman SGS, Seshadri SK (2009) Thermal oxidation of CP–Ti: evaluation of characteristics and corrosion resistance as a function of treatment time. Mater Sci Eng C 29(6):1942–1949
29. Liu XY, Chu PK, Ding CX (2004) Surface modification of titanium, titanium alloys, and related materials for biomedical applications. Mater Sci Eng R Rep 47(3–4):49–121
30. Hryniewicz T, Rokicki R, Rokosz K (2009) Corrosion and surface characterization of titanium biomaterial after magnetoelectropolishing. Surf Coating Technol 203(10–11):1508–1515
31. Habibzadeh S, Li L, Shum-Tim D, Davis EC, Omanovic S (2014) Electrochemical polishing as a 316L stainless steel surface treatment method: towards the improvement of biocompatibility. Corrosion Sci 87:89–100
32. De Nardo L, Altomare L, Del Curto B, Cigada A, Draghi L (2012) Chapter 4 – electrochemical surface modifications of titanium and titanium alloys for biomedical applications. In: Driver M (eds) Coatings for biomedical applications. Woodhead Publishing, Cambridge, UK, pp 106–142
33. Shabalovskaya S, Anderegg J, Van Humbeeck J (2008) Critical overview of Nitinol surfaces and their modifications for medical applications. Acta Biomaterialia 4(3):447–467
34. Clarke B, Carroll W, Rochev Y, Hynes M, Bradley D, Plumley D (2006) Influence of nitinol wire surface treatment on oxide thickness and composition and its subsequent effect on corrosion resistance and nickel ion release. J Biomed Mater Res Part A 79A(1):61–70
35. http://www.numis.northwestern.edu/Research/Projects/Hip.shtml
36. Ashby MF, Ferreira PJ, Schodek DL (eds) (2009) Chapter 1: nanomaterials and nanotechnologies: an overview, Nanomaterials, nanotechnologies and design: an introduction for engineers and architects. Elsevier Butterworth-Heinemann, Burlington, MA, pp 1–16
37. Kostoff RN, Koytcheff RG, Lau GY (2007) Global nanotechnology research literature overview. Technol Forecast Soc Change 74:1733–1747
38. Pitkethly MJ (2004) Nanomaterials-the driving force. Mater Today 7:20–29
39. Ashby MF, Ferreira PJ, Schodek DL (eds) (2009) Chapter 8: nanomaterials: synthesis and characterization, Nanomaterials, nanotechnologies and design: an introduction for engineers and architects. Elsevier Butterworth-Heinemann, Burlington, MA, pp 257–290

40. Ashby MF, Ferreira PJ, Schodek DL (eds) (2009) Chapter 11: nanomaterials and nanotechnologies in health and the environment, Nanomaterials, nanotechnologies and design: an introduction for engineers and architects. Elsevier Butterworth-Heinemann, Burlington, MA, pp 467–500
41. Van Hove MA (2009) Atomic-scale structure: from surface to nanomaterials. Surf Sci 603:1301–1305
42. Zäch M, Hägglund C, Chakarov D, Kasemo B (2006) Nanoscience and nanotechnology for advanced energy systems. Curr Opin Solid State Mater Sci 10:132–143
43. Balasundaram G, Webster TJ (2006) A perspective on nanophase materials for orthopedic implant applications. J Mater Chem 16:3737–3745
44. Stevens MM, George JH (2005) Exploring and engineering the cell surface interface. Science 310:1135–1138
45. Wilson CJ, Clegg RE, Leavesley DI, Pearcy MJ (2005) Mediation of biomaterial-cell interactions by adsorbed proteins: a review. Tissue Eng 11(1–2):1–18
46. Webster TJ, Ejiofor JU (2004) Increased osteoblast adhesion on nanophase metals: Ti, Ti6Al4V, and CoCrMo. Biomaterials 25:4731–4739
47. Price RL, Waid MC, Haberstroh KM, Webster TJ (2003) Selective bone cell adhesion on formulations containing carbon nanofibers. Biomaterials 24:1877–1887
48. Webster TJ, Smith TA (2005) Increased osteoblast function on PLGA composites containing nanophase titania. J Biomed Mater Res Part A 74:677–686. doi:10.1002/jbm.a.30358
49. Manjubala I, Scheler S, Bossert J, Jandt KD (2006) Mineralisation of chitosan scaffolds with nano-apatite formation by double diffusion technique. Acta Biomaterilia 2(1):75–84
50. Aizenberg J (2005) A bio-inspired approach to controlled crystallization at the nanoscale. Bell Labs Tech J 10(3):129–141
51. Wagner T, Neinhuis C, Barthlott W (1996) Wettability and contaminability of insect wings as a function of their surface sculptures. Acta Zoologica 77:213–225. doi:10.1111/j.1463-6395.1996.tb01265.x
52. Lee W, Jin MK, Yoo WC, Lee JK (2004) Nanostructuring of a polymeric substrate with well-defined nanometer-scale topography and tailored surface wettability. Langmuir 20(18): 7665–7669
53. Valiev RZ (2004) Nanostructuring of metals by severe plastic deformation for advanced properties. Nat Mater 3:511–516
54. Faghihi S, Azari F, Zhilyaev AP, Szpunar JA, Vali H, Tabrizian M (2007) Cellular and molecular interactions between MC3T3-E1 pre-osteoblasts and nanostructured titanium produced by high-pressure torsion. Biomaterials 28:3887–3895
55. Zhilyaev AP, Langdon TG (2008) Using high-pressure torsion for metal processing: fundamentals and applications. Progr Mater Sci 53:893–979
56. Valiev RZ, Islamgaliev RK, Alexandrov IV (2000) Bulk nanostructured materials from severe plastic deformation. Progr Mater Sci 45(2):103–189
57. Minárik P, Král R, Janeček M (2013) Effect of ECAP processing on corrosion resistance of AE21 and AE42 magnesium alloys. Appl Surf Sci 281:44–48
58. Suresh KS, Geetha M, Richard C, Landoulsi J, Ramasawmy H, Suwas S, Asokamani R (2012) Effect of equal channel angular extrusion on wear and corrosion behavior of the orthopedic Ti–13Nb–13Zr alloy in simulated body fluid. Mater Sci Eng C 32:763–771
59. Li SY, Beyerlein IJ, Bourke MAM (2005) Texture formation during equal channel angular extrusion of fcc and bcc materials: comparison with simple shear. Mater Sci Eng A 394(1–2):66–77
60. Ahna SH, Chunb YB, Yuc SH, Kima KH, Hwang SK (2010) Microstructural refinement and deformation mode of Ti under cryogenic channel die compression. Mater Sci Eng A 528: 165–171
61. Rosen GI, Jensen DJ, Hughes DA, Hansen N (1995) Microstructure and local crystallography of cold rolled aluminum. Acta Metallurgica Materialia 43(7):2563–2579
62. Hughes DA, Hansen N (1997) High angle boundaries formed by grain subdivision mechanisms. Acta Materialia 45(9):3871–3886

63. Momeni A, Abbasi SM (2011) Repetitive thermomechanical processing towards ultra fine grain structure in 301, 304 and 304L stainless steels. J Mater Sci Technol 27(4):338–343
64. Shakhova I, Dudko V, Belyakov A, Tsuzaki K, Kaibyshev R (2012) Effect of large strain cold rolling and subsequent annealing on microstructure and mechanical properties of an austenitic stainless steel. Mater Sci Eng A 545:176–186
65. González M, Peña J, Gil FJ, Manero JM (2014) Low modulus Ti–Nb–Hf alloy for biomedical applications. Mater Sci Eng C 42:691–695
66. del Valle JA, Pérez-Prado MT, Ruano OA (2003) Texture evolution during large-strain hot rolling of the Mg AZ61 alloy. Mater Sci Eng A 355:68–78
67. Li X, Qi W (2013) Effect of initial texture on texture and microstructure evolution of ME20 Mg alloy subjected to hot rolling. Mater Sci Eng A 560:321–331
68. Luo J, Yan H, Chen RS, Han EH (2014) Effects of Gd concentration on microstructure, texture and tensile properties of Mg–Zn–Gd alloys subjected to large strain hot rolling. Mater Sci Eng A 614:88–95
69. Ortiz AL, Tian JW, Villegas JC, Shaw LL, Liaw PK (2008) Interrogation of the microstructure and residual stress of a nickel-base alloy subjected to surface severe plastic deformation. Acta Materialia 56(3):413–426
70. Zahrani EM, Fathi MH (2009) The effect of high-energy ball milling parameters on the preparation and characterization of fluorapatite nanocrystalline powder. Ceram Int 35:2311–2323
71. Nouri A, Hodgson PD, Wen C (2011) Effect of ball-milling time on the structural characteristics of biomedical porous Ti–Sn–Nb alloy. Mater Sci Eng C 31:921–928
72. Nasiri-Tabrizi B, Fahami A, Ebrahimi-Kahrizsangi R (2013) Effect of milling parameters on the formation of nanocrystalline hydroxyapatite using different raw materials. Ceram Int 39:5751–5763
73. Rakovsky A, Gotman I, Rabkin E, Gutmanas EY (2013) Strong bioresorbable Ca phosphate-PLA nanocomposites with uniform phase distribution by attrition milling and high pressure consolidation. J Mech Behav Biomed Mater 18:37–46
74. Hignett B, Andrew TC, Downing W, Duwell EJ, Belanger J, Tulinski EH (1987) Surface cleaning, finishing and coating. In: Wood WG (ed) Metals handbook. American Society for Metals, Metals Park, pp 107–127
75. Kern M, Thompson VP (1994) Sandblasting and silica coating of a glass-infiltrated alumina ceramic – volume loss, morphology, and changes in the surface-composition. J Prosthet Dent 71:453–461
76. Kern M, Thompson VP (1994) Effects of sandblasting and silica-coating procedures on pure titanium. J Dent 22:300–306
77. Wennerberg A (1998) The importance of surface roughness for implant incorporation. Int J Mach Tool Manufact 38:657–662
78. Wen X, Wang X, Zhang N (1996) Microrough surface of metallic biomaterials: a literature review. J Biomed Mater Eng 6:173–189
79. Citeau A, Guicheux J, Vinatier C, Layrolle P, Nguyen TP, Pilet P, Daculsi G (2005) In vitro biological effects of titanium rough surface obtained by calcium phosphate grid blasting. Biomaterials 26:157–165
80. Kubo M, Fijishima A, Hotta Y, Kunii J, Shimakura Y, Shimidzu T, Kawawa T, Miyazaki T (2006) Production method of resin-bonded titanium crown by CAD/CAM. The 19th proceedings of society titanium, research. p 42
81. Miyakawa O, Watanabe K, Okawa S, Kanatani M, Nakano S, Kobayashi M (1996) Surface contamination of titanium by abrading treatment. Dent Mater 15:11–21
82. Mandelbrot BB (1983) The fractal geometry of nature. Freeman, New York, p 34
83. Chesters S, Wen HY, Lundin M, Kasper G (1989) Fractal-based characterization of surface texture. Appl Surf Sci 40:185–192
84. Sayles RS, Thomas TR (1978) Surface topography as a non-stationary random process. Nature 271:431–434
85. Oshida Y, Munoz CA, Winkler MM, Hashem A, Ito M (1993) Fractal dimension analysis of aluminum oxide particle for sandblasting dental use. J Biomed Mater Eng 3:117–126

86. Park JH, Olivares-Navarrete R, Baier RE, Meyer AE, Tannenbaum R, Boyan BD, Schwartz Z (2012) Effect of cleaning and sterilization on titanium implant surface properties and cellular response. Acta Biomaterialia 8(5):1966–1975
87. Guo ZX, Wang XL, Huang H (2010) Plasma-mediated ablation of biofilm contamination. Appl Surf Sci 257(4):1247–1253
88. Cooper LF, Zhou YS, Takebe J, Guo JL, Abron A, Holmén A, Ellingsen JE (2006) Fluoride modification effects on osteoblast behavior and bone formation at TiO_2 grit-blasted c.p. titanium endosseous implants. Biomaterials 27(6):926–936
89. Peutzfeld A, Asmussen E (1996) Distortion of alloy by sandblasting. Am J Dent 9:65–66
90. Multigner M, Ferreira-Barragáns S, Frutos E, Jaafar M, Ibáñez J, Marín P, Pérez-Prado MT, González-Doncel G, Asenjo A, González-Carrasco JL (2010) Superficial severe plastic deformation of 316 LVM stainless steel through grit blasting: effects on its microstructure and subsurface mechanical properties. Surf Coating Tech 205(7):1830–1837
91. Aparicio C, Gil FJ, Fonseca C, Barbosa M, Planell JA (2003) Corrosion behaviour of commercially pure titanium shot blasted with different materials and sizes of shot particles for dental implant applications. Biomaterials 24(2):263–273
92. Hashemi B, Yazdi MR, Azar V (2011) The wear and corrosion resistance of shot peened–nitrided 316L austenitic stainless steel. Mater Des 32:3287–3292
93. Sealy MP, Guo YB (2010) Surface integrity and process mechanics of laser shock peening of novel biodegradable magnesium–calcium (Mg–Ca) alloy. J Mech Behav Biomed Mater 3:488–496

Chapter 3
Recent Development of Metal Nanoparticles Catalysts and Their Use for Efficient Hydrogenation of Biomass-Derived Levulinic Acid

Kai Yan and Huixia Luo

Abstract In this chapter we concentrate our attention on the green processes of metal nanoparticles and utilization for catalytic hydrogenation of biomass-derived levulinic acid, from the pioneering studies to the present state of the art. An overview of the different methods and recent advances for the fabrication of metal nanoparticles, especially for the green methods, are commented and compared. Challenges and areas that need improvement are also highlighted in the corresponding area. The resulting catalysts are commented for the catalytic upgrading of levulinic acid which is a chemical building block from lignocellulosic biomass for the production of transportation fuels, as well as useful chemicals. Specific examples are reviewed with emphasis on different synthetic methods, comparing the behavior of different metal catalysts.

Keywords Green processes • Metal nanoparticle • Development • Hydrogenation • Levulinic acid

3.1 Introduction

Due to the diminishing of fossil fuels and its associated seriously environmental issues, sustainable alternatives have been taken for environmental protection and rational utilization of renewable energy [1–5]. Lignocellulosic biomass is the renewable and abundant source that can be used as a replacement for fossil resources in the sustainable production of transportation fuels and chemicals [6–8]. However, the high concentration of oxygen functionalized units in biomass presents a challenge for the development of biomass-based processes [9–12]. Over the

K. Yan (✉)
School of Engineering, Brown University, 182 Hope Street, Providence, RI 02912, USA
e-mail: kai_yan@brown.edu

H. Luo
Department of Chemistry, Princeton University, Princeton, NJ 08544, USA

V.A. Basiuk, E.V. Basiuk (eds.), *Green Processes for Nanotechnology*,
DOI 10.1007/978-3-319-15461-9_3

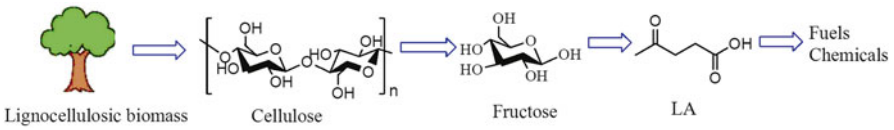

Fig. 3.1 Production route of fuels and chemicals from lignocellulosic biomass

last several decades, it has been demonstrated that one of the most effective methodology is to transform the high concentration of oxygen functionalized biomass to levulinic acid (LA) that has low oxygen content, followed by catalytic conversion of LA into fuels and valuable chemicals as shown in Fig. 3.1. Besides, LA has been identified as one of the most promising top-12 building blocks for the sustainable production of fuels and useful chemicals in the replacement of fossil resources [13, 14]. Homogeneous catalytic conversion of LA is very efficient and selective due to the easy access to the catalytic active center [6, 15], but it often suffers from the difficulty in the removal of the catalyst from the reaction media and its relatively poor thermal stability [16]. To develop a green processes, environment-friendly catalysts with low-cost and high-performance should be designed for easy removal from the reaction media and recycling [17–19]. In this context, the use of metal nanoparticles (NPs) in catalysis is crucial and thereby brings enhanced selectivity and efficiency [20].

Metal nanoparticles with small size and uniform distribution exhibit interesting chemical and physical properties due to their attractive properties and high surface area [21–24]. They have attracted enormous attentions among all nanostructured materials due to their fascinating properties and potential applications in daily lives [25]. The progress of nanoscience and nanotechnology has resulted in the development of various synthesis methods for the synthesis of metal nanoparticles with different morphologies and controllable sizes. Due to these unique properties of metal nanoparticles, they have been widely used as catalysts in the energy processing, fine chemical production and air pollution control [26–29]. Especially for Ru, Cu, Pd, and Pt, they have deeply attracted researchers and industry owing to their capability of using fewer catalysts to achieve higher catalytic activity. For example, Pd nanoparticles have been utilized in the selective production of hydrogen from alcohols, Fischer–Tropsch synthesis, CO oxidation, and NOx reduction [30–32]. The utilized metal nanoparticles are usually dispersed finely on metal oxide support to prevent particle growth and aggregation, where the metal oxide support can enhance the surface area, light absorption, and charge-carrier separation [24, 33, 34]. In the regard, the support for metal nanoparticles catalysts should have stable chemical, mechanical, and thermal properties [35]. On the other hand, the high surface area to volume ratio can lead to modifications in structure and properties. The uniform nanoparticle distributions will undoubtedly benefit the catalytic reaction [30]. This chapter is an up-to-date review of the literature available on the subject of hydrogenation of biomass-derived LA platform using metal nanoparticles synthesized by various green methods.

3.2 Typical and Green Methods for Synthesis of Metal Nanoparticles

Over the last decades, several routes have been used to synthesize supported metal catalysts including chemical co-precipitation, vapor deposition, incipient wetness impregnation-reduction, and others [24, 30, 36, 37]. One important aspect of the synthesis of supported catalysts is that many different sizes will exhibit slightly different properties. For example, in the catalysis of CO to CO_2, gold nanoparticles that were supported on a substrate must be within the size distribution of about 2–5 nm [38–40]. In the following sections are the discussions on the different approaches to synthesize nanoscale catalysts, followed by some modern approaches. It has become the goal of many researchers to obtain nanoparticles with predictable and uniform sizes through a green route. Despite the availability of all these synthetic methods, control of different morphologies, nanoparticle size, shape, and composition has been a major challenge in catalyst development [41].

3.2.1 Co-precipitation Method

Co-precipitation method is often based on the slow addition of a mixed solution containing the metal precursor into a reactor. A second solution (alkaline solution) was added in the reactor to maintain the pH at a selected value leading to the co-precipitation of the two metallic salts, which is followed by filtering, washing, and drying [42–45]. This yielded fairly substantial amounts of products within a reasonable period of time [2]. This method offers high degree of control for process parameters such as pH, temperature, aging time, mixing rate, ratio of metal precursor's concentration [46–48]. This method conventionally caters for synthesis of hydrotalcite-like compounds as our previous reports [18, 45, 49–51]. Depending on these precipitations conditions, it can generally obtain well crystallized hydrotalcite phases and also control the properties of hydrotalcite particles including crystallinity, size, size distribution, purity, and stability.

In the synthesis of metal nanoparticles, a suspension of substrates (e.g., TiO_2, SiO_2, Al_2O_3, etc.) is kept with continuous stirring [52, 53]. A soluble metal solution [such as $Pd(NO_3)_2$] was added and combined under vigorous stirring at a tuned pH value, which caused the dissolved metal to begin to be reduced. After the metal particles were formed and deposited on the substrate, the resulting solution was dried or centrifuged to obtain the final metal nanoparticles [54, 55]. Co-precipitation method is very powerful for the synthesis of high percent loading. Besides, the particles are directly deposited on the surface of the substrate, which greatly shorten the preparation time [56]. However, the disadvantage of this method is that the deposited metal nanoparticles are easy to aggregate and difficult to control the shapes [57].

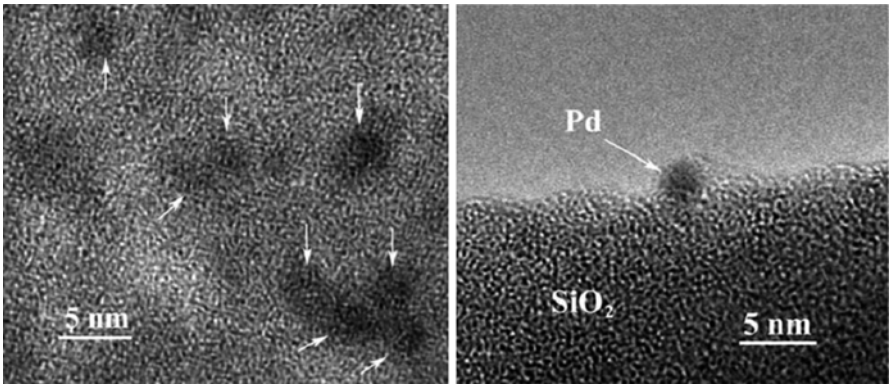

Fig. 3.2 High-resolution transmission electron microscopy (HR-TEM) images of Pd nanoparticles on the silica support (*right*) and on the edges of the silica support (*left*). Reprinted from ref. [34] with permission by American Chemical Society

Benito et al. [58] studied the preparation procedure and the La_2O_3/Pd weight ratio of a series of Pd/La_2O_3/SiO_2 catalysts (5 wt% Pd). If the precipitation procedure leaded to La_2O_3 deposition in the final step, the coverage of Pd particles by La_2O_3 patches would occurs which would negatively affect the activity. Co-precipitation of La and Pd at fixed pH was found to result in an optimized interaction of Pd with La_2O_3 and thus to an optimized use of expensive Pd. Recently, we have also employed the co-precipitation method to initially produce Cu-hydrotalcite and then obtain Cu-catalysts by reduction, the resulting metal catalysts display high selectivity and high efficiency for the hydrogenation of biomass-derived LA [22, 23, 59]. Barau et al. [34] recently prepared supported Pd metal nanoparticles on mesoporous silica and the typical HR-TEM images are show in Fig. 3.2. Such metallic Pd nanoparticles, with particle sizes around 4–5 nm, were found to be relatively well dispersed on the surface of silica. They also show a tendency to aggregate on the surface of the mesoporous silica at higher loadings and the nanoparticles were less homogeneously dispersed.

3.2.2 Incipient Wetness Impregnation-Reduction

In incipient wetness impregnation process, the active metal precursor was initially dissolved in an aqueous or organic solution with a suspended support (having a known porous volume) under stirring condition. The solution of the dissolved metal was usually made with a volume equal to the pore size of the support [60, 61]. Through the slow capillary action, the solubilized metal was adsorbed into the pores of the used support. The solution was then dried either through evaporation at room temperature or calcined to drive off the volatile components within the solution, leaving the metal precursor suspended on the surface or confined inside the porous structure. The maximum loading was limited by the solubility of the precursor in the solution.

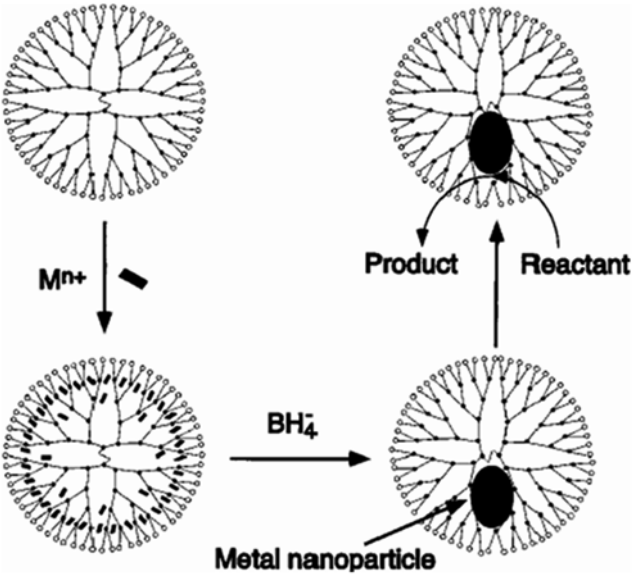

Fig. 3.3 Synthesis process of dendrimer-encapsulated metal (M) nanoparticles. Reprinted from ref. [66] with permission by American Chemical Society

The concentration profile of the impregnated compound depended on the mass transfer conditions within the pores during impregnation and drying [62–64].

In the followed reduction section, the remaining solids were dried or calcined in air at the specific temperature for some time, and subsequently reduced in flowing H_2 (mixed in N_2 or Ar) after which it was finally cooled to room temperature under a flow of pure Ar or N_2. Another reduction method is the chemical reduction using chemical agents such as formaldehyde, $NaBH_4$, and $LiAlH_4$. For example, $NaBH_4$ was the most often used as reducing agent to prepare Pt deposited surface [65]. One synthetic diagram of the dendrimer-encapsulated metal nanoparticles is shown in Fig. 3.3 [66].

Recently, we employed the palladium precursors (e.g., palladium nitrate, palladium (II) acetylacetonate) to fabricate Pd nanoparticles confined in the mesoporous supports or loaded on multi-walled carbon nanotubes using incipient wetness impregnation-reduction method [67, 68]. Through careful control, Pd nanoparticle can be highly dispersed on the surface of multi-walled carbon nanotubes (Fig. 3.4a, b) or confined inside the mesoporous channels of SiO_2 supports (Fig. 3.4c, d). Taking the synthesis of 3 wt% Pd supported on multi-walled carbon nanotubes (CNT) for example, the typical procedure was performed as following [68]: firstly, a definite amount of CNT support (~0.3 g), ethanol (5 mL) and the pre-calculated amount of $Pd(acac)_2$ was added into a 50 mL glass-bottle under argon environment. The mixture was impregnated under the stirring condition with a speed of 1,000 rpm for 12 h to ensure the high dispersion of the $Pd(acac)_2$ on the CNT support at room temperature. After this, 5 mL $NaBH_4$ (0.5 M) was added inside for the reduction of 1 h at 80 °C under argon environment. The obtained solution was centrifuged at a rate of

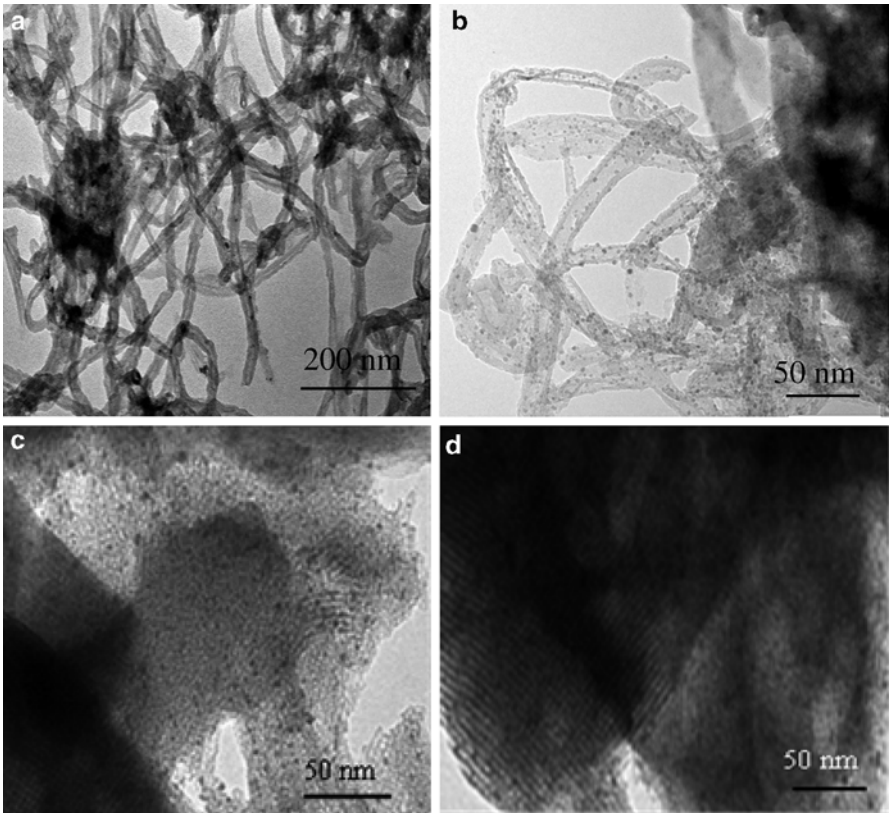

Fig. 3.4 TEM images of 3 wt% Pd/CNT images (**a** and **b**). Reprinted from ref. [68] with permission, Copyright 2013 Springer; 5 wt% Pd nanoparticles on MCM-41 (**c**) and TiMCM-41(**d**). Reprinted from ref. [67] with permission, Copyright 2014 Elsevier

3,500 rpm for 10 min and the obtained gel was dried at 90 °C for 6 h under argon environment. Table 3.1 summarizes some typical works of common metal nanoparticle synthesis by incipient wetness impregnation-reduction method.

Although this method is very useful for the synthesis of readily active catalysts, it also suffers from many of the same drawbacks. The resulting particles typically have a broad distribution in size. Besides, some organic materials or excess solvents may need to be driven away at high temperature, which causes an increase in the size of the particles [20].

3.2.3 Chemical Vapor Deposition

In a typical Chemical Vapor Deposition (CVD) process, the wafer (substrate) is exposed to one or more volatile precursors, which react and/or decompose on the substrate surface to produce the desired deposit. The process is often used in the

Table 3.1 Summary of common metal nanoparticle synthesis by the incipient wetness impregnation-reduction method

No.	Catalyst	Precursor	Particle size (nm)	References
1	5 wt% Ru/C	$RuCl_3$	6.0	[69]
2	5 wt% Ru/C	$RuCl_3$	1.7	[70]
3	2 wt% Ru/C	$RuCl_3$	3.3	[71]
4	1.5 wt% Ru/C	$Ru(NO)(NO_3)_3$	1.5–2.2	[72]
5	3 wt% Pd/CNT	$Pd(acac)_2$	2.8	[68]
6	3 wt% Pd/CNT	$Pd(acac)_2$	4.5	[68]
7	0.6 wt% Au–0.65 wt% Pd/SiO_2	$HAuCl_4$, $PdCl_2$	6.2	[73]
8	0.5 wt% Au–0.5 wt% Pd/C	$HAuCl_4$, $PdCl_2$	~6	[74]
9	5 wt% Ru/Al_2O_3	$RuCl_3$	15.2	[69]
10	5 wt% Ru/Al_2O_3	$Ru(NO)(NO_3)_3$	10.8	[75]
11	2.5 wt% Au–2.5 wt% Pd/C	$HAuCl_4$, $PdCl_2$	4.6	[76]
12	2.5 wt% Au–2.5 wt% Pd/Al_2O_3	$HAuCl_4$, $Pd(NO_3)_2$	2–10	[77]
13	5 wt % Pd/MCM-41	$Pd(NO_3)_2$	2–10	[67]
14	5 wt % Pd/TiMCM-41	$Pd(NO_3)_2$	2–10	[67]
15	2.5 wt% Au–2.5 wt% Pd/Al_2O_3	$HAuCl_4$, $Pd(NO_3)_2$	1–8	[78]

semiconductor industry to produce thin films. In a chemical vapor deposition method to fabricate metal nanoparticles, particle formation often occurs in a gas phase flow that is usually heated to induce decomposition of one or more precursor compounds, generating vapor-phase atoms or reactive molecules [79]. Evaporation of solvent, evaporation or sublimation of precursor compounds, precursor decomposition, particle nucleation, growth, and aggregation may all be involved in the synthesis process [80]. Haruta et al. studied different methods for the preparation of gold catalysts on various oxide supports (e.g., TiO_2, Al_2O_3, SiO_2, MgO, ZnO, or Fe_2O_3): liquid-phase methods using $HAuCl_4$ precursor and $[Au(CH_3)_2(acac)]$ as volatile precursor for chemical vapor deposition [81–83]. They reported the deposition of active gold nanoparticles with relatively high dispersion of 2–6 nm gold nanoparticles. Synthesis of nanoparticles in the vapor phase is usually a continuous method that can provide better controllability and reproducibility compared to batch methods. In such pure vapor-phase methods, solid nanoparticles nucleate directly from the vapor phase. For this to occur, the vapor phase mixture must be thermodynamically unstable relative to formation of solid particles. The product nanoparticles nucleate from a supersaturated vapor of atoms or reactive molecular fragments [84]. High temperature is usually applied to drive precursor decomposition. For this method, a nebulizer is required to generate small enough droplets (nano/micro-sized), which are then carried by gas flow and experience solvent evaporation and solute precipitation. Therefore, the size of produced particles with this mechanism depends mainly on the size of original droplets. Vapor phase methods have been applied to produce a variety of metal particles (e.g., Pt, Pd, Cu, Ru) [85–89].

Liang et al. [90] reported Pd nanoparticle/functionalized carbon anno fiber (CNF) composites were synthesized by a two-step chemical vapor deposition using

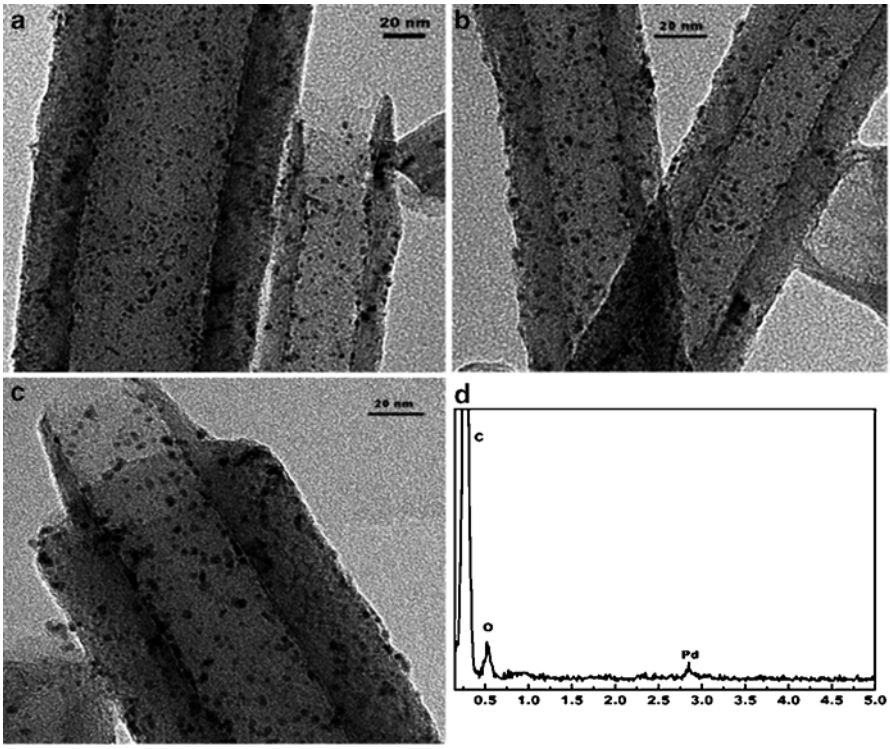

Fig. 3.5 TEM images and EDX analysis of Pd particles supported on the functionalized CNF composites. 2.04 % Pd/CNFs (**a**); 3.22 % Pd/CNFs (**b**); 4.30 % Pd/CNFs (**c**); EDX analysis of 2.04 % Pd/CNFs (**d**). Reprinted from ref. [90] with permission by American Chemical Society

cyclopentadienyl allyl palladium [Pd(allyl)(Cp)] as precursor at atmospheric pressure. They found that the Pd(allyl)(Cp) precursor could be dissociatively adsorbed on the surface of the CNF by the reaction between the ligands and the surface oxygen groups. Further reduction in H_2 would produce the Pd/CNF nanocomposites. TEM results (Fig. 3.5) show that highly dispersed and evenly distributed Pd particles with diameters of 2–4 nm could be prepared by this two-step CVD method.

3.2.4 Chemical Fluid Deposition

Chemical Fluid Deposition (CFD) involves the chemical reduction of organometallic compounds in supercritical fluid (e.g., CO_2) to yield high purity metal deposits [91]. Typically, the reaction was initiated upon the addition of H_2 or other reducing agent. The advantages of chemical fluid deposition over most conventional deposition techniques were due to the unique properties of the supercritical fluids, where it involved the chemical reduction of organometallic compounds inside to yield high

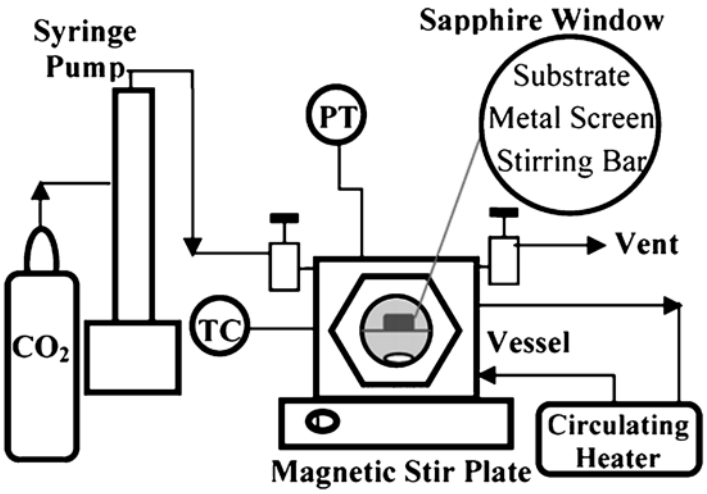

Fig. 3.6 Schematic diagram for supercritical impregnation. Reprinted from ref. [96] with permission by American Chemical Society

purity deposits [92]. The environmentally benign CO_2 in its liquid or supercritical state ($scCO_2$) has a tremendous potential as a green reaction medium for the sustainable preparation of nanoparticles because it is nonflammable, nontoxic and it has convenient critical parameters (Tc = 31 °C, Pc = 73.8 bar) [32, 93]. The low surface tension of liquid CO_2 (from 4.5 dyn/cm at 0 °C to zero at the critical point of 7.38 MPa at 31.1 °C) makes it as an excellent wetting agent [94, 95].

The pioneering CFD-studies by *Watkins* were dedicated towards the formation of metallic films on supports [97, 98]. The process involves the dissolution of a metallic precursor in a supercritical fluid, its sorption onto a support and the conversion to metal ensembles by reduction in H_2 or other reducing agent. The typical setup is shown in Fig. 3.6 [96], a certain amount of organometallic precursor platinum dimethyl (cyclooctadiene) [$PtMe_2COD$], a stirring bar, and a certain amount of support were placed into the high-pressure vessel. The vessel was sealed and heated to the desired temperature (often over 60 °C), then CO_2 was slowly purged inside and impregnated for several hours. After this, hydrogen was often input for chemical reduction of Pt precursor into Pt(0). In the final step, the Pt(0) supported on the substrate can be achieved after the release of gas. HR-TEM was used to study the textural structure of the resulting nanoparticles as shown in Fig. 3.7. In each case, these micrographs reveal uniformly dispersed metal nanoparticles with a mean particle size of 1.2–6.4 nm and a narrow particle size distribution. Comparison of the micrographs obtained from sample E and sample F, as well as those from samples G and H, show that higher metal contents result in larger particle sizes and broader distributions.

The approach has been used to prepare a wide variety of metallic films including Pt, Pd, Ru and Rh on various types of supports [24, 99–101]. Although the $scCO_2$

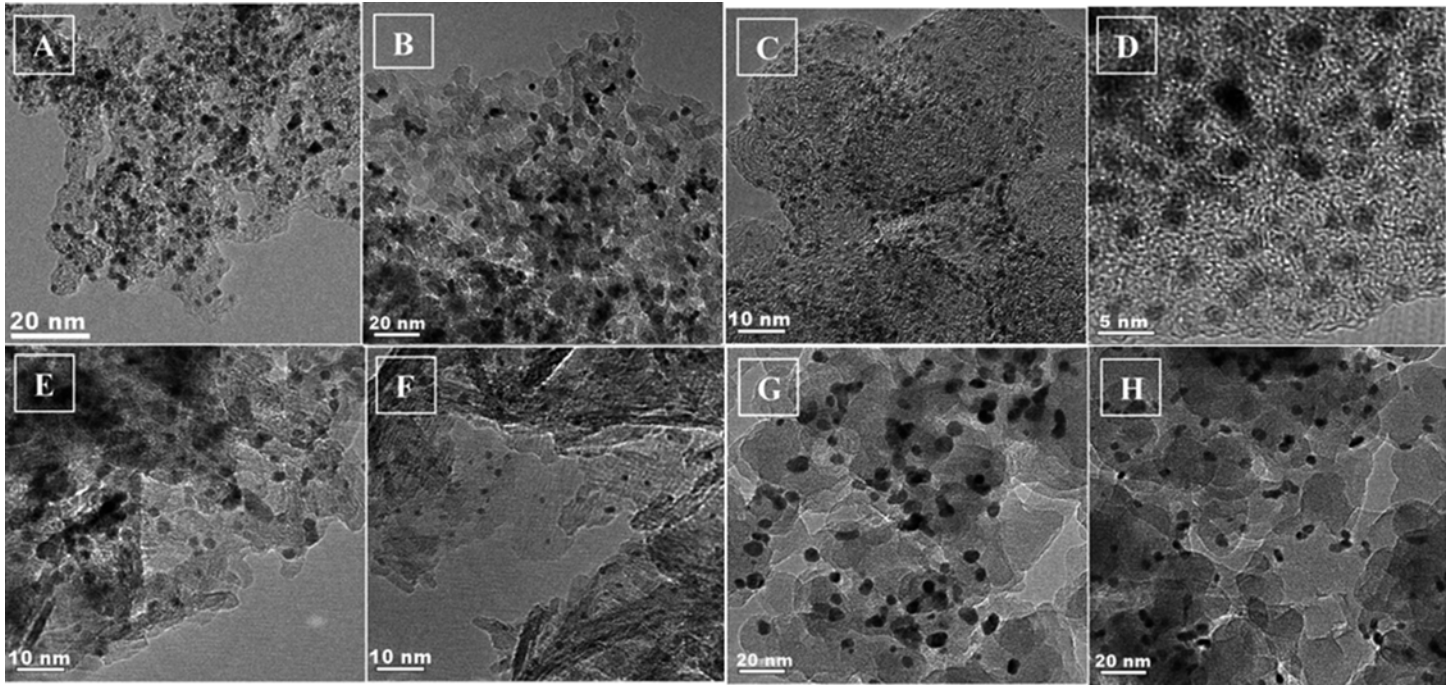

Fig. 3.7 HR-TEM micrographs of supported Ru and Pt nanoparticles on different substrates obtained from samples: (**a**) 40 wt% Pt on carbon aerogel, (**b**) 12 wt% Pt on silica aerogel, (**c**) 16.2 wt% Pt on carbon black, (**d**) 8.8 wt% Pt on Nafion (**e**) 11.6 wt% Pt on Al_2O_3, (**f**) 3.0 wt% Pt on Al_2O_3, (**g**) 9.5 wt% Pt on SiO_2, (**h**) 5.1 wt% Pt on SiO_2. Reprinted from ref. [96] with permission by American Chemical Society

Table 3.2 Summary of representative studies from literatures for the preparation of metal nanoparticles using chemical fluid deposition method

No.	Catalysts	Precursor	Reaction conditions	References
1	Pd/Al_2O_3	$Pd(hfac)_2$	H_2, CO_2, 75 °C (impregnation), 250 °C (reduction)	[104]
2	Pd/Al_2O_3	$Pd(hfac)_2$	H_2, CO_2, 28.5 °C (impregnation), 75 °C (reduction)	[95]
3	Pd/SiO*x*	$Pd(hfac)_2$	H_2, CO_2, 40–150 °C	[94]
4	Pd/SBA-15	$Pd(hfac)_2$	H_2, CO_2, 40 °C	[105]
5	Pd/CNT	$Pd(hfac)_2$	H_2, CO_2	[103]
6	Pd/MCM-41	$Pd(acac)_2$	H_2, CO_2, 200 °C	[106]
7	Pt-Cu/CNT	$Pt(acac)_2$, $Cu(hfac)_2$	H_2, CO_2, 200 °C	[103]
8	Pt/CNT	$Pt(acac)_2$	H_2, CO_2, 200 °C	[103]
9	Pt/MCM-41	$Pd(hfac)_2$	H_2, CO_2, 60 °C	[107]
10	Pt/C	(cod) $Pt(Me)_2$	H_2, CO_2, 80 °C (impregnation), 200 °C (reduction)	[96]
11	Ru/C	$Ru(acac)_3$	H_2, CO_2, 80–200 °C	[101]
12	Ru/MCM-41	$Ru(acac)_3$	H_2, CO_2, 200 °C	[106]

Note: CNT: carbon nanotubes

derived CFD method was advanced, the employed supercritical fluid often associated with high temperature and high pressure, which often presented high requirement toward the reaction fixture and increasing the corresponding cost. Thus, the CFD method based on liquid carbon dioxide was also developed. Kim et al. [94, 95] reported the first use of liquid carbon dioxide (L-CO_2) in the preparation of supported metal catalysts. The low surface tension of liquid CO_2 may help increase the dispersion of metal precursors. However, a liquid CO_2-derived method often limited to the metal precursor is sufficiently soluble in this medium. Table 3.2 presents the typical works of metal nanoparticles synthesis using chemical fluid deposition methods. In general, the chemical fluid method are very attractive since it offered many advantages rather than the traditional impregnation method, including the minimization of liquid waste generation, avoiding the use of aqueous means, enhancing the environmental benignity, and rapid separation of final nanoparticles [28, 102, 103].

The understanding of the catalytic activities and other technological applications of nanoparticles and catalysts requires a combination analysis of the particle size, shape, morphology, and surface properties. Various spectroscopic, microscopic, crystallographic and other physical techniques have been utilized for the characterization of nanostructured materials and their reactivity. Examples of these techniques include Fourier transform infrared spectroscopy, ultraviolet-visible spectroscopy, fluorescence spectroscopy, Raman spectroscopy, X-ray photoelectron spectroscopy, transmission electron microscopy, scanning electron microscopy, powder X-ray diffraction, as well as many other methods [20, 35].

3.3 Hydrogenation of Levulinic Acid on Metal Nanoparticles

Catalytic hydrogenation using hydrogen gas and metal nanoparticles catalysts can be considered as the most important catalytic method in the synthesis of fine chemicals on both laboratory and production scales. The classical hydrogenation catalysts (e.g., Noble metals, Raney nickel, and supported Ni and Cu) have been often utilized [41, 66, 108]. The design of new eco-friendly catalysts with low cost for efficient transformation of natural or biomass-derived platform chemicals is one of the promising approaches for the sustainable development [109, 110]. For most of the approaches being investigated, platform intermediate levulinic acid (LA), which are traditionally produced from renewable lignocellulosic biomass [111–113], are often employed as feedstock for the production of value-added chemicals and biofuels [28, 59, 114, 115].

Biofuel γ-valerolactone (GVL) and 2-methyltetrahydrofuran (MTHF) coupled with value-added pentanoic acid (PA) can be produced through the hydrogenation of LA on metal nanoparticles (Nps) catalysts as shown in Fig. 3.8. It has recently been demonstrated that GVL, a frequently used food additive, exhibits the most important characteristics of an ideal sustainable liquid, including the possibility to utilize it for the production of either energy or carbon-based consumer products [116]. In addition, GVL does not hydrolyze under neutral conditions and no measurable amount of peroxides was formed in a glass flask under air in weeks, making it a safe material for large scale use [116, 117]. A comparative evaluation of GVL and ethanol as fuel additives [116], with a mixture of 10 v/v% GVL or EtOH and 90 v/v% 95-octane gasoline, exhibited very similar fuel properties. Since GVL did not form an azeotrope with water, resulting in a less energy demanding process for the production of GVL than that of absolute ethanol [117, 118], which has attractive applications as a liquid fuel.

However, it was reported that GVL has the problem in blending limits for use in conventional combustion engines, thus it may be more attractive to convert GVL

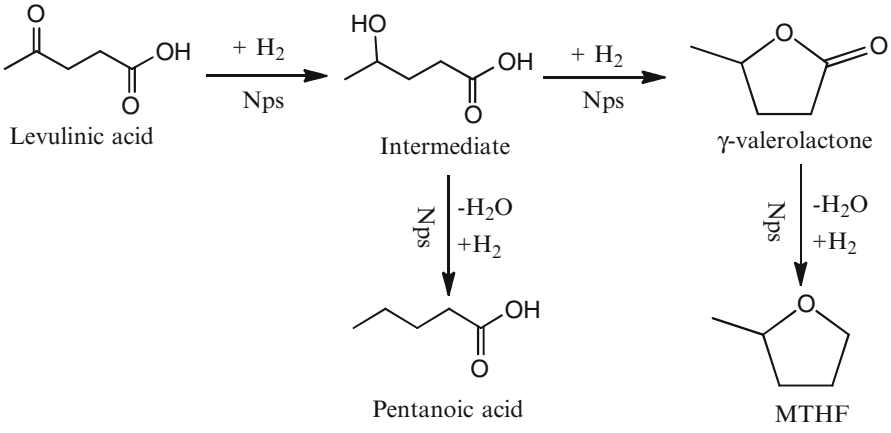

Fig. 3.8 Various fuels and chemicals derived from the hydrogenation of levulinic acid [116]

into liquid alkenes (or alkanes) [109]. GVL went through the ring-opening and further got decarboxylated to produce butane, which can be oligomerized at elevated pressures. One of benefit allowing GVL to be a practical biofuel is that it is relatively inexpensive to produce. Using a cheap feedstock (e.g., glucose), this biofuel can be produced at prices between 2 and 3 US$/gallon [116]. A group of researchers at Shell Global Solutions have shown the conversion of glucose-derived GVL to the valeric biofuels, like alkyl valerate esters, where valeric fuels are produced in four steps [119, 120].

In general, GVL can be worked as solvent, fuels, fuel additives, or fuel precursors. How to efficiently produced GVL has becoming crucial. The hydrogenation of LA to GVL using the homogeneous Ru-complex derived catalysts, appeared attractive, high conversion as well as good selectivity were often obtained [6, 121, 122]. However, the recovery of expensive metal catalysts from reaction residues remains still a challenge. Due to its relatively easy recycle and separation, heterogeneous catalysts appeared more attractive and the supported transitional metal catalysts have been often employed, the typical hydrogenation of LA to GVL have been performed in solvent free [123, 124] or in organic solvents like dioxane, ethylether. Over 99 % yield of GVL was achieved on Ru/Al_2O_3 catalyst under the condition of 200 °C, 20 MPa molecular hydrogen and water coupled with supercritical CO_2 as the reaction medium [123]. Manzer reported that 97 % yield of GVL was obtained using Ru/C catalyst at 150 °C and 34.5 bar hydrogen in dioxane [124]. Recently, we have reported the synthesis of a series of Pd nanoparticles on SiO_2 using CO_2-assisted chemical fluid deposition method and the resulting Pd nanoparticles display highly efficient performance in the selective production of GVL [28, 102]. Carmen et al. report the synthesis of Ru nanoparticles on a DOWEX 50WX2-100 gel-type resin using the incipient wetness impregnation-reduction method and the resulting Ru nanoparticles (2.8 ± 0.8 nm) are highly efficient for the hydrogenation of LA [125].

Understanding the reaction mechanisms will certainly progress technological development of GVL application. At present, one of the biggest issues with the catalytic transformation of LA to GVL or other commodity chemicals is the high yield of coke produced during the process. Efficiently addressing the formation of intractable coke and efficient conversion of LA are attracting numerous attentions from researchers and industry. Jesse and coworkers [126] have studied the hydrogenation mechanism of LA to GVL using the Ru/C catalyst, they initially envisaged two different pathways for the transformation as shown in Fig. 3.9. Pathway 1 illustrated the sequence initiated by hydrogenation of the ketone group in LA to form 4-hydroxypentanoic acid (HPA), which would went through acid-catalyzed, intramolecular esterification to form the thermodynamically preferred lactone, GVL. Alternatively, angelicalactones (AL) can form via endothermic dehydration of LA, and they become increasingly prevalent in acidic media and at elevated temperatures (pathway 2). They thought angelicalactones are anticipated to rapidly hydrogenate, forming GVL in the presence of Ru/C and under H_2 atmospheres.

They further investigated the turnover frequencies of LA hydrogenation over Ru/C as a function of time on-stream at different reaction temperature as shown in Fig. 3.10 [126]. As shown in Fig. 3.10a, LA hydrogenation rates decreased rapidly

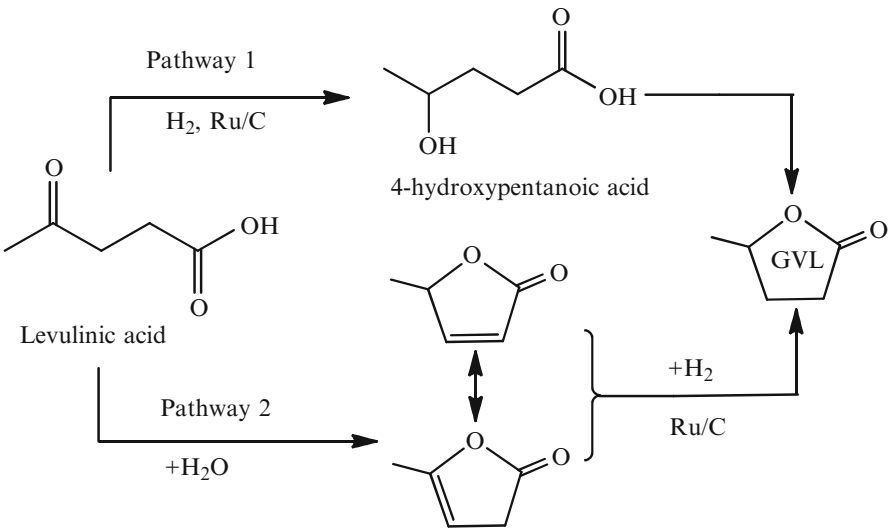

Fig. 3.9 Pathways for the hydrogenation of LA to GVL [126]

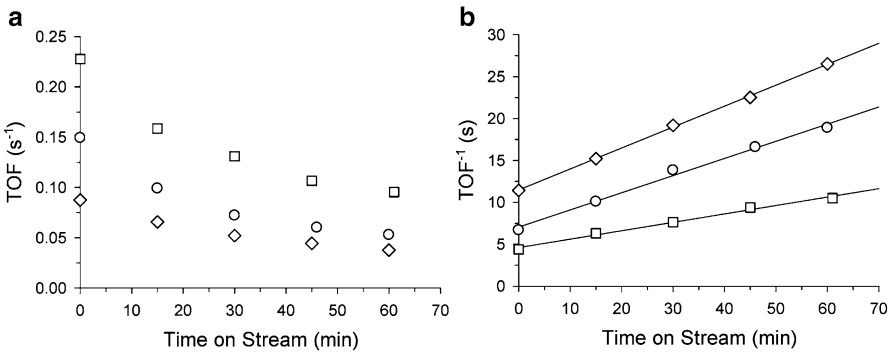

Fig. 3.10 (**a**) Rates of LA hydrogenation over Ru/C at 323 K (*open diamond*), 343 K (*open circle*), and 363 K (*open square*) as a function of time on-stream. (**b**) Linearized rate data illustrating second-order deactivation and method employed for estimation of rates at zero time on-stream. For all experiments summarized here, the aqueous phase concentrations of LA and H_2 were 0.50 and 0.016 M. Reprinted from ref. [126] with permission by American Chemical Society

in the aqueous-phase system, even at mild temperatures (323 K). At low temperatures, intramolecular esterification of HPA appeared to control the rate of GVL formation, whereas at high temperatures, mass transfer limited the rate of hydrogenation. They also reported the independent of the reaction conditions, the time decay of hydrogenation rates at short times on-stream (less than 8 h) by a second-order model (Fig. 3.10b). The pronounced deactivation of monometallic Ru/C even started under mild conditions. Through the further calculation of reaction kinetics and comparison between experimental and predicted models, they got the conclusion that LA can be hydrogenated at near ambient temperature, proceeding primarily through a HPA-

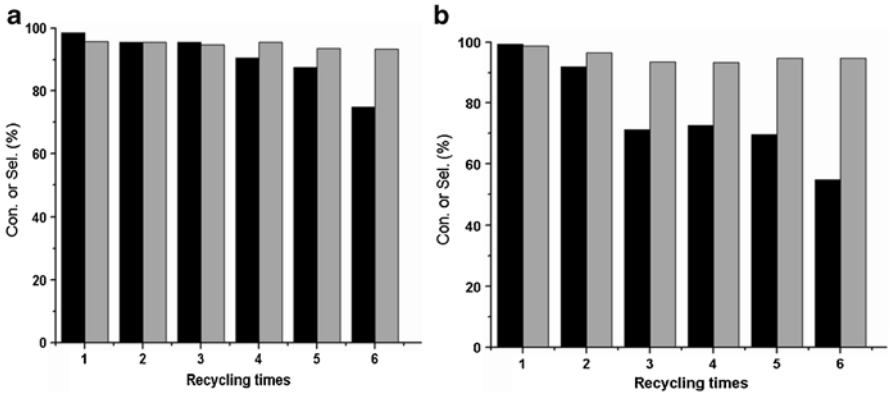

Fig. 3.11 The effect of recycling times on LA hydrogenation over RQ-Ni (**a**) and Raney Ni (**b**) (*black square* of LA conversion, *grey square* of the selectivity of GVL). Reaction conditions: Cat. 200 mg, LA 500 mg, isopropanol 20 ml, 373 K, 1.5 MPa, 4 h. Reproduced from ref. [127], Springer 2014

mediated pathway in which hydrogenation occurred first and was followed by acid-catalyzed dehydration. They also pointed out for the future metal nanoparticles design, where LA hydrogenation was best suited to bifunctional catalysts exhibiting hydrogenation functionality alongside acidity.

The employed Ru catalysts display good performance, but the high cost and relatively easy deactivation of Ru catalysts make them difficult to be utilized in practice. Developing an effective, stable, cheap, and eco-friendly catalyst with high efficiency spurges the exploration of more robust catalysts. Recently, Rong et al. [127] employed a series of Raney Ni, Raney Co, Raney Cu, and Raney Fe catalysts for the hydrogenation of LA, Raney Ni catalysts display the highest activity in terms of GVL yields (82 %). They fabricated RQ-Ni nanoparticle catalyst, and it presented ~94 % yield, which has a clear enhancement in comparison with the commercial Raney Ni catalysts. Subsequently, the authors performed the stability tests on the fabricated RQ-Ni and commercial Raney Ni catalysts over six runs (Fig. 3.11). It was evident that there are declines on LA conversion as well as GVL selectivity. However, RQ-Ni metal nanoparticles display much better stability than that of commercial Raney Ni catalysts.

Due to the tunable composition, size, and electronic properties linked to various applications including magnetism, electronics, photonics, and especially catalysis, bimetallic nanoparticles are of great importance [129]. Yang et al. [128] reported an elegant metal complex-involved multicomponent assembly route to highly efficient Ru-Ni bimetallic nanoparticles in ordered mesoporous carbons (OMC), which displayed high activity for the hydrogenation of LA as shown in Fig. 3.12. The fabrication of composition-tuned Ru-Ni bimetallics in OMC (Ru_xNi_{1-x}-OMC, $x = 0.5 - 0.9$) was facilely realized via in situ construction of CTAB-directed cubic Ia3d chitosan–ruthenium–nickel–silica mesophase before pyrolysis and silica removal (Fig. 3.13) (More representative studies for the hydrogenation of levulinic acid using metal nanoparticles have been summarized in Table 3.3).

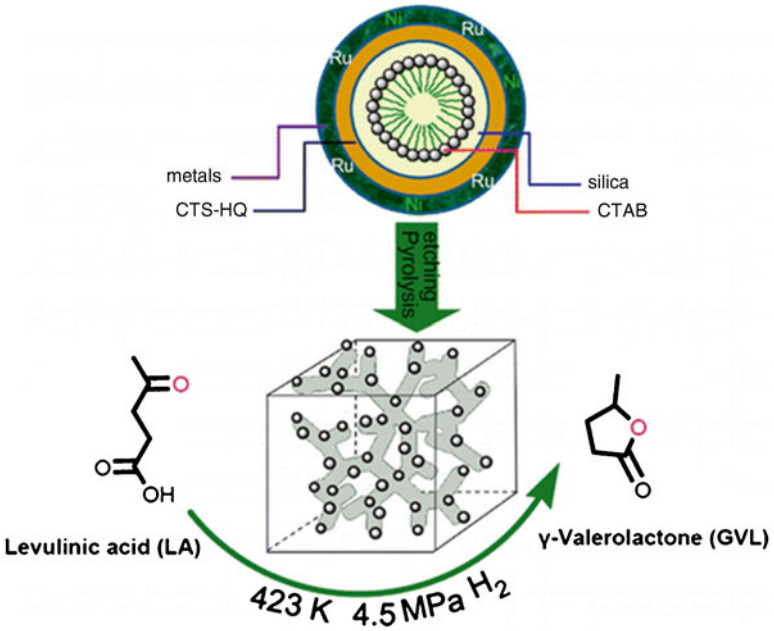

Fig. 3.12 Synthesis of Ru-Ni bimetallic nanoparticles in ordered mesoporous carbons for the hydrogenation of LA. Reproduced from ref. [128], American Chemistry Society

Table 3.3 Representative studies for hydrogenation of levulinic acid using metal nanoparticles

No.	Catalyst	Reaction conditions	Y (GVL)/%	References
1	5 % Ru/C	150 °C, 800 psi H_2, 2 h, 1,4-Dixoane	72	[124]
2	Raney Ni	~200 °C, 48.3 bar H_2	94	[123]
3	5 % Ru/C	130 °C, 1.2 Mpa H_2, 160 min, methanol solvent	91.3	[130]
4	5 %Ru/Al_2O_3	70 °C, 3.0 Mpa H_2, acid-assisted, H_2O solvent	56.2	[131]
5	5 % Ru/C	265 °C, 1–25 bar H_2, 50 h, 1,4-Dioxane	98.6	[132]
6	5 % Pd/C	265 °C, 1–25 bar H_2, 50 h, 1,4-Dioxane	90	[132]
7	5 % Pt/C	265 °C, 1–25 bar H_2, 50 h, 1,4-Dioxane	30	[132]
8	Raney Ni	220 °C, 48 bar H_2, 3 h	94	[133]
9	5 wt% Ru/C	180 °C, WHSV = 1.2, propyl guaiacol solvent, formic acid	93	[134]
10	5 wt% Ru/C	130 °C, 1.2 Mpa H_2, methanol solvent	91.1	[135]

(continued)

Table 3.3 (continued)

No.	Catalyst	Reaction conditions	Y (GVL)/%	References
11	5 % Pt/SiO_2	180 °C, 9 MPa, 6 h, water solvent	97.3	[102]
12	1 mol % Au/ZrO_2	150 °C, 6 h, equimolar amount of LA and formic acid	>99	[136]
13	3 wt% Pd/Al_2O_3	160 °C, 6 h, H_2O	46.3	[28]
14	Ru/C	150 °C, 6 h, 580 psi H_2, 1 h, formic acid	67	[137]
15	Ru/TiO_2	150 °C, 6 h, 580 psi H_2, 1 h, formic acid	63	[137]
16	5 wt% Ru/hydroxyapatite	70 °C, 5 bar H_2, 38 mL H_2O	99	[138]
17	5 wt% Pd/hydroxyapatite	70 °C, 5 bar H_2, 38 mL H_2O	23.4	[138]
18	5 wt% Pt/hydroxyapatite	70 °C, 5 bar H_2, 38 mL H_2O	37.0	[138]

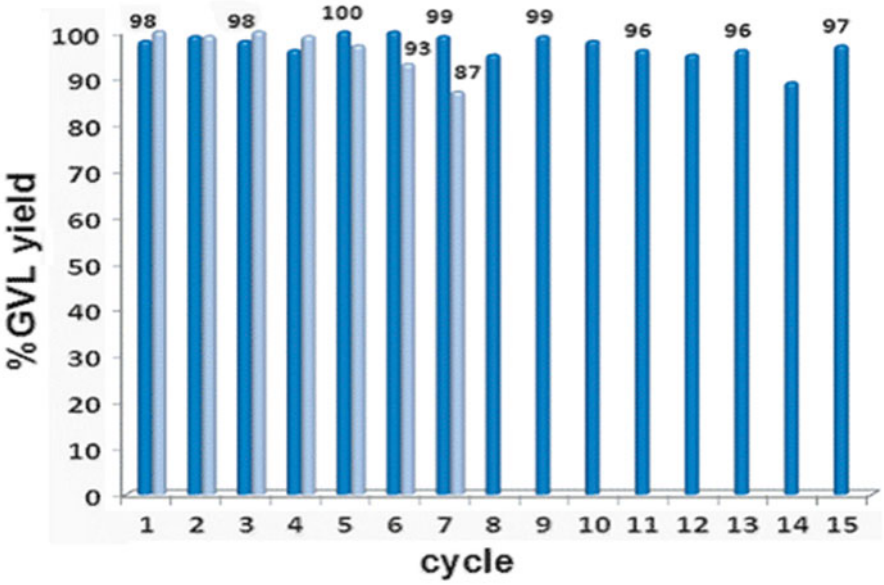

Fig. 3.13 Recyclability test for $Ru_{0.9}Ni_{0.1}$-OMC (*blue*) and $Ru_{0.7}Ni_{0.3}$-OMC (*gray*). Reaction conditions: LA (5.0 g), catalyst (15 mg), H_2 (4.5 MPa), 423 K, and 2 h [128]. Reproduced from ref. [128] with permission of American Chemistry Society

Overall, the confinement of metal nanoparticles in the mesoporous channel could prevent the potential metal leach or aggregation, which could enhance the stability of metal nanoparticles in the processes. Many of these processes for the highly selective hydrogenation of LA are still early in their development, and would benefit greatly from additional research.

3.4 Conclusion and Outlook

Recent progress in the design and preparation of supported metal nanoparticles suggested that a numerous variety of metal nanoparticles can nowadays be synthesized through different preparation routes. However, the preparation of supported metal nanoparticles should be performed in a more sustainable way, with less waste generation, avoiding the toxic compounds and decreasing the production costs. The direct supercritical fluid (e.g., CO_2) deposition method of making bimetallic nanoparticles appears to provide a simple way of preparing and studying catalytic properties of various bimetallic nanocatalysts. The technology itself represents a green chemistry approach for nanomaterials synthesis. Monodisperse metal NPs (1–10 nm) including bimetallic and trimetallic NP catalysts, most often more efficient than those containing only one type of metal, are attracting for many current reactions with great catalytic efficiency.

The selective conversion of lignocellulosic biomass provides a possible approach to the sustainable production of fuels and chemical products. The catalysts developed should fully use a variety of catalytic functions, including acid sites, basic sites, and metal hydrogenation sites, to accomplish the common goal of selectively removing oxygen functional groups. By identifying and tuning important catalyst parameters, more effective catalytic materials are designed with improved selectivity to desirable products and increased rate of reaction. Future attention may also focus more on the metal nanoparticles catalysts deactivation and regeneration; mechanical stability; and economic viability.

References

1. Cao Z, Jiang H, Luo H, Baumann S, Meulenberg WA, Assmann J, Mleczko L, Liu Y, Caro J (2013) Natural gas to fuels and chemicals: improved methane aromatization in an oxygen-permeable membrane reactor. Angew Chem Int Ed 52:13794–13797
2. Luo H, Efimov K, Jiang H, Feldhoff A, Wang H, Caro J (2011) CO_2-stable and cobalt-free dual-phase membrane for oxygen separation. Angew Chem Int Ed 50:759–763
3. Climent MJ, Corma A, Iborra S (2014) Conversion of biomass platform molecules into fuel additives and liquid hydrocarbon fuels. Green Chem 16:516–547
4. Corma A, de la Torre O, Renz M, Villandier N (2011) Production of high-quality diesel from biomass waste products. Angew Chem Int Ed 50:2375–2378
5. Cao Z, Jiang H, Luo H, Baumann S, Meulenberg WA, Voss H, Caro J (2012) Simultaneous overcome of the equilibrium limitations in BSCF oxygen-permeable membrane reactors: water splitting and methane coupling. Catal Today 193:2–7
6. Geilen F, Engendahl B, Harwardt A, Marquardt W, Klankermayer J, Leitner W (2010) Selective and flexible transformation of biomass-derived platform chemicals by a multifunctional catalytic system. Angew Chem Int Ed 49:5510–5514
7. Geilen FMA, vom Stein T, Engendahl B, Winterle S, Liauw MA, Klankermayer J, Leitner W (2011) Highly selective decarbonylation of 5-(hydroxymethyl)furfural in the presence of compressed carbon dioxide. Angew Chem Int Ed 50:6831–6834
8. vom Stein T, Grande P, Sibilla F, Commandeur U, Fischer R, Leitner W, Domínguez de Maria P (2010) Salt-assisted organic-acid-catalyzed depolymerization of cellulose. Green Chem 12: 1844–1849

9. Yan K, Wu G, Lafleur T, Jarvis C (2014) Production, properties and catalytic hydrogenation of furfural to fuel additives and value-added chemicals. Renew Sustain Energy Rev 38:663–676
10. Huber GW, Dumesic JA (2006) An overview of aqueous-phase catalytic processes for production of hydrogen and alkanes in a biorefinery. Catal Today 111:119–132
11. Huber GW, Iborra S, Corma A (2006) Synthesis of transportation fuels from biomass: chemistry, catalysts, and engineering. Chem Rev 106:4044–4098
12. Yan K, Wu X, An X, Xie X (2013) Facile synthesis of reusable CoAlhydrotalcite catalyst for dehydration of biomass-derived fructose into platform chemical 5-hydroxymethylfurfural. Chem Eng Commun 201:456–465
13. Werpy T, Petersen G, Aden A, Bozell J, Holladay J, White J, Manheim A, Eliot D, Lasure L, Jones S (2004) Top value added chemicals from biomass volume I—results of screening for potential candidates from sugars and synthesis Gas. No. DOE/GO-102004-1992. Department of Energy Washington DC
14. Tong X, Ma Y, Li Y (2010) Biomass into chemicals: conversion of sugars to furan derivatives by catalytic processes. Appl Catal Gen 385:1–13
15. Qiao Y, Li H, Hua L, Orzechowski L, Yan K, Feng B, Pan Z, Theyssen N, Leitner W, Hou Z (2012) Peroxometalates immobilized on magnetically recoverable catalysts for epoxidation. ChemPlusChem 77:1128–1138
16. Widegren JA, Finke RG (2003) A review of the problem of distinguishing true homogeneous catalysis from soluble or other metal-particle heterogeneous catalysis under reducing conditions. Journal of Molecular Catalysis A: J Mol Catal A Chem 198:317–341
17. Yan K, Chen A (2013) Environmentally benign NiAlCe-hydrotalcite for efficient synthesis of benzoin ethyl ether. Environ Chem Lett 11:171–175
18. Yan K, Liao J, Wu X, Xie X (2013) Facile synthesis of eco-friendly Cu-hydrotalcite catalysts for highly selective synthesis of furfural diethyl acetal and benzoin ethyl ether. Adv Mater Lett 4:702
19. Yan K, Wu G, Jarvis C, Wen J, Chen A (2014) Facile synthesis of porous microspheres composed of TiO_2 nanorods with high photocatalytic activity for hydrogen production. Appl Catal Environ 148–149:281–287
20. Campelo JM, Luna D, Luque R, Marinas JM, Romero AA (2009) Sustainable preparation of supported metal nanoparticles and their applications in catalysis. ChemSusChem 2:18–45
21. Sankar M, Dimitratos N, Miedziak PJ, Wells PP, Kiely CJ, Hutchings GJ (2012) Designing bimetallic catalysts for a green and sustainable future. Chem Soc Rev 41:8099–8139
22. Yan K, Chen A (2013) Efficient hydrogenation of biomass-derived furfural and levulinic acid on the facilely synthesized noble-metal-free Cu-Cr catalyst. Energy 58:357–363
23. Yan K, Chen A (2014) Selective hydrogenation of furfural and levulinic acid to biofuels on the ecofriendly Cu–Fe catalyst. Fuel 115:101–108
24. Cangül B, Zhang LC, Aindow M, Erkey C (2009) Preparation of carbon black supported Pd, Pt and Pd-Pt nanoparticles using supercritical CO_2 deposition. J Supercrit Fluid 50:82–90
25. Campbell CT, Parker SC, Starr DE (2002) The effect of size-dependent nanoparticle energetics on catalyst sintering. Science 298:811–814
26. Hu L, Zhao G, Hao W, Tang X, Sun Y, Lin L, Liu S (2012) Catalytic conversion of biomass-derived carbohydrates into fuels and chemicals via furanic aldehydes. RSC Adv 2:11184–11206
27. West RM, Kunkes EL, Simonetti DA, Dumesic JA (2009) Catalytic conversion of biomass-derived carbohydrates to fuels and chemicals by formation and upgrading of mono-functional hydrocarbon intermediates. Catal Today 147:115–125
28. Yan K, Jarvis C, Lafleur T, Qiao Y, Xie X (2013) Novel synthesis of Pd nanoparticles for hydrogenation of biomass-derived platform chemicals showing enhanced catalytic performance. RSC Adv 3:25865–25871
29. Jin T, Guo S, Zuo J-l, Sun S (2013) Synthesis and assembly of Pd nanoparticles on graphene for enhanced electrooxidation of formic acid. Nanoscale 5:160–163
30. Herves P, Perez-Lorenzo M, Liz-Marzan LM, Dzubiella J, Lu Y, Ballauff M (2012) Catalysis by metallic nanoparticles in aqueous solution: model reactions. Chem Soc Rev 41:5577–5587

31. Hou Z, Theyssen N, Brinkmann A, Leitner W (2005) Biphasic aerobic oxidation of alcohols catalyzed by poly(ethylene glycol)-stabilized palladium nanoparticles in supercritical carbon dioxide. Angew Chem Int Ed 117:1370–1373
32. Hou Z, Theyssen N, Leitner W (2007) Palladium nanoparticles stabilised on PEG-modified silica as catalysts for the aerobic alcohol oxidation in supercritical carbon dioxide. Green Chem 9:127–132
33. Astruc EBD (ed) (2008) Nanoparticles and catalysis. Wiley-VCH Verlag GmbH & Co. KGaA, Weinheim
34. Barau A, Budarin V, Caragheorgheopol A, Luque R, Macquarrie D, Prelle A, Teodorescu V, Zaharescu M (2008) A simple and efficient route to active and dispersed silica supported palladium nanoparticles. Catal Lett 124:204–214
35. Campbell CT (2013) The energetics of supported metal nanoparticles: relationships to sintering rates and catalytic activity. Acc Chem Res 46:1712–1719
36. Chen A, Holt-Hindle P (2010) Platinum-based nanostructured materials: synthesis, properties, and applications. Chem Rev 110:3767–3804
37. Bavykin D, Lapkin A, Plucinski P, Torrente-Murciano L, Friedrich J, Walsh F (2006) Deposition of Pt, Pd, Ru and Au on the surfaces of titanate nanotubes. Top Catal 39:151–160
38. Chen M, Goodman DW (2006) Catalytically active gold: from nanoparticles to ultrathin films. Acc Chem Res 39:739–746
39. Diao P, Guo M, Zhang Q (2008) How does the particle density affect the electrochemical behavior of gold nanoparticle assembly? J Phys Chem C 112:7036–7046
40. Liu Y, Jia C-J, Yamasaki J, Terasaki O, Schüth F (2010) Highly active iron oxide supported gold catalysts for CO oxidation: how small must the gold nanoparticles be? Angew Chem Int Ed 49:5771–5775
41. Shiju NR, Guliants VV (2009) Recent developments in catalysis using nanostructured materials. Appl Catal Gen 356:1–17
42. Cavani F, Trifirò F, Vaccari A (1991) Hydrotalcite-type anionic clays: preparation, properties and applications. Catal Today 11:173–301
43. Clause O, Rebours B, Merlen E, Trifiró F, Vaccari A (1992) Preparation and characterization of nickel-aluminum mixed oxides obtained by thermal decomposition of hydrotalcite-type precursors. J Catal 133:231–246
44. Xie X, Yan K, Li J, Wang Z (2008) Efficient synthesis of benzoin methyl ether catalyzed by hydrotalcite containing cobalt. Catal Commun 9:1128–1131
45. Yan K, Xie X, Li J, Wang X, Wang Z (2007) Preparation, characterization, and catalytical application of MgCoAl-hydrotalcite-like compounds. J Nat Gas Chem 16:371–376
46. Yan K, Lafleur T, Liao J, Xie X (2014) Highly selective one-pot synthesis of benzoin ether compounds on Ni- AlCe-hydrotalcite catalysts. Curr Catal 3:73–81
47. Yan K, Wu X, An X, Xie X (2013) Novel preparation of nano-composite CuO-Cr_2O_3 using Ctab-template method and efficient for hydrogenation of biomass-derived furfural. Funct Mater Lett 06, 1350007
48. Luo H, Jiang H, Klande T, Cao Z, Liang F, Wang H, Caro J (2012) Novel cobalt-free, noble metal-free oxygen-permeable 40Pr0.6Sr0.4FeO3-δ-60Ce0.9Pr0.1O2-δ dual-phase membrane. Chem Mater 24:2148–2154
49. Yan K, Wu X, An X, Xie X (2013) Facile synthesis and catalytic property of spinel ferrites by a template method. J Alloy Comp 552:405–408
50. Xie X, An X, Yan K, Wu X, Song J, Wang Z (2010) A new way to synthesize benzoin isopropyl ether on Cu-Fe-hydrotalcite. J Nat Gas Chem 19:77–80
51. Xie X, Yan K, Hu QX, Song JL,Wang Z (2008) Preparation and catalytic application of copper-containing hydrotalcite-like compounds. Chin J Inorg Chem 24:32–36
52. Neri G, Rizzo G, De Luca L, Donato A, Musolino MG, Pietropaolo R (2009) Supported Pd catalysts for the hydrogenation of campholenic aldehyde: influence of support and preparation method. Appl Catal Gen 356:113–120

53. Cukic T, Kraehnert R, Holena M, Herein D, Linke D, Dingerdissen U (2007) The influence of preparation variables on the performance of Pd/Al2O3 catalyst in the hydrogenation of 1,3-butadiene: building a basis for reproducible catalyst synthesis. Appl Catal Gen 323:25–37
54. Zhang H, Watanabe T, Okumura M, Haruta M, Toshima N (2012) Catalytically highly active top gold atom on palladium nanocluster. Nat Mater 11:49–52
55. Meier DC, Goodman DW (2004) The influence of metal cluster size on adsorption energies: CO adsorbed on Au clusters supported on TiO2. J Am Chem Soc 126:1892–1899
56. Chen M, Kumar D, Yi C-W, Goodman DW (2005) The promotional effect of gold in catalysis by palladium-gold. Science 310:291–293
57. Tao AR, Habas S, Yang P (2008) Shape control of colloidal metal nanocrystals. Small 4:310–325
58. Mul G, Hirschon AS (2001) Effect of preparation procedures on the activity of supported palladium/lanthanum methanol decomposition catalysts. Catal Today 65:69–75
59. Yan K, Liao J, Wu X, Xie X (2013) A noble-metal free Cu-catalyst derived from hydrotalcite for highly efficient hydrogenation of biomass-derived furfural and levulinic acid. RSC Adv 3:3853–3856
60. Chen L-F, Guo P-J, Zhu L-J, Qiao M-H, Shen W, Xu H-L, Fan K-N (2009) Preparation of Cu/SBA-15 catalysts by different methods for the hydrogenolysis of dimethyl maleate to 1,4-butanediol. Appl Catal Gen 356:129–136
61. Wang H, Zhao F, Fujita S-I, Arai M (2008) Hydrogenation of phenol in scCO2 over carbon nanofiber supported Rh catalyst. Catal Commun 9:362–368
62. Crooks RM, Zhao M (1999) Dendrimer-encapsulated Pt nanoparticles: synthesis, characterization, and applications to catalysis. Adv Mater 11:217–220
63. Niu Y, Crooks RM (2003) Dendrimer-encapsulated metal nanoparticles and their applications to catalysis. C R Chim 6:1049–1059
64. Yang C-M, Liu P-H, Ho Y-F, Chiu C-Y, Chao K-J (2002) Highly dispersed metal nanoparticles in functionalized SBA-15. Chem Mater 15:275–280
65. Nie L, Yu J, Li X, Cheng B, Liu G, Jaroniec M (2013) Enhanced performance of NaOH-modified Pt/TiO2 toward room temperature selective oxidation of formaldehyde. Environ Sci Technol 47:2777–2783
66. Crooks RM, Zhao M, Sun L, Chechik V, Yeung LK (2000) Dendrimer-encapsulated metal nanoparticles: synthesis, characterization, and applications to catalysis. Acc Chem Res 34:181–190
67. Yan K, Lafleur T, Jarvis C, Wu G (2014) Clean and selective production of γ-valerolactone from biomass-derived levulinic acid catalyzed by recyclable Pd nanoparticle catalyst. J Clean Prod 72:230–232
68. Yan K, Lafleur T, Liao J (2013) Facile synthesis of palladium nanoparticles supported on multi-walled carbon nanotube for efficient hydrogenation of biomass-derived levulinic acid. J Nanopart Res 15:1–7
69. Feng J, Fu H, Wang J, Li R, Chen H, Li X (2008) Hydrogenolysis of glycerol to glycols over ruthenium catalysts: effect of support and catalyst reduction temperature. Catal Commun 9:1458–1464
70. Lin B, Wei K, Ma X, Lin J, Ni J (2013) Study of potassium promoter effect for Ru/AC catalysts for ammonia synthesis. Catal Sci Technol 3:1367–1374
71. Viniegra M, Gomez R, Gonzalez RD (1988) The role of support in the catalytic hydrogenation of benzene over ruthenium catalysts. J Catal 111:429–432
72. Oliviero L, Barbier J, Duprez D, Guerrero-Ruiz A, Bachiller-Baeza B, Rodríguez-Ramos I (2000) Catalytic wet air oxidation of phenol and acrylic acid over Ru/C and Ru-CeO2/C catalysts. Appl Catal Environ 25:267–275
73. Venezia AM, Liotta LF, Pantaleo G, La Parola V, Deganello G, Beck A, Koppány Z, Frey K, Horváth D, Guczi L (2003) Activity of SiO2 supported gold-palladium catalysts in CO oxidation. Appl Catal Gen 251:359–368
74. Lopez-Sanchez JA, Dimitratos N, Miedziak P, Ntainjua E, Edwards JK, Morgan D, Carley AF, Tiruvalam R, Kiely CJ, Hutchings GJ (2008) Au-Pd supported nanocrystals prepared by

a sol immobilisation technique as catalysts for selective chemical synthesis. Phys Chem Chem Phys 10:1921–1930
75. Basagiannis AC, Verykios XE (2008) Influence of the carrier on steam reforming of acetic acid over Ru-based catalysts. Appl Catal Environ 82:77–88
76. Edwards JK, Solsona B, Landon P, Carley AF, Herzing A, Watanabe M, Kiely CJ, Hutchings GJ (2005) Direct synthesis of hydrogen peroxide from H2 and O2 using Au-Pd/Fe2O3 catalysts. J Mater Chem 15:4595–4600
77. Solsona BE, Edwards JK, Landon P, Carley AF, Herzing A, Kiely CJ, Hutchings GJ (2006) Direct synthesis of hydrogen peroxide from H_2 and O_2 using Al_2O_3 supported Au-Pd catalysts. Chem Mater 18:2689–2695
78. Kesavan L, Tiruvalam R, Rahim MHA, bin Saiman MI, Enache DI, Jenkins RL, Dimitratos N, Lopez-Sanchez JA, Taylor SH, Knight DW, Kiely CJ, Hutchings GJ (2011) Solvent-free oxidation of primary carbon-hydrogen bonds in toluene using Au-Pd alloy nanoparticles. Science 331:195–199
79. Feng M, Puddephatt RJ (2003) Chemical vapor deposition of macroporous platinum and palladium-platinum alloy films by using polystyrene spheres as templates. Chem Mater 15:2696–2698
80. Anjana Devi JG, Lakshmi R, Shivashankar SA (1998) A novel Cu(II) chemical vapor deposition precursor: synthesis, characterization, and chemical vapor deposition. J Mater Res 13:687–692
81. Haruta M (1997) Size- and support-dependency in the catalysis of gold. Catal Today 36:153–166
82. Okumura M, Tanaka K, Ueda A, Haruta M (1997) The reactivities of dimethylgold(III) β-diketone on the surface of TiO2: a novel preparation method for Au catalysts. Solid State Ion 95:143–149
83. Bond GC, Thompson DT (1999) Catalysis by gold. Catal Rev 41:319–388
84. Jeon NL, Lin W, Erhardt MK, Girolami GS, Nuzzo RG (1997) Selective chemical vapor deposition of platinum and palladium directed by monolayers patterned using microcontact printing. Langmuir 13:3833–3838
85. Becht M, Dahmen KH, Atamny F, Baiker A (1995) Surface morphology and electrical properties of copper thin films prepared by MOCVD. Fresenius J Anal Chem 353:718–722
86. Chen RS, Chen YS, Huang YS, Chen YL, Chi Y, Liu CS, Tiong KK, Carty AJ (2003) Growth of IrO2 films and nanorods by means of CVD: an example of compositional and morphological control of nanostructures. Chem Vap Deposition 9:301–305
87. Forde MM, Kesavan L, bin Saiman MI, He Q, Dimitratos N, Lopez-Sanchez JA, Jenkins RL, Taylor SH, Kiely CJ, Hutchings GJ (2013) High activity redox catalysts synthesized by chemical vapor impregnation. ACS Nano 8:957–969
88. Hierso JC, Serp P, Feurer R, Kalck P (1998) MOCVD of rhodium, palladium and platinum complexes on fluidized divided substrates: novel process for one-step preparation of noble-metal catalysts. Appl Organomet Chem 12:161–172
89. Vahlas C, Delmas M (2008) Platinum protective coatings processed by organometallic CVD. Chem Vap Deposition 14:103–106
90. Liang C, Xia W, van den Berg M, Wang Y, Soltani-Ahmadi H, Schlüter O, Fischer RA, Muhler M (2009) Synthesis and catalytic performance of Pd nanoparticle/functionalized CNF composites by a two-step chemical vapor deposition of Pd(allyl)(Cp) precursor. Chem Mater 21:2360–2366
91. Watkins JJ, Blackburn JM, McCarthy TJ (1999) Chemical fluid deposition: reactive deposition of platinum metal from carbon dioxide solution. Chem Mater 11:213–215
92. Long DP, Blackburn JM, Watkins JJ (2000) Chemical fluid deposition: a hybrid technique for low-temperature metallization. Adv Mater 12:913–915
93. Leitner W (2002) Supercritical carbon dioxide as a green reaction medium for catalysis. Acc Chem Res 35:746–756
94. Kim J, Roberts GW, Kiserow DJ (2006) Supported Pd catalyst preparation using liquid carbon dioxide. Chem Mater 18:4710–4712

95. Kim J, Kelly MJ, Lamb HH, Roberts GW, Kiserow DJ (2008) Characterization of palladium (Pd) on alumina catalysts prepared using liquid carbon dioxide. J Phys Chem C 112: 10446–10452
96. Zhang Y, Kang D, Saquing C, Aindow M, Erkey C (2005) Supported platinum nanoparticles by supercritical deposition. Ind Eng Chem Res 44:4161–4164
97. Blackburn JM, Long DP, Cabanas A, Watkins JJ (2001) Deposition of conformal copper and nickel films from supercritical carbon dioxide. Science 294:1–7
98. Romang AH, Watkins JJ (2010) Supercritical fluids for the fabrication of semiconductor devices: emerging or missed opportunities? Chem Rev 110:459–478
99. Bozbag SE, Yasar NS, Zhang LC, Aindow M, Erkey C (2011) Adsorption of Pt(cod)me2 onto organic aerogels from supercritical solutions for the synthesis of supported platinum nanoparticles. J Supercrit Fluid 56:105–113
100. Zhang Y, Erkey C (2006) Preparation of supported metallic nanoparticles using supercritical fluids: a review. J Supercrit Fluid 38:252–267
101. Zhang Y, Kang D, Aindow M, Erkey C (2005) Preparation and characterization of ruthenium/carbon aerogel nanocomposites via a supercritical fluid route. J Phys Chem B 109: 2617–2624
102. Yan K, Lafleur T, Wu G, Liao J, Ceng C, Xie X (2013) Highly selective production of value-added γ-valerolactone from biomass-derived levulinic acid using the robust Pd nanoparticles. Appl Catal Gen 468:52–58
103. Yen CH, Shimizu K, Lin Y-Y, Bailey F, Cheng IF, Wai CM (2007) Chemical fluid deposition of Pt-based bimetallic nanoparticles on multiwalled carbon nanotubes for direct methanol fuel cell application. Energy Fuel 21:2268–2271
104. Kelly M, Kim J, Roberts G, Lamb H (2008) Characterization of Pd/γ-Al2O3 catalysts prepared using [$Pd(hfac)_2$] in liquid CO_2. Top Catal 49:178–186
105. Morère J, Tenorio MJ, Torralvo MJ, Pando C, Renuncio JAR, Cabañas A (2011) Deposition of Pd into mesoporous silica SBA-15 using supercritical carbon dioxide. J Supercrit Fluid 56:213–222
106. Yen CH, Lin HW, Phan TD, Tan CS (2011) Chemical fluid deposition of monometallic and bimetallic nanoparticles on ordered mesoporous silica as hydrogenation catalysts. J Nanosci Nanotechnol 11:2465–2469
107. Yan K, Lafleur T, Liao J, Xie X (2014) Facile green synthesis of palladium nanoparticles for efficient liquid-phase hydrogenation of biomass-derived furfural. Sci Adv Mater 6:135–140
108. Rylander P (2012) Catalytic hydrogenation over platinum metals. Elsevier, Amsterdam
109. Bond JQ, Alonso DM, Wang D, West RM, Dumesic JA (2010) Integrated catalytic conversion of γ-valerolactone to liquid alkenes for transportation fuels. Science 327:1110–1114
110. Xinghua Z, Tiejun W, Longlong M, Chuangzhi W (2010) Aqueous-phase catalytic process for production of pentane from furfural over nickel-based catalysts. Fuel 89:2697–2702
111. Gao Y, Wang X-H, Yang H-P, Chen H-P (2012) Characterization of products from hydrothermal treatments of cellulose. Energy 42:457–465
112. Kruse A, Funke A, Titirici MM (2013) Hydrothermal conversion of biomass to fuels and energetic materials. Curr Opin Chem Biol 17:515–521
113. Toor SS, Rosendahl L, Rudolf A (2011) Hydrothermal liquefaction of biomass: a review of subcritical water technologies. Energy 36:2328–2342
114. Akhtar J, Amin NAS (2011) A review on process conditions for optimum bio-oil yield in hydrothermal liquefaction of biomass. Renew Sustain Energy Rev 15:1615–1624
115. Chareonlimkun A, Champreda V, Shotipruk A, Laosiripojana N (2010) Reactions of C5 and C6-sugars, cellulose, and lignocellulose under hot compressed water (HCW) in the presence of heterogeneous acid catalysts. Fuel 89:2873–2880
116. Horvath IT, Mehdi H, Fabos V, Boda L, Mika LT (2008) [gamma]-Valerolactone—a sustainable liquid for energy and carbon-based chemicals. Green Chem 10:238–242
117. Fabos V, Koczo G, Mehdi H, Boda L, Horvath IT (2009) Bio-oxygenates and the peroxide number: a safety issue alert. Energ Environ Sci 2:767–769

118. Nasirzadeh K, Zimin D, Neueder R, Kunz W (2004) Vapor-pressure measurements of liquid solutions at different temperatures: apparatus for use over an extended temperature range and some new data. J Chem Eng Data 49:607–612
119. Lange J-P, van de Graaf WD, Haan RJ (2009) Conversion of furfuryl alcohol into ethyl levulinate using solid acid catalysts. ChemSusChem 2:437–441
120. Lange JP, Price R, Ayoub PM, Louis J, Petrus L, Clarke L, Gosselink H (2010) Valeric biofuels: a platform of cellulosic transportation fuels. Angew Chem Int Ed Engl 49:4479–4483
121. Braca G, Raspolli Galletti AM, Sbrana G (1991) Anionic ruthenium iodorcarbonyl complexes as selective dehydroxylation catalysts in aqueous solution. J Organomet Chem 417:41–49
122. Mehdi H, Fabos V, Tuba R, Bodor A, Mika LT, Horvath IT (2008) Integration of homogeneous and heterogeneous catalytic processes for a multi-step conversion of biomass: from sucrose to levulinic acid, gamma-valerolactone, 1,4-pentanediol, 2-methyl-tetrahydrofuran, and alkanes. Top Catal 48:49–54
123. Bourne RA, Stevens JG, Ke J, Poliakoff M (2007) Maximising opportunities in supercritical chemistry: the continuous conversion of levulinic acid to γ-valerolactone in CO_2. Chem Commun 44:4632–4634
124. Manzer LE (2004) Catalytic synthesis of [alpha]-methylene-[gamma]-valerolactone: a biomass-derived acrylic monomer. Appl Catal Gen 272:249–256
125. Moreno-Marrodan C, Barbaro P (2014) Energy efficient continuous production of [gamma]-valerolactone by bifunctional metal/acid catalysis in one pot. Green Chem 16:3434–3438
126. Abdelrahman OA, Heyden A, Bond JQ (2014) Analysis of kinetics and reaction pathways in the aqueous-phase hydrogenation of levulinic acid to form γ-valerolactone over Ru/C. ACS Catal 4:1171–1181
127. Rong Z, Sun Z, Wang L, Lv J, Wang Y, Wang Y (2014) Efficient conversion of levulinic acid into γ-valerolactone over Raney Ni catalyst prepared from melt-quenching alloy. Catal Lett 144:1766–1771
128. Yang Y, Gao G, Zhang X, Li F (2014) Facile fabrication of composition-tuned Ru–Ni bimetallics in ordered mesoporous carbon for levulinic acid hydrogenation. ACS Catal 4:1419–1425
129. Alonso DM, Wettstein SG, Dumesic JA (2012) Bimetallic catalysts for upgrading of biomass to fuels and chemicals. Chem Soc Rev 41:8075–8098
130. Gong Y, Lin L, Yan Z (2011) Catalytic hydrogenation and oxidation of biomass-derived levulinic acid. BioResources 6:686–699
131. Galletti AMR, Antonetti C, De Luise V, Martinelli M (2012) A sustainable process for the production of [gamma]-valerolactone by hydrogenation of biomass-derived levulinic acid. Green Chem 14:688–694
132. Upare PP, Lee J-M, Hwang DW, Halligudi SB, Hwang YK, Chang J-S (2011) Selective hydrogenation of levulinic acid to [gamma]-valerolactone over carbon-supported noble metal catalysts. J Ind Eng Chem 17:287–292
133. Christian RV, Brown HD, Hixon RM (1947) Derivatives of γ-valerolactone, 1,4-pentanediol and 1,4-Di-(β-cyanoethoxy)-pentane. J Am Chem Soc 69:1961–1963
134. Azadi P, Carrasquillo-Flores R, Pagan-Torres YJ, Gurbuz EI, Farnood R, Dumesic JA (2012) Catalytic conversion of biomass using solvents derived from lignin. Green Chem 14: 1573–1576
135. Yan Z-P, Lin L, Liu S (2009) Synthesis of γ-valerolactone by hydrogenation of biomass-derived levulinic acid over Ru/C catalyst. Energ Fuel 23:3853–3858
136. Du X-L, He L, Zhao S, Liu Y-M, Cao Y, He H-Y, Fan K-N (2011) Hydrogen-independent reductive transformation of carbohydrate biomass into γ-valerolactone and pyrrolidone derivatives with supported gold catalysts. Angew Chem Int Ed 50:7815–7819
137. Deng L, Zhao Y, Li J, Fu Y, Liao B, Guo Q-X (2010) Conversion of levulinic acid and formic acid into γ-valerolactone over heterogeneous catalysts. ChemSusChem 3:1172–1175
138. Sudhakar M, Lakshmi Kantam M, Swarna Jaya V, Kishore R, Ramanujachary KV, Venugopal A (2014) Hydroxyapatite as a novel support for Ru in the hydrogenation of levulinic acid to γ-valerolactone. Catal Commun 50:101–104

Chapter 4
Green Synthesis of Metallic and Metal Oxide Nanoparticles and Their Antibacterial Activities

P.C. Nagajyothi and T.V.M. Sreekanth

Abstract In recent years, the development of metallic and metal oxide nanoparticles in an eco-friendly manner using plant materials has attracted considerable attention. The biogenic reduction of metal ions to the base metal is quite rapid, can be conducted readily at room temperature under sunlight conditions, can be scaled up easily, and the method is eco-friendly. The reducing agents involved include various water-soluble metabolites (e.g., alkaloids, terpenoids, polyphenolic compounds) and coenzymes. Noble metals (silver and gold) have been the main focus of plant-based synthesis. These green synthesized nanoparticles have a range of shapes and sizes compared to those produced by other organisms. The advantages of using plant-derived materials for nanoparticle synthesis have attracted the interest of researchers to investigate the mechanisms of metal ions uptake and bio-reduction by plants. These biosynthesized metallic and metal oxide nanoparticles have a wide range of biological applications. This chapter, however, discusses only the antibacterial activities.

Keywords Green synthesis • Eco-friendly • Antiparticles • Antibacterial activities

4.1 Introduction

Nanotechnology or nanoscale technology normally considers sizes below 100 nm. Nanoscience studies the phenomena, properties and responses of materials at the atomic, molecular, and macromolecular scales, usually at sizes between 1 and 100 nm [1]. At this size range, materials exhibit remarkable properties and are

P.C. Nagajyothi
Department of Physiology, College of Oriental Medicine, Dongguk University, Gyeongju 780-714, Republic of Korea

T.V.M. Sreekanth (✉)
Department of Life Chemistry, Catholic University of Daegu, Gyeongsan 712-702, Republic of Korea
e-mail: tvmsreekanth@gmail.com; sreekanth@cu.ac.kr

V.A. Basiuk, E.V. Basiuk (eds.), *Green Processes for Nanotechnology*,
DOI 10.1007/978-3-319-15461-9_4

gaining importance in the areas of mechanics, optics, biomedical sciences, chemical industry, electronics, drug-gene delivery, energy science, catalysis [2, 3] optoelectronics [4, 5] photo electrochemical applications [6], and nonlinear optical devices [7, 8]. Therefore, the production of nanoparticles with innovative applications can be achieved by controlling the size and shape on the nanometer scale. Nanoparticles can exhibit size and shape-dependent properties, which are of interest for applications ranging from biosensing and catalysts to optics, antimicrobials, and modern electronics. These particles also have applications in a range of fields, such as medical imaging, drug delivery, nanocomposites, and hyperthermia of tumors [9–12]. AuNPs and AgNPs are most common NPs in biomedical applications and interdisciplinary field of nanobiotechnology [13, 14]. AuNPs have been used for a range of purposes, such as markers for biological screening and immunoassay [15], protein assay [16] anticancer [17], antimicrobial activities [18–21], antimelanoma [19] tyrosinase inhibitory [19], and capillary electrophoresis [22]. AgNPs have extensive applications in areas, such as integrated circuits [23], sensors [24], biolabelling filters [24], antimicrobial deodorant fibers [25], antimicrobials [26–29], cell electrodes [30], antioxidants [28], and antiproliferative activities [29]. These AgNPs have potential antimicrobial effects against infectious organisms, such as *Escherichia coli*, *Bacillus subtilis*, *Vibrio cholera*, *Pseudomonas aeruginosa*, *Syphilis typhus*, and *Staphylococcus aureus* [31, 32]. ZnO NPs are used widely in industrial applications, such as pigments [33], dye-sensitized solar cells [34], photo-catalysts [35], and sensors [36]. ZnO is a wide bandgap semiconductor (II–IV) with an energy gap of 3.37 eV at room temperature, and ZnO NPs have a great advantage in their application as catalysts owing to their large surface area and high catalytic activity [37], as well as their antibacterial, antioxidant, and cytotoxic activities [38].

4.2 Synthesis of Nanoparticles

Nanoparticles can be synthesized using two methods: "top-down (Fig. 4.1)" approach or "bottom-up" approach. In the "top-down" approach, the bulk materials are broken down gradually to nanosized materials (lithographic techniques, e.g., grinding, milling), whereas in bottom-up approach, atoms or molecules are assembled to molecular structures in the nanometer range [39].

In bottom-up synthesis, nanoparticles are constructed from smaller entities, e.g., by joining atoms, molecules, and smaller particles [40]. In bottom-up synthesis, the nanostructured building blocks of nanoparticles form first and then assemble to produce the final particle [41]. Figure 4.2 shows the probable mechanism of nanoparticle synthesis by a bottom-up approach.

Of the biological methods of synthesis, methods based on microorganisms have been reported widely [22–25, 42]. Microbial synthesis is of course readily scalable, environmentally benign, and compatible with the use of the product for medical applications. On the other hand, these methods require multiple purification steps, or the maintenance of microbial cell cultures is more cost-incurring.

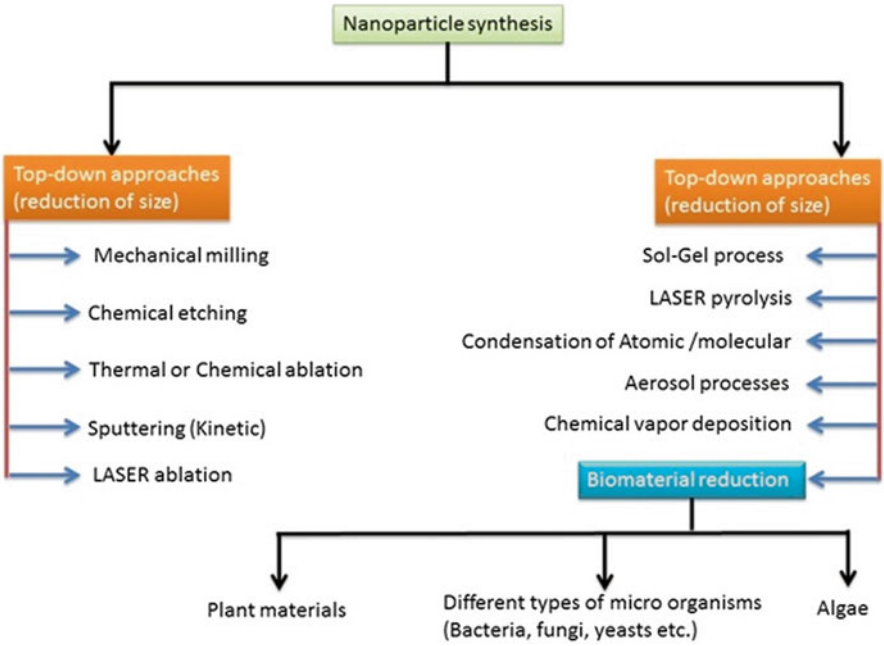

Fig. 4.1 Various approaches for making nanoparticles and cofactor dependent bioreduction with slight modifications. Reprinted from ref. [39] with permission from Elsevier

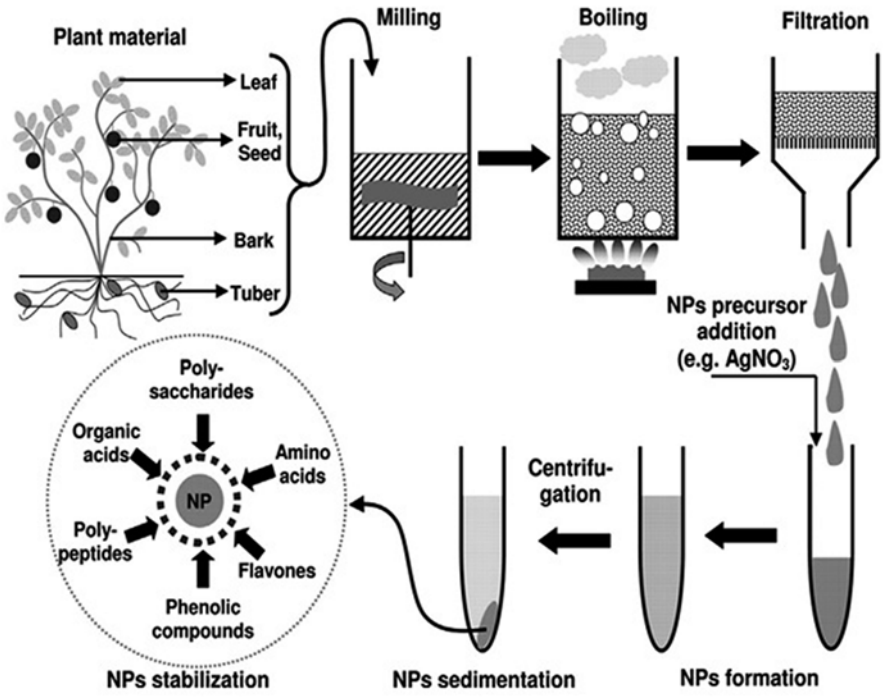

Fig. 4.2 Schematic representation of nanoparticle synthesis from plant extracts

4.2.1 Plant Biomass/Living Plant for Nanoparticle Synthesis (Green Synthesis; Fig. 4.3)

The use of plant materials is considered a green route and a reliable method for green synthesis of nanoparticles owing to its eco-friendly nature. Plants have been exploited successfully for rapid and extracellular biosynthesis of noble metallic and metal oxide nanoparticles [43–50]. Table 4.1 summarizes some of the reports pertaining to metallic and metal oxide nanoparticle synthesized by using various plant extracts, including their size and shape.

4.2.2 Silver Nanoparticles (AgNPs)

AgNPs have been synthesized from various types of plant extracts (Fig. 4.4), yeast, fungi, and bacteria. The use of plant extracts for the synthesis of AgNPs can be advantageous over other environmentally benign biological processes by

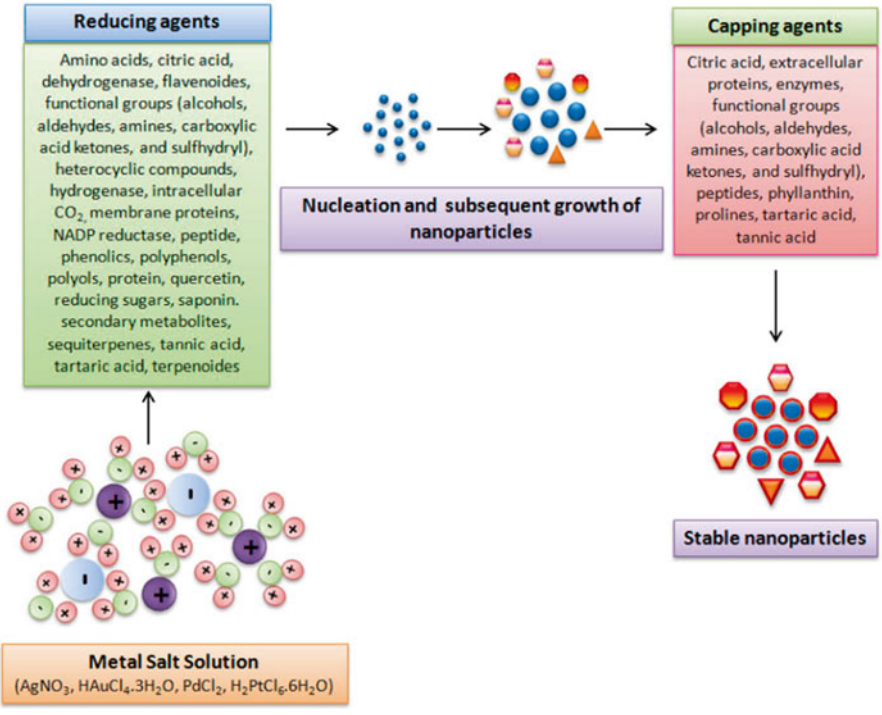

Fig. 4.3 Schematic diagram showing the mechanisms behind the biogenic synthesis of metallic nanoparticles. Reprinted from ref. [46] with permission from the American Chemical Society

Table 4.1 Green synthesis of metallic and metal oxide nanoparticles from different plant extracts and their size and shapes

Plant name	Type of NPs	Shape and size	Tested microorganism	Reference
Soybean–garlic aqueous extract	AuNPs	Spherical (7–12.4 nm)	*S. aureus*, *P. aeruginosa*, and *A. baumannii/haemolyticus*	El-Batal et al. [124]
Dioscorea batatas rhizome	AuNPs	Triangular, hexagonal, rod, and irregular (18.48–56.18 nm)	*S. aureus*, *S. epidermidis*, and *E. coli*	Sreekanth et al. [125]
Grapes fruit	AuNPs	Spherical (–)	*S. aureus*, *C. koseri*, *B. cereus*, *P. aeruginosa*, *E. coli*, and *C. albicans*	Lokina and Narayanan [126]
Aerva lanata flower	AuNPs	Spherical (48.4 nm)	*S. aureus*, *B. cereus*, and *P. aeruginosa*	Kirubha and Alagumuthu [127]
Senna siamea leaf	AuNPs	Spherical and hexagonal (70 nm)	*S. aureus*, *B. subtilis*, *E. coli*, *P. aeruginosa*, and *K. pneumonia*	Rajasekhar et al. [128]
Tephrosia purpurea leaf	AuNPs	Spherical (~100 nm)	*E. coli*, *E. faecalis*, and *K. pneumonia*	Jisha et al. [129]
Caesalpinia pulcherrima flower	AuNPs	Spherical (10–50 nm)	*A. niger*, *A. flavus*, *E. coli*, and *Streptobacillus* sp.	Nagaraj et al. [130]
Bacopa monnieri plant		Spherical (15–35 nm)	*E. coli*, *S. aureus*, *B. subtilis*, and *Enterococcus*	Mahitha et al. [131]
Plumeria alba flower	AuNPs	Spherical 20–30 nm and 80–150 nm	*A. niger*, *A. flavus*, *E. coli* and *Streptobacillus* sp.	Nagaraj et al. [132]
Ziziphus Jujuba fruit	AuNPs	Spherical (34.8 nm)	*E. coli*, *S. aureus*, *B. cereus*, and *P. aeruginosa*	Kirubha and. Alagumuthu [133]
Abelia grandiflora root	AgNPs	Spherical (10–30 nm)	*E. coli*, *B. megaterium*, *B. subtilis*, *S. aureus*, *K. pneumonia*, and *P. vulgaris*	Sharma et al. [134]
Mimusops elengi leaf	AgNPs	Spherical (55–80 nm)	*K. pneumonia*, *S. aureus*, and *Micrococcus luteus*	Prakash et al. [135]
Vanda Tessellate leaves	AgNPs	Cubic, hexagonal (10–50 nm)	*E. coli*, *Salmonella* sp, and *S. aureus*	Manjunath et al. [136]
Nelumbo nucifera seed	AgNPs	Spherical (2.76–16.62 nm)	*B. cereus*, *S. typhimurium*, *S. epidermidis*, *B. megaterium*	Nguyen Thi Mai Tho et al. [137]
Lycopersicon esculentum	AgNPs	Square (10–45 nm)	*E. coli*	Smaranika Das et al. [138]
Carob leaf	AgNPs	Spherical (5–40 nm)	*E. coli*	Awwad et al. [139]

(continued)

Table 4.1 (continued)

Plant name	Type of NPs	Shape and size	Tested microorganism	Reference
Bacopa monnieri whole plant	AgNPs	Spherical (22 nm)	*S. aureus*, *B. subtilis*, *E. coli*, *K. pneumoniae*	Mahitha et al. [140]
Phyllanthus amarus whole plant	AgNPs	Spherical (8–24 nm)	*P. aeruginosa*	Singh et al. [141]
Pomegranate peel	AgNPs	5–50 nm	*S. aureus*, *P. aeruginosa*, and *E. coli*	Shanmugavadivu et al. [142]
Elaeagnus indica leaves	AgNPs	Mono-dispersive (30 nm)	*E. coli*, *P. putida*, *B. subtilis* and *S. aureus*, *A. flavus* and *F. oxysporum*	Natarajan et al. [143]
Aloe leaf	ZnONPs	Spherical (25–55 nm)	*S. aureus*, *S. marcescens*, *P. mirabilis*, and *C. freundii*	Sangeetha et al. [144]
Solanum nigrum leaf	ZnONPs	Quasi-spherical (29.79 nm)	*S. aureus*, *S. paratyphi*, *V. cholera*, and *E. coli*	Ramesh et al. [145]
Aloe vera	ZnONPs	Irregular, triangular (69 nm)	*S. aureus*, *S. pyogenes*, *P. aeruginosa*, *E. coli*, and *S. typhi*	Ayeshamariam et al. [146]

eliminating the need for elaborate processes of maintaining cell cultures. Plants/plant extracts can act as both reducing and stabilizing agents in the synthesis of nanoparticles. Jose-Yacaman et al. first reported the formation of gold and silver nanoparticles synthesized from living plants [44, 45]. Triangular, hexagonal, cubic, and circular AgNPs were synthesized from a *Pseudocydonia sinensis* fruit extract [46]. Sathiskumar et al. [47] examined the ability of the extracts of powder and bark of *Curcuma longa* towards the formation of AgNPs, and reported that a bark extract can produce a large amount of AgNPs compared to the powder extract. The resulting nanoparticles varied in shape and size but exhibited strong antibacterial activity against *E. coli*. Sreekanth et al. [51] reported the formation of spherical AgNPs using a *Citrus reticulata* juice extract. Similarly, many other studies have synthesized AgNPs from the leaf extract of *Argemone mexicana* [52], bran powder of Sorghum spp., [53], and the leaf extracts of *Allium cepa* [54] and *Euphorbia hirta* [55].

Sreekanth et al. [56] reported the synthesis of AgNPs using *Nelumbo nucifera* root extract, in which AgNPs were predominantly spherical and had a mean size of 16.7 nm. Quite recently, AgNPs have been synthesized using a variety of plants, such as banana (spherical shape), neem (triangular), and tulsi (cuboidal shape) [57], *Abelia grandiflora* (spherical shape and mean size of 10–30 nm) [58], *Malus domestica* fruit extract [59], *Zingiber officinale* root extract (spherical and size ranging from 10 to 20 nm) [60], orange peel extract (spherical and a mean size of 91.89 nm) [61], *Sterculia foetida* L young leaves (spherical, irregular and nanoparticle size

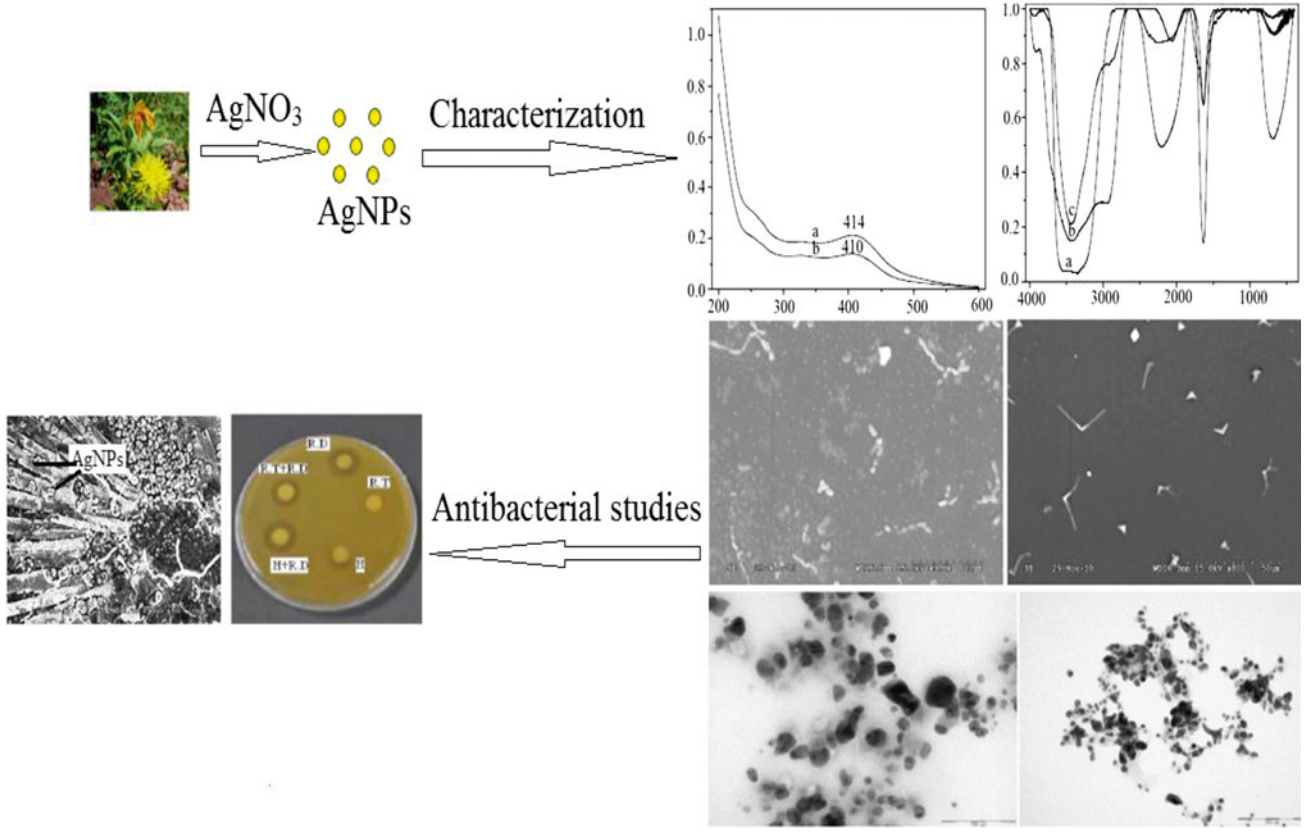

Fig. 4.4 Schematic of the procedure followed to synthesize AgNPs by using *Carthamus tinctorius* flower extracts and to study their antibacterial properties. Reprinted from ref. [51] with permission from the Bentham Sciences

ranges from 30 to 50 nm) [62], *Ocimum tenuiflorum* (spherical particles with a mean size of 29 nm), and *Catharanthus roseus* (spherical shape nanoparticles with a mean size of 19 nm) [63], respectively.

4.2.3 Gold Nanoparticles (AuNPs)

AuNPs are the most attractive noble metal nanoparticles because of their potential applications in catalysis, optics nanoelectronics, gene expression, and clinical diagnosis [64].

Huang et al. [65] reported the formation of gold nanoparticles from the sun-dried leaves of *Cinnamomum camphora*. Narayanan and Sakthivel [66] reported the extracellular synthesis of gold nanoparticles using the leaf extract of *Coriandrum sativum*. They found that the synthesized nanoparticles were triangular, truncated and decahedral in morphology with a mean size of 6.7–57.9 nm. Ramezani et al. [67] tested the leaf extracts of three different plants, i.e., *Eucalyptus camaldulensis, Pelargonium roseum*, and *A. indica*, for the reduction of aqueous chloroaurate solutions. The results indicated that all the leaf extracts tested could produce gold nanoparticles, but a significant increase in reduction was observed when the menthol extracts of *E. camaldulensis* and *P. roseum* were used compared to the *A. indica* leaf extract. Raghunandan et al. [68] reported that the addition of a microwave-exposed aqueous extracellular guava leaf extract to an aqueous gold chloride solution yielded stable poly-shaped gold nanoparticles with high purity. Ankamwar [69] reported the formation of highly stable gold nanoparticles (10–35 nm) when the leaf extract of *Terminalia catappa* was exposed to an aqueous chloroaurate solution. Gold nanoparticles with various sizes were also obtained using the dried leaf extract of *Stevia rebaudiana* [70]. Moreover, Thirumurugan et al. [71] also produced the gold nanoparticles using the leaf extract of *A. indica*.

Recently, Singh and Bhakat [72] reported the synthesis of gold nanoparticles using the leaves and bark of Ficus carica. In addition, the synthesis of spherical gold nanoparticles by the reduction of $AuCl_4^-$ by the leaf extracts of *Sphaeranthus amaranthoides* [73] and *Putranjiva roxburghii* [74] was reported. The syntheses of gold nanoparticles with different sizes in the range of 15 – 25 nm were obtained by controlling the synthetic parameters using the leaf extract of fenugreek [75].

Several studies have independently reported the reduction of aqueous chloroaurate solution using a variety of plant parts (Fig. 4.5). The formation of gold nanowires was reported from the pulp extract of *Beta vulgaris* [76]. Similarly, spherical-shaped crystalline gold nanoparticles were synthesized using the flower extract of *Nycanthes arbor-tristis* [77] and the leaf extract of *Mangifera indica* [78].

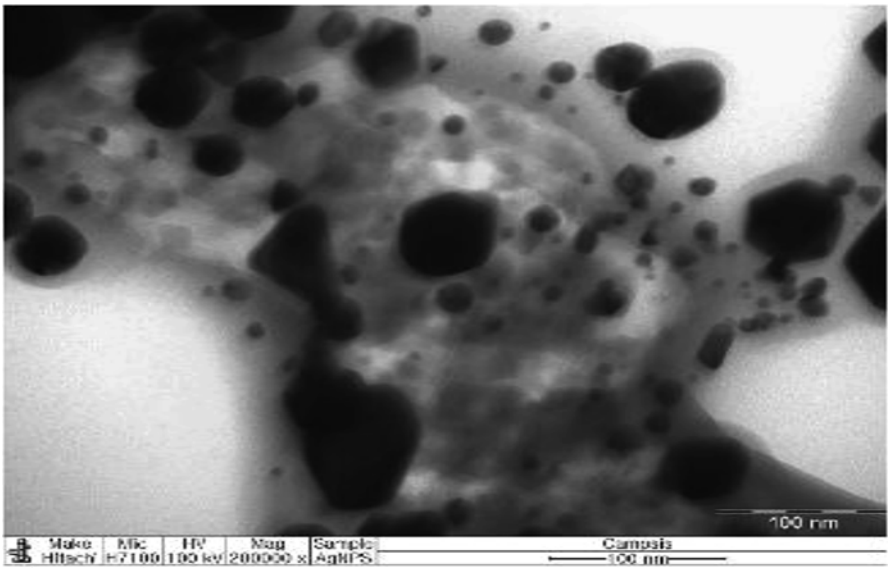

Fig. 4.5 Green-synthesized AuNPs from *Nelumbo nucifera* seed extract. Reprinted from ref. [137] with permission from the Slovenian Chemical Society

4.2.4 Zinc Oxide Nanoparticles (ZnONPs)

ZnONPs is an attractive semiconductor material for nano-electronic and photonic applications [79]. ZnO NPs are used widely in industrial applications, such as pigments, dye-sensitized solar cells [80], photocatalysts [40], and sensors [41]. ZnO is a wide band-gap semiconductor (II–IV) with an energy gap of 3.37 eV at room temperature, and ZnO NPs have great advantage in catalyst applications owing to their large surface area and high catalytic activity [42].

Nagajyothi et al. [38] reported ZnO NPs synthesized using a Coptidis rhizoma root extract and studied the antibacterial, antioxidant, and cytotoxic activities, and observed nanoparticles with a mean size of 8.50 nm and spherical and rod shapes (Fig. 4.6). They also synthesized ZnO NPs from *P. trifoliata* fruits and examined the catalytic activity using the Claisen–Schmidt condensation reaction [81], (Fig. 4.7).

Similarly, there are many reports on ZnO NPs. Divya et al. [48] synthesized ZnO NPs using *Hibiscus rosa-sinensis* leaf extract and examined their antibacterial activity against *Staphylococcus* aureus, *Escherichia coli*, *Pseudomonas aeruginosa, Klebsiella pneumonia*. The ZnO NPs showed the least activity against *Klebsiella pneumonia*. Vijayakumar et al. [49] reported ZnO NPs synthesized using a *Plectranthus amboinicus* leaf extract and studied S*taphylococcus aureus*. An *Eichhornia crassipes* leaf extract was used for the synthesis of ZnONPs with a mean size of 32 ± 4 nm [50]. Salam et al. [82] synthesized ZnONPs from *Ocimum basilicum* L.; the nanoparticles were hexagonal and less than 20 nm in size.

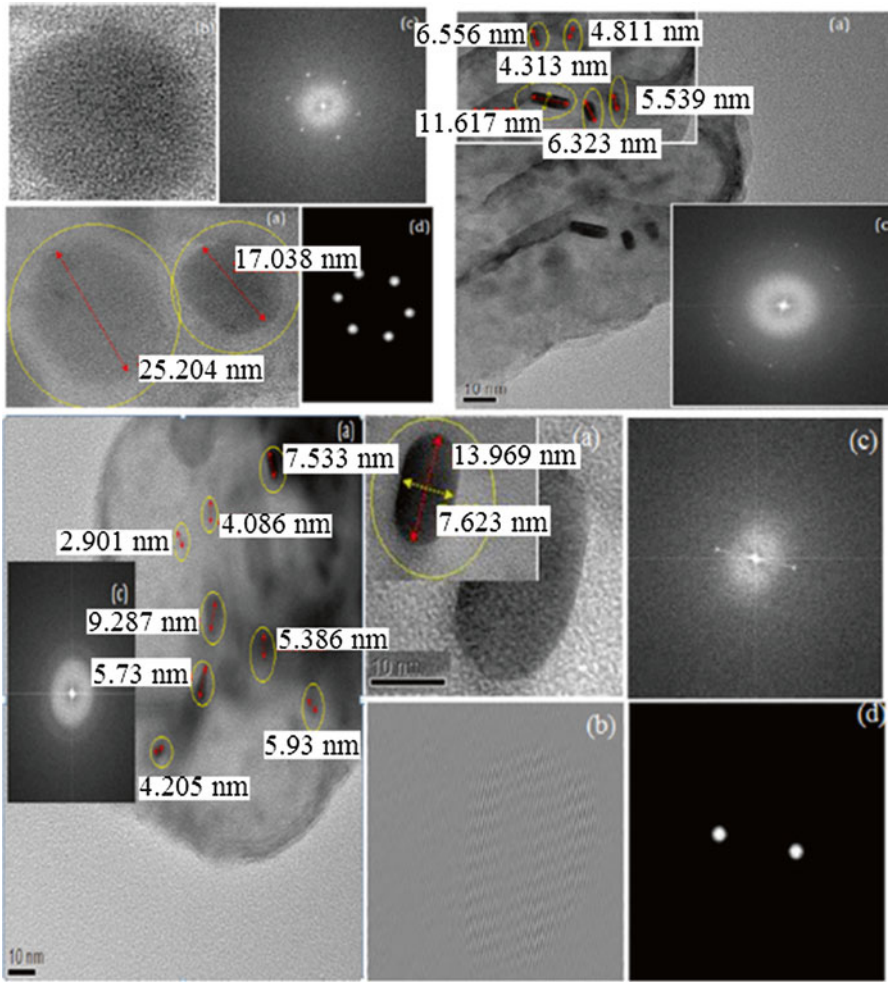

Fig. 4.6 Green-synthesized ZnO NPs from coptidis rhizoma: (**a**) TEM images (**b**) high resolution TEM image (**c**, **d**) selected area electron diffraction (SAED). Reprinted from ref. [38] with permission from Elsevier

Recently, ZnO NPs have been synthesized using different plants, such as *Camellia sinensis* (16 nm) [83], *Borassus flabellifer* fruit extract (rod shape and size ranged from 50 to 60 nm) [84], *Coriandrum sativum* leaf extract (flower shape with a mean size of 66 nm) [85, 86], *Citrus paradisi* peel extract (spherical shape and particle sizes ranging from 12 to 72 nm) [87, 88], leaves of *Adhatoda vasica* (discoid in shape with a mean size of 19–60 nm) [87], *Olea europaea* leaf extract (nanosheets or nanoplatelets with sizes in the range, 18–30 nm) [88], *Azadirachta indica* (nanoflowers of 51 nm), and *Emblica officinalis* (nanoflakes, 16 nm in size) [89] respectively.

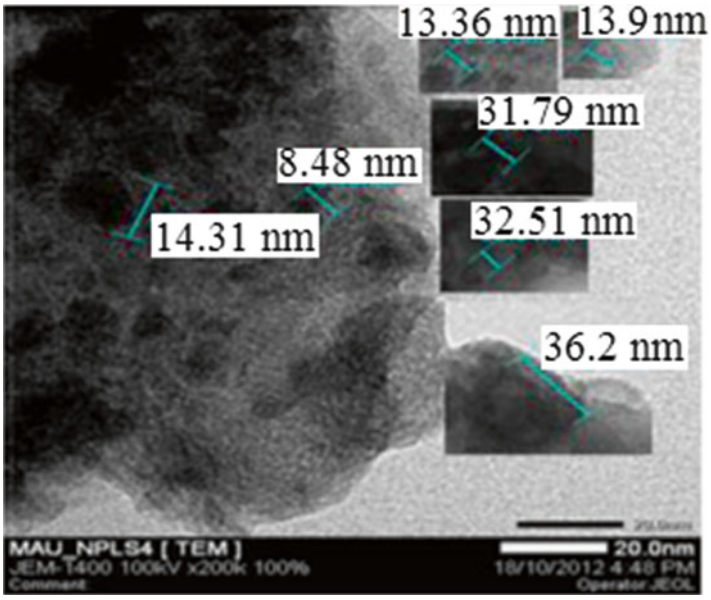

Fig. 4.7 Green-synthesized ZnO NPs from *Poncirus trifoliata.* Reprinted from ref. [81] with permission from Elsevier

4.3 Characterization of Nanoparticles

Nanoparticles are generally characterized by their shape, size, surface area, and disparity. In addition, the homogeneity of these properties is important for many applications. The common instruments used for characterization are as follows [18–21, 28, 29]:

1. UV–Visible spectroscopy.
2. Fourier transform infrared (FT-IR) spectroscopy.
3. Scanning electron microscopy (SEM).
4. Energy dispersive X-ray spectroscopy (EDS).
5. Transmission electron microscopy (TEM).
6. Atomic force microscopy (AFM).
7. X-ray diffraction (XRD).
8. Dynamic light scattering (DLS).

UV–Visible spectroscopy is a commonly used technique. The light wavelengths in the range, 200–700 nm, are generally used to characterize a range of metallic and metal oxide nanoparticles. Spectrophotometric absorption measurements in the wavelength ranges of 400–450, 500–550, and 300–400 nm are used to characterize Ag, Au, and ZnO nanoparticles, respectively.

FTIR spectroscopy is useful for characterizing the surface chemistry. Organic functional groups (e.g., carbonyls, hydroxyls) attached to the surface of nanoparticles and the other surface chemical residues are detected by FTIR spectroscopy.

When the synthesis is completed, the size, shape, and dispersion state of metal and metal oxide nanoparticles are normally measured by SEM, TEM, and AFM.

SEM and TEM are used for morphological characterization on the nanometer to micrometer scale. TEM has a 1,000-fold higher resolution than SEM. The elemental composition of metal nanoparticles is commonly established using energy dispersive spectroscopy (EDS).

AFM offers visualization in three dimensions. The resolution in the vertical, or *Z*-axis, is limited by the vibration environment of the instrument, whereas the resolution in the horizontal, or *X*–*Y*-axis, is limited by the diameter of the tip used for scanning. AFM provides surface characterization on the atomic scale.

XRD is used for phase identification and characterization of the crystal structure of nanoparticles. X-rays penetrate into the nanomaterial and the resulting diffraction pattern is compared with standards to obtain structural information.

DLS is used to characterize the surface charge and size distribution of particles suspended in a liquid.

4.4 Antibacterial Studies of AuNPs

The antibacterial activity of AuNPs with antibiotics exhibit a larger zone of inhibition compared to standard antibiotics [90]. Another study reported similar results for the Marigold flower [91]. The efficacy of the antibacterial activity of AuNPs can be increased by the addition of antibiotics [92]. Williams et al. [93] reported that gold NPs do not affect bacterial growth or functional activity, whereas conjugates of vancomycin to AuNPs decrease the number of growing bacterial cells [94] Gu et al. [95] synthesized gold NPs covered with an antibiotic (vancomycin) and reported significant enhancement of the antibacterial activity for this conjugate compared to the activity of the free antibiotic. Ciprofloxacin with gold nanoshells showed high antibacterial activity against *E. coli* [96, 97]. The coating of aminoglycosidic antibiotics with AuNPs had a significant antibacterial effect on gram-positive and gram-negative bacteria [97]. Cefaclor (a second-generation β-lactam antibiotic)-reduced AuNPs exhibited potent antibacterial activity on both gram-positive (*S. aureus*) and gram-negative bacteria (*E. coli*) compared to Cefaclor and AuNPs alone [98].

4.4.1 Mechanism of the Bactericidal Action of AuNPs

The mechanism of the inhibitory effects of metallic nanoparticles on microorganisms is partially known, but there are still some questions on the mechanism of action along with the spectrum of antibacterial activity [99].

Grace and Pandian [97] reported that the AuNPs have a great bactericidal effect and possess well-developed surface chemistry, chemical stability, and an appropriate smaller size, which make them easier to interact with microorganisms. The nanoparticles bind to the building elements of the outer membrane causing structural changes, degradation, and finally cell death.

Every AuNP is surrounded by a number of stabilizer molecules, which prevent agglomeration and reduce the surface area and interfacial free energy of the nanoparticles, thereby maintaining the particle reactivity [100]. This makes the particles interact easily with the outer membrane components of the cell, and causes significant changes and damage to their surfaces leading to cell death.

Chwalibog et al. [101] reported that the interaction between AuNPs and *Staphylococcus aureus* was prevented by a biofilm and the substance released by the cells caused distortions of the cell wall. AuNPs bind closely to the surface of the microorganisms, causing visible damage to the cells, which can minimize the treatment durations and side effects of drugs [102]. AuNPs generate holes in the cell wall, resulting in leakage of the cell contents and finally cell death. In another way, it can bind to the DNA of bacteria and inhibit DNA transcription [98].

4.5 Antibacterial Studies of AgNPs

Among the non-organic antibacterial agents, Ag ions or Ag NPs are strong antimicrobial agents. A minute amount of silver is harmless to human cells but is biocidal to microbial cells [103].

Priya et al. [104] reported that AgNPs synthesized from banana leaf extract exhibits the maximum inhibition for gram-positive bacteria (*Bacillus*). Silver ions and AgNPs have also inhibitory and lethal effects on both gram-positive and gram-negative bacteria (*E. coli*, and *S. aureus*) [104]. *E. coli* (gram-negative) was less sensitive to Ag NPs compared to gram-positive bacteria *S. aureus*. Similar results were observed by Sondi and Salopek-Sondi [105]. On the other hand, Kim et al. [106] reported that gram-positive *S. aureus* was less affected by AgNPs compared to *E. coli*, even at high concentrations. The AgNPs were tested against both gram-positive and gram-negative bacteria (*E. coli*, *S. aureus*, and *B. substilis*) in liquid systems. The concentrations tested (50, 70, and 90 μg/μL) produced inhibition percentages of 11.43, 40.26, and 51.53; 9.94, 11.95, and 43.64; and 8.69, 12.5, and 44.63 mm, respectively [51]. Agar well diffusion studies showed that green synthesized AgNPs exhibited effective inhibitory action against *S. aureus*, *B. cereus*, *L. monocytogenes*, and *S. flexneri* [107]. The effects of AgNPs, penicillin and tetracycline against both gram-negative (*E. coli and P. mirabilis*) and gram-positive bacteria (*S. epidermidis*) were examined using the disk diffusion method. The antibacterial activity of penicillin against gram-negative and gram-positive bacteria was greater in the presence of AgNPs than tetracycline. The largest increase in the fold area was observed against *S. epidermidis* (75 %) followed in order by *E. coli* (46.66 %) and *P. mirabilis* (13.63 %). Tetracycline in combination with AgNPs

produced an increase in the fold area against *S. epidermidis* (42.85 %) followed in order by *E. coli* (31.57 %) and *P. mirabilis* (9.09 %) [28]. Raffin et al. [108] reported that 16 nm silver nanoparticles were completely cytotoxic to the gram-negative bacteria, *E. coli*, at low concentrations (60 μg/mL).

4.5.1 Mechanism of the Bactericidal Action of AgNPs

The antibacterial mechanism(s) of AgNPs are not completely understood, but various studies have shown that Ag NPs can attach to the surface of the cell membrane, thereby disturbing the permeability and respirational functions of the cell [109]. Furthermore, AgNPs interact with the surface of a membrane and can penetrate the bacterium [110].

Wang et al. [111] reported that AgNPs react with sulfur-containing proteins in the interior of the cells, and those phosphorous-containing compounds, such as vital enzymes and DNA bases, will affect the respiratory chain and cell division in bacteria, ultimately causing cell death.

Key factors such as size (surface area) and particle shape affect the antibacterial activity of AgNPs [112]. Pal et al. reported that triangular AgNPs are more effective against the gram-negative bacteria, *E. coli*, than spherical and rod-shaped AgNPs, suggesting that the shape of AgNPs should be considered when developing highly efficient antibacterial agents [113].

4.6 Antibacterial Studies of ZnO NPs

Among the several metal oxides studied for their antibacterial activity, ZnO NPs exhibit selective toxicity to bacteria but have a minimal effect on human cells [114–117]. Jayaseelan et al. [118] reported that the green synthesized ZnO NPs showed the maximum inhibition zones in the ZnO NPs (25 μg/mL) *P. aeruginosa* (22 ± 1.8 mm) and *A. flavus* (19 ± 1.0 mm). *A. hydrophila*, *E. coli*, *E. faecalis*, and *C. albicans* exhibited a minimum inhibitory concentration at 1.2, 1.2, 1.5, and 0.9 μg/mL. The antibacterial activity of ZnO NPs was evolved against gram-negative and -positive bacteria using the resazurin incorporation method. The MICs of ZnO NPs against *E. coli*, *P. aeruginosa*, and *S. aureus* were observed at 500 μg/mL, 500 μg/mL, and 125 μg/mL, respectively, by the resazurin incorporation method [119]. The MIC of the ZnO nanoparticles against *E. coli* was found to be 500 μg/mL using the disk diffusion method [119]. ZnONPs had a much stronger antibacterial effect on gram-positive bacteria than on gram-negative bacteria [120, 121]. Other reports have confirmed the strong antimicrobial activity of ZnO NPs in the food-borne bacteria, *Salmonella typhimurium* and *Staphylococcus aureus* [122]. In another report, 12 nm ZnO NPs inhibited the growth of *E. coli* by disintegrating the cell membrane and increasing the membrane permeability [123]. Nagajyothi et al. [38] reported the

maximum antibacterial activity against *E. coli* (11 mm) according to the disk diffusion method with much less activity against *B. megaterium* (10 mm), *B. pumilus* (9 mm), and *B. cereus* (9 mm). Sawai [120] reported that ZnO is a biocidal agent and that the antibacterial activity was dependent on the agent concentration.

4.6.1 Mechanism of the Bactericidal Action of ZnO NPs

The production of hydrogen peroxide from the surface of ZnO is considered as an efficient means for the inhibition of bacterial growth [121]. The number of ZnO powder particles per unit volume of powder slurry increases with decreasing particle size, resulting in an increased surface area and increased generation of hydrogen peroxide. The antibacterial activity of ZnO was attributed to the release of Zn^{2+} ions, which damage the cell membrane and interact with the intracellular contents [114]. The antibacterial activity of nanoparticles depends on its size, by which ZnO NPs smaller in size than the pore size in the bacteria can cross the cell membrane without hindrance [121].

4.7 Conclusions

This chapter summarizes recent research works on the synthesis of gold, silver, and zinc oxide nanoparticles using plant extracts and their potential applications in the field of biology. Chemical synthesis methods have enjoyed a colorful history in the production of metallic and metal oxide nanoparticles. These chemically produced nanoparticles have however been implicated in cellular and tissue toxicity. Moreover, the production is environmentally unfriendly and quite expensive. This has made the use of plants the preferred alternatives. Green synthesized gold, silver, and zinc oxide nanoparticles have demonstrated mild to exceptional antimicrobial activities over the past few years. However, one major challenge confronting this biogenic method is the attachment of biological materials onto the nanostructure. Further studies are therefore warranted into the green synthesis of unadulterated nanostructures which may further improve activity and reduce the unlikely probability of toxicity.

References

1. Logothetidis S (ed) Nanostructured materials and their applications. NanoScience and Technology. Springer-Verlag Berlin Heidelberg 2012. doi:10.1007/978-3-642-22227-6_1
2. Schmid G (1992) Chem Rev 92:1709–1727
3. Hoffman AJ, Mills G, Yee H, Hoffmann M (1992) J Phys Chem 96:5546–5552
4. Colvin VL, Schlamp MC, Alivisatos A (1994) Nature 370:354–357
5. Wang Y, Herron N (1991) J Phys Chem 95:525–532

6. Mansur HS, Grieser F, Marychurch MS, Biggs S, Urquhart RS, Furlong D (1995) J Chem Soc Faraday Trans 91:665–672
7. Wang Y (1991) Acc Chem Res 24:133–139
8. Yoffe A (1993) Adv Phys 42:173–266
9. Tan M, Wang G, Ye Z, Yuan J (2006) Lumin 117:20–28
10. Lee HY, Li Z, Chen K, Hsu AR, Xu C, Xie J, Sun S, Chen X (2008) J Nucl Med 49:1371–1379
11. Pissuwan D, Valenzuela SM, Cortie MB (2006) Trends Biotechnol 24:62–67
12. Panigrahi S, Kundu S, Ghosh S, Nath S, Pal T (2004) J Nanopart Res 6:411–414
13. Cai W, Gao T, Hong H, Sun J (2008) Nanotechnol Sci Appl 1:17–32
14. Sperling RA, Gil PR, Zhang F, Zanella M, Parak WJ (2008) Chem Soc Rev 37:1896–1908
15. Liu X, Dai Q, Austin L, Coutts J, Knowles G, Zou J, Chen H, Huo Q (2008) J Am Chem Soc 130:2780–2782
16. Tang D, Yuan R, Chai Y (2007) Biosens Bioelectron 22:1116–1120
17. Medley CD, Smith JE, Tang Z, Wu Y, Bamrungsap S, Tan W (2008) Anal Chem 80: 1067–1072
18. Nagajyothi PC, Lee KD, Sreekanth TVM (2014) Synth React Inorg Metal-Org Nano-Metal Chem 4:1011–1018
19. Tetty CO, Nagajyothi PC, Lee SE, Ocloo A, Minh An TN, Sreekanth TVM, Lee KD (2012) Int J Cosm Sci 34:150–154
20. Sreekanth TVM, Nagajyothi PC, Lee KD (2012) Adv Sci Lett 6:63–69
21. Nagajyothi PC, Sreekanth TVM, Prasad TNVKV, Lee KD (2012) Adv Sci Lett 5:124–130
22. Tseng WL, Huang MF, Huang YF, Chang HT (2005) Electrophoresis 26:3069–3075
23. Kotthaus S, Gunther BH, Hang R, Schafer H (1997) IEEE Trans Compon Packag Manuf Technol Part A 20:15–20
24. Cao G (2004) Nanostructures and nanomaterials: synthesis, properties and applications. Imperial College Press, London
25. Zhang W, Wang G (2003) New Chem Mater 31:42–44
26. Krishnaraj C, Jagan EG, Rajasekar S, Selvakumar P, Kalaichelvan PT, Mohan N (2010) Colloids Surf B 76:50–56
27. Elumalai EK, Prasad TNVKV, Hemachandran J, Viviyan Therasa S, Thirumalai T, David E (2010) J Pharm Sci Res 2:549–554
28. Nagajyothi PC, Sreekanth TVM, Jae-il Lee, Kap Duk Lee (2014) J Photochem Photobiol B Biol 130:299–304
29. Klaus-Joerger T, Joerger R, Olsson E, Granqvist CG (2001) Trends Biotechnol 19:15–20
30. Mukherjee P, Ahmad A, Mandal D, Senapati S, Sainkar SR, Khan MI (2001) Nano Lett 1:515–519
31. Thakkar KN, Mhatre SS, Parikh RY (2010) Nanomed Nanotechnol Biol Med 6:257–262
32. Dura'n N, Marcato PD, De S, Gabriel IH, Alves OL, Esposito E (2007) J Biomed Nanotechnol 3:203–208
33. Adlim M, Bakar MA, Liew KY, Ismail J (2004) J Mol Catal A 212:141–149
34. Chakraborty S, Raj CR (2009) Biosens Bioelectron 24:3264–3268
35. Venu R, Ramalu TS, Znandakumar S, Rani VS, Kim CG (2011) Colloids Surf A 384: 733–738
36. Lin X, Wu M, Kuga S, Endo T, Huang Y (2011) Green Chem 13:283–287
37. Čechalova V, Kalendova A (2007) J Phys Chem Solids 68:1096–1100
38. Nagajyothi PC, Sreekanth TVM, Tettey CO, Yang In June, Shin Heung Mook (2014) Bioorg Med Chem Lett 24:4298–4303
39. Mittal AK, Chisti Y, Banerjee UB (2013) Biotechnol Adv 31:346–356
40. Suliman AE, Tang Y, Xu L (2007) Sol Energy Mater Sol Cell 91:1658–1662
41. Parida KM, Dash SS, Das DP (2006) J Colloid Interface Sci 298:787–793
42. Gao T, Wang TH (2005) Appl Phys A 80:1451–1454
43. Gardea-Torresdey JL, Parsons JG, Dokken K, Peralta-Videa J, Troiani HE, Santiago P, Jose-Yacaman M (2002) Nano Lett 2:397–401

44. Gardea-Torresdey JL, Gomez E, Peralta-Videa J, Parsons JG, Troiani HE, Jose Yacaman M (2003) Langmuir 19:1357–1361
45. Nagajyoyhi PC, Sreekanth TVM, Lee KD (2012) Synt React Inorg Metal-Org Nano-Metal Chem 42:1339–1344
46. Akhtar MS, Panwar J, Yun Y-S (2013) ACS Sustain Chem Eng 1:591–602
47. Sathishkumar M, Krishnamurthy S, Yun YS (2010) Biores Technol 101:7958–7965
48. Divya MJ, Sowmia C, Joona K, Dhanya KP (2013) Res J Pharm Biol Chem Sci 4:1137–1142
49. Vijayakumar S, Vinoj G, Malaikozhundan B, Shanthi S, Vaseeharan B (2015) Spectrochim Acta Part A Mol Biomol Spectros 137:886–891
50. Vanathi P, Rajiv P, Narendhran S, Rajeshwari S, Rahman KSM, Venckatesh R (2014) Mat Lett 134:13–15
51. Sreekanth TVM, Kap Duk Lee (2013) Curr Nanosci 9:457–462
52. Singh A, Jain D, Upadhyay MK, Khandelwal N, Verma HN (2010) Dig J Nanomater Biostruct 5:483–489
53. Njagi EC, Huang H, Stafford L, Genuino H, Galindo HM, Collins JB, Hoag GE (2010) Langmuir 27:264–271
54. Saxena A, Tripathi RM, Singh RP (2010) Dig J Nanomater Biostruct 5:427–432
55. Bipinchandra KS, Shin J, Shailesh SS, Alkotaini B, Lee S, Kim BS (2014) Korean J Chem Eng 31:2035–2040
56. Sreekanth TVM, Ravikumar S, Eom IY (2014) J Photochem Photobiol B Biol 141:100–105
57. Priya B, Mantosh S, Aniruddha M, Papita D (2014) Bioresou Bioprocess 1:1–10
58. Sharma G, Jasuja ND, Rajgovind, Singhal P, Josh SC (2014) J Microb Biochem Technol 6:1–3
59. Umoren SA, Obot IB, Gase ZM (2014) J Mater Environ Sci 5:907–914
60. Velmurugan P, Krishnan A, Manoharan M, Kui-Jae L, Min Cho, Sang-Myeong L, Jung-Hee P, Sae-Gang Oh, Keuk-Soo Bang, Byung-Taek Oh (2014) Bioproc Biosyst Eng 37: 1935–1943
61. Manal AA, Awatif Hendi A, Khalid Ortashi MO, Dalia Elradi FA, Nada Eisa E, Lamia A, Al-lahieb M, Shorog, Al-Otiby, Nada M, Merghani, Abdelelah Awad AG (2014) Int J Phys Sci 9:34–40
62. Shivakumar PS, Vidyasagar GM (2014) Int J Green Chem Bioprocess 4:1–5
63. Saikia D (2014) Int J Latest Res Sci Technol 3:132–135
64. Umesh Kumar P, Nayak PL (2012) World J Nano Sci Technol 1:10–25
65. Huang J, Li Q, Sun D, Lu Y, Su Y, Yang X, Wang H, Wang Y, Shao W, He N, Hong J, Chen C (2007) Nanotechnology 18:104–105
66. Narayanan KB, Sakthivel N (2008) Mater Lett 62:4588–4590
67. Ramezania N, Ehsanfara Z, Shamsab F, Aminc G, Shahverdid HR, Esfahanic HRM, Shamsaiea A, Bazazb RD, Shahverdi AR (2008) Z Naturforsch 63b:903–908
68. Raghunandan D, Bedre D, Mahesh S, Basavaraja SD, Balaji SY, Manjunath Venkataraman A (2011) J Nanopart Res 13:2021–2028
69. Balaprasad A (2010) E-J Chem 7:1334–1339
70. Anuj Mishra N, Bhadauria S, Mulayam Gaur S, Pasricha R, Kushwah SB (2010) Int J Green Nanotechnol Phys Chem 1:118–124
71. Thirumurugan A, Jiflin GJ, Rajagomathi G, Tomy NA, Ramachandran S, Jaiganesh R (2010) Int J Biol Technol 1:75–77
72. Singh PP, Chittaranjan B (2012) Int J Sci Res 2:1–4
73. Nellore J, Pauline PC, Amarnath K (2012) Dig J Nanomater Biostruct 7:123–133
74. Badole MR, Dighe VV (2012) Int J Drug Disco Herb Res 2:275–278
75. Aromal SA, Philip D (2012) Spectrochim Acta Part A Mol Biomol Spect 97:1–5
76. Laura Castro M, Blázquez L, González F, Jesús A (2010) Chem Eng J 164:92–97
77. Ratul Kumar D, Nayanmoni G, Utpal B (2011) Bioprocess Biosyst Eng 34:615–619
78. Daizy P (2010) Spectrochimica Acta Part A 77:807–810

79. Yi GC, Wang C, Park WI (2005) Semicond Sci Technol 20:22–34
80. Senthil TS, Muthukumarasamy N, Misook Kang (2014) Bull Korean Chem Soc 35:1050–1056
81. Nagajyothi PC, Minh An TN, Sreekanth TVM, Jae-il Lee, Dong Joo Lee, Lee KD (2013) Mater Lett 108:160–163
82. Salam HA, Sivaraj R, Venckatesh R (2014) Mat Lett 131:16–18
83. Senthilkumar SR, Sivakumar T (2014) Int J Pharm Pharm Sci 6:461–465
84. Vimalaa K, Sundarraj S, Paulpandi M, Vengatesan S, Kannan S (2014) Proc Biochem 49:160–172
85. Gnanasangeetha D, SaralaThambavani D (2013) Res J Mater Sci 1:1–8
86. Kumar B, Smita K, Cumbal L, Debut A (2014) Bioinorg Chem Appl Article ID 523869, 7 p
87. Bhumi G, Ratna Raju Y, Savithramma N (2014) Int J Drug Dev Res 6:97–104
88. Awwad MA, Albiss B, Ahmad L (2014) Adv Mater Lett 5:520–524
89. Gnanasangeetha D, Thambavani SD (2014) Int J Pharma Sci Res 5:2866–2873
90. Liny P, Divya T, Barasa Malakar, Nagaraj B, Krishnamurthy NB, Dinesh R (2012) Int J Pharma Biosci 3:439–446
91. Krishnamurthy N, Nagaraj B, Barasa Malakar, Liny P, Dinesh R (2012) Int J Pharma Biosci 3:212–221
92. Burygin GL (2009) Nanoscale Res Lett 4:794–801
93. Williams DN, Ehrman SH, Holoman TRP (2006) J Nanobiotechnol 4:1–8
94. Huang WC, Tsai PJ, Chen YC (2007) Nanomedicine 2:777–787
95. Gu H, Ho PL, Tong E, Wang L, Xu B (2003) Nano Lett 3:1261–1263
96. Rosemary MJ, MacLaren I, Pradeep T (2006) Langmuir 22:10125–10129
97. Grace NA, Pandian K (2007) Colloids Surf A Physicochem Eng Asp 297:63–70
98. Rai A, Prabhune A, Perry CC (2010) J Mater Chem 20:6789–6798
99. Choi O, Deng KK, Kim NJ, Ross L Jr, Surampalli RY, Hu Z (2008) Water Res 42: 3066–3074
100. Valodkar M, Rathore PS, Jadeja RN, Thounaojam M, Devkar RV, Thakore S (2012) J Hazard Mater 201:244–249
101. Chwalibog A, Sawosz E, Hotowy A, Szeliga J, Mitura S, Mitura K (2010) Int J Nanomed 5:1085–1094
102. Zawrah MF, Abd el-moez SI (2011) Life Sci 8:37–44
103. Kateryna Kon, Mahendra Rai (2013) J Comp Clin Path Res 2:160–174
104. Priya B, Satapathy M, Mukhopahayay A, Das P (2014) Bioresou Bioprocess 1:1–10
105. Sondi I, Salopek-Sondi B (2004) J Colloid Interf Sci 275:177–182
106. Kim JS, Kuk E, Yu KN, Kim JH, Park SJ, Lee HJ, Kim SH, Park YK, Park YH, Hwang CY, Kim YK, Lee YS, Jeong DH, Cho MH (2007) Nanomed Nanotech Biol Med 3:95–101
107. Murugan K, Senthilkumar B, Al-Sohaibani S (2014) Int J Nanomed 9:2431–2438
108. Raffin M, Hussain F, Bhatti TM, Akhter JI, Hameed A, Hasan MM (2008) J Mater Sci Technol 24:192–196
109. Kvitek L, Panacek A, Soukupova J, Kolar M, Vecerova R, Prucek R (2008) J Phys Chem C 112:5825–5834
110. Morones JR, Elechiguerra JL, Camacho A, Holt K, Kouri J, Ramirez JT (2005) Nanotechnology 16:1353–2346
111. Wang G, Shi C, Zhao N, Du X (2007) Mater Lett 61:3795–3797
112. Rai MK, Deshmukh SD, Ingle AP, Gade AK (2012) J Appl Microbiol 112:841–852
113. Pal S, Tak YK, Song JM (2007) Appl Environ Microbiol 73:1712–1720
114. Brayner R, Ferrari-Iliou R, Brivois N, Djediat S, Benedetti MF, Fievet F (2006) Nano Lett 6:866–870
115. Thill A, Zeyons O, Spalla O, Chauvat F, Rose J, Auffan M, Flank AM (2006) Environ Sci Technol 40:6151–6156
116. Reddy KM, Feris K, Bell J, Wingett DG, Hanley C (2007) Appl Phys Lett 90: 2139021–2139023

117. Zhang LL, Jiang YH, Ding YL, Povey M, York D (2007) J Nanopart Res 9:479–489
118. Jayaseelan C, Abdul Rahuman A, Vishnu Kirthi A, Marimuthu S, Santhoshkumar T, Bagavan A, Gaurav K, Karthik L, Bhaskara Rao KV (2012) Spectrocemica Acta Part A 90:78–84
119. Mariappan P, Krishnamoorthy K, Kadarkaraithangam J, Govindasamy M (2011) Nanotechnol Biol Med 7:184–192
120. Sawai JJ (2003) Microbiol Meth 54:177–182
121. Yamamoto O (2001) Int J Inorg Mater 3:643–646
122. Liu Y, He L, Mustapha A, Li H, Hu ZQ, Lin M (2009) J Appl Microbiol 107:1193–1201
123. Jin T, Sun D, Su JY, Zhang H, Sue HJ (2008) J Food Sci 74:M46–M52
124. El-Batal AI, Hashem AA, Abdelbaky NM (2013) Springerplus 23:129–142
125. Sreekanth TVM, Nagajyothi PC, Supraja N, Prasad TNVKV (2014) Appl Nano Sci DOI 10.1007/s13204-014-0354-x
126. Lokina S, Narayanan V (2013) Chem Sci Trans 2(S1):S105–S110
127. Kirubhan R, Alagumuthu G (2014) Int J Pharm 4:195–200
128. Rajasekhar Reddy G, Jayakumar C, Morais AB, Sreenivasn D, Gandhi NN (2012) Int J Green Chem Bioprocess 2:1–5
129. Jisha ER, Balamurugan G, Edison N, Selvakumar P, Rathiga R (2012) Int J Pharm Tech Res 4:1323–1331
130. Nagaraj B, Divya TK, Malakar B, Krishnamurthy NB, Dinesha R, Negrila CC, Ciobanu CS, Iconaru SL (2012) Dig J Nanomater Biostr 7:899–905
131. Mahitha B, Raju BDP, Madhavi T, Lakshmi CNDM, Sushma NJ (2013) Ind J Adv Chem Sci 1(2):94–98
132. Nagaraj B, Barasa M, Divya TK, Krishnamurthy NB, Liny P, Dinesh R (2012) Int J Res 4:144–150
133. Kirubha R, Alagumuthu G (2014) World J Pharm Sci 2(11):1469–1474
134. Sharma G, Rajgovind NDJ, Suresh PS, Joshi C (2014) J Microbial Biochem Technol 6:274–278
135. Prakash P, Gnaprakash R, Emmanuel R, Arokiyaraj M, Saravanan M (2013) Colloids Surf B Biointerf 108:255–259
136. Manjunath Hullikere M, Joshi CG, Peethambar SK (2014) Res J Pharma Biol Chem Sci 5:395–401
137. Sreekanth TVM, Nagajyothi PC, Supraja N, Prasad, TNVKV (2014) Appl Nanosci. doi:10.1007/s13204-014-0354-x
138. Smaranika D, Parida UK, Bindhani BK (2014) Int J Pharm Bio Sci 5:307–322
139. Awwad AM, Salem NM, Abdeen AO (2013) Int J Indust Chem 4:1–6
140. Mahitha B, Raju BDP, Dillip GR, Madhukar Reddy C, Mallikarjuna K, Manoj L, Priyanka S, Jayantha Rao K, John Sushma N (2011) Dig J Nanomater Biostr 6:135–142
141. Singh K, Panghal M, Kadyan S, Chaudhary U, Yadav JP (2014) J Nanobiotechnol 12:1–9
142. Shanmugavadivu M, Kuppusamy S, Ranjithkuma R (2014) AJADD 2:174–182
143. Natarajan RK, Nayagam AAJ, Gunagarajan S, Ekambaram MN, Manimaran A (2013) World Appl Sci J 23:1314–1321
144. Sangeetha G, Rajeshwari S, Rajendranb V (2012) Mater Int 22:693–700
145. Ramesh M, Anbuvannan M, Viruthagir G (2014) Spectrochimica Acta Part A Mol Biomol Spectros. doi:10.1016/j.saa.2014.09.105
146. Ayeshamariam A, Kashif M, Vidhya VS, Sankaracharyulu MGV, Swaminathan V, Bououdina M, Jayachandran M (2014) J Optoelect Biomed Mater 6:85–99

Chapter 5
Green Synthesis: Properties and Potential Applications in Nanomaterials and Biomass Nanocomposites

Ming-Guo Ma

Abstract Development of green processes for nanotechnology is of great importance for broadening and improving the industrial applications of nanomaterials and nanocomposites. This chapter focuses on the recent developments in green synthesis, its properties, and its potential applications in nanomaterials and biomass nanocomposites. Among the various green processes for nanotechnology, we pay more attention to the microwave-assisted method, which has been accepted as a promising green methodology in the synthesis of nanomaterials and nanocomposites. Undoubtedly, the microwave-assisted method conforms to the principles of green chemistry such as "*minimize the use of solvents and other auxiliary substances*" and "*minimize energy use*" due to its characteristics of reduced energy consumption, reduced pollution, shorter reaction time, and higher product yield.

In recent years, rapid progress has been made in the preparation of nanomaterials and nanocomposites by a microwave-assisted method. In this chapter, the green microwave-assisted synthesis of various nanomaterials including metal nanomaterials, metal oxides nanomaterials, metal chalcogenides nanomaterials, bio-nanomaterials, nanocomposites, and biomass nanocomposites is reviewed. Some typical examples by our research group and by other groups are introduced, which would favor the understanding of the green microwave processes for nanotechnology. Finally, we propose the future perspectives of this green methodology for the fabrication of nanomaterials and nanocomposites.

Keywords Green • Nanomaterials • Nanocomposites • Microwave • Biomass

M.-G. Ma (✉)
Engineering Research Center of Forestry Biomass Materials and Bioenergy, Beijing Key Laboratory of Lignocellulosic Chemistry, College of Materials Science and Technology, Beijing Forestry University, Beijing 100083, People's Republic of China
e-mail: mg_ma@bjfu.edu.cn

V.A. Basiuk, E.V. Basiuk (eds.), *Green Processes for Nanotechnology*,
DOI 10.1007/978-3-319-15461-9_5

5.1 Introduction

In general, green production refers to realizing reasonable utilization of resources and reducing harm to the environment and humans, which includes the main ways of comprehensive utilization of resources and waste, green production process, and the improvement and development of green technology. Recently, green processes for nanotechnology have been receiving more and more attention, which has favored environmental protection and sustainable economic development. Various green processes for nanotechnology have been reported such as hydrothermal/solvothermal method, sol–gel method, microwave-assisted method, and ultrasound agitation method. Among these reported green methods, microwave-assisted method has characteristics of reduced energy consumption, reduced pollution, shorter reaction time, and higher product yield, which has been widely accepted as a promising greener methodology for nanotechnology. In early 2003, a review on the application of microwave chemistry appeared in *Nature* [1]. In our previous review paper, we described the recent developments in the synthesis of nanomaterials by means of the microwave-assisted ionic-liquid method [2]. This review covered the research work done on the microwave synthesis of nanomaterials in ionic liquids. We discussed most typical examples including noble metals, metal oxides, complex metal oxides, metal sulfides, and other nanomaterials. More recently, Zhu and Chen reviewed the microwave-assisted preparation of inorganic nanostructures in liquid phase in *Chemical Reviews* [3]. They reviewed most inorganic nanostructured materials including metals, semimetals, alloys, metal oxides, metal sulfides, metal selenides, metal tellurides, calcium-based salts and other oxysalts, inorganic–inorganic nanocomposites, and inorganic–organic nanocomposites, in various solvents including water, polyols, ionic liquids, and mixed solvents prepared by microwave heating. This review also compared the differences between microwave heating and conventional heating in the formation of inorganic nanostructures in liquid phase and suggested the future prospects and challenges for microwave-assisted preparation of inorganic nanostructures in liquid phase. This chapter highlights the recent progress of the nanomaterials and nanocomposites especially biomass nanocomposites via the microwave-assisted method. More importantly, some typical examples are introduced in our research group and by other groups. We believe that this chapter contributes an interesting content emphasizing the topic of the book "*Green Processes for Nanotechnology*: *From Inorganic to Bioinspired Nanomaterials*".

5.2 Green Synthesis, Properties, and Potential Applications of Nanomaterials

5.2.1 Microwave-Assisted Synthesis of Metal Nanomaterials

The metal nanomaterials have been the topic of intensive research due to their unique properties and promising applications. It is reported that green and rapid microwave-assisted method is used for the synthesis of various transition-metal nanomaterials

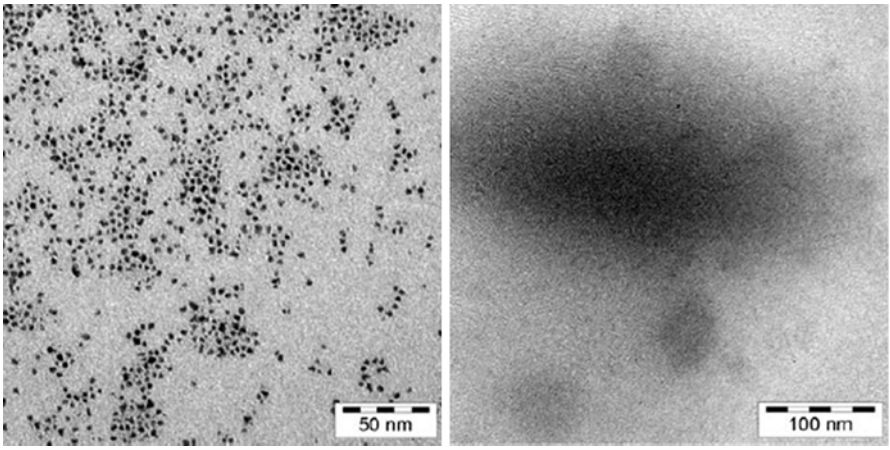

Fig. 5.1 Re-nanoparticles from $[Re_2(CO)_{10}]$ by microwave method (*left*) and photolytic decomposition (*right*). From ref. [4]. Reprinted with permission from Wiley-VCH

including chromium, molybdenum, tungsten, manganese, rhenium, ruthenium, osmium, cobalt, rhodium, and iridium nanoparticles with a very small (0.8–5 nm) and uniform size under an argon atmosphere from their metal–carbonyl precursors [M*x*(CO)*y*] in the ionic liquid (IL, 1-butyl-3-methylimidazolium tetrafluoroborate, [Bmim][BF_4]) for 3 min [4]. Experimental results revealed ruthenium, rhodium, or iridium nanoparticle/IL dispersions as highly active and easily recyclable catalysts for biphasic liquid–liquid hydrogenation of cyclohexene to cyclohexane with activities of up to 522 (mol product) $(\text{mol Ru})^{-1}\,\text{h}^{-1}$ and 884 (mol product) $(\text{mol Rh})^{-1}\,\text{h}^{-1}$, which gave almost quantitative conversion within 2 h at 10 bar H_2 and 90 °C. Especially, in comparison to UV-photolytic (1,000 W, 15 min) or conventional thermal decomposition (180–250 °C, 6–12 h) method, metal nanomaterials with smaller size and better dispersion were obtained by microwave method (Fig. 5.1). However, the only fly in the ointment is that [Bmim][BF_4] is a toxic solvent. Choosing nontoxic IL favors the green synthesis of transition-metal nanomaterials.

One-dimensional rod-like nanostructures composed of Rh(0) and Rh(I) were synthesized on the glass surface by microwave-assisted method using cetyltrimethylammonium bromide (CTAB) as a reducing agent as well as soft template of reduction of Rh(III) ions from boiling aqueous solution only in the 1990s [5]. More importantly, it obtained a high yield of gram quantity sample. pH was reported to have a remarkable influence on the alteration of aspect ratio and sharpening of the edges of Rh nanorods. It was reported that interesting shape transformation from nanorods and nanowires to octahedral or spherical particles was observed categorically by deploying a redox reaction in a selective redox environment. The authors suggested that all the oxide layer, Rh(I), and the surface of redox environment, carbon-coated Cu grid surface, were the main factors for rod-to-octahedral shape transformation; the oxidized rhodium species got adsorbed on (100) facets of the nanocubes and were reduced during the oxidation of metallic Cu present in the grids; Rh nanorods were transformed into small spherical particles even in the solution phase and were

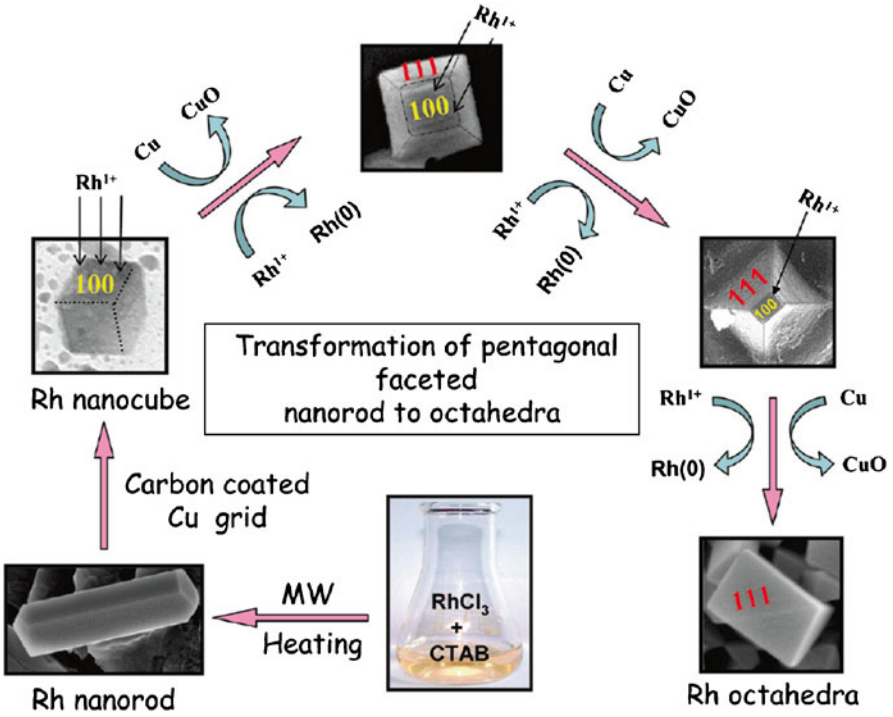

Fig. 5.2 Mechanistic pathway showing the ex situ transformation of pentagonal faceted nanorod to octahedra. From ref. [5]. Reprinted with permission from ACS

deposited on the Cu wire surfaces (Fig. 5.2). Cyclic voltammetric measurement indicated that Rh nanonetwork and spherical showed almost the behavior of the glassy carbon electrode and as-prepared Rh nanorods displayed high current generation at lower potential, compared to the blank glassy carbon electrode, which could be used as a potential candidate for oxygen evolution.

A microwave-assisted method was used for the rapid synthesis of uniform and ultralong chemically stable single-crystalline tellurium (Te) nanowires in aqueous solution [6]. Te nanowires were observed with high aspect ratios, an average diameter of 20 nm, and lengths up to tens of micrometers (Fig. 5.3a). The dispersion of Te nanowires in water is deep blue (the inset of Fig. 5.3a). The selected area electron diffraction (SAED) pattern of a typical nanowire revealed it to be single crystalline (inset in Fig. 5.3b). From the HR-TEM, the lattice spacing was ca. 5.9 Å, 4.0 Å, and 3.2 Å, corresponding to the lattice spacings of the (001), (100), and (101) planes for hexagonal tellurium, respectively, suggesting that the Te nanowires grow along [001] direction. It was found that polyvinylpyrrolidone (PVP), pH value, reaction time, and a suitable surfactant all were key parameters for the formation of high-quality Te nanowires with a high aspect ratio. The as-prepared hydrophilic Te nanowires were reported to display a broadened luminescent emission from short-wave ultraviolet to visible region under the vacuum-ultraviolet (VUV) excitation at

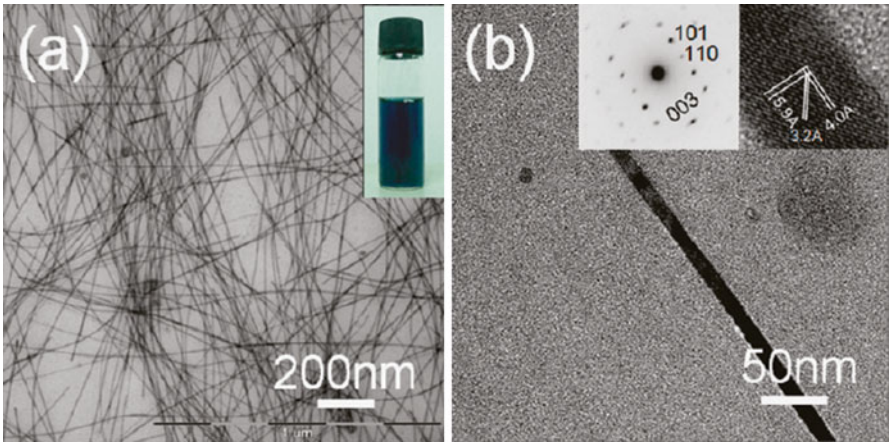

Fig. 5.3 TEM images of Te nanowires. (**a**) TEM image of the Te nanowires. (**b**) TEM image of a single nanowire. The *inset* of (**a**) displays the digital photograph of Te nanowires and *inset* of (**b**) shows the corresponding HR-TEM and the corresponding SAED pattern obtained from the single nanowire. The electron beam was focused along [010] axis. The sample was prepared from 2 mL solution by microwave heating at 150 °C for 15 min, which was taken from a 38 mL mother solution made of 33 mL of deionized water, 1.0 g of PVP, 0.0922 g of Na_2TeO_3, 3.33 mL of aqueous ammonia, and 1.67 mL of hydrazine hydrate. From ref. [6]. Reprinted with permission from ACS

room temperature, and they were more easily oxidized by storing in water than that synthesized by hydrothermal process.

Microwave radiation method was reported in the synthesis of Ag nanoparticles in aqueous media by reduction of the diaminesilver(I) complex, $[Ag(NH_3)_2]^+$ with carboxymethylcellulose (CMC) in both batch-type and continuous-flow reactor systems [7]. It was reported that Ag nanoparticles with sizes spanning the range of 1–2 nm and 1.4–3.6 nm (average size ~3 nm) were obtained using 390-Watt microwaves (MW-390 W/Cool protocol) and 170-Watt microwaves (no cooling; MW-170 W protocol), respectively. The microwave radiation method is compared to a conventional heating method in detail. Experimental results revealed clear differences in the heating mechanisms between conventional heating and microwave heating by the dielectric characteristics of the aqueous media and the Ag colloidal sol in the reactor. After a 4-min and 5-min heating time, the UV-visible spectra revealed an LSPR band at 417 nm and 424 nm for microwave method and 413 nm and 421 nm for oil bath heating method, respectively (Fig. 5.4a, b). A fairly monodispersed particle size distribution from microwave heating (1.8–3.6 nm; average size ~3 nm) and a broader size distribution (1–5 nm) from conventional heating (Fig. 5.4c, d) were observed. Light scattering measurements indicated a size distribution in the range 1–2.3 nm by microwave heating (Fig. 5.4e) and polydispersed nanoparticles mostly in the 3–5.7 nm range by conventional heating (Fig. 5.4f).

A rapid microwave-assisted green approach was developed for highly fluorescent Ag nanoclusters with favorable monodispersity and good stability in aqueous solution as a novel fluorescence probe for Cr^{3+} sensing with high sensitivity and

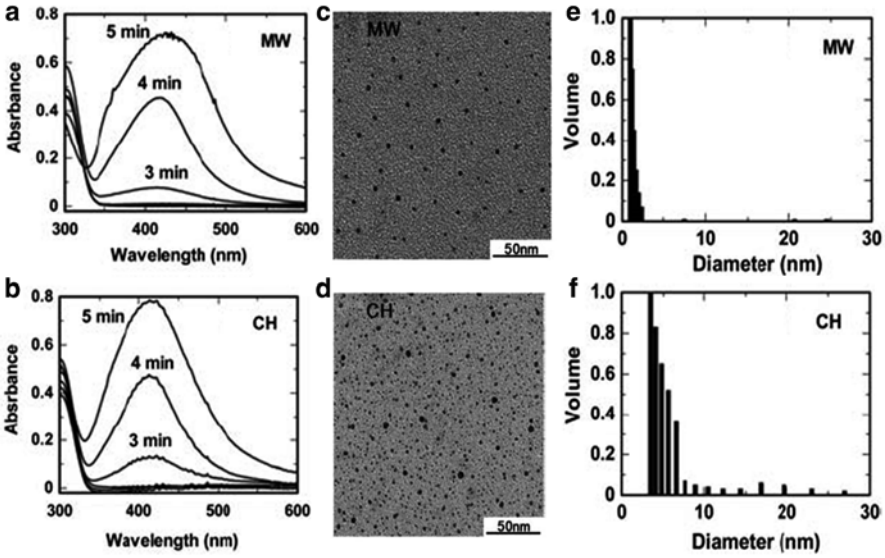

Fig. 5.4 UV-visible absorption spectra, TEM images and particle size distribution with light scattering of the silver nanoparticles produced by microwave and oil bath heating methods (microwave heating, **a**, **c**, and **e**; oil bath heating, **b**, **d**, and **f**). Note that the 5-min UV-visible absorption bands of the samples were obtained after a fourfold dilution of the respective colloidal sols. Concentrations: CMC, 0.05 % w/v and diaminesilver(I) aqueous solution, 60 mM. From ref. [7]. Reprinted with permission from RSC

excellent selectivity [8], which exhibited bright and photostable emission excited by visible light. Ag nanoclusters were known to have widespread applications in bioimaging, chemical, and single-molecule studies. Microwave irradiation was used for the synthesis of an average size of 1.6 nm for water-soluble fluorescent Ag nanoclusters in aqueous solution with red fluorescence emission around 608 nm and a characteristic absorption peak at about 508 nm [9].

A comparison of initiation methods (thermal, microwave assisted, hard ultraviolet light, and sonication) in relation to the size, monodispersity, and shape of nearly monodisperse Au nanoparticles formed by the Turkevich method using a constant concentration of auric acid (0.28 mM) and varying concentrations of tri-sodium citrate (0–3.88 mM) has been demonstrated [10]. Au nanoparticles have the average size of 11.0–11.9 nm in thermal reactions, 16.9–18.0 nm in sonolysis reactions, 11.3–17.2 nm in microwave-assisted reactions, and 8.0–10.9 nm in hard ultraviolet light initiated reactions. Monodisperse Au nanoparticle colloids with significantly varying average size (8.0–18.0 nm) were obtained by simply changing the initiation method.

A green microwave-assisted method has been developed for the preparation of fluorescent bovine serum albumin (BSA)-stabilized and HAS protected Au nanoclusters with strong red emission and excellent stability in both solution and solid forms by employing BSA as a reducing and capping agent within a very short time

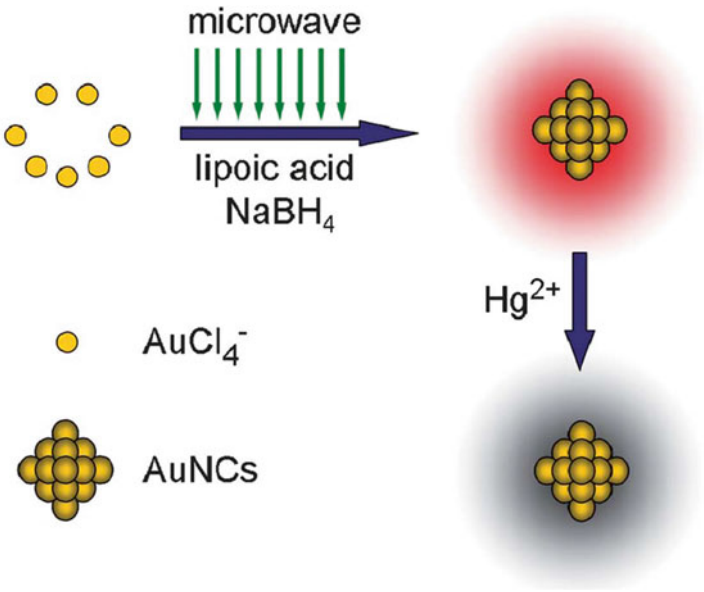

Scheme 5.1 Schematic illustration of microwave-assisted synthesis of fluorescent AuNCs and their fluorescence quenching upon interaction with Hg^{2+} ions. From ref. [13]. Reprinted with permission from RSC

(several minutes) [11], which has applications in fluorescent biosensors, bioanalysis, and medicine fields. A one-step green microwave-assisted method is also used for the synthesis of highly stable BSA-protected small Au nanoclusters from a BSA–$HAuCl_4$ aqueous solution as a fluorescence enhanced sensor for detection of silver (I) ions with high selectivity and sensitivity [12].

A green microwave-assisted strategy was also introduced for synthesizing dihydrolipoic acid (DHLA) capped fluorescent Au nanoclusters [13], which possessed ultrasmall size, good photophysical property, low cytotoxicity, and good cell membrane permeability. Microwave irradiation was found to enhance the fluorescence quantum yield of Au nanoclusters by about fivefold and shortened the reaction time from hours to several minutes (Scheme 5.1). The as-prepared DHLA-Au nanoclusters were capable of sensing Hg^{2+} through the specific interaction between Hg^{2+} and Au^{+} on the surface of Au nanoclusters.

A rapid microwave-assisted green method was introduced for the preparation of metal Ag, Au, Pt, and Pd nanoparticles in aqueous solutions using beet juice as both a reducing and a capping reagent [14]. The as-prepared Ag nanoparticles prepared by beet juice were found to exhibit higher catalytic activity and durability than those prepared using $NaBH_4$ for the reduction of 4-nitrophenol to 4-aminophenol. Before the reaction only the peak of 4-nitrophenol at 400 nm was observed and then the peak of 4-nitrophenol disappeared, and a new peak of 4-aminophenol appeared at 290 nm after the addition of Ag nanoparticles (Fig. 5.5). The as-prepared Ag

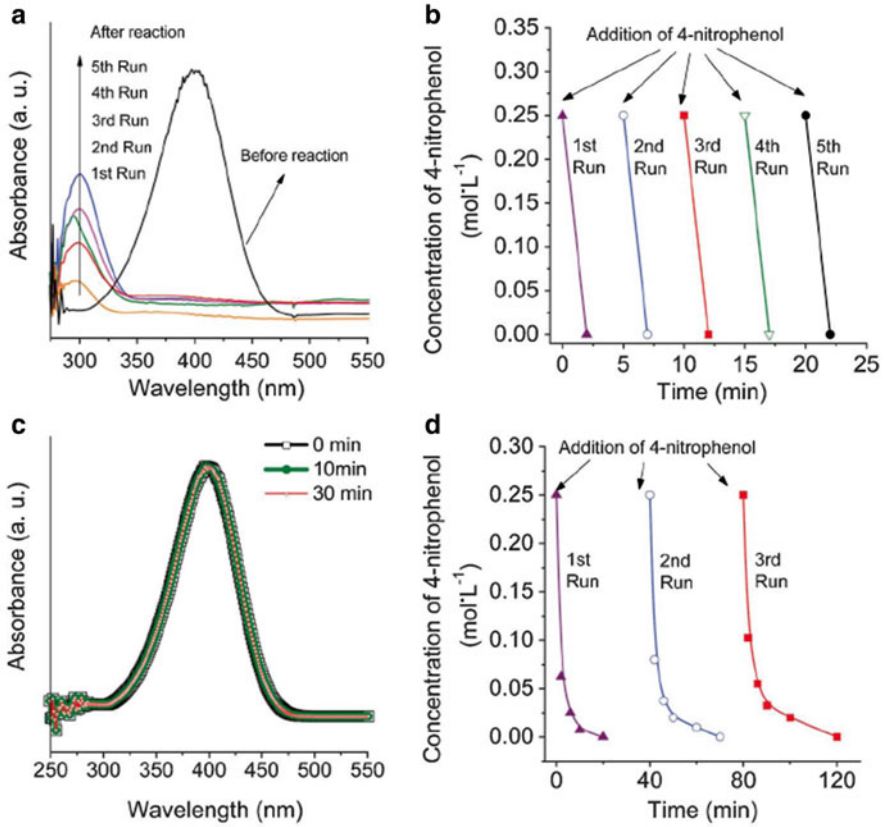

Fig. 5.5 Catalytic reduction of 4-nitrophenol: (**a**) UV–Vis spectra of solutions of reaction mixture in the presence of Ag nanoparticles prepared by beet juice; (**b**) catalytic activity and recyclability of Ag nanoparticles prepared by beet juice; (**c**) UV–Vis spectra of solutions without catalyst; (**d**) catalytic activity and recyclability of Ag nanoparticles prepared by $NaBH_4$. From ref. [14]. Reprinted with permission from RSC

nanoparticles quickly exhibited excellent stable catalytic reduction efficiency of 100 % within 2 min after every addition even after five runs. No change was observed for absorption peak of 4-nitrophenol even after 30 min without catalyst (Fig. 5.5c). The complete conversion of 4-nitrophenol needed 20 min for Ag sample prepared by $NaBH_4$ (Fig. 5.5d).

A microwave-assisted method was also developed for highly efficient and large scale synthesizing uniform single-crystal Cu nanowires using ascorbic acid in hexadecylamine (HDA) [15]. Cu nanowires have an average diameter of 50 ± 10 nm and lengths of longer than 10 mm (Fig. 5.6). It was observed that the fringes had lattice spacings of 2.12 Å, 2.58 Å, and 1.85 Å, corresponding to the {111}, {110}, and {200} plane, respectively, indicating the growth direction of <1-10> (Fig. 5.6d). The as-obtained Cu nanowires were found to show outstanding conductivity, comparable with electrospun copper nanofibers.

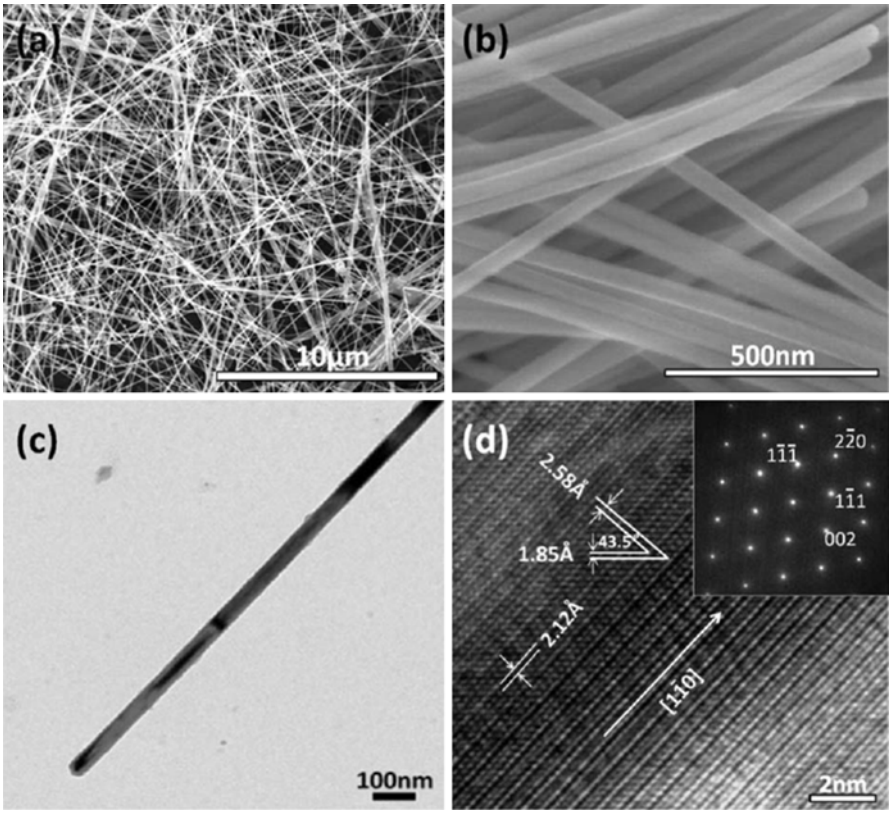

Fig. 5.6 Structural and morphological characterization of Cu nanowires: (**a**) SEM image; (**b**) magnified SEM image; (**c**) TEM image; and (**d**) high resolution TEM image. The *inset* in (**d**) shows an SAED image of single Cu nanowire in (**c**). From ref. [15]. Reprinted with permission from RSC

5.2.2 Microwave-Assisted Synthesis of Metal Oxides Nanomaterials

Considerable progress has been made in green microwave-assisted synthesis of various metal oxides nanomaterials. A microwave-assisted approach was used for the synthesis of silver indium tungsten oxide $AgIn(WO_4)_2$ mesocrystals with high hierarchical structures [16], which displayed high and selective photocatalytic activity for the degradation of different organic dyes under UV and visible light irradiation. The $AgIn(WO_4)_2$ mesocrystals showed a pure monoclinic structure (JCPDS card No. 77-2098) (Fig. 5.7d) and displayed the high hierarchy of the caterpillar-like architectures uniform with diameters of 350–500 nm at the middle part and lengths of 800–1,000 nm (Fig. 5.7a–c). It was reported that pH played an important role in the phase formation and shape evolution process.

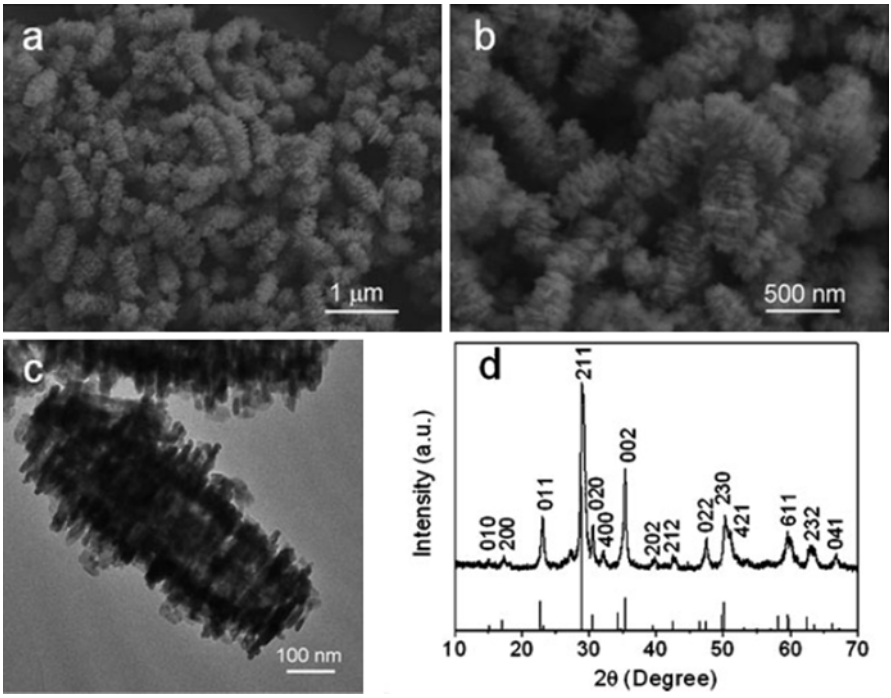

Fig. 5.7 (**a**) and (**b**) SEM images of $AgIn(WO_4)_2$ mesocrystals prepared by microwave-assisted synthesis at 180 °C for 20 min. (**c**) TEM image of individual caterpillar-like particle. (**d**) XRD pattern of the $AgIn(WO_4)_2$ mesocrystals. From ref. [16]. Reprinted with permission from RSC

Highly crystalline SnO_2 quantum dots with a narrow size distribution (4.27 ± 0.67 nm) was achieved by microwave-assisted decomposition of $Sn(OtBu)_4$ in IL [17], which showed typical semiconducting I–V behaviors and gas sensing properties as ink-jet printing nano-bridges between gold electrodes on polycarbonate and on silicon chip as well.

A microwave-assisted hydrothermal technique is presented to prepare cryptomelane-type manganese oxide octahedral molecular sieves for 10 s [18]. Reaction time and temperature are found to determine the formation conditions of manganese oxide octahedral molecular sieves. Amorphous manganese oxide below 80 °C and crystalline phase manganese oxide octahedral molecular sieves at 100 °C or above were obtained. Efficient microwave-assisted hydrothermal synthesis of CuO sea urchin-like architectures was also reported via a mesoscale self-assembly in water [19]. The tenorite phase of CuO with amonoclinic structure (JCPDS 48-1548; Fig. 5.8a) was found. As-obtained CuO was composed of urchin-like architectures with diameters of around 2.2 mm (Fig. 5.8b). The bright diffraction points corresponding SAED pattern can be indexed by the monoclinic structure of CuO resultant to the diffraction of (110), (11-2), and (00-2) planes (Fig. 5.8c). HR-TEM image indicated the same crystallographic orientation (like a single crystal) (Fig. 5.8d).

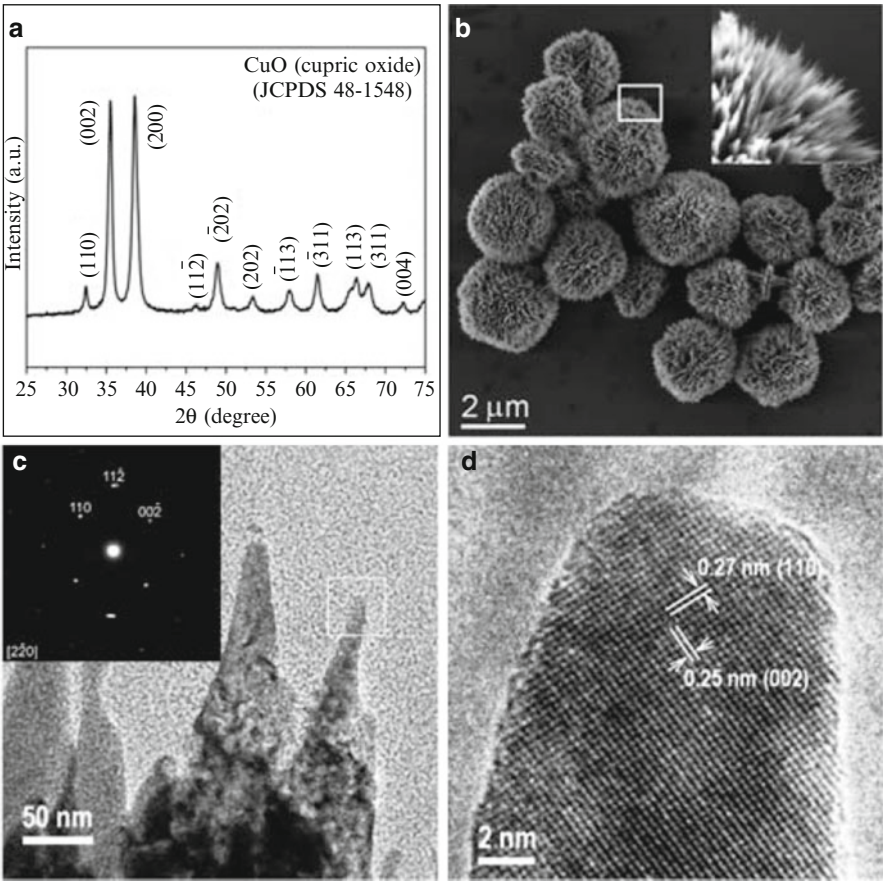

Fig. 5.8 (**a**) Powder XRD pattern recorded for CuO synthesized by microwave-assisted hydrothermal method in 15 min, and (**b**) FE-SEM image, (**c**) TEM image, *inset* a SAD pattern, and (**d**) HR-TEM image of a single plate of the CuO sea urchin-like microcrystal. From ref. [19]. Reprinted with permission from RSC

The interfringe distance was found to be 0.27 nm for plane (110) and 0.25 nm for plane (002), indicating that the [11-2] direction is the bisector of the triangle.

Green microwave-assisted hydrothermal method was used for the synthesis of a self-assembled photocatalytically active rutile TiO_2 mesocrystals assembled with ultralong nanowires using $TiCl_3$ at 200 °C for only 1 min [20]. TiO_2 mesocrystals have the BET specific surface area of 16 $m^2\ g^{-1}$ and exhibit an obvious red-shift of 0.2 eV with aspect to that of pure rutile TiO_2, ascribing to the high aspect ratio of rutile nanowires. The mesocrystals show excellent photocatalytic activity for NO removal in air and the activity is well maintained after three cycles and gold modification on the rutile TiO_2 results in a 50 % improvement in the photocatalytic performance. The TiO_2 was assigned to a pure tetragonal rutile phase with high purity

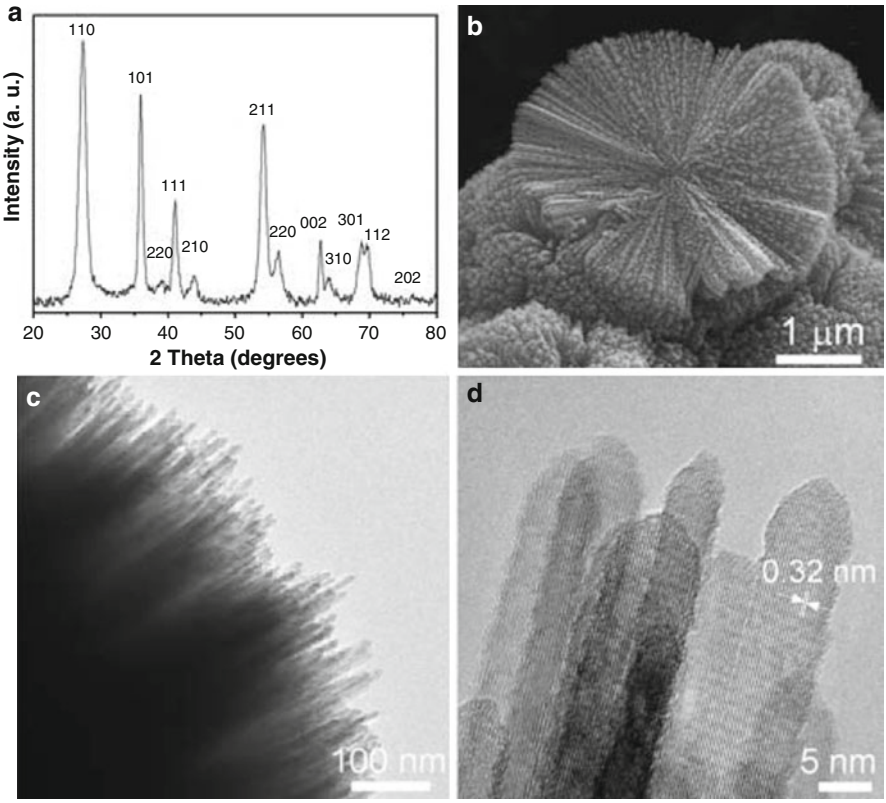

Fig. 5.9 XRD pattern (**a**), SEM (**b**), TEM (**c**) and HR-TEM (**d**) image of the self-assembled rutile TiO_2 by microwave heating $TiCl_3$ at 200 °C for 1 min suggest that the mesocrystals are promising photocatalyst for solar driven applications. From ref. [20]. Reprinted with permission from RSC

and good crystallinity (JCPDS card, 21-1276, Fig. 5.9a). It was observed that the 2 mm nanowire arrays grow radially from a cross section of a hemisphere (Fig. 5.9b). The superstructure is composed of individual nanowires (Fig. 5.9c). The HR-TEM image (Fig. 5.9d) indicated the growth direction of the nanowires along the (001) direction and the periodic fringe spacing of ~0.32 nm corresponding to the interplanar spacing between the (110) plane.

A convenient microwave-hydrothermal synthesis of nanostructured Cu^{2+}-substituted $ZnGa_2O_4$ spinels was reported [21]. Moreover, hexagonal WO_3 nanowires with high aspect ratio of 625 and specific surface area of 139 $m^2\ g^{-1}$ were prepared for the first time by a microwave-assisted hydrothermal method at 150 °C for 3 h in a solution containing $(NH_4)_2SO_4$ as a capping reagent and Na_2WO_4 as a starting material [22]. WO_3 nanowires had a diameter of 5–10 nm and lengths of up to several micrometers. WO_3 was found to have excellent electrocatalytic activity for hydrogen evolution reaction with high activity and stability in water by cyclic voltammetry and linear sweep voltammetry.

Vanadium pentoxide (V_2O_5) nanomaterials with excellent catalytic activities were prepared by a facile microwave-assisted refluxing reaction of $VOSO_4$ and $(NH_4)_2S_2O_8$ solutions under atmospheric pressure at 100 °C for 1 h under atmospheric pressure [23]. The as-synthesized V_2O_5 nanomaterials were found to display excellent catalytic performance for the oxidative cyanation of *N*,*N*-dimethylaniline to *N*-methyl-*N*-phenylcyanamide. The conversion of *N*,*N*-dimethylaniline to *N*-methyl-*N*-phenylcyanamide was found to increase with an increase in the amount of V_2O_5 catalyst.

Microwave-assisted heating was also reported to prepare unique lamellar sodium/potassium iron oxide nanosheets nanomaterials with unique architectures and multifunctionalities, ferromagnetic properties and electrochemical properties consisting of two-dimensional iron oxide building blocks using the suspension of iron(II) sulfate, sodium thiosulfate, and sodium/potassium hydroxide within 5 min [24]. $Na_{2.4}Fe_{10.99}O_{16.03}$ nanosheets were assembled from thin nanosheets into a three-dimensional flower-like architecture with an edge length of more than 500 nm in both dimensions (Fig. 5.10a). HR-TEM image indicated some edge and screw dislocations in nanosheets (Fig. 5.10e, f), and the fringe spacings of about 4.1 for the (015) plane and 4.4 Å for the (104) plane (Fig. 5.10).

The preparation of flower-like Bi_2WO_6 with a good thermal stability was reported via a simple, rapid, microwave-assisted solution phase process [25]. The time-dependent experiments were found to show an Ostwald ripening mechanism in the crystal growth process. The as-prepared Bi_2WO_6 was reported to have excellent photocatalytic activities for the degradation of Rhodamine B (RhB) under visible light irradiation.

Microwave-assisted solution-phase approach was applied for the preparation of monodisperse erythrocyte-like $Cd_2Ge_2O_6$ superstructures by employing $Cd(Ac)_2{\cdot}2H_2O$ and GeO_2 as the reactants in the presence of hydrazine monohydrate [26]. Monoclinic phase $Cd_2Ge_2O_6$ erythrocyte-like microstructures were found to have a relatively good dispersion and uniform diameters of ~8 mm (Fig. 5.11a) and be constructed by abundant single crystalline nanoneedles (Fig. 5.11b, c). HR-TEM image displayed the lattice fringes of single crystalline nature and the neighboring planes correspond to the (1-10) and (001) plane of $Cd_2Ge_2O_6$ (Fig. 5.11d). Experimental results discovered that $Cd_2Ge_2O_6$ had the absorption edge of 318 nm and a band gap of ~3.91 eV.

A rapid and facile microwave-assisted route was developed for the synthesis of rhombic dodecahedral Fe_3O_4 nanocrystals for the first time in the presence of ILs at temperatures as low as 90 °C within 15 min [27]. The magnetic study reveals that the T_B of the Fe_3O_4 nanocrystals is found to be at 120 K, and the saturation magnetization is 86 emu g^{-1} at room temperature. Furthermore, it was observed that the rhombic dodecahedral Fe_3O_4 nanocrystals bound with 12 high-energy {110} facets probably lead to future prospects toward their potential applications such as conspicuous catalytic activity.

Microwave-assisted hydrothermal synthesis was used to synthesize titanium–tin oxide solid solutions from a solution containing $TiCl_3$ and $SnCl_4$ [28]. Single-phase rutile-type $TixSn_{1-x}O_2$ solid solutions are achieved by annealing in air.

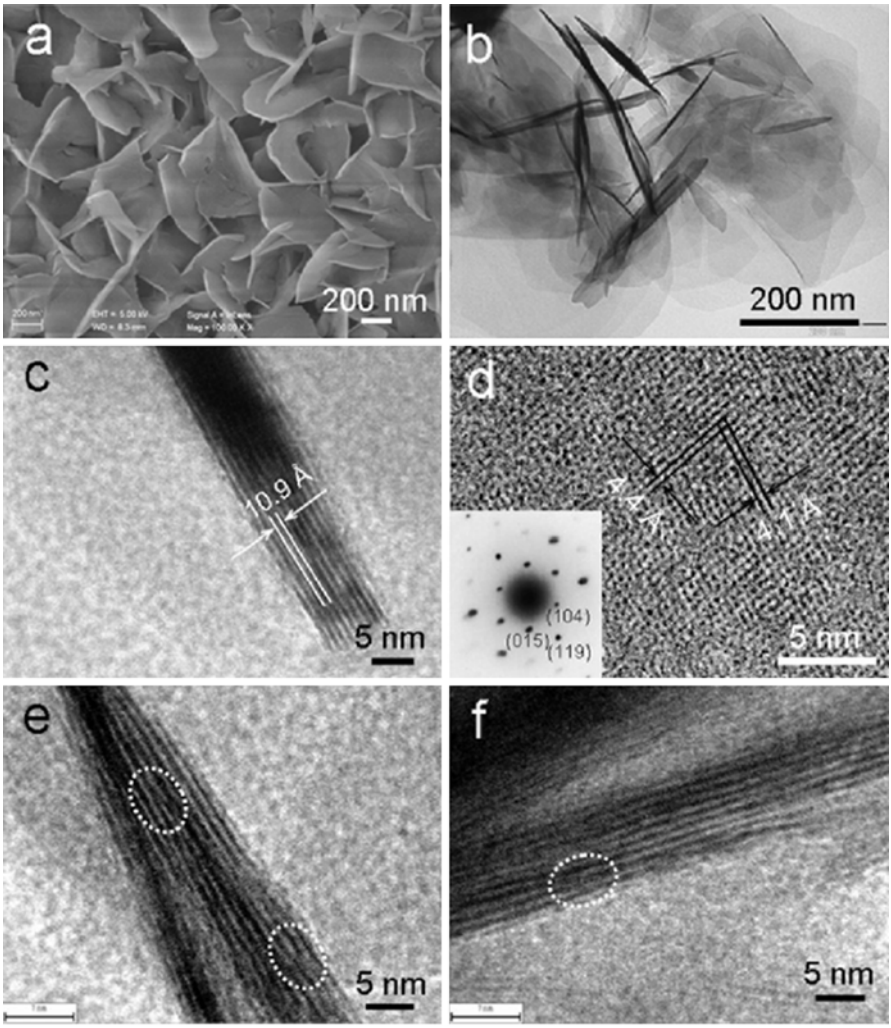

Fig. 5.10 (**a**) SEM image and (**b**) TEM image of the as-prepared $Na_{2.4}Fe_{10.99}O_{16.03}$ nanosheets via microwave-assisted synthesis at 180 °C for 5 min. HRTEM images of (**c**) a vertical and (**d**) a planar $Na_{2.4}Fe_{10.99}O_{16.03}$ nanosheet (*inset* is the SAED pattern). (**e**) and (**f**) HRTEM images of different vertical $Na_{2.4}Fe_{10.99}O_{16.03}$ nanosheets. Dislocations in the layered structures are marked by the *dashed ellipses*. From ref. [24]. Reprinted with permission from ACS

Co_3O_4 nanowires could be synthesized in conventional reflux and microwave-assisted methods under homogeneous precipitation conditions [29]. Co_3O_4 with randomly distributed thin nanowires were obtained by the conventional reflux method and higher-dimensional and arranged nanowires by the microwave reflux method. The lower-dimensional nanowires were more ferromagnetic than the higher-dimensional Co_3O_4 nanowires. Co_3O_4 shows better high rate cyclic stability due to its more rigid orientated nanowire structure using the microwave-assisted method.

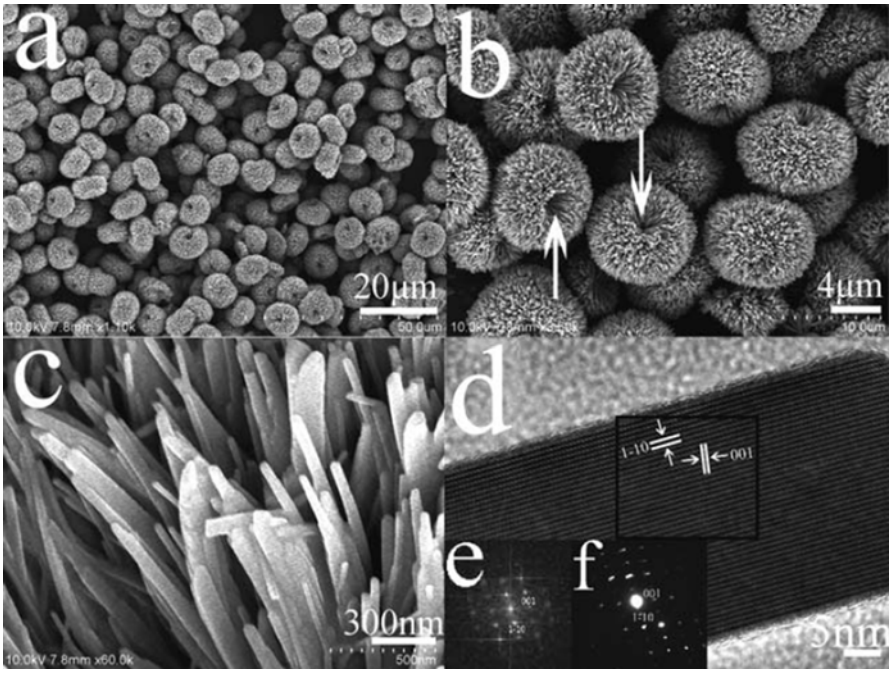

Fig. 5.11 (**a**–**c**) SEM images, (**d**) HR-TEM image, (**e**) the corresponding fast Fourier transformation image and (**f**) the SAED pattern of the as prepared $Cd_2Ge_2O_6$ erythrocyte-like superstructures (The FFT and SAED images were taken from the *marked area* in Fig. 5.3d). From ref. [26]. Reprinted with permission from RSC

α-Fe_2O_3 nanomaterials with a surface area of around 173.0 $m^2\ g^{-1}$ was synthesized by a microwave-assisted hydrothermal reaction of $Fe(NO_3)_3$ and urea at 120 °C for 30 min [30]. α-Fe_2O_3 nanomaterials were reported to display excellent catalytic performance for the oxidation of CO and 2-propanol to CO_2 and adsorption performance for the removal of As(III) of 51.8 mg g^{-1} at room temperature in water treatment. Magnetic nanorods with aspect ratio 3.2 were prepared in water by a simple and fast microwave-assisted reduction using akaganeite β-FeOOH nanorods and hydrazine as precursors and redactor only in 2 min [31].

$Li_4Ti_5O_{12}$ microspheres composed of nanoflakes were rapid synthesized within 1 h by a combination of a microwave-assisted hydrothermal method and a microwave post-annealing process [32]. The electrode using CMC as binder had better high-rate capability, much lower charge transfer resistance, lower apparent activation energy, and lower apparent diffusion activation energy than the one with polyvinylidene fluoride binder. Unique porous ZnO polygonal nanoflakes with excellent NO_2 sensing performances were also synthesized by the microwave hydrothermal method with a subsequent annealing process [33].

Single-crystal α-MnO_2 nanotubes were synthesized by microwave-assisted hydrothermal of potassium permanganate in the presence of hydrochloric acid [34]. The as-synthesized MnO_2 nanostructures are reported to be incorporated in air cathodes

of lithium-air batteries as electrocatalysts for the oxygen reduction and evolution reactions. The electrodes made of single-crystalline α-MnO_2 nanotubes were found to exhibit much better stability than those made of α-MnO_2 nanowires and δ-MnO_2 nanosheet-based microflowers in both charge and discharge processes.

CeO_2 nanoparticles were synthesized by a microwave-assisted hydrothermal method under different synthesis temperatures [35]. The synthesis temperature was found to effect morphology of the samples. Spherical particles of about 5 nm at 80 °C, a mix of spherical and rod-like nanoparticles at 120 °C, nanorods with 10 nm average diameter and 70 nm length at 160 °C were obtained.

Rod-like $FeWO_4$ nanocrystals with wolframite-type monoclinic structures were carried out by the microwave hydrothermal method at 170 °C for 45 min [36]. $FeWO_4$ nanocrystals prepared with polyethylene glycol-200 have a partial preferential orientation in the (011) plane in relation to other nanocrystals prepared with sodium bis(2-ethylhexyl)sulfosuccinate and water. Experimental results show that nanocrystals grow by self-assembly, an oriented attachment process and the aggregation of small nanocrystals with a further growth of rod-like $FeWO_4$ crystals. PL properties of these nanocrystals are found to be dependent on distortions in octahedral [FeO_6]/[WO_6] clusters and partial preferential orientation in the (011) crystallographic plane of these nanocrystals.

Preparation of lanthanide (Eu^{3+}, Tb^{3+}, Sm^{3+}, and Dy^{3+}) phosphors luminescent materials (red, green, orange-red, and blue-yellow) one-dimensional nanorods with diameters of 10–20 nm and lengths of up to 200 nm were achieved at low temperature (70 °C) in 45 min using simultaneous supersonic and microwave irradiation [37].

Micronano self-assembled $NaY(WO_4)_2$ hierarchical dumbbells were synthesized by a microwave-assisted hydrothermal approach, followed by a heat treatment [38]. It was found that the amount of trisodium citrate plays a crucial role in the assembly process of the precursor. Yb^{3+}/Er^{3+}, Yb^{3+}/Tm^{3+}, and Yb^{3+}/Ho^{3+} codoped $NaY(WO_4)_2$ were found to exhibit strong green, blue, and yellow emissions under 980 nm excitation, respectively. The luminescence colors of $Yb^{3+}/Ho^{3+}/Tm^{3+}$ tridoped $NaY(WO_4)_2$ can be tuned from blue through white to yellow by simply adjusting the doping concentrations of the activator ions under 980 nm excitation.

A fast and facile microwave-assisted hydrothermal process is reported for the preparation of perovskite $NaTaO_3$ nanocrystals with Ta_2O_5 and NaOH as starting materials [39], which showed photocatalytic activity for overall water splitting more than two times greater than those prepared under conventional hydrothermal conditions.

Visible light-activated $SnNb_2O_6$ nanosheets with a thickness of 1–4 nm versus several hundred nanometres in lateral size were prepared by a microwave-assisted template-free hydrothermal method without exfoliation for the first time [40]. Authors suggested that the formation mechanism of $SnNb_2O_6$ nanosheets reasonably follows a synergy interaction of reaction–crystallization and dissolution–recrystallization processes. $SnNb_2O_6$ nanosheets show much higher photocatalytic activities for the degradation of rhodamine B (RhB), compared with their counterparts prepared by the traditional solid-state reaction, due to the unique morphology, larger surface area, smaller crystallites, and stronger redox ability of the photogenerated hole–electron pair. It was reported that the reaction rate is enhanced by over 4 times

and the RhB molecule can be mineralized into CO_2 and H_2O over $SnNb_2O_6$ nanosheets. Highly crystalline and single phase Zn_2SnO_4 quantum dots with a good crystallinity and a narrow size distribution were also achieved by microwave-assisted hydrothermal synthesis [41].

Copper oxides have been widely used as catalysts, gas sensors, adsorbents, and electrode materials. Urchin-like architectured CuO nanomaterials with excellent catalytic and electrochemical performance were synthesized via a facile microwave-assisted hydrothermal process in $Cu(CH_3COO)_2$ (0.1 M)/urea(0.5 M) and $Cu(NO_3)_2$ (0.1 M)/urea(0.5 M) aqueous systems at 150 °C for 30 min [42]. CuO nanoparticles, spheroidal form (CuO-1) in $Cu(CH_3COO)_2$/urea aqueous solution, and CuO nanorods (CuO-2) in the $Cu(NO_3)_2$/urea aqueous system were observed. Experimental results indicated that CuO nanomaterials exhibit excellent catalytic activities for the epoxidation of alkenes and the oxidation of CO to CO_2. The conversions of styrene and norbornene were observed to reach 100 % with selectivity of about 45 % and 100 % after 24 h of catalytic reaction, respectively. The conversions of trans-β-methylstyrene were observed to approach 97 % with selectivity of 100 % with the reaction proceeded for 8 h.

A microwave-assisted hydrothermal method was introduced to monitor the growth process of $SrTiO_3$ nanospheres by taking "snapshots" of reaction intermediates [43]. Authors proposed a possible formation mechanism based on dehydration of titanium and strontium clusters followed by mesoscale transformation and a self-assembly process along an oriented attachment mechanism resulting in spherical-like shape.

The microwave-assisted hydrothermal method was also reported for the synthesis of Sn^{2+}-doped $ZnWO_4$ nanocrystals with controlled particle sizes and lattice structures for tunable optical and photocatalytic properties [44]. Sn^{2+}-doped $ZnWO_4$ nanocrystals greatly enlarged the BET surface areas from 40.1 to ~110 $m^2\ g^{-1}$. An abnormal band gap narrowing of Sn^{2+}-doped $ZnWO_4$ nanocrystals as a consequence of bulk and surface doping effects as well as lattice variations was observed.

Nanostructured $Cu_xZn_{1-x}Al_2O_4$ with a Cu:Zn ratio of 1/4:3/4, an average size of approximately 5 nm and a high specific surface area (above 250 $m^2\ g^{-1}$) was prepared as a precursor for $Cu/ZnO/Al_2O_3$-based catalysts by a microwave-assisted hydrothermal method at 150 °C [45].

Visible-light-induced antibacterial activity of carbon-doped anatase-brookite titania nano-heterojunction photocatalysts were synthesized by microwave-assisted method at 100 °C [46]. The most active photocatalyst was obtained after 60 min of microwave irradiation, which was found to exhibit a twofold higher visible-light induced photocatalytic activity in contrast to the standard commercial photocatalyst Evonik-Degussa P-25.

A microwave hydrothermal reaction is presented for the synthesis of highly crystallized anisotropic TiO_2 single nanocrystals for high performance dye-sensitized solar cells within 60 min [47]. The photoelectrode consisting of anisotropic nanorods and V-shaped twins was found to have a significant advantage for achieving an appreciable incident photon-to-current conversion efficiency of 85.6 % for the dye-sensitized solar cell.

5.2.3 *Microwave-Assisted Synthesis of Metal Chalcogenides Nanomaterials*

Metal chalcogenides nanomaterials are important functional materials and widely used in various fields. A green microwave synthesis route is described for the $Cu(In_{1-}xGax)Se_2$ nanoparticles with an average crystallite size of 3 nm and variable Ga content in an aqueous solution containing mercapto-acetic acid for the first time [48]. UV-visible absorption confirmed the tunable optical properties and could be applied in high density photovoltaic films and other optoelectronic applications.

Two methods were compared for the synthesis of hierarchical nanostructured $CdIn_2S_4$ resembling marigold flowers in aqueous medium and $CdIn_2S_4$ nanotubes in methanol medium using a hydrothermal method more than 24 h, and $CdIn_2S_4$ with mixed morphologies (flowers, spheres and pyramids) using a microwave method within 15 min [49]. It was found that $CdIn_2S_4$ had the band gap of 2.27 eV using the microwave method and 2.23 eV using the hydrothermal method. Experimental results indicated that the marigold flowers, nanoparticle spheres, and nanopyramids of $CdIn_2S_4$ synthesized by microwave method showed excellent photocatalytic activity and gave almost 30 % enhancement in the degradation of methylene blue (MB) as compared to CdS under direct sunlight.

Water soluble and optically active penicillamine (Pen) capped CdSe nanocrystals quantum dots with broad spectral distribution (430–780 nm) of photoluminescence were produced by microwave irradiation [50]. The nanoparticles show a very broad distribution of photoluminescence, attributing to emission from surface defect states.

Highly emissive CdSe, CdSe/CdS, and CdSe/CdS/ZnS quantum dots with size control, narrowing of size distributions, and improved quantum yields were fabricated under fine-tuned microwave-hydrothermal conditions using a synthetic microwave reactor for dielectric heating that provides both kinetic control, and in situ monitoring of temperature and pressure [51]. The optical characteristics were obtained after growth of CdS (ii), ZnS (iii), and CdS/ZnS (iv) shells at CdSe cores (i) (Fig. 5.12). Shell growth showed characteristic red shifts and notable increases in quantum yields from ~3 to 20–40 % with *r* and annealing time (Fig. 5.12a, b).

An ideal illustration of the automated microwave irradiation based synthesis setup employed (Fig. 5.13a), as well as the in situ temperature (Fig. 5.13b) and systems pressure characteristics (Fig. 5.13c) profiles obtained during a typical synthesis of CdSe quantum dots at temperatures of 60–180 °C, is shown. Both heating and cooling rates are rapid. One can observe the rapid increase in hydrothermal temperature (T_H) to a desired set-point (region-i), followed by a stable annealing temperature (region-ii), and the rapid temperature quenching (region-iii) due to absence of microwave irradiation coupled with high flow rate purging of the microwave cavity by compressed N_2. A similar profile is shown for the systems pressure characteristics (Fig. 5.13c).

A facile two-step, microwave-assisted method was described for the synthesis of the C@CdS core–shell hybrid spheres with the good dispersity and uniformity [52].

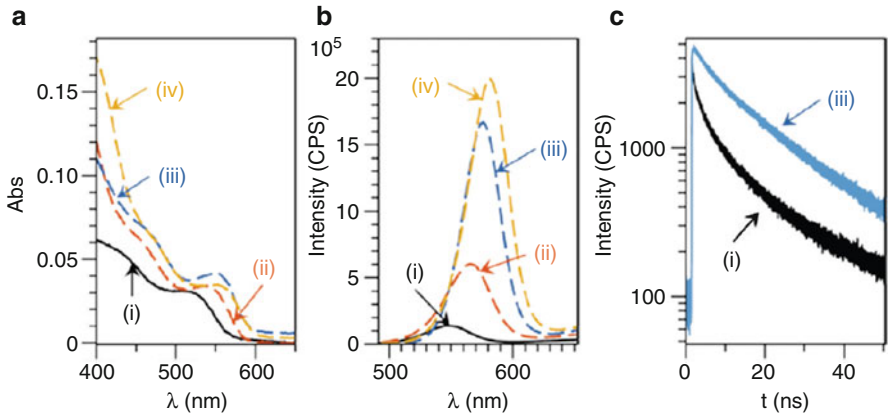

Fig. 5.12 A representative set of the UV–Vis (**a**) and PL emission (**b**) for CdSe-cores synthesized at 160 °C (*i*), and after CdS (*ii*), ZnS (*iii*), and CdS/ZnS (*iv*) shell growth at T_H = 120 °C. The TCSPC results (**c**) for the as-synthesized CdSe-cores before (*i*) and after ZnS shell growth (*iii*) with 420 nm excitation. From ref. [51]. Reprinted with permission from ACS

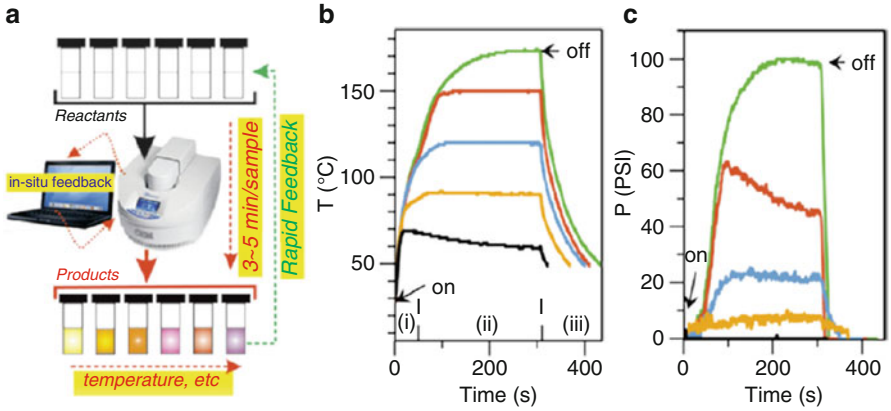

Fig. 5.13 A schematic illustration (**a**) of the synthesis strategy employed. Microwave irradiation based dielectric heating to hydrothermal temperatures allows for automated synthesis, high throughput, and in situ monitoring of reaction temperature (**b**), and pressure (**c**) during hydrothermal quantum dot synthesis. From ref. [51]. Reprinted with permission from ACS

The thickness of the CdS nanoparticles shell could be varied or controlled by the irradiation time. C@CdS core–shell hybrid spheres showed a higher photocatalytic degradation activity when exposed to visible light irradiation than that of CdS nanospheres under the same conditions, which have potential applications in photocatalytic cleaners, optoelectronic devices, water purification, environmental cleaning, and solar energy conversion.

A facile and rapid microwave-assistance approach was also reported for the fabrication of CdTe/poly(*N*-methylolacrylamide) (CdTe/PNMA) and CdTe/poly (*N*-methylolacrylamide-co-dimethyl diallyl ammonium chloride) (CdTe/poly (NMA-co-DMDAAC)) hydrogels with a high quantum yield and excellent photoluminescence stability [53]. The CdTe/PNMA hydrogels are responsive to different kinds of heavy metal ions including Pb^{2+}, Cd^{2+}, Zn^{2+}, and Mn^{2+}, and the CdTe/poly(NMA-co-DMDAAC) fluorescent slices exhibit selective fluorescent sensing toward organoamines of *n*-propylamine (PPA), triethylamine (TEA), and *N*,*N*-dimethylaniline (DMA).

A microwave-assisted process was used for the rapid synthesis of highly luminescent thiol-capped CdTe nanocrystals with high photoluminescence intensity in an IL based on a universal growth model under the assumption that the growth rate exponentially converges as the reaction proceeds [54]. The microwave irradiation was found to play a pivotal role in the limiting step of the growth of nanocrystals including the activation of nanocrystal precursor and the subsequent formation of nuclei.

A microwave-assisted synthesis method was used to prepare water-soluble and highly luminescent glutathione-capped $Zn_{1-x}Cd_xTe$ alloyed quantum dots with excellent biocompatibility using pollutant-free sodium tellurite (Na_2TeO_3) as the Te source [55]. It was observed that the size could be tuned from 500 to 610 nm and the photoluminescent quantum yield can reach up to 90 %. The cytotoxicity of the glutathione-capped $Zn_{1-x}Cd_xTe$ alloyed quantum dots towards living cells can be reduced to a small extent due to the incorporation of the Zn ions as shown by in vitro cytotoxicity studies (MTT-assay). The authors suggested that high-performance $Zn_{1-x}Cd_xTe$ alloyed quantum dots are highly promising biological fluorescent labels in biological applications.

The optical properties of glutathione-capped $Zn_{1-x}Cd_xTe$ alloyed quantum dots showed the quantum size effect by through the temporal evolution of UV-visible and PL spectra (Fig. 5.14). PL peaks of the samples are dominated by the band-edge emission without a broad deep-trap emission peak with the Cd/Zn feed ratio of 3:2 and the reaction time from 10 min to 5 h (Fig. 5.14b). Increase in size with a longer growth time and a narrow size distribution of alloyed quantum dots were observed. Moreover, the as-prepared alloyed quantum dots are transparent under visible light, suggesting that these alloyed quantum dots are well-dispersed in aqueous phase without further treatment (Fig. 5.14c). The as-prepared alloyed quantum dots solutions emit bright fluorescence of cyan blue, green, yellow, orange, and red under UV irradiation (Fig. 5.14d).

5.2.4 Microwave-Assisted Synthesis of Bio-nanomaterials

Bio-nanomaterials have wide applications in the biomedical fields. A rapid microwave-assisted hydrothermal method has been developed for the preparation of highly stable amorphous calcium phosphate (ACP) porous nanospheres with a relatively uniform size and an average pore diameter of about 10 nm by using $CaCl_2 \cdot 2H_2O$

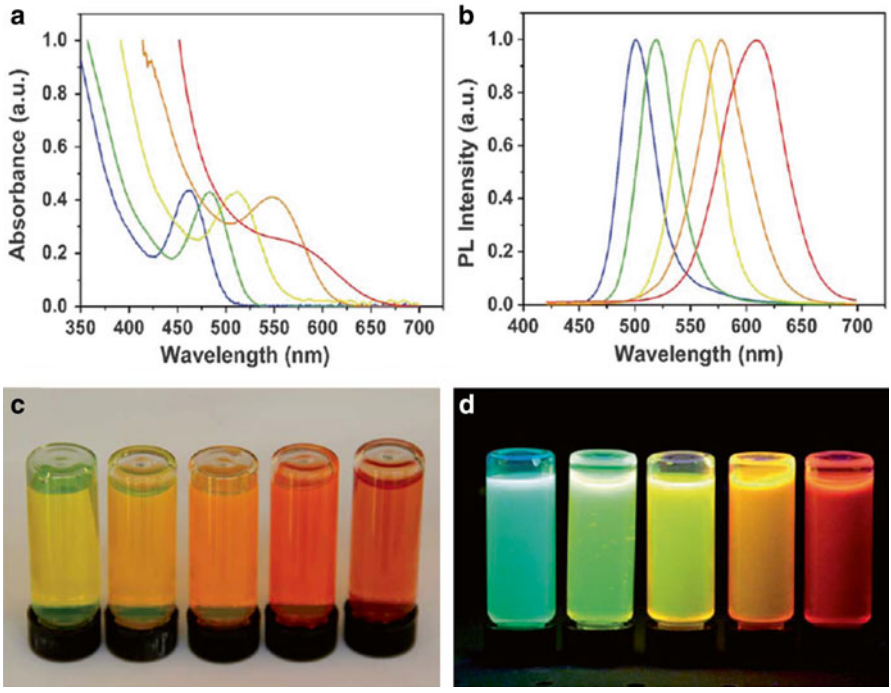

Fig. 5.14 Temporal evolution of (**a**) UV–Vis absorption and (**b**) PL emission spectra of glutathione-capped $Zn_{1-x}Cd_xTe$ alloyed quantum dots. Photographs of GSH capped $Zn_{1-x}Cd_xTe$ alloyed quantum dots under visible light (**c**) and 365 nm UV light (**d**). (reaction time: 10 min, 30 min, 1 h, 2 h, 5 h, from *left* to *right*). From ref. [55]. Reprinted with permission from RSC

as the calcium source and adenosine 5′-triphosphate disodium salt (ATP) as the phosphorus source and stabilizer [56]. The as-prepared ACP porous nanospheres are found to be efficient for anticancer drug (docetaxel) loading and release, and a high ability to damage tumor cells.

The experimental parameters were found to affect the size of ACP porous nanospheres. ACP porous nanospheres had relatively uniform in size with an average diameter of (260 ± 51) nm at 100 °C for 30 min (Fig. 5.15a), (257 ± 37) nm at 120 °C for 30 min (Fig. 5.15b), (238 ± 35) nm at 120 °C for 10 min, (320 ± 53) nm with 50 mm Ca^{2+} (Fig. 5.15c), (400 ± 76) nm at pH 10 (Fig. 5.15d), and (227 ± 28) nm with 25 mm Ca^{2+} at 120 °C for 60 min (Fig. 5.15e).

A microwave-assisted hydrothermal method was also reported for the rapid and sustainable synthesis of hydroxyapatite (HA) hierarchically nanostructured porous hollow microspheres with specific surface area of 87.3 $m^2\ g^{-1}$ and average pore size of 20.6 nm by using biocompatible creatine phosphate disodium salt as an organic phosphorus source in aqueous solution [57]. It was observed that HA hierarchically nanostructured porous hollow microspheres within the range of 0.8–1.5 mm consisted of nanosheets or nanorods as the building blocks. Using creatine phosphate as

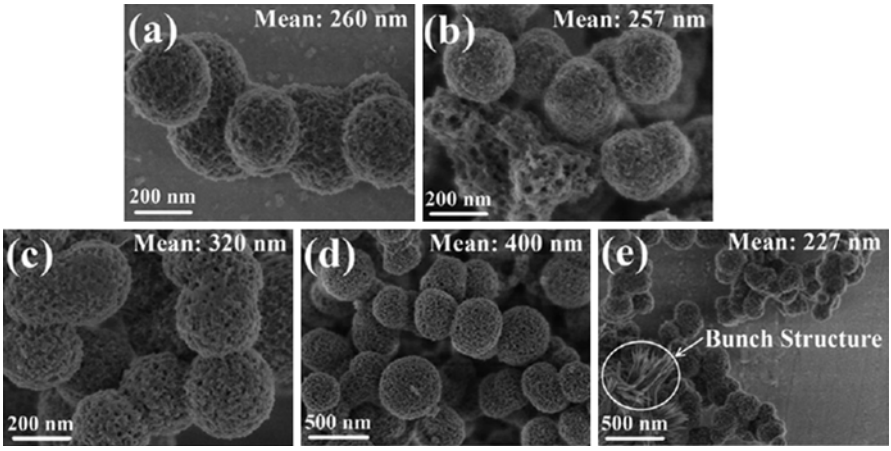

Fig. 5.15 SEM micrographs of ACP porous nanospheres synthesized by using $CaCl_2 \cdot 2H_2O$ as the calcium source and ATP as both the phosphorus source and stabilizer by the microwave-assisted hydrothermal method under different conditions: (**a**) 25 mm Ca^{2+}, pH 5, 100 °C for 30 min; (**b**) 25 mm Ca^{2+}, pH 5, 120 °C for 30 min; (**c**) 50 mm Ca^{2+}, pH 5, 120 °C for 30 min; (**d**) 25 mm Ca^{2+}, pH 10, 120 °C for 30 min; (**e**) 25 mm Ca^{2+}, pH 5, 120 °C for 60 min. From ref. [56]. Reprinted with permission from Wiley-VCH

the organic phosphorus source, nanosheets/nanorods hierarchically were assembled into nanostructured porous hollow microspheres with a relatively uniform size and the diameters of HA porous hollow microspheres were about 1 mm (Fig. 5.16c–f). The control sample consisted of a mixture of nanorods and nanosheets and no porous hollow microspheres were observed (Fig. 5.16a, b). The as-prepared porous hollow microspheres have been found to show a relatively high drug-loading capacity and protein-adsorption ability, as well as sustained drug and protein release, by using ibuprofen as a model drug and hemoglobin (Hb) as a model protein, respectively.

A surfactant-free rapid microwave-assisted hydrothermal method was reported for the synthesis of HA nanosheet-assembled flower-like hierarchical nanostructures with a high protein and DNA loading capacity and pH-controlled protein release function [58]. The morphology from flower-like to polyhedra can be varied by adjusting the microwave heating temperature. The loading capacities obtained for bovine serum albumin (BSA), hemoglobin (Hb), and fish sperm DNA were 165 mg g^{-1}, 164 mg g^{-1}, and 112 mg g^{-1}, respectively.

One-pot microwave-assisted hydrothermal method was also reported for the biocompatible europium-doped calcium HA and fluoroapatite nanophosphors functionalized with poly(acrylic acid) through a from aqueous basic solutions containing calcium nitrate, sodium phosphate monobasic, as well as sodium fluoride in the case of the fluoroapatite particles [59]. The size of the nanospindles was 191(32)×40(5) nm for calcium HA and 152(24)×38(6) nm for calcium fluoroapatite. The as-prepared samples showed a very high colloidal stability in 2-(*N*-morpholino) ethanesulfonic acid at pH 6.5.

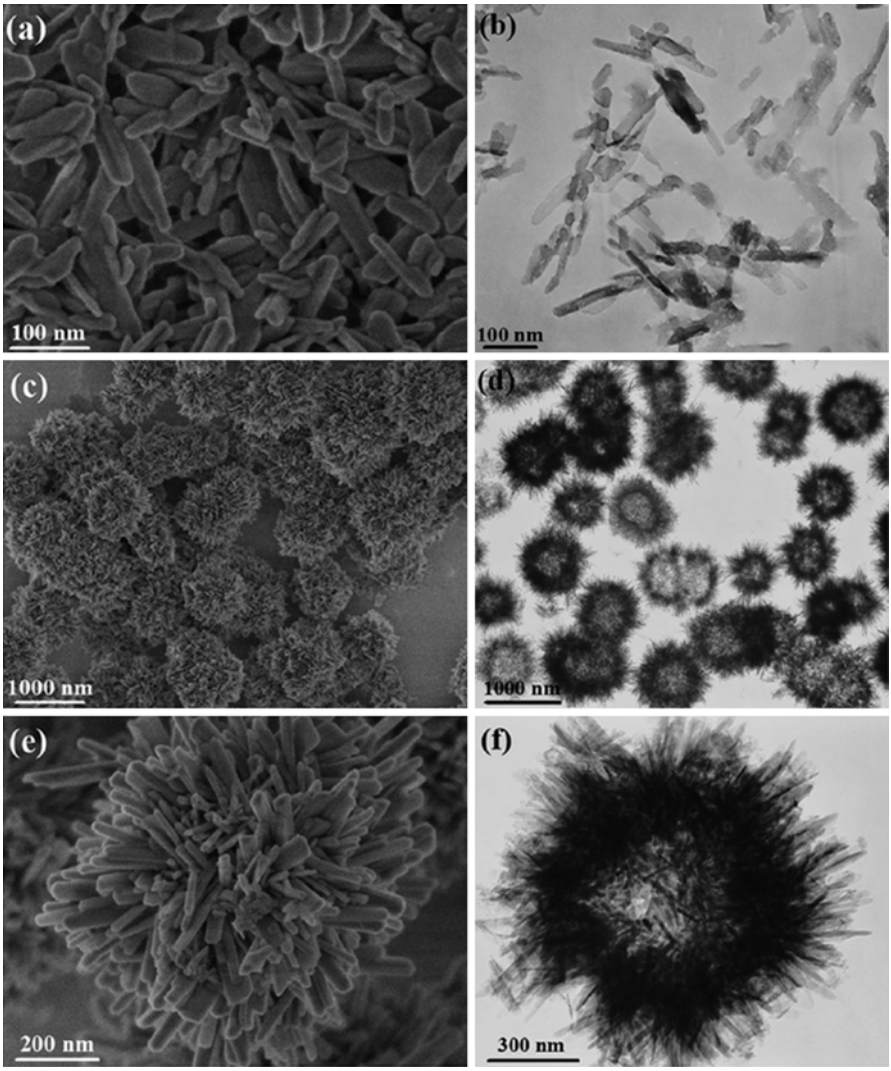

Fig. 5.16 SEM (*left*) and TEM images (*right*): (**a**, **b**) Control sample that was obtained by using $Na_2HPO_4 \cdot 12H_2O$ in the absence of creatine phosphate; (**c**–**f**) HAP hierarchically nanostructured porous hollow microspheres that were prepared by using $CaCl_2$ and creatine phosphate in aqueous solution through a microwave-assisted hydrothermal method at 120 °C for 10 min. From ref. [57]. Reprinted with permission from Wiley-VCH

5.2.5 Microwave-Assisted Synthesis of Nanocomposites

Green microwave-assisted method was also reported to the synthesis of various nanocomposites. A green and rapid microwave-assisted synthetic procedure is presented for the preparation of low-toxic Mn: ZnSe/ZnS core/shell nanocrystals with

good crystallizability and favorable monodispersity to label antibodies for selective detection of human immunoglobulin G based on fluorescence resonance energy transfer between the Mn: ZnSe/ZnS and Au nanoparticles [60].

Three-dimensional Pd@Pt core–shell nanostructures with controllable shape and composition were synthesized using a microwave heating method [61]. Pd@Pt electrocatalysts were found to exhibit higher catalytic activity than pure Pd and pure Pt catalysts for both the oxygen electroreduction reaction and methanol electrooxidation reaction, and the highest activity are obtained at the Pd@Pt electrocatalyst with a Pd/Pt molar ratio of 1:3.

Dope submicrometer carbon spheres with Ag nanoparticles was used to fabricate Ag nanoparticles–C composites via microwaving suspensions of nanoporous carbon spheres in aqueous $Ag(NH_3)_2^+$ solutions with poly(*N*-vinylpyrrolidone) as reducer in high yield within a short reaction time [62]. The composite spheres were reported to exhibit not only a tunable plasmon resonance shift but also an excellent catalytic activity toward the reduction of 4-nitrophenol by sodium borohydride using controlling the Ag doping.

Reduced graphene oxide–Fe_2O_3 nanocomposite was prepared as a high-performance anode material for lithium ion batteries using a facile two-step synthesis by homogeneous precipitation and subsequent reduction of the G-O with hydrazine under microwave irradiation to yield reduced graphene oxide platelets decorated with Fe_2O_3 nanoparticles [63]. Graphene oxide–Fe_2O_3 nanocomposite exhibited the first discharge and charge capacities of 1,693 mA h g^{-1} and 1,227 mA h g^{-1} at a current density of 100 mA h g^{-1}, respectively. It shows good capacity retention with 1,027 mA h g^{-1} after the 50th discharge, as well as ~800 mA h g^{-1} of discharge capacity even at the current density of 800 mA g^{-1}.

Microwave-assisted method was used to synthesize a core–shell multiwalled carbon nanotubes/graphene oxide nanoribbons heterostructure with excellent electrochemical performance for electrochemically detect ascorbic acid, dopamine, and uric acid [64]. The authors attributed this to the unique electronic structure of a high density of unoccupied electronic states above the Fermi level and enriched oxygen-based functionality at the edge of the graphene-like structures.

CdS-reduced graphene oxide nanocomposites are synthesized via the microwave-assisted reduction of graphite oxide in a CdS precursor solution [65]. These composites exhibit enhanced photocatalytic performance for the reduction of Cr(VI) with a maximum removal rate of 92 % under visible light irradiation as compared with pure CdS (79 %) due to the increased light absorption intensity and the reduction of electron–hole pair recombination in CdS with the introduction of reduced graphene oxide.

Preparation of ZnO–ZnS core–shell nanorods was described via microwave-assisted method in situ surface sulfidation of ZnO nanorods [66]. ZnO–ZnS core–shell nanorods possess significantly higher visible light photocatalytic activity, which is twice that of the original ZnO nanorods. The thickness and nanoparticle size of the ZnS shell can be conveniently varied or controlled by the concentration of the organo-sulfur source thioacetamide. The pure ZnO hexangular rods of about 120 nm in diameter with smooth surface (Fig. 5.17a). The surface of the ZnO

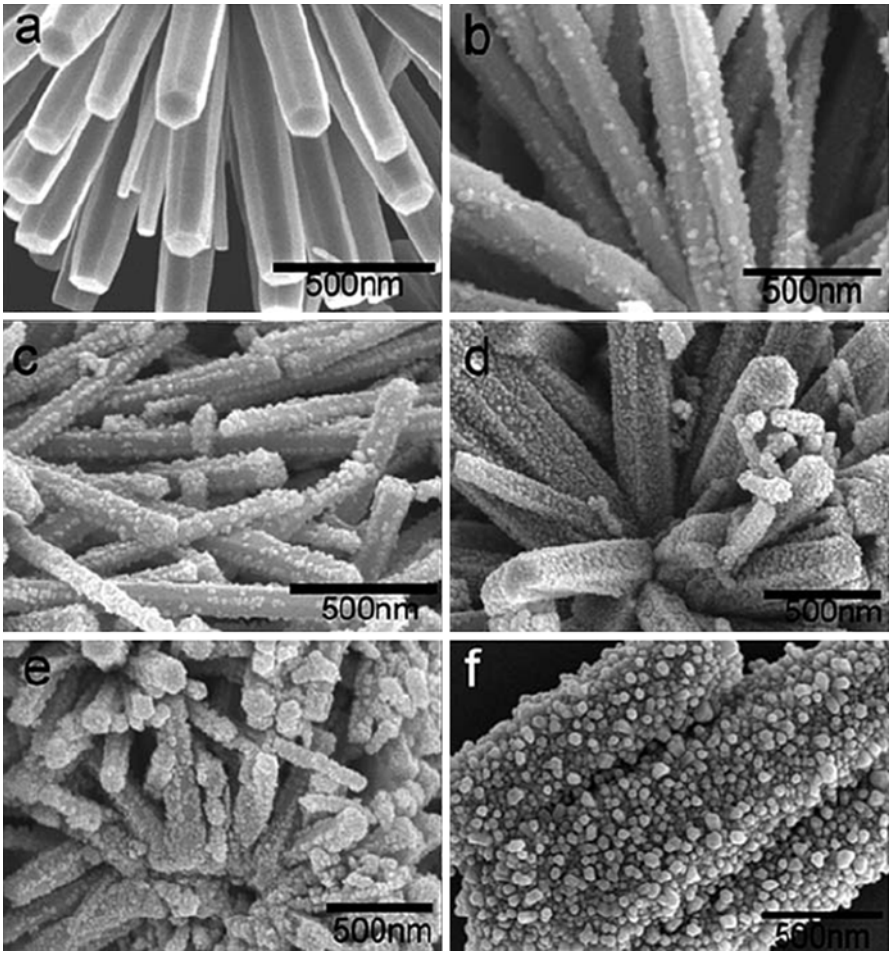

Fig. 5.17 Typical SEM images of as-prepared (**a**) pure ZnO nanorods and ZnO–ZnS core–shell nanorods obtained via microwave irradiation with different concentration of thioacetamide: (**b**) 0.0025 M, (**c**) 0.0075 M, (**d**) 0.0125 M (**e**) 0.0175 M and (**f**) 0.0225 M. From ref. [66]. Reprinted with permission from RSC

nanorods became rougher and thicker, implying an increasing conversion from ZnO to ZnO/ZnS hybrid structures via the surface sulfidation with increasing concentration of thioacetamide (Fig. 5.17b–f). The as-prepared products were reported to exhibit narrowed band gap and strong orange luminescence at 621 nm, due to the interstitial oxygen ion defect present in hydrothermally grown ZnO. It was also reported that the PL intensity gradually decreases with the increase of the thickness of ZnS shell, indicating charge transfer between the two components of the ZnO–ZnS hybrids. The ZnO–ZnS hybrid structures evinced a significantly higher (by 100 % increase) photocatalytic activity in the degradation of RhB than that of pure ZnO NRs under the same conditions.

SnO_2–graphene composites were synthesized as a superior anode for lithium-ion batteries by an ultrafast and environmentally friendly microwave autoclave method, consisting of a few layers of graphene nanosheets sandwiching SnO_2 nanoparticles with a highly uniform distribution, which show significantly improved cycle lives, compared with the bare SnO_2 electrode due to the active function of the graphene nanosheets in the composites [67]. It was reported that SnO_2–graphene composites with a graphene content of 33.3 wt% exhibits a very stable capacity of about 590 mA h g^{-1} without noticeable fading for up to 200 cycles.

Formation of bimetallic Au–Pd and Au–Pt nanoparticles was reported at 110 and 130 °C by the reduction of chlorocomplexes of gold (III) from muriatic solutions by nanocrystal powders of palladium and platinum under hydrothermal conditions and microwave irradiation [68].

TiO_2-reduced graphene oxide composites are synthesized via the microwave-assisted reduction of graphite oxide in a TiO_2 suspension [69]. The composites exhibit enhanced photocatalytic performance for the reduction of Cr(VI) with a maximum removal rate of 91 % under UV light irradiation as compared with pure TiO_2 (83 %) and commercial TiO_2 P25 (70 %) due to the increased light absorption intensity and range as well as the reduction of electron–hole pair recombination in TiO_2 with the introduction of reduced graphene oxide.

A microwave-assisted synthesis technique was also used to produce copper-doped and ^{64}Cu-doped iron oxide nanoparticles with a dextran coating within only 5 min [70]. Highly luminescent and low toxic glutathione-capped CdSeTe@ZnS–SiO_2 quantum dots were synthesized for the detection of Cu(II) via a microwave-assisted method [71]. The as-prepared quantum dots showed high luminescence, low toxicity and good water solubility.

Hollow ZnO core/ZnS shell structures with enhanced photocatalytic properties were prepared by microwave hydrothermal method [72]. The Kirkendall effect and an Ostwald ripening process were suggested for the fabrication of core/ZnS shell structures. The ZnO/ZnS heterostructures fill the surface defects of ZnO crystals and improve the stability of the photocatalysts by overcoming the photocorrosion effect of a single ZnO photocatalyst under UV light irradiation.

A green rapid microwave-assisted method was reported for the synthesis of ZnO–Au hybrids with excellent control over the morphology, loading and interface nature using just water as the solvent and reducing agent for CO oxidation [73]. The hybrids exhibit good catalytic activity for CO oxidation, compared to similar hybrids reported in the literature.

Microwave irradiation technique was employed for the synthesis of small-sized highly luminescent CdSeS–ZnS core–shell quantum dots for live cell imaging [74]. The prepared CdSeS–ZnS core–shell quantum dots showed significantly enhanced luminescence and photostability than that of CdSeS core quantum dots. The small size quantum dots were localized predominantly in the nuclear compartment of Hela cells with negligible cytotoxicity, even at a concentration of 300 μg mL^{-1} after 24 h incubation.

Porous CdO–CdS core–shell nanoboxes with uniform morphology and good structural stability were prepared by microwave-assisted in situ surface sulfidation

of $CdCO_3$ nanocubes followed by annealing treatment [75]. The as-obtained products exhibit much higher visible-light-driven photocatalytic activity in the reduction of aqueous Cr(VI) than pure CdS.

$LiFePO_4$–C–graphene composites as cathode materials for Li-ion batteries with enhanced rate capability were synthesized by a rapid, one-pot, microwave-assisted hydrothermal method within 15 min at 200 °C, followed by sintering at 600 °C for 2 h under a H_2–Ar (5:95, v/v) atmosphere [76]. The $LiFePO_4$–C–graphene composite exhibited a discharge capacity of 165 mA h g^{-1} at 0.1 °C and 88 mA h g^{-1} at 10 °C, respectively.

Biocompatible hollow doughnut-like ZnO–Au nanocomposites were synthesized with the coordination and selective adsorption effect of trisodium citrate through a fast one-step microwave-assisted hydrothermal route [77]. The hollow ZnO–Au nanocomposites are photostable with a strong resonance Raman signal. ZnO–Au nanomaterials have low biological cytotoxicity on human colon cancer cells (LOVO cells) at the concentration of 50 μg mL^{-1}.

Porous ZnO nanostructures were synthesized by a microwave-assisted hydrothermal reaction then converted into porous ZnO–ZnSe nanocomposites by a microwave-assisted dissolution-recrystallization process using an aqueous solution containing selenium ions [78]. The porous ZnO–ZnSe nanocomposites had much higher activities than the porous ZnO nanostructures. The main photocatalytic activity of the synthesized nanostructures arose from photoexcitation of the semiconductor (ZnO or ZnSe) via absorption of light of energy equal to or exceeding the band gap energy.

Microwave-assisted method was also developed to fabricate SnO_2-reduced graphene oxide–carbon nanotube composites for lithium ion batteries [79]. The as-prepared composites with 60 wt% SnO_2 achieve a maximum capacity of 502 mA h g^{-1} after 50 cycles at 100 mA g^{-1} and a capacity of 344 mA h g^{-1} at a high current density of 1,000 mA g^{-1}.

5.3 Green Synthesis of Biomass Nanocomposites

Biomass is generated in organisms by photosynthesis and has characters of renewal, biodegradation, low pollution, and widespread distribution. Nanocomposites consisted of two or more than two kinds of components, which produced new properties to meet the industrial requirements by synergistic effect between components. Biomass nanocomposites were obtained by combining the advantages of biomass and nanocomposites. Green microwave-assisted method was applied for the synthesis of biomass nanocomposites in accordance with the principles of green chemistry including biodegradation, low toxicity, environment-friendly, economy-friendly, and energy-saving. Cellulose is typical biomass composed of glucose molecules. In this section, cellulose nanocomposites were used as the typical examples for the green synthesis of biomass nanocomposites. Our research group has done a lot of work on the green synthesis of biomass nanocomposites by microwave-assisted method.

As early as 2010, the green microwave-assisted method was developed for preparation of cellulose–carbonated hydroxyapatite (CHA) nanocomposites only within 15 min [80]. The cellulose nanocomposites were obtained in NaOH-urea aqueous solution without organic solvents. Microcrystalline cellulose was known to have irregular flake shape. CHA nanostructures were found to be dispersed in the cellulose matrix. Then, microwave-assisted method was used to prepare the cellulose–CHA nanocomposites in IL [81], which combined the advantages of microwave, IL, and biomass. It is well known that IL is the solvent for dissolution of cellulose and the better solvent for absorbing microwave. CHA was observed to display the aggregated nanorods and cellulose nanocomposites had rough surface. Experimental results showed that different shape and crystallinity were observed using microwave and oil heating method. Some loose particles and pore structures were observed by oil heating at 130 °C for 24 h. Moreover, different thermal stabilities were shown using microwave and oil heating method. The regenerated cellulose had ~69.1 % of weight loss. Cellulose–CHA nanocomposites had ~20.3 and 35.9 % of weight losses by microwave method with 2 and 5 wt% microcrystalline cellulose. Nanocomposites had ~26.1, 23.3, and 14.2 % of weight losses using oil heating method with 2, 4, and 5 wt% microcrystalline cellulose.

After that, microwave-assisted ILs method was also applied to synthesize the cellulose–F-substituted hydroxyapatite (FHA) nanocomposites [82]. Experimental results indicated he cellulose–CaF nanocomposites at high NaF concentration. FHA particles were found to be embedded in the cellulose matrix or dispersed on the surface of cellulose matrix. The F-substituted HA particles were embedded in the cellulose matrix without IL (Fig. 5.18a). F-substituted HA were dispersed on the surface of cellulose matrix using 0.5 g IL (Fig. 5.18b). FHA particles were dispersed on the surface of irregular cellulose fibers using 1.0 g IL (Fig. 5.18c, d). The size of FHA particles increased and the number decreased with 2.0 g IL (Fig. 5.18e, f). Obviously, IL had an effect on the FHA in cellulose nanocomposites.

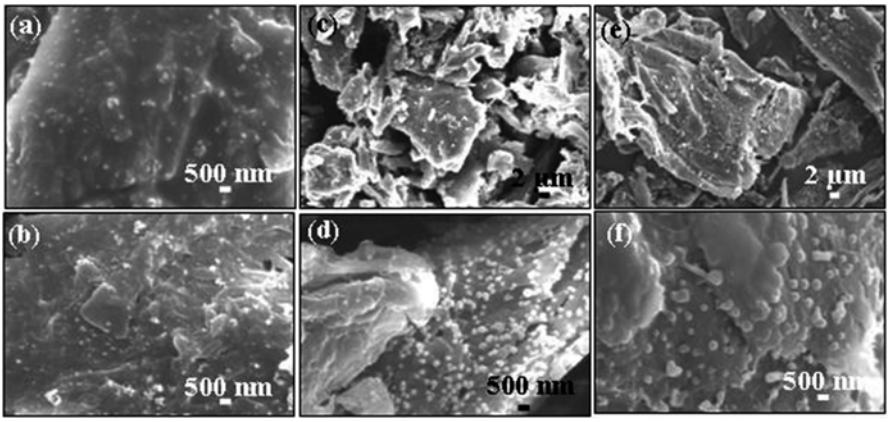

Fig. 5.18 SEM images of the cellulose–FHA nanocomposites using different concentrations of IL: (**a**) 0 g; (**b**) 0.5 g; (**c**, **d**) 1.0 g; (**e**, **f**) 2.0 g. From ref. [82]. Reprinted with permission from Elsevier

It is known that $CaCO_3$ is the major inorganic components of shells and limestone. The cellulose–$CaCO_3$ composites are also reported as the biomedical materials and have biological activities such as protein-adhesive properties, cell compatibility, and hard tissue compatibility. Microwave-assisted method was also employed to synthesize the cellulose–$CaCO_3$ composites [83]. Cellulose has various types such as wood fiber, plant fiber, microcrystalline cellulose, microfibrillated cellulose, nanofibrillated cellulose, cellulose nanocrystals, bacterial cellulose, and so on. Cellulose types of alkali extraction cellulose and microcrystalline cellulose were found to play an important role in the microstructure and morphologies of the cellulose–$CaCO_3$ composites. It was observed that the sample had better crystallinity using microcrystalline cellulose than that using alkali extraction cellulose. Using microcrystalline cellulose, cellulose with irregular shape and $CaCO_3$ microspheres was observed. The cellulose fibers and $CaCO_3$ particles were observed using alkali extraction cellulose.

Microwave-assisted IL method is also applied for the preparation of cellulose–$CaCO_3$ nanocomposites using alkali extraction cellulose [84]. $CaCO_3$ is well-crystallized calcite with the hexagonal structure. The crystallinity of calcite dramatically increased with increasing alkali extraction cellulose concentration. The regenerated cellulose had fiber-like shape with clear surface and some pores structure. The change process of morphology was observed from polyhedral to cubes to particles. $CaCO_3$ with polyhedral-like shape was observed on the surface of cellulose using 2 wt% alkali extraction cellulose. $CaCO_3$ crystals with cube-like shape embedded in the cellulose matrix were observed using 5 wt% alkali extraction cellulose. With 10 wt% alkali extraction cellulose, $CaCO_3$ particles dispersed on the surface of cellulose were shown.

Cytotoxicity experiments demonstrated that the cellulose–$CaCO_3$ nanocomposites have good biocompatibility, which can be used as a safe biomaterial for biomedical applications. Cell cytotoxicity of the cellulose nanocomposites was tested via 5-dimethylthiazol-2-yl-2,5-diphenyltetrazolium bromide (MTT) assay. The samples were synthesized in IL (Fig. 5.19B) and ethylene glycol (Fig. 5.19A) using the alkali extraction cellulose concentration (5 %) by microwave-assisted method. Cell viability values were 91.3, 94.6, 86.9, 82.7, and 84.9 % with the increasing nanocomposites concentrations from 0.1 to 1 to 10 to 100 to 500 μg mL^{-1} (Fig. 5.19B). Using ethylene glycol as solvent, the cell viability values were 91.7 %, 94.6 %, 92.1 %, 85.3 %, and 89.2 % (Fig. 5.19A), respectively. Cytotoxicity experiments indicated that cellulose–$CaCO_3$ nanocomposites had essentially no in vitro cytotoxicity and biologically safe for the application in biomedical field.

These wood nanocomposites can utilize the main valid components of biomass and can be a candidate for biomedical applications. A green microwave-assisted method was developed for the preparation of $CaCO_3$ particles-filled wood powder nanocomposites using dewaxed wood powder in the NaOH/urea solution [85]. The urea acted as part of the CO_3^{2-} source and provided a basic condition for the synthesis of $CaCO_3$. Heating time was reported to play an important role in the morphology and dispersion of $CaCO_3$ in the nanocomposites. The $CaCO_3$ congregates with rice-like shape grew on wood powder as substrate in a heating time of 10 min.

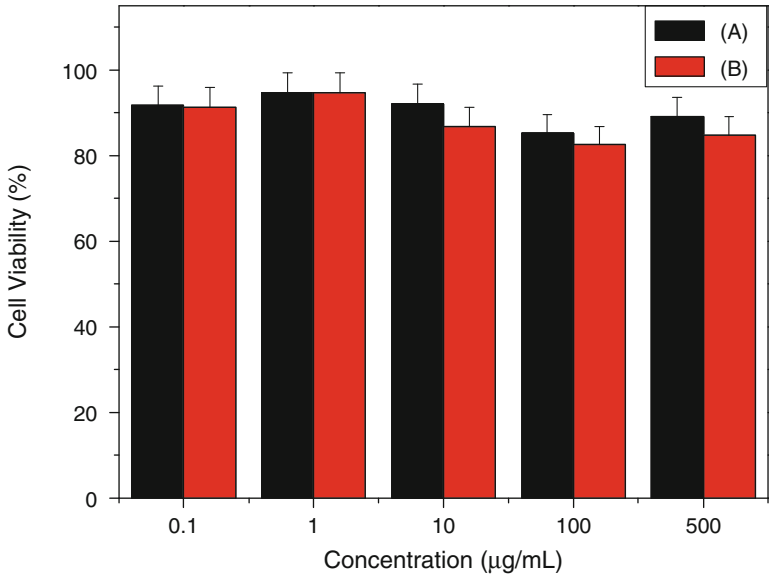

Fig. 5.19 Viabilities of normal human fibroblasts incubated with the cellulose–$CaCO_3$ nanocomposites: (*A*) using ethylene glycol and (*B*) using ionic liquid. They were determined by survival cells per well relative to that of untreated cells. The error bars stand for standard deviations. From ref. [84]. Reprinted with permission from Elsevier

It was shown that $CaCO_3$ congregates and particles were obtained for 30 min. When the heating time was 1 h, one can observe powder fibers with $CaCO_3$ congregates and particles.

Calcium silicate has good biocompatibility, bioactivity, and degradability, and wide applications in drug delivery and bone tissue engineering field. A rapid and green microwave-assisted method was used for the synthesis of the cellulose–calcium silicate nanocomposites in ILs and recycled ILs [86]. It was observed that the calcium silicate nanoparticles or nanosheets homogeneously dispersed in the cellulose matrix with slight differences for ILs and recycled ILs. The cross polarization magic angle spinning (CP/MAS) ^{1}H NMR spectrum of the starting IL has the noticeable signals in the region between 0.50 and 11.00 ppm, which attributed to the typical peaks of different hydrogens of IL (Fig. 5.20a). Similar ^{1}H NMR spectra of the recycled IL (Fig. 5.20b–d) were observed. The slight differences at 10.37 ppm was observed between starting IL and recycled IL. The peaks moved among the recycled IL due to the existence of ethanol and cellulose. IL was found to have an effect on the morphology of the cellulose–calcium silicate nanocomposites. Cellulose–calcium silicate nanocomposites with calcium silicate nanoparticles dispersed in the cellulose matrix using IL, and cellulose–calcium silicate nanocomposites with calcium silicate nanosheets dispersed in the cellulose matrix using recycled IL.

Ag has known to have strong antimicrobial activity against nearly 650 types of bacteria and has potential applications in various fields such as antibacterial filters, wound dressing materials, and food packaging field. Cellulose–Ag nanocomposites

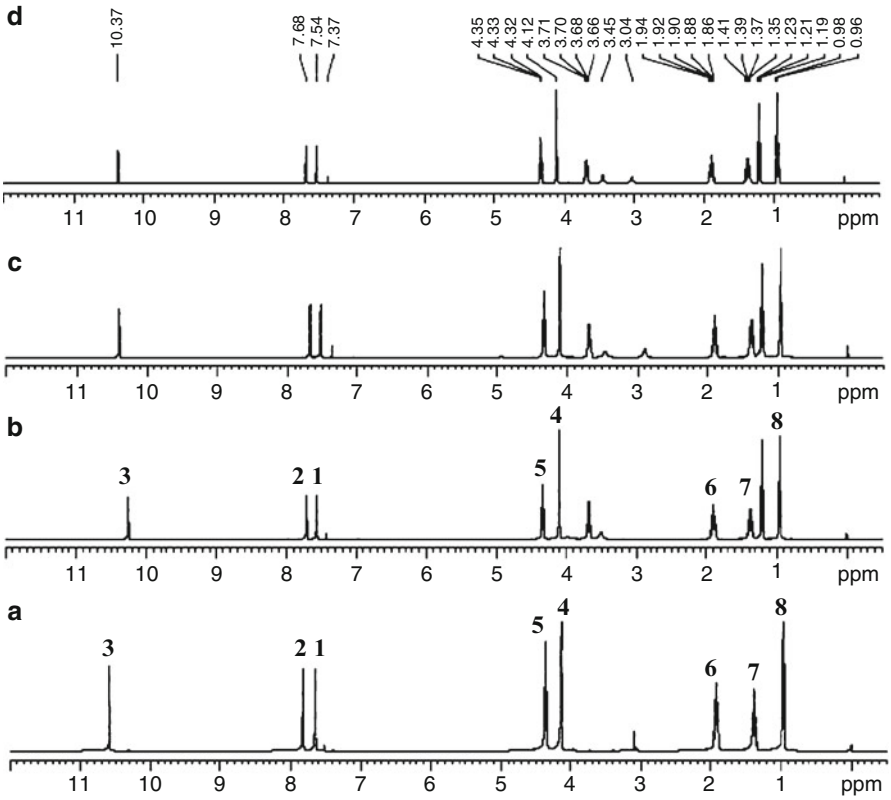

Fig. 5.20 CP/MAS ^{1}H NMR spectra of (*a*) the starting ionic liquids and (*b–d*) the recycled ionic liquids. From ref. [83]. Reprinted with permission from Elsevier

were also fabricated by the green microwave-assisted method using reducing silver nitrate in ethylene glycol (EG), which was acted as a solvent, a reducing reagent, and a microwave absorber [87]. It was observed that Ag particles with diameters of about 100 nm homogeneously dispersed in the cellulose substrate. The cellulose–Ag nanocomposites were found to exhibit a strong antibacterial activity against both *E. coli* (gram-negative bacteria) and *S. aureus* (gram-positive bacteria). The cellulose–Ag nanocomposites displayed inhibition zones of 10 mm and 2.5 mm for *E. coli* and *S. aureus* with low concentration (0.075 g) (Fig. 5.21a, b), and inhibition zones of 12.5 mm and 6.5 mm for *E. coli* and *S. aureus* with high concentration (0.150 g), respectively (Fig. 5.21c, d).

Silver chloride (AgCl), as a photosensitive material, has wide applications in photometry, plating, electrochemical, and biomedical fields. Cellulose and AgX (X = Cl, Br) hybrids were carried out by microwave-assisted ionic liquids method [88], in which ILs acted simultaneously as a solvent, a microwave absorber, and a reactant by providing Cl^- or Br^- to the synthesis of AgCl or AgBr crystals.

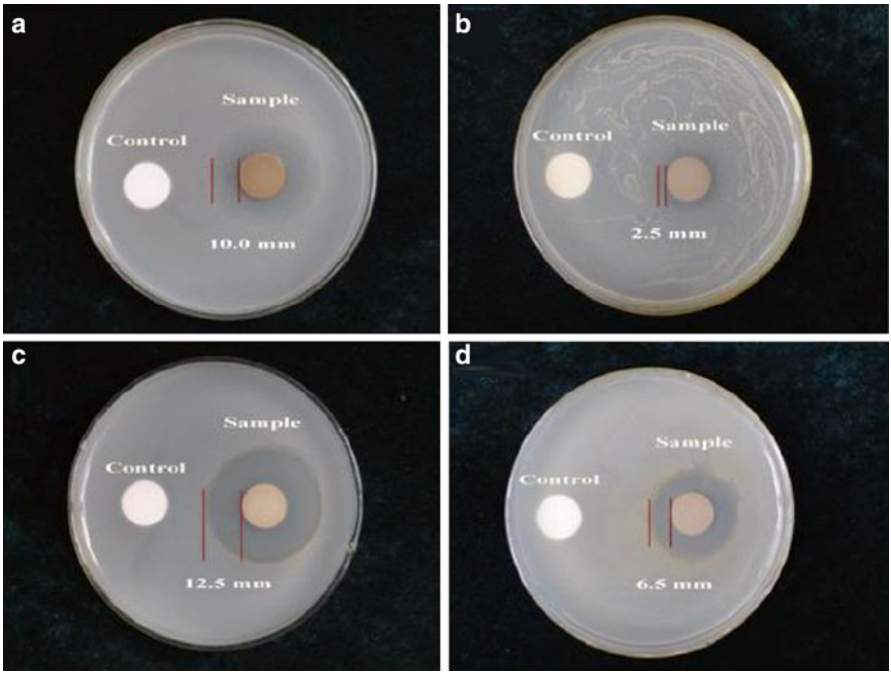

Fig. 5.21 Antimicrobial activities of the cellulose–Ag nanocomposites: (**a**, **c**) *E. coli* and (**b**, **d**) *S. aureus*. From ref. [87]. Reprinted with permission from Elsevier

The cellulose–Ag/AgCl hybrid and cellulose–Ag/AgBr hybrid were found to be synthesized using cellulose–AgCl and cellulose–AgBr hybrids as precursors.

It was found that well-crystallized AgCl with a cubic structure was obtained using [Bmim]Cl and [Amim]Cl as solvents (Fig. 5.22a, b). Using [Bmim]Br chosen as solvent, well-crystallized AgBr with a cubic structure was observed (Fig. 5.22c). Using [Bmim]Cl as solvent, mechanical mixture of AgCl crystals and cellulose was obtained (Fig. 5.23a). The AgCl crystals were embedded in the cellulose substrate using [Amim]Cl (Fig. 5.23b). AgBr crystals with dendrite-like shape using [Bmim]Br (Fig. 5.23d–f) were observed. The melting point and viscosity of IL were found to have an effect on the formation of cellulose and AgX (X = Cl, Br) hybrids.

Cellulose–AgCl and cellulose–AgBr hybrids were found to have different chemical stability. Cellulose–AgCl hybrids had no obvious change using cellulose–AgCl hybrid as precursor and ascorbic acid as the reducing reagent in [Amim]Cl via microwave heating at 130 °C for 30 min (Fig. 5.24a). The as-obtained cellulose–AgCl hybrids had highly chemical stability. Cellulose–AgCl/Ag hybrids were observed using $AgNO_3$ and ascorbic acid in ionic liquid at 130 °C for 30 min via microwave heating (Fig. 5.24b). Cellulose–Ag/AgBr hybrid was shown using cellulose–AgBr hybrid as precursor and ascorbic acid as the reducing reagent in [Bmim]Br via microwave heating at 130 °C for 30 min (Fig. 5.24c). Cellulose–AgBr hybrid was shown

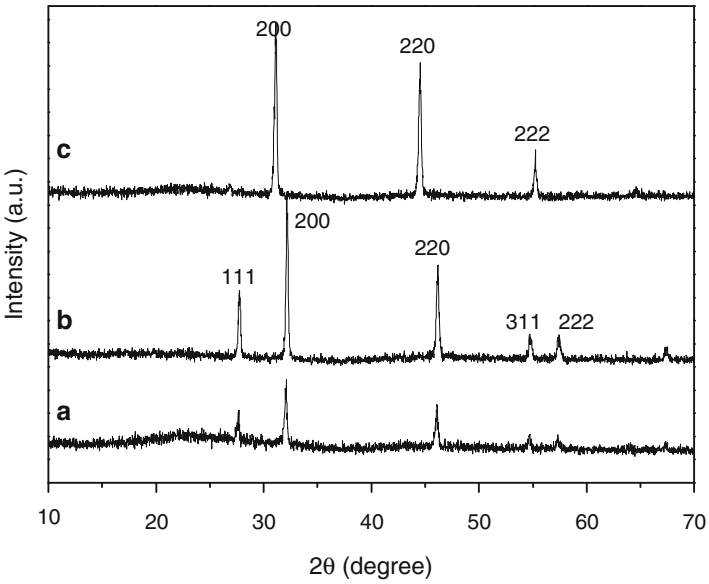

Fig. 5.22 XRD patterns of (*a*, *b*) the cellulose–AgCl and (*c*) cellulose–AgBr hybrids prepared by microwave heating using different types of ionic liquids: (*a*) [Bmim]Cl; (*b*) [Amim]Cl; (*c*) [Bmim]Br. From ref. [88]. Reprinted with permission from Elsevier

using $AgNO_3$ and ascorbic acid in ionic liquid at 130 °C for 30 min via microwave heating (Fig. 5.24d). Experimental results indicated that the cellulose played an important role in the chemical stability of cellulose hybrids.

CuO, as a transition metal oxide with a narrow band gap (Eg = 1.2 eV), has unique electronic, photoconductive, and photochemical properties and wide applications in photovoltaic thin film solar cells, a photocatalyst for water splitting, high-temperature superconductors, and magnetoresist materials. The microwave-assisted IL route was used for the preparation of cellulose–CuO nanocomposites [89]. CuO crystals were formed by thermal treatment of the cellulose–CuO nanocomposites at 800 °C for 3 h in air. It was found that the ratio of cellulose solution to ionic liquid had an effect on the shapes of CuO in nanocomposites.

Experimental results revealed that the CuO shape changed from nanosheets to bundles and to particles with increasing heating time. CuO crystals with bundle-like shape consisting of nanosheets grew on cellulose substrate in IL (10 mL)/cellulose solution (10 mL) by microwave heating at 100 °C for 20 min (Fig. 5.25). CuO crystals displayed relatively uniform size and consisted of regular nanosheets with a heating time of 10 min. CuO particles with diameters of about 300 nm for 40 min were obtained. Obviously, choosing an appropriate heating time is important for the formation of the cellulose–CuO nanocomposites.

ZnO, a wide band gap II-VI semiconducting material, has unique properties such as large exciton binding energy (60 meV), optical transparency, electric conductivity,

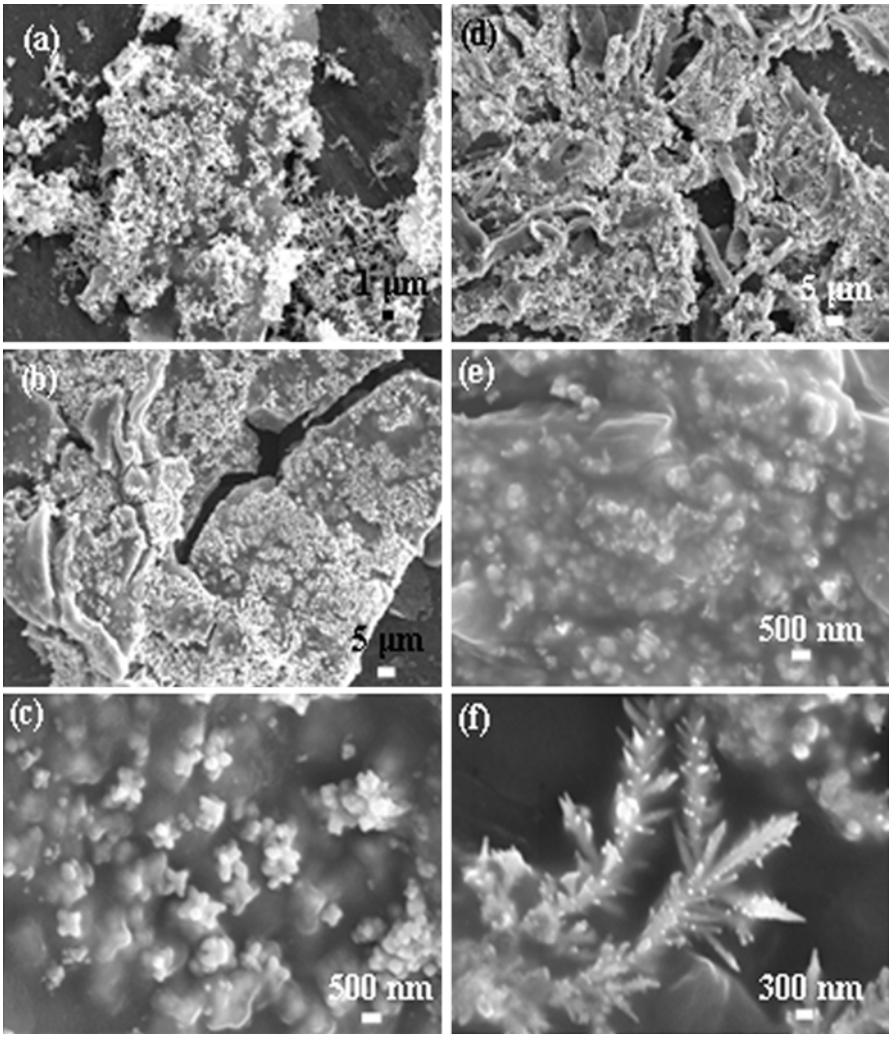

Fig. 5.23 SEM images of (**a**–**c**) the cellulose–AgCl and (**d**–**f**) cellulose–AgBr hybrids prepared by microwave heating using different types of ionic liquids: (**a**) [Bmim]Cl; (**b**) and (**c**) [Amim]Cl; (**d**–**f**) [Bmim]Br. From ref. [88]. Reprinted with permission from Elsevier

piezoelectricity and possible applications in short-wavelength optoelectronics, gas sensors, solar energy conversion, and field emission. Microwave-assisted method was developed for the fabrication of $Zn_5(OH)_8Cl_2{\cdot}H_2O$ sheets using microcrystalline cellulose as matrix from $ZnCl_2 \cdot 3H_2O$ (Fig. 5.26) [90]. ZnO crystals were formed by the thermal decomposition of the $Zn_5(OH)_8Cl_2{\cdot}H_2O$ at 600 °C for 3 h in air.

The cellulose was found to have fiber-like shape by oil heating (Fig. 5.26a). $Zn_5(OH)_8Cl_2{\cdot}H_2O$ hexagonal sheets with the thickness of about 70 nm and the average size of about 1.2 μm were obtained on the surface of cellulose by microwave

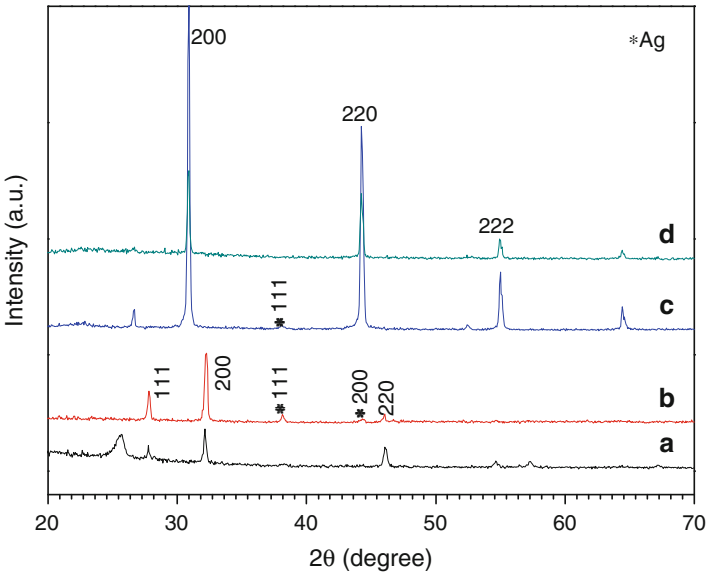

Fig. 5.24 XRD patterns of the cellulose–AgX/Ag hybrids prepared by microwave heating using different types of ionic liquids: (*a*) and (*b*) [Amim]Cl; (*c*) and (*d*) [Bmim]Br. From ref. [88]. Reprinted with permission from Elsevier

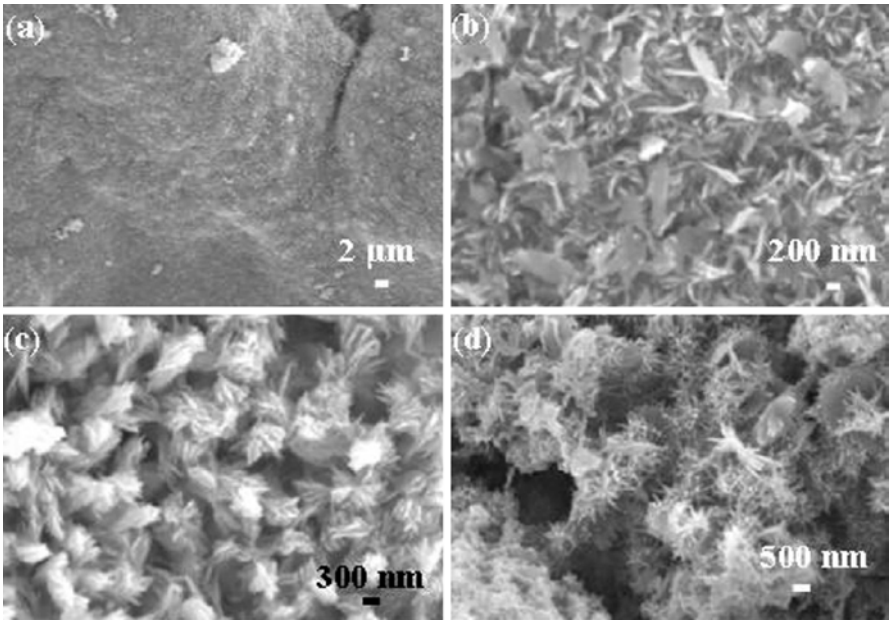

Fig. 5.25 SEM images of the cellulose–CuO nanocomposites prepared in ionic liquid (10 mL)/cellulose solution (10 mL) by microwave heating at 100 °C for 20 min. From ref. [89]. Reprinted with permission from Elsevier

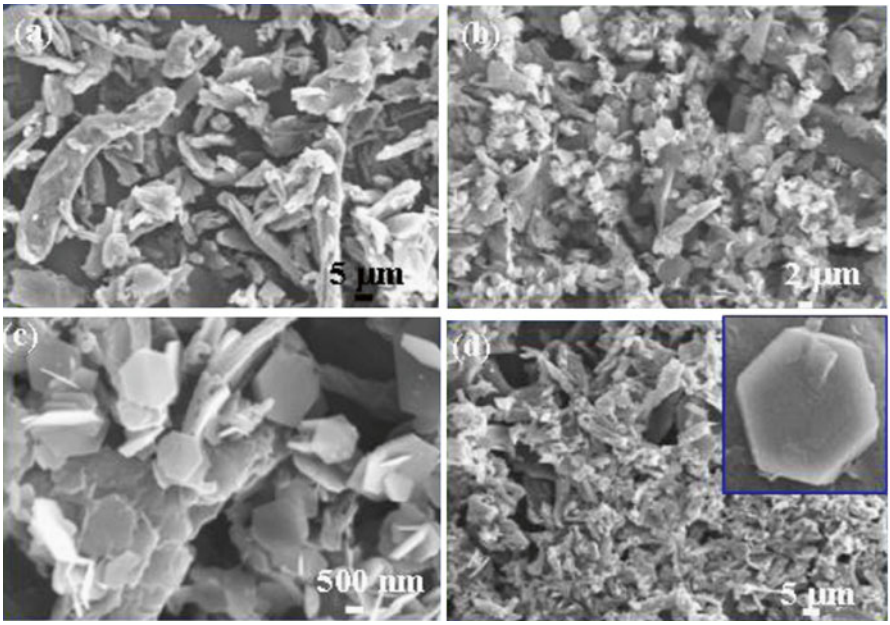

Fig. 5.26 SEM images of the $Zn_5(OH)_8Cl_2{\cdot}H_2O$ sheets prepared (**a**) by oil heating and (**b**–**d**) by microwave heating for different times: (**b**, **c**) 30 min; (**d**) 60 min. From ref. [90]. Reprinted with permission from Elsevier

heating (Fig. 5.26b–d). The size of $Zn_5(OH)_8Cl_2{\cdot}H_2O$ hexagonal sheets was observed to increase with heating time.

Green microwave-assisted method was also developed for the synthesis of the manganese-containing cellulose nanocomposites using microcrystalline cellulose and $Mn(CH_3COO)_2 \cdot 4H_2O$ in the NaOH/urea aqueous solutions [91]. Microcrystalline cellulose pretreated with NaOH/urea aqueous solutions was found to play an important role in the phase, shape, and thermal stability of cellulose nanocomposites. Well-crystalline manganese oxides during the synthetic procedure were not observed before and after thermal treatment (Fig. 5.27). The interesting restrain effect of cellulose treated with NaOH/urea aqueous solutions was found.

It was reported that cellulose treated with NaOH/urea was known to display an irregular flake-like shape. Irregular cellulose flakes and aggregated nanosheets were observed for 10 min (Fig. 5.28a–c). The nanosheets with the dramatically decreasing size were observed to grow on the cellulose substrate for 40 min (Fig. 5.28d–f). The nanosheets bundles were found at the surface of cellulose for 60 min (Fig. 5.28g–i).

Based on the abovementioned experimental results, one can deduce that green microwave-assisted method can be widely employed for the synthesis of various biomass nanocomposites such as cellulose–metal, cellulose–metal oxides, cellulose–metal complex oxides nanocomposites, and so on. However, the properties, mechanism, and potential applications of these biomass nanocomposites still need

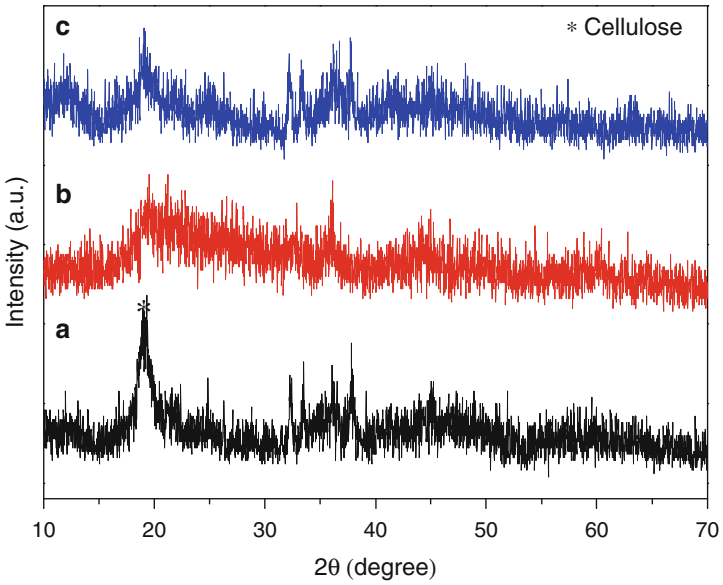

Fig. 5.27 XRD patterns of the samples prepared at 80 °C for (*a*) 10 min, (*b*) 40 min, and (*c*) 60 min. From ref. [91]. Reprinted with permission from Elsevier

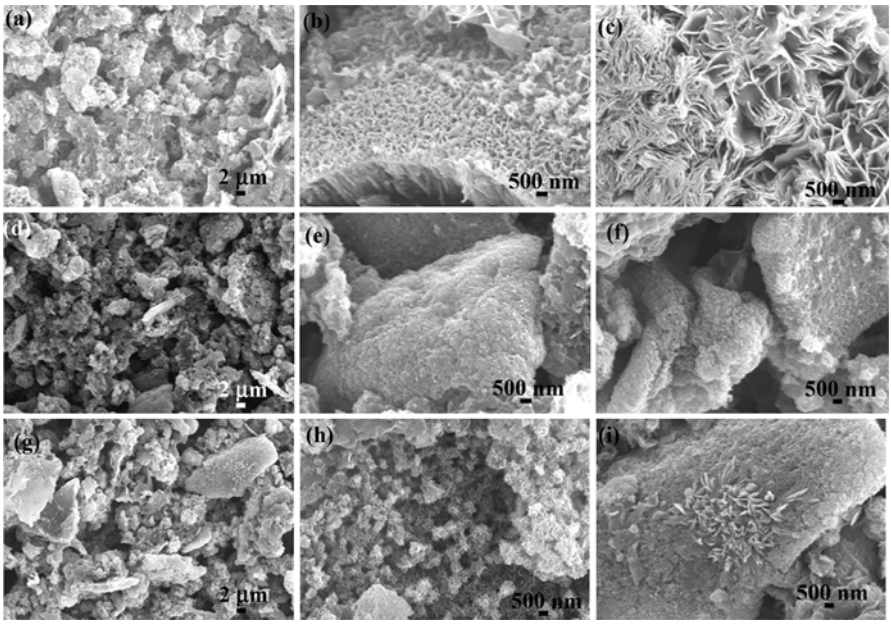

Fig. 5.28 SEM images of the manganese-containing cellulose nanocomposites prepared at 80 °C for (**a**–**c**) 10 min, (**d**–**f**) 40 min, and (**g**–**i**) 60 min. From ref. [91]. Reprinted with permission from Elsevier

to be further explored in the near future. The improved properties and wide potential applications of biomass nanocomposites reflect real advantages of green strategies including method, solvent, materials, and procedure.

5.4 Future Prospects

The abovementioned works have indicated that there are several research works on the nanomaterials and nanocomposites via the microwave-assisted method. In comparison to other green processes, this microwave-assisted method has exhibited obvious advantages, obtained different results, and had wide potential applications. The different results and improved properties could open new applications of nanomaterials and nanocomposites. In the near future, more and more examples would be provided, which may display the advantages of green microwave-assisted method.

As mentioned in our earlier review [2] and the review by Zhu and Chen [3], the near future research trends and directions should be focused including the in-depth understanding of the detailed mechanisms under microwave-assisted method, comparative studies between the microwave heating and conventional heating, theoretical and computer simulations of microwave effects and microwave mechanisms, and microwave-assisted large-scale production, and so on.

It is well known that the green processes are system concepts. The synthetic method only is a part of the green processes. Besides green synthetic route, the other green processes such as green solvents, green resources, green materials, green design, and green production also should be considered. In some examples, toxic solvent such as [Bmim][BF_4] was used.

5.5 Summary

In summary, this chapter describes the green microwave-assisted method for the preparation of nanomaterials and nanocomposites. As described above, there are many reports on the research of various nanomaterials including metal nanomaterials, metal oxides nanomaterials, metal chalcogenides nanomaterials, bio-nanomaterials, nanocomposites, and biomass-based nanocomposites via this green process. The as-obtained nanomaterials and nanocomposites display excellent properties and have wide potential applications such as biomedical, gas sensing, photocatalyst, printing, drug delivery, protein/DNA adsorption, adsorbents, dye-sensitized solar cells, antibacterial materials, and anode materials especially for lithium-ion battery. Obviously, the green microwave-assisted method is a promising process for nanotechnology.

Acknowledgments Financial support from the Fundamental Research Funds for the Central Universities (No. JC2013-3), Beijing Nova Program (Z121103002512030), the Program for New Century Excellent Talents in University (NCET-11-0586), and National Natural Science Foundation of China (31070511) is gratefully acknowledged.

References

1. Adam D (2003) Microwave chemistry: out of the kitchen. Nature 421:571–572
2. Ma MG, Zhu JF, Zhu YJ, Sun RC (2014) The microwave-assisted ionic-liquid method: a promising methodology in nanomaterials. Chem Asian J 9:2378–2391
3. Zhu YJ, Chen F (2014) Microwave-assisted preparation of inorganic nanostructures in liquid phase. Chem Rev 114:6462–6555
4. Vollmer C, Redel E, Abu-Shandi K, Thomann R, Manyar H, Hardacre C, Janiak C (2010) Microwave irradiation for the facile synthesis of transition-metal nanoparticles (NPs) in ionic liquids (ILs) from metal–carbonyl precursors and Ru-, Rh-, and Ir-NP/IL dispersions as biphasic liquid-liquid hydrogenation nanocatalysts for cyclohexene. Chem Eur J 16:3849–3858
5. Pradhan M, Sarkar S, Sinha AK, Basu M, Pal T (2010) High-yield synthesis of 1D Rh nanostructures from surfactant mediated reductive pathway and their shape transformation. J Phys Chem C 114:16129–16142
6. Liu JW, Chen F, Zhang M, Qi H, Zhang CL, Yu SH (2010) Rapid microwave-assisted synthesis of uniform ultralong Te nanowires, optical property, and chemical stability. Langmuir 26:11372–11377
7. Horikoshi S, Abe H, Torigoe K, Abe M, Serpone N (2010) Access to small size distributions of nanoparticles by microwave-assisted synthesis. Formation of Ag nanoparticles in aqueous carboxymethylcellulose solutions in batch and continuous-flow reactors. Nanoscale 2:1441–1447
8. Liu SH, Lu F, Zhu JJ (2011) Highly fluorescent Ag nanoclusters: microwave-assisted green synthesis and Cr^{3+} sensing. Chem Commun 47:2661–2663
9. Li RQ, Wang CL, Bo F, Wang ZY, Shao HB, Xu SH, Cui YP (2012) Microwave-assisted synthesis of fluorescent Ag nanoclusters in aqueous solution. ChemPhysChem 13:2097–2101
10. Uppal MA, Kafizas A, Ewing MB, Parkin IP (2010) The effect of initiation method on the size, monodispersity and shape of gold nanoparticles formed by the Turkevich method. New J Chem 34:2906–2914
11. Yan L, Cai YQ, Zheng BZ, Yuan HY, Guo Y, Xiao D, Choi MMF (2012) Microwave-assisted synthesis of BSA-stabilized and HSA-protected gold nanoclusters with red emission. J Mater Chem 22:1000–1005
12. Yue Y, Liu TY, Li HW, Liu ZY, Wu YQ (2012) Microwave-assisted synthesis of BSA-protected small gold nanoclusters and their fluorescence-enhanced sensing of silver(I) ions. Nanoscale 4:2251–2254
13. Shang L, Yang LX, Stockmar F, Popescu R, Trouillet V, Bruns M, Gerthsen D, Nienhaus GU (2012) Microwave-assisted rapid synthesis of luminescent gold nanoclusters for sensing Hg^{2+} in living cells using fluorescence imaging. Nanoscale 4:4155–4160
14. Kou JH, Varma RS (2012) Beet juice utilization: expeditious green synthesis of noble metal nanoparticles (Ag, Au, Pt, and Pd) using microwaves. RSC Adv 2:10283–10290
15. Liu YQ, Zhang M, Wang FX, Pan GB (2012) Facile microwave-assisted synthesis of uniform single-crystal copper nanowires with excellent electrical conductivity. RSC Adv 2:11235–11237
16. Hu B, Wu LH, Liu SJ, Yao HB, Shi HY, Li GP, Yu SH (2010) Microwave-assisted synthesis of silver indium tungsten oxide mesocrystals and their selective photocatalytic properties. Chem Commun 46:2277–2279
17. Xiao LS, Shen H, von Hagen R, Pan J, Belkoura L, Mathur S (2010) Microwave assisted fast and facile synthesis of SnO_2 quantum dots and their printing applications. Chem Commun 46:6509–6511
18. Huang H, Sithambaram S, Chen CH, Kithongo CK, Xu LP, Iyer A, Garces HF, Suib SL (2010) Microwave-assisted hydrothermal synthesis of cryptomelane-type octahedral molecular sieves (OMS-2) and their catalytic studies. Chem Mater 22:3664–3669
19. Volanti DP, Orlandi MO, Andrés J, Longo E (2010) Efficient microwave-assisted hydrothermal synthesis of CuO sea urchin-like architectures via a mesoscale self-assembly. CrystEngComm 12:1696–1699

20. Zhang DQ, Li GS, Wang F, Yu JC (2010) Green synthesis of a self-assembled rutile mesocrystalline photocatalyst. CrystEngComm 12:1759–1763
21. Conrad F, Zhou Y, Yulikov M, Hametner K, Weyeneth S, Jeschke G, Gunther D, Grunwaldt JD, Patzke GR (2010) Microwave-hydrothermal synthesis of nanostructured zinc-copper gallates. Eur J Inorg Chem 2010:2036–2043
22. Phuruangrat A, Ham DJ, Hong SJ, Thongtem S, Lee JS (2010) Synthesis of hexagonal WO_3 nanowires by microwave-assisted hydrothermal method and their electrocatalytic activities for hydrogen evolution reaction. J Mater Chem 20:1683–1690
23. Qiu G, Dharmarathna S, Genuino H, Zhang Y, Huang H, Suib SL (2011) Facile microwave-refluxing synthesis and catalytic properties of vanadium pentoxide nanomaterials. ACS Catal 1:1702–1709
24. Wu LH, Yao HB, Hu B, Yu SH (2011) Unique lamellar sodium/potassium iron oxide nanosheets: facile microwave-assisted synthesis and magnetic and electrochemical properties. Chem Mater 23:3946–3952
25. Cao XF, Zhang L, Chen XT, Xue ZL (2011) Microwave-assisted solution-phase preparation of flower-like Bi_2WO_6 and its visible-light-driven photocatalytic properties. CrystEngComm 13:306–311
26. Zhang L, Cao XF, Chen XT, Xue ZL (2011) Fast preparation and growth mechanism of erythrocyte-like $Cd_2Ge_2O_6$ superstructures via a microwave-hydrothermal process. CrystEngComm 13:2464–2471
27. Li XY, Liu DP, Song SY, Wang X, Ge X, Zhang HJ (2011) Rhombic dodecahedral Fe_3O_4: ionic liquid-modulated and microwave-assisted synthesis and their magnetic properties. CrystEngComm 13:6017–6020
28. Yang YL, Hu CC, Hua CC (2011) Preparation and characterization of nanocrystalline $Ti_xSn_{1-x}O_2$ solid solutions via a microwave-assisted hydrothermal synthesis process. CrystEngComm 13:5638–5641
29. Meher SK, Rao GR (2011) Effect of microwave on the nanowire morphology, optical, magnetic, and pseudocapacitance behavior of Co_3O_4. J Phys Chem C 115:25543–25556
30. Qiu GH, Huang H, Genuino H, Opembe N, Stafford L, Dharmarathna S, Suib SL (2011) Microwave-assisted hydrothermal synthesis of nanosized α-Fe_2O_3 for catalysts and adsorbents. J Phys Chem C 115:19626–19631
31. Milosevic I, Jouni H, David C, Warmont F, Bonnin D, Motte L (2011) Facile microwave process in water for the fabrication of magnetic nanorods. J Phys Chem C 115:18999–19004
32. Chou SL, Wang JZ, Liu HK, Dou SX (2011) Rapid synthesis of $Li_4Ti_5O_{12}$ microspheres as anode materials and its binder effect for lithium-ion battery. J Phys Chem C 115:16220–16227
33. Chen M, Wang ZH, Han DM, Gu FB, Guo GS (2011) Porous ZnO polygonal nanoflakes: synthesis, use in high-sensitivity NO_2 gas sensor, and proposed mechanism of gas sensing. J Phys Chem C 115:12763–12773
34. Truong TT, Liu YZ, Ren Y, Trahey L, Sun YG (2012) Morphological and crystalline evolution of nanostructured MnO_2 and its application in lithium-air batteries. ACS Nano 6:8067–8077
35. Araújo VD, Avansi W, de Carvalho HB, Moreira ML, Longo E, Ribeiro C, Bernardi MIB (2012) CeO_2 nanoparticles synthesized by a microwave-assisted hydrothermal method: evolution from nanospheres to nanorods. CrystEngComm 14:1150–1154
36. Almeida MAP, Cavalcante LS, Morilla-Santos C, Dalmaschio CJ, Rajagopal S, Li MS, Longo E (2012) Effect of partial preferential orientation and distortions in octahedral clusters on the photoluminescence properties of $FeWO_4$ nanocrystals. CrystEngComm 14:7127–7132
37. Wang QM, Zhang ZY, Zheng YH, Cai WS, Yu YF (2012) Multiple irradiation triggered the formation of luminescent $LaVO_4$: Ln^{3+} nanorods and in cellulose gels. CrystEngComm 14:4786–4793
38. Zhang JC, Wang W, Li BX, Zhang XH, Zhao XD, Liu XY, Zhao M (2012) Self-assembled $NaY(WO_4)_2$ hierarchical dumbbells: microwave-assisted hydrothermal synthesis and their tunable upconversion luminescent properties. Eur J Inorg Chem 2012:2220–2225
39. Shi JY, Liu GJ, Wang N, Li C (2012) Microwave-assisted hydrothermal synthesis of perovskite $NaTaO_3$ nanocrystals and their photocatalytic properties. J Mater Chem 22:18808–18813

40. Liang SJ, Zhu SY, Chen Y, Wu WM, Wang XC, Wu L (2012) Rapid template-free synthesis and photocatalytic performance of visible light-activated $SnNb_2O_6$ nanosheets. J Mater Chem 22:2670–2678
41. Lehnen T, Zopes D, Mathur S (2012) Phase-selective microwave synthesis and inkjet printing applications of Zn_2SnO_4 (ZTO) quantum dots. J Mater Chem 22:17732–17736
42. Qiu GH, Dharmarathna S, Zhang YS, Opembe N, Huang H, Suib SL (2012) Facile microwave-assisted hydrothermal synthesis of CuO nanomaterials and their catalytic and electrochemical properties. J Phys Chem C 116:468–477
43. Moreira ML, Longo VM, Avansi W Jr, Ferrer MM, Andrés J, Mastelaro VR, Varela JA, Longo É (2012) Quantum mechanics insight into the microwave nucleation of $SrTiO_3$ nanospheres. J Phys Chem C 116:24792–24808
44. Su YG, Zhu BL, Guan K, Gao SS, Lv L, Du CF, Peng LM, Hou LC, Wang XJ (2012) Particle size and structural control of $ZnWO_4$ nanocrystals via Sn^{2+} doping for tunable optical and visible photocatalytic properties. J Phys Chem C 116:18508–18517
45. Conrad F, Massue C, Küehl S, Kunkes E, Girgsdies F, Kasatkin I, Zhang BS, Friedrich M, Luo Y, Armbrüester M, Patzke GR, Behrens M (2012) Microwave-hydrothermal synthesis and characterization of nanostructured copper substituted ZnM_2O_4 (M=Al, Ga) spinels as precursors for thermally stable Cu catalysts. Nanoscale 4:2018–2028
46. Etacheri V, Michlits G, Seery MK, Hinder SJ, Pillai SC (2013) A highly efficient $TiO_{2-x}C_x$ nano-heterojunction photocatalyst for visible light induced antibacterial applications. ACS Appl Mater Interfaces 5:1663–1672
47. Manseki K, Kondo Y, Ban T, Sugiura T, Yoshida T (2013) Size-controlled synthesis of anisotropic TiO_2 single nanocrystals using microwave irradiation and their application for dye-sensitized solar cells. Dalton Trans 42:3295–3299
48. Al Juhaiman L, Scoles L, Kingston D, Patarachao B, Wang DS, Bensebaa F (2010) Green synthesis of tunable $Cu(In_{1-x}Gax)Se_2$ nanoparticles using non-organic solvents. Green Chem 12:1248–1252
49. Apte SK, Garaje SN, Bolade RD, Ambekar JD, Kulkarni MV, Naik SD, Gosavi SW, Baeg JO, Kale BB (2010) Hierarchical nanostructures of $CdIn_2S_4$ via hydrothermal and microwave methods: efficient solar-light-driven photocatalysts. J Mater Chem 20:6095–6102
50. Gallagher SA, Moloney MP, Wojdyla M, Quinn SJ, Kelly JM, Gun'ko YK (2010) Synthesis and spectroscopic studies of chiral CdSe quantum dots. J Mater Chem 20:8350–8355
51. Han H, Di Francesco G, Maye MM (2010) Size control and photophysical properties of quantum dots prepared via a novel tunable hydrothermal route. J Phys Chem C 114:19270–19277
52. Hu Y, Liu Y, Qian HS, Li ZQ, Chen JF (2010) Coating colloidal carbon spheres with CdS nanoparticles: microwave-assisted synthesis and enhanced photocatalytic activity. Langmuir 26:18570–18575
53. Guo X, Wang CF, Fang Y, Chen L, Chen S (2011) Fast synthesis of versatile nanocrystal-embedded hydrogels toward the sensing of heavy metal ions and organoamines. J Mater Chem 21:1124–1129
54. Hayakawa Y, Nonoguchi Y, Wu HP, Diau EWG, Nakashima T, Kawai T (2011) Rapid preparation of highly luminescent CdTe nanocrystals in an ionic liquid via a microwave-assisted process. J Mater Chem 21:8849–8853
55. Du J, Li XL, Wang SJ, Wu YZ, Hao XP, Xu CW, Zhao X (2012) Microwave-assisted synthesis of highly luminescent glutathione-capped $Zn_{1-x}Cd_xTe$ alloyed quantum dots with excellent biocompatibility. J Mater Chem 22:11390–11395
56. Qi C, Zhu YJ, Zhao XY, Lu BQ, Tang QL, Zhao J, Chen F (2013) Highly stable amorphous calcium phosphate porous nanospheres: microwave-assisted rapid synthesis using ATP as phosphorus source and stabilizer, and their application in anticancer drug delivery. Chem Eur J 19:981–987
57. Qi C, Zhu YJ, Lu BQ, Zhao XY, Zhao J, Chen F, Wu J (2013) Hydroxyapatite hierarchically nanostructured porous hollow microspheres: rapid, sustainable microwave-hydrothermal synthesis by using creatine phosphate as an organic phosphorus source and application in drug delivery and protein adsorption. Chem Eur J 19:5332–5341

58. Zhao XY, Zhu YJ, Chen F, Lu BQ, Wu J (2013) Nanosheet-assembled hierarchical nanostructures of hydroxyapatite: surfactant-free microwave hydrothermal rapid synthesis, protein/DNA adsorption and pH-controlled release. CrystEngComm 15:206–212
59. Escudero A, Calvo ME, Rivera-Fernández S, de la Fuente JM, Ocaña M (2013) Microwave-assisted synthesis of biocompatible europium-doped calcium hydroxyapatite and fluoroapatite luminescent nanospindles functionalized with poly(acrylic acid). Langmuir 29:1985–1994
60. Zhu D, Jiang XX, Zhao C, Sun XL, Zhang JR, Zhu JJ (2010) Green synthesis and potential application of low-toxic Mn: ZnSe/ZnS core/shell luminescent nanocrystals. Chem Commun 46:5226–5228
61. Zhang H, Yin YJ, Hu YJ, Li CY, Wu P, Wei SH, Cai CX (2010) Pd@Pt core-shell nanostructures with controllable composition synthesized by a microwave method and their enhanced electrocatalytic activity toward oxygen reduction and methanol oxidation. J Phys Chem C 114:11861–11867
62. Tang SC, Vongehr S, Meng XK (2010) Carbon spheres with controllable silver nanoparticle doping. J Phys Chem C 114:977–982
63. Zhu XJ, Zhu YW, Murali S, Stollers MD, Ruoff RS (2011) Nanostructured reduced graphene oxide/Fe_2O_3 composite as a high-performance anode material for lithium ion batteries. ACS Nano 5:3333–3338
64. Sun CL, Chang CT, Lee HH, Zhou JG, Wang J, Sham TK, Pong WF (2011) Microwave-assisted synthesis of a core-shell MWCNT/GONR heterostructure for the electrochemical detection of ascorbic acid, dopamine, and uric acid. ACS Nano 5:7788–7795
65. Liu XJ, Pan LK, Lv T, Zhu G, Sun Z, Sun CQ (2011) Microwave-assisted synthesis of CdS-reduced graphene oxide composites for photocatalytic reduction of Cr(VI). Chem Commun 47:11984–11986
66. Hu Y, Qian H, Liu Y, Du G, Zhang F, Wang L, Hu X (2011) A microwave-assisted rapid route to synthesize ZnO/ZnS core-shell nanostructures via controllable surface sulfidation of ZnO nanorods. CrystEngComm 13:3438–3443
67. Zhong C, Wang JZ, Chen ZX, Liu HK (2011) SnO_2-raphene composite synthesized via an ultrafast and environmentally friendly microwave autoclave method and its use as a superior anode for lithium-ion batteries. J Phys Chem C 115:25115–25120
68. Belousov OV, Belousova NV, Sirotina AV, Solovyov LA, Zhyzhaev AM, Zharkov SM, Mikhlin YL (2011) Formation of bimetallic Au-Pd and Au-Pt nanoparticles under hydrothermal conditions and microwave irradiation. Langmuir 27:11697–11703
69. Liu XJ, Pan LK, Lv T, Zhu G, Lu T, Sun Z, Sun CQ (2011) Microwave-assisted synthesis of TiO_2-reduced graphene oxide composites for the photocatalytic reduction of Cr(VI). RSC Adv 1:1245–1249
70. Wong RM, Gilbert DA, Liu K, Louie AY (2012) Rapid size-controlled synthesis of dextran-coated, ^{64}Cu-doped iron oxide nanoparticles. ACS Nano 6:3461–3467
71. Shen YY, Li LL, Lu Q, Ji J, Fei R, Zhang JR, Abdel-Halim ES, Zhu JJ (2012) Microwave-assisted synthesis of highly luminescent CdSeTe@ZnS-SiO_2 quantum dots and their application in the detection of Cu(II). Chem Commun 48:2222–2224
72. Chen W, Ruan H, Hu Y, Li DZ, Chen ZX, Xian JJ, Chen J, Fu XZ, Shao Y, Zheng Y (2012) One-step preparation of hollow ZnO core/ZnS shell structures with enhanced photocatalytic properties. CrystEngComm 14:6295–6305
73. Kundu P, Singhania N, Madras G, Ravishankar N (2012) ZnO-Au nanohybrids by rapid microwave-assisted synthesis for CO oxidation. Dalton Trans 41:8762–8766
74. Zhan HJ, Zhou PJ, He ZY, Tian Y (2012) Microwave-assisted aqueous synthesis of small-sized, highly luminescent CdSeS/ZnS core/shell quantum dots for live cell imaging. Eur J Inorg Chem 2012:2487–2493
75. Yang WL, Liu Y, Hu Y, Zhou MJ, Qian HS (2012) Microwave-assisted synthesis of porous CdO-CdS core-shell nanoboxes with enhanced visible-light-driven photocatalytic reduction of Cr(VI). J Mater Chem 22:13895–13898
76. Shi Y, Chou SL, Wang JZ, Wexler D, Li HJ, Liu HK, Wu YP (2012) Graphene wrapped $LiFePO_4$/C composites as cathode materials for Li-ion batteries with enhanced rate capability. J Mater Chem 22:16465–16470

77. Geng J, Song GH, Jia XD, Cheng FF, Zhu JJ (2012) Fast one-step synthesis of biocompatible ZnO/Au nanocomposites with hollow doughnut-like and other controlled morphologies. J Phys Chem C 116:4517–4525
78. Cho S, Jang JW, Lee JS, Lee KH (2012) Porous ZnO-ZnSe nanocomposites for visible light photocatalysis. Nanoscale 4:2066–2071
79. Chen TQ, Pan LK, Liu XJ, Yu K, Sun Z (2012) One-step synthesis of SnO_2-reduced graphene oxide-carbon nanotube composites via microwave assistance for lithium ion batteries. RSC Adv 2:11719–11724
80. Jia N, Li SM, Zhu JF, Ma MG, Xu F, Wang B, Sun RC (2010) Microwave-assisted synthesis and characterization of cellulose-carbonated hydroxyapatite nanocomposites in NaOH-urea aqueous solution. Mater Lett 64:2223–2225
81. Ma MG, Jia N, Li SM, Sun RC (2011) Nanocomposites of cellulose/carbonated hydroxyapatite by microwave-assisted fabrication in ionic liquid: characterization and thermal stability. Iran Polym J 20:413–421
82. Jia N, Li SM, Ma MG, Sun RC (2012) Rapid microwave-assisted fabrication of cellulose/F--substituted hydroxyapatite nanocomposites using green ionic liquids as additive. Mater Lett 68:44–46
83. Ma MG, Fu LH, Sun RC, Jia N (2012) Compare study on the cellulose/$CaCO_3$ composites via microwave-assisted method using different cellulose types. Carbohydr Polym 90:309–315
84. Ma MG, Dong YY, Fu LH, Li SM, Sun RC (2013) Cellulose/$CaCO_3$ nanocomposites: microwave ionic liquid synthesis, characterization, and biological activity. Carbohydr Polym 92:1669–1676
85. Ma MG, Deng F, Yao K, Tian CH (2014) Microwave-assisted synthesis and characterization of $CaCO_3$ particles-filled wood powder nanocomposites. Bioresources 9:3909–3918
86. Jia N, Li SM, Ma MG, Sun RC, Zhu L (2011) Green microwave-assisted synthesis of cellulose/calcium silicate nanocomposites in ionic liquids and recycled ionic liquids. Carbohydr Res 346:2970–2974
87. Li SM, Jia N, Ma MG, Zhang Z, Liu QH, Sun RC (2011) Cellulose-silver nanocomposites: microwave-assisted synthesis, characterization, their thermal stability, and antimicrobial property. Carbohydr Polym 86:441–447
88. Dong YY, He J, Sun SL, Ma MG, Fu LH, Sun RC (2013) Environmentally-friendly microwave ionic liquids synthesis of hybrids from cellulose and AgX (X = Cl, Br). Carbohydr Polym 98:168–173
89. Ma MG, Qing SJ, Li SM, Zhu JF, Fu LH, Sun RC (2013) Microwave synthesis of cellulose/CuO nanocomposites in ionic liquids and its thermal transformation to CuO. Carbohydr Polym 91:162–168
90. Fu LH, Dong YY, Ma MG, Li SM, Sun SL, Sun RC (2013) $Zn_5(OH)_8Cl_2{\cdot}H_2O$ sheets formed using cellulose as matrix via microwave-assisted method and its transformation to ZnO. Mater Lett 92:136–138
91. Ma MG, Deng F, Yao K (2014) Manganese-containing cellulose nanocomposites: microwave synthesis, characterization, and the restrain effect of cellulose. Carbohydr Polym 111:230–235

Chapter 6
Solvent-Free Functionalization of Carbon Nanomaterials

Elena V. Basiuk and Vladimir A. Basiuk

Abstract Meeting the growing needs for more ecologically friendly, "green" processes for the functionalization of carbon nanomaterials (CNMs), a variety of chemical reactions proceeding under solvent-free conditions were proposed. Significant advances were achieved in the solvent-free covalent functionalization of carbon nanotubes (CNTs): a number of reactions were proposed to introduce organic moieties into the nanotube ends and sidewalls, which can be initiated by temperature, plasma, or mechanochemical treatment. In a number of instances, however, the concept "solvent-free" is applied to the *reaction* conditions only, whereas the entire synthetic protocol still requires auxiliary purification steps, which consume organic solvents along with an additional time, labor, and equipment. Our group systematically worked on the development of *totally* solvent-free functionalization techniques, with an emphasis on the covalent modification of CNTs, and attempting to further apply the same solvent-free protocols to other CNMs, nanodiamond in particular. The functionalization protocols designed by us are based on thermally activated reactions of amidation and nucleophilic addition with chemical compounds (mainly amines and thiols), which are stable and volatile at 150–200 °C under reduced pressure. Among main advantages of this approach is that not only the reactions per se take place at a high rate but also excess reagents are spontaneously removed from the functionalized material, thus making its additional purification unnecessary. As regards other CNMs, while the research effort undertaken for the chemical modification of ND, graphene, and graphene oxide as a whole is significant, the possibility of using solvent-free techniques for this purpose remains strongly underexplored.

Keywords Carbon nanomaterials • Fullerenes • Carbon nanotubes • Nanodiamond • Graphene • Functionalization • Solvent-free

E.V. Basiuk
Centro de Ciencias Aplicadas y Desarrollo Tecnológico, Universidad Nacional Autónoma de México, Circuito Exterior C.U., 04510 México, DF, Mexico

V.A. Basiuk (✉)
Instituto de Ciencias Nucleares, Universidad Nacional Autónoma de México, Circuito Exterior C.U., 04510 Mexico, DF, Mexico
e-mail: basiuk@nucleares.unam.mx

V.A. Basiuk, E.V. Basiuk (eds.), *Green Processes for Nanotechnology*,
DOI 10.1007/978-3-319-15461-9_6

6.1 Introduction

Among the most important materials for modern nanoscience and nanotechnology are carbon nanomaterials (CNMs), comprising fullerenes, carbon nanotubes (CNTs), nanodiamond (ND), graphene, and graphene oxide (GO). The areas of their already existing and potential applications include electronics, energy generation and storage, catalysis, composites, and biomedicine (see, for example, the chapters in the refs. [1–3]).

One of the properties of most of CNMs is that they are poorly soluble in organic and especially aqueous solvent media, which is especially typical for fullerenes, graphene and all the known types of CNTs, namely single-walled, double-walled, and multi-walled nanotubes (SWNTs, DWNTs, and MWNTs, respectively). For example, CNTs tend to agglomerate into bundles, in which individual nanotubes stick together due to strong hydrophobic interactions and are extremely difficult to separate from each other. This trend to agglomeration grossly complicates processability of CNMs and, in particular, makes virtually impossible their integration into aqueous-based biological media, which is indispensable for biomedical applications. Other specific areas, in which mechanical handling of individual carbon nanoparticles is required, are the fabrication of CNT-based probes for atomic force microscopy (AFM), scanning tunneling microscopy (STM), nanoelectronic and nanoelectromechanical devices.

The solubility/dispersibility, and thus processability, of CNMs can be dramatically enhanced by means of their chemical modification (see the refs. [4–7]). The term of chemical modification implies intentional changes of the local chemical nature of nanoparticles (NPs) and other materials in order to tune their chemical, physical, mechanical, and other properties. In the case of CNMs, this can be done by attaching new chemical groups to the fullerene cage [4], to CNT sidewalls and/or ends [5], to the surface of ND particles [6], and finally to the planes and/or edges of graphene and GO sheets [7]. This can be afforded in different ways, and as a result, a large number of both covalent and noncovalent techniques of chemical modification have been designed up to now.

The reader can be confused with other two terms commonly used along with or instead of "chemical modification," which are "functionalization" and "derivatization." The difference between the three terms is sometimes rather vague and subtle, without any strict guidelines of how to use them. In some cases, "chemical modification" can be performed by exploring weak (van der Waals and π–π stacking) noncovalent interactions with relatively unreactive molecules. The term "functionalization" is also used in the above context, though more frequently implies covalent bonding of reactive functional groups to the nanostructure. The term "derivatization" (that is, the covalent formation of chemical derivatives) can be often found as a synonym of "functionalization"; at the same time, its narrower meaning is a further chemical conversion of the functional groups already introduced into the nanoparticle.

Despite the fact that noncovalent modification can be very useful and even optimal for some applications, a major research effort is done toward the design of new and efficient covalent linking techniques. One of the best illustrative examples is the covalent derivatization based on the chemistry of oxygenated functionalities, where carboxylic groups COOH prevail. In the case of CNTs and graphene, they can be generated at the nanotube tips and sidewall defect sites by means of oxidation in strong acidic media. Carboxylic groups are intrinsic to detonation ND, and their concentration can be further increased by the oxidation. Regardless of their origin and of CNM considered, COOH groups are relatively inert under ambient conditions, and therefore need to be activated for a further derivatization step. Their treatment with such activating reagents as thionyl chloride $SOCl_2$ or carbodiimides produces reactive groups, which can be converted into amides by reacting with amines of variable structure and molecular weight [5, 8–13]. In this way, the amide derivatization is inevitably performed in two steps. But what is worse, the whole reaction sequence requires the use of large amounts of organic solvents; it is very tedious and labor-consuming due to a number of auxiliary steps such as washing, centrifugation, and drying; if $SOCl_2$ is employed as an activating reagent, its corrosive and toxic properties must be added to the above list. Many other currently used techniques of CNM covalent modification exhibit similar characteristics.

Within the global trend of looking for more ecologically friendly, "green" processes and technologies, the chemistry of CNMs is no exception. All twelve basic principles of green chemistry formulated by Anastas and Warner [14] are applicable to nanocarbons, but we draw the reader's attention to three of them:

Principle 1. *Prevention*: It is preferable to prevent waste than to treat or clean up waste after it has been created.

Principle 3. *Less hazardous chemical syntheses*: Wherever practicable, synthetic techniques should be designed to use and generate substances that possess low or no toxicity to human health and the environment.

Principle 5. *Safer solvents and auxiliaries*: The use of auxiliary substances (solvents, separation agents, etc.) should be minimized wherever possible and innocuous when used.

These principles clearly imply the importance of reducing, or even better avoiding, the consumption of organic solvents for a chemical process. In our studies on the chemistry of carbon nanomaterials, we systematically addressed and emphasized this aspect. The present review focuses on the application of solvent-free techniques for covalent and noncovalent functionalization of SWNTs, MWNTs, ND, graphene, and GO with organic (as well as some inorganic) compounds obtained up to now, with a limited consideration of the relevant data for fullerenes.

6.2 Fullerenes

While fullerenes are often mentioned as a class of CNMs, sensu stricto they belong to molecular materials due to a well-defined and constant molecular structure (C_{60}, C_{70}, C_{80}, etc.), as opposed to CNTs and graphene. A reader interested in the solvent-free techniques for chemical modification of fullerenes with organic compounds can be addressed to other sources of bibliographic information, for example to the review [15] focusing on mechanochemistry of fullerenes. Here we only consider some experimental results on the gas-phase procedures which are more or less equally applicable for the functionalization of fullerenes and other CNMs (CNTs in particular).

C_{60} is the most common and best studied fullerene in all regards, including its extremely rich chemistry. The most widely employed approaches to its covalent functionalization with organic compounds are based on the nucleophilic addition reactions. Among these reactions, which take advantage of a strong electrophilic nature of C_{60}, one of the first explored was the addition of aliphatic amines [16, 17]. The amine addition onto C_{60} cage was performed by several research groups [16–23] under variable experimental conditions. Most implementations of this reaction are unable to fully control the stoichiometry, and produce complex mixtures of adducts with a variable number of amine molecules added onto C_{60} and of uncertain stereochemistry, which are very difficult (if possible at all) to separate. On average, the number of amine addends may vary between two and six, depending on the amine and reaction conditions used.

In our first report on the solvent-free amination of C_{60} [24], the latter was first impregnated from solution onto the surface of silica gel, then the silica-supported fullerene was treated with nonylamine (NA) vapor at about 150 °C under reduced pressure. Our consideration was that the dispersion of crystalline C_{60} over an inert solid surface can significantly enhance the yield of addition products. High-performance liquid chromatographic analysis found that the reaction produced a complex mixture of addition products. According to the C:N ratio calculated from elemental analysis, the number of NA molecules attached to C_{60} was 3 on average, whereas field-desorption mass spectrometric study detected a number of molecular and fragment ions corresponding to the molecular species with up to six NA moieties added to C_{60}.

The regioselectivity of gas-phase amine polyaddition onto C_{60} (and higher fullerenes) is an important aspect, but unfortunately, it is very difficult to study experimentally. The only relevant information was obtained using density functional theory (DFT) calculations [25], by performing a systematic analysis of possible nucleophilic addition sites of one to six methylamine molecules onto C_{60} cage. By comparing the formation energies for different possible isomeric adducts, we found that the thermodynamically favorable additions are always observed on the 6,6 C=C bonds, and never on the 5,6 junctions. A preferable polyaddition pattern is the one where $–NHCH_3$ and –H addends form an aligned chain, with the C atoms to which

they are attached alternating in a zigzag order. Later, we also approached the problem of regioselectivity in C_{60} fullerene using general-purpose reactivity indicators [26]. While higher fullerenes are of limited interest for nanotechnology due to their much higher cost as compared to that of C_{60}, their reactivity characteristics are of definite scientific interest as well. To provide an insight, we performed DFT modeling of the gas-phase functionalization of C_{80} by methylamine through successive reactions with up to three methylamine molecules [27] and found that the addition preferentially takes place onto the 5,6 bonds (in contrast to what was observed for C_{60} [25]) and that the preferred addition sites are C atoms of the 5,6 bonds of the five-membered ring next to the pentagon of previous addition.

The gas-phase addition of more complex amines, including aliphatic and aromatic mono and diamines, onto C_{60} bulk material and thin films was explored as well. The functionalization of C_{60} with 1,8-diaminooctane (1,8-DAO) at 150–170 °C was employed to prepare cross-linked thin films of fullerene capable of binding silver nanoparticles (AgNPs) [28, 29]. The latter were attached to 1,8-DAO-functionalized films through the Ag coordination to the N donor atoms of diamine. High-resolution transmission electron microscopy (HRTEM) imaging showed that AgNPs had an average diameter of about 5 nm on the functionalized C_{60}, whereas when deposited onto pristine C_{60}, they had much more variable dimensions and showed a trend to twinning.

In another study [30], thin films of C_{60} were first deposited onto silicon substrates and then either functionalized with 1,8-DAO or, for comparison, polymerized by UV pulsed laser irradiation; their comparative characterization was carried out by AFM, optical reflectance, transmittance, and photoluminescence spectroscopies, as well as by measuring the photovoltaic response and electrical parameters of Au/C_{60}/Si heterostructures. The highest photoluminescence efficiency and light transmittance, along with the lowest photocurrent of diode structure, were observed for the chemically functionalized films. Further measurements [31] showed that the decoration of pristine and 1,8-DAO-functionalized C_{60} films with AgNPs did not change the photocurrent spectra as compared to those for undecorated films, but lowered the values of internal quantum efficiency.

The gas-phase functionalization with 1,5-diaminonaphthalene (DAN) as a representative of aromatic amines was proposed as a simple way to modify electronic properties of C_{60} thin films [32]. A temperature of about 190 ° C and reaction time of 4 h were chosen as optimal reaction conditions. Similarly to the functionalization with aliphatic bifunctional 1,8-DAO, two amino groups of DAN were expected to cross-link neighboring fullerene cages. The resulting oligomeric and/or polymeric adducts exhibited a reduced solubility in toluene as compared to pristine C_{60} films, as well as a lower surface roughness as found by AFM. DAN molecules were able to penetrate into the C_{60} bulk, and thus provided an efficient and uniform functionalization. As a result, the DAN-functionalized films acquired better electrical conductivity as compared to that of pristine films not only along the surface layer but also through the entire phase of C_{60}, by one and four orders of magnitude, respectively. Further characterization of optical, photoluminescence and photoelectric

properties of C_{60} fullerene films covalently functionalized with DAN (and with aromatic monoamines 1-aminopyrene and 1-pyrenemethylamine, for comparison) was undertaken for Au/C_{60}/Si photodiode heterostructures [33].

Chemical mechanisms of the gas-phase cross-linking of C_{60} molecules with 1,8-DAO and DAN were studied in detail by means of DFT calculations and different experimental techniques [34], where two alternative mechanisms of the amination reaction via polyaddition and cross-linking were considered. In terms of the calculated relative energies of formation, the cross-linking mechanism turned to be more exothermically preferred than that the diaddition pathway. The experimental techniques used were laser desorption/ionization time-of-flight mass spectrometry (LDI-TOF MS), thermogravimetric analysis (TGA), and AFM. LDI-TOF mass spectra confirmed the covalent attachment of 1,8-DAO and DAN to C_{60}. Both mechanisms were equally efficient in the case of DAN (Fig. 6.1), where the peaks due to $(C_{60})_2$ + DAN, $(C_{60})_2$ + $(DAN)_2$, and $(C_{60})_2$ + $(DAN)_3$ were clearly seen in LDI-TOF mass spectra. At the same time, the polyaddition pathway seems to be more preferable in the case of 1,8-DAO, where the attachment of up to four diamine molecules was observed, without evident presence of cross-linked C_{60} molecules (Fig. 6.2).

Thiols were found to add onto fullerene cage similarly to amines, even though sulfhydryl groups SH are less active nucleophiles as compared to NH_2 groups. The addition reaction was exemplified by the solvent-free functionalization C_{60} thin films with 1,8-octanedithiol (1,8-ODT) at about 140 °C [35]. The dithiol-functionalized films obtained were used as supports for stable and homogeneous deposition of Au nanoparticles (AuNPs), whose average size was about 5 nm according to HRTEM observations. Further comparative optical and photoelectrical characterization of the Au/C_{60}/Si heterostructures [36–38] was performed for different types of C_{60} thin films: pristine, 1,8-DAO and 1,8-ODT-functionalized, without and with deposited AgNPs and AuNPs, respectively. The direct band (or mobility) gap value of C_{60} showed almost no change after diamine and dithiol functionalization, with a slight decrease after further deposition of metal nanoparticles [38]. Both types of functionalization changed the optical gap value, but in a different way: 1,8-DAO functionalization increased, whereas 1,8-ODT functionalization decreased the optical gap. The deposition of AgNPs and AuNPs decreased all the optical parameters as a result of reducing structural disorder in the functionalized films.

In the context of fullerene functionalization, a class of compounds of special interest is porphyrins and related macrocyclic systems, which is due to a significant research effort toward the design of new efficient light-harvesting systems (for example, see reviews [39–41] and references cited therein). The applicability of solvent-free functionalization technique is limited here due to very low volatility of porphyrin-type compounds, unless high-vacuum conditions are employed. As a consequence, instead of functionalizing crystalline fullerene powders, the macrocyclic compounds are deposited onto C_{60} films by means of physical vapor deposition (PVD), and therefore, only noncovalent interactions are explored. In the porphyrin–fullerene hybrid films obtained by PVD, a structural aspect of particular interest is self-assembled monolayers (SAMs) of porphyrins. In our report [42],

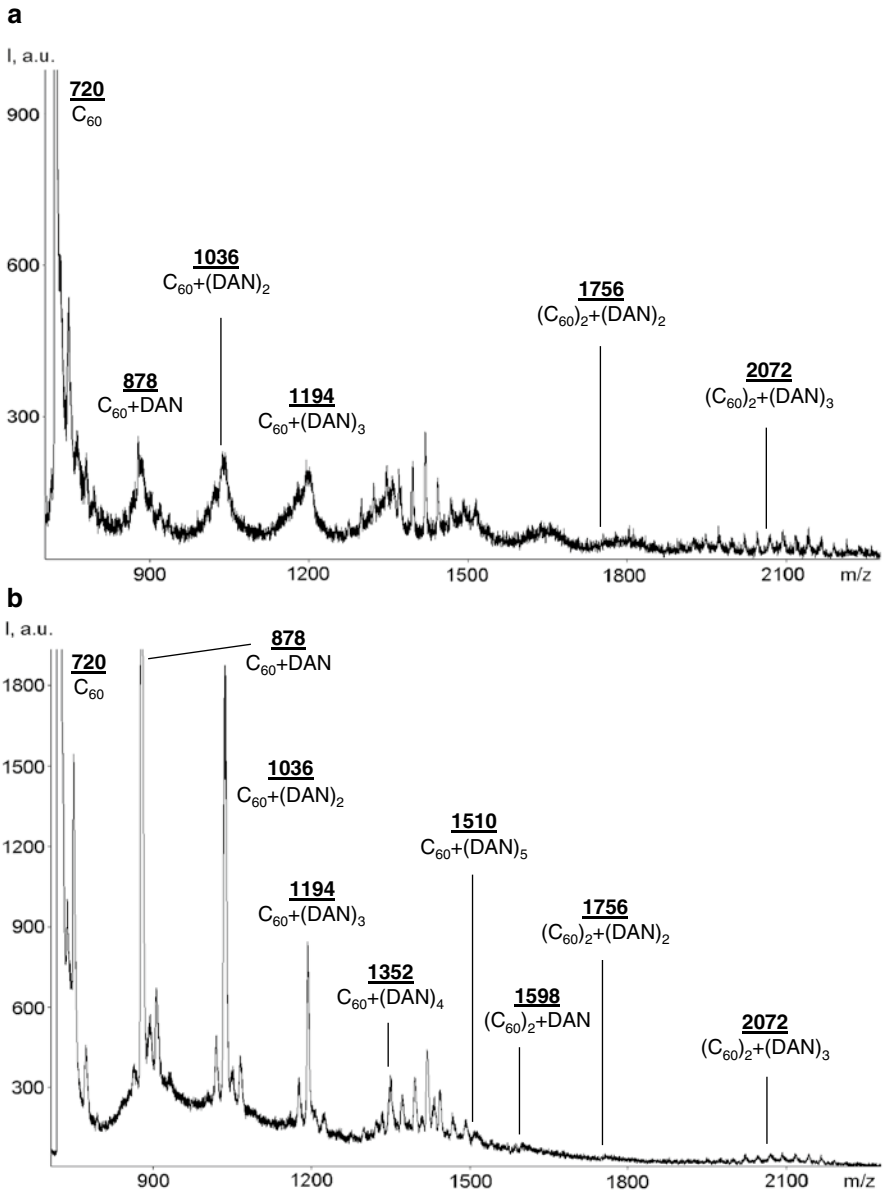

Fig. 6.1 Representative positive (**a**) and negative ion (**b**) LDI-TOF mass spectra of 1,5-diaminonaphthalene-functionalized fullerene C_{60} [34]. Reprinted with permission from the American Chemical Society

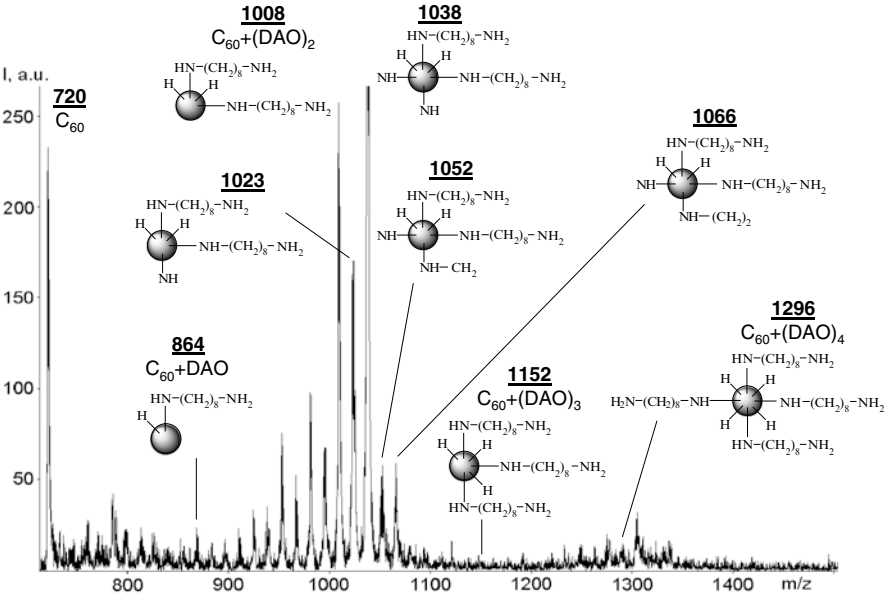

Fig. 6.2 Representative negative ion LDI-TOF mass spectra of 1,8-diaminooctane-functionalized fullerene C_{60}. For convenience, fullerene cages are shown as balls, and 1,8-DAO is abbreviated as DAO [34]. Reprinted with permission from the American Chemical Society

we performed combined theoretical–experimental analysis of the behavior of *meso*-tetraphenylporphine (also called 5,10,15,20-tetraphenyl-21*H*,23*H*-porphine, or H_2TPP) and its transition metal complexes with Ni(II) and Co(II) (NiTPP and CoTPP, respectively), adsorbed from the gas phase onto C_{60} films supported on highly oriented pyrolytic graphite (C_{60}@HOPG). The results of STM imaging of adsorbed porphyrin molecules were compared with theoretical models, consisting of graphene sheets covered with a dense monolayer of C_{60} (C_{60}@G) and accommodating H_2TPP molecules in different ways, whose geometry was optimized by using MM+ molecular mechanics. NiTPP and CoTPP molecules were found to form ordered surface arrangements on C_{60}@HOPG films (Fig. 6.3), whose basic structural elements included equilateral triangles or parallel rows formed by porphyrin species. At the same time, the assemblies covered very limited areas, evidently due to the fact that the fullerene films are composed of overlapping 20–70 nm-sized clusters, and each individual cluster exhibits additional imperfections, thus preventing the formation of extended porphyrin arrays. In addition to the molecular mechanics modeling [42], a number of theoretical studies attempted DFT description of noncovalent porphyrin–fullerene interactions; however, due to computational limitations the model systems were limited to porphyrin–C_{60} dyads and triads (see refs. [41, 43–48] and references therein).

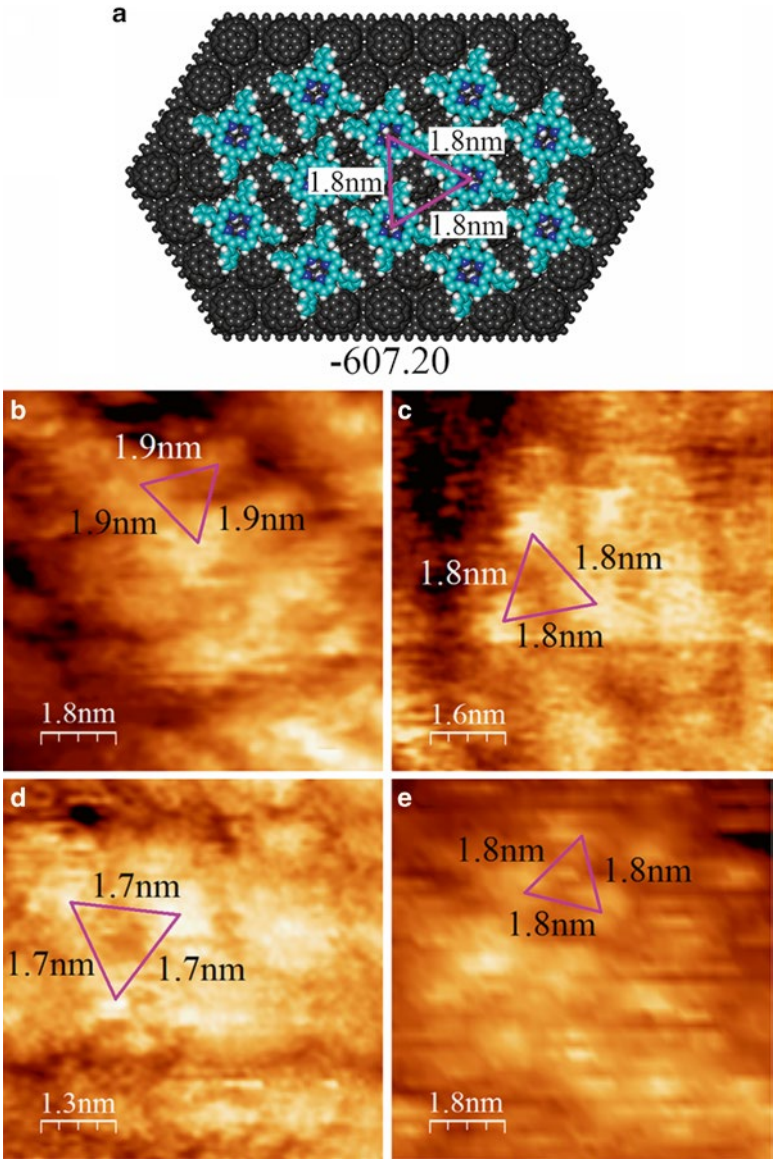

Fig. 6.3 Comparison between (**a**) MM+ optimized model for the most energetically favorable arrangement of 12 H_2TPP molecules on C_{60}@G (formation energy in kcal mol^{-1}), and STM topographic images of experimentally observed self-assemblies of (**b**, **c**) CoTPP (I_T = 0.8 nA, V = −0.8 V, and I_T = 0.8 nA, V = −0.5 V, respectively) and (**d**, **e**) NiTPP (I_T = 0.7 nA, V = −0.5 V, and I_T = 0.8 nA, V = −0.5 V, respectively) formed on the surface of C_{60}@HOPG thin film. The theoretical model predicts the formation of interacting equilateral triangles or parallel rows of porphyrins with a 1.8 nm periodicity. The STM images show similar geometries of assembly, with periodicities of 1.8–1.9 nm for CoTPP, and 1.7–1.8 nm for NiTPP, that is in good agreement with the modeling results. Reprinted from ref. [42], with permission by Elsevier

6.3 Carbon Nanotubes

Both covalent and noncovalent modification with organic (as well as with some inorganic) compounds can help to dramatically improve solubility/dispersibility and therefore processability of CNTs [5, 9–11] crucial for many applications. A particularly important circumstance from the point of view of biomedical uses is that pristine and oxidized CNTs can cause toxic effects in most living organisms and cells (see refs. [49–51] and references therein), which can be mitigated by "masking" nanotube sidewalls by various functionalizing chemical species.

A large number of both noncovalent and covalent procedures to the functionalization of CNTs was proposed up to now, which, unfortunately, often require large amounts of organic solvents. Thus, the importance of developing alternative, solvent-free functionalization techniques cannot be overestimated [52].

6.3.1 Nanotube Sidewalls

Among the most explored techniques of chemical modification of CNTs [52] is fluorination [53–78], for a number of reasons. For example, fluorinated SWNTs produce metastable solutions in dimethylformamide, tetrahydrofuran, and alcohols after ultrasonication. Fluorination strongly modifies conductivity properties of CNTs, which can be important for their electronic applications. In addition, fluorination can serve as a chemical gateway to further chemical conversions on the nanotube sidewalls. In most cases, the fluorination was performed by reaction of solid CNTs with fluorine gas, although other fluorinating reagents were found to be efficient such as CF_4 plasma [66, 72, 76, 77], gas mixtures of BrF_3 and Br_2 [68], as well as of F_2, O_2, and N_2 [70]. As opposed to traditional fluorination with F_2 and other aggressive gaseous reagents, the reaction of MWNTs with xenon difluoride XeF_2, which takes place at ambient temperature under the sunlight or halogen lamp illumination [71], can be considered as the most ecologically friendly implementation of nanotube fluorination due to its extreme simplicity in performance and safety.

The in situ reaction of reactive aryl diazonium species, obtained from 4-substituted anilines (R-C_6H_4-NH_2, where R = Cl, Br, *tert*-butyl, CO_2CH_3, NO_2, etc.) through the addition of isoamyl nitrite or sodium nitrite in sulfuric or acetic acid, was a technique proposed to covalently functionalize SWNT sidewalls in the absence of common organic solvents [79–81]: instead, isoamyl nitrite, H_2SO_4, and acetic acid are liquids serving as the reaction medium. A mechanochemical variety of the same functionalization reaction for SWNTs employed ball milling [79]. The reaction of SWNTs with diazonium salts performed in imidazolium and pyridinium-based ionic liquids instead of common organic solvents, results in functionalized individual nanotubes, whose properties are comparable to those of the SWNTs functionalized under harsh reaction conditions [82]. The latter procedure explores the unique solvent properties of ionic liquids and can be completed in minutes at ambient temperature. Thus, despite the fact that this method does employ solvents, it allows for an obvious gain from the point of view of green chemistry.

A scalable solvent-free process yielding highly functionalized and dispersible MWNTs was developed by using in situ generated aryl diazonium salts in the presence of ammonium persulfate and 2,2′-azoisobutyronitrile [83]. Sidewalls of both MWNTs and SWNTs can be functionalized under solvent-free conditions with azobenzene and anthraquinone residues possessing redox activity, for potential applications in functional catalysis and memory storage devices [84].

Polyurethane-grafted SWNTs were obtained by the coupling reaction of alkyne moiety-decorated nanotubes with azide moiety containing polyurethane using Cu(I) catalyzed Huisgen [3+2] cycloaddition [85], where alkyne functionalization of SWNTs was performed through their reaction with *p*-aminophenyl propargyl ether using a solvent-free diazotization procedure.

Brunetti et al. [86] proposed a facile approach which uses microwave irradiation to functionalize CNTs through 1,3-dipolar cycloaddition of aziridines under solvent-free conditions. The efficiency of microwave treatment was demonstrated by comparison to a similar protocol under classical conditions for the azomethine ylides in dimethylformamide: under the classical conditions, the reaction was completed in 5 days versus 1 h under microwave irradiation, and the functionalization degree was considerably lower. Solvent-free, one-pot functionalization of MWNTs based on the 1,3-dipolar cycloaddition of azomethine ylides using *N*-benzyloxycarbonyl glycine and formaldehyde was reported in ref. [87]. A straightforward solvent-free synthetic procedure for delta-1-pyrroline grafted onto MWNTs by the 1,3-dipolar cycloaddition of the mesoionic 4-methyl-2-phenyloxazol-5(4*H*)-one was described by Grassi et al. [88]. One more fast and reproducible approach to the solvent-free, microwave-assisted 1,3-dipolar cycloaddition to SWNTs used carbonyl ylides generated from a series of oxiranes [89]. The treatment of SWNTs with benzylidenmalononitrile epoxide gave rise to a *gem*-dicyano derivative, which is convenient for further transformation into esters or amides via the Pinner reaction. In a recent implementation of covalent functionalization of SWNTs sidewalls through 1,3-dipolar cycloaddition [90], 3-phenyl-phthalazinium-1-olate was employed, which is a stable and reactive azomethine imine; in this case, microwave heating was found to be more efficient than conventional and solvent-free heating.

Covalent functionalization of nanotube sidewalls with 4-vinylaniline under solvent-free conditions was used as a preliminary step in the preparation of SWNT–polystyrene composites [91]. Another example of CNT sidewall modification with alkenes employed gas phase reagents, thus providing a clean, efficient, and scalable methodology [92]. Covalent functionalization of SWNTs with alcohols was performed under microwave irradiation [93], where an electrophilic addition reaction between a series of alcohols and nanotube sidewalls resulted in the attachment of alkyl and OH groups.

Ye et al. [94] designed solvent-free, one-step functionalization of aligned MWNTs using initiated chemical vapor deposition (CVD), where aligned MWNTs were uniformly functionalized with an epoxy polymer. Electrically conducting poly(3,4-ethylenedioxythiophene)/MWNT composites were prepared by in situ oxidative polymerization of ethylenedioxythiophene in the presence of nanotubes in supercritical carbon dioxide as a reaction medium [95]; prior to the polymerization, MWNTs were modified with 3-(trimethoxysilyl)propyl methacrylate to improve

their dispersibility in CO_2. Covalent attachment of 2,2′-(ethylenedioxy)-diethylamine to MWNTs was shown to yield amino-functionalized nanotubes which behaved like liquids at ambient temperature, and therefore could be homogeneously dispersed and chemically embedded in an epoxy matrix through a solvent-free process [96]. As was exemplified by the solvent-free deposition of tertiary phosphines onto SWNTs, the dispersibility in common organic solvents can be also enhanced by means of noncovalent functionalization of nanotubes [97].

A number of reports dealt with the solvent-free functionalization of CNTs with inorganic compounds. The authors of the works [98, 99] looked for a controllable route to stable titania layers on MWNT surfaces, where precursor compounds such as $TiBr_4$, $TiCl_4$, $Ti(O\textit{i}\text{-}Pr)_4$, and $Ti(OEt)_4$ were used to cover nanotubes under solvent-free conditions. Microwave irradiation was shown to be an efficient energy source for the rapid decomposition of organic metal salts (for example, Fe(II), Co(II), Ni(II), Ag(I), and Pd(II) acetates) in solid mixtures with SWNTs and MWNTs under completely solvent-free conditions [100]. The rapid and local Joule heating of nanotube substrates resulted in the instantaneous formation of metal (e.g., Ag, Au, Co, Ni, Pd, Pt) and metal oxide (Fe_3O_4, MnO, TiO_2, etc.) nanoparticles on CNT surfaces in high yields within seconds of microwave exposure. Cobalt molybdate ($CoMoO_4$) nanoplatelets with a crystalline–amorphous core–shell structure were anchored to MWNTs in a similar way, where the microwave treatment took 15 min only [101]. Ruthenium nanoparticles uniformly dispersed on CNT supports were obtained by using solvent-free microwave-assisted thermolysis of dodecacarbonyltriruthenium precursor [102].

An energy source alternative to conventional and microwave heating is plasma ionization. We already mentioned above the possibility to use it for CNT fluorination by means of CF_4 plasma treatment [66, 72, 76, 77]. Further applicability of the plasma technique was demonstrated by Felten et al. [77]. In particular, the use of O_2 and NH_3 atmosphere instead of CF_4 allowed for grafting O- and N-containing functionalities to MWNTs: functional groups formed in this way at the nanotube surface included OH, C=O, COOH, NH_2, etc., whose specific type and concentration depended on the plasma conditions.

A cold plasma approach under NH_3 atmosphere was also used to functionalize SWNTs by Khare et al. [103]. FTIR spectra proved successful functionalization as short as after 20 min of discharge; infrared features detected were due to N–H stretching and bending vibrations of primary and secondary amines, as well as due to C=N and C–H bonds. The same research group later exposed SWNTs to microwave-generated N_2 plasma [104]. The results strongly depended on the distance between the discharge source and SWNT sample, due to the possibility of N atom loss due to recombination. The chemical groups generated in this way were very similar to those identified in the study with NH_3 glow discharge [103].

The approach proposed by Chen et al. [105] for chemical modification of aligned MWNTs employed radio frequency glow-discharge plasma activation with acetaldehyde or ethylenediamine vapor. As a result of plasma-initiated polymerization, a concentric layer of homogeneous polymer film formed around each of the aligned nanotubes. A hollow cathode glow discharge was used for the solvent-free

functionalization of SWNTs [106]. This low temperature, facile and fast treatment can be used to efficiently generate a variety of functional groups including COOH, OH, NH_2, NO_2, and NO to the open ends and sidewalls of SWNTs. The functionalities obtained open the possibility for the further attachment to nanotubes of such complex species as enzymes and antibodies.

Mechanochemical treatment is one more way to covalently functionalize CNTs [15]. This approach can produce local high-pressure spots and therefore bring the reacting species into the closest contact to initiate novel chemical reactions. Apparently, Kónya et al. [107] were first to demonstrate the efficiency of this type of treatment for the chemical modification of CNTs. Their experiments consisted in a large-scale ball-milling production of short MWNTs with simultaneous attachment of thiol, amine, amide, carbonyl, and other chemical groups, by supplying a suitable reactant gas (H_2S, NH_3, Cl_2, CO, CH_3SH, or $COCl_2$) to MWNT sample during the entire ball-milling process. Mechanochemical modification of SWNTs was also undertaken with halocarbons exemplified by trifluoromethane, trichloromethane, tetrachloroethylene, and hexafluoropropene, which can easily produce reactive radical species [108].

While the latter two studies employed reagents, which are gaseous or easily volatile under ambient temperature, Li et al. [109] showed that even nonvolatile compounds such as fullerenes can be used for the chemical modification of CNTs, giving rise to C_{60}-decorated nanotubes. Likewise, Pan et al. [110] employed the high-speed vibration mill technique for the reaction of SWNTs with potassium hydroxide, where a simple milling SWNTs and KOH together under ambient atmosphere and temperature for 2 h produced highly hydrophilic nanotubes with covalently attached OH groups. A more detailed survey of the use of mechanochemical treatment for functionalization of CNTs was presented in the recent review [15].

There are a large number of compounds, which are nonvolatile at room temperature but can sublime without decomposition under vacuum at elevated temperatures. Their particular representatives, which can be used for the gas-phase functionalization of CNTs, are simpler synthetic porphyrins, phthalocyanines, and even fullerenes. Among the most interesting examples illustrating a high-temperature limit of the gas-phase procedure one should mention the works [111, 112], in which cobalt(II) phthalocyanine (CoPc) was encapsulated in DWNTs and MWNTs. In this rather rare example of noncovalent endohedral modification of CNTs, the open-end nanotubes were treated with CoPc vapor under 370–375 °C and high vacuum during 3 days. CoPc deposited on the outside nanotube walls was removed by repeated rinsing with a mixture of chloroform and 1 % trifluoroacetic acid, resulting in endohedrally functionalized materials; their structure was confirmed by TEM, and the corresponding images are presented in Fig. 6.4.

A simpler representative of tetraazamacrocyclic annulene complexes is Ni(II) complex of 5,7,12,14-tetramethyldibenzo-1,4,8,11-tetraazacyclotetradeca-3,5,7,10,12,14-hexaene (also called Ni(II)-tetramethyldibenzotetraaza[14]annulene, or NiTMTAA for simplicity; Fig. 6.5). The gas-phase noncovalent functionalization of both open-end SWNTs and pristine MWNTs with NiTMTAA was tested at two selected temperatures of 220 and 270 °C [113]. The nanohybrid materials obtained

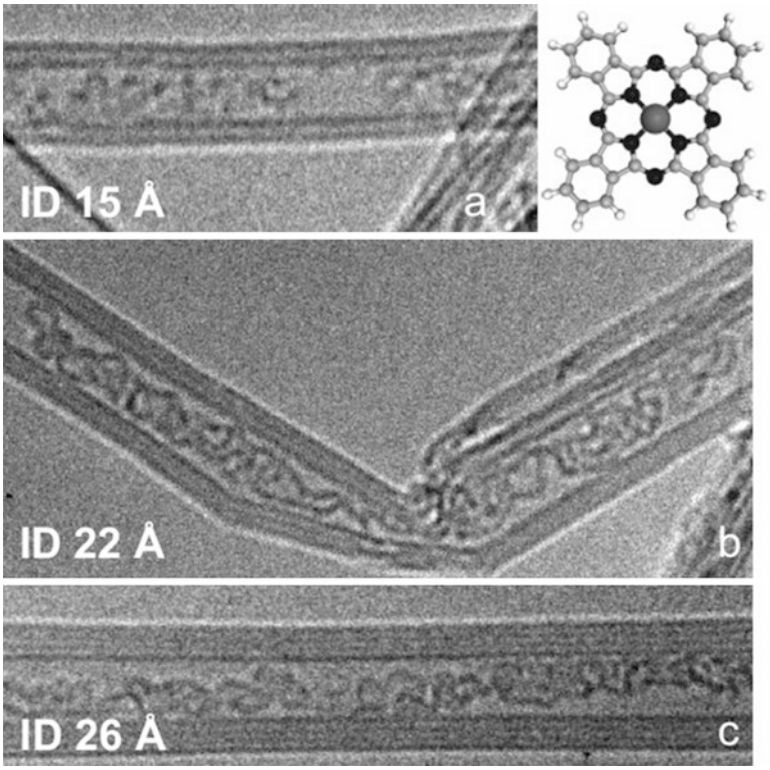

Fig. 6.4 TEM images of CoPc filled nanotubes: (**a**) the narrowest observed DWNT (15 Å inner diameter) filled with CoPc; (**b**, **c**) two MWNTs showing a near optimal degree of filling. Note that all nanotubes have pristine surfaces. *Inset*: schematic drawing of a CoPc molecule, central ion: cobalt, *black*: nitrogen, *grey*: carbon, *white*: hydrogen. Reprinted from ref. [112], with permission by WILEY-VCH Verlag GmbH & Co

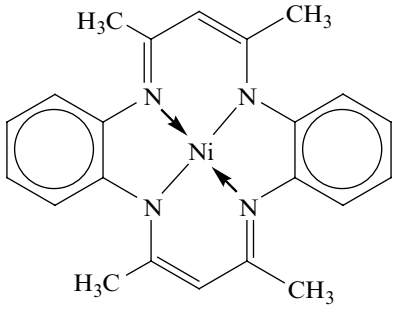

Fig. 6.5 Ni(II) complex of 5,7,12,14-tetramethyldibenzo-1,4,8,11-tetraazacyclotetradeca-3,5,7,10,12,14-hexaene, also called Ni(II)-tetramethyldibenzotetraaza[14]annulene, or NiTMTAA for simplicity

were characterized by means of a number of electron microscopic and spectroscopic techniques, as well as TGA. Thermogravimetric analysis found interesting differences in their composition. In the case of MWNTs (Fig. 6.6b) the separation at about 380 °C between the two weight losses was rather straightforward, whereas for SWNTs (Fig. 6.6a) an additional minor step until ca. 480 °C was observed. These results were interpreted as follows. Pristine MWNTs have closed ends and thus their inner cavities are inaccessible for NiTMTAA. As a result, the latter was adsorbed on the external sidewalls only: this adsorbed form is decomposed until 380 °C producing relatively homogeneous weight loss. On the other hand, SWNTs were acid-purified, had open ends and therefore accessible inner cavities: accordingly, NiTMTAA can adsorb on both external sidewalls and inside the nanotubes, producing two weight loss steps. Increasing the temperature of sublimation reduced adsorption on the external surface, but helped NiTMTAA to penetrate into the nanotube cavities. For comparison, H_2TPP, its metal complexes and hemin, which were deposited onto the same open-end SWNTs from solution and whose molecular size is considerably larger than that of NiTMTAA, did not show any signs of endohedral adsorption [114]. The possibility of both exohedral and endohedral adsorption is an important factor to bear in mind in noncovalent functionalization of CNTs with relatively small chemical species. Unfortunately, it is usually ignored, unless endohedral functionalization is intentional, as it was in the case of CoPc [111, 112].

Speaking in a broader sense, the term "solvent-free" functionalization may be applied not only to a process in which the liquid reaction medium was totally absent but also to the one which did not employ an *organic* solvent. That is, the functionalization carried out in aqueous solutions can be considered as solvent-free as well. This type of functionalization is particularly common in the noncovalent attachment of biomolecules, especially proteins [115–117], since the latter simply do not dissolve in organic solvents. CNTs with strongly adsorbed proteins can serve as templates for the further deposition of metal nanoparticles. For example, this was demonstrated for human serum albumin (HSA) adsorbed on MWNTs, which was used for the decoration with AgNPs [117] generated by reduction of silver nitrate $AgNO_3$ with citric acid [28]. AgNPs deposited onto HSA-functionalized MWNTs (TEM images shown in Fig. 6.7) had a controlled diameter of about 2 nm and a narrow size distribution.

6.3.2 Oxidized Carbon Nanotubes

The functionalization techniques considered in the previous section explore mainly the chemistry of CNT sidewalls. At the same time, a number of methods for nanotube chemical modification employ the chemistry of oxidized defects. The commonly used strong-acid purification processes open the nanotube ends generating there oxygen-containing functionalities, in which carboxylic groups prevail [5, 9–11, 118–120]. And it is COOH groups which can be subjected to further derivatization reactions. The most common approach among the latter is the formation of

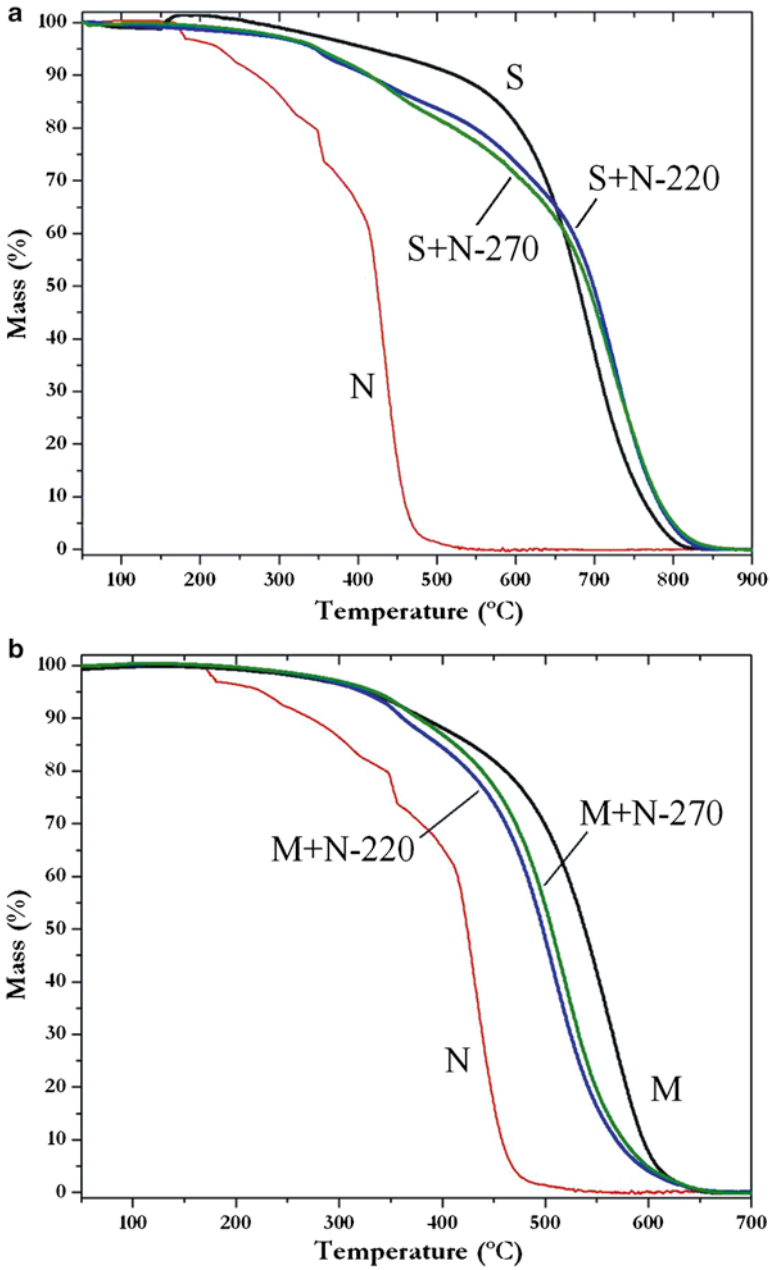

Fig. 6.6 TGA curves for (**a**) SWNTs and (**b**) MWNTs (denoted as S and M, respectively) noncovalently functionalized with NiTMTAA (N) at 220 and 270 °C, in comparison with the curves for pure components [113]. Reprinted with permission from Elsevier

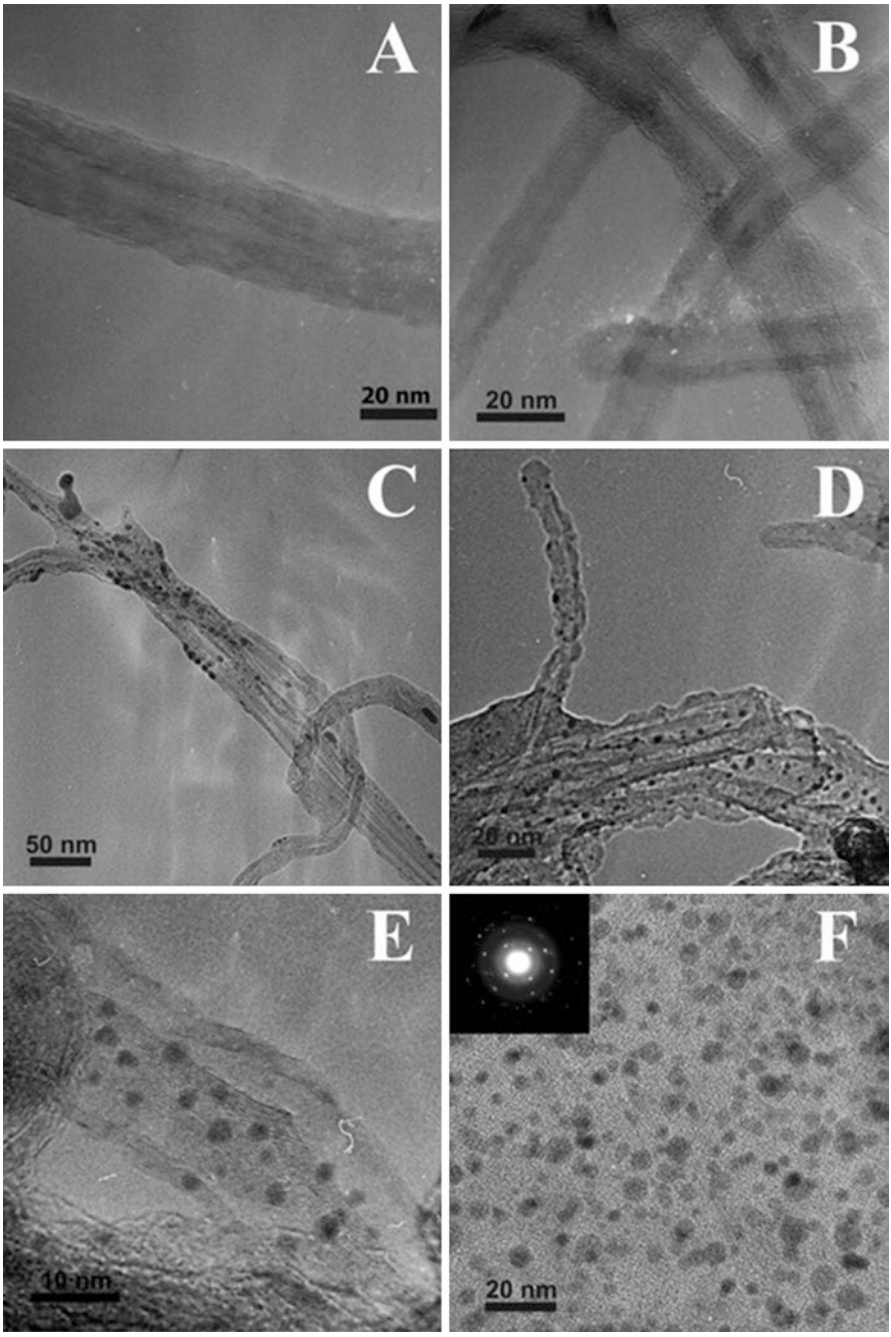

Fig. 6.7 TEM images at of (**a**) pristine MWNTs; (**b**) HSA – MWNT hybrid; (**c**–**e**) AgNP/HSA–MWNT hybrid material at different magnifications; (**f**) AgNPs deposited onto a TEM grid without HSA–MWNTs. *Inset* in (**f**) shows selected area fast-Fourier-transform diffraction pattern for AgNPs. Reprinted from ref. [117] with permission from the Canadian Society for Chemical Engineering

amide derivatives. Nevertheless, COOH groups by themselves are relatively inert at room temperature and thus require activation. It is conventionally performed via the treatment with thionyl chloride $SOCl_2$ in an aprotic organic solvent, which converts carboxylic groups into the corresponding acid chlorides C(=O)-Cl. At the second step, the acid chlorides react with aliphatic and aromatic amines producing amide derivatives as explained in Scheme 1:

$$\mathrm{CNT-C(=O)\text{-}OH + SOCl_2 \rightarrow CNT-C(=O)\text{-}Cl \xrightarrow[\text{-HCl}]{\mathrm{H_2NR}} CNT-C(=O)\text{-}NHR} \quad \text{(Scheme 1)}$$

where R is alkyl or aryl substituent. Thionyl chloride is known to be a corrosive and toxic compound, and is sometimes substituted with less ecologically unfriendly carbodiimides, which are soft amide-coupling agents widely used in peptide and protein chemistry. The only *pro* for $SOCl_2$ is its volatility, due to which its excess can be easily removed, whereas substituted ureas (final products of carbodiimide-coupling reactions) are not volatile, and need an additional washing off to be removed. A very similar esterification reaction can be carried out by substituting amine reagent with an alcohol HOR, under the same reaction conditions as for the amidation derivatization:

$$\mathrm{CNT-C(=O)\text{-}OH + SOCl_2 \rightarrow CNT-C(=O)\text{-}Cl \xrightarrow[\text{-HCl}]{\mathrm{HOR}} CNT-C(=O)\text{-}OR} \quad \text{(Scheme 2)}$$

As an alternative to the liquid-phase protocol, the acid chloride-activated SWNTs were derivatized with long-chain amines exemplified by octadecylamine (ODA) $CH_3(CH_2)_{17}NH_2$ and 4-dodecyl-aniline ($4\text{-}CH_3(CH_2)_{13}C_6H_4NH_2$) under solvent-free conditions at elevated temperature of 100 °C for 4 days [121, 122]. The same coupling between amino groups of ODA and COOH groups of oxidized SWNTs was carried out with the help of dicyclohexylcarbodiimide (DCC) as carboxyl activation reagent [123–125]. In the reports [126, 127], the solvent-free reaction conditions were employed for amidation and esterification according to Scheme 1 and Scheme 2, respectively, of acid chloride-activated SWNTs and MWNTs with lipophilic and hydrophilic dendron species; in this case, the protocol included heating of the component mixture at 75 °C and vigorous stirring for 48 h under N_2 protection.

Looking for the formation of carboxylate salts through a simple acid–base interaction (Scheme 3), Chen et al. [128] directly heated ODA with carboxylated SWNTs:

$$\mathrm{SWNT\text{-}COOH + H_2N(CH_2)_{17}CH_3 \rightarrow SWNT\text{-}COO^{-+}NH_3(CH_2)_{17}CH_3} \quad \text{(Scheme 3)}$$

The mixture of SWNTs with ODA (whose melting point is 55–57 °C) was heated for 4–8 days at 120–130 °C. Nevertheless, the authors did not account for one of the fundamental properties of carboxylic acids and amines: they can form amides under higher temperatures (>100 °C) directly via *thermal* activation, without any additional *chemical* activation of COOH groups. In other words, the reaction of

oxidized CNTs with amines in this case should be described by Scheme 4 instead of Scheme 3:

$$\mathrm{CNT-C(=O)\text{-}OH + H_2NR \xrightarrow[-H_2O]{} CNT-C(=O)\text{-}NHR} \qquad \text{(Scheme 4)}$$

Therefore, the authors [128] must have unintentionally obtained the amide derivatives of ODA instead of its carboxylate salts. On the contrary, Lin et al. [129] intentionally used the solvent-free melting treatment to derivatize oxidized MWNTs with poly-(propionylethylenimine-*co*-ethylenimine) through amidation reaction. The derivatization was first carried out at 160–180 °C for 12 h under N_2 atmosphere [129]; however, later it was found to be equally efficient when treating the melts at 165 °C for as short as 20 min [130, 131].

While the latter techniques of CNT amidation and esterification employ solvent-free *reaction* conditions, the derivatized nanotubes still need further purification from the excess organic reagent. The purification implies such auxiliary operations as extraction, centrifugation, precipitation, filtration, solvent evaporation, and drying (often in vacuum), which are quite tedious and typically take an incomparably longer time than the derivatization reaction per se, not to mention the need for additional instruments (centrifuges, filtration systems, rotary evaporators, ovens, etc.). As a result, from the point of view of green chemistry, the gain afforded is insignificant. This circumstance motivated us to look for more simplified solvent-free techniques for the amide derivatization of oxidized CNTs, which would also minimize the auxiliary purification steps.

A suitable approach was already tested and proved to be efficient, though in a quite distant area: namely, in the chemical modification of silica gel-based stationary phases for liquid chromatography. Systematic efforts were undertaken on the design of the solvent-free, gas-phase covalent modification of silica with polyazamacrocyclic ligands, pyrimidine bases, and low-molecular-weight carboxylic acids [132–135], which are crystalline and nonvolatile compounds under ambient temperature and pressure. We found that decreasing the pressure to a moderate vacuum and simultaneously increasing the temperature to >150 °C makes all the above compounds sublime and form efficiently the covalently bonded derivatives on silica surface. In the context of CNT functionalization, the most relevant example is the reaction between silica-bonded aminopropyl groups and carboxylic acid vapor giving rise to the formation of surface amides, similar to the one described by Scheme 4. This *temperature*-activated amidation proceeds readily at 150–180 °C without the need for *chemical* activation of the COOH groups: the whole procedure takes about 1 h and produces high yields of the amide derivatives (>50 % based on the starting surface concentration of aminopropyl functionalities). Excess of the derivatizing reagent is spontaneously removed from the hot reaction zone due to the heating under dynamic (and in some cases static) vacuum, thus making purification of the derivatized material and the use of solvents unnecessary. In other words, the entire process turns to be 100 % solvent-free.

As applied to CNT functionalization, this gas-phase protocol was first tested for the direct amidation of oxidized SWNT defects (Scheme 4) [136, 137], where the reaction is typically carried out at 150–170 °C for 1–2 h. Other authors [138] later found that the reaction temperature can be even lower, for example 110 °C, but then the treatment time should be substantially prolonged, to 40 h. Amide-derivatized SWNTs acquired an enhanced solubility/dispersibility in many organic solvents; the strongest effect was found for ODA [137], although the derivatization with shorter amines such as nonylamine gave good results as well [136]. An important aspect we addressed both experimentally and theoretically is that solubility and other characteristics of the derivatized nanotubes can be influenced by the presence of physically adsorbed amine molecules; energetically preferable sites for their adsorption are most likely the nanotube cavities [136, 139]. The improved solubility is usually a positive effect; however, there are other CNT properties which might be compromised due to the presence of unaccounted adsorption species. For example, when biomedical applications are targeted, the excess reagent can be released into an organism in an uncontrolled way and produce adverse or even toxic effects, depending on its chemical nature. These considerations are equally valid for the liquid-phase functionalization of CNTs.

If the amidation reaction is performed with a diamine, the second NH_2 group can remain dangling and thus available for another derivatization step. We demonstrated this possibility by using 1,8-DAO-amide derivatized SWNTs for the second amidation with L-alanine and ε-caprolactam [140], according to the reactions explained in Fig. 6.8. The volatility of ε-caprolactam is relatively high, and the derivatization can be performed under static vacuum at about 160 °C, whereas the reaction with L- alanine requires constant evacuation (i.e., dynamic vacuum) and higher temperatures of 160–200 °C due to a poor volatility of α-amino acids. The reaction with ε-caprolactam turned to be especially interesting, where we found clear indications of its polymerization into nylon 6 apparently initiated by the dangling amino groups of 1,8-DAO (Fig. 6.8; last reaction). SEM imaging revealed dramatic changes in the structure of SWNT bundles: while oxidized SWNTs exhibit a typical fluffy morphology with numerous single nanotubes and thin bundles coming out of the bulk

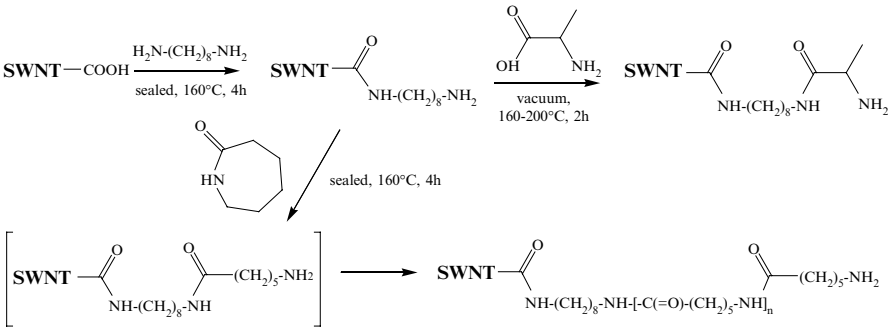

Fig. 6.8 Amide attachment of 1,8-diaminooctane to oxidized SWNTs and further solvent-free derivatization reactions with L-alanine and ε-caprolactam [140]

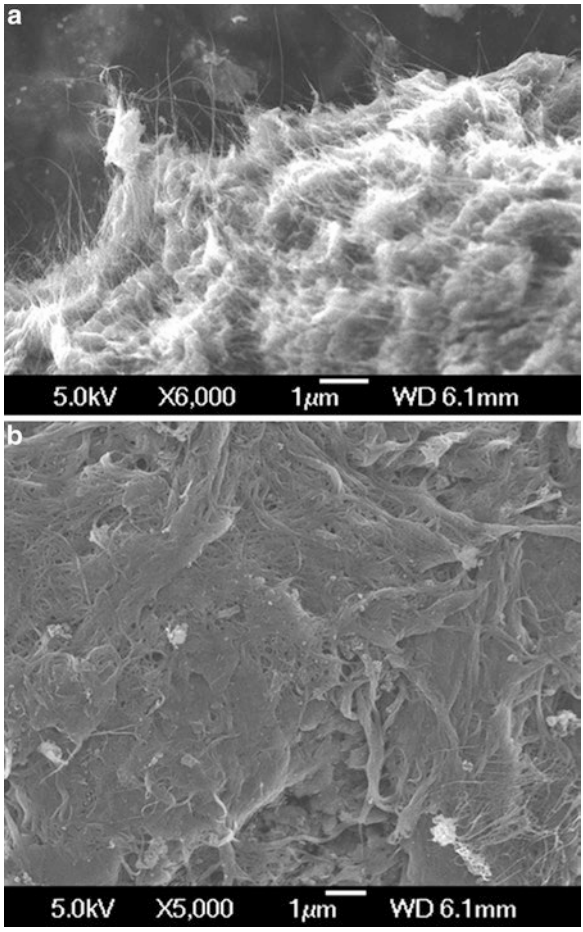

Fig. 6.9 Comparison of SEM images of oxidized SWNTs (**a**) before and (**b**) after two-step derivatization with 1,8-diaminooctane and ε-caprolactam. Reprinted from ref. [140] with permission by the Royal Society of Chemistry

(Fig. 6.9a), the polymeric phase formed in the ε-caprolactam-treated nanotubes "glues" them together and makes the samples look much more compact and less porous (Fig. 6.9b). Covalent cross-linking of this kind might be useful for improving mechanical properties of CNT–polymer composites.

6.3.3 Pristine Multi-walled Carbon Nanotubes

Pristine MWNTs produced by CVD have certain advantages as compared to open-end acid-oxidized SWNTs. First, the former are synthesized with a high degree of purity, and thus already do not require the acid purification, which makes same-quality SWNTs so expensive (usually two orders of magnitude more expensive than pristine MWNTs). Another reason is that the ends of pristine MWNTs are closed

with fullerene-type caps, and therefore, organic reagents and solvents can hardly penetrate inside the nanotubes: in this way, uncontrolled endohedral adsorption is minimized (Interestingly, the ends of catalytic CVD-grown MWNTs can be opened without the oxidative treatment, but instead by means of microwave irradiation in vacuum, which apparently makes metal catalyst particles remaining at the nanotube ends after the CVD synthesis to "explode" [141].).

As regards their chemical reactivity, pristine MWNTs do not have heteroatom-containing functional groups similar to COOH, which could be subjected to derivatization. However, instead they have pentagonal, heptagonal, and apparently larger-ring cyclic defects, which are responsible for the spherical curvature of the closed caps, as well as for the nanotube kinking and junctions if they are present in the sidewalls. Their high reactivity explains the fact that it is these sites which are oxidized first under the strong-acid treatment, and as a result, these structural elements cannot be found anymore in the purified nanotubes.

It was quite logical and natural to expect that the nucleophilic addition of primary and secondary amines, well explored for spherical fullerenes [16–23], can occur in a similar way at the closed caps of pristine MWNTs, and that the solvent-free conditions of amine functionalization of C_{60} [24, 28, 32, 34] discussed in Sect. 6.2 can be successfully applied to the closed-end nanotubes.

This type of functionalization was first attempted with octadecylamine [142]. The successful attachment of hydrophobic long-chain ODA to MWNTs manifested itself in a significant increase in the nanotube solubility/dispersibility in organic solvents. In particular, 20-min ultrasonication of ODA-MWNTs obtained in isopropanol produced stable dispersions which did not exhibit visible precipitation for more than one month; for comparison, pristine MWNTs started to precipitate almost immediately after ultrasonication. Other monofunctional amines tested afterwards for the functionalization of pristine MWNTs were NA, dodecylamine, and 4-phenyl-butylamine [143].

TGA results for the amine-functionalized MWNTs [142, 143] and their comparison with the relevant data published by other authors [144] helped to make preliminary conclusions that (1) the amine species are found mainly in covalently bonded state, and (2) their major fraction is distributed along MWNT sidewalls. The second explanation is hardly compatible with the chemistry of *ideal*, defect-free nanotube sidewalls, which are known to be chemically inert with respect to chemical reagents like amines. Instead, it suggested the existence of reactive structural defects distributed along the sidewalls of pristine MWNTs. The hypothesis on the addition sites was supported by TEM observations of ODA-MWNTs [142]. As it is shown in Fig. 6.10a, pristine MWNTs were composed of about 10 coaxial tubes, with their closed ends having an irregular shape. Similar closed ends were clearly seen in ODA-MWNTs; however, they were covered with about 2-nm layer of an amorphous material (Fig. 6.10b), which apparently originated from high-energy electron beam degradation of ODA molecules covalently bonded to the pentagons and/or other defect sites. More interestingly, TEM observation of the sidewalls of ODA-MWNTs found similar amorphous formations (Fig. 6.10c) located at the sites with well-pronounced curvature (or kinks). On the contrary, almost ideal MWNT

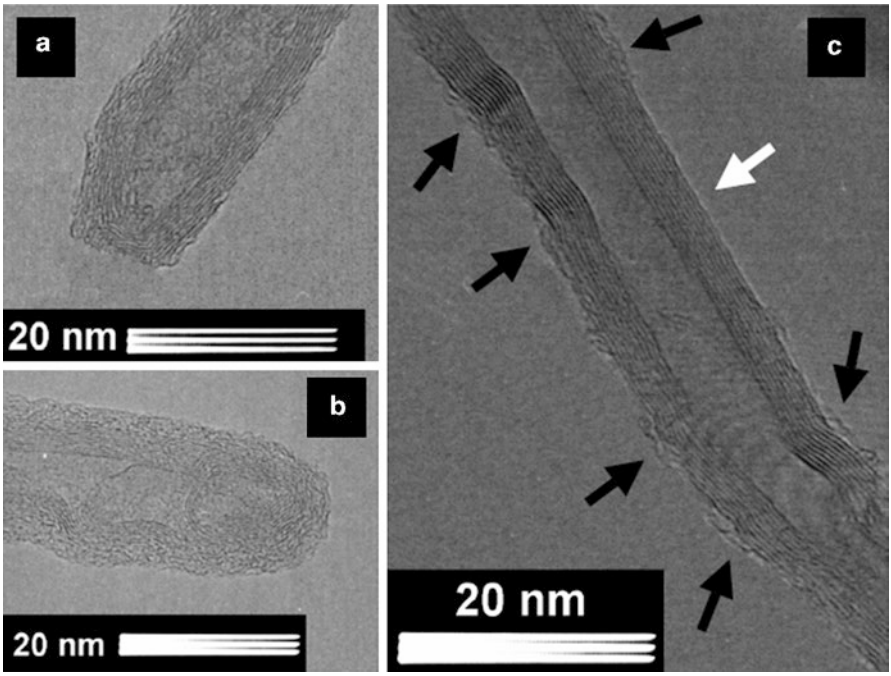

Fig. 6.10 HRTEM images showing closed ends of pristine MWNTs (**a**), of ODA-MWNTs (**b**), and sidewalls of ODA-MWNTs (**c**). *Black arrows* point to an amorphous material originating from ODA molecules bound to the defect sites; *white arrow* points to almost ideal sidewalls where no similar material can be observed. Reprinted from ref. [142] with permission by the American Chemical Society

sidewalls did not contain visible amounts of any additional material. The reactivity of pentagonal defects in the nanotubes toward amines was supported by our semiempirical calculations [142] and later DFT results by Lin et al. [145]. The applicability of Raman spectroscopy to differentiate between pristine and amine-functionalized MWNTs was discussed in ref. [146].

The use of bifunctional and polyfunctional amine reagents for the solvent-free functionalization of pristine MWNTs was explored as well. Even polymeric amines such as polyethylene glycol diamine (PEGDA) and polyethylenimine (PEI) can be employed for this purpose [147, 148]. Since the polymeric amines are nonvolatile and cannot be used for the *gas-phase* functionalization, the procedure had to be modified by performing it under melt conditions. Unfortunately, the advantages of the gas-phase functionalization were lost in part, since unreacted amine cannot be removed by heating and pumping out, but instead repeated washing in water, centrifugation, decantation and drying under vacuum had to be done. On the other hand, even though the latter auxiliary steps were necessary, no solvents except for water were used.

The case of diamines is especially interesting and attractive, from different points of view [149]. For example, CNT functionalization with diamines can facilitate a

number of biomedical applications, where strong electrostatic interactions between amino groups and biological components can ensure reliable immobilization of biological compounds onto the nanotube surface. Speaking of electronic applications, the chemical functionalization with bifunctional molecules can be envisioned as a way to cross-link and integrate CNTs into complex networks for nanoscale electronic circuits. Moreover, the mechanical stability of non-functionalized CNT agglomerates is limited due to relatively weak van der Waals interaction between individual nanotubes, whereas covalent cross-linking can dramatically enhance their mechanical strength.

With these considerations in mind, we undertook a morphological analysis of cross-linking effects in MWNTs covalently functionalized via the gas-phase technique with three aliphatic diamines 1,8-DAO, 1,10-diaminodecane (1,10-DAD), and 1,12-diaminododecane (1,12-DAD), as well as with aromatic DAN [149]. We found manifestations of nanotube cross-linking in different experiments, including a simple solubility/dispersibility test, where the diamine functionalization made MWNTs totally insoluble in isopropanol in the case of 1,8-DAO, 1,10-DAD, and 1,12-DAD, and strongly reduced nanotube dispersibility in the case of DAN. Dramatic changes in the morphology of MWNT agglomerates were observed by conventional TEM. While in pristine MWNTs well-distinguishable individual nanotubes had a typical random orientation, diamine-functionalized MWNTs appeared as very dense yarn-like structures (Fig. 6.11) with some degree of ordering. High-resolution TEM found the presence of amorphous matter at the sites of closed contact between MWNTs (Fig. 6.12) originating from the cross-linking diamine molecules. The most interesting effect was observed in AFM images (Fig. 6.13), in which all the diamine-functionalized MWNTs exhibited a strong trend to self-assembly through their rectification and arrangement into parallel aggregates. This phenomenon was interpreted as cross-linking of MWNTs with diamine interlinkers according to three different patterns, namely "side-to-side," "end-to-side," and "end-to-end" interconnections (Fig. 6.14).

Despite the cross-linking effects described in the previous paragraph, there are no indications that *all* the diamine molecules have *both* NH_2 termini forming covalent bonds with nanotubes. Therefore, a possibility exists that the dangling NH_2 groups can be further derivatized in a way similar to the one discussed in Sect. 6.3.2 for the case of 1,8-DAO-amide functionalized SWNTs [140] and explained in Fig. 6.8. The same reaction sequence was applied for the two-step covalent modification of pristine MWNTs (Fig. 6.15), under the reaction conditions similar to those employed for SWNT functionalization. And again, we found clear indications of ε-caprolactam polymerization into nylon 6 initiated by the amino groups of 1,8-DAO attached to MWNTs. This result seemed to be especially interesting and potentially useful from the point of view of polymer–nanotube composites, and in a subsequent study [150] we attempted to approach optimal reaction conditions for the solvent-free polymerization of ε-caprolactam on 1,8-DAO-MWNTs.

To conclude on the amino functionalization of pristine MWNTs with amines, one should mention two reports [50, 151] on biocompatibility properties, which showed that MWNTs functionalized with ODA, 1,8-DAO, L-alanine, and nylon 6

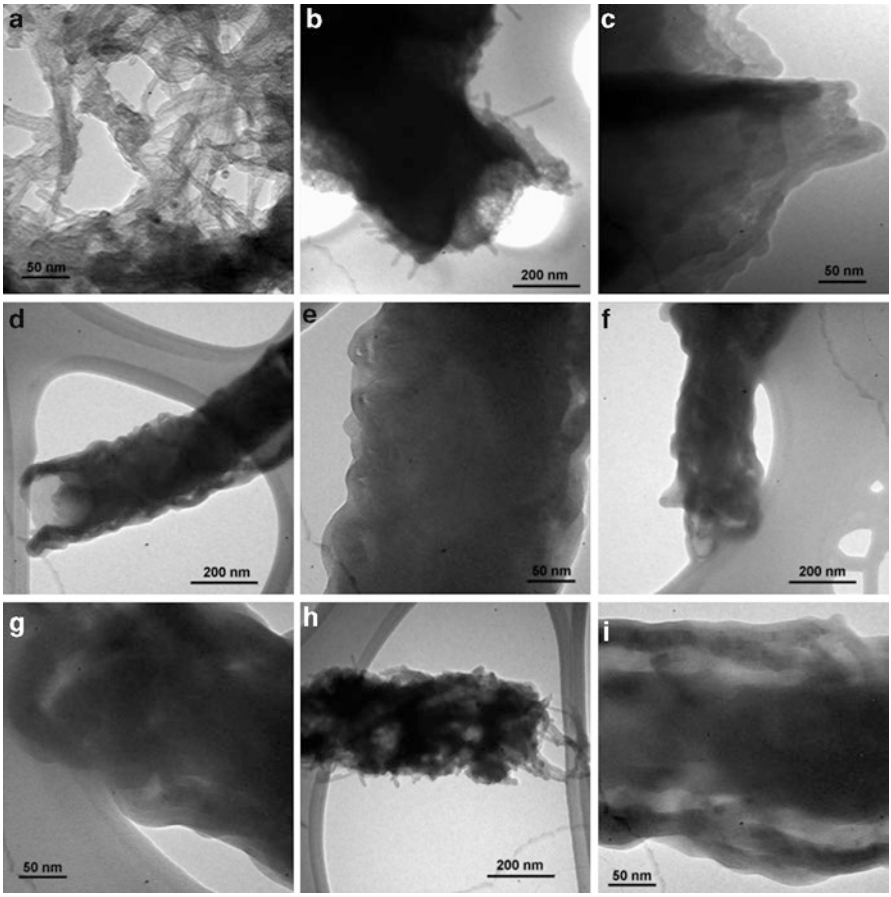

Fig. 6.11 Representative TEM images for (**a**) pristine MWNTs and diamine-functionalized nanotube samples at different magnifications: (**b**, **c**) 1,8-DAO-MWNTs; (**d**, **e**) 1,10-DAD-MWNTs; (**f**, **g**) 1,12-DAD-MWNTs; (**h**, **i**) DAN-MWNTs. Reprinted from ref. [149] with permission by Elsevier

by using the solvent-free gas-phase technique have considerably improved biocompatibility as compared to pristine MWNTs.

Amines are not the only nucleophilic reagents which can add onto the defect sites of pristine MWNTs. SH groups can act as nucleophiles as well, and this property was used for the gas-phase solvent-free addition of bifunctional aliphatic thiols to pristine MWNTs [152, 153]. The reaction conditions were very similar to those for the functionalization with volatile amines, since all the reagents tested (1,4-butanedithiol, 1,6-hexanedithiol, 1,8-octanedithiol, and 2-aminoethanethiol) are volatile under reduced pressure and elevated temperature. MWNTs functionalized in this way were further used as supports for the deposition of AuNPs [153]. Small Au particles, with a narrow size distribution around 1.7 nm, were obtained on 1,6-hexanedithiol-modified

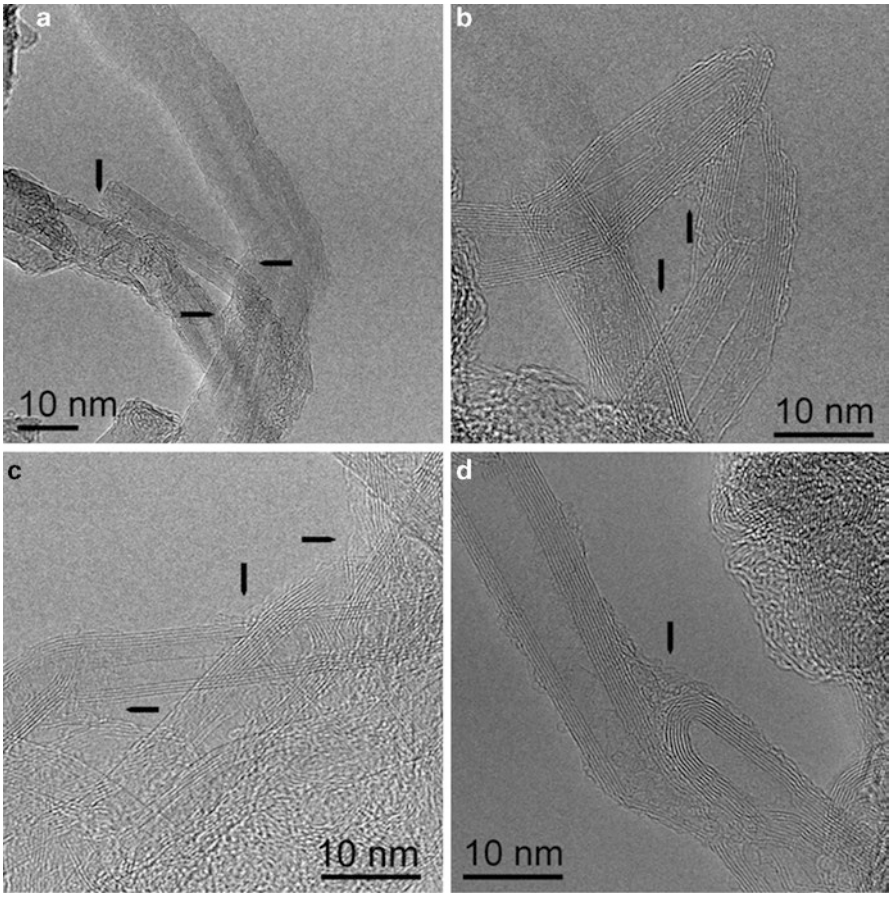

Fig. 6.12 High-resolution TEM images showing the sites (*arrows*) of MWNT cross-linking with diamine molecules: (**a**) 1,8-DAO-MWNTs; (**b**) 1,10-DAD-MWNTs; (**c**) 1,12-DAD-MWNTs; (**d**) DAN-MWNTs. Reprinted from ref. [149] with permission by Elsevier

MWNTs (Fig. 6.16a, c). For MWNTs functionalized with 2-aminoethanethiol, the average size of AuNPs was larger, of about 5.5 nm (Fig. 6.16b, d), which was explained by their higher mobility and coalescence phenomena. A Gatan image filter coupled to TEM helped to obtain the filtered images around sulfur *L* edge (165 eV) and carbon *K* edge (284 eV) pointing to the location of S-containing moieties. Figure 6.17a shows a bent nanotube with an AuNP of about 6-nm size. The corresponding filtered images at carbon *K* edge and sulfur *L* edge peak are presented in Fig. 6.17b, c, respectively. In the latter image one can see that S element is present at the nanotube surface; however, its distribution is inhomogeneous, with a notably higher S concentration observed around the AuNP location.

In addition to the deposition of metal NPs, dithiol groups covalently attached to pristine MWNTs via the solvent-free functionalization can be suggested for the uses

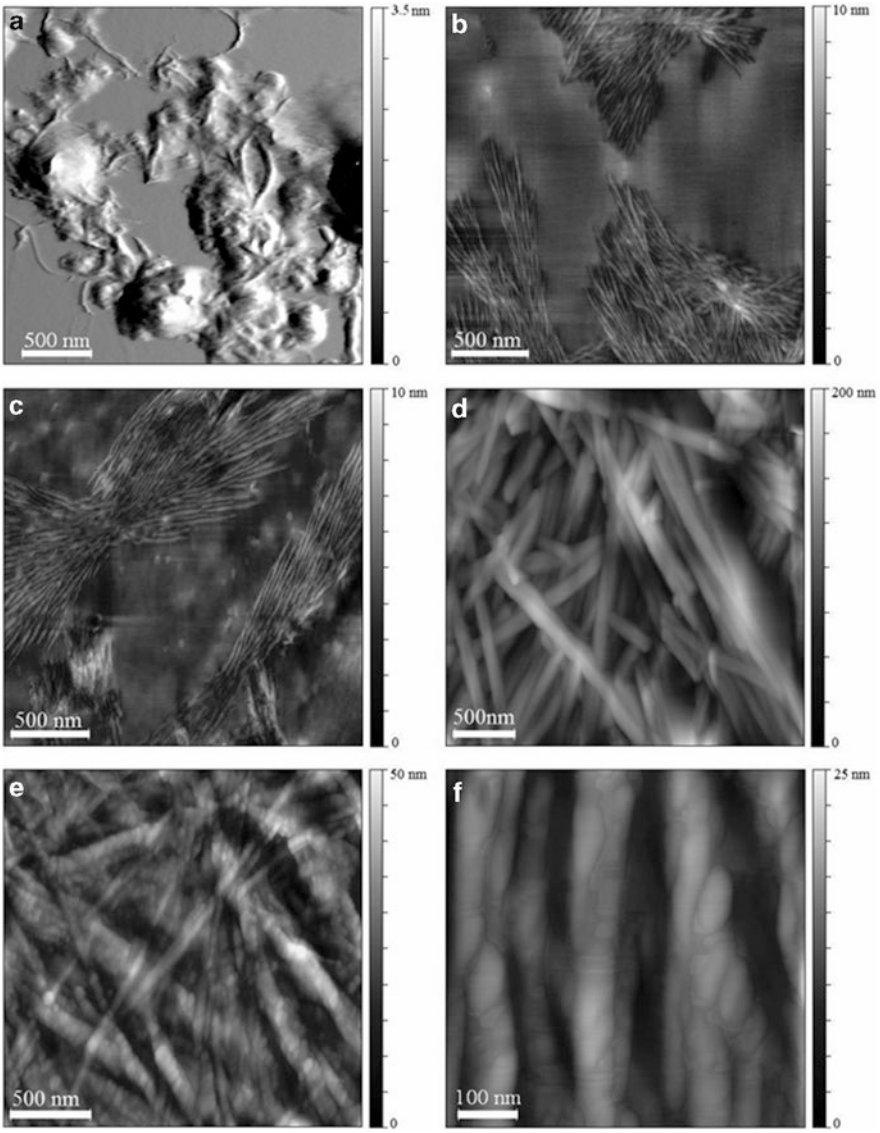

Fig. 6.13 AFM topography images (on Si/SiO_2 substrates) for (**a**) pristine MWNTs, (**b**) 1,8-DAO-MWNTs, (**c**) 1,10-DAD-MWNTs, (**d**) 1,12-DAD-MWNTs, and (**e**, **f**) DAN-MWNTs at different magnifications. Reprinted from ref. [149] with permission by Elsevier

as chemical linkers for anchoring metal complexes, attaching the nanotubes to gold tips for scanning probe microscopies, as well as for adsorption and concentration of trace metal ions. Similarly to amine-functionalized MWNTs, thiol-functionalized nanotubes have a better biocompatibility as compared to non-functionalized, pristine MWNTs [151].

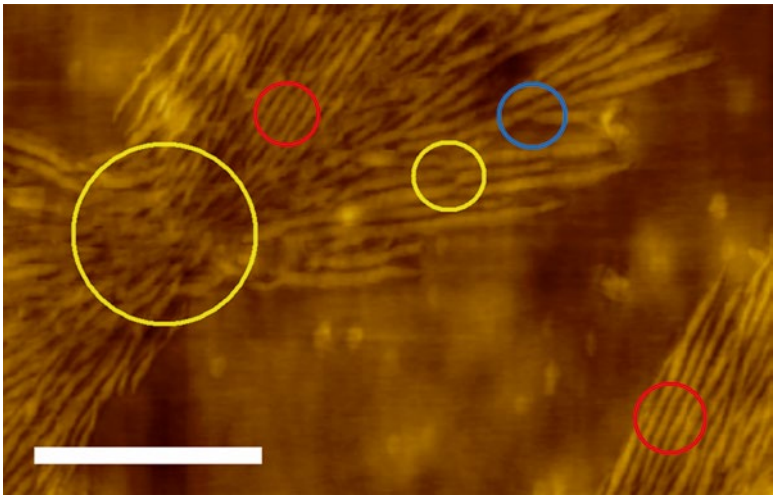

Fig. 6.14 Amplified AFM topography image (on Si/SiO_2 substrate) for 1,10-DAD-MWNTs exemplifying three possible cross-linking patterns, indicated with circles of different colors: *yellow*, "end-to-end," *red*, "side-to-side"; *blue*, "end-to-side." Scale bar, 500 nm. Reprinted from ref. [149] with permission by Elsevier

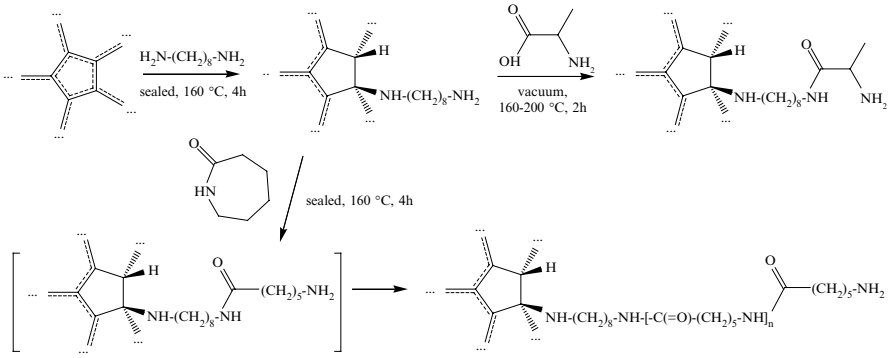

Fig. 6.15 Chemical attachment of 1,8-diaminooctane to pristine MWNTs and further solvent-free derivatization reactions with L-alanine and ε-caprolactam [140]

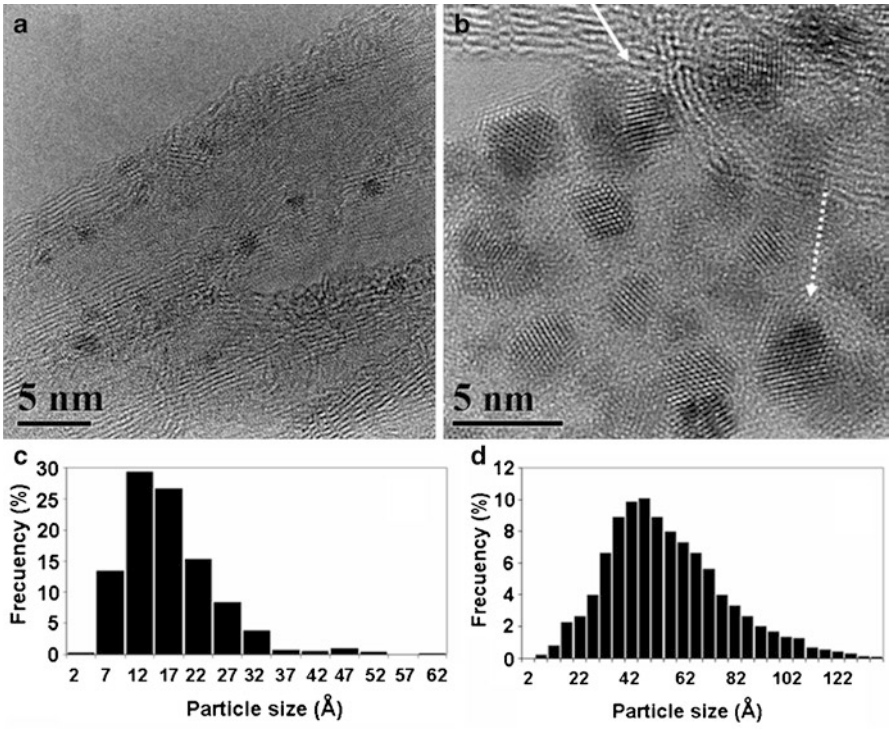

Fig. 6.16 HRTEM images of gold nanoparticles on (**a**) 1,6-hexanedithiol-functionalized and (**b**) 2-aminoethanethiol-functionalized MWNTs, along with the corresponding size histograms for AuNPs (**c** and **d**, respectively). *White solid* and *dashed arrows* in (**b**) point to examples of overlapping and coalescing AuNPs on 2-aminoethanethiol-functionalized MWNTs. Adapted from ref. [153] with permission by the American Chemical Society

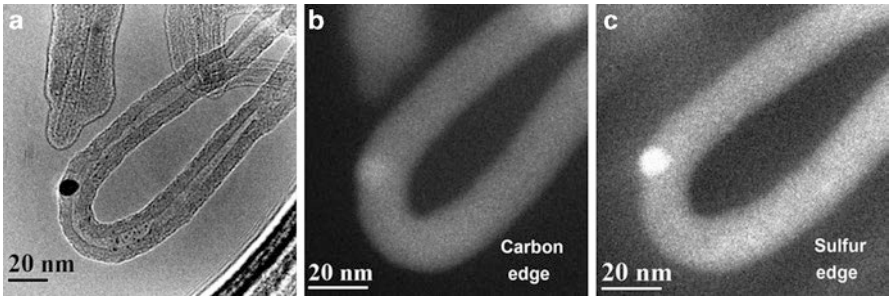

Fig. 6.17 (**a**) TEM image of a bent MWNT with a gold nanoparticle of about 6-nm size; (**b**) the corresponding image filtered around carbon *K*-edge (284 eV), and (**c**) filtered image around the sulfur L-edge (165 eV). Reprinted from ref. [153] with permission by the American Chemical Society

6.4 Nanodiamond

The main hybridization state of carbon atoms in ND is sp^3, which makes this nanomaterial very distinct from sp^2-dominated fullerenes and CNTs in terms of bulk structure, electronic, optical, mechanical, and other properties. Nevertheless, one feature makes ND have much in common with oxidized CNTs: the presence of oxygen-containing functionalities, including carboxylic groups, on its surface [6, 13, 154]. ND surface functionalization is of great interest for improving the particles dispersion, changing their wettability and adhesion characteristics, improving catalytic and biocompatibility properties, among others. At the same time, while the research effort undertaken for ND chemical modification as a whole is significant (for example, see recent reviews [155–157] and references therein), the possibility of using solvent-free techniques for this purpose remains underexplored.

Adopting the solvent-free amidation protocol described above for the derivatization of oxidized SWNTs (Sect. 6.3.2, Scheme 4) proved to be a very efficient approach to change the chemical nature of ND surface. A number of amines was tested for the temperature-activated conversion of COOH groups of ND into respective amide derivatives, which include 1,8-DAO, 1,10-DAD, 1,12-DAD, DAN, PEGDA, and PEI [149, 158]. According to solubility/dispersibility tests in water and isopropanol, the functionalization of ND increased its lipophilicity [158]. However, the functionalization with aliphatic diamines 1,8-DAO, 1,10-DAD, and 1,12-DAD reduced suspension stability due to the cross-linking effect [149]. The organic content, as estimated from TGA curves, strongly depended on the amine employed: while the content of covalently bonded 1,8-DAO, 1,10-DAD, and 1,12-DAD moieties spanned from <10 % for 1,12-DAD-ND to almost 20 % for 1,8-DAO-ND, the organic content in DAN-ND was lower by roughly one order of magnitude.

As it can be observed by SEM [149], both pristine and functionalized ND samples exist as large agglomerates of a few micrometers in size. Nevertheless, the big difference between them is that for pristine ND it was possible to discern 10^1–10^2 nm-sized primary agglomerates, whereas for 1,8-DAO-ND, 1,10-DAD-ND, and 1,12-DAD-ND the μm-sized grains exhibited smoother surfaces with less evident fine structure, which was attributed to the cross-linking phenomenon and further confirmed by AFM imaging (Fig. 6.18). The 10^1–10^2 nm-sized primary agglomerates were seen by AFM in all ND samples. In agreement with the SEM results, they appeared more dispersed and “fluffy” in pristine ND (Fig. 6.18a), whereas in all the diamine-functionalized samples the agglomerates were considerably denser with a smooth globular shape (Fig. 6.18b–f). DAN-ND (Fig. 6.18f) represented an intermediate case, with smaller primary agglomerates than for aliphatic diamine-functionalized NDs. The latter observation was explained by a lower diamine content and consequently by a lower degree of cross-linking.

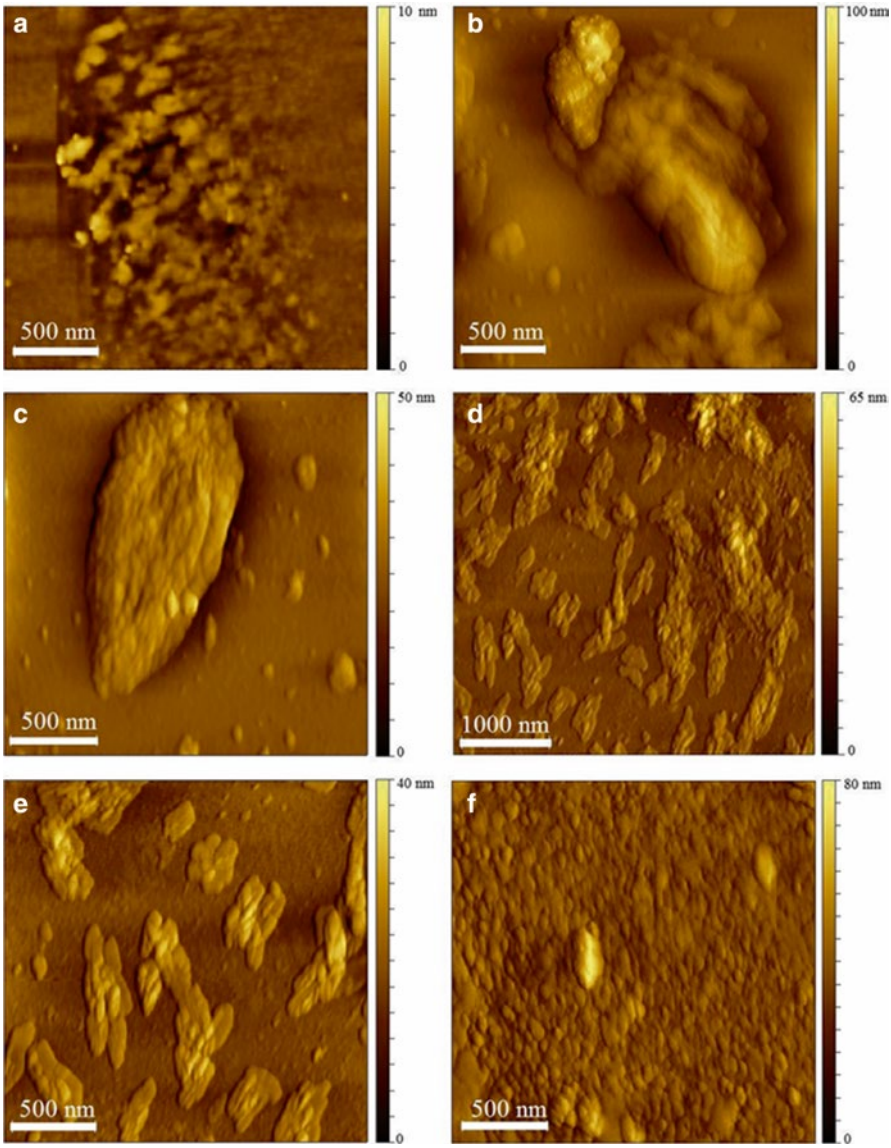

Fig. 6.18 AFM topography images (on Si/SiO_2 substrates) for (**a**) pristine ND, (**b**) 1,8-DAO-ND, (**c**) 1,10-DAD-ND, (**d**, **e**) 1,12-DAD-ND at different magnifications, and (**f**) DAN-ND. Reprinted from ref. [149] with permission by Elsevier

6.5 Graphene and Graphene Oxide

Strictly speaking, the possibility of applying the solvent-free functionalization methodology to graphene seems to be very problematic. Contrary to fullerenes, CNTs and ND, which keep their intrinsic properties both in solution/suspension and in solid state (powder), the highly exfoliated state which distinguishes graphene from graphite presupposes the existence of a dispersing solvent. That is, the very concepts of "graphene" and "solvent-free" are generally incompatible. Single graphene sheets deposited from solution/dispersion or CVD-grown on solid supports are an exception: in this case the solvent-free technique is definitely applicable. On the other hand, the resulting minute-size samples can hardly be characterized by TGA and most spectral techniques, which is indispensable to prove successful functionalization. The solvent-free functionalization of graphene oxide would not represent any problem in principle.

Nevertheless, graphene and GO are by more than one decade "younger" than CNTs, and correspondingly, less time was available to propose and refine suitable techniques for their functionalization. Especially this is true as regards the solvent-free techniques. One of the useful approaches can employ mechanochemical reactions: for example, ball milling of graphite with solid inorganic compounds such as KOH, $KMnO_4$, $(NH_4)_2S_2O_8$, SO_3, and dry ice gives rise to graphene and GO with a different degree of oxidation and different types of oxidized groups (see refs. [15, 159] and references therein).

The solvent-free microwave irradiation was shown to be widely applicable to various organic metal salts (mainly acetates) with graphene, forming substrate-supported metal (e.g., Ag, Au, Co, Ni, Pd, Pt) or metal oxide (e.g., Fe_3O_4, MnO, TiO_2) nanoparticles in high yields within as short duration of microwave irradiation as about 1–2 min [100]. As shown in the TEM images in Fig. 6.19, the products contained few-layered graphene structures with surfaces decorated with NPs of various average sizes: for example, from <5 nm Pt and TiO_2 nanoparticles to 5–15 nm Pd and Fe_3O_4 NPs. Other works on using microwave irradiation for the deposition of inorganic nanoparticles described the decoration of graphene with molybdenum disulfide (MoS_2) NPs with effective hydrodesulfurization activity for carbonyl sulfide conversion at low temperature [160]; facile synthesis of magnetic FeNPs on graphene by means of microwave treatment of GO–ferrocene mixtures, for heavy metal removal and disinfection control of drinking water [161]; and the synthesis of AuNPs–reduced GO composites using ascorbic acid as eco-friendly reducing agent [162]. Also, stable Ru and Rh metal NPs were supported on graphene surfaces by microwave decomposition of the respective metal carbonyl precursors in the ionic liquid 1-butyl-3-methylimidazolium tetrafluoroborate [163].

Interesting holey nanostructures for potential uses as fillers for polymeric composites were synthesized in a study by Lin et al. [164]. First, the deposition of AgNPs onto the graphene sheet surface was carried out by solid-state mixing of silver acetate with graphene, with subsequent thermal treatment under a nitrogen atmosphere to decompose the acetate. Then, the Ag catalyst-loaded graphene sam-

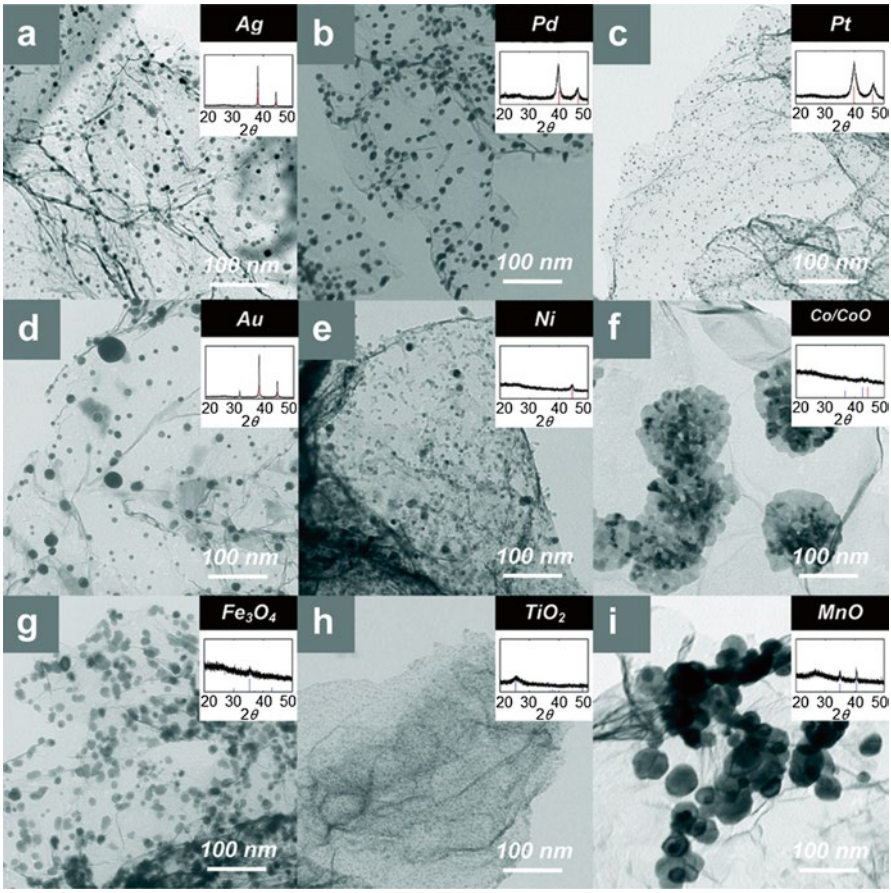

Fig. 6.19 TEM images of various metal or metal oxide nanoparticle-decorated graphene samples from modulated microwave heating (maximum power = 50 W, set temperature = 300 °C) of the corresponding salt/graphene solid mixtures, with the corresponding XRD patterns in the insets: (**a**) Ag, (**b**) Pd, (**c**) Pt, (**d**) Au, (**e**) Ni, (**f**) Co/CoO, (**g**) Fe_3O_4, (**h**) TiO_2, and (**i**) MnO. The metal-to-C contents in all samples were ~10 mol % except for **c** and **d**, which were both ~5 mol %. Reprinted from ref. [100] with permission by the American Chemical Society

ples were subjected to thermal treatment in air: in this way, the graphitic carbon in contact with AgNPs was selectively oxidized into gaseous byproducts CO and/or CO_2, leaving holes in the graphene surface. At the last step, the Ag was removed by refluxing in diluted nitric acid to obtain the final holey graphene products.

As regards the solvent-free functionalization of graphene with organic compounds, the number of relevant research reports is rather limited. Besides, even though the chemical procedures were presented as "solvent-free" due to performing the functionalization reactions in aqueous media, they required further auxiliary operations of redispersing, ultrasonication, filtering, washing, etc., usually employing organic solvents. The works to be mentioned include the diazotization of

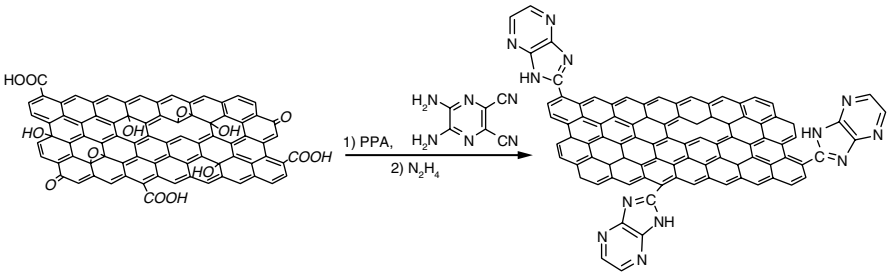

Fig. 6.20 Scheme of the covalent attachment of 5,6-diaminopyrazine-2,3-dicarbonitrile to GO in the presence of polyphosphoric acid with simultaneous hydrolysis of cyano groups, and further reduction of the remaining oxygen-containing groups with hydrazine [167]

graphene with 4-ethynylaniline–isoamyl nitrite mixture [165] and 4-chloroaniline/$NaNO_2$ mixture [166]. An example of more complex covalent chemistry was described by Du et al. [167], where 5,6-diaminopyrazine-2,3-dicarbonitrile was grafted on the graphene sheets through the cyclization reaction between COOH groups of GO and the amino groups of 5,6-diaminopyrazine-2,3-dicarbonitrile in the presence of polyphosphoric acid, with simultaneous hydrolysis of cyano groups (Fig. 6.20); at the second step, the functionalized GO was reduced by hydrazine to remove the remaining oxygen-containing groups.

6.6 Conclusions

Meeting the needs for more ecologically friendly, "green" processes in the chemistry of CNMs, a variety of chemical reactions proceeding under solvent-free conditions have been proposed for their functionalization. In turn, the main emphasis was up to now on the covalent chemical modification of CNTs: these reactions can be exemplified by fluorination, additions of reactive aryl diazonium and other radical species, which can be initiated by temperature, plasma, or mechanochemical treatment. Similarly to the conventional liquid-phase reactions, the solvent-free approaches allow for the introduction of organic moieties into the nanotube ends and sidewalls. The resulting materials exhibit improved solubility/dispersibility in organic and aqueous solvents, enhanced reactivity required for further chemical derivatization, among other potentially useful properties. In a number of instances, however, the concept "solvent-free" is applied to the *reaction* conditions only: while the use of typical large amounts of solvents is grossly reduced, the entire synthetic protocol still requires auxiliary purification steps (washing, filtering, drying, centrifugation, etc.), which consume organic solvents along with an additional time, labor, and equipment.

For more than one decade, our research group systematically has worked on the development of *totally* solvent-free functionalization techniques, with an emphasis on the covalent modification of CNTs, and attempting to further apply the same

solvent-free protocols to other forms of nanocarbon, ND in particular. The functionalization protocols designed by us are based on thermally activated reactions of amidation and nucleophilic addition with chemical compounds (mainly amines and thiols), which are stable and volatile at 150–200 °C under reduced pressure. Among main advantages of this approach is that not only the reactions per se take place at a high rate but also excess reagents are spontaneously removed from the functionalized material, thus making its additional purification unnecessary.

As a last general comment, significant advances have been achieved in the solvent-free functionalization of CNTs with important implications for different application areas. As regards other CNMs, while the research effort undertaken for the chemical modification of ND, graphene and GO as a whole is significant, the possibility of using solvent-free techniques for this purpose remains strongly underexplored and, in our opinion, should be duly addressed in the near future.

Acknowledgements Financial support from the National Council of Science and Technology of Mexico (grant CONACYT- 127299) and from the National Autonomous University of Mexico (grants DGAPA-IN100815 and IN101313) is greatly appreciated.

References

1. Bhushan B (ed) (2012) Encyclopedia of nanotechnology, vol 1–4. Springer, New York, NY
2. Nalwa HS (ed) (2004) Encyclopedia of nanoscience and nanotechnology, vol 1–10. American Scientific Publishers, Stevenson Ranch, CA
3. Nalwa HS (2011) Encyclopedia of nanoscience and nanotechnology, vol 11–25. American Scientific Publishers, Stevenson Ranch, CA
4. Langa F, Nierengarten J-F (eds) (2012) Fullerenes: principles and applications. Royal Society of Chemistry, Cambridge, UK
5. Basiuk VA, Basiuk EV (eds) (2008) Chemistry of carbon nanotubes, vol 1–3. American Scientific Publishers, Stevenson Ranch, CA
6. Shenderova OA, Gruen DM (eds) (2012) Ultrananocrystalline diamond: synthesis, properties and applications, 2nd edn. Elsevier, Oxford, UK
7. Rao CNR, Sood AK (eds) (2013) Graphene: synthesis, properties, and phenomena. Wiley-VCH, Weinheim
8. Liu J, Rinzler AG, Dai H, Hafner JH, Bradley RK, Boul PJ, Lu A, Iverson T, Shelimov K, Huffman CB, Rodriguez-Macias F, Shon Y-S, Lee TR, Colbert DT, Smalley RE (1998) Fullerene pipes. Science 280:1253
9. Sun Y-P, Fu K, Lin Y, Huang W (2002) Functionalized carbon nanotubes: properties and applications. Acc Chem Res 35:1096
10. Hirsch A, Vostrowsky O (2005) Functionalization of carbon nanotubes. Top Curr Chem 245:193
11. Karousis N, Tagmatarchis N, Tasis D (2010) Current progress on the chemical modification of carbon nanotubes. Chem Rev 110:5366
12. Georgakilas V, Otyepka M, Bourlinos AB, Chandra V, Kim N, Kemp KC, Hobza P, Zboril R, Kim KS (2012) Functionalization of graphene: covalent and non-covalent approaches, derivatives and applications. Chem Rev 112:6156
13. Mochalin VN, Shenderova O, Ho D, Gogotsi Y (2012) The properties and applications of nanodiamonds. Nat Nanotechnol 7:11
14. Anastas PT, Warner JC (1998) Green chemistry: theory and practice. Oxford University Press, New York, NY, p 30

15. Zhu S-E, Li F, Wang G-W (2013) Mechanochemistry of fullerenes and related materials. Chem Soc Rev 42(7535)
16. Hirsch A, Li Q, Wudl F (1991) Globe-trotting hydrogens on the surface of the fullerene compound C60H6(N(CH2CH2)2O)6. Angew Chem Int Ed Engl 30:1309
17. Wudl F, Hirsch A, Khemani KC, Suzuki T, Allemand PM, Koch HE, Srdanov G, Webb HM (1992) Survey of chemical reactivity of C60, electrophile and dieno—polarophile par excellence, In: Hammond GS, Kuck VJ (eds) Fullerenes: synthesis, properties and chemistry of large carbon clusters. ACS Symp Ser Vol. 48, Chapter 11, p 161
18. Seshadri R, Govindaraj A, Nagarajan R, Pradeep T, Rao CNR (1992) Addition of amines and halogens with fullerenes C60 and C70. Tetrahedron Lett 33:2069
19. Kampe KD, Egger N, Vogel M (1993) Diamino and tetraamino derivatives of buckminsterfullerene C60. Angew Chem Int Ed Engl 32:1174
20. Troshina AO, Thoshin PA, Peregudov AS, Kozlovski VI, Lyubovskaya RN (2006) Photoaddition of N-substituted piperazines to C60: an efficient approach to the synthesis of water-soluble fullerene derivatives. Chem Eur J 12:5569
21. Isobe H, Tomita N, Nakamura E (2000) One-step multiple-addition of amine to [60]fullerene. Synthesis of tetra(amino)fullerene epoxide under photochemical aerobic conditions. Org Lett 2:3663
22. Lawson GE, Kitaygorodskiy A, Ma B, Bunker CE, Sun YP (1995) Photoinduced Inter- and Intra-molecular electron transfer reactions of [60]fullerene and a tertiary amine. Formation of the cycloadduct N-ethyl-trans-2′,5′-dimethylpyrrolidino[3′,4′:1,2][60]fullerene. J Chem Soc Chem Commun 21:2225
23. Wang GW, Chen XP, Cheng X (2006) Unexpected reactions of [60]fullerene involving tertiary amines and insight into the reaction mechanisms. Chem Eur J 12:7246
24. Basiuk (Golovataya-Dzhymbeeva) EV, Basiuk VA, Shabel'nikov VP, Golovatyi VG, Flores JO, Saniger JM (2003) Reaction of silica-supported fullerene C60 with nonylamine vapor. Carbon 41:2339
25. Amelines-Sarria O, Basiuk VA (2009) Multiple addition of methylamine to fullerene C60: a density functional theory study. J Comput Theor Nanosci 6:73
26. Contreras-Torres FF, Basiuk VA, Basiuk EV (2008) Regioselectivity in azahydro[60]fullerene derivatives: application of general-purpose reactivity indicators. J Phys Chem A 112:8154
27. Amelines-Sarria O, Basiuk VA (2009) A DFT study of methylamine polyaddition to C80 fullerene. Superlattice Microst 46:302
28. Meza-Laguna V, Basiuk (Golovataya-Dzhymbeeva) EV, Alvarez-Zauco E, Acosta-Najarro D, Basiuk VA (2007) Cross-linking of C60 films with 1,8-diaminooctane and further decoration with silver nanoparticles. J Nanosci Nanotechnol 7:3563
29. Basiuk EV, Zauco EA, Basiuk VA (2006) Chemical cross-linking in C60 thin films (Chapter 20). In: Mahalik NP (ed) Micromanufacturing and Nanotechnology. Springer, Berlin, p 453
30. Dmitruk NL, Borkovskaya OY, Mamontova IB, Kondratenko OS, Naumenko DO, Basiuk (Golovataya-Dzhymbeeva) EV, Alvarez-Zauco E (2007) Optical and electrical characterization of chemically and photopolymerized C60 thin films on silicon substrates. Thin Solid Films 515:7716
31. Dmitruk NL, Borkovskaya OY, Mamykin SV, Naumenko DO, Berezovska NI, Dmitruk IM, Meza-Laguna V, Alvarez-Zauco E, Basiuk EV (2008) Fullerene C60-silver nanoparticles hybrid structures: optical and photoelectric characterization. J Nanosci Nanotechnol 8:5958
32. Martínez-Loran E, Alvarez-Zauco E, Basiuk VA, Basiuk EV, Bizarro M (2011) Fullerene thin films functionalized by 1,5-diaminonaphthalene: preparation and properties. J Nanosci Nanotechnol 11:5569
33. Dmitruk NL, Borkovskaya OY, Naumenko DO, Mamontova IB, Berezovska NI, Dmitruk IM, Meza-Laguna V, Basiuk EV (2011) Effect of thin C60 films modification with aminosubstituted polycyclic aromatic hydrocarbons and meso-tetraphenylporphine on optical and photoelectric properties of Au/C60/Si photodiode structures. Mol Cryst Liq Cryst 535:10
34. Contreras-Torres FF, Basiuk EV, Basiuk VA, Meza-Laguna V, Gromovoy TY (2012) Nanostructured diamine-fullerene derivatives: computational DFT study and experimental evidence for their formation via gas-phase functionalization. J Phys Chem A 116:1663

35. Meza-Laguna V, Basiuk (Golovataya-Dzhymbeeva) EV, Alvarez-Zauco E, Gromovoy TY, Amelines-Sarria O, Bassiouk M, Puente-Lee I, Basiuk VA (2008) Fullerene C60 films cross-linked with octane-1,8-dithiol: preparation, characterization and the use as template for chemical deposition of gold nanoparticles. J Nanosci Nanotechnol 8:3828
36. Dmitruk NL, Borkovskaya OY, Mamykin SV, Naumenko DO, Meza-Laguna V, Basiuk (Golovataya-Dzhymbeeva) EV, Puente Lee I (2010) Optical and photoelectrical studies of gold nanoparticle-decorated C60 films. Thin Solid Films 518:1737
37. Dmitruk N, Borkovskaya O, Naumenko D, Berezovska N, Dmitruk I, Meza-Laguna V, Alvarez-Zauco E, Basiuk E (2009) Optical and photoluminescent properties of nanostructured hybrid films based on functional fullerenes and metal nanoparticles. Semicond Phys Quantum Electron Optoelectron 12:205
38. Dmitruk NL, Borkovskaya OY, Havrylenko TS, Naumenko DO, Petrik P, Meza-Laguna V, Basiuk (Golovataya-Dzhymbeeva) EV (2010) Effect of chemical modification of thin C60 fullerene films on the fundamental absorption edge. Semicond Phys Quantum Electron Optoelectron 13:180
39. Ito O, D'Souza F (2012) Recent advances in photoinduced electron transfer processes of fullerene-based molecular assemblies and nanocomposites. Molecules 17:5816
40. D'Souza F, Ito O (2012) Photosensitized electron transfer processes of nanocarbons applicable to solar cells. Chem Soc Rev 41:86
41. Basiuk VA, Contreras-Torres FF, Bassiouk M, Basiuk EV (2009) Interactions of porphyrins with low-dimensional carbon materials. J Comput Theor Nanosci 6:1383
42. Bassiouk M, Álvarez-Zauco E, Basiuk VA (2013) Adsorption of *meso*-tetraphenylporphines on thin films of C60 fullerene. Appl Surf Sci 275:374
43. Kolokoltsev Y, Amelines-Sarria O, T. Yu G, Basiuk VA (2010) Interaction of mesotetraphenylporphines with C60 fullerene: comparison of several density functional theory functionals implemented in DMol3 module. J Comput Theor Nanosci 7:1095
44. Amelines-Sarria O, Kolokoltsev Y, Basiuk VA (2010) Noncovalent 1:2 complex of *meso*tetraphenylporphine with C60 fullerene: a density functional theory study. J Comput Theor Nanosci 7:1996
45. Basiuk VA, Amelines-Sarria O, Kolokoltsev Y (2010) A density functional theory study of porphyrin–pyridine–fullerene triad ZnTPP·Py·C60. J Comput Theor Nanosci 7:2322
46. Basiuk VA, Kolokoltsev Y, Amelines-Sarria O (2011) Noncovalent interaction of *meso*tetraphenylporphine with C60 fullerene as studied by several DFT methods. J Nanosci Nanotechnol 11:5519
47. Basiuk VA, Henao-Holguín LV (2013) Effects of orbital cutoff in DMol3 DFT calculations: a case study of *meso*-tetraphenylporphine–C60 complex. J Comput Theor Nanosci 10:1266
48. Basiuk VA, Henao-Holguín LV (2014) Dispesion-corrected DFT calculations of *meso*- tetraphenylporphine–C60 complex by using DMol3 module. J Comput Theor Nanosci 11:1609
49. Basiuk EV, Ochoa-Olmos OE, De la Mora-Estrada LF (2011) Ecotoxicological effects of carbon nanomaterials on algae, fungi and plants. J Nanosci Nanotechnol 11:3016
50. Ochoa-Olmos OE, Montero-Montoya R, Serrano-García L, Basiuk EV (2009) Genotoxic properties of nylon-6/MWNTs nanohybrid. J Nanosci Nanotechnol 9:4727
51. Basiuk VA, Basiuk EV, Shishkova S, Dubrovsky JG (2013) Systemic phytotoxic impact of as-prepared carbon nanotubes in long-term assays: a case study of *Parodia ayopayana* (Cactaceae). Sci Adv Mater 5:1337
52. Basiuk EV (2008) Solvent-free techniques for covalent chemical modification of carbon nanotubes (chapter 4). In: Basiuk VA, Basiuk EV (eds) Chemistry of carbon nanotubes, 2nd edn. American Scientific Publishers, Stevenson Ranch, CA, p 55
53. Khabashesku VN, Billups WE, Margrave JL (2002) Fluorination of single-wall carbon nanotubes and subsequent derivatization reactions. Acc Chem Res 35:1087
54. Stevens JL, Huang AY, Peng H, Chiang IW, Khabashesku VN, Margrave JL (2003) Side wall amino-functionalization of single-walled carbon nanotubes through fluorination and subsequent reactions with terminal diamines. Nano Lett 3:331
55. Kawasaki S, Komatsu K, Okino F, Touhara H, Kataura H (2004) Fluorination of open- and closed-end single-walled carbon nanotubes. Phys Chem Chem Phys 6:1769

56. Mickelson ET, Huffman CB, Rinzler AG, Smalley RE, Hauge RH, Margrave JL (1998) Fluorination of single-wall carbon nanotubes. Chem Phys Lett 296:188
57. Gu Z, Peng H, Hauge RH, Smalley RE, Margrave JL (2002) Cutting single-wall carbon nanotubes through fluorination. Nano Lett 2:1009
58. Zhu J, Kim JD, Peng H, Margrave JL, Khabashesku VN, Barrera EV (2003) Improving the dispersion and integration of single-walled carbon nanotubes in epoxy composites through functionalization. Nano Lett 3:1107
59. Kelly KF, Chiang IW, Mickelson ET, Hauge RH, Margrave JL, Wang X, Scuseria GE, Radloff C, Halas N (1999) Insight into the mechanism of sidewall functionalization of single-walled nanotubes: an STM study. Chem Phys Lett 313:445
60. Marcoux PR, Schreiber J, Batail P, Lefrant S, Renouard J, Jacob G, Albertini D, Mevellec JY (2002) A spectroscopic study of the fluorination and defluorination reactions on single-walled carbon nanotubes. Phys Chem Chem Phys 4:2278
61. Mickelson ET, Chiang IW, Zimmerman JL, Boul PJ, Lozano J, Liu J, Smalley RE, Hauge RH, Margrave JL (1999) Solvation of fluorinated single-wall carbon nanotubes in alcohol solvents. J Phys Chem B 103:4318
62. Peng H, Gu Z, Yang J, Zimmerman JL, Willis PA, Bronikowski MJ, Smalley RE, Hauge RH, Margrave JL (2001) Fluorotubes as cathodes in lithium electrochemical cells. Nano Lett 1:625
63. Pehrsson PE, Zhao W, Baldwin JW, Song C, Liu J, Kooi S, Zheng B (2003) Thermal fluorination and annealing of single-wall carbon nanotubes. J Phys Chem B 107:5690
64. Zhao W, Song C, Zheng B, Liu J, Viswanathan T (2002) Thermal recovery behavior of fluorinated single-walled carbon nanotubes. J Phys Chem B 106:293
65. An KH, Heo JG, Jeon KG, Bae DJ, Jo C, Yang CW, Park C-Y, Lee YH, Lee YS, Chung YS (2002) X-ray photoemission spectroscopy study of fluorinated single-walled carbon nanotubes. Appl Phys Lett 80:4235
66. Plank NOV, Jiang L, Cheung R (2003) Fluorination of carbon nanotubes in CF4 plasma. Appl Phys Lett 83:2426
67. Hamwi A, Alvergnat H, Bonnamy S, Béguin F (1997) Fluorination of carbon nanotubes. Carbon 35:723
68. Yudanov NF, Okotrub AV, Shubin YV, Yudanova LI, Bulusheva LG (2002) Fluorination of arc-produced carbon material containing multiwall nanotubes. Chem Mater 14:1472
69. Hayashi T, Terrones M, Scheu C, Kim YA, Ruhle M, Nakajima T, Endo M (2002) NanoTeflons: structure and EELS characterization of fluorinated carbon nanotubes and nanofibers. Nano Lett 2:491
70. Park S-J, Jeong H-J, Nah C (2004) A study of oxyfluorination of multi–walled carbon nanotubes on mechanical interfacial properties of epoxy matrix nanocomposites. Mater Sci Eng A 385:13
71. Unger E, Liebau M, Duesberg GS, Graham AP, Kreupl F, Seidel R, Hoenlein W (2004) Fluorination of carbon nanotubes with xenon difluoride. Chem Phys Lett 399:280
72. Valentini L, Puglia D, Armentano I, Kenny JM (2005) Sidewall functionalization of single-walled carbon nanotubes through CF4 plasma treatment and subsequent reaction with aliphatic amines. Chem Phys Lett 403:385
73. Muramatsu H, Kim YA, Hayashi T, Endo M, Yonemoto A, Arikai H, Okino F, Touhara H (2005) Fluorination of double-walled carbon nanotubes. Chem Commun 15:2002
74. Ziegler KJ, Gu Z, Shaver J, Chen Z, Flor EL, Schmidt DJ, Chan C, Hauge RH, Smalley RE (2005) Cutting single-walled carbon nanotubes. Nanotechnology 16:S539
75. Wang Y-Q, Sherwood PMA (2004) Studies of carbon nanotubes and fluorinated nanotubes by X-ray and ultraviolet photoelectron spectroscopy. Chem Mater 16:5427
76. Valentini L, Armentano I, Mengoni F, Puglia D, Pennelli G, Kenny JM (2005) Chemical gating and photoconductivity of CF4 plasma-functionalized single-walled carbon nanotubes with adsorbed butylamine. J Appl Phys 97:114320–114321
77. Felten A, Bittencourt C, Pireaux JJ, Van Lier G, Charlier JC (2005) Radio-frequency plasma functionalization of carbon nanotubes surface O2, NH3, and CF4 treatments. J Appl Phys 98:074308–1

78. Zhang W, Bonnet P, Dubois M, Ewels CP, Guerin K, Petit E, Mevellec JY, Vidal L, Ivanov DA, Hamwi A (2012) Comparative study of SWCNT fluorination by atomic and molecular fluorine. Chem Mater 24:1744
79. Dyke CA, Tour JM (2003) Solvent-free functionalization of carbon nanotubes. J Am Chem Soc 125:1156
80. Dyke CA, Tour JM (2004) Overcoming the insolubility of carbon nanotubes through high degrees of sidewall functionalization. Chem Eur J 10:813
81. Dyke CA, Stewart MP, Maya F, Tour JM (2004) Diazonium-based functionalization of carbon nanotubes: XPS and GC-MS analysis and mechanistic implications. Synlett 1:155
82. Price BK, Hudson JL, Tour JM (2005) Green chemical functionalization of single-walled carbon nanotubes in ionic liquids. J Am Chem Soc 127:14867
83. Chen XH, Wang HF, Zhong WB, Feng T, Yang XG, Chen JH (2008) A scalable route to highly functionalized multi-walled carbon nanotubes on a large scale. Macromol Chem Phys 209:846
84. Sadowska K, Roberts KP, Wiser R, Biernat JF, Jablonowska E, Bilewicz R (2009) Synthesis, characterization, and electrochemical testing of carbon nanotubes derivatized with azobenzene and anthraquinone. Carbon 47:1501
85. Rana S, Cho JW, Kumar I (2010) Synthesis and characterization of polyurethane-grafted singlewalled carbon nanotubes via click chemistry. J Nanosci Nanotechnol 10:5700
86. Brunetti FG, Herrero MA, Munoz JDM, Giordani S, Diaz-Ortiz A, Filippone S, Ruaro G, Meneghetti M, Prato M, Vazquez E (2007) Reversible microwave-assisted cycloaddition of aziridines to carbon nanotubes. J Am Chem Soc 129:14580
87. Paiva MC, Simon F, Novais RM, Ferreira T, Proenca MF, Xu W, Besenbacher F (2010) Controlled functionalization of carbon nanotubes by a solvent-free multicomponent approach. ACS Nano 4:7379
88. Grassi G, Scala A, Piperno A, Iannazzo D, Lanza M, Milone C, Pistone A, Galvagno S (2012) A facile and ecofriendly functionalization of multiwalled carbon nanotubes by an old mesoionic compound. Chem Commun 48:6836
89. Tagliapietra S, Cravotto G, Gaudino EC, Visentin S, Mussi V (2012) Functionalization of single-walled carbon nanotubes through 1,3-cycloaddition of carbonyl ylides under microwave irradiation. Synlett 10:1459
90. Bayazit MK, Coleman KS (2012) Probing the selectivity of azomethine imine cycloaddition to single-walled carbon nanotubes by resonance Raman spectroscopy. Chem Asian J 7:2925
91. Nayak RR, Lee KY, Shanrnugharaj AM, Ryu SH (2007) Synthesis and characterization of styrene grafted carbon nanotube and its polystyrene nanocomposite. Eur Polym J 43:4916
92. Menzel R, Tran MQ, Menner A, Kay CWM, Bismarck A, Shaffer MSP (2010) A versatile, solvent-free methodology for the functionalisation of carbon nanotubes. Chem Sci 1:603
93. Tian R, Wang XB, Li MJ, Hu HT, Chen R, Liu FM, Zheng H, Wan L (2008) An efficient route to functionalize singe-walled carbon nanotubes using alcohols. Appl Surf Sci 255:3294
94. Ye YM, Mao Y, Wang F, Lu HB, Qu LT, Dai LM (2011) Solvent-free functionalization and transfer of aligned carbon nanotubes with vapor-deposited polymer nanocoatings. J Mater Chem 21:837
95. Yuvaraj H, Jeong YT, Lee WK, Lim KT (2009) Synthesis of MWNT/PEDOT composites for the application of organic light emitting diodes. Mol Cryst Liq Cryst 514:366
96. Yang YK, Yu LJ, Peng RG, Huang YL, He CE, Liu HY, Wang XB, Xie XL, Mai YW (2012) Incorporation of liquid-like multiwalled carbon nanotubes into an epoxy matrix by solvent-free processing. Nanotechnology 23:225701
97. Suri A, Chakraborty AK, Coleman KS (2008) A facile, solvent-free, noncovalent, and nondisruptive route to functionalize single-wall carbon nanotubes using tertiary phosphines. Chem Mater 20:1705
98. Németh Z, Réti B, Dieker C, Akos K, Alexander DTL, Seo JW, Forró L, Hernadi K (2010) Preparation of homogeneous titania coatings on the surface of MWNTs. Phys Status Sol B 247:2683
99. Németh Z, Dieker C, Kukovecz A, Alexander D, Forró L, Seo JW, Hernadi K (2011) Preparation of homogeneous titania coating on the surface of MWNT. Compos Sci Tech 71:87

100. Lin Y, Baggett DW, Kim JW, Siochi EJ, Connell JW (2011) Instantaneous formation of metal and metal oxide nanoparticles on carbon nanotubes and graphene via solvent-free microwave heating. ACS Appl Mater Interfaces 3:1652
101. Xu ZW, Li Z, Tan XH, Holt CMB, Zhang L, Amirkhiz BS, Mitlin D (2012) Supercapacitive carbon nanotube-cobalt molybdate nanocomposites prepared via solvent-free microwave synthesis. RSC Adv 2:2753
102. Ni XJ, Zhang BS, Li C, Pang M, Su DS, Williams CT, Liang CH (2012) Microwave- assisted green synthesis of uniform ru nanoparticles supported on non-functional carbon nanotubes for cinnamaldehyde hydrogenation. Catal Commun 24:65
103. Khare BN, Wilhite P, Quinn RC, Chen B, Schingler RH, Tran B, Imanaka H, So CR, Bauschlicher CW Jr, Meyyappan M (2004) Functionalization of carbon nanotubes by ammonia glow-discharge: experiments and modeling. J Phys Chem B 108:8166
104. Khare B, Wilhite P, Tran B, Teixeira E, Fresquez K, Nna Mvondo D, Bauschlicher C Jr, Meyyappan M (2005) Functionalization of carbon nanotubes via nitrogen glow discharge. J Phys Chem B 109:23466
105. Chen Q, Dai L, Gao M, Huang S, Mau A (2001) Plasma activation of carbon nanotubes for chemical modification. J Phys Chem B 105:618
106. Bystrzejewski M, Rummeli MH, Gemming T, Pichler T, Huczko A, Lange H (2009) Functionalizing single-wall carbon nanotubes in hollow cathode glow discharges. Plasma Chem Plasma Process 29:79
107. Kónya Z, Vesselenyi I, Niesz K, Kukovecz A, Demortier A, Fonseca A, Delhalle J, Mekhalif Z, Nagy JB, Koós AA, Osváth Z, Kocsonya A, Biró LP, Kiricsi I (2002) Large scale production of short functionalized carbon nanotubes. Chem Phys Lett 360:429
108. Barthos R, Méhn D, Demortier A, Pierard N, Morciaux Y, Demortier G, Fonseca A, Nagy JB (2005) Functionalization of single-walled carbon nanotubes by using alkyl-halides. Carbon 43:321
109. Li X, Liu L, Qin Y, Wu W, Guo Z-X, Dai L, Zhu D (2003) C60 modified single-walled carbon nanotubes. Chem Phys Lett 377:32
110. Pan H, Liu L, Guo ZX, Dai L, Zhang F, Zhu D, Czerw R, Carroll DL (2003) Carbon nanotubols from mechanochemical reaction. Nano Lett 3:29
111. Schulte K, Yan C, Ahola-Tuomi M, Stróżecka A, Moriarty PJ, Khlobystov AN (2008) Encapsulation of cobalt phthalocyanine molecules in carbon nanotubes. J Phys Conf Ser 100:012017
112. Schulte K, Swarbrick JC, Smith NA, Bondino F, Magnano E, Khlobystov AN (2007) Assembly of cobalt phthalocyanine stacks inside carbon nanotubes. Adv Mater 19:3312
113. Basiuk VA, Henao-Holguín LV, Álvarez-Zauco E, Bassiouk M, Basiuk EV (2013) Gas- phase noncovalent functionalization of carbon nanotubes with a Ni(II) tetraaza[14]annulene complex. Appl Surf Sci 270:634
114. Bassiouk M, Basiuk VA, Basiuk EV, Álvarez-Zauco E, Martínez-Herrera M, Rojas- Aguilar A, Puente-Lee I (2013) Noncovalent functionalization of single-walled carbon nanotubes with porphyrins. Appl Surf Sci 275:168
115. Nepal D, Geckeler KE (2007) Proteins and carbon nanotubes: close encounter in water. Small 3:1259
116. Rodríguez-Galván A, Contreras-Torres FF, Basiuk EV, Alvarez-Zauco E, Heredia A, Basiuk VA (2011) Aggregation of human serum albumin on graphite and single-walled carbon nanotubes as studied by scanning probe microscopies. J Nanosci Nanotechnol 11:5491
117. Rodríguez-Galván A, Contreras-Torres FF, Basiuk EV, Heredia A, Basiuk VA (2013) Deposition of silver nanoparticles onto human serum albumin-functionalized multi-walled carbon nanotubes. Can J Chem Eng 91:264
118. Bahr JL, Tour JM (2002) Covalent chemistry of single-wall carbon nanotubes. J Mater Chem 12:1952
119. Hirsch A (2002) Functionalization of single-walled carbon nanotubes. Angew Chem Int Ed 41:1853

120. Basiuk VA, Basiuk (Golovataya-Dzhymbeeva) EV (2004) Chemical derivatization of carbon nanotube tips. In: Nalwa HS (ed) Encyclopedia of nanoscience and nanotechnology, 1st edn. American Scientific Publishers, Stevenson Ranch CA, p 761
121. Chen J, Hamon MA, Hu H, Chen Y, Rao AM, Eklund PC, Haddon RC (1998) Solution properties of single-walled carbon nanotubes. Science 282:95
122. Hamon MA, Chen J, Hu H, Chen Y, Itkis ME, Rao AM, Eklund PC, Haddon RC (1999) Dissolution of single-walled carbon nanotubes. Adv Mater 11:834
123. Lian Y, Maeda Y, Wakahara T, Akasaka T, Kazaoui S, Minami N, Shimizu T, Choi N, Tokumoto H (2004) Nondestructive and high-recovery-yield purification of single-walled carbon nanotubes by chemical functionalization. J Phys Chem B 108:8848
124. Lian Y, Maeda Y, Wakahara T, Nakahodo T, Akasaka T, Kazaoui S, Minami N, Shimizu T, Tokumoto H (2005) Spectroscopic study on the centrifugal fractionation of soluble single-walled carbon nanotubes. Carbon 43:2750
125. Jia H, Lian Y, Ishitsuka MO, Nakahodo T, Maeda Y, Tsuchiya T, Wakahara T, Akasaka T (2005) Centrifugal purification of chemically modified single-walled carbon nanotubes. Sci Technol Adv Mater 6:571
126. Sun YP, Huang W, Lin Y, Fu K, Kitaygorodskiy A, Riddle LA, Yu YJ, Carroll DL (2001) Soluble dendron-functionalized carbon nanotubes: preparation, characterization, and properties. Chem Mater 13:2864
127. Fu K, Huang W, Lin Y, Riddle LA, Carroll DL, Sun YP (2001) Defunctionalization of functionalized carbon nanotubes. Nano Lett 1:439
128. Chen J, Rao AM, Lyuksyutov S, Itkis ME, Hamon MA, Hu H, Cohn RW, Eklund PC, Colbert DT, Smalley RE, Haddon RC (2001) Dissolution of full-length single-walled carbon nanotubes. J Phys Chem B 105:2525
129. Lin Y, Rao AM, Sadanadan B, Kenik E, Sun YP (2002) Functionalizing multiple-walled carbon nanotubes with aminopolymers. J Phys Chem B 106:1294
130. Czerw R, Guo Z, Ajayan PM, Sun YP, Carroll DL (2001) Organization of polymers onto carbon nanotubes: a route to nanoscale assembly. Nano Lett 1:423
131. Riggs JE, Guo Z, Carroll DL, Sun YP (2000) Strong luminescence of solubilized carbon nanotubes. J Am Chem Soc 122:5879
132. Basiuk VA, Chuiko AA (1990) Gas-phase synthesis, properties and some applications of acylamide stationary phases for high-performance liquid chromatography. J Chromatogr 521:29
133. Basyuk VA (1991) Preparation and properties of functionalized sorbents based on bromobutyliminopropyl silica gel for high-performance liquid chromatography. J Anal Chem USSR-Engl Tr 46:401
134. Basiuk VA, Khil'chevskaya EG (1991) Gas-phase acylation of aminopropyl silica gel in the synthesis of some chemically bonded silica materials for analytical applications. Anal Chim Acta 255:197
135. Basiuk VA, Chuiko AA (1993) Selectivity of bonded stationary phases containing uracil derivatives for liquid chromatography of nucleic acid components. J Chromatogr Sci 31:120
136. Basiuk EV, Basiuk VA, Bañuelos JG, Saniger-Blesa J-M, Pokrovskiy VA, Gromovoy TY, Mischanchuk AV, Mischanchuk BG (2002) Interaction of oxidized single-walled carbon nanotubes with vaporous aliphatic amines. J Phys Chem B 106:1588
137. Basiuk VA, Kobayashi K, Kaneko T, Negishi Y, Basiuk EV, Saniger-Blesa J-M (2002) Irradiation of single-walled carbon nanotubes with high-energy protons. Nano Lett 2:789
138. Hadjiev VG, Lagoudas DC, Oh E-S, Thakre P, Davis D, Files BS, Yowell L, Arepalli S, Bahr JL, Tour JM (2006) Buckling instabilities of octadecylamine functionalized carbon nanotubes embedded in epoxy. Compos Sci Tech 66(128)
139. Basiuk VA (2003) ONIOM studies of chemical reactions on carbon nanotube tips: effects of the lower theoretical level and mutual orientation of the reactants. J Phys Chem B 107:8890
140. Basiuk VA, Salvador-Morales C, Basiuk EV, Jacobs RMJ, Ward M, Chu BT, Sim RB, Green MLH (2006) "Green" derivatization of carbon nanotubes with nylon 6 and *L*-alanine. J Mater Chem 16:4420

141. Alvarez-Zauco E, Basiuk VA, Acosta-Najarro D, Flores-Morales C, Puente-Lee I, Bassiouk M, Gromovoy TY, Mischanchuk BG, Basiuk EV (2010) Microwave irradiation of pristine multi-walled carbon nanotubes in vacuum. J Nanosci Nanotechnol 10:448
142. Basiuk EV, Monroy-Peláez M, Puente-Lee I, Basiuk VA (2004) Direct solvent-free amination of closed-cap carbon nanotubes: a link to fullerene chemistry. Nano Lett 4:863
143. Basiuk EV, Gromovoy TY, Datsyuk A, Palyanytsya BB, Pokrovskiy VA, Basiuk VA (2005) Solvent-free derivatization of pristine multi-walled carbon nanotubes with amines. J Nanosci Nanotechnol 5:984
144. Chattopadhyay D, Galeska I, Papadimitrakopoulos F (2003) A route for bulk separation of semiconducting from metallic single wall carbon nanotubes. J Am Chem Soc 125:3370
145. Lin T, Zhang W-D, Huang J, He C (2005) A DFT study of the amination of fullerenes and carbon nanotubes: reactivity and curvature. J Phys Chem B 109:13755
146. Sato R, Basiuk EV, Saniger-Blesa JM (2006) Application of principal component analysis to discriminate the Raman spectra of functionalized multi-walled carbon nanotubes. J Raman Spectrosc 37:1302
147. Basiuk (Golovataya-Dzhymbeeva) EV, Ochoa-Olmos O, Contreras-Torres FF, Meza-Laguna V, Alvarez-Zauco E, Puente-Lee I, Basiuk VA (2011) "Green" functionalization of pristine multi-walled carbon nanotubes with long-chain aliphatic amines. J Nanosci Nanotechnol 11:5546
148. Contreras-Torres FF, Ochoa-Olmos OE, Basiuk EV (2009) Amine-functionalized multi-walled carbon nanotubes: an atomic force microscopy study. J Scan Probe Microsc 4:100
149. Basiuk EV, Basiuk VA, Meza-Laguna V, Contreras-Torres FF, Martínez M, Rojas-Aguilar A, Salerno M, Zavala G, Falqui A, Brescia R (2012) Solvent-free covalent functionalization of multi-walled carbon nanotubes and nanodiamond with diamines: looking for cross-linking effects. Appl Surf Sci 259:465
150. Basiuk EV, Solis-González OA, Alvarez-Zauco E, Puente-Lee I, Basiuk VA (2009) Nanohybrids of nylon 6 with multi-walled carbon nanotubes: solvent-free polymerization of ε- caprolactam under variable experimental conditions. J Nanosci Nanotechnol 9:3313
151. Salvador-Morales C, Basiuk EV, Basiuk VA, Green MLH, Sim RB (2008) Effects of covalent functionalisation on the biocompatibility characteristics of multi-walled carbon nanotubes. J Nanosci Nanotechnol 8:2347
152. Basiuk EV, Puente-Lee I, Claudio-Sánchez J-L, Basiuk VA (2006) Solvent-free derivatization of pristine multi-walled carbon nanotubes with dithiols. Mater Lett 60:3741
153. Zanella R, Basiuk EV, Santiago P, Basiuk VA, Mireles E, Puente-Lee I, Saniger JM (2005) Deposition of gold nanoparticles onto thiol-functionalized multi-walled carbon nanotubes. J Phys Chem B 109:16290
154. Jiang T, Xu K (1995) FTIR study of ultradispersed diamond powder synthesized by explosive detonation. Carbon 33:1663
155. Shakun A, Vuorinen J, Hoikkanen M, Poikelispää M, Das A (2014) Hard nanodiamonds in soft rubbers: past, present and future–a review. Compos Part A 64:49
156. Yakovlev RY, Solomatin AS, Leonidov NB, Kulakova II, Lisichkin GV (2014) Detonation diamond-a perspective carrier for drug delivery systems. Russ J Gen Chem 84:379
157. Moosa B, Fhayli K, Li S, Julfakyan K, Ezzeddine A, Khashab NM (2014) Applications of nanodiamonds in drug delivery and catalysis. J Nanosci Nanotechnol 14:332
158. Basiuk EV, Santamaría-Bonfil A, Meza-Laguna V, Gromovoy TY, Alvares-Zauco E, Contreras-Torres FF, Rizo J, Zavala G, Basiuk VA (2013) Solvent-free covalent functionalization of nanodiamond with amines. Appl Surf Sci 275:324
159. Posudievsky OY, Khazieieva OA, Koshechko VG, Pokhodenko VD (2012) Preparation of graphene oxide by solvent-free mechanochemical oxidation of graphite. J Mater Chem 22:12465
160. Liu N, Wang X, Xu W, Hu H, Liang J, Qiu J (2014) Microwave-assisted synthesis of MoS2/graphene nanocomposites for efficient hydrodesulfurization. Fuel 119:163

161. Gollavelli G, Chang C-C, Ling Y-C (2013) Facile synthesis of smart magnetic graphene for safe drinking water: heavy metal removal and disinfection control. ACS Sustain Chem Eng 1:462
162. Sharma P, Darabdhara G, Reddy TM, Borah A, Bezboruah P, Gogoi P, Hussain N, Sengupta P, Das MR (2013) Synthesis, characterization and catalytic application of Au NPs-reduced graphene oxide composites material: an eco-friendly approach. Catal Commun 40:139
163. Marquardt D, Vollmer C, Thomann R, Steurer P, Mülhaupt R, Redel E, Janiak C (2011) The use of microwave irradiation for the easy synthesis of graphene-supported transition metal nanoparticles in ionic liquids. Carbon 49:1326
164. Lin Y, Watson KA, Kim J-W, Baggett DW, Working DC, Connell JW (2013) Bulk preparation of holey graphene via controlled catalytic oxidation. Nanoscale 5:7814
165. Castelaín M, Shuttleworth PS, Marco C, Ellis G, Salavagione HJ (2013) Comparative study of the covalent diazotization of graphene and carbon nanotubes using thermogravimetric and spectroscopic techniques. Phys Chem Chem Phys 15:16806
166. Mondal T, Bhowmick AK, Krishnamoorti R (2012) Chlorophenyl pendant decorated graphene sheet as a potential antimicrobial agent: synthesis and characterization. J Mater Chem 22:22481
167. Du Z-Z, Ai W, Zhao J-F, Xie L-H, Huang W (2014) Synthesis and characterization of amphiphilic graphene. Sci China Technol Sci 57:244

Chapter 7
Green Chemical and Biological Synthesis of Nanoparticles and Their Biomedical Applications

Mehdi Razavi, Erfan Salahinejad, Mina Fahmy, Mostafa Yazdimamaghani, Daryoosh Vashaee, and Lobat Tayebi

Abstract To generate nanoparticles with particular shapes and dimensions, various techniques including physicochemical and biological routes have been developed. The physical and chemical processes are typically expensive and require hazardous chemicals. In this chapter, we introduce current advancements in the green synthesis of nanoparticles as eco-friendly, cost-effective, and simple approaches. The microbial synthesis of nanoparticles using bacteria, fungi, and viruses; phototrophic eukaryotes including plants, diatoms, and algae; heterotrophic human cell lines and some

M. Razavi
Helmerich Advanced Technology Research Center, School of Material Science and Engineering, Oklahoma State University, Tulsa, OK 74106, USA

Biomaterials Research Group, Department of Materials Engineering, Isfahan University of Technology, Isfahan 84156-83111, Iran

Dental Materials Research Center, Isfahan University of Medical Sciences, Isfahan, Iran

E. Salahinejad
Faculty of Materials Science and Engineering, K.N. Toosi University of Technology, Tehran, Iran

M. Fahmy
Marquette University School of Dentistry, Milwaukee, WI 53233, USA

M. Yazdimamaghani
Helmerich Advanced Technology Research Center, School of Material Science and Engineering, Oklahoma State University, Tulsa, OK 74106, USA

D. Vashaee
School of Electrical and Computer Engineering, North Carolina State University, Raleigh, NC 27606, USA

L. Tayebi (✉)
Department of Developmental Sciences, Marquette University School of Dentistry, Milwaukee, WI 53233, USA

Biomaterials and Advanced Drug Delivery Laboratory, Stanford University, Palo Alto, CA 94304, USA
e-mail: lobat.tayebi@marquette.edu

V.A. Basiuk, E.V. Basiuk (eds.), *Green Processes for Nanotechnology*,
DOI 10.1007/978-3-319-15461-9_7

other biological agents is especially emphasized in this review. It also declares the applications of these nanomaterials in a broad range of potential areas, such as medical biology, labeling, sensors, drug delivery, dentistry, and environmental cleanup.

Keywords Green chemistry • Bio-inspired synthesis • Nanoparticle • Green synthesis

7.1 Introduction

During the last decade, nanotechnology has become a cutting edge and highly interdisciplinary research area including basic sciences, material science and medicine. The word "nano" has been derived from a Greek word "nanos" translated from "dwarf" and refers to the size of one billionth (10^{-9} m). Due to the more surface atoms and larger surface energy of nanomaterials, compared to bulk materials, they present considerable changes in physical, mechanical, chemical, electrical, magnetic, optical, and biological properties [1, 2]. Recently, nano-biotechnology, as one of the most imperative areas, has attracted much attention in the nanoscience. Typically, nanomaterials are considered as the next generation of biosensors and various bioelectronic applications, as a result of enhanced Rayleigh scattering and quantum size effects [3].

Latest innovations in nanotechnology have resulted in the synthesis of nanomaterials with different shapes, such as wires, tubes, and particles for doable applications in different fields. Nanoparticles with dimensions smaller than 100 nm is normally produced by using two following techniques: top-down and bottom-up [4]. Bulk materials are little-by-little collapsed to nanoparticles in top-down methods; conversely, in bottom-up approaches, a nanomaterial is constructed by bonding of atoms or molecules. The latter route is generally comprised of chemical and biological techniques. In view of the fact that the size, shape and crystallinity of nanomaterials may be a vital effectual parameter of their physicochemical properties, the preparation of monodispersed particles with desirable dimensions and shapes for different applications is a main challenge [5]. For this purpose, particular techniques have been employed to produce nanoparticles with specific shapes and sizes. Unfortunately, in common wet methods, different unsafe initial precursors, for example tetrakis(hydroxymethyl)phosphonium chloride, poly-*N*-vinyl pyrrolidone, and sodium borohydride, are normally utilized. On the other hand, in dry methods, UV, lithography, and aerosol are not regarded as environment-friendly techniques. Remained toxic elements on the surface of the synthesized materials lead to restrictions in clinical applications. Hence, an increasing tendency has been created to develop biocompatible materials by environment-friendly routes [5, 6], simultaneously considering economical issues for future commercial purposes.

The growing knowledge in the direction of green chemistry has led to a necessity to expand plain, inexpensive, and environment-friendly procedures [5]. Green nanotechnology aims to design novel materials having profits on financial, medicine, and environment issues, in order to solve the negative aspects of nano from the commencement [7]. To assemble an enhanced command for using nanoparticles in medicine, nanoparticles are required to be produced throughout "green" techniques

with minor toxic materials. It is necessary to widen capable green synthesis routes, given that the majority of applied methods involve organic solvents, low materials conversion, toxic reducing agents, difficult and wasteful purifications. Employing apt solvents, reducing and stabilizing agents in the preparation of nanoparticles via green technologies are different from other methods. Thus, there is a strange prospect to employ science and engineering to develop new products which take human and environmental health into the consideration. Following this opportunity has resulted in the development of the "Green Nanoscience" idea [8]. Although green processes are regarded as harmless, inexpensive, sustainable, and biocompatible, they comprise some shortcomings in handling microbes and in providing improved features over dimension distribution, form, and crystallinity. Furthermore, the nanoparticles synthesized by biological techniques have no monodispersity and involve a time-consuming process. However, the aforementioned points could be organized by the optimization of parameters, including pH, temperature, time, and the quantityof biological materials [9]. In this chapter, we aim to focus on the production of nanoparticles using different techniques in the scope of green nanotechnology.

7.2 Categorization of Nanomaterials

A wide range of nanomaterials with different physical and chemical behaviors has been developed. The classification of nanomaterials is continually being changed, due to new inventions in nanotechnology. Nanomaterials can be divided into a number of various groups, including nanoclusters, nanopowders, nanocrystals, nanoparticles, nanorods, nanospheres, nanodiamonds, and quantum dots [10].

7.3 Physicochemical Synthesis of Nanoparticles

To synthesize metallic nanoparticles (MNPs), several techniques including laser ablation [11], sol–gel [12], ion sputtering [13], solvothermal [14], and chemical reduction [9] have been employed. Moreover, micropatterning, photolithography, and ink jet printing have been introduced as known examples for top-down approaches [9].

7.3.1 Laser Ablation

Laser ablation is considered as a "green technique" for attaining noble MNPs. In this method, a bulk plate is immersed into a solution and nanoparticles are formed with a plasma plume produced by the laser ablation. The high energy needed and the slight control over the growth rate of the produced nanoparticles may be considered as the main weaknesses of the laser ablation technique [11].

7.3.2 Inert Gas Condensation

Inert gas condensation (IGC) has been considerably utilized to produce metallic nanoparticles [15]. Through the IGC technique, the metal is placed in a high vacuum chamber. He and Ar gases are usually employed at the pressure of around a few hundred Pascal. The metal is evaporated through this process and again condensed as a result of losing its kinetic energy though collisions with the gas atoms in the environment. As a result, nanocrystals are formed by the Brownian coagulation and coalescence. The synthesis of Au/Pd nanoparticles with a controlled dimension has been reported by this technique [16].

7.3.3 Sol–Gel Method

As a wet chemical route, the sol–gel method has been recently developed in the nanomaterials science. Inorganic nanoparticles are produced by the sol–gel technique, through a sequential process including the formation of a colloidal suspension (sol) and gelation in a continuous liquid state (gel). The size and stability of nanoparticles can be controlled by adjusting parameters and adding different mixtures. However, the basic crisis of aqueous sol–gel methods is the complexity of the procedure and is the fact that the as-synthesized products normally have an amorphous structure. Another mode of the sol–gel process can be done via a nonaqueous chemistry route, whereas the transformation of the initial materials occurs in an organic solvent. The non-hydrolytic methods are able to surmount some of the foremost constraints of aqueous modes, thereby signifying a powerful and multipurpose choice. The benefits are a direct outcome of the manifold function of organic constituents in the reaction system (e.g., solvent, surfactants). Currently, the family of nanoparticles, ranging from plain binary metal oxides to multi-metal and doped systems, is preferred to be synthesized by nonaqueous techniques [9, 12].

7.3.4 Hydrothermal and Solvothermal Synthesis

The hydrothermal and solvothermal synthesis processes of inorganic materials are considered as a prominent technique in the preparation of nanomaterials. In hydrothermal techniques, the synthetic process happens in an aqueous solution over the boiling temperature of water, while in solvothermal techniques the reaction is performed in organic solvents at about 200–300 °C above their boiling temperatures. Although the hydrothermal and solvothermal methods have a long history, these methods have been recently employed in materials production processes. Generally, hydrothermal and solvothermal reactions are preformed in a particularly sealed container or autoclave. In the mentioned states, the solubility of reactants is notably

enhanced, facilitating the reaction to happen at lower temperatures. Amongst several instances, TiO_2 photocatalysts have been synthesized throughout a hydrothermal route [17]. Due to the inexpensive cost and energy expenditure, hydrothermal methods may be applicable for industrial manufacturing. Furthermore, solvothermal techniques enable the selection amongst various solvents or blends thereof, thereby rising the adaptability of the synthesis. For instance, nanostructured TiO_2 have been produced using solvents HF and 2-propanol [18].

7.3.5 Colloidal Methods

Crystallographic features on the nucleation and growth of metallic nanoparticles has broadly been accomplished by means of colloidal systems. Overall, metallic nanoparticles are synthesized by reducing precursor salts with compositions similar to hydrazine, borohydride, citrate, etc., followed by surface modification with appropriate capping ligands to avoid aggregation and to present superior surface characteristics. The particular applications of organic solvents in this synthetic way regularly increase environmental matters. Multi-shaped nanoparticles are produced using the mentioned technique which needs differential centrifugation and thus possesses a low yield. Consequently, the expansion of trustworthy experimental protocols for synthesizing of the nanomaterials, over a range of chemical composition, size, and enough monodispersity, demands concerns in the modern nanotechnology [19, 20]. In this situation, current researches focus on the development of green and biosynthetic technologies for making nanocrystals with a needed size and a desired shape.

7.4 Green Chemistry Synthesis of Nanoparticles

7.4.1 Tollens Process

The tollens synthesis is a one-step method that, for example, can yield Ag nanoparticles with a controlled size [21, 22]. Through a study conducted on the saccharide reduction of Ag^+ ions by the tollens process [22], it was found that small particles of 57 nm is size are formed with glucose at low ammonia concentrations (0.005 M). Different particle sizes can be achieved by varying the concentration of ammonia, whereas the higher concentration of ammonia would lead to a larger particle size [23]. Le et al. [24] also pointed out a modified tollens technique, in which oleic acid is added as a stabilizer and a UV radiation is simultaneously used with treatment by glucose during the reduction process, to attain silver nanoparticles with a controlled size. Yin et al. [21] examined the potential of the tollens method in preparing silver nanoparticles. In another method described by Yin and colleagues [24], there is a delay period greater than 5 min, which allows the complete mixing of reactants. Most have concluded that, the synthesis by the tollens method is environmentally green, due to the use of nontoxic chemicals.

7.4.2 Microwave Irradiation

Microwave (MW) heating of particles was discovered in 1940s and has become successful in the food industry with applications in chemistry [25]. Microwave irradiation is an electromagnetic radiation between frequencies of 0.3–300 GHz. Microwave chemistry is based on the principle of dielectric heating [26]. There are two main mechanisms for microwave irradiation, namely dipolar polarization and ionic conduction mechanisms. The irradiation of matter in turn causes the alignment of dipoles or ions in the electric field [27]. Because electromagnetic radiations (EMR) produce an oscillating field, these dipoles or ions attempt to realign themselves within this field and produce heat through molecular friction [27]. Using microwaves to heat the samples is a green method for the synthesis of nanoparticles, while it also yields desirable features, including shorter reaction periods and better product yields [28].

Microwave irradiation has several advantages within the realm of chemical synthesis. For instance, in the preparation of inorganic nanoparticles, conductive heating is carried out by using an external heat source; however, this method is slow and relatively inefficient. In contrast, microwave irradiation produces efficient internal heating, while uniformly raising the temperature of the entire reaction mixture. Furthermore, microwave heating increases the reaction rate; for instance, Au nanowires have been synthesized under the microwave irradiation method within 2–3 min [29]. Moreover, the heat source does not come into direct contact with reactants, allowing the precise control of reaction parameters and the reduction of chemical wastes. There are also limitations to the use of irradiation techniques, including the short penetration depth [30]. MW-assisted heating has been used for the preparation of nanostructures, including Ag, Au, Pt, and Au–Pd. In addition to spherical nanoparticles, crystalline polygonal plates, sheets, rods, and wires have also been prepared within only a few minutes under MW irradiation conditions [31]. Besides requiring less energy, microwave irradiation should be more environment-friendly than conventional heating methods [32].

7.4.3 Use of Polyoxometalates

Polyoxometalates (POMs) are anionic structures composed of early transition metal elements in their highest oxidation state [33]. Since POMs are soluble in water and have the capability of undergoing stepwise, multielectron redox reactions without disturbing their structure have the potential for synthesizing Ag nanoparticles [33, 34]. Ag nanoparticles with different shapes and sizes can be obtained by using different POMs, in which POMs serve as a reductant as well as a stabilizer [23]. Zhang et al. [35] described a synthesis method of metal nanoparticles. They found that for the efficient synthesis of Pd and Pt nanoparticles, reduced POMs were constructive, as both reducing and capping agents at room temperature in water.

Georgakilas et al. [36] focused on the process of decorating carbon nanotubes (CNTs) with nanoparticles in order to produce novel nanohybrid materials for a wider range of applications. The attachment of Au nanoparticles to CNTs' sidewalls has shown to be promising for highly efficient electrochemical cells and photoelectronic sensor devices. POMs serve as reducing, encapsulating and bridging molecules and avoid the introduction of other organic toxic molecules. The nanohybrids produced using the POMs enhance photocatalytic activities under visible light irradiations.

7.5 Bio-inspired Green Synthesis of Nanomaterials

Green chemistry is gradually incorporated into up-to-date developments in maintenance with a worldwide attempt to decrease the production of dangerous wastes and to develop energy-efficient synthesis methods. To do so, any synthetic means or chemical procedures have to deal with the basic standards of green chemistry, by using environmentally kind solvents and nontoxic chemicals [37]. The green synthesis of nanoparticles ought to encompass main steps, which are consistent with green chemistry outlooks with regard to the choice of: biocompatible and nontoxic solvents, environmentally reducing materials, and nontoxic agents for stabilizing the produced nanoparticles. Applying the aforementioned decisions into nanoscience will aid the processing of intrinsically safer nanomaterials and nanostructured devices. Consequently, green nanotechnology aims to apply green chemistry theories in developing nanoscale materials, and to design production techniques with decreased dangerous waste generation and safer applications [38].

Moreover, biochemical processes can occur at low temperatures, as a result of the high specificity of biocatalysts. Thus, a synthetic method containing one or more biological steps would cause the energy saving and lesser environmental impacts, compared to conventional techniques. In order to optimize safer nanoparticle fabrication, it is popular to use bio-based techniques minimizing the dangerous forms of material production. Using examples from nature, the fact that living organisms create inorganic materials during bio-guided routes should be adopted as an advanced approach to nanomaterials assembly [39]. Typically, biomineralization methods develop biomolecular models, which relate to nano-scaled inorganic materials, leading to very competent and controlled syntheses. The structures of these materials are well controlled at both nano- and macro-scale levels, allowing the design of multifunctional behaviors. Simpler organisms including bacteria, algae, and fungi, have developed plans for biominerals production throughout 100 millions of years of advancement. The objective of templating biomolecules in the mineralization process is to present an artificial microenvironment in which the inorganic phase morphology is firmly controlled by a range of low-range interactions.

Nature has devised a variety of progressions for the creation of nano- and microscaled inorganic materials, contributing to the improvement of fairly innovative (Fig. 7.1) and mostly unexplored research areas in regard to the biosynthesis of

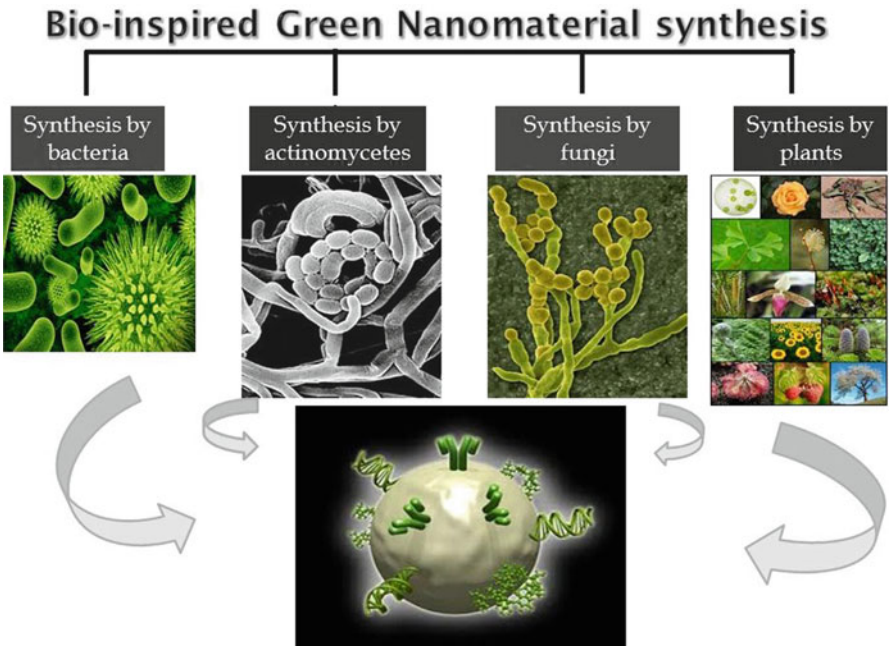

Fig. 7.1 A schematic representation of bio-inspired green synthesis of nanomaterials. Reprinted from ref. [9] with permission by Elsevier

nanomaterials [9, 40]. Biosynthesis of nanoparticles is a category of bottom-up methods in which the foremost chemical reaction is reduction and oxidation. Antioxidant and reducing agents in microbial enzymes or plant phytochemicals are typically considered for reducing metal constituents into nanoparticles [41].

7.5.1 Microbial Synthesis of Nanoparticles

The microbial synthesis of nanoparticles is considered as a green chemistry method that correlates between nanoscience and microbial biotechnology. Biosynthesis of Au, Ag, Au–Ag alloy, Se, Pt, Pd, SiO_2, TiO_2, ZrO_2, quantum dots, magnetite, and uraninite nanoparticles using bacteria, fungi, yeasts, viruses, and actinomycetes have been reported. However, biological nanoparticles, in spite of stability, are not monodispersed and their synthesis rate is time-consuming. To conquer these crises, numerous factors including microbial cultivation techniques and extraction methods are useful, where combinatorial approaches, for example photobiological methods, may be utilized. Cellular, biochemical, and molecular mechanisms that contribute to the preparation of biological nanoparticles need to be assessed in depth to enhance the production rate and to improve nanoparticle properties.

Due to the rich biodiversity of microbes, they as biological materials for nanoparticle production are still up for investigation investigated. Investigating natural secrets for the production of nanoparticles by microbes is considered as strong eco-friendly green nanofactories. The synthesis of nanoparticles using microbial techniques has appeared as a talented research area in the nanobiotechnology field, which interconnects biotechnology and nanotechnology [6].

The chemical detoxification and ion efflux from cells by membrane proteins may be the main reason for the resistance of the majority of toxic heavy metals to microbes. The solubility alteration may be another reason for the microbial resistance. Hence, microbial systems are able to detoxify metal ions by reduction and deposition processes. Additionally, the inorganic toxic ions convert to metal nontoxic nanoclusters [6]. Microbial detoxification may be prepared by extracellular biomineralization, complexation, biosorption, precipitation, or intracellular bioaccumulation.

Extracellular synthesis of metal nanoparticles possesses further commercial uses in different fields. Since polydispersity is the main issue, it is essential to consider the optimization parameters for monodispersity in a biological process [42]. Regarding the intracellular approach, the accumulated particles have specific sizes with a lesser amount of polydispersity. However, further steps including ultrasound processes or reactions with appropriate detergents are needed for intracellularly synthesized nanoparticles. This may be employed in the recovery of expensive metals from wastes and leachates. Moreover, bio-matrix metal nanoparticles as catalysts in chemical reactions will aid to maintain nanoparticles for permanent applications in bioreactors [43]. Microbial production of metal nanoparticles is related to the localization of cell reductive constituents. Once reductive enzymes in cell walls or secreted enzymes are engaged in the reduction of metal ions, it is clear to get metal nanoparticles extracellularly. Compared to intracellular approaches, extracellular synthesis has been found to have wide applications in electronics and bio imaging.

7.5.2 Biosynthesis of Nanoparticles by Bacteria

Bacteria play a vital role in biogeochemical cycling and metal mineral creations in surface [44]. Employing microbial cells for the synthesis of nanosized materials is accounted as a new advancement for the production of metal nanoparticles. While attempts for the biosynthesis of nanomaterials are being currently made, relations between microorganisms and metals have been well reported and the capacity of microorganisms to extract metals is applied in commercial biotechnological approaches including bioleaching and bioremediation [45].

Bacteria usually synthesize inorganic materials, using intracellular or extracellular mechanisms. Microorganisms are regarded as a possible biofactory for the manufacturing of nanoparticles like Au, Ag and CdS. As known bacteria, prokaryotic *Escherichia coli*, *Pseudomonas stutzeri*, *Pseudomonas aeruginosa*, *Plectonema boryanum*, *Salmonella typhi*, *Staphylococcus currens*, *Vibrio cholerae* have attracted

much attention for the synthesis of metallic nanoparticles through extracellular and intracellular processes [46]. Moreover, some bacteria for the production of inorganic nanoparticles have been recognized, such as magnetotactic bacteria which are employed for magnetic nanoparticles and S-layer bacteria for producing gypsum and calcium carbonate layers [47].

A number of microorganisms are able to live and grow at the high concentrations of metal ions, owing to their resistance to the metal. The mechanisms involve: efflux systems, solubility alteration and toxicity, bioaccumulation, biosorption, an extracellular complex at the precipitation of metals and the lack of particular metal transport systems [48].

Recently, bacterial activity has been used in the precipitation of mineral ores. For Fe- and Mn-oxide precipitation processes, Pedomicrobium-like budding bacteria in an Alaskan placer has previously been utilized; also, it has recently been employed to synthesize Au [1, 16]. *Bacillus subtilis* 168 reduces water-soluble Au^{+3} ions to Au^0, synthesizing octahedral structures in the cell walls with the size of around 5–25 nm [49]. Also, the bioreduction of chloroauric acid to Au^0 nanoparticles by means of *Escherichia coli* DH5α has been recently reported [50]. The produced nanoparticles on the surface of cells were mainly sphere-shaped with a few other features of triangles and hexagonals. These cell-bound nanoparticles have been recognized as a suitable choice in describing the electrochemistry of hemoglobin and proteins [50].

As a typical instance, Fig. 7.2 indicates a dark-field TEM photomicrograph of S-algae cells accompanied by Pt nanoparticles deposited in a periplasmic space. At the ambient temperature and neutral pH, S-algae were placed anaerobically in a H_2PtCl_6 solution. In the existence of lactate as the electron donor, $PtCl_6^{-2}$ ions were converted to 5 nm Pt nanoparticles within 1 h [51].

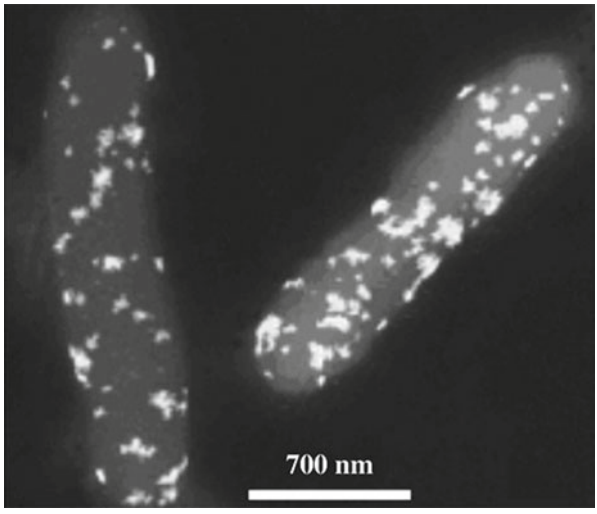

Fig. 7.2 Dark-field TEM image of S-algae cells with platinum nanoparticles deposited in the periplasmic space. Reprinted from ref. [51] with permission by Elsevier

7.5.3 Biosynthesis of Nanoparticles by Fungi

The production of fungal-mediated metal nanoparticles is a quite modern research area. Fungi have been considerably employed for the biosynthesis of nanoparticles, where the mechanistic characteristics governing the nanoparticle synthesis have been considered for a small number of them. Nanoparticles with monodispersity and appropriate dimensions may be achieved using fungi. Fungi could be utilized as a source for the synthesis of a huge quantity of nanoparticles against bacteria, since fungi produce the higher amounts of proteins leading to higher nanoparticle production [40]. As an Ascomycetes class of fungi, yeast has presented an excellent ability for nanoparticle production. Fungi are more favorable in comparison to other microorganisms, plants, and bacteria in regard to easier handling, simpler fabrication ability, withstanding flow pressure and agitation in bioreactors.

Nowadays, fungi such as *Colletotrichum* sp. [52], *Fusarium oxysporum* [53], *Trichothecium* sp., *Trichoderma asperellum*, *T. viride* [54], *Phanerochaete chrysosporium* [55], *F. solani* USM 3799 [56], *A. fumigatus* [57], *F. semitectum* [56], *Aspergillus niger* [58], *Coriolus versicolor* [59], *Phoma glomerata* [60], *Penicillium brevicompactum* [61], and *Penicillium fellutanum* [62] are used for producing nanoparticles. For example, Au nanoparticles have been intracellularly produced by the *Verticillium luteoalbum* fungus [40]. The production rate and the size of nanoparticles can be controlled by adjusting pH, temperature, concentration of Au, and incubation time. A biological process with this ability to rigorously control the particle shape would be a significant benefit.

The extracellular secretions of reductive proteins can be simply handled in downstream processing. In addition, given that the nanoparticles form at the outer layer of the cells and unneeded cellular constituents are avoided, it can be directly employed in different applications. The nanoparticles formed by the extracellularly reduced approaches is larger than those formed within microorganisms. Thus, the size limit could have been corresponded to the nucleation of particles inside the organisms [6].

Mukherjee et al. [63] focused on the use of eukaryotic microorganisms in the biological production of Au nanoparticles using *Verticillium* sp. (AAT-TS-4). According to this research, the Au nanoparticles of about 20 nm in size, well-defined dimensions and good dispersity were reported on the surface of the cytoplasmic membrane of fungal mycelium. TEM analyses indicated ultrathin sections of fungal mycelia, with nanoparticles of triangles and hexagonal morphologies on the cell walls and of quasi-hexagonal morphologies on the cytoplasmic membrane. *Trichothecium* sp. was also used to synthesize Au nanoparticles intracellularly [64].

The synthesis of nanoparticles in cell outer layers (extracellularly) has many usages, since it evades adjoining cellular constituents from the cell. Typically, fungi are considered as organisms that synthesize nanoparticles extracellularly, due to their vast range of secretory components, which involve in decreasing particle size and capping of nanoparticles. Shankar et al. [52] found an endophytic fungus, *Colletotrichum* sp. isolated from the leaves of geranium plants (*Pelargonium graveolens*), which

quickly reduced Au ions to zero-valent Au nanoparticles with a polydispersed spherical morphology. These Au nanoparticles had a combination of disk and rod-like structures. Glutathiones as the capping agents of Au nanoparticles bind with free amine groups or cysteine residues [65].

As one of the classifications of prokaryotes, Actinomycetes have main characteristics of fungi. Additionally, a new extremophilic actinomycete, *Thermomonospora* sp. was found to produce extracellular monodispersed Au nanoparticles. These synthesized Au nanoparticles had a spherical morphology with a size of around 8 nm [66].

7.5.4 Virus-Mediated Biosynthesis of Nanoparticles

A few biomolecules similar to amino acids, fatty acids, and polyphates are utilized for the synthesis of semiconductor nanostructures. Especially, through a change in the ratio of fatty acids, various shapes of CdSe, CdTe, and CdS nanocrystals can be obtained [67]. Moreover, there exists other biological materials for the environment-friendly production of inorganic materials such as DNA [68], protein cages [69], viroid capsules [70], biolipid cylinders [71], bacterial rapidosomes [72], multicellular superstructures [73] and S-layers [74]. By using glutamate and aspartate on the outer layer of virus, tobacco mosaic virus (TMV) has been utilized to produce iron oxides by hydrolysis, co-crystallization of CdS and PbS, and the sol–gel synthesis of silica [75]. For the synthesis of quantum dot nanowires, the self-assembled viral capsid of genetically engineered viruses was exploited as biological templates.

A7 and J140 peptides with the capability of ZnS and CdS nanocrystal nucleation were expressed as pVIII proteins into the crystalline capsid of viruses. ZnS nanocrystals were assembled on the viral capsid with a size of about 5 nm and hexagonal wurtzite morphology, and CdS nanowires were assembled with a size of 3–5 nm. Hybrid nanowires including ZnS and CdS were obtained with a dual peptide virus engineered to express A7 and J140 within the same viral capsid [76, 77] (Fig. 7.3).

7.5.5 Biosynthesis of Metal Nanoparticles by Terrestrial Phototrophic Eukaryotes (Plants)

Since phototrophs are sustainable supplies, they may be utilized mostly in the green synthesis of nanoparticles. In this regard, the green chemistry method is an alternate method for producing biocompatible nanoparticles with chemical synthesis, which is the most recent doable route of linking material science and biotechnology in the field of nanobiotechnology [5]. Nanobiotechnology has more benefits compared to usual techniques, because of the availability of more constituents by biological bodies for the formation of nanostructures. The rich biodiversity of such biological bodies needs to be studied for the production of bionanomaterials. Molecular cloning and engineering of genes encoding particular enzymes, that facilitate the bioreduction of metals, are investigated to help the simplistic manufacturing of nanomaterials [5].

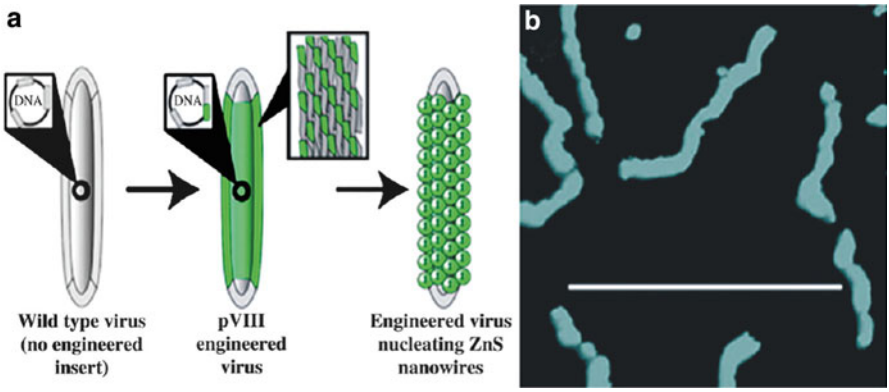

Fig. 7.3 A7-pVIII-engineered viruses related to the synthesis of ZnS nanocrystals. (**a**) The diagram showing A7 peptide expression on pVIII protein upon phage amplification and assembly, then the consequent nucleation of ZnS nanocrystals. (**b**) ADF STEM images that show the morphology of ZnS-virus nanowires. Reprinted from ref. [77] with permission by the National Academy of Sciences

Until today, different phototrophic eukaryotes including plants, microbes (diatoms), algae, and heterotrophic human cell lines and some biocompatible agents, which are considered as effective environment-friendly green nanofactories, have been notably employed for the synthesis of different inorganic nanoparticles. Phototrophic eukaryotes including plants, algae, diatoms and heterotrophic human cell lines and other biocompatible agents have been expressed to produce green nanoparticles such as Co, Cu, Ag, Au, SiO_2, Pd, Pt, Ir, bimetallic alloys, magnetite, and quantum dots. Due to their variety and sustainability, applying phototrophic, heterotrophic eukaryotes and biocompatible agents for the development of nanomaterials is still to be entirely investigated [5].

In the past, only prokaryotes had been used for the biosorption and bioreduction of insoluble toxic metal ions to soluble nontoxic metal salts or valency changes. However, it was understood that highly developed organisms such as plants, algae, diatoms, human cells and other components of eukaryotes have the ability to reduce metal ions to metal nanoparticles. Eukaryotes give further information in their genetic material to encode a variety of reducing/stabilizing agents that facilitate the production of metal nanoparticles. Phototrophic eukaryotes obtain energy from sunlight, using photosynthesis, and thereby fix inorganic carbon into organic materials, while heterotrophic eukaryotes similar to human cells employ organic carbon synthesized by other organisms for growth. Terrestrial environments comprise predominant phototrophs like plants, algae, and diatoms in aquatic environments [5].

The benefit of plants for the synthesis of nanoparticles is that they are accessible, harmless to handle and have a wide variability of metabolites that help in reduction. Some of the plants have been recently explored for their function in the production of nanoparticles (Fig. 7.4) [9]. Au nanoparticles with a size variety between 2 and 20 nm have been produced by live Alfalfa plants [78]. Moreover, Ag, Co, Ni, Zn,

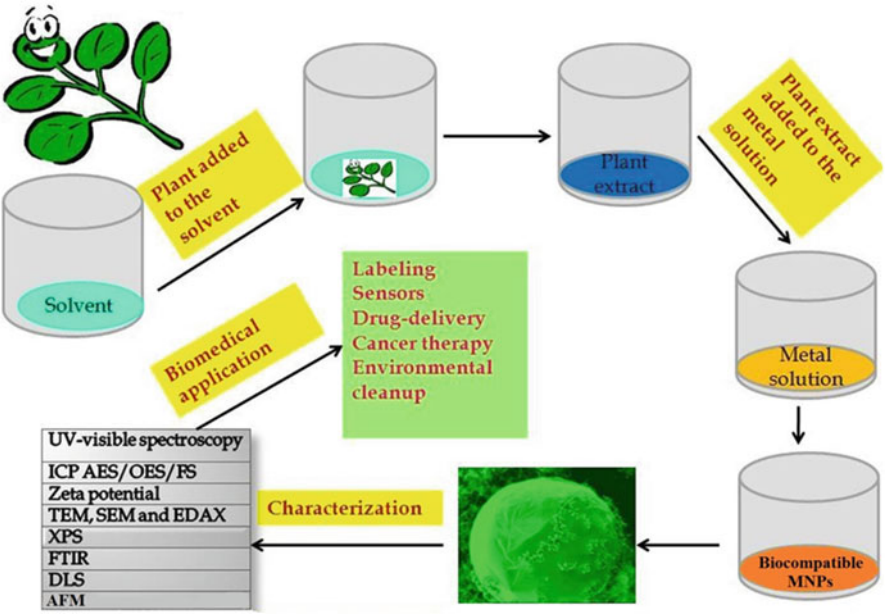

Fig. 7.4 A schematic representation of plants as a source of green nanosynthesis, its characterization and biomedical applications. Reprinted from ref. [9] with permission by Elsevier

and Cu nanoparticles have been produced in the live plants of Alfalfa, *Brassica juncea* (Indian mustard), and *Helianthus annuus*. Some of the plants, for example *B. juncea*, have been known as hyperaccumulators, synthesizing more concentrations of metal ions, as compared to others [79].

Today, much research has been conducted on the reduction of metal nanoparticles with plants and the particular function of phytochemicals. The main water-soluble phytochemicals such as organic acids, flavones, and quinines which can conduct reduction processes. The phytochemicals existing in *Cyprus* sp. (Mesophytes), *Bryophyllum* sp. (Xerophytes), and *Hydrilla* sp. (Hydrophytes) were investigated for their role in the production of Ag nanoparticles. The Xerophytes consist of emodin as an anthraquinone, which could undergo redial tautomerization, resulting in the precipitation of Ag nanoparticles. Currently, Au nanoparticles have been produced using the extracts of *Magnolia kobus* and *Diospyros kaki* leaf extracts. The influence of temperature on the synthesis process of nanoparticles was examined, and it was reported that at lower temperatures, polydispersed particles with a size of between 5 and 300 nm was acquired, whilst the formation of smaller spherical particles happens at higher temperatures [80].

Although the synthesis of metal ions by using microbes, including fungi and bacteria, requires a relatively longer reduction duration, water soluble phytochemicals perform it in a much lesser period. Accordingly, in comparison to the microbes,

the plants are superior selections for the production of nanoparticles. Fahmy et al. [81] pointed out green nanotechnology as an entrance technique for the beneficiation of natural cellulose fibers. Plant tissue culture routes and downstream processing mediate in manufacturing metallic and oxide nanoparticles on a trade scale, once matters such as the metabolic status of the plant etc. are correctly addressed.

Plants are considered principal photosynthetic autotrophs as the high level and food chain manufacturers, with a high biomass production in terrestrial environments. Plants receive about 75 % of light energy from sun and convert it into the chemical energy of glucose. In comparison to prokaryotic microbes which require costly techniques for maintaining microbial cultures and downstream processing, the plants and their products are regarded as sustainable and renewable resources for the production of nanoparticles. Phytomining has been known as an inexpensive and eco-friendly approach compared to conventional chemical routes. Phytomining employs the plants in order to recover noble metals from ore mines and runoffs. Compared to other chemical routes which are less effectual for producing the low levels of metals, it is able to synthesize even a very low level of metal accumulated in tissues.

Nontoxic chelators, such as thiourea, iodide, bromide, thiocyanate, cyanide, and thiosulfate, can solubilize metals from ores and mediate a proper uptake by plants. Accumulation of metal ions in plants is mostly utilized in phytoremediation which has been considered as a cost-effective, environment-friendly, and proficient method for the cleanup of polluted sites [82]. In phytomining, plants that bioconcentrate metal ions into their biomass from a large volume of soil are hunted for, which can be harvested and recovered from contaminated sites. In *Berkheya coddii* and *Brassica juncea*, hyperaccumulation of Au was found with thiocyanate solution as the solubilizer, whereas *B. juncea* and chicory hyperaccumulated Au with bromide, iodide, cyanide, thiosulfate, or thiocyanate solutions. The solubilizer, cyanide induced a higher accumulation of Au in leaves and stems of *B. juncea* and *B. coddii*, while the accumulation was found to be higher in roots with the addition of thiocyanate. As a result of the effect of plant's internal pH on complexes, the mentioned distinctions in the translocation abilities between cyanide and thiocyanate are observed [83]. Many investigations have been performed in order to eliminate high concentrations of Au (III) ions from solutions and soils with different solubilizers.

Several metal nanoparticles possess catalytic activities, and in homogeneous solutions they are hard to recover after the downstream procedures of chemical reactions. Sharma et al. [43] used the roots and shoots of *Sesbania drummondii* for the intracellular synthesis of Au nanoparticles, when grown in sterile aqueous agar containing Au ions. The reduction process was believed to be facilitated by the existence of secondary metabolites in the cells. TEM results of the root cells indicated the existence of monodispersed nanoparticles with a size of 6–20 nm in organelles and multiple spherical nanoparticles surrounding the cell organelles in the cytoplasm. In this regard, for the reduction of industrially toxic pollutants like 4-nitrophenol, the biomatrixed nanomaterial containing Au nanoparticles was employed as the stable catalyst (Fig. 7.5).

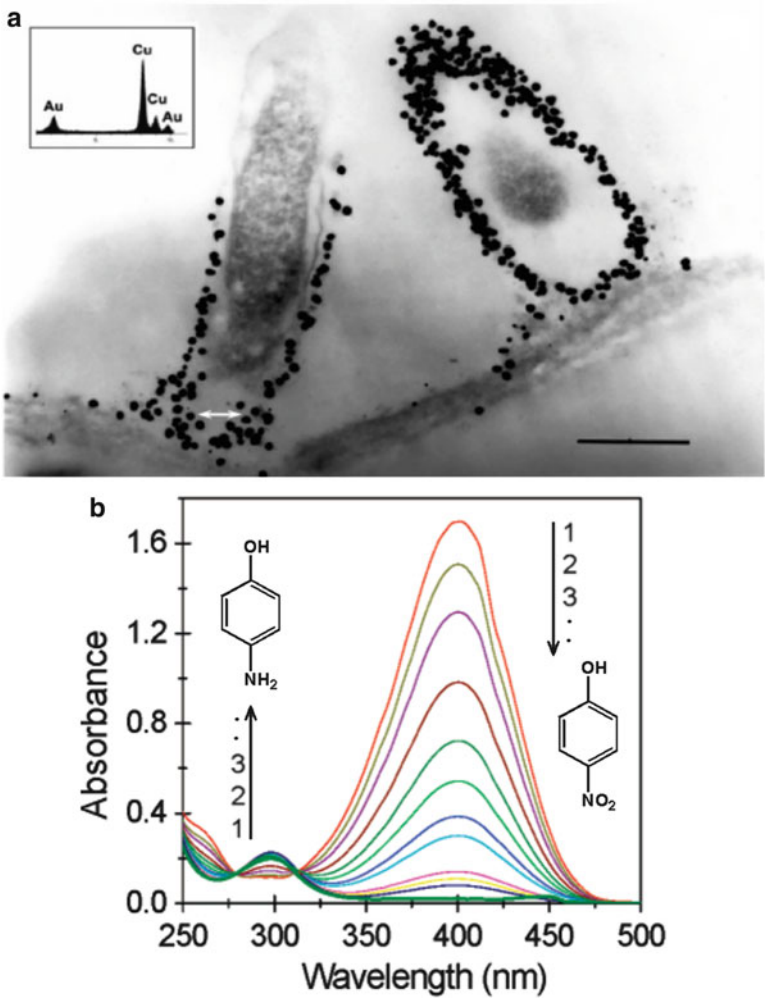

Fig. 7.5 (**a**) TEM micrograph of *Sesbania drummondii* root, which shows gold nanoparticles that surround organelles (scale marker = 500 nm). (**b**) UV–visible absorption spectra during the successive reduction of 4-nitrophenolate ions by gold nanoparticle-rich biomatrix. Reprinted from ref. [43] with permission by the American Chemical Society

As previously mentioned, plant biomass is a renewable energy supply attained from living or dead plants. These are usually utilized to produce electricity, biofuel, biogas, etc. Thus, the use of biomass wastes in the production of nanoparticles is of high importance. Commonly, the generation of biomass by phototrophs is cost-effective, as it only requires sunlight, water, carbon dioxide, and inorganic salts. In the situation of the alarming rise of global warming, the fabrication of plant biomass is a natural bioprocess of carbon sequestration from the air. Alfalfa biomass produces Au nanoparticles of ~100 nm and irregular shapes by the reduction of Au

(III) ions in a pH-dependent mode [84]. Also, Herrera et al. [85] reported the binding of Ag (I) ions by alfalfa biomass from an aqueous solution in a pH-dependent mode.

The existence of different reducing agents including secondary metabolites, proteins, and enzymes is normally involved in the production of metal nanoparticles by plant components. In bioaccumulation, the nanoparticle localization is according to the attendance of specific enzymes or proteins. The recovery of these nanoparticles from plant components is time-consuming and costly, and requires enzymes to surround and then degrade cellulosic materials [86]. Accordingly, the production of different metal nanoparticles by plant extracts is simple in downstream and scaling up processing of nanoparticles. Most recently, plant extracts are extensively utilized as a practical and simplistic approach for the production of metal nanoparticles, compared to physical and chemical routes. Geranium plant extracts from stem, leaf, and root have been reported for the extracellular synthesis of Au nanoparticles. Shankar et al. [52] reported the biological reduction of Au ions to Au nanoparticles, by using geranium leaf broth, with the size of 20–40 nm and multiply twinned particles. In the reduction process of Au ions, the ethanol groups of terpenoids are oxidized to carbonyl, and an amide (II) band of proteins was involved in stabilizing molecules in the formation of nanoparticles. Nanoparticles with a size of around 14 nm and a spherical morphology were formed by geranium stem extracts [52]. Shankar et al. [47] showed the synthesis of Ag nanoparticles with adding $Ag(NO_3)$ to the leaf extract of neem after 4 h. Since the redox has lesser ability for the reduction of Ag ions to metallic Ag compared to Au, this process takes a long duration. Ag nanoparticles with a size range of 5–35 nm and spherical morphology have been produced using terpenoids in the leaf extract, which facilitate the reduction of Ag ions by the oxidation of aldehyde groups in molecules to carboxylic acid.

Dried powder of alfalfa was also employed in the production of new nanomaterials, according to bimetallic particles such as Eu–Au nanoparticles, which has a broad application in nuclear medicine and nanophotonics. Europium (Eu) is a material with low oxidation resistance and most reactive among rare elements. Eu–Au bimetallic nanoparticle with the size range of 2–20 nm was synthesized by the reduction of Eu^{+3} and Au^{+3} into MTP clusters of Eu^0/Au^0 at pH = 8.0 [87]. There are some plants which produce several kinds of nanoparticles. For example, the leaf extract of *Azadirachta indica* is employed for the production of Au, Ag, and Au core–Ag shell nanoparticles. The synthesized Au–Ag core–shell structure had a mixture of Ag and Au ions in the ratio of 1:1, with spherical shape and a size of 50–100 nm [47].

Platinum group metals (PGMs) are valuable D-block transition metals, which have a tendency to come together in mineral deposits having remarkable chemical catalytic properties for the transformation of toxic elements and in electronic devices. The aqueous extract of the fruit of Gardenia was utilized in the bioreduction of $PdCl_2$ to Pd nanoparticles as the catalytic hydrogenation of p-nitrotoluene with the size of 3–5 nm and uniform distribution. Antioxidants such as geniposide, chlorogenic acid, crocetin, and crocins reduced and stabilized nanoparticles [88].

7.5.6 Biosynthesis of Nanoparticles by Aquatic Phototrophic Eukaryotes (Algae)

Algae are eukaryotic aquatic oxygenic photoautotrophs, which generate their food using sunlight photosynthesis with the production of O_2. Their photosynthesis mechanism has been developed from cyanobacteria via endosymbiosis, which is of the main producers in many aquatic environments. Amongst a variety of algae, *Chlorella* sp. was found to synthesize different heavy metals such as Cd [89], U, Cu, and Ni [90]. *Chlorella vulgaris* is a single-celled green alga belonging to phylum Chlorophyta, and its extracts indicated antitumor performances [91]. Dried algal cells were understood to present a strong binding ability to tetrachloroaurate (III) ions in order to produce algal-bound Au, which was afterward reduced to form Au (0). Almost 88 % of algal-bound Au reached the metallic state and Au crystals were synthesized in the inner and outer layer of the cell surfaces with tetrahedral, icosahedral, and decahedral structures.

In this approach, the optimization of parameters such as pH, temperature and metal ions (solute) concentration for accelerating the biological accumulation of nanoparticles with thin sizes and appropriate shapes is compulsory. Up to now, only very few researches have been focused on optimization in biological processes. For synthesizing Au nanoparticles with a controlled size and shape, and a hexagonal morphology, a 28-kDa "gold shape-directing protein (GSP)" in the extract of green alga, *C. vulgaris* has been employed, where with the increase of concentration in GSP, Au plates with lateral sizes up to micrometers were accumulated [92].

7.5.7 Biosynthesis of Nanoparticles by Aquatic Phototrophic Eukaryotes (Diatoms)

As the nonmotile and unicellular eukaryotic photosynthetic algae, diatoms are encased inside a silica unique cell wall. Diatoms are also a manufacturer of around 25 % of the world net primary production from solar energy. Diatoms are different nanostructures producing organisms, by finding the correlation between morphogenesis and the diatom genome. Controlling the 3D shape and pattern of diatoms leads to the appearance of a new research area called "diatom nanobiotechnology." Marine diatom cells of *Cyclotella meneghiniana*, *Glyphodiscus stellatus*, *Isthmia nervosa*, and *Roperia tesselata* that create amorphous clear silica glass valves with special shapes and sizes in microscale or nanoscale structures have found broad applications such as biomedical, electronic, optical, semiconductor nanolithography, sensing, and drug delivery (Fig. 7.6) [93].

The heavy metal pollution of water bodies from industries like metal smelting, casting, electroplating, and mining waste materials is currently a vital issue. The application of microalgae for removing the heavy metals contamination, even at low amounts, is more than that of plants, algae, bacteria, and fungi. It is the cost effective and environmentally friendly process, and the use of the microalgae that synthesize

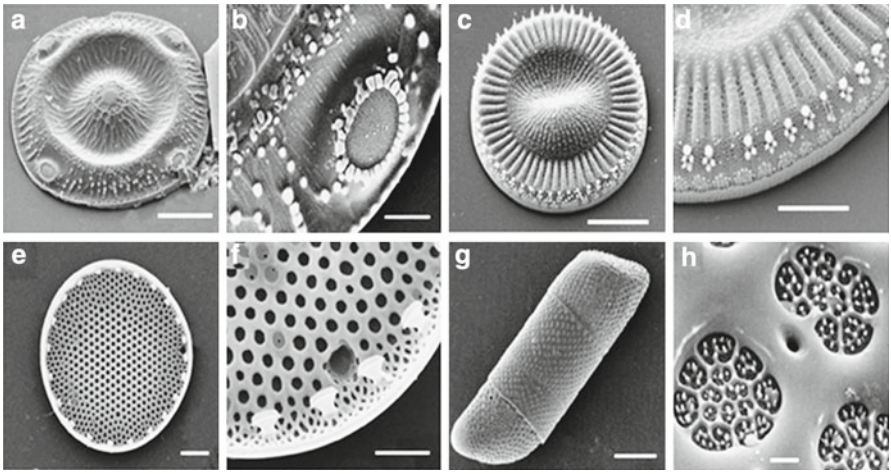

Fig. 7.6 Transmission electron microscopic images of marine centric diatoms and close-ups of surface features, courtesy of Mary Ann Tiffany. (**a** and **b**) *Glyphodiscus stellatus*, (**c** and **d**) *Cyclotella meneghiniana*, (**e** and **f**) *Roperia tesselata*, and (**g** and **h**) *Isthmia nervosa*. Reprinted from ref. [93] with permission by Elsevier

metal nanoparticles from insoluble heavy metal pollutants which has dual benefits in the recovery and production of valuable nanoparticles. Similar to a microbial biomass, microalgae adsorb confiscate heavy metal ions by the production of phytochelatin [94]. However, the microalgal biomass synthesis is more costly compared to terrestrial plants.

Diatoms usually make silica for their cell wall during the biomineralization processes, together with particular organic macromolecules including silaffins to form a complex microscopic configuration. These silaffins that diatoms exploit to direct silica precipitation could be utilized in the semiconductor industry. In the same way, in diatom, *Coscinodiscus granii* and cationic polypeptides quickly induce the deposition of silica from silicic acid in vitro. Furthermore, adding polyamines produces silica by the precipitation of silicic acid. The formed nanostructured materials are monodispersed particles of 100–200 nm in size with a spherical morphology. Therefore, the research on the components involved in the biosilica of diatoms aids to biomimic the natural process and results in the precipitation of complex nanostructures at ambient conditions and neutral pH [95].

7.5.8 Biosynthesis of Nanoparticles by Heterotrophic Eukaryotic Cell Lines (Human)

Human cells are heterotrophic in nutrition and require to be supplied with energy for their survival. Human cancerous and noncancerous cells, mimicking the natural environment of cells are able to synthesize some metal nanoparticles in vitro intracellularly.

By using a tetrachloroaurate solution (1 mM), cancer cells such as SiHa (malignant cervical epithelial cells), HeLa (malignant cervical epithelial cells), and SKNSH (human neuroblastoma) and non-cancer cells like HEK-293 (nonmalignant human embryonic kidney cells) have produced Au nanoparticles with sizes between 20 and 100 nm. These nanoparticles were produced in the cytoplasm and in the nucleus of the cells. The size of these nanoparticles in nucleus was smaller than that of the cytoplasmic particles [96].

7.6 Applications of Metal Nanoparticles in Medical Biology

In the research field of nanomaterials, metal nanoparticles have attracted very much interest because of their broad uses in catalysis, electronics, photonics, sensing, environmental cleanup, imaging, and drug delivery [9, 97]. The reason why nanoparticles are attractive for biomedical applications is due to their distinctive properties including high surface-to-mass ratio compared to other particles, their quantum properties and their ability to adsorb and bring other compounds such as drugs, probes and protein to determined locations. The biological application of metal nanoparticles has indicated a fast advancement in the area of labeling, delivery, heating, and sensing. Typically, the optical properties of colloidal Au nanoparticles have been employed for new biomedical applications with an importance on cancer diagnostics and therapeutics [9].

7.6.1 Labeling

Metal nanoparticles are used to produce contrast due to their electron absorbing properties. Au nanoparticles are suitable as a contrasting agent in transmission electron microscopy, since they highly absorb electrons. In addition, due to the same size of nanoparticles with proteins, they are utilized for bio tagging or labeling [98]. Au nanoparticles provide a very high spatial resolution and so have been applied in some of labeling applications, as a result of their small size and functionalizing properties, i.e., with antibodies (immunostaining) [99]. Furthermore, optical detection methods are extensive in the biological field, due to the change in the optical or fluorescence properties of nanomaterials. Correspondingly, the optical properties of particles including strong absorption, scattering and particularly plasmon resonance, make them valuable for light-based methods such as photothermal or photo-acoustic imaging. Moreover, radioactive Au nanoparticles make it applicable for sensitive detection and as an X-ray contrast agent [9].

7.6.2 Sensors

Metal nanoparticles can be utilized as sensors. The electronic and optical sensing properties of biomaterial surfaces is a usual practice in analytical biochemistry. Thus, the immobilization of biomolecule–nanoparticle conjugates on the surface

provides a broad approach for the development of optical or electronic biosensors. Metal nanoparticles like Au or Ag indicate plasmon absorbance bands in the visible spectral region, which are controlled by the particles size. Their optical behavior can be altered by binding to special molecules, allowing the ion detection and quantification of analytes. The absorption properties of Au nanoparticles change considerably when agglomeration occurs. Many researches have been documented on bioassay labeling and tissue staining, using metal particles as an approach to observing biological processes. Espectral shifts which come from agglomerated metal nanoparticles, like Au, are considered in the development of biosensors, based on a hybrid system being composed of biomolecule and nanoparticles. For example, nanoparticles that were functionalized with two types of nucleic acid, which were matching to two parts of an analyzed DNA, were hybridized with analyzed DNA, resulting in agglomeration of the nanoparticles and in the detection of a red shifted interparticle plasmon absorbance of the agglomerated nanoparticle [100].

7.6.3 Drug Delivery

Nanoparticles have an appropriate prospect in the form of drug therapies [101]. An effective dose of drugs could be reached to a definite targeted tissue but engineered to deliver in a planned time period in order to ensure the highest efficiency as well as the patient's safety. Due to the nontoxicity and nonimmunogenicity and functionalization properties, Au nanoparticles are superlative for the preparation of scaffolds and vehicles for drug delivery. Aubin-Tam et al. [102] designed a drug delivery system with Au nanoparticles and infrared light which released multiple drugs in a controlled fashion, since the different shapes of nanoparticles respond to various infrared wavelengths. For example, nanobones and nanocapsules are melted at light wavelengths corresponding to 1,100 and 800 nm, respectively. Thus, excitation at a specific wavelength can melt specific kinds of Au nanorods and release a specific kind of DNA strand. Brown et al. [103] also conducted research on Au nanoparticles for an improved anticancer property of the active component of oxaliplatin. To do so, naked Au nanoparticles were functionalized with a thiolated poly(ethyleneglycol) (PEG) monolayer capped with a carboxylate group, and then [Pt(1*R*,2*R*diaminocyclohexane)$(H_2O)_2]_2NO_3$ was added to the PEG surface to make a supramolecular complex with drug molecules. The cytocompatibility, drug uptake, and localization in lung epithelial cancer cell line (A549) and colon cancer cell lines (HCT116, HCT15, HT29, and RKO) were studied for platinum-tethered nanoparticles. The platinum-tethered nanoparticles presented a significant improvement in biocompatibility, compared to oxaliplatinal in all of the mentioned cell lines, and an extraordinary ability to infiltrate the nucleus in the lung cancer cells. The light absorbing behavior of Au nanoparticles formulate it appropriate as heat mediating objects, where the absorbed light energy is scattered into the particles environment, producing a high temperature in their surrounding area. This result may be utilized to open polymer microcapsules for drug delivery applications and even destroy cancerous cells. Moreover, nanoparticles are functionalized with antibodies

corresponding to cancerous cells. These nanoparticles specifically attach to targeting cells, which are then killed by hyperthermal therapy.

It is worth noting that, for such in vivo purposes, the cell compatibility of the nanoparticles might be considered as an issue and should be studied with care. Due to biocompatibility of Au nanoparticles and their hyperthermal activity, this material has found an extensive application for treating malignant cancerous cells [104]. Recently, Melancon et al. [105] showed the photothermal influence of hollow Au nanoshells with the diameter of around 30 nm bound to monoclonal antibody on the destruction of cancerous cells. Au nanoshells directed to the epidermal growth factor receptor (EGFR) and the resulting anti-EGFR-Au indicated a good colloidal stability and proficient photothermal influence in the near-infrared region. The irradiation of A431 tumor cells treated with anti-EGFR-Au with near-infrared laser led to cell death. Au nanoparticles have also been employed to increase the biorecognition of anticancer drugs. Dacarbazine [5-(3,3-dimethyl-1-triazeno)imidazole-4-carboxamide; DTIC] is usually utilized as an anticancer drug. Au nanoparticles are negatively charged by PPh3 and the oxidized DTIC is positive charged. Therefore, DTIC could be simply assembled onto the surface of Au nanoparticles, and the particular interactions between anticancer drug DTIC and DNA or DNA bases are facilitated by Au nanoparticles.

7.6.4 Nanoparticles in Medicine and Dentistry

In bone implants, if the surface is left smooth, the body will try to reject it. This is due to the fact that the smooth surface will likely cause the production of a fibrous tissue, covering the surface of the implant. This fibrous layer in turn reduces the contact area between the implant and bone, which may lead to loosening of the implant and inflammation in that area. It was shown that having nano-sized features on the surface of the prosthesis could reduce the chances of rejection, in addition to stimulating the production of osteoblasts [99].

Furthermore, in the realm of dentistry, titanium is extensively used, because of its high fracture resistance, and ductility. However, it lacks bioactivity, so that it does not support cell adhesion and growth. Apatite coatings have been used in the past due to their bioactivity and ability to bond to the bone. However, the thickness and nonuniformity of apatite coatings on titanium are considered as limitations. Moreover, porous structures are needed to support nutrient transport. Ceramic nanoparticles are used to prepare an artificial hybrid material which could be placed on the tooth surface to improve scratch resistance [99, 106].

Nanoparticles have been also shown to have antimicrobial properties, due to their large surface area. Metallic nanoparticles can be used to effectively inhibit growth in a number of microorganisms and thereby have numerous applications in medicine and dentistry. Specifically, in dental materials, nanoparticles can be used as

active antibacterial agents. Secondary caries are found to be the main reason for restoration failure and are primarily caused by the invasion of plaque bacteria such as *Streptococcus mutans* and *Lactobacillus* in the presence of fermentable carbohydrates. In order to ensure a long-lasting restoration and the possible control of oral infections, the use of nanoparticles to make antimicrobial materials should be explored [107].

7.6.5 Environmental Cleanup as Defense Against Environmental Challenges to Medical Biology

Although metal nanoparticles are widely being used in various areas, their application in environmental biotechnology is still restricted. One of the important environmental issues is the pollution of water bodies by various chemicals, because of different anthropogenic and industrial wastes. One of the most fascinating use of metal nanoparticles is refinement of drinking water polluted with heavy metals. Recent restrictions in the elimination of heavy metals have been aimed to be conquered by the adsorption process on metal nanoparticles via the formation of alloys. Au and Hg are found in numerous phases including AuHg, Au_3Hg, and $AuHg_3$. The relation of Ag nanoparticles with Hg^{2+} ions was examined due to the increased ability of Ag to form alloys in different phases. It was found that the surface plasmon of Ag nanoparticles blue shifted with a reduction in intensity, directly after adding Hg^{2+} ions [108]. The partial oxidation of Ag nanoparticles to Ag ions is responsible for the reduction in intensity, so that the shift is due to the integration of Hg into Ag nanoparticles. The potential of Ag nanoparticles to decrease heavy metals can also be viewed as a technique for alloy nanoparticles preparation, for example Ag–Hg bimetallic nanoparticles. Currently, the colorimetric detection of heavy metals like As, Hg, Pb, etc., has also been investigated by using metal nanoparticles.

One of the key properties indicated by functionalized metal nanoparticles surfaces is the recognition of heavy metals. In this technique, heavy metal biomolecule functionalized Au nanoparticles can be used. An instance of this method is the interaction of metal ions with nucleotides, whereas Hg^{2+} facilitates the thymine–thymine base pairs formation [109]. In related ways, ligands such as (gallic acid (Pb^{2+}), cysteine (Hg^{2+}, Cu^{2+}), and mercaptoundecanoic acid (Pb^{2+}, Cd^{2+}, Hg^{2+})) functionalized metal nanoparticles have been utilized for identifying particular metal ions, leading to the formation of ligand–metal ion complex and the changes in optical properties at low level concentrations (ppm) [110]. The removal of pesticides by metal nanoparticles is an innovative idea to this research area. Amongst other pollutants, the existence of pesticide residue in drinkable water higher than permissible limit is of big alarms to public health. This occurs as a result of the discriminate use of pesticide, in particular belonging to organophosphorus groups, in agricultural applications. It is necessary to decrease the amount of pesticide in drinkable water, which

is difficult to reach by conventional chemical routes, owing to the broad variation of their chemical structures. To address the mentioned environmental issues, recent research focused on planning techniques based on nanotechnology. Das et al. [111] showed the adsorption of various organophosphorous pesticides on the surface of Au nanoparticles. Au nanoparticles produced on the surface of the *R. oryzae* mycelia in a single set were then employed for the adsorption of different *organophosphorous* pesticides. Following the adsorption of these pesticides, the surface morphology obviously changes compared to the unadsorbed nanomaterial, as confirmed with atomic force microscopic photomicrographs.

7.7 Conclusions

Nanomaterials, with typical dimensions in the range of 1–100 nm, are at the leading edge of nanoscience and nanotechnology. Recently, nanomaterials, particularly metal nanoparticles, have attracted special interest in the diverse field of applied science ranging from material science to biotechnology. Moreover, exponentially growing attention has been observed in the biological synthesis of nanomaterials. The knowledge increase towards green chemistry and biological approaches has resulted in the use of eco-friendly techniques for the manufacturing of nontoxic and biocompatible nanomaterials. The development of environment-friendly routes in the production of material is of significant importance to enlarge their biological purposes. Recently, a range of green nanoparticles with definite chemical compositions, sizes, and structures have been produced by various techniques, and their uses in many cutting-edge technological areas have been examined. Different biological bodies have been developed in the biosynthetic methods of metal nanoparticles and the use of organisms or constituents that facilitate the synthesis of monodispersed metallic nanoparticles. Consequently, the simplistic biosynthesis of nanoparticles with controlled dimensions and shapes by using molecular cloning and genetic engineering approaches and other photobiological techniques will be a marvelous expansion in the nanobiotechnology area. Expediting research on such organisms, biocomponents, or parameters will eject such conservative dangerous processes. Terrestrial and aquatic phototrophic eukaryotes, heterotrophic eukaryotes, and biocompatible agents have enormous capability to create metal nanoparticles. Phototrophic eukaryotes such as plants, algae and diatoms are considered as potentially sustainable and renewable biofactories for the production of nanoparticles. Nanomaterials by renewable bioresources and biocompatible agents with exceptional physicochemical, optoelectronics, and electronic properties are of immense significance for wider purposes in the areas of chemistry, medicine, electronics, and agriculture.

References

1. Schmid G (1992) Large clusters and colloids. Metals in the embryonic state. Chem Rev 92:1709–1727
2. Daniel M-C, Astruc D (2004) Gold nanoparticles: assembly, supramolecular chemistry, quantum-size-related properties, and applications toward biology, catalysis, and nanotechnology. Chem Rev 104:293–346
3. Ramanavičius A, Kaušaitė A, Ramanavičienė A (2005) Polypyrrole-coated glucose oxidase nanoparticles for biosensor design. Sens Actuators B Chem 111:532–539
4. Fendler JH (2008) Nanoparticles and nanostructured films: preparation, characterization, and applications. Wiley, New York
5. Narayanan KB, Sakthivel N (2011) Green synthesis of biogenic metal nanoparticles by terrestrial and aquatic phototrophic and heterotrophic eukaryotes and biocompatible agents. Adv Colloid Interface Sci 169:59–79
6. Narayanan KB, Sakthivel N (2010) Biological synthesis of metal nanoparticles by microbes. Adv Colloid Interface Sci 156:1–13
7. Hutchison JE (2008) Greener nanoscience: a proactive approach to advancing applications and reducing implications of nanotechnology. ACS Nano 2:395–402
8. Mckenzie LC, Hutchison JE (2004) Green nanoscience: an integrated approach to greener products, processes, and applications. Chimica oggi. Chemistry Today. http://pages.uoregon.edu/cgnn/nanoscience.pdf
9. Nath D, Banerjee P (2013) Green nanotechnology–a new hope for medical biology. Environ Toxicol Pharmacol 36:997–1014
10. Chakrabarti S, Fathpour S, Moazzami K, Phillips J, Lei Y, Browning N et al (2004) Pulsed laser annealing of self-organized InAs/GaAs quantum dots. J Electron Mater 33:L5–L8
11. Mafuné F, Kohno J-y, Takeda Y, Kondow T, Sawabe H (2001) Formation of gold nanoparticles by laser ablation in aqueous solution of surfactant. J Phys Chem B 105:5114–5120
12. Shukla S, Seal S (1999) Cluster size effect observed for gold nanoparticles synthesized by sol-gel technique as studied by X-ray photoelectron spectroscopy. Nanostruct Mater 11: 1181–1193
13. Raffi M, Rumaiz AK, Hasan M, Shah SI (2007) Studies of the growth parameters for silver nanoparticle synthesis by inert gas condensation. J Mater Res 22:3378–3384
14. Rosemary M, Pradeep T (2003) Solvothermal synthesis of silver nanoparticles from thiolates. J Colloid Interface Sci 268:81–84
15. Gleiter H (1989) Nanocrystalline materials. Prog Mater Sci 33:223–315
16. Pérez-Tijerina E, Pinilla MG, Mejía-Rosales S, Ortiz-Méndez U, Torres A, José-Yacamán M (2008) Highly size-controlled synthesis of Au/Pd nanoparticles by inert-gas condensation. Faraday Discuss 138:353–362
17. Ren W, Ai Z, Jia F, Zhang L, Fan X, Zou Z (2007) Low temperature preparation and visible light photocatalytic activity of mesoporous carbon-doped crystalline TiO_2. Appl Catal B Environ 69:138–144
18. Yang HG, Sun CH, Qiao SZ, Zou J, Liu G, Smith SC et al (2008) Anatase TiO_2 single crystals with a large percentage of reactive facets. Nature 453:638–641
19. Tao AR, Habas S, Yang P (2008) Shape control of colloidal metal nanocrystals. Small 4:310–325
20. Brust M, Kiely CJ (2002) Some recent advances in nanostructure preparation from gold and silver particles: a short topical review. Colloids Surf A Physicochem Eng Asp 202:175–186
21. Yin Y, Li Z-Y, Zhong Z, Gates B, Xia Y, Venkateswaran S (2002) Synthesis and characterization of stable aqueous dispersions of silver nanoparticles through the Tollens process. J Mater Chem 12:522–527
22. Kvítek L, Prucek R, Panáček A, Novotný R, Hrbáč J, Zbořil R (2005) The influence of complexing agent concentration on particle size in the process of SERS active silver colloid synthesis. J Mater Chem 15:1099–1105

23. Sharma VK, Yngard RA, Lin Y (2009) Silver nanoparticles: green synthesis and their antimicrobial activities. Adv Colloid Interface Sci 145:83–96
24. Le A-T, Huy P, Tam PD, Huy TQ, Cam PD, Kudrinskiy A et al (2010) Green synthesis of finely-dispersed highly bactericidal silver nanoparticles via modified Tollens technique. Curr Appl Phys 10:910–916
25. Luque R, Baruwati B, Varma RS (2010) Magnetically separable nanoferrite-anchored glutathione: aqueous homocoupling of arylboronic acids under microwave irradiation. Green Chem 12:1540–1543
26. Bilecka I, Niederberger M (2010) Microwave chemistry for inorganic nanomaterials synthesis. Nanoscale 2:1358–1374
27. Kappe CO (2004) Controlled microwave heating in modern organic synthesis. Angew Chem Int Ed 43:6250–6284
28. Nadagouda MN, Speth TF, Varma RS (2011) Microwave-assisted green synthesis of silver nanostructures. Acc Chem Res 44:469–478
29. Polshettiwar V, Varma RS (2008) Microwave-assisted organic synthesis and transformations using benign reaction media. Acc Chem Res 41:629–639
30. Kappe CO (2006) The use of microwave irradiation in organic synthesis. From laboratory curiosity to standard practice in twenty years. CHIMIA Int J Chem 60:308–312
31. Polshettiwar V, Nadagouda MN, Varma RS (2009) Microwave-assisted chemistry: a rapid and sustainable route to synthesis of organics and nanomaterials. Aust J Chem 62:16–26
32. Wang Y, Yin L, Palchik O, Hacohen YR, Koltypin Y, Gedanken A (2001) Sonochemical synthesis of layered and hexagonal yttrium-zirconium oxides. Chem Mater 13:1248–1251
33. Rhule JT, Hill CL, Judd DA, Schinazi RF (1998) Polyoxometalates in medicine. Chem Rev 98:327–358
34. Troupis A, Hiskia A, Papaconstantinou E (2002) Synthesis of metal nanoparticles by using polyoxometalates as photocatalysts and stabilizers. Angew Chem Int Ed 41:1911–1914
35. Zhang G, Keita B, Dolbecq A, Mialane P, Sécheresse F, Miserque F et al (2007) Green chemistry-type one-step synthesis of silver nanostructures based on MoV–MoVI mixed-valence polyoxometalates. Chem Mater 19:5821–5823
36. Georgakilas V, Gournis D, Tzitzios V, Pasquato L, Guldi DM, Prato M (2007) Decorating carbon nanotubes with metal or semiconductor nanoparticles. J Mater Chem 17:2679–2694
37. Anastas PT, Warner JC (2000) Green chemistry: theory and practice. Oxford University Press, Oxford
38. Dahl JA, Maddux BL, Hutchison JE (2007) Toward greener nanosynthesis. Chem Rev 107:2228–2269
39. Mann S (1993) Molecular tectonics in biomineralization and biomimetic materials chemistry. Nature 365:499–505
40. Mohanpuria P, Rana NK, Yadav SK (2008) Biosynthesis of nanoparticles: technological concepts and future applications. J Nanoparticle Res 10:507–517
41. Durán N, Marcato PD, Durán M, Yadav A, Gade A, Rai M (2011) Mechanistic aspects in the biogenic synthesis of extracellular metal nanoparticles by peptides, bacteria, fungi, and plants. Appl Microbiol Biotechnol 90:1609–1624
42. Bao C, Jin M, Lu R, Zhang T, Zhao YY (2003) Preparation of Au nanoparticles in the presence of low generational poly (amidoamine) dendrimer with surface hydroxyl groups. Mater Chem Phys 81:160–165
43. Sharma NC, Sahi SV, Nath S, Parsons JG, Gardea-Torresde JL, Pal T (2007) Synthesis of plant-mediated gold nanoparticles and catalytic role of biomatrix-embedded nanomaterials. Environ Sci Technol 41:5137–5142
44. Southam G, Saunders JA (2005) The geomicrobiology of ore deposits. Econ Geol 100: 1067–1084
45. Gericke M, Pinches A (2006) Biological synthesis of metal nanoparticles. Hydrometallurgy 83:132–140
46. Klaus T, Joerger R, Olsson E, Granqvist C-G (1999) Silver-based crystalline nanoparticles, microbially fabricated. Proc Natl Acad Sci 96:13611–13614

47. Shankar SS, Rai A, Ahmad A, Sastry M (2004) Rapid synthesis of Au, Ag, and bimetallic Au core–Ag shell nanoparticles using Neem (*Azadirachta indica*) leaf broth. J Colloid Interface Sci 275:496–502
48. Husseiny M, El-Aziz MA, Badr Y, Mahmoud M (2007) Biosynthesis of gold nanoparticles using *Pseudomonas aeruginosa*. Spectrochim Acta A Mol Biomol Spectrosc 67:1003–1006
49. Beveridge T, Murray R (1980) Sites of metal deposition in the cell wall of *Bacillus subtilis*. J Bacteriol 141:876–887
50. Du L, Jiang H, Liu X, Wang E (2007) Biosynthesis of gold nanoparticles assisted by *Escherichia coli* DH5α and its application on direct electrochemistry of hemoglobin. Electrochem Commun 9:1165–1170
51. Konishi Y, Ohno K, Saitoh N, Nomura T, Nagamine S, Hishida H et al (2007) Bioreductive deposition of platinum nanoparticles on the bacterium *Shewanella algae*. J Biotechnol 128:648–653
52. Shankar SS, Ahmad A, Pasricha R, Sastry M (2003) Bioreduction of chloroaurate ions by geranium leaves and its endophytic fungus yields gold nanoparticles of different shapes. J Mater Chem 13:1822–1826
53. Uddin I, Adyanthaya S, Syed A, Selvaraj K, Ahmad A, Poddar P (2008) Structure and microbial synthesis of sub-10 nm Bi_2O_3 nanocrystals. J Nanosci Nanotechnol 8:3909–3913
54. Fayaz AM, Balaji K, Girilal M, Yadav R, Kalaichelvan PT, Venketesan R (2010) Biogenic synthesis of silver nanoparticles and their synergistic effect with antibiotics: a study against gram-positive and gram-negative bacteria. Nanomed Nanotechnol Biol Med 6:103–109
55. Vigneshwaran N, Kathe AA, Varadarajan P, Nachane RP, Balasubramanya R (2006) Biomimetics of silver nanoparticles by white rot fungus, *Phanerochaete chrysosporium*. Colloids Surf B: Biointerfaces 53:55–59
56. Ingle A, Rai M, Gade A, Bawaskar M (2009) Fusarium solani: a novel biological agent for the extracellular synthesis of silver nanoparticles. J Nanoparticle Res 11:2079–2085
57. Basavaraja S, Balaji S, Lagashetty A, Rajasab A, Venkataraman A (2008) Extracellular biosynthesis of silver nanoparticles using the fungus *Fusarium semitectum*. Mater Res Bull 43: 1164–1170
58. Gade A, Bonde P, Ingle A, Marcato P, Duran N, Rai M (2008) Exploitation of *Aspergillus niger* for synthesis of silver nanoparticles. J Biobased Mater Bioenergy 2:243–247
59. Sanghi R, Verma P (2009) Biomimetic synthesis and characterisation of protein capped silver nanoparticles. Bioresour Technol 100:501–504
60. Birla S, Tiwari V, Gade A, Ingle A, Yadav A, Rai M (2009) Fabrication of silver nanoparticles by *Phoma glomerata* and its combined effect against *Escherichia coli*, *Pseudomonas aeruginosa* and *Staphylococcus aureus*. Lett Appl Microbiol 48:173–179
61. Shaligram NS, Bule M, Bhambure R, Singhal RS, Singh SK, Szakacs G et al (2009) Biosynthesis of silver nanoparticles using aqueous extract from the compactin producing fungal strain. Process Biochem 44:939–943
62. Kathiresan K, Manivannan S, Nabeel M, Dhivya B (2009) Studies on silver nanoparticles synthesized by a marine fungus, *Penicillium fellutanum* isolated from coastal mangrove sediment. Colloids Surf B: Biointerfaces 71:133–137
63. Mukherjee P, Ahmad A, Mandal D, Senapati S, Sainkar SR, Khan MI et al (2001) Bioreduction of $AuCl_4^-$ ions by the fungus, *Verticillium* sp. and surface trapping of the gold nanoparticles formed. Angew Chem Int Ed 40:3585–3588
64. Ahmad A, Senapati S, Khan MI, Kumar R, Sastry M (2005) Extra-/intracellular biosynthesis of gold nanoparticles by an Alkalotolerant fungus, *Trichothecium* sp. J Biomed Nanotechnol 1:47–53
65. Gole A, Dash C, Soman C, Sainkar S, Rao M, Sastry M (2001) On the preparation, characterization, and enzymatic activity of fungal protease-gold colloid bioconjugates. Bioconjug Chem 12:684–690
66. Ahmad A, Senapati S, Khan MI, Kumar R, Sastry M (2003) Extracellular biosynthesis of monodisperse gold nanoparticles by a novel extremophilic actinomycete, *Thermomonospora* sp. Langmuir 19:3550–3553

67. Henglein A (1989) Small-particle research: physicochemical properties of extremely small colloidal metal and semiconductor particles. Chem Rev 89:1861–1873
68. Braun E, Eichen Y, Sivan U, Ben-Yoseph G (1998) DNA-templated assembly and electrode attachment of a conducting silver wire. Nature 391:775–778
69. Wong KK, Douglas T, Gider S, Awschalom DD, Mann S (1998) Biomimetic synthesis and characterization of magnetic proteins (magnetoferritin). Chem Mater 10:279–285
70. Douglas T, Young M (1998) Host–guest encapsulation of materials by assembled virus protein cages. Nature 393:152–155
71. Archibald DD, Mann S (1993) Template mineralization of self-assembled anisotropic lipid microstructures. Nature 364:430–433
72. Pazirandeh M, Baral S, Campbell J (1992) Metallized nanotubules derived from bacteria. Biomimetics 1:41–50
73. Davis SA, Burkett SL, Mendelson NH, Mann S (1997) Bacterial templating of ordered macrostructures in silica and silica-surfactant mesophases. Nature 385:420–423
74. Shenton W, Pum D, Sleytr UB, Mann S (1997) Synthesis of cadmium sulphide superlattices using self-assembled bacterial S-layers. Nature 389:585–587
75. Shenton W, Douglas T, Young M, Stubbs G, Mann S (1999) Inorganic–organic nanotube composites from template mineralization of tobacco mosaic virus. Adv Mater 11:253–256
76. Lee S-W, Mao C, Flynn CE, Belcher AM (2002) Ordering of quantum dots using genetically engineered viruses. Science 296:892–895
77. Mao C, Flynn CE, Hayhurst A, Sweeney R, Qi J, Georgiou G et al (2003) Viral assembly of oriented quantum dot nanowires. Proc Natl Acad Sci 100:6946–6951
78. Gardea-Torresdey J, Parsons J, Gomez E, Peralta-Videa J, Troiani H, Santiago P et al (2002) Formation and growth of Au nanoparticles inside live alfalfa plants. Nano Lett 2:397–401
79. Bali R, Razak N, Lumb A, Harris A (2006) The synthesis of metallic nanoparticles inside live plants. Nanoscience and nanotechnology, 2006 ICONN'06 international conference on IEEE
80. Song JY, Jang H-K, Kim BS (2009) Biological synthesis of gold nanoparticles using Magnolia kobus and Diospyros kaki leaf extracts. Process Biochem 44:1133–1138
81. Fahmy TY, Mobarak F (2011) Green nanotechnology: a short cut to beneficiation of natural fibers. Int J Biol Macromol 48:134–136
82. Terry N, Zayed A (1998) Phytoremediation of selenium. In: Frankenberger WT Jr, Engberg RA (eds) Environmental chemistry of selenium. Dekker, New York, pp 633–655
83. Lamb A, Anderson C, Haverkamp R (2001) The induced accumulation of gold in the plants *Brassica juncea*, *Berkheya coddii* and chicory
84. Gardea-Torresdey J, Tiemann K, Gamez G, Dokken K, Tehuacanero S, Jose-Yacaman M (1999) Gold nanoparticles obtained by bio-precipitation from gold (III) solutions. J Nanoparticle Res 1:397–404
85. Herrera I, Gardea-Torresdey J, Tiemann K, Peralta-Videa J, Armendariz V, Parsons J (2003) Binding of silver (I) ions by alfalfa biomass (*Medicago sativa*): batch pH, time, temperature, and ionic strength studies. J Hazard Subst Res 4:1–16
86. Marshall AT, Haverkamp RG, Davies CE, Parsons JG, Gardea-Torresdey JL, van Agterveld D (2007) Accumulation of gold nanoparticles in *Brassica juncea*. Int J Phytoremediation 9: 197–206
87. Ascencio J, Mejia Y, Liu H, Angeles C, Canizal G (2003) Bioreduction synthesis of Eu-Au nanoparticles. Langmuir 19:5882–5886
88. Jia L, Zhang Q, Li Q, Song H (2009) The biosynthesis of palladium nanoparticles by antioxidants in *Gardenia jasminoides* Ellis: long lifetime nanocatalysts for p-nitrotoluene hydrogenation. Nanotechnology 20:385601
89. Awadalla FT, Pesic B (1992) Biosorption of cobalt with the AMT TM metal removing agent. Hydrometallurgy 28:65–80
90. Wilde EW, Benemann JR (1993) Bioremoval of heavy metals by the use of microalgae. Biotechnol Adv 11:781–812

91. Hosea M, Greene B, Mcpherson R, Henzl M, Dale Alexander M, Darnall DW (1986) Accumulation of elemental gold on the alga *Chlorella vulgaris*. Inorg Chim Acta 123: 161–165
92. Xie J, Lee JY, Wang DI, Ting YP (2007) Identification of active biomolecules in the high-yield synthesis of single-crystalline gold nanoplates in algal solutions. Small 3:672–682
93. Drum RW, Gordon R (2003) Star Trek replicators and diatom nanotechnology. Trends Biotechnol 21:325–328
94. Gekeler W, Grill E, Winnacker E-L, Zenk MH (1988) Algae sequester heavy metals via synthesis of phytochelatin complexes. Arch Microbiol 150:197–202
95. Noll F, Sumper M, Hampp N (2002) Nanostructure of diatom silica surfaces and of biomimetic analogues. Nano Lett 2:91–95
96. Anshup A, Venkataraman JS, Subramaniam C, Kumar RR, Priya S, Kumar TS et al (2005) Growth of gold nanoparticles in human cells. Langmuir 21:11562–11567
97. Guo R, Song Y, Wang G, Murray RW (2005) Does core size matter in the kinetics of ligand exchanges of monolayer-protected Au clusters? J Am Chem Soc 127:2752–2757
98. Sperling RA, Gil PR, Zhang F, Zanella M, Parak WJ (2008) Biological applications of gold nanoparticles. Chem Soc Rev 37:1896–1908
99. Salata OV (2004) Applications of nanoparticles in biology and medicine. J Nanobiotechnol 2:3
100. Huo Q (2007) A perspective on bioconjugated nanoparticles and quantum dots. Colloids Surf B: Biointerfaces 59:1–10
101. Ghosh P, Han G, De M, Kim CK, Rotello VM (2008) Gold nanoparticles in delivery applications. Adv Drug Deliv Rev 60:1307–1315
102. Aubin-Tam M-E, Hamad-Schifferli K (2008) Structure and function of nanoparticle–protein conjugates. Biomed Mater 3:034001
103. Brown SD, Nativo P, Smith J-A, Stirling D, Edwards PR, Venugopal B et al (2010) Gold nanoparticles for the improved anticancer drug delivery of the active component of oxaliplatin. J Am Chem Soc 132:4678–4684
104. Dickerson EB, Dreaden EC, Huang X, El-Sayed IH, Chu H, Pushpanketh S et al (2008) Gold nanorod assisted near-infrared plasmonic photothermal therapy (PPTT) of squamous cell carcinoma in mice. Cancer Lett 269:57–66
105. Melancon MP, Lu W, Yang Z, Zhang R, Cheng Z, Elliot AM et al (2008) In vitro and in vivo targeting of hollow gold nanoshells directed at epidermal growth factor receptor for photothermal ablation therapy. Mol Cancer Ther 7:1730–1739
106. De La Isla A, Brostow W, Bujard B, Estevez M, Rodriguez JR, Vargas S et al (2003) Nanohybrid scratch resistant coatings for teeth and bone viscoelasticity manifested in tribology. Mater Res Innov 7:110–114
107. Hamouda IM (2012) Current perspectives of nanoparticles in medical and dental biomaterials. Journal of Biomedical Research 26:143–151
108. Bootharaju M, Pradeep T (2010) Uptake of toxic metal ions from water by naked and monolayer protected silver nanoparticles: an X-ray photoelectron spectroscopic investigation. J Phys Chem C 114:8328–8336
109. Ono A, Togashi H (2004) Highly selective oligonucleotide-based sensor for mercury (II) in aqueous solutions. Angew Chem Int Ed 43:4300–4302
110. Huang CC, Yang Z, Lee KH, Chang HT (2007) Synthesis of highly fluorescent gold nanoparticles for sensing mercury (II). Angew Chem 119:6948–6952
111. Das SK, Das AR, Guha AK (2009) Gold nanoparticles: microbial synthesis and application in water hygiene management. Langmuir 25:8192–8199

Chapter 8
Nanoparticle Synthesis by Biogenic Approach

Sarvesh Kumar Srivastava, Chiaki Ogino, and Akihiko Kondo

Abstract Biological synthesis of nanoparticles has been present in living organisms over the course of evolution to serve a variety of purposes. In this chapter, we discuss the latest trends and application for nanoparticle synthesis via plants, algae, yeast, bacteria, fungi, etc. There exists several review articles among others documenting studies about various biogenic sources and associated nanoparticle synthesis; we have rather emphasized on recent research works which probed into novel applications of these bio-nanoparticles along with some important historical findings. Also, we have discussed the challenges faced by biogenic methods along with possible areas to tweak in order to standardize this synthesis technique. Biogenic synthesis of nanoparticles has the potential to provide cost-effective, eco-friendly alternative to work as "biological nanofactories"/functionalization method once the attention has been shifted to understand the underlying mechanism, its in vitro replication and obtaining shape/size control over the nanoparticles being synthesized.

Keywords Biosynthesis • Bioinspired materials • Biogenic synthesis • Green chemistry • Nanoparticles • Nanotechnology

8.1 Introduction

In recent years, nanoscience and nanotechnology has made considerable progress towards synthesis and characterization of new materials due to their widespread application in everyday life. Nanoparticles in particular have revolutionized almost all the spheres of our life: catalysis, drug delivery, sensors, paints, surface coatings, energy systems, electronics, cosmetics/clothing/accessories, aerospace/defence, etc. During the last decade, exhaustive research has been carried out in understanding more about these nanoparticles and their possible applications.

S.K. Srivastava • C. Ogino • A. Kondo (✉)
Department of Chemical Science and Engineering, Graduate School of Engineering, Kobe University, 1-1 Rokkodai-cho, Nada-ku, Kobe, Hyogo 657-8501, Japan
e-mail: akondo@kobe-u.ac.jp

V.A. Basiuk, E.V. Basiuk (eds.), *Green Processes for Nanotechnology*,
DOI 10.1007/978-3-319-15461-9_8

Today, nanoparticles are not only responsible for miniaturization of devices but also for the development of several key-enabled technologies which could not have been possible without them. As per the National Nanotechnology Initiative, nanotechnology can be defined as the manipulation of matter with at least one dimension in the size range from 1 to 100 nm or 10^{-9} of a metre. This miniaturization allows them to exhibit novel and significantly improved physical, chemical, and biological properties, phenomena and processes owing to their size. When characteristic structural features are intermediate between isolated atoms and bulk materials in the range of about 1–100 nm, the objects often display physical attributes substantially different from those displayed by either atoms or bulk materials. The properties of material changes as their size approaches the nanoscale and as the percentage of atoms at the surface of a material becomes significant at the nanoscale size-dependent properties are observed. These interesting and sometimes unexpected properties of nanoparticles (NPs) are therefore largely due to the large surface area of the material which governs the contribution made by the small bulk of material [1].

Important behavioural changes are caused not only by continuous modification of characteristics with diminishing size but also by the emergence of totally new phenomena such as quantum confinement [2], a typical example of which is that the colour of light emitting from semiconductor nanoparticles depends on their sizes.

Generally speaking, the first way is to start with a bulk material and then break it into smaller pieces using mechanical, chemical or other form of energy (top-down). An opposite approach is to synthesize the material from atomic or molecular species via chemical reactions, allowing for the precursor particles to grow in size (bottom-up). Then there are functional approaches like Biogenic techniques, which seek to develop components of desired functionality without less control on how they might be assembled. Last two decades have witnessed rapid increase in environmentally sustainable processes in material development and chemical engineering as a result of worldwide problems associated with environmental contamination. Nature has been the oldest and largest producer of several nano-structures which are not only organized at multiple scales but, in many ways, adapted to the environment [3]. These materials are generally formed in mild conditions like neutral pH, minimal temperature control and low reactant concentrations. Furthermore, these processes are highly efficient with the continuous recycling of materials and minimal toxicity to surrounding environment. Keeping our discussion limited for nanoparticles only, there exists several “natural systems” around us which produce nanoparticles of different size and functions: silica shells of diatoms, heavy metal remediation by microbes, uptake of mineral and elements by plants, etc. In fact, ever since inception of life on planet Earth, biological entities have been in constant touch with organic/inorganic materials present in the atmosphere (volcanoes, oceans, mineral deposits, etc.) resulting in life as we see today. The rise in alchemy resulted in the intentional addition of different metals and their salts (e.g. Au, Pb, Cu, Ag, As and Hg) to food and plant extracts, which were then “formulated” into medicinal potions, potentially yielding complex mixtures of nano-biocomposites [4]. Some of these can still be seen today in form of Roman Chalice, Chichen Itza statue

(Mayan blue dye) and several ancient medicinal formulations (like bhasma in Ayurveda) [5]. It is evident that biogenic nanomaterials and its application has always been a part of human history albeit not scientifically well understood/analyzed as we can do today and will be righteous to understand the face that despite our great advances in synthetic materials, nature still has plenty to teach us [6].

Biogenic synthesis of nanomaterials revolves around the philosophy of utilizing active compounds present in our nature for synthesizing/imparting novel properties which in turn can provide a breakthrough in its application [7, 8]. With the help of nature's molecules, chemical engineers have found ways to create new materials that can do everything ranging from bone/tissue regeneration, cancer treatment, efficient chemical catalysis and clean energy production [9]. This requires identification and extraction of active biomolecules which may originate from any living system or part of living system with the possibility of creating bio-nano hybrid systems [10]. Also, due to its biological origin, these nanomaterials are generally observed to be eco-friendly and non-toxic thereby proving to be excellent material for drug delivery [11] and clean energy [12]. This subset of bio-nanotechnology can be defined as a field representing all facets of research at the intersection of biology and material science generally following the principles of green chemistry. These biogenic materials tend to inherit specific chemical/material properties either in form of functional activity or passively incorporated as an inert coating/layer or scaffolding material. It is important to note that although there exists several physical and chemical methods to produce monodisperse nanoparticles, they require extensive process control including surfactants (for stability) and use of toxic chemicals (reductants). Also, the traces of toxic chemicals over the nanoparticle surface and non-polar solvents in their synthesis medium limit their application in the clinical field.

Nanoparticles can be classified into two major categories namely organic and inorganic nanoparticles. Carbon nanoparticles/carbonaceous substrates comprises for organic nanoparticles. Metal nanoparticles which for the majority of nanoparticle applications as stated above falls under the category of inorganic nanoparticles. This chapter is focused on inorganic nanoparticle synthesis by biogenic agents including both eukaryotic and prokaryotic sources. With abundant biological resources available in the nature in form of plants/phytochemicals, algae, fungi, yeast, bacteria, etc., we have emphasized on developing industrially feasible, cost-efficient and environmentally benign processes for nanoparticles synthesis with the inherent potential to be developed into biomimetic systems.

Although, each biogenic agent has a specific reaction mechanism, they essentially work in the same manner where we a "complex broth" results in formation of desired nanostructures. Apart from characterization of such nanostructures, emphasis should be laid on extraction and analysis of the involved biological (macro)-molecules in order to use them as templates for the nanomaterial synthesis, better described as "biomimetic materials". Although still in its infancy, some biogenic methods have evolved into biomimetic approach giving rise to complex bionanohybrid materials, self-assembled functional materials, advanced biomedical applications, etc. In this chapter, we provide an overview on different classes of biogenic

agents that can be used to synthesize a vast array of nanoparticles. It should be noted that there have been tremendous developments in the field of biogenic production of nanoparticles and their applications over the last decade. Therefore, we have focused our discussion on the groundbreaking approaches/applications of these nanoparticles. At the end of this chapter, we have discussed in brief about recent studies showing successful transformation of biogenic approach into biomimetic model for nanoparticle synthesis and application. This paradigm shift from using a "broth mixture" to pinning the active molecules for a stand-alone assembly is the need and challenge for biogenic nanomaterials.

8.2 Biogenic Synthesis of Nanoparticles

8.2.1 Bacteria and Yeast

As discussed above, the use of biological systems has emerged as a radical technology for synthesizing nanoparticles with an aim to control nanoparticle morphology and imparting value-added properties. Bacteria have an innate ability to reduce metallic ions to their respective metallic nanoparticles functioning as "green" nanofactories. This reduction mechanism in bacteria is due to their chemical detoxification acting as a defence [13] mechanism as well as due to energy-dependent ion efflux from the cell by membrane proteins that function either as ATPase or ion-transporters [14]. In fact, interactions between metals and microbes have been used for such biological applications [15] as biomineralization, bioremediation, bioleaching and biocorrosion leading to microbial synthesis of nanoparticles.

Examples include the formation of magnetic nanoparticles by magnetotactic bacteria, synthesis of gold nanoparticles with varying shape and sizes by several fungal species, the production of silver nanoparticles within the periplasmic space of *Pseudomonas stutzeri*, synthesis of nanoscale, semi-conducting CdS crystals in the yeast *Schizosaccharomyces pombe,* the formation of palladium nanoparticles using sulphate reducing bacteria in the presence of an exogenous electron donor, etc. The interest also extends to the synthesis of other nanostructures like nanowires and the assembly of nanoparticles using biological templates such as DNA, proteins, S-layers and viruses [15–17].

Bacteria can produce inorganic nanoparticles either intracellularly or extracellularly with a well-defined shape and monodispersity. Nanoparticle production by microorganisms can be broadly divided into three categories: chemolithotrophy for energy production, use of such particles for specialized functions and detoxification for survival in toxic environments [18]. Detoxification of its immediate environment is vital for bacteria's survival and to overcome the same, it either reduces the ions or form water insoluble complexes by incorporating hydrophobic moieties as a defence mechanism [19]. The exact mechanism of bioreduction however will largely depend on the bacterial strain and growth conditions of the reaction mixture. Also, bacterial structural diversity in its morphology such as bacillus, coccus,

spirillum, fusiform bacilli, star-shaped bacteria [20] can be utilized for template based synthesis as discussed later. It is interesting to note that starting from the earlier reporting of silver nanoparticle (35–45 nm) produced by a silver-resistant strain isolated from a silver mine, we have witnessed biomimetic synthesis of silver nanoparticles [21] using silver-binding peptides identified from a combinatorial phage display peptide library. Extracellular reductases (NADH-dependent, nitrate-dependent, etc.) produced by the microorganisms tends to reduce the silver ions. The reductase enzyme gets its electrons from NADH, which is then oxidized to NAD+. Also, certain genes have been identified which suggests molecular evidence of silver resistance in bacteria [22]. Silver nanoparticles of the size range of 10–15 nm [23] were produced with the dried cells of *Corynebacterium* sp. were treated with diamine silver complex. The ionized carboxyl group of amino acid residues and the amide of peptide chains and some reducing groups, such as aldehyde and ketone were the main groups found responsible for trapping $[Ag(NH_3)_2]^+$ onto the cell wall. They were associated with the subsequent bioreduction of the ions to nanoparticles. Similarly, gold nanoparticles have been synthesized extensively from various biogenic agents. Klaus et al. observed that variation in incubation conditions may lead to different particle sizes [24]. In another bacteria (*R. capsulate*) mediated synthesis of Au NPs, the shape of the gold nanoparticles was found to be pH dependent. Gold nanoparticles of size range 10–20 nm were formed at pH 7 while nanoplates/spherical gold nanoparticles were observed at pH 4 [25]. In another study, Ahmad et al. showed extracellular synthesis of gold nanoparticle by an extremophile (*Thermomonospora* sp.) [26], while Lahr et al. demonstrated Surface-Enhanced Raman Spectroscopy (SERS) cellular imaging of intracellularly biosynthesized (*Pseudokirchneriella subcapitata*) gold nanoparticles [27]. Sloick et al. presented cowpea chlorotic mottle viral templates for gold nanoparticle synthesis where the viral capsid actively carried out the reduction of $AuCl_4^-$ by electron transfer from surface tyrosine residue [28]. In another "biogenic to biomimetic" transition, Kim et al. published peptide-mediated shape- and size-tunable synthesis of gold nanostructures which linked single amino acid change greatly influencing the size of nanoparticle (~100 nm) being synthesized [29]. We also demonstrated an array of monometallic nanoparticles (Ag, Pd, Fe, Rh, Ni, Ru, Pt, Co and Li) synthesized from *Pseudomonas aeruginosa* SM1 as shown in Fig. 8.1.

This first of its kind study showed room-temperature synthesis of several important catalytically active nanoparticles produced in a very efficient and low-cost manner.

In another study, we successfully utilized the *E. coli* extracellular matrix in a fixed column reactor for continuous production of Au NPs. Similarly, semiconductor nanoparticles like that of CdS have been formed by *E. coli* (intracellularly) as well as extracellularly by *Rhodopseudomonas palustris* [31]. Shenton et al. demonstrated synthesis of cadmium sulphide superlattices (5 nm) using self-assembled bacterial S-layers [32]. Nucleation of the inorganic phase was confined to the pores between subunits in the S-layers. Platinum nanoparticles (5 nm) has been reportedly produced by *S. algae* (in the periplasm) when hexachloroplatinate ions were introduced in presence of lactate as electron donor [33]. In another study, Riddin et al.

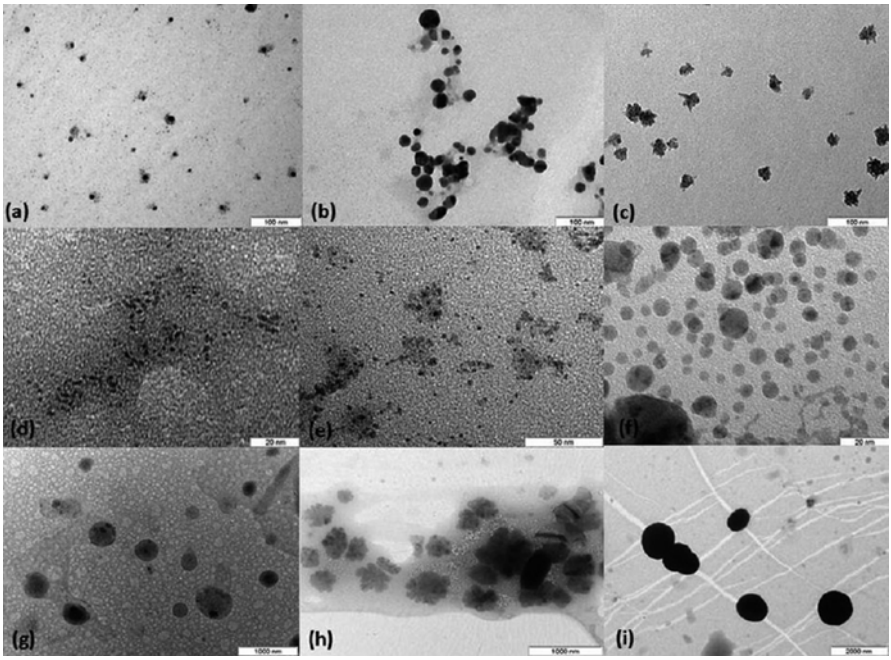

Fig. 8.1 Room temperature synthesis of (**a**) Ag, (**b**) Pd, (**c**) Fe, (**d**) Rh, (**e**) Ni, (**f**) Ru, (**g**) Pt, (**h**) Co, (**i**) Li. Reprinted from ref. [30] with permission by Springer Science + Business Media B.V.

demonstrated cell-free, cell-soluble protein extract from a consortium of sulphate-reducing bacteria in the biosynthesis of geometric Pt(0) nanoparticles [34]. Similarly, Bharde et al. demonstrated magnetite nanoparticle synthesis by *Actinobacter*, a nonmagnetotactic bacterium, using iron precursors under aerobic conditions [35]. While earlier studies were very slow (about 1 week) and required strictly anaerobic conditions, this study tends to ease the required process control, one of the several benefits of biogenic synthesis.

Apart from monometallic nanoparticles, bacterial have shown unique properties for producing an altogether different and complex nanoparticles. Li et al. showed in-situ CdS nanoparticles (8 nm) synthesis and via bacterial cellulose (BC) nanofibers [36]. In another study, Bao et al. showed biosynthesis of CdTe quantum dots using *E. coli* [37] and yeast cells. In this process, yeast secreted proteins coordinated with Cd_2^+ and Te_2^+ ions forming caps on the surface of the QDs (~3 nm) thereby improving the biocompatibility as well as high fluorescent properties as shown in Fig. 8.2 [38].

This work provides a cost-effective green approach to synthesize highly fluorescent biocompatible CdTe QDs with high quantum yield ~33 % at a reaction temperature of 35 °C as compared to high quality CdTe nanocrystals obtained under hydrothermal conditions 180 °C [39], indicating that the biosynthesized CdTe QDs area good candidate for bio-imaging. It is worth noting that yeasts can accumulate

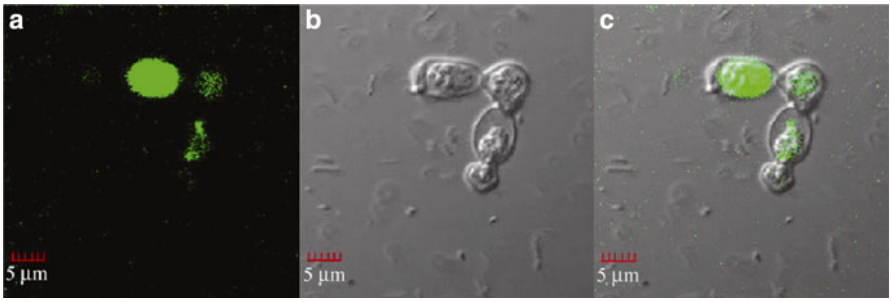

Fig. 8.2 Confocal image of CdTe QDs (**a**) excited by 488 nm laser (**b**) bright-field image (**c**) overlaid image. Reprinted from ref. [38] with permission by Springer Science + Business Media B.V.

significantly high amounts of toxic metals. This species has developed different mechanism to overcome the toxic effects of heavy metals including enzymatic oxidation or reduction, sorption at the cell wall, chelating with extracellular peptides or polysaccharides, controlled cell membrane transport of heavy metals towards or their active efflux from the cell. Ability of yeast to produce CdS and PbS has earned them the tag of green factories for semi-conductor crystals [40]. While discussing complex nanoparticles, it is worth noting that microbial systems have shown capability to produce bimetallic nanoparticles as well. Hosseinkhani et al. showed synthesis of bimetallic Pd-Au nanoparticles via *Cupriavidus necator* cells as support material [41]. The synthesis was carried out in two steps where monometallic Pd(0) and Au(0) layer was formed on *Cupriavidus necator* cell surface followed by formate assisted reduction of Au(III)/Pd(II) on to the pre-formed core. In another interesting study, Deplance et al. reported a novel biochemical method based on sacrificial hydrogen strategy to synthesize core/shell Pd@Au NPs as shown in Fig. 8.3 [42]. They utilized the ability of *E. coli* cells supplied with H2 as electron donor to precipitate Pd(II) ions from solution followed by the reduction of soluble Au(III) over its surface thereby generating characteristic core-shell morphology with high catalytic activity in oxidation of benzyl alcohol.

In another study by Carmona et al. magneto-optical bacteria were produced using probiotic *Lactobacillus fermentum* [43]. By exploiting metal-reduction properties (to produce gold nanoparticles) and their capacity to incorporate iron oxide nanoparticles at their external surface, they reported living magneto-optical bacteria behaving as a magnet at room temperature. Biogenic inorganic NP synthesis has several advantages due to their flexibility in terms of minimal process control, benign reaction conditions, minimal by-products and non-toxic nanomaterials. Bacteria and yeast in particular are an interesting class to function as green nanofactory mainly because while former has high multiplication rate the latter happens to be one of the most researched living system. Bacterial cultures can be easily scaled up depending upon the strain type and large amounts of required extracellular proteins/surfactants responsible for certain type of nanomaterial synthesis can be extracted at high purity. Similarly, yeast offers an additional advantage to act as a host for genetic modifications leading to highly specific bio-nano hybrids including

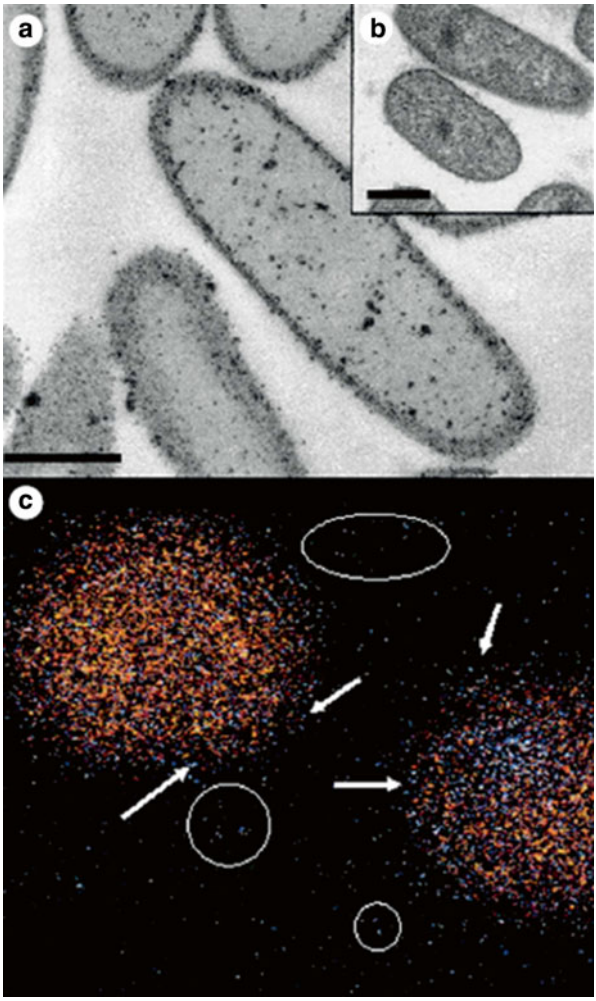

Fig. 8.3 *E.coli* mediated synthesis of bimetallic Au-Pd nanoparticles. (**a**) TEM image following sequential reduction of Pd (II) and (**b**) Au (III) (**c**) EDX mapping of two Pd–Au particles showing superimposed Au and Pd distributions. Reprinted from ref. [42] with permission by the Royal Society

special function nanoparticles. However, there are several challenges which need to be addressed before microbial assisted nanoparticles synthesis can become an industrially viable alternative for nanomaterial production. The first and foremost, similar to other biogenic agents, nanomaterial synthesis happens by a complex mixture of broth where one or more chemical entities may be responsible for the synthesis/functioning of the desired nanomaterial. There exists a plethora of reports where "mix n match" approach of utilizing different strain with different metal ion solution results in certain type of precipitation/reduction leading to colloidal nanoparticle solution. However, not much is being been done in pinning the active biomolecules which are responsible for the nanoparticle/nanomaterial synthesis. The aim biogenic synthesis should remain the same as with almost all the domains

Table 8.1 Summary of nanoparticles synthesized by biogenic approach

Microbe	Nanoparticle type and morphology	Reference
Escherichia coli	Au (50 nm, circular)	Srivastava et al. [44]
Rhodopseudomonas capsulata	Au nanowires (10–20 nm)	He et al. [45]
Lactobacillus sp.	Au (20–50 nm, Hexagonal)	Nair et al. [46]
Clostridium thermoaceticum	CdS	Cunningham et al. [47]
Actinobacter sp.	Magnetite (10–40 nm)	Bharde et al. [35]
Shewanella oneidensis	Uranium (IV) extracellular	Marshall et al. [48]
Desulfovibrio desulfuricans	Pd (~50 nm)	Yong et al. [49]
Klebsiella pneumoniae	Ag (5–30 nm)	Shahverdi et al. [50]
Pseudomonas aeruginosa	Ag (13 nm, spherical)	Ganesh Kumar et al. [51]
Streptomyces sp.	$MnSO_4$ and $ZnSO_4$ (10–20 nm)	Waghmare et al. [52]
Candida glabrata	CdS (200 nm)	Dameron et al. [53]
Pichia jadinii	Au (~100 nm)	Gericke et al. [54]
Yarrowia lipolytica	Au	Agnihotri et al. [55]
Torulopsis sp.	PbS (2–5 nm)	Kowshik et al. [56]

of science, i.e. to evolve into a more concrete and standard practice. Further, bacterial synthesis of nanoparticles generally results in coating of extracellular biomolecules (resulting in stabilization) over the nanoparticle being synthesized. This may not be required for certain specific applications along with the probability of initiating step for purification of resulting nanoparticles. Therefore, biogenic chemists should focus on developing "standard operating procedures" which can create a benchmark for homogeneity of the process among similar strains and culture conditions. As of now, production of nanoparticle by microbial strain has been established. Therefore, microbial synthesis of nanoparticle needs a little more than just synthesis characterization and generic application to combat its existing challenges. Emphasis should be laid on understanding the biochemical mechanism of nanoparticle synthesis via proteomic, genetic or metabolomics analysis. With the advent of biomimetic materials and template assisted synthesis of nanomaterials, these well-studied and well-developed biogenic systems will play a key-role in the future of green processes for nanotechnology. Similarly, there exists a vast plethora of bacteria and yeast mediated nanoparticle synthesis as shown in Table 8.1.

8.2.2 Fungi and Algae

Fungi and algae are among the prominent key players for biogenic synthesis of nanoparticles. In fact, fungi offer some distinct advantages as compared to other biogenic agents in terms of high enzymatic production, ability to scale-up (e.g. thin substrate fermentation method) and high tolerance against metals. High

extracellular proteins/enzymes results in high yield of nanoparticles. Mukherjee et al. reported biosynthesis of silver nanoparticles (25 ± 12 nm) using *Verticillium* sp [57]. While exposure to fungal biomass in presence of aqueous Ag^+ ions solution resulted in the intracellular reduction of the metal ions, the cells continued to multiply after biosynthesis of the silver nanoparticles showing high metal resistance. This study was important as silver nanoparticles are generally regarded as the panache for antimicrobial agent. Similarly, Ahmad et al. reported extracellular synthesis of CdS nanoparticles by *Fusarium oxysporum* via extracellular sulphate reductase enzymes [58]. The enzyme mixture was responsible for the conversion of sulphate ions to sulphide ions that subsequently reacted with aqueous Cd_2^+ ions to yield highly stable CdS nanoparticles.

High extracellular protein yield from fungal systems were also utilized for the synthesis of gold nanocrystals with varied morphology including spherical, regular nanoplates, spiral nanoplates, nanowalls, lamellar nanoagglomerates, and spherical nanoagglomerates via mycelia-free spent medium (*Aspergillus niger*) which were found to be temperature and pH dependent [59]. Similarly, heat treatment of cell-free filtrate (*T. koningii*) indicated that the presence of aromatic and aliphatic amines (Cysteine, Tyrosine, etc.) is responsible for the nanoparticle production and stabilization [60, 61]. This extracellular yield of enzyme/proteins from fungal system with its ability to grow on mineral media (metal ions) is a key feature for biogenic synthesis of nanoparticles via fungal strains. A SDS-PAGE study on Au NP synthesized via *Rhizopus oryzae* confirmed that two proteins of 45 and 42 kDa participate in gold reduction, while an 80 kDa protein serves as a capping agent [62]. This "capping agent" property from fungus was also utilized in the synthesis of core-shell nanoparticle (silver-protein; 30.5 ± 4.0 nm) synthesis by spent mushroom substrate [63]. *Fusarium oxysporum* provided some interesting results by producing Pt NPs (5–30 nm) via "two-cycle two-electron mechanism" for Pt NP formation. H_2PtCl_6 with its octahedral structure was may fit into the hydrolase active site, and then subsequently getting reduced at the surface of the enzyme to form Pt^{+2}. Next, $PtCl_2$ moves to the hydrophobic channel of the hydrolase active site and is reduced at pH 7.5 and 38 °C. This study further reaffirms the importance of reaction parameters like pH and temperature as stated above since H_2PtCl_6 was unreactive at pH 7.5, 38 °C; $PtCl_2$ was unreactive at pH 9, 65 °C [64]. Also, a fungal strains of *Fusarium* sp. found to produce Au–Ag bimetallic nanoparticles and silica nanoparticles. In another study, magnetite nanoparticles were produced by *Verticillium* sp. and subsequent SDS-PAGE analysis suggested cationic 55 kDa protein may be responsible for the hydrolysis of the $[Fe(CN)_6]_3$ and $[Fe(CN)_6]_4$ precursors; The presence of the 13 kDa protein, which was suggested to be induced by the presence of the iron complexes. Therefore, as evident, despite a decade long research of utilizing fungal strains for nanoparticle production and being able to establish some key-findings regarding the "extracellular synthesis" route, biogenic synthesis is in dire need of identifying the underlying mechanism of such processes. Although a few studies reported preliminary SDS-PAGE analysis asserting extracellular proteins responsible for nanoparticle production, it is vital to establish the proteomic/genetic route of such biogenic studies. Since, biogenic synthesis is an established

route of nanomaterial synthesis (as is the case now), a collective effort is needed to mimic the underlying molecular machinery so that the same advantages can be achieved more "controlled" manner. Also, it should be noted that a majority of filamentous fungi that have been reported for nanoparticle synthesis are plant and/or human pathogen. This makes handling and disposal of the biomass a major inconvenience toward commercialization of the process. Further, lack of proper control studies to ascertain the mechanism behind nanoparticle production is a major challenge which microbial biogenic synthesis needs to assess [60, 61]. Diatoms have been long regarded as a perfect "natural design" with highly efficient metabolism to remove large amounts of carbon dioxide, a major greenhouse gas. The very interesting design trait includes their cell wall which is made up entirely of glass, i.e. silica or silicon dioxide. The shell of these unicellular organisms are ornately patterned with features just tens of nanometers in size. With thousands of different species of diatoms, we have virtually a large library of extracellular design patterns waiting to be explored and utilized for nano-motors, nano-scale reactors, etc. Kröger et al. provided the first of its kind study to utilize polycationic peptides from diatom biosilica to direct silica nanosphere formation [65]. This set of polycationic peptides better known as silaffins were isolated from diatom cell walls and were responsible to form a network of silica nanospheres when added to a solution of silicic acid within a few seconds. Since, silaffins contain covalently modified lysine-lysine elements; this not only suggested the role of primary/secondary amines for catalytic structure formation but was able to confirm the underlying mechanism within a few years. The study done by Kröger et al. is all the more important since it addressed the major issue of biogenic synthesis, i.e. not only to synthesize/characterize the material but to provide in-depth analysis of the underlying mechanism in subsequent studies. Among early studies, Torres et al. also reported biosynthesis of gold nanoparticles by a single-step room temperature method of aqueous chloroaurate ions by brown seaweed (*Fucus spiralis*) [66]. Similarly, several algal strains have been found to produce Au, Ag and Pt NPs. Also, a batch reactor study of *Chlorella vulgaris* for silver nanoparticle synthesis in a continuously stirred non-aerated culture assembly was carried out to produce polydispersed (8–20 nm) Ag NPs [67]. On a slightly different perspective, alginate which is an algal polysaccharide has found application in the synthesis of ferromagnetic nanoparticles as well as an efficient catalyst matrix for oxidation reactions [24]. In another study, Govindaraju et al. investigated interaction of single-cell protein of *Spirulina platensis* for the synthesis of Ag, Au and Au core—Ag shell nanoparticles [68].

8.2.3 Plant Derived Materials

Plants have the tendency (often required as micronutrients and macronutrients) to uptake very low levels of metals and accumulate in tissues compared to the chemical methods, which is less effective in low levels of metals. It is interesting to note that although the biological reduction of metals by plant extracts has been known since

the early 1900s, the synthesis of nanoparticles using plant materials has only recently been studied within the decade [69]. The synthesis of metal nanoparticles using biological materials has been shown to produce nanoparticles of the same shapes and sizes as those produced through chemical or physical methods. An added advantage with using plants as biogenic agent is often their compatibility with living systems. A recent study by Zhang et al. reported that exosome-like nanoparticles from inexpensive, edible plants might be used to make nanovectors to bypass toxicity and cost related challenges. The nanoparticles from the juice of grapefruits, grapes and tomatoes were undertaken for this study [11]. However, the current chapter discusses important plant mediated nanoparticle synthesis strategies and reaction parameters required for obtaining desired nanoparticle morphology. In fact, the accumulation of metal ions in plants has been largely used in phytoremediation for about three decades or so, which has been a low-cost eco-friendly and efficient environmental clean-up technique [70]. This also resulted in phytomining technique where plants were used to extract mineral traces from below the Earth's surface [71]. In 2002, Gardea-Torresday et al. reported formation and growth of Au NP inside live alfalfa plant where they presented the possibility of using live plants for fabrication of nanoparticles. As claimed in this report, this indeed opened up a new and exciting method to fabricate nanoparticles with successive contribution for the now emerging field of nanobiotechnology. With nanoanalytical instruments and imaging coming into focus, subsequent years reported several reports of nanocrystalline metal in plants suggesting plant phytochemicals has not only the potential to reduce but also to stabilize the resulting nanoparticles [72]. Marshall et al. utilized *B. juncea* to report accumulation of metallic gold as nanoparticles (5–50 nm) [73]. Similarly, among earlier studies, Gardea-Torresdey et al. reported silver nanoparticles synthesis in alfalfa seedlings [74]. They reported that when seedlings were grown under aseptic conditions in a basal medium containing silver nitrate, silver(I) ions were reduced and accumulated as Ag(0) nanoparticles at physiological pH (5.8) both in roots and shoots. However, as expected from other biogenic agents, extracellular nanoparticle synthesis is what we are looking for. One major advantage of using plant extracts as biogenic agent for nanoparticle synthesis is that in comparison to microorganisms, the phytosynthesis method does not require complex processes like microbial isolation, culturing, maintenance, etc., thereby making it an ideal choice for cost-effective bulk production of nanoparticles. Also, there have been studies claiming that that the rate of nanoparticle synthesis is faster and more stable using plants as compared to microbes [75]. Shankar et al. reported formation of gold nanotriangles by lemongrass leaf extract [76]. They reported that the nanotriangles seem to grow by a process involving rapid reduction, assembly and room-temperature sintering of "liquid-like" spherical gold nanoparticles. In addition, leaf extracts of several plants including lemongrass, neem, tamarind, geranium, *Aloe vera*, and *Capsicum annuum* have been reported to demonstrated their potential in formation of Au and Ag nanoparticles [77] In another study, Gangula et al. reported synthesis of Gold (Au) and Silver (Ag) nanoparticles (NPs) from the stem extract of *Breynia rhamnoides* [78]. The phenolic glycosides and reducing sugars present in the extract were reported to be responsible for the rapid reduction rates of Au^{3+} ions to AuNPs.

Similarly, Huang et al. reported Au NP formation from the sun-dried leaves of *Cinnamomum camphora* [79]. Song et al. claimed first report of Pt nanoparticles using the leaf extract of *Diospyros kaki* from aqueous $H_2PtCl_6 \cdot 6H_2O$ solution [80]. This study also highlighted the fact that biogenic nanoparticle synthesis may not necessarily be an enzyme dependent process. Likewise, syntheses of platinum and palladium nanoparticles have been reported using extracts of several different plant species [81, 82]. Jia et al. reported formation of Pd nanocatalyst for p-Nitrotoluene hydrogenation with *Gardenia jasminoides* stating 100 % conversion efficiency under specified reaction conditions [83]. This study highlighted that geniposide, chlorogenic acid, crocins and crocetin played an important part in reduction and stabilization of Pd nanoparticles (temperature dependent). Coccia et al. also reported one-pot synthesis of platinum and palladium nanoparticles using lignin isolated from red pine (*Pinus resinosa*) [84]. Likewise, bimetallic nanoparticles have also been synthesized using plant extracts. Lu et al. reported Ag – Pd alloy nanoparticles (NPs) using the aqueous extract of *Cacumen platycladi* leaves and its application as a catalyst for hydrogenation of 1,3-butadiene [85]. The results reported that biomolecules including saccharides, polyphenols, or carbonyl compounds were involved in the reduction process with (NH)C = O groups were responsible for the stabilization of the NPs. Similarly, Zhang et al. reported synthesis of bimetallic Au-Pd nanoparticles (~7 nm) with *Cacumen platycladi* leaf extract in aqueous environment [86]. Preliminary investigation suggested C = O and C-O groups in the plant extract responsible for capping the nanoparticles. Similarly, bimetallic nanoparticle synthesis of Au-Ag nanoparticles have been reported using dried leaf extract of *Anacardium occidentale* where water soluble biomolecules like polyols and proteins were suggested to be responsible for the bio-reduction [87]. In another study, Patel et al. demonstrated high-performance nanothermite composites derived from superreactive CuO nanorods oxidizers fabricated by simple biogenic routes using *Aloe vera* plant extracts [88].

Recently, Nolasco-Arizmendi et al. reported silk–gold nanocomposite fabric by reduction of gold ions using aqueous extract of grapefruit pulp (*Citrus paradisi*) suggesting potential in development of functional fibres/fabrics using plant mediated biogenic method [89]. Carbohydrates and organic acids, present in *C. paradisi* were believed to be responsible for the formation of nanoparticles [89]. Also, Hang et al. reported bimetallic Au–Pd/TiO_2 catalysts for solvent-free oxidation of benzyl alcohol (BzOH) to benzaldehyde (BzH) with *Cacumen platycladi* (*CP*) extract [90]. With high BzOH conversion (~78 %) and selectivity (~96 %), recycling tests showed that even after seven recycles, the catalyst still remained suggesting excellent durability and reusability leading towards industrial application [90].

Although with tremendous development shown towards plant mediated synthesis of inorganic nanoparticles, among prime challenges, it is important to understand the underlying mechanism and functional biomolecules involved for its subsequent developmental stage of biomimetic nanomaterial synthesis. Several researchers have reported that larger nanoparticles are formed at lower pH (2–4) while smaller nanoparticles are formed as the pH level increases [82, 83]. This was presumed as at low pH (pH 2 in case of Au NPs) they tend to aggregate to form

larger nanoparticles rather than to nucleate and form new nanoparticles. In contrast, at pH 3 and 4, a greater number of functional groups (carbonyl and hydroxyl) are available to act as nucleation sites, thereby producing nanoparticles of relatively small size. Similarly, it was reported that nanoparticles are formed at a higher rate with increase in temperatures. Grecke and Pinches observed that Au nanorods and platelets were synthesized at higher temperatures, while spherical-shaped nanoparticles were formed at lower temperatures [91]. This is understandable as with increase in temperature, the rate of reaction also increases, thereby enhancing the synthesis of nanoparticles [92, 93].

However, as evident from plant being used as biogenic agents, there exists no core proof underlining the reaction mechanism with purified active compound and the assessment of its catalytic binding site. This is detrimental for the growth of plants as biogenic agents since numerous plant extracts were randomly used to make metallic nanoparticles (Au and Ag due to their ease in synthesis and SPR related preliminary observation). Chemical groups including flavonoids, terpenoids, primary/secondary amines, polysaccharides, carbonyl and sulfhydryl groups, etc. have all been reported for NP synthesis. In absence of any process control, plant biogenic synthesis needs standardized protocols where the focus should shift from mere chemical groups (as provided from FTIR study) to actual extraction, purification and assessment of phytoactive chemicals. Very recently, a number of reports have been published on the synthesis of noble metal nanoparticles from plants with possible mechanism studies [94–96].

8.3 Challenges for Biogenic Synthesis of Nanoparticles

Similar to any other nascent technology, biogenic synthesis of nanomaterials (or nanoparticles in particular) has several challenges which it needs to address before being considered as a viable alternative for industrial production of nanomaterials/nanoparticles. In this concluding section, our aim is highlight some key-challenges which need to be addressed for biogenic synthesis being evolved into biomimetic synthesis. It is interesting to note that although a plethora of scientific articles have been published in field of biogenic synthesis of nanoparticles within a decade, the challenges being highlighted here remains as important as they were before and for the future.

8.3.1 Protocol Designing: Stringent Control Setup

The first and foremost caution for biogenic synthesis is the designing of synthesis experiment. In a very recent article, Liu et al. showed synthesis of nanoparticles (Au) and reduced graphene oxide by using chemically defined microbe culture media alone, without the involvement of microbes [97]. These studies in one go highlighted

what many studies may have claimed in the past to be achieved microbiologically, could have been a mere control error. As this paper correctly points out that "using this article to alert researchers in the microbial nanosynthesis field to carefully design control experiments to avoid the misunderstanding of the microbial synthesis mechanisms and realize the implementation of complete green methods to fabricate technologically important nanomaterials." This is indeed an important issue which needs to be addressed systematically and providing video evidence (with time-lapsed study) to prove only the sought biogenic agent is being active is very important.

8.3.2 Putting Emphasis on Reaction Kinetics and Process Control: Understanding Reaction Mechanism

As of now, it is an established fact that biogenic agents can be used to produce metallic nanoparticles. As highlighted throughout this chapter, several eukaryotic and prokaryotic organisms have been utilized to synthesize an array of nanoparticles. Therefore, upcoming studies must focus on standardizing the protocol, understanding of reaction mechanism and controlling the morphology of nanoparticles in liquid media. The overexploitation of biogenic agents merely to report the synthesis aspect should be accompanied by the factors controlling the study. This can be better understood by the fact that as of now several plants/bacteria has been identified to produce nanoparticles while exact mechanism still largely remains elusive or rather process dependent. Although, utilizing a dozen different species to catalogue the nanoparticles being produced makes sense provided each of it undergoes to establish the rigorous process parameters for a more comprehensive and new set of information. Too often reports have been published where nanoparticle synthesis has been reported by a biogenic agent with the change of strain, part of the plant, culture condition, etc. This can be the initial foundation of the study but then needs greater information to be built upon before scientific community can transform such studies into more accurate biomimetic platforms. This can be better understood by the fact that recently Bhaduri et al. claimed Ag NP synthesis by sunlight [98]. Similarly, Kim et al. showed sunlight based synthesis of gold nanoparticles [99].

Therefore, what we see here is some studies which claim to achieve the nanoparticle synthesis just like biogenic agents with no requirement of laborious microorganism screening, plant culturing/Soxhlet extraction, cultivating and complex downstream separation processing can be eliminated. Our intention here is to highlight the importance that merely changing the biogenic substrate (knowing well that they are indeed capable of producing nanoparticles) and subsequent characterization of nanoparticles may not be sufficient considering the sheer amount of publications within the last decade. We need to address the underlying mechanism by carrying out proteomic and metabolomics studies as and when required. In place of multiple publications by utilizing different biogenic agents to produce Au/Ag or any nanoparticles, emphasis should be laid on advancing the already established bio-

genic agents with greater process control so that they can be mimicked into the lab for real applications. Although we have cited several biomimetic studies in this chapter, a good example at this point will be liposomes which are composed of lipid membranes just like cell-membrane with the ability to control the reaction kinetics at nano/micro scale [100]. While the first part of the issue is scientific where there is need to study the underlying mechanism, the latter is more ethical where the "quality and impact" of a study is considered into account.

8.3.3 Importance of the "Choice of Characterization" Studies

"There is no doubt that SPR from Au NPs can serve as the preliminary indicator for Au NP synthesis. However, as of now, where ample of studies has been done indicating the same, there is need to dwell deeper and extract more meaningful information like reaction kinetics or time-dependent stability of nanoparticles etc." The above statement highlights another important challenge for biogenic nanoparticle synthesis, i.e. the need to set a higher benchmark when it comes to characterization of nanomaterials. Another example of it can be TEM images where several biogenic synthesis studies claimed the nanoparticles to be "highly monodispersed" but did not provided a bell-graph study confirming the same. Obtaining highly monodisperse nanoparticles is a challenge for biogenic systems since there are several parameters acting upon. Studies done by Bastús et al. [101] and Perrault et al. [102] can be used as a benchmark while reporting reaction process dependent nanoparticle morphology and associated kinetics. Another key-feature as we have seen across most of the biogenic studies is the inclusion of FT-IR data generally confirming some active chemical groups (primary amines, secondary amines, thiols, etc.) which may be responsible for the chemical reaction. This needs to be further confirmed and complemented by more conclusive analytical studies including SDS-PAGE followed by 2D-PAGE and if possible, protein sequencing. This is important because as of now, it is already established that almost all sorts of active proteins in aqueous condition have the capacity to produce nanoparticles (especially Au NPs because of its low reduction potential). Therefore, there is an urgent need to raise the necessary scientific evidence from mere detection to its "extraction-purification and subsequent characterization" so that biogenic synthesis can match pace with the ever-growing need of biomimetic materials. Another important point is utilization of EDX data while confirming reduction taking place. It should be noted that EDX can detect the element even if it is present in its compound (salt) form and may not necessarily means reduction taking place or associated quantitative changes. Therefore, it is important to utilize XPS among others which given an edge over (EDX and FT-IR) by providing information about the chemical state of all the elements involved in the reaction.

References

1. Gan Y, Sun L, Banhart F (2008) One- and two-dimensional diffusion of metal atoms in graphene. Small 4:587–591. doi:10.1002/smll.200700929
2. Hong W, Bai H, Xu Y et al (2010) Preparation of gold nanoparticle/graphene composites with controlled weight contents and their application in biosensors. J Phys Chem C 114: 1822–1826. doi:10.1021/jp9101724
3. Sowerby SJ, Holm NG, Petersen GB (2001) Origins of life: a route to nanotechnology. Biosystems 61:69–78. doi:10.1016/S0303-2647(01)00130-7
4. Arvizo RR, Bhattacharyya S, Kudgus RA, Giri K, Bhattacharyaa R, Mukherjee P (2012) Intrinsic therapeutic applications of noble metal nanoparticles: past, present and future. Chem Soc Rev 41:2943–2970. doi:10.1039/C2CS15355F
5. Stylios GK, Giannoudis PV, Wan T (2005) Applications of nanotechnologies in medical practice. Injury 36(Suppl 4):S6–S13. doi:10.1016/j.injury.2005.10.011
6. Goodsell DS (2004) Bionanotechnology: lessons from nature. Wiley-VCH Verlag GmbH & Co KGaA, Weinheim
7. Liu K, Zhang J-J, Cheng F-F et al (2011) Green and facile synthesis of highly biocompatible graphene nanosheets and its application for cellular imaging and drug delivery. J Mater Chem 21:12034. doi:10.1039/c1jm10749f
8. Fratzl P (2007) Biomimetic materials research: what can we really learn from nature's structural materials? J R Soc Interface 4:637–642. doi:10.1098/rsif.2007.0218
9. Pompe W, Rodel G, Weiss H, Mertig M (2013) Bio-nanomaterials. Wiley-VCH Verlag GmbH & Co KGaA, Weinheim
10. Eduardo R-H, Margarita D, Pilar A (2008) An introduction to Bio-nanohybrid materials. In: Katsuhiko Ariga YML (ed) Eduardo ruiz-hitzky Bio-inorganic hybrid nanomater. Strateg. Synth. Charact. Appl. Wiley-VCH Verlag GmbH & Co KGaA, Weinheim, pp 1–40
11. Wang Q, Zhuang X, Mu J et al (2013) Delivery of therapeutic agents by nanoparticles made of grapefruit-derived lipids. Nat Commun 4:1867. doi:10.1038/ncomms2886
12. Chen S-Y, Lu Y-Y, Shih F-Y et al (2013) Biologically inspired graphene-chlorophyll phototransistors with high gain. Carbon 63:23–29. doi:10.1016/j.carbon.2013.06.031
13. Hallmann J, Hallmann AQ, Mahaffee WFKJ (1997) Bacterial endophytes in agricultural crops. Can J Microbiol 43:895–914
14. Bruins MR, Kapil S, Oehme FW (2000) Microbial resistance to metals in the environment. Ecotoxicol Environ Saf 45:198–207. doi:10.1006/eesa.1999.1860
15. Klaus-Joerger T, Joerger R (2001) Bacteria as workers in the living factory: metal-accumulating bacteria and their potential for materials science. Trends Biotechnol 19:15–20
16. Wahl R, Mertig M, Raff J et al (2001) Electron-beam induced formation of highly ordered palladium and platinum nanoparticle arrays on the S layer of Bacillus sphaericus NCTC 9602. Adv Mater 13:736–740. doi:10.1002/1521-4095(200105)13:10<736::AID-ADMA736>3.0.CO;2-N
17. Blum AS, Soto CM, Wilson CD et al (2004) Cowpea mosaic virus as a scaffold for 3-D patterning of gold nanoparticles. Nano Lett 4:867–870. doi:10.1021/nl0497474
18. Romano C, D'Imperio S, Woyke T et al (2013) Comparative genomic analysis of phylogenetically closely related Hydrogenobaculum sp. Isolates from Yellowstone National Park. Appl Environ Microbiol 79:2932–2943. doi:10.1128/AEM. 03591-12
19. Gadd GM (2010) Metals, minerals and microbes: geomicrobiology and bioremediation. Microbiology 156:609–643. doi:10.1099/mic. 0.037143-0
20. Young KD (2006) The selective value of bacterial shape. Microbiol Mol Biol Rev 70:660–703. doi:10.1128/MMBR. 00001-06
21. Naik RR, Stringer SJ, Agarwal G et al (2002) Biomimetic synthesis and patterning of silver nanoparticles. Nat Mater 1:169–172. doi:10.1038/nmat758
22. Parikh RY, Singh S, Prasad BLV et al (2008) Extracellular synthesis of crystalline silver nanoparticles and molecular evidence of silver resistance from Morganella sp.: towards

understanding biochemical synthesis mechanism. Chembiochem 9:1415–1422. doi:10.1002/cbic.200700592
23. Zhang H, Li Q, Lu Y et al (2005) Biosorption and bioreduction of diamine silver complex by Corynebacterium. J Chem Technol Biotechnol 80:285–290. doi:10.1002/jctb.1191
24. Saha S, Pal A, Kundu S et al (2010) Photochemical green synthesis of calcium-alginate-stabilized Ag and Au nanoparticles and their catalytic application to 4-nitrophenol reduction. Langmuir 26:2885–2893. doi:10.1021/la902950x
25. He S, Guo Z, Zhang Y et al (2007) Biosynthesis of gold nanoparticles using the bacteria Rhodopseudomonas capsulata. Mater Lett 61:3984–3987. doi:10.1016/j.matlet.2007.01.018
26. Ahmad A, Senapati S, Khan MI et al (2003) Extracellular biosynthesis of monodisperse gold nanoparticles by a novel extremophilic actinomycete, Thermomonospora sp. Langmuir 19:3550–3553
27. Lahr RH, Vikesland PJ (2014) Surface-enhanced Raman spectroscopy (SERS) cellular imaging of intracellularly biosynthesized gold nanoparticles. ACS Sustain Chem Eng 2:1599–1608. doi:10.1021/sc500105n
28. Slocik JM, Naik RR, Stone MO, Wright DW (2005) Viral templates for gold nanoparticle synthesis. J Mater Chem 15:749. doi:10.1039/b413074j
29. Kim J, Rheem Y, Yoo B et al (2010) Peptide-mediated shape- and size-tunable synthesis of gold nanostructures. Acta Biomater 6:2681–2689. doi:10.1016/j.actbio.2010.01.019
30. Srivastava SK, Constanti M (2012) Room temperature biogenic synthesis of multiple nanoparticles (Ag, Pd, Fe, Rh, Ni, Ru, Pt, Co, and Li) by Pseudomonas aeruginosa SM1. J Nanoparticle Res 14:831. doi:10.1007/s11051-012-0831-7
31. Bai HJ, Zhang ZM, Guo Y, Yang GE (2009) Biosynthesis of cadmium sulfide nanoparticles by photosynthetic bacteria Rhodopseudomonas palustris. Colloids Surf B: Biointerfaces 70:142–146. doi:10.1016/j.colsurfb.2008.12.025
32. Shenton W, Pum D, Sleytr UB (1997) Letters to Nature: Synthesis of cadmium sulphide superlattices using bacterial S-layers. Nature 389:585–587
33. Konishi Y, Ohno K, Saitoh N et al (2007) Bioreductive deposition of platinum nanoparticles on the bacterium Shewanella algae. J Biotechnol 128:648–653. doi:10.1016/j.jbiotec.2006.11.014
34. Riddin T, Gericke M, Whiteley CG (2010) Biological synthesis of platinum nanoparticles: effect of initial metal concentration. Enzyme Microb Technol 46:501–505. doi:10.1016/j.enzmictec.2010.02.006
35. Bharde A, Wani A, Shouche Y et al (2005) Bacterial aerobic synthesis of nanocrystalline magnetite. J Am Chem Soc 127:9326–9327. doi:10.1021/ja0508469
36. Hu W, Chen S, Li X et al (2009) In situ synthesis of silver chloride nanoparticles into bacterial cellulose membranes. Mater Sci Eng C 29:1216–1219. doi:10.1016/j.msec.2008.09.017
37. Bao H, Lu Z, Cui X et al (2010) Extracellular microbial synthesis of biocompatible CdTe quantum dots. Acta Biomater 6:3534–3541. doi:10.1016/j.actbio.2010.03.030
38. Bao H, Hao N, Yang Y, Zhao D (2010) Biosynthesis of biocompatible cadmium telluride quantum dots using yeast cells. Nano Res 3:481–489. doi:10.1007/s12274-010-0008-6
39. Zhang H, Wang L, Xiong H et al (2003) Hydrothermal synthesis for high-quality CdTe nanocrystals. Adv Mater 15:1712–1715. doi:10.1002/adma.200305653
40. Sweeney RY, Mao C, Gao X et al (2004) Bacterial biosynthesis of cadmium sulfide nanocrystals. Chem Biol 11:1553–1559
41. Hosseinkhani B, Søbjerg LS, Rotaru A-E et al (2012) Microbially supported synthesis of catalytically active bimetallic Pd-Au nanoparticles. Biotechnol Bioeng 109:45–52. doi:10.1002/bit.23293
42. Deplanche K (2012) Microbial synthesis of core/shell gold/palladium nanoparticles for applications in green chemistry. J R Soc Interface 9:1705–1712
43. Carmona F, Mart M, Ga N, Dominguez-vera JM (2014) Bioinspired magneto-optical bacteria. Inorg Chem 53:8565–8569
44. Srivastava SK, Yamada R, Ogino C, Kondo A (2013) Biogenic synthesis and characterization of gold nanoparticles by Escherichia coli K12 and its heterogeneous catalysis in degradation of 4-nitrophenol. Nanoscale Res Lett 8:70. doi:10.1186/1556-276X-8-70

45. He S, Zhang Y, Guo Z, Gu N (2008) Biological synthesis of gold nanowires using extract of Rhodopseudomonas capsulata. Biotechnol Prog 24:476–480. doi:10.1021/bp0703174
46. Nair B, Pradeep T (2002) Coalescence of nanoclusters and formation of submicron crystallites assisted by Lactobacillus strains. Cryst Growth Des 2:293–298
47. Cunningham D, Lundie L (1993) Precipitation of cadmium by Clostridium thermoaceticum. Appl Environ Microbiol 59:7–14
48. Marshall MJ, Beliaev AS, Dohnalkova AC et al (2006) c-Type cytochrome-dependent formation of U(IV) nanoparticles by Shewanella oneidensis. PLoS Biol 4:268. doi:10.1371/journal.pbio.0040268
49. Yong P, Rowson NA, Farr JPG et al (2002) Bioreduction and biocrystallization of palladium by Desulfovibrio desulfuricans NCIMB 8307. Biotechnol Bioeng 80:369–379. doi:10.1002/bit.10369
50. Shahverdi AR, Fakhimi A, Shahverdi HR, Minaian S (2007) Synthesis and effect of silver nanoparticles on the antibacterial activity of different antibiotics against Staphylococcus aureus and Escherichia coli. Nanomedicine 3:168–171. doi:10.1016/j.nano.2007.02.001
51. Kumar CG, Mamidyala SK (2011) Extracellular synthesis of silver nanoparticles using culture supernatant of Pseudomonas aeruginosa. Colloids Surf B: Biointerfaces 84:462–466. doi:10.1016/j.colsurfb.2011.01.042
52. Waghmare S, Deshmukh A (2011) Biosynthesis and characterization of manganese and zinc nanoparticles. Univers J Environ Res Technol 1:64–69
53. Dameron CT, Reese RN, Mehra RK, Kortan AR, Carroll PJSM (1989) Biosynthesis of cadmium sulphide quantum semiconductor crystallites. Nature 338:596–597
54. Gericke M, Pinches A (2006) Microbial production of gold nanoparticles. Gold Bull 39:22–28. doi:10.1007/BF03215529
55. Agnihotri M, Joshi S, Kumar AR et al (2009) Biosynthesis of gold nanoparticles by the tropical marine yeast Yarrowia lipolytica NCIM 3589. Mater Lett 63:1231–1234. doi:10.1016/j.matlet.2009.02.042
56. Kowshik M, Vogel W, Urban J (2002) Microbial synthesis of semiconductor PbS nanocrystallites. Adv Mater 14:815–818
57. Mukherjee P, Ahmad A, Mandal D et al (2001) Fungus-mediated synthesis of silver nanoparticles and their immobilization in the mycelial matrix: a novel biological approach to nanoparticle synthesis. Nano Lett 1:515–519. doi:10.1021/nl0155274
58. Ahmad A, Mukherjee P, Mandal D et al (2002) Enzyme mediated extracellular synthesis of CdS nanoparticles by the fungus, Fusarium oxysporum. J Am Chem Soc 124:12108–12109. doi:10.1021/ja027296o
59. Xie J, Lee JY, Wang DIC, Ting YP (2007) High-yield synthesis of complex gold nanostructures in a fungal system. J Phys Chem C 111:16858–16865. doi:10.1021/jp0752668
60. Maliszewska I, Aniszkiewicz Ł, Sadowski Z (2009) Biological synthesis of gold nanostructures using the extract of Trichoderma koningii. Acta Phys Pol A 116:S163–S165
61. Vigneshwaran N, Kathe AA, Varadarajan PV et al (2006) Biomimetics of silver nanoparticles by white rot fungus, Phaenerochaete chrysosporium. Colloids Surf B: Biointerfaces 53:55–59. doi:10.1016/j.colsurfb.2006.07.014
62. Das SK, Liang J, Schmidt M et al (2012) Biomineralization mechanism of gold by zygomycete fungi Rhizopus oryzae. ACS Nano 6:6165–6173. doi:10.1021/nn301502s
63. Vigneshwaran N, Kathe AA, Varadarajan PV et al (2007) Silver—protein (core—shell) nanoparticle production using spent mushroom substrate. Langmuir 23:7113–7117
64. Govender Y, Riddin T, Gericke M, Whiteley CG (2009) Bioreduction of platinum salts into nanoparticles: a mechanistic perspective. Biotechnol Lett 31:95–100. doi:10.1007/s10529-008-9825-z
65. Kröger N, Deutzmann R, Sumper M (1999) Polycationic peptides from diatom biosilica that direct silica nanosphere formation. Science 286:1129–1132
66. Mata YN, Torres E, Blázquez ML, Ballester A, González F, Muñoz JA (2009) Gold(III) biosorption and bioreduction with the brown alga Fucus vesiculosus. J Hazard Mater 166(2–3):612–618. doi:10.1016/j.jhazmat.2008.11.064

67. Satapathy S, Shukla SP, Sandeep KP et al (2014) Evaluation of the performance of an algal bioreactor for silver nanoparticle production. J Appl Phycol. doi:10.1007/s10811-014-0311-9
68. Govindaraju K, Basha SK, Kumar VG, Singaravelu G (2008) Silver, gold and bimetallic nanoparticles production using single-cell protein (Spirulina platensis) Geitler. J Mater Sci 43:5115–5122. doi:10.1007/s10853-008-2745-4
69. Parsons JG, Peralta-Videa JR, Gardea-Torresdey JL (2007) Chapter 21 Use of plants in biotechnology: Synthesis of metal nanoparticles by inactivated plant tissues, plant extracts, and living plants. In: Dibyendu Sarkar RD and RHBT-D in ES (ed) Concepts Appl. Environ. Geochemistry. Elsevier, pp 463–485
70. Hersrald RL, Ftnll BJ, Ni AJ (1969) Extractability of nickel added to soils and its concentration in plants. Can J Soil Sci 49:335–342
71. Sheorana V, Sheoranb AS, Pooniaa P (2009) Phytomining: A review. Minerals Engineering 22:12, 1007. doi:10.1016/j.mineng.2009.04.001
72. Mucalo MR, Bullen CR, Manley-harris M (2002) Arabinogalactan from the Western larch tree: A new, purified and highly water-soluble polysaccharide-based protecting agent for maintaining precious metal nanoparticles in colloidal suspension. J Mater Sci 37:493–504
73. Marshall AT, Haverkamp RG, Davies CE et al (2007) Accumulation of gold nanoparticles in Brassic juncea. Int J Phytoremediation 9:197–206. doi:10.1080/15226510701376026
74. Gardea-Torresdey JL, Gomez E, Peralta-Videa JR et al (2003) Alfalfa sprouts: a natural source for the synthesis of silver nanoparticles. Langmuir 19:1357–1361. doi:10.1021/la020835i
75. Iravani S (2011) Green synthesis of metal nanoparticles using plants. Green Chem 13:2638. doi:10.1039/c1gc15386b
76. Shankar SS, Rai A, Ahmad A et al (2005) Controlling the optical properties of lemongrass extract synthesized gold nanotriangles and potential application in infrared-absorbing optical coatings. Chem Mater 17:566–572
77. Shankar SS, Rai A, Ahmad A et al (2012) Synthesis of metal nanoparticles in living plants. Ital J Agron 7:577–583. doi:10.4081/ija.2012.e37
78. Gangula A, Podila R, Ramakrishna M et al (2011) Catalytic reduction of 4-nitrophenol using biogenic gold and silver nanoparticles derived from Breynia rhamnoides. Langmuir 27:15268–15274
79. Huang J, Li Q, Sun D et al (2007) Biosynthesis of silver and gold nanoparticles by novel sundried Cinnamomum camphora leaf. Nanotechnology 18:105104. doi:10.1088/0957-4484/18/10/105104
80. Song JY, Kwon E-Y, Kim BS (2010) Biological synthesis of platinum nanoparticles using Diospyros kaki leaf extract. Bioprocess Biosyst Eng 33:159–164. doi:10.1007/s00449-009-0373-2
81. Parker HL, Rylott EL, Hunt AJ et al (2014) Supported palladium nanoparticles synthesized by living plants as a catalyst for Suzuki-Miyaura reactions. PLoS One 9:e87192. doi:10.1371/journal.pone.0087192
82. Soundarrajan C, Sankari A, Dhandapani P et al (2012) Rapid biological synthesis of platinum nanoparticles using Ocimum sanctum for water electrolysis applications. Bioprocess Biosyst Eng 35:827–833. doi:10.1007/s00449-011-0666-0
83. Jia L, Zhang Q, Li Q, Song H (2009) The biosynthesis of palladium nanoparticles by antioxidants in Gardenia jasminoides Ellis: long lifetime nanocatalysts for p-nitrotoluene hydrogenation. Nanotechnology 20:385601. doi:10.1088/0957-4484/20/38/385601
84. Coccia F, Tonucci L, Bosco D et al (2012) One-pot synthesis of lignin-stabilised platinum and palladium nanoparticles and their catalytic behaviour in oxidation and reduction reactions. Green Chem 14:1073. doi:10.1039/c2gc16524d
85. Li Q (2014) Plant-mediated synthesis of Ag – Pd alloy nanoparticles and their application as catalyst toward selective hydrogenation. ACS Sustain Chem Eng 2:1212–1218
86. Zhang G, Du M, Li Q et al (2013) Green synthesis of Au–Ag alloy nanoparticles using Cacumen platycladi extract. RSC Adv 3:1878. doi:10.1039/c2ra22442a

87. Sheny DS, Mathew J, Philip D (2011) Phytosynthesis of Au, Ag and Au-Ag bimetallic nanoparticles using aqueous extract and dried leaf of Anacardium occidentale. Spectrochim Acta A Mol Biomol Spectrosc 79:254–262. doi:10.1016/j.saa.2011.02.051
88. Patel VK, Bhattacharya S (2013) High-performance nanothermite composites based on aloe-vera-directed CuO nanorods. ACS Appl Mater Interfaces 5:13364–13374. doi:10.1021/am404308s
89. Nolasco-Arizmendi V, Morales-Luckie R, Sanchez-Mendieta V et al (2012) Formation of silk-gold nanocomposite fabric using grapefruit aqueous extract. Text Res J 83:1229–1235. doi:10.1177/0040517512461697
90. Hong Y, Jing X, Huang J et al (2014) Biosynthesized bimetallic Au – Pd nanoparticles supported on TiO 2 for solvent-free oxidation of benzyl alcohol. ACS Sustain Chem Eng 2: 1752–1759
91. Gericke M, Pinches A (2006) Biological synthesis of metal nanoparticles. Hydrometallurgy 83:132–140. doi:10.1016/j.hydromet.2006.03.019
92. Dwivedi AD, Gopal K (2010) Biosynthesis of silver and gold nanoparticles using Chenopodium album leaf extract. Colloids Surf A Physicochem Eng Asp 369:27–33. doi:10.1016/j.colsurfa.2010.07.020
93. Philip D (2009) Biosynthesis of Au, Ag and Au-Ag nanoparticles using edible mushroom extract. Spectrochim Acta A Mol Biomol Spectrosc 73:374–381. doi:10.1016/j.saa.2009.02.037
94. Zheng B, Kong T, Jing X et al (2013) Plant-mediated synthesis of platinum nanoparticles and its bioreductive mechanism. J Colloid Interface Sci 396:138–145. doi:10.1016/j.jcis.2013.01.021
95. Mittal AK, Bhaumik J, Kumar S, Banerjee UC (2014) Biosynthesis of silver nanoparticles: elucidation of prospective mechanism and therapeutic potential. J Colloid Interface Sci 415:39–47. doi:10.1016/j.jcis.2013.10.018
96. Haverkamp RG, Marshall AT (2008) The mechanism of metal nanoparticle formation in plants: limits on accumulation. J Nanoparticle Res 11:1453–1463. doi:10.1007/s11051-008-9533-6
97. Liu L, Shao Z, Ang HM et al (2014) Are microorganisms indispensable in green microbial nanomaterial synthesis? RSC Adv 4:14564. doi:10.1039/c4ra00555d
98. Bhaduri GA, Little R, Khomane RB et al (2013) Green synthesis of silver nanoparticles using sunlight. J Photochem Photobiol A Chem 258:1–9. doi:10.1016/j.jphotochem.2013.02.015
99. Kim J-H, Twaddle KM, Hu J, Byun H (2014) Sunlight-induced synthesis of various gold nanoparticles and their heterogeneous catalytic properties on a paper-based substrate. ACS Appl Mater Interfaces 6:11514–11522. doi:10.1021/am503745w
100. Genç R, Clergeaud G, Ortiz M, O'Sullivan CK (2011) Green synthesis of gold nanoparticles using glycerol-incorporated nanosized liposomes. Langmuir 27:10894–10900. doi:10.1021/la201771s
101. Bastús NG, Merkoçi F, Piella J, Puntes V (2014) Synthesis of highly monodisperse citrate-stabilized silver nanoparticles of up to 200 nm: kinetic control and catalytic properties. Chem Mater 26:2836–2846. doi:10.1021/cm500316k
102. Perrault SD, Chan WCW (2009) Synthesis and surface modification of highly monodispersed, spherical gold nanoparticles of 50–200 nm. J Am Chem Soc 131:17042–17043

Chapter 9
Green Synthesis of Metal Nanoparticles by Plants: Current Trends and Challenges

Luciano Paulino Silva, Ivy Garcez Reis, and Cínthia Caetano Bonatto

Abstract Metal nanoparticles (MNPs) have been widely used in a range of recent scientific and technological applications. They can be produced by conventional chemical synthesis or green synthesis methods. Green synthesis consists of a myriad of promising approaches for the production of MNPs with desired properties. Plants represent the most explored group of living organisms for the green synthesis of MNPs, and to date, hundreds of species have been used. However, several factors that should be taken into account when performing green synthesis of MNPs remain underestimated or unexplored. This chapter does not focus on any specific plant species or experimental conditions leading to the synthesis of MNPs since there are numerous recent publications reviewing the literature in this outstanding field. The present chapter instead focuses on the trends and challenges in MNPs synthesis using plants which include reproducibility, scale-up, predictability, and development of strategies for effective management of governance, regulatory, and

L.P. Silva (✉)
Embrapa Genetic Resources and Biotechnology, Laboratory of Mass Spectrometry, Nanobiotechnology Room, Nanotechnology and Synthetic Biology Group, Brasilia 70770-917, DF, Brazil

Postgraduate Program in Animal Biology, Institute of Biological Sciences, University of Brasilia, Brasilia 70910-900, DF, Brazil

Postgraduate Program in Nanoscience and Nanobiotechnology, Institute of Biological Sciences, University of Brasilia, Brasilia 70910-900, DF, Brazil
e-mail: luciano.paulino@embrapa.br; lucianopaulinosilva@gmail.com

I.G. Reis
Embrapa Genetic Resources and Biotechnology, Laboratory of Mass Spectrometry, Nanobiotechnology Room, Nanotechnology and Synthetic Biology Group, Brasilia 70770-917, DF, Brazil

Biotechnology, Institute of Biological Sciences, University of Brasilia, Brasilia 70910-900, DF, Brazil

C.C. Bonatto
Embrapa Genetic Resources and Biotechnology, Laboratory of Mass Spectrometry, Nanobiotechnology Room, Nanotechnology and Synthetic Biology Group, Brasilia 70770-917, DF, Brazil

Postgraduate Program in Animal Biology, Institute of Biological Sciences, University of Brasilia, Brasilia 70910-900, DF, Brazil

V.A. Basiuk, E.V. Basiuk (eds.), *Green Processes for Nanotechnology*,
DOI 10.1007/978-3-319-15461-9_9

compliance risks. Finally, the major aim of this chapter is to provide an overview of relevant concerns raised or neglected by the available scientific literature regarding the green synthesis of MNPs using plants.

Keywords Metal nanoparticles • Green synthesis • Plants

9.1 Green Nanotechnology for Sustainable Development

Green nanotechnology is an emerging and powerful nanotechnology field that is supporting the development of innovative, reliable, and sustainable solutions to address global issues through research, development, and innovation. Indeed, green nanotechnology is based on lowering the risk of producing and applying nanomaterials [1]. The goal of the green nanotechnology is to use whole biological organisms or their parts (molecules, cells, tissues, or organs) as bioengineers or raw materials to develop novel and valuable nanomaterials with sustainable benefits.

The unique physical, chemical, and biological properties of nanomaterials developed through eco-friendly routes, such as catalytic potential [2], electrical conductivity [3], optical sensitivity [4], magnetic behavior [5], or biological reactivity [6], emerge from factors such as shape, size, surface charge, surface area, chemical composition, crystallinity, and agglomeration/aggregation properties of nanoscale featured materials. Currently, a myriad of nanostructured materials and nano-objects have been produced by sustainable methods and without the use of organic solvents and chemical reagents harmful to the environment [7]. Among the nano-objects that have been synthesized by green nanotechnology approaches, perhaps the most promising are the metal nanoparticles (MNPs) which are widely used as functional materials due to the properties uniquely accessible by these nanostructures [8].

In fact, the new properties of MNPs originated from atomic ordering to the nanoscale are largely different from those of their individual atoms or bulk metallic materials [9]. The current applications of MNPs include their use as: catalysts [10]; delivery systems for drugs [11]; enhancing contrast agents [12]; active food packaging materials [13]; components aiming the construction of nanobiosensors [14]; gene transfer systems [11]; antibiotics, antiseptics, and disinfectants aiming the control of pathogens and pests [15]; and nanoelectronic components [16].

9.2 Green Synthesis of MNPs: General Considerations

Most often, the synthesis of MNPs involves the chemical reduction of metal ions from salt solutions in the presence of a strong base (reducing agent), such as sodium borohydride or sodium hydroxide (Fig. 9.1), followed by the addition of a stabilizing agent, also called as capping agent or stabilizer [9]. However, the reagents used as reducing agents and the solvents used to dissolve the stabilizers are commonly toxic substances which may have adverse and deleterious health and environmental

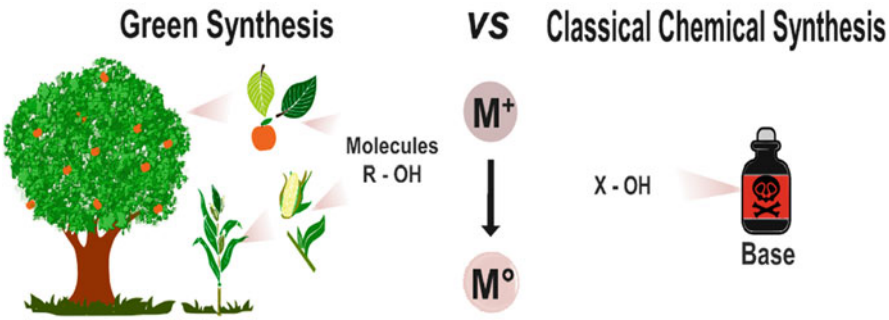

Fig. 9.1 Schematic illustration of the two main approaches used for the synthesis of metal nanoparticles: Green and Chemical (Classical) synthesis. Additional details are shown for the green synthesis of metal nanoparticles using dicotyledons and monocotyledons via reduction of metal salts using plant parts as reducing and stabilizing agents

effects if residues of them are present in the final nanosystems [17]. Thus, this may lead to several concerns regarding safety applications of MNPs as well as to search for novel alternative approaches aiming their synthesis [18]. One of these alternatives is the green synthesis of MNPs using biological systems that is based on the principles of green chemistry [19–22].

The green synthesis of MNPs may be performed using prokaryotic [23] or eukaryotic [4] organisms (including microorganisms, plants, and animals) or parts thereof, and can occur through intracellular [24] or extracellular [25] pathways. The biological components (primary and secondary metabolites) act as agents to promote the reduction of a target metal ion resulting in the formation of MNPs (Fig. 9.1). These same reducing compounds or other surrounding molecules may also form a stabilizing layer (coating) on the surface of MNPs, preventing or at least minimizing them to agglomerate/aggregate or grow in a disorderly manner during their production [26]. Furthermore, specific experimental conditions (temperature, pH, and reagents concentration) can modulate the production and properties of MNPs obtained by green synthesis approaches [3].

Most of the MNPs obtained from green synthesis strategies show as desirable characteristics under the sustainability perspective the fact that they are eco-friendly (use of lesser toxic reagents and solvents); are simple and rapid to produce (smaller number of steps); are biocompatible (can be used directly to target applications without prior purification steps); are biodegradable (can be hydrolyzed by biological pathways); and have low cost of production and high yield.

9.3 Green Synthesis of MNPs by Plants

Living organisms representing all biological kingdoms may have potential for use in green synthesis of MNPs. Fortunately, many of these organisms that can be used in green synthesis, beyond being species of the biodiversity; they are also grown or

raised for food and feed purposes. Plants are typically the first choice of researchers aiming the green synthesis of MNPs due to their biomass abundance, species diversity, and molecular repertoires [26–28]. Plants use primary and secondary metabolites for various aspects related to their surviving strategies (e.g., seasonality changes and reproductive behavior) and physiological responses to stressor agents (e.g., herbivores, pathogens, and climate changes). These same molecules are responsible for making the plant one of the major bioreactors and molecule suppliers for green synthesis approaches [28].

In fact, it is now well accepted that plants produce a wide range of metabolites that can act synergistically in the reduction of metal ions to their metallic counterparts and/or the stabilization of MNPs surface [26]. It is believed that the primary compounds responsible for the reduction of metal ions by plants are amino acids [29], citric acid [5], flavonoids [30], phenolic compounds [31], terpenoids [32], heterocyclic compounds [33], enzymes [34], peptides [35], polysaccharides [36], saponins [37], tannins [38], among others.

Green synthesis of MNPs mediated by plants use extracts of organs/tissues or the whole organisms [27, 39]. Indeed, an important aspect concerning the green synthesis of MNPs by plants is the fact that different plant parts (e.g., leaves, seeds, barks, roots, fruits, and others) may produce nano-objects with different characteristics [40, 41], and for this reason should be considered separately. For each plant part, there is a specific phytochemical profile with different composition or concentration according to the needs of each organ, and the type of biotic or abiotic stress to which a plant may be subjected.

9.3.1 Current Trends

Green synthesis using plants consists of a contemporary nanobiotechnology field that can help researchers studying MNPs understand the molecular mechanisms orchestrating bioreduction, nucleation, growth, and stabilization. Researchers first attempts were based on the utilization of plant extracts selected empirically from the endemic or global biodiversity. In those studies, MNPs were synthesized using extracts from different plant species and parts in the presence of metal salts and producing structures with different compositions, shapes, sizes, and activities (Fig. 9.2). Several studies describing green synthesis of MNPs using plants were based on the reduction of noble metals [3, 26, 27, 42, 43], including gold (Au), silver (Ag), platinum (Pt), and copper (Cu). The MNPs shape usually observed in the green synthesis using plants are spheres [3, 44–46] and triangles [45, 47]. The size of the greenly synthesized MNPs is commonly in the range of 15–50 nm of hydrodynamic diameter [48]. Among the biological activities of MNPs obtained by green synthesis using plants include antibacterial [49, 50], antifungal [3], anticancer [51], larvicidal [52], among others.

Leaves' extract is the most common choice for performing green synthesis of MNPs from plant organs, but the application of seed, bark, flower, fruit, tuber, and

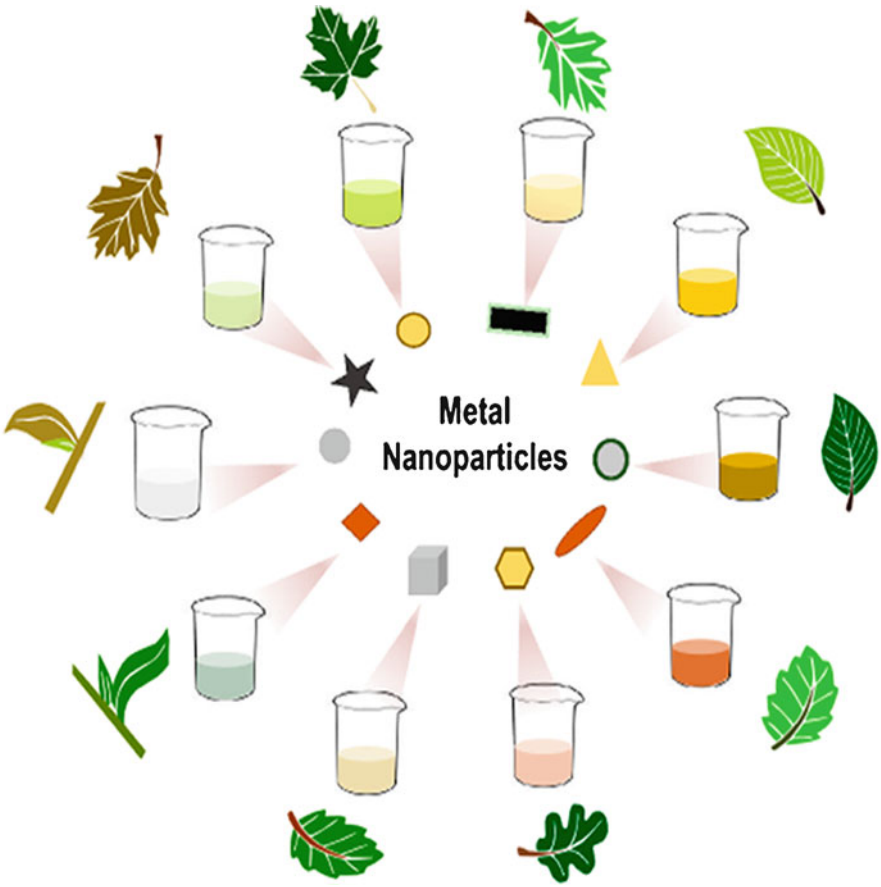

Fig. 9.2 Green synthesis of metal nanoparticles using extracts obtained from leaves of different plant species leading to the production of structures with different compositions, shapes, and sizes

root extracts has also been reported [26]. Leaves are commonly the major source of metabolites aiming the green synthesis of MNPs due to the fact that they are renewable, non-destructive, and abundant, unlike other plant tissues. Therefore, the parent material (plant part), in association with the season or the place of collection of a plant organ as well as the presence of abiotic (cold, water, presence of metals, or pesticides) or biotic (presence of pests or pathogens) stressor agents may have major influence on the synthesis and characteristics of the MNPs. Surprisingly, almost all these plant features are solely neglected in almost all experimental designs in spite of the fact that they would be crucial for reproducibility and scaling-up of MNPs production.

Moreover, besides the variety of nanoscale features obtained by MNPs synthesized using different plant extracts, researchers can alter a number of other synthesis conditions. Reaction time [53, 54], concentration of extracts [45, 55] and/or metal

ions [53–55], temperature [3, 42, 54, 55], and pH [53–56] are some of the tunable parameters which help researchers to optimize the efficiency and speed of the green synthesis of MNPs even resembling the typical features of conventional chemical synthesis. Therefore, it is worth mentioning the importance of variation of the synthesis parameters for obtaining MNPs with the desired characteristics. In addition, they also provide insight into formation mechanisms of the MNPs [49, 50, 57].

Green synthesis of MNPs can also occur with the plant in vivo [58, 59]. It is documented that plants respond to the stress generated by the presence of metals by a process of binding and complexation with phytochelatins and secondary metabolites [60–63]. However, this process is slower and has a higher cost than exploit plant extracts when performing the synthesis of MNPs.

9.3.2 Challenges in Green Synthesis of MNPs by Plants

9.3.2.1 Reproducibility

Achieving high reproducibility is a challenging component of the green synthesis of MNPs using plants. In the course of the solar year, the plants are under a variety of environmental pressures including water stress [28], lack [28] or excess [64] of essential nutrients, changes in the soil pH [65], herbivores and parasites attack [30], competition among species [66], excess [67] or lack [68] of light exposure, among others. Beyond the environmental pressures there is also the incidental (e.g., pollution) and intentional (e.g., use of herbicides and pesticides) anthropic actions [69]. In response to those stimuli the plant metabolism is altered to propitiate improved conditions for the survival of the plant, maximizing its fitness [70]. For this reason, the production of primary and secondary metabolites is upregulated or downregulated according to the stimulus [71].

Moreover, the age of a plant organ (e.g., young or senescent leaves) also may influence in the concentration and presence of metabolites (Fig. 9.3). The genetic background of the plant material is another factor that should be considered during the selection of a candidate but it has been absolutely neglected during the green synthesis of MNPs. This plant physiology scenario ends up leaving the extract with a different final composition, depending on each season or stimulus suffered by the plant.

The metabolites found in a plant are the reducing agents and stabilizers used for the green synthesis of MNPs using plants [27, 34, 72]. If the composition and\or the concentration of the metabolites in a plant extract are different, distinct profiles of MNPs will be formed in the synthesis. Therefore, the care with the season in which the biological material was collected is an essential requirement aiming the reproducibility of the synthesis. Several studies do not pay any attention to reporting the period of the year in which the plant material for the MNPs synthesis was collected,

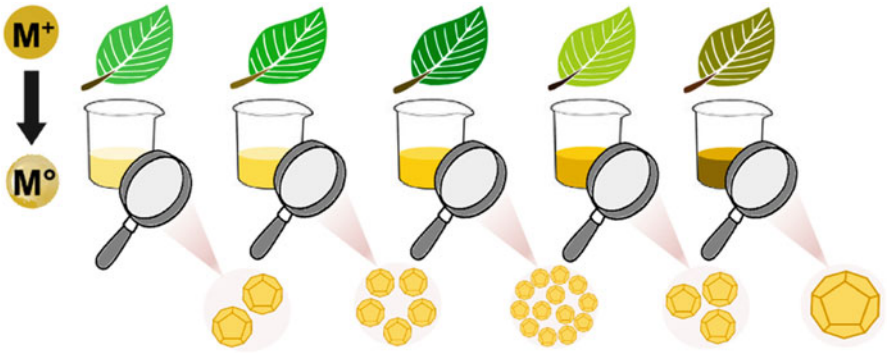

Fig. 9.3 Different metabolic states/ages of leaves from a same plant species when used in the green synthesis of metal nanoparticles and may lead to the formation of structures with different sizes and thereby interfering in the reproducibility of the reactions

describing the conditions of growth wherein the plant was cultivated or collected, and quantifying the major metabolites present in the extract. All those information must be considered essential for the reproducibility of the process and to understand the mechanisms culminating in the formation of MNPs.

After the elucidation of the molecular mechanisms underlying the formation of MNPs, researchers could select plants that contain high concentration of the structuring agents and even combine two or more plant extracts with additive or complementary properties. In this case, plants can also be cultivated and multiplied in greenhouses with biotic and abiotic factors strictly controlled, under stress-regulated conditions, aiming the production of metabolites with key roles in the synthesis of MNPs. Another approach aiming the controlled production of metabolites that remains unexplored would be the use of tissue culturing techniques. Plant tissues cultured in vitro are not only ecologically viable, but also allow higher yields, hence lowering the need for seeding and cropping [73]. This is a facile and rapid model to obtain the molecules responsible for the reduction of the metallic ions with no need to wait for the growth of the plant and the synthesis and accumulation of the metabolites by the plant organs (e.g., leaves). If using this method, the key metabolites could be directly secreted in the growth medium, providing a controlled production of those molecules that could be involved in the green synthesis of MNPs.

It is also possible to obtain plants as bioreactors for production of pre-selected molecules through metabolic pathways engineering [73–75] and these genetically modified organisms (GMOs) could be used for the green synthesis of MNPs. Therefore, by integrating synthetic biology approaches based on GMOs with green nanotechnology, the fine tuning of the molecular components guiding the MNPs assembly and structure will be possible.

9.3.2.2 Scale-Up

The scale-up is probably one of the challenging steps involved in the production of nanostructures [45]. The challenges of scaling up the MNPs' green synthesis using plants include the low abundance of raw materials (e.g., non-cultivated plants), lack of appropriate equipment to render the necessary amounts, difficulty to control the molecular composition, and the heterogeneity of plant extracts.

The extraction of the metabolites which will form a plant extract should be done in the same conditions for all the plants under comparison or a batch of the plant material in order to obtain a considerable homogeneity. However, it would not be surprising if a plant species previously identified as a potent green synthesis driver could be further considered inexpressive or vice versa due to the presence of enhancers or inhibitors. Any modification on the metabolites production and extraction method could yield molecules that would not be necessarily the same with the best performance in green synthesis of MNPs. If the molecules present in an extract are obtained directly from non-cultivated plants in order to obtain large amounts of plant biomass it would be expected dramatic differences in metabolic profile among different batches that finally could produce MNPs with distinct physicochemical characteristics. This fact occurs since each harvest cycle would expose the plant to different stress profiles. In order to avoid or at least minimize such limitations, the metabolites extraction aiming green synthesis of MNPs should be done in each cycle with plants grown under similar conditions, which could let the processes impracticable due to the growth time and the fact that a number of species do not grow easily under controlled conditions.

The use of plant tissue cultures is probably a first-class choice to the large scale production of MNPs, since this method offers independent and uniform biochemical products. The biotic and abiotic elements that directly influence the production of metabolites can be strictly controlled in vitro, including pathogens, temperature, humidity, and some chemicals products that can mimic the interaction with other living organisms and the environment. The plant tissues cultivation is simpler than plant crops since it does not depends on the climatic conditions, soil, and others regional characteristics. The reproducibility and productivity of a plant tissue cultured in vitro under strictly controlled conditions can always be close to the theoretical maximum due to the tuning of the reaction medium and has an excellent yield since they are commonly faster and more efficient in extracting primary and secondary metabolites from plant tissue cultures than the entire plants. Unfortunately, there are plant metabolites which are only produced by specific organs of whole plants or present in a preferential site of bioaccumulation and lack the ability to accumulate in dedifferentiated cells, similar to those from explants [74].

In addition to homogenization of the metabolites profile, the application of automated synthesis reactors with volumes from few milliliters to several liters which are based on batch and flow processes can lead to rapid, scalable and reproducible large scale synthesis of MNPs using plant extracts (Fig. 9.4). However, there are only few commercial instruments available which are applicable or at least adaptable to the synthesis of MNPs under controlled conditions and novel developments are expected in the coming years. Forthcoming instruments will revolutionize the means by which manufacturers produce MNPs.

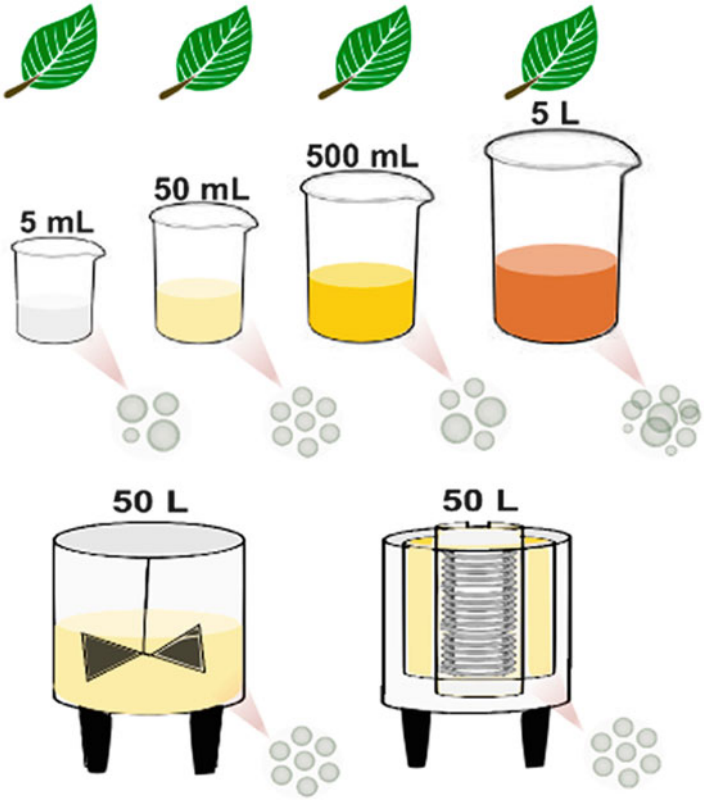

Fig. 9.4 Scale-up of the green synthesis of metal nanoparticles using plant leaves of a same species. There are dramatic differences on reproducibility of the produced structures using reservoirs with different volume capacity (5 mL–5 L). The use of reactors (batch or flow) can produce higher amounts (up to 50 L) and standardize the shape and size of the synthesized structures

9.3.2.3 Predictability

Predictability of nanostructures formation and activity represents a recent trend in nanotechnology [76]. One option is to perform a high-throughput screening to identify novel species that enable green synthesis of MNPs, characterize the synthesized nanostructures from physical, chemical, and biological viewpoints, and compile such metadata into easily manageable databases. Thus, these data would be useful to translate into benefits in terms of the development of simulators based on mathematical modeling of nanoscale phenomena. The utilization of simulations to predict the factors critically influencing the process of green synthesis of MNPs by plants has potential to revolutionize the way by which researchers design, conceive, and perform their experiments. Therefore, it makes sense to replace the empirical process by the use of mathematical modeling and computer-aided design (Fig. 9.5). The next few years will demonstrate whether or not simulators will have a feasible application in the green synthesis of MNPs.

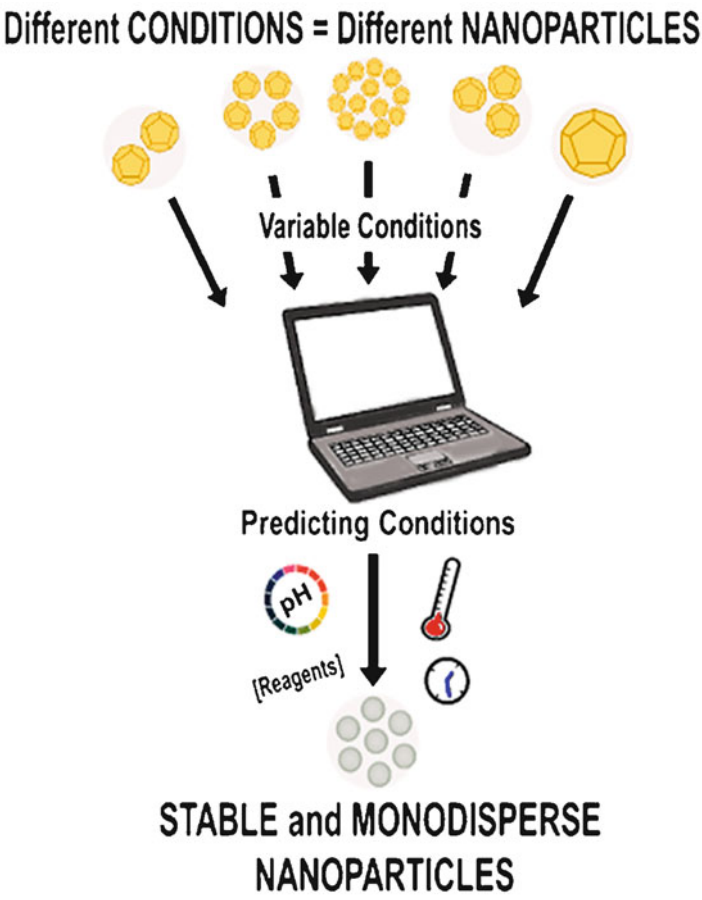

Fig. 9.5 Schematic illustration of the use of mathematical modeling and rational experimental design by computer-assisted predictability of the synthesis routes of metal nanoparticles using plants aiming higher homogeneity and reproducibility of the reactions

9.3.3 Challenges for Applicability of MNPs Obtained by Green Synthesis Using Plants

9.3.3.1 Risk Assessment and Risk Management

Taking into account the increased interest and development of nanomaterials in recent years, emerges a field of the nanotechnology research, termed nanotoxicology, whose foremost focus is to evaluate the interactions between the nanomaterials and the three domains of living organisms, and environment [77, 78]. Thus, there is an absolutely urgent need for policies to regulate the safe use of nanomaterials,

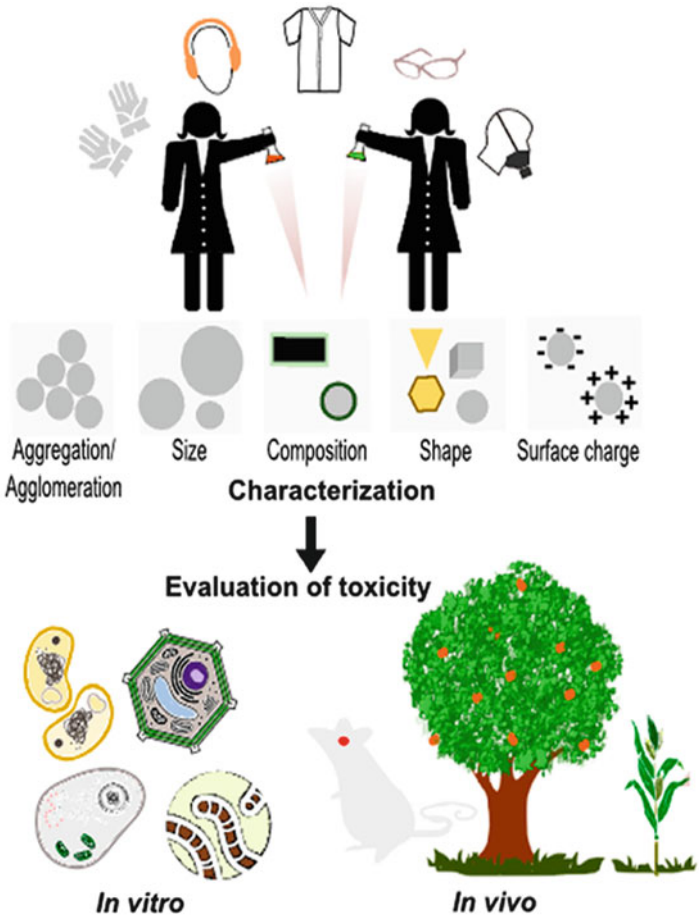

Fig. 9.6 Schematic illustration of the personal protective equipments that are commonly recommended for nanotechnology workers to reduce the risks of exposition to nanomaterials with different physical and chemical characteristics. In addition, the safety potential of the nanomaterials, including metal nanoparticles, must be assessed by in vitro and in vivo assays

including MNPs synthesized by green chemistry approaches. This need is related to the minimization of exposure of the researchers, workers, and consumers, as well as the environment to potentially hazardous nanosystems (Fig. 9.6).

The steps which can be considered as essentials in the process of understanding these questions include: firstly, it is necessary to define the applicability of a nanomaterial; secondly, it is necessary to identify the physicochemical properties of the nanomaterial (e.g., mean size and size distribution, shape, charge, chemical composition, potential for agglomeration/aggregation, crystallinity, solubility, density, stability, porosity, and surface area); thirdly, it is necessary to determine the mechanism(s) of interaction between the nanomaterial and living systems at

molecular, cellular, tissue, systemic, and ecosystems levels using in silico, in vitro, and in vivo assays (Fig. 9.6); and lastly, the critical training of the population towards the understanding of regulatory issues related to the use of nanoparticles and nanostructured materials is necessary.

An adequate characterization is necessary in order to minimize the possibilities of leading to an incorrect result. The most used parameter is the size, but it alone does not provide sufficient information to forecast the possible interactions between the MNPs and the biological medium [79]. The surface charge and the agglomeration/aggregation range of the MNPs can also indicate in which conditions could the adsorption of metabolites (e.g., proteins) or interaction with others components present in the organism or environment, like ions and others dispersed solutes, occur [80]. The absorption peak associated with the surface plasmon resonance of the MNPs can exclude multiple tests that use the same wavelength range of absorption to quantify the activity [26].

Beyond the interaction between the nanomaterial and the compounds available in the system, the dose and the knowledge of the mechanism of action are fundamental to predict the nanotoxicity and consequently the therapeutic range to the MNPs produced using plants. Unfortunately, the separation of the toxicity from the therapeutic use is not a trivial challenge. Determining the dose is a key point to separate the toxicity from the therapeutic range [81]; oftentimes an excessive concentration of MNPs is applied in the biological assays due the difficulty to quantify the correct dose, which leads to a widespread toxicity caused by the nanoparticles and not a treatment as expected.

In the current global scenario, it is clear that there is the need for improvement and development of conceptual, experimental, and computational methodologies that could be considered standards to interpret and understand the majority of the trusted and reliable data on the physical, chemical, biological, and toxicological interactions of MNPs [82].

9.3.3.2 Regulatory Challenges

Currently, for almost all the countries neither chemically nor greenly synthesized MNPs have been subject to special regulations regarding production, handling, storage, or disposal [83]. Currently, the managing risk is determined for the bulk materials rather than describe the potential impacts from the nanostructuring [84]. Regulatory bodies are starting to devote additional attention to nano-objects, including MNPs, but their discussions are far to compare and mainly differentiate MNPs produced by classical chemistry and green chemistry syntheses (Fig. 9.7). The forthcoming years will be essential to define the standards to be used by the regulatory agencies, but regardless of anything, a factor that should be considered is that green synthesis methods are not only much less toxic and environment friendly but also cost-effective, rapid, and simple to perform.

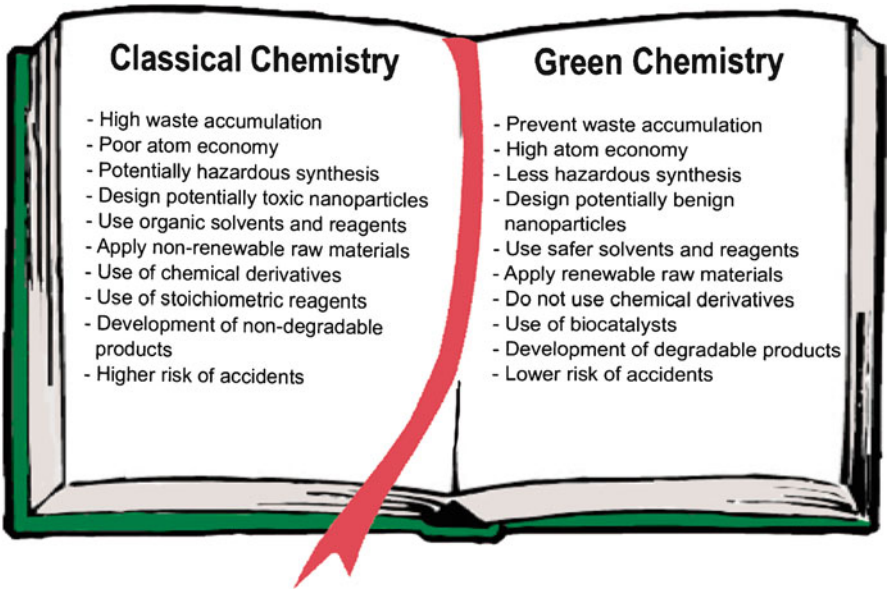

Fig. 9.7 Comparison of the principles and consequences of classical chemistry and green chemistry aiming the development of metal nanoparticles

9.4 Conclusion

This chapter covers several concerns and trends that should be kept in mind when performing green synthesis of MNPs using plants. It is possible that the challenges addressed in this chapter may not be resolved by any single researcher or even a team of researchers. In order to increase the confidence of the green synthesis of MNPs by plants, some paradigm shift must take place. Firstly, researchers have to understand the mechanisms underlying the bioreduction, nucleation, growth, and stabilization of MNPs using plants and accept that this task could not be satisfactorily accomplished without a consideration of the phenomenon as whole and including all related variables. Secondly, they should prospect innovative solutions for current and future challenges towards the reliable and efficient use of MNPs synthesized using plants. Finally, researchers must prove that green synthesis of MNPs using plants is predictable, reproducible, scalable, and safe to be used on multiple threads.

References

1. Hutchison JE (2008) Greener nanoscience: a proactive approach to advancing applications and reducing implications of nanotechnology. ACS Nano 2(3):395–402. doi:10.1021/nn800131j
2. Dahl JA, Maddux BLS, Hutchison JE (2007) Toward greener nanosynthesis. Chem Rev 107(6):2228–2269. doi:10.1021/cr050943k

3. Bonatto CC, Silva LP (2014) Higher temperatures speed up the growth and control the size and optoelectrical properties of silver nanoparticles greenly synthesized by cashew nutshells. Ind Crop Prod 58:46–54. doi:10.1016/j.indcrop.2014.04.007
4. Quester K, Avalos-Borja M, Vilchis-Nestor A et al (2013) SERS properties of different sized and shaped gold nanoparticles biosynthesized under different environmental conditions by Neurospora crassa extract. PLoS One 8(10):1–8. doi:10.1371/journal.pone.0077486
5. Yehia M, Labib S, Ismail SM (2014) Structural and magnetic properties of nano-NiFe2O4 prepared using green nanotechnology. Physica B Condens Matter 446:49–54. doi:10.1016/j.physb.2014.04.032
6. Sharma VK, Yngard RA, Lin Y (2009) Silver nanoparticles: green synthesis and their antimicrobial activities. Adv Colloid Interface Sci 145(1–2):83–96. doi:10.1016/j.cis.2008.09.002
7. Nadagouda MN, Varma RS (2009) Risk reduction via greener synthesis of noble metal nanostructures and nanocomposites. Nato Sci Peace Secur 3:209–217. doi:10.1007/978-1-4020-9491-0_15
8. Raveendran P, Fu J, Wallen SL (2003) Completely "Green" synthesis and stabilization of metal nanoparticles. J Am Chem Soc 125(46):13940–13941. doi:10.1021/ja029267j
9. Murphy CJ, Sau TK, Gole AM et al (2005) Anisotropic metal nanoparticles: synthesis, assembly, and optical applications. J Phys Chem B 109(29):13857–13870. doi:10.1021/jp0516846
10. Narayanan R, El-Sayed MA (2005) Catalysis with transition metal nanoparticles in colloidal solution: nanoparticle shape dependence and stability. J Phys Chem B 109(26):12663–12676. doi:10.1021/jp051066p
11. McBrain SC, Yiu HHP, Dobson J (2008) Magnetic nanoparticles for gene and drug delivery. Int J Nanomedicine 3(2):169–180
12. Liao H, Nehl CL, Hafner JH (2006) Biomedical applications of plasmon resonant metal nanoparticles. Nanomedicine 1(2):201–208. doi:10.2217/17435889.1.2.201
13. Llorens A, Lloret E, Picouet PA et al (2012) Metallic-based micro and nanocomposites in food contact materials and active food packaging. Trends Food Sci Tech 24(1):19–29. doi:10.1016/j.tifs.2011.10.001
14. Lazarides AA, Kelly KL, Jesen TR et al (2000) Optical properties of metal nanoparticles and nanoparticle aggregates important in biosensors. J Mol Struct Theochem 529(1–3):59–63. doi:10.1016/S0166-1280(00)00532-7
15. Rai M, Yadav A, Gade A (2009) Silver nanoparticles as a new generation of antimicrobials. Biotechnol Adv 27:76–83. doi:10.1016/j.biotechadv.2008.09.002
16. Wiederrecht GP, Wurtz GA, Hranisavljevic J (2004) Coherent coupling of molecular excitons to electronic polarizations of noble metal nanoparticles. Nano Lett 4(11):2121–2125. doi:10.1021/nl0488228
17. Bystrzejewska-Piotrowska G, Golimowski J, Urbana PL (2009) Nanoparticles: their potential toxicity, waste and environmental management. Waste Manage 29(9):2587–2595. doi:10.1016/j.wasman.2009.04.001
18. Gericke M, Pinches A (2006) Biological synthesis of metal nanoparticles. Hydrometallurgy 83(1–4):132–140. doi:10.1016/j.hydromet.2006.03.019
19. Lenerdão EJ, Freitag RA, Batista MJD et al (2003) Green chemistry - the 12 principles of green chemistry and it insertion in the teach and research activities. Quim Nova 26(1):123–129
20. Tang SY, Bourne RA, Smith RL et al (2008) The 24 principles of green engineering and green chemistry: "Improvements productively". Green Chem 10:268–269. doi:10.1039/B719469M
21. Anastas P, Eghbali N (2009) Green chemistry: principles and practice. Chem Soc Rev 39:301–312. doi:10.1039/B918763B
22. Rajawat S, Qureshi MS (2014) Electrolytic deposition of silver nanoparticles under "Principles of Green Chemistry". Arab J Sci Eng 39:563–568. doi:10.1007/s13369-013-0879-4
23. Srivastava P, Bragança J, Ramanan SR et al (2013) Synthesis of silver nanoparticles using haloarchaeal isolate Halococcus salifodinae BK3. Extremophiles 17(5):821–831. doi:10.1007/s00792-013-0563-3

24. El-Said WA, Cho H, Yea C et al (2014) Synthesis of metal nanoparticles inside living human cells based on the intracellular formation process. Adv Mater Interfaces 26(6):910–918. doi:10.1002/adma.201303699
25. Senapati S, Ahmad A, Khan MI et al (2005) Extracellular biosynthesis of bimetallic Au-Ag alloy nanoparticles. Small 1(5):517–520. doi:10.1002/smll.200400053
26. Iravani S (2011) Green synthesis of metal nanoparticles using plants. Green Chem 13:2638–2650. doi:10.1039/C1GC15386B
27. Kumar V, Yadav SK (2009) Plant-mediated synthesis of silver and gold nanoparticles and their applications. J Chem Technol Biotechnol 84(2):151–157. doi:10.1002/jctb.2023
28. Jha AK, Prasad AKJ, Prasad K et al (2009) Plant system: nature's nanofactory. Colloids Surf B Biointerfaces 73:219–223. doi:10.1016/j.colsurfb.2009.05.018
29. Shao Y, Jin Y, Dong S (2004) Synthesis of gold nanoplates by aspartate reduction of gold chloride. Chem Commun 9:1104–1105. doi:10.1039/B315732F
30. Shankar SS, Ahmad A, Pasricha S (2003) Bioreduction of chloroaurate ions by geranium leaves and its endophytic fungus yields gold nanoparticles of different shapes. J Mater Chem 13:1822–1826. doi:10.1039/B303808B
31. Sivaraman SK, Elango I, Kumar S et al (2009) A green protocol for room temperature synthesis of silver nanoparticles in seconds. Curr Sci 97(7):1055–1059
32. Thakkar NK, Mhatre SS, Parikh RY (2010) Biological synthesis of metallic nanoparticles. Nanomedicine 6(2):257–262. doi:10.1016/j.nano.2009.07.002
33. Huang J, Chen C, He N et al (2007) Biosynthesis of silver and gold nanoparticles by novel sundried Cinnamomum camphora leaf. Nanotechnology 18:105–106. doi:10.1088/0957-4484/18/10/105104
34. Narayanan KB, Sakthivel N (2011) Green synthesis of biogenic metal nanoparticles by terrestrial and aquatic phototrophic and heterotrophic eukaryotes and biocompatible agents. Adv Colloid Interface Sci 169(2):59–79. doi:10.1016/j.cis.2011.08.004
35. Tan YN, Lee JY, Wang DI (2010) Uncovering the design rules for peptide synthesis of metal nanoparticles. J Am Chem Soc 132(16):5677–5686. doi:10.1021/ja907454f
36. Park Y, Hong YN, Weyers A et al (2011) Polysaccharides and phytochemicals: a natural reservoir for the green synthesis of gold and silver nanoparticles. IET Nanobiotechnol 5(3):69–78. doi:10.1049/iet-nbt.2010.0033
37. Arunachalam KD, Annamalai SK, Hari S (2013) One-step green synthesis and characterization of leaf extract-mediated biocompatible silver and gold nanoparticles from Memecylon umbellatum. Int J Nanomedicine 8:1307–1315, http://dx.doi.org/10.2147/IJN.S36670
38. Huang X, Wu H, Pu S et al (2011) One-step room-temperature synthesis of Au@Pd core-shell nanoparticles with tunable structure using plant tannin as reductant and stabilizer. Green Chem 13:950–957. doi:10.1039/c0gc00724b
39. Marchiol L (2012) Synthesis of metal nanoparticles in living plants. IJA 7(37):274–282
40. Rai M, Yadav A, Gade A (2008) CRC 675 - current trends in phytosynthesis of metal nanoparticles. Crit Rev Biotechnol 28(4):277–284
41. Kharissova OV, Dias HVR, Kharisov BI et al (2013) The greener synthesis of nanoparticles. Trends Biotechnol 31(4):240–248. doi:10.1016/j.tibtech.2013.01.003
42. Song JY, Kim BS (2009) Rapid biological synthesis of silver nanoparticles using plant leaf extracts. Bioprocess Biosyst Eng 32:79–84. doi:10.1007/s00449-008-0224-6
43. Vinod VT, Saravanan P, Sreedhar B et al (2011) A facile synthesis and characterization of Ag, Au and Pt nanoparticles using a natural hydrocolloid gum kondagogu (Cochlospermum gossypium). Colloids Surf B Biointerfaces 83(2):291–298. doi:10.1016/j.colsurfb.2010.11.035
44. Bar H, Bhui DK, Sahoo GP et al (2009) Green synthesis of silver nanoparticles using latex of Jatropha curcas. Colloids Surf A Physicochem Eng Asp 339(1–3):134–139. doi:10.1016/j.colsurfa.2009.02.008
45. Smitha SL, Philip D, Gopchandran KG (2009) Green synthesis of gold nanoparticles using Cinnamomum zeylanicum leaf broth. Spectrochim Acta A Mol Biomol Spectrosc 74(3):735–739. doi:10.1016/j.saa.2009.08.007

46. Philip D (2010) Rapid green synthesis of spherical gold nanoparticles using Mangifera indica leaf. Spectrochim Acta Mol Biomol 77(4):807–810. doi:10.1016/j.saa.2010.08.008
47. Chandran SP, Chaudhary M, Pasricha R et al (2006) Synthesis of gold nanotriangles and silver nanoparticles using Aloe vera plant extract. Biotechnol Prog 22:577–583. doi:10.1021/bp0501423
48. Veeraputhiran V (2013) Bio-catalytic synthesis of silver nanoparticles. Int J Chem Tech Res 5(5):2555–2562
49. Singh A, Jain D, Upadhyay MK et al (2010) Green synthesis of silver nanoparticles using Argemone mexicana leaf extract and evaluation of their antimicrobial activities. Dig J Nanomater Bios 5(2):483–489
50. Singh AK, Talat M, Singh DP et al (2010) Biosynthesis of gold and silver nanoparticles by natural precursor clove and their functionalization with amine group. J Nanopart Res 12: 1667–1675. doi:10.1007/s11051-009-9835-3
51. Mollick MMR, Bhowmick B, Mondal D et al (2014) Anticancer (in vitro) and antimicrobial effect of gold nanoparticles synthesized using Abelmoschus esculentus (L.) pulp extract via a green route. RSC Adv 4:37838–37848. doi:10.1039/C4RA07285E
52. Borase HP, Patil CD, Salunkhe RB et al (2014) Mosquito larvicidal and silver nanoparticles synthesis potential of plant latex. J Entomol Acarol Res 46(2):59–65, http://dx.doi.org/10.4081/jear.2014.1920
53. Philip D (2010) Green synthesis of gold and silver nanoparticles using Hibiscus rosa sinensis. Physica E Low Dimens Syst Nanostruct 42(5):1417–1424. doi:10.1016/j.physe.2009.11.081
54. Dubey SP, Lahtinen M, Sillanpää M (2010) Tansy fruit mediated greener synthesis of silver and gold nanoparticles. Process Biochem 45(7):1065–1071. doi:10.1016/j.procbio.2010.03.024
55. Dwivedi AD, Gopal K (2010) Biosynthesis of silver and gold nanoparticles using Chenopodium album leaf extract. Colloids Surf A Physicochem Eng Asp 369(1–3):27–33. doi:10.1016/j.colsurfa.2010.07.020
56. Armendariz V, Herrera I, Jose-yacaman M et al (2004) Size controlled gold nanoparticle formation by Avena sativa biomass: use of plants in nanobiotechnology. J Nanopart Res 6(4):377–382
57. Sau TK, Murphy CJ (2004) Room temperature, high-yield synthesis of multiple shapes of gold nanoparticles in aqueous solution. J Am Chem Soc 126(28):8648–8649. doi:10.1021/ja047846d
58. Harris AT, Bali R (2008) On the formation and extent of uptake of silver nanoparticles by live plants. J Nanopart Res 10:691–695. doi:10.1007/s11051-007-9288-5
59. Marchiol L, Mattiello A, Poscic F et al (2014) In vivo synthesis of nanomaterials in plants: location of silver nanoparticles and plant metabolism. Nanoscale Res Lett 9:101. doi:10.1186/1556-276X-9-101
60. Zenk MH (1996) Heavy metal detoxification in higher plants-a review. Gene 179(1):21–30. doi:10.1016/S0378-1119(96)00422-2
61. Cobbett CS (2000) Phytochelatin biosynthesis and function in heavy-metal detoxification. Curr Opin Plant Biol 3(3):211–216. doi:10.1016/S1369-5266(00)80067-9
62. Yadav SK (2010) Heavy metals toxicity in plants: an overview on the role of glutathione and phytochelatins in heavy metal stress tolerance of plants. S Afr J Bot 76(2):167–179. doi:10.1016/j.sajb.2009.10.007
63. Rascio N, Navari-Izzo F (2011) Heavy metal hyperaccumulating plants: how and why do they do it? And what makes them so interesting? Plant Sci 180(2):169–181. doi:10.1016/j.plantsci.2010.08.016
64. Lisar SYS, Motafakkerazad R, Hossain MM et al (2012) Water stress. In: Rahman IMM (ed) Water stress in plants: causes, effects and responses. Intech, Croatia, pp 1–14
65. Wang W, Vinocur B, Altman A (2003) Plant responses to drought, salinity and extreme temperatures: towards genetic engineering for stress tolerance. Planta 218(1):1–14
66. Wardle DA, Nilsson MC, Gallet C et al (1998) An ecosystem-level perspective of allelopathy. Biol Rev 73(3):305–319. doi:10.1111/j.1469-185X.1998.tb00033.x

67. Demming-Adams B, Adams WW (1992) Photoprotection and other responses of plants to high light stress. Annu Rev Plant Physiol Plant Mol Biol 43:599–626
68. Ruban AV (2009) Plants in light. Commun Integr Biol 2(1):50–55
69. Schwitzguébel JP (2001) Hype or hope: the potential of phytoremediation as an emerging green technology. Remed J 11(4):63–78. doi:10.1002/rem.1015
70. Wang WX, Vinocur B, Shoseyov O et al (2000) Biotechnology of plant osmotic stress tolerance physiological and molecular considerations. Acta Hort 560:285–292, Paper presented at the IV International symposium on in vitro culture and horticultural breeding
71. Cheong YH, Chang HS, Gupta R et al (2002) Transcriptional profiling reveals novel interactions between wounding, pathogen, abiotic stress, and hormonal responses in Arabidopsis. Plant Physiol 129(2):661–677, http://dx.doi.org/10.1104/pp.002857
72. Mittal AK, Chisti Y, Banerjee UC (2013) Synthesis of metallic nanoparticles using plant extracts. Biotechnol Adv 31(2):346–356. doi:10.1016/j.biotechadv.2013.01.003
73. Rao SR, Ravishankar GA (2002) Plant cell cultures: chemical factories of secondary metabolites. Biotechnol Adv 20(2):101–153. doi:10.1016/j.biotechadv.2008.09.002
74. Hussain MS, Fareed S, Ansari S et al (2012) Current approaches towards production of secondary plant metabolites. J Pharm Bioallied Sci 4(1):10–20. doi:10.4103/0975-7406.92725
75. Verpoorte R, Van Der Heijden R, Ten HJG et al (1999) Metabolic engineering of plant secondary metabolite pathways for the production of fine chemicals. Biotechnol Lett 21(6):467–479. doi:10.1023/A:1005502632053
76. Viswanath B, Kundu P, Mukherjee B et al (2008) Predicting the growth of two-dimensional nanostructures. Nanotechnology 19(19):195603–195610. doi:10.1088/0957-4484/19/19/195603
77. Oberdörster G (2009) Safety assessment for nanotechnology and nanomedicine: concepts of nanotoxicology. J Int Med 267:89–105. doi:10.1111/j.1365-2796.2009.02187.x
78. Oberdörster G, Oberdörster E, Oberdörster J (2005) Nanotoxicology: an emerging discipline evolving from studies of ultrafine particles. Environ Health Perspect 113(7):823–839
79. Karlsson HL, Gustafsson J, Cronholm P et al (2009) Size-dependent toxicity of metal oxide particles - a comparison between nano- and micrometer size. Toxicol Lett 188(2):112–118. doi:10.1016/j.toxlet.2009.03.014
80. Kroll A, Pillukat MH, Hahn D et al (2009) Current in vitro methods in nanoparticle risk assessment: limitations and challenges. Eur J Pharm Biopharm 72(2):370–377. doi:10.1016/j.ejpb.2008.08.009
81. Elsaesser A, Howard CV (2012) Toxicology of nanoparticles. Adv Drug Deliver Rev 64:129–137. doi:10.1016/j.addr.2011.09.001
82. Puzyn T, Rasulev B, Gajewicz A et al (2011) Using nano-QSAR to predict the cytotoxicity of metal oxide nanoparticles. Nat Nanotech 6:138–139. doi:10.1038/nnano.2011.10
83. Seaton A, Tran L, Aitken R et al (2009) Nanoparticles, human health hazard and regulation. J R Soc Interface 10:1–11. doi:10.1098/rsif.2009.0252.focus
84. Auffan M, Rose J, Bottero J et al (2009) Towards a definition of inorganic nanoparticles from an environmental, health and safety perspective. Nat Nanotechnol 4:634–641. doi:10.1038/nnano.2009.242

Chapter 10
Biomimetic Soft Polymer Nanomaterials for Efficient Chemical Processes

Matt McTaggart, Manish Jugroot, and Cecile Malardier-Jugroot

Abstract Nanostructured soft materials combine structure and function to produce effects inspired by natural systems. Recent innovations in polymer science and supramolecular chemistry have led to the development of materials that can respond to and control their microenvironment, allowing them to increase the efficiency of chemical processes while decreasing their ecological impact. Size effects are profound at the nanoscale, allowing for a broad range of applications. This chapter features synthetic biomimetic nanosystems at different size regimes and match them with biological counterparts from tissues through cell walls to vesicles and proteins. The application of soft, bioinspired nanomaterials in fields ranging from medicine to sustainable energy represents a fundamental advancement in science and technology.

10.1 Introduction

Nearly every biological process depends on soft, self-assembling nanostructures that sense or alter the local environment to ensure efficient and selective action. Living organisms routinely produce highly structured macromolecules to accomplish functions that humanity performs through industry: energy collection, fuel production and storage, material transport, and detoxification of waste products among them [1]. Soft matter in nature, ranging from tissues through cellular membranes to proteins, is therefore an obvious source of inspiration for addressing the technological challenges that arise as we seek to improve the efficiency of industrial processes. Although the effectiveness of natural materials has long been recognized, it is only in recent decades that we have developed the methods needed to measure

M. McTaggart • C. Malardier-Jugroot (✉)
Department of Chemistry and Chemical Engineering, Royal Military College of Canada, Kingston, ON, Canada K7K7B4
e-mail: Cecile.Malardier-Jugroot@rmc.ca

M. Jugroot
Department of Mechanical Engineering, Royal Military College of Canada, Kingston, ON, Canada K7K7B4

V.A. Basiuk, E.V. Basiuk (eds.), *Green Processes for Nanotechnology*,
DOI 10.1007/978-3-319-15461-9_10

their structure and dynamics or indeed to begin to reproduce them synthetically [2]. Biomimicry, whether by adapting natural molecules to new purposes or by recreating the chemical and physical properties of biological systems in new materials, is an emerging area in material science [3]. Biomimetic soft materials represent a fundamental advancement in fields as far reaching as medicine, energy, and chemical catalysis towards efficient and environmentally friendly processes.

Because of their simple synthesis, low cost, tunable mechanical properties, and generally inert reactivity, polymers are ubiquitous as macroscopic structures, but lately new nanoscale structural and functional properties have been discovered [4]. Conductive polymers permit electrochemical processes to occur in disperse networks free from metals [5], both important considerations for maximizing efficiency and minimizing toxicity [6]. Copolymer arrangements of charged, hydrophobic, or hydrogen-bonding monomers interact in solution to produce specific effects similar to those of proteins—complex natural polymers of amino acids. Like their biological counterparts, the conformation of synthetic polymers containing surface active groups can be very sensitive to changes in the physical environment [7]. Polymers can be finely tuned to adsorb or shed solvent molecules through changes in temperature or light, to alter electrostatic bonds by changes to ionic strength, and to change conformation of weak acid or base containing polymers in relation to pH [8]. Both naturally occurring and synthetic soft nanomaterials can produce very precise nanoarchitectures through the self-assembly of small molecules [9]. Amphiphilic surfactants may be similarly used to build micelles of varying shapes from tens to hundreds of nanometers in radius through a process that mimics self-assembly of the lipid bilayer that composes cellular membranes [10].

It is obvious to say but bears mentioning that the size of individual components, as well as their proportional contributions, becomes increasingly important as the size of the system decreases. At the microscale, materials in applications such as tissue scaffolding and sensing actuators may express dramatic statistical effects on the performance of the system by the random inclusion of a small percentage of functional polymer fibres. Systems in the 10–100 nm size regime, such as selective membranes and encapsulating reaction vessels, contain highly organized functional elements and have precisely determined functions. With dimensions less than 10 nm, self-assembling materials composed of single molecules or supramolecular structures can produce emergent properties that mimic functional proteins or enzymes. This review surveys applications in each of these three size regimes to illustrate the advantages of using soft nanomaterials to sense and alter their local chemical and physical environment to improve the efficiency and sustainability of processes.

10.2 Structures from 100 to 1,000 nm

Nanostructured materials near the micrometre range are able to influence or respond to environmental conditions such as temperature, pH, light, and electrical stimulation. The specific mechanical and electrical response of polymer-based materials in this regime can be tailored according to application.

10.2.1 Tissue Engineering

Inherently conductive polymers have been subject to intense study in recent decades for application in microelectronics, optics, and fuel cells among others. Given the crowded and conductive nature of the extracellular matrix (ECM) in living organisms, conductive polymers were tested as a scaffold for tissue regeneration and engineering [11] In addition to conduction, in vivo applications have specific toxicity, inflammatory, and mechanical demands that must be met. Due to its high conductivity, polypyrrole is of particular interest although poor solubility, degradability, and elasticity limit its usefulness.

Fonner et al. [12] examined the effect of polypyrrole's synthesis method on its morphology, conduction, and suitability for medical implant. They found that surface roughness and choice of counter ion play important roles in cell adhesion and long-term viability; changing the dopant allows the material to be altered to suit the application. For example, tosylate (ToS) produces a more conductive polymer than doping with chloride (Cl) or polystyrene sulfonate (PSS) and so is better suited for electrochemical coatings. PSS treated polypyrrole films are more stable in aqueous environments making it the preferred choice for long-term in vivo implantation. Chloride counter ions, as presented in Fig. 10.1, were observed to improve cell viability on thicker films due to enhanced surface roughness.

By coating a polymer exhibiting more desirable mechanical properties with polypyrrole researchers have improved cell development and adhesion to tissue engineering scaffolds. Polypyrrole–polylactide blends from 5 to 10 % have been used for electrical stimulation-enhanced tissue regeneration, the results of which are shown in Fig. 10.2 [13]. Cell size, adhesion, viability, and cytokine release were all improved in the presence of mild electrical stimulation. Because of its

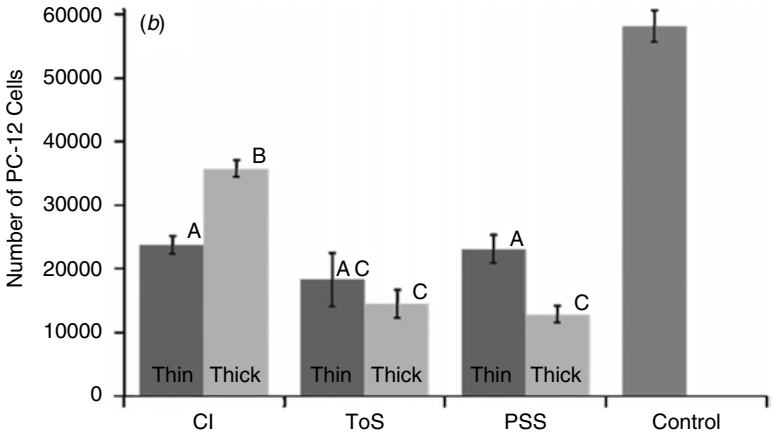

Fig. 10.1 Viability of PC-12 cells cultured on polypyrrole films of 150 nm (*thin*) and 650 nm (*thick*) using three different counter ion dopants. (Reproduced from Fonner et al. [12] with permission by IOP Science)

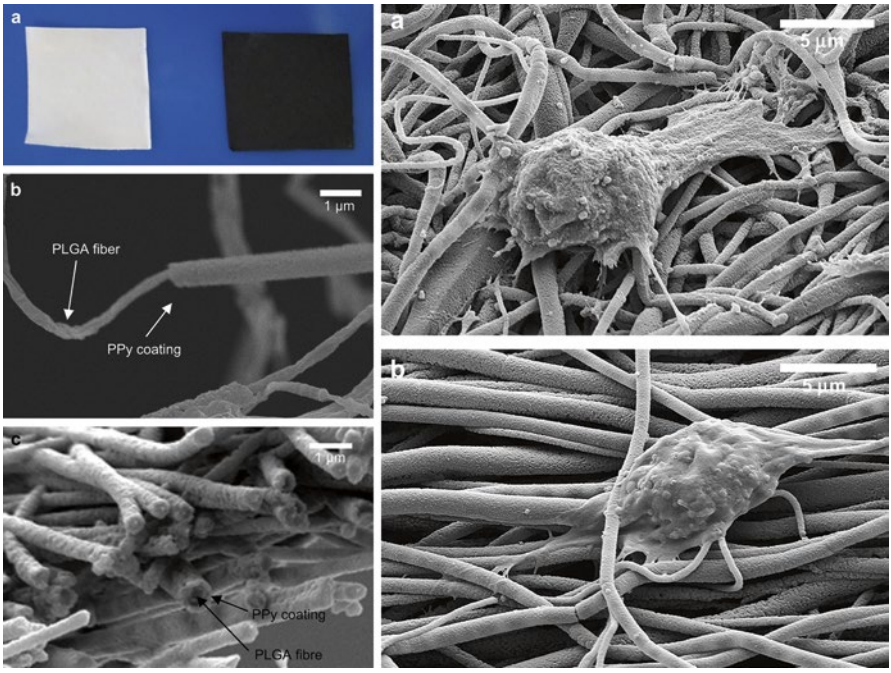

Fig. 10.2 Images of PC-12 cell growth on polypyrrole-coated poly(lactic-co-glycolic acid) fibres. A potential of 10 mV/cm stimulated increased neurite formation and length by 40–90 % and 40–50 % respectively (neurites indicated by *black arrows*). Fibre alignment (**b**, *lower right*) also improved these factors over a random mesh (**a**, *upper right*). (Reproduced from Lee et al. [13] with permission by Elsevier)

non-degradability in vivo, it is preferable to minimize the amount of polypyrrole per supporting polymer structure. Fibres containing as little as a 1:39 ratio of polypyrrole to chitosan were found to sufficiently maintain the positive mechanical and conductive aspects of each.

10.2.2 Sensing Membranes

Reactive polymers can sense changes in their environment such as pH, temperature, and ionic concentration [14]. Figure 10.3 shows examples of thin films of responsive polyelectrolyte hydrogels. Light or thermoresponsive polymers can be produced by tuning its relationship with its solvent so that its conformation changes in response to transition through the critical solution temperature [15]. As the polymer's relative affinity to itself and its solvent changes, solvent molecules will be either drawn into the polymer matrix or expelled from it. The volume and permeability of the matrix will change accordingly. The rate of responsiveness is limited by diffusion so thin layer depositions are ideal.

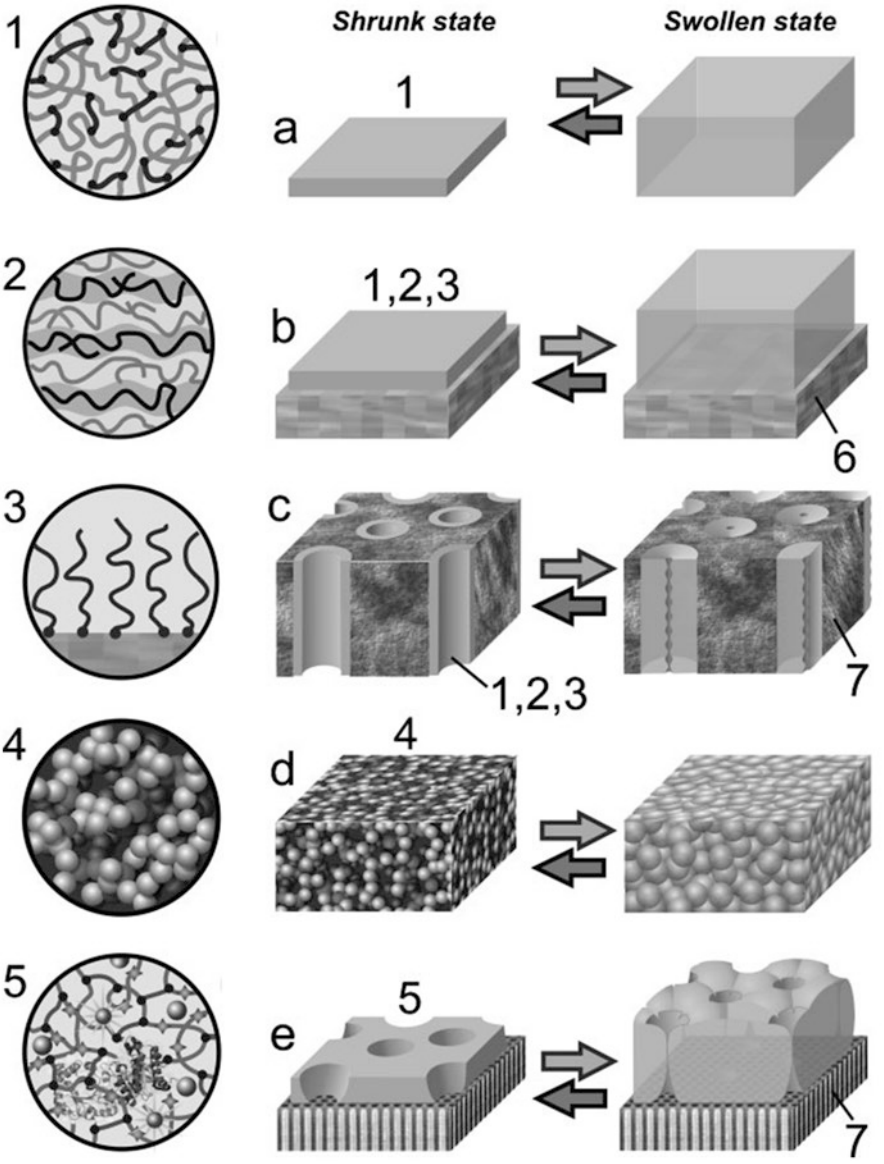

Fig. 10.3 Responsive polymer gating materials: (**a**) self-standing bulk gel film, (**b**) surface-attached planar thin film, (**c**) thin film immobilized on the walls of a porous substrate, (**d**) self-standing composite film with inclusions of stimuli-sensitive polymer, and (**e**) thin-film gel membrane on top of a porous substrate. (Reproduced from Tokarev and Minko [8] with permission by Wiley)

Similarly, polymer affinity for a specific solute can produce a measurable response in the material and act as a reusable sensor for that molecule. An example of this is a 200 nm electropolymerized m-acrylamidophenyl-boronic acid with acrylamide reported by Gabai et al. [16]. The film acts as an ion gate governed by

the presence of glucose: boronic acid sites will bond preferentially to glucose and swell the polymer matrix, increasing permeability to a redox couple that is readily measured. The selectivity of sensing and switching mechanisms near the microscale suffers due to the random nature of its matrix. As permeability increases in the above sample, more and more varied chemical species are able to traverse the membrane. In addition, glucose may not be the only molecule, or indeed the only sugar, capable of bonding to boronic acid, leaving open the possibility for false positives or mismanagement of cross-membrane exchange.

10.3 Structures from 10 to 100 nm

As in nature, polymer or amphiphilic monomer membranes can enclose a volume and isolate it from interaction with bulk solvent [17]. Membranes of cells and cellular organelles perform this function and incorporate selective and responsive pores in the membrane to precisely control traffic into and out of the enclosed space. If a catalytic centre is included in the membrane or enclosed within it, the reactions it promotes will be enhanced by confinement. In fact, confinement can be a determining factor for reaction energetics and major products depending on the size of the system under study. Integration into a membrane, whether enclosed or porous, can also enhance the rate of multi-step reactions by coordinating the placement of catalysts, cofactors, and substrates.

10.3.1 Selective Membranes

Membranes enclosing nanoscale volumes can control the flow of solutes by the inclusion of pores. Active and passive gate proteins in the cellular membrane are critical for the functioning of biological processes by ensuring the appropriate concentration balance of ions and reaction substrates in and outside of the cell. Unlike the sensing membranes described above, the membranes themselves remain impermeable but selective gates at nanopores selectively control solute exchange in response to environmental conditions.

Lin et al. [18] describe a method for monitoring glucose according to ion current through an enzyme decorated nanochannel (Fig. 10.4). Ion track etching was used to produce a 20 nm hourglass-shaped channel in a 12 μm polyimide membrane. Using NaOCl as the chemical etching agent produces carboxyl groups along the channel whose negative charges maintain the channel aperture and create high cation selectivity. Functionalizing the channel with glucose oxidase (GOx) and horseradish peroxidase (HRP) produces the following reaction to the presence of glucose:

$$\text{Glucose} + O_2 + H_2O \xrightarrow{GO_x} \text{Gluconic acid} + H_2O_2 \xrightarrow{HRP} O_2 + H_2O \qquad (10.1)$$

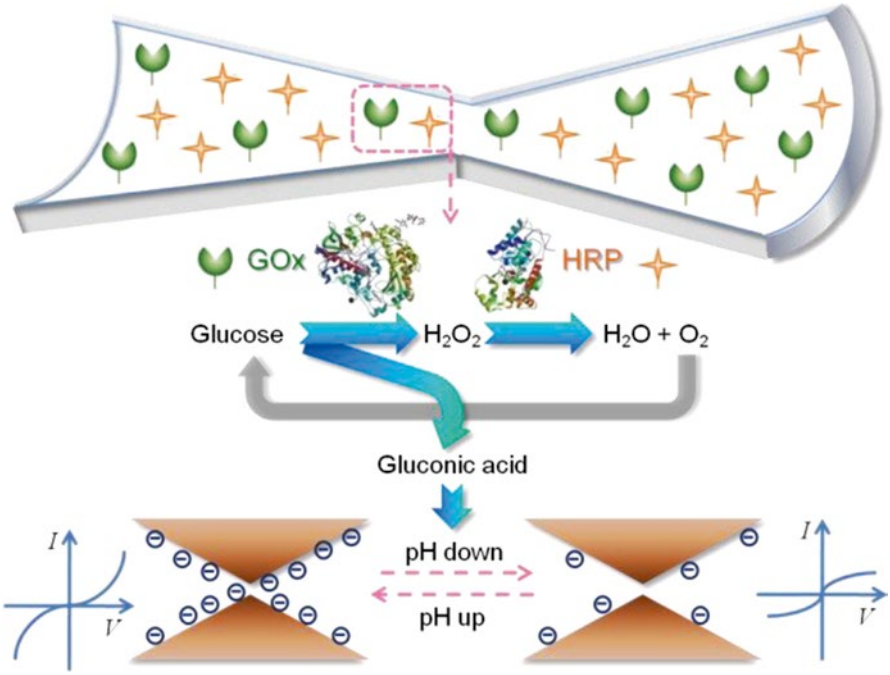

Fig. 10.4 Chemically etched double-conical nanochannel modified with GOx and HRP. Presence of glucose in the test produced gluconic acid and H_2O_2 by GOx catalysis; H_2O_2 was then decomposed into H_2O and O_2 by HRP. Accumulation of gluconic acid decreased channel pH and negative charge density leading to a current decline. (Reproduced from Lin et al. [18] with permission by the American Chemical Society)

The reduction of pH in channel produced by the local concentration of gluconic acid neutralizes the carboxyl groups, narrowing the channel and reducing its cation affinity in proportion to the amount of glucose present. Ion current is thereby reduced or increased by a reduction or increase in channel pH. Since the glucose oxidase enzyme is known to be highly selective for glucose, cation passage serves as an equally selective glucose sensor (Fig. 10.5).

10.3.2 Vesicle-Like Confinement

Reaction sites within a cell are located in crowded, confined spaces. Confinement in a small volume improves the reaction rates and efficiency of catalyzed reactions by restricting diffusion, reducing rotational and translational energy loss, and increasing the effective molarity of the catalyst's local environment.

Minten and co-workers [19] used the capsid of the Cowpea Chlorotic Mottle Virus (CCMV) to encapsulate enzymes and investigate the role of confinement on

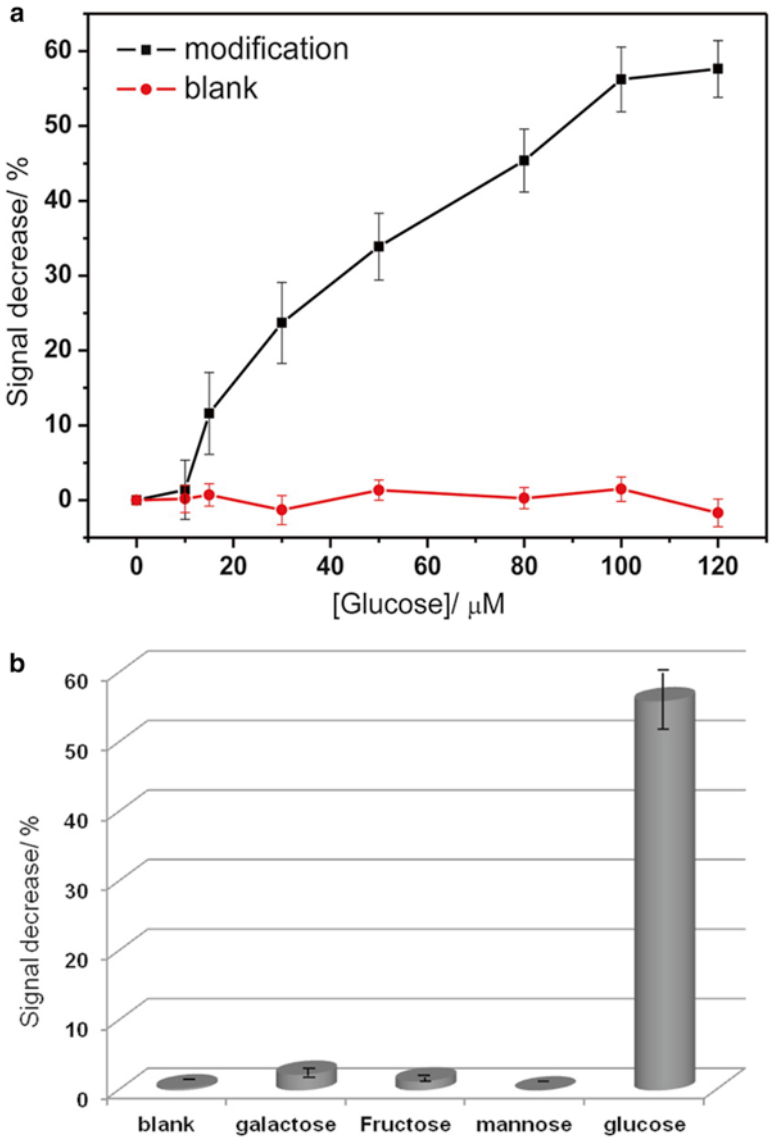

Fig. 10.5 (**a**) Dose response of bare and functionalized nanochannels. (**b**) Selectivity analysis for glucose response. The galactose, fructose, and mannose molarity were 1 mM each; the strongly selective glucose response was achieved with only 0.1 mM . (Reproduced from Lin et al. [18] with permission by the American Chemical Society)

enzyme reaction rates. The CCMV capsid comprises 180 identical proteins which separate into 90 dimers at pH 7.5 and self-assemble when returned to pH 5. This reversible association permits the simple removal of viral RNA and its replacement with a molecule of interest, in this case the acid-tolerant enzyme PalB.

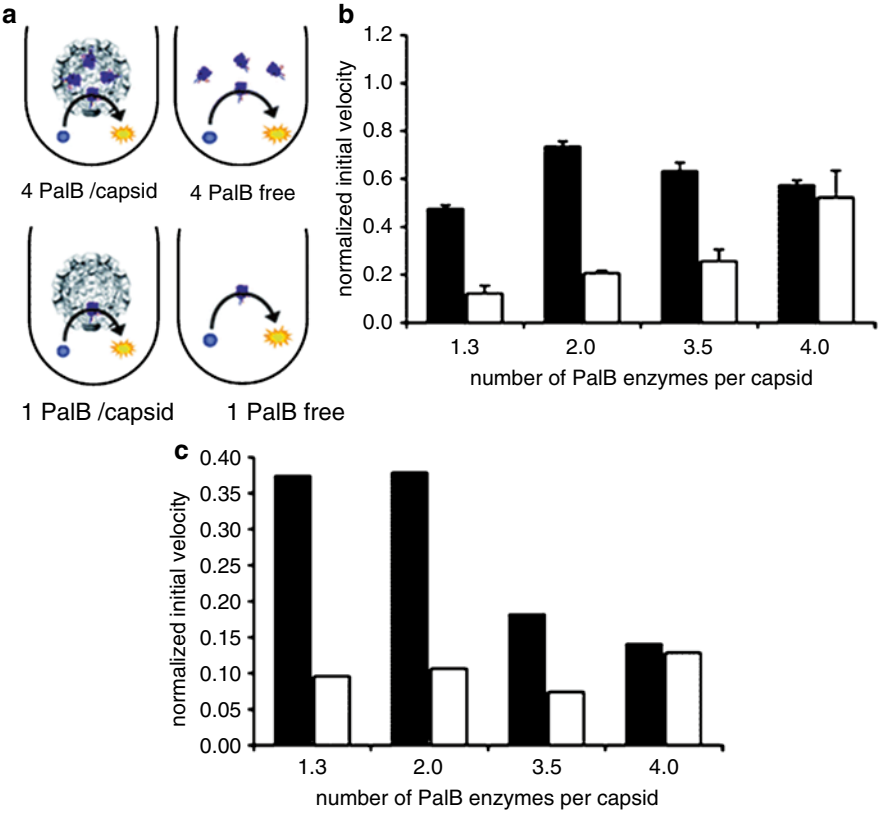

Fig. 10.6 Kinetics of PalB encapsulation. The concentration of capsid is the same in all samples. (**a**) Schematic representation of the experimental set-up. (**b**) Normalized initial rates with respect to 1.3 PalB/capsid experiment. *Black bars* represent initial rates of samples with encapsulated PalB, *white bars* indicate the rate for free PalB. (**c**) Normalized initial rates per PalB and per capsid. (Reproduced from Minten et al. [19] with permission by Royal Society of Chemistry)

Figure 10.6 shows the results from testing enzymatic catalysis in saturating substrate concentrations and demonstrates that the encapsulated enzymes outperform their unconfined counterparts. Furthermore, the molarity within confinement spaces containing a single substrate molecule was increased by a factor of 10^4 and enzyme concentration was effectively 25 times greater than the bulk. Consequently, the likelihood of finding more than one substrate molecule within a given capsid was negligibly low, removing any advantage of including more than one enzyme in the confinement space. Minten did, however, show that different enzymes could be encapsulated in a single capsid, opening the potential for highly coordinated cascade reactions.

The effect of confinement can also be significant on the sensitivity and efficiency of physical processes like photon emission. Chemoluminescence is used for many analytical applications due to its high sensitivity to dilute samples.

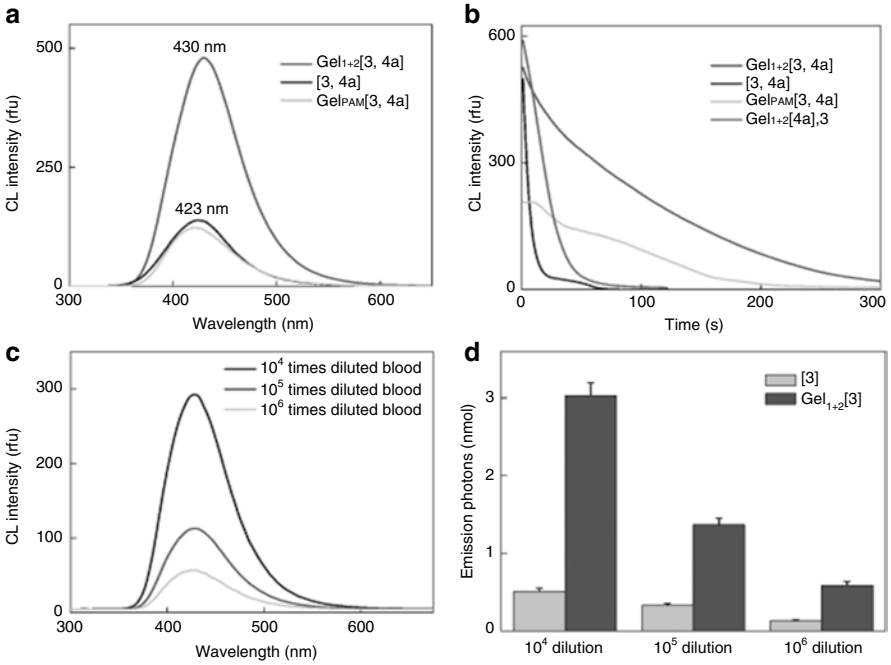

Fig. 10.7 (**a**) The chemoluminescent (CL) emission spectra of the 0.025 mm luminol and 0.0375 mm Hb in the supramolecular hydrogel, PAM hydrogel, or solution initiated by adding 0.25 mm H_2O_2, respectively; (**b**) the time-dependent CL intensity curve of various systems; (**c**) the CL emission spectra catalyzed by rabbit blood at various dilutions; (**d**) the numbers of photons emitted from the CL reactions of luminol in hydrogel ($Gel_{1+2}[3]$) or free ([3]) with H_2O_2 catalyzed by blood at various dilutions from an initial concentration of 11.9 mg Hb mL^{-1} (Reproduced from Wang et al. [20] with permission by Wiley)

Luminol fluoresces in the presence of haemoglobin but generally achieves no better than 1 % quantum yield in solution. The quantum yield of bioluminescent systems, alternately, is much higher: 88 % of the light-generating reactions in fireflies are reported to successfully produce photon emission. Wang et al. [20] were able to significantly increase the quantum yield of luminol reactions while extending their half life by mimicking the intercellular environment with supramolecular hydrogels (Fig. 10.7). For example, (9-fluoroethylmethyl) carbamate peptides in water, mixed with luminol and met-haemoglobin increased the quantum yield to 11.22 % from 1.02 % without the hydrogel. Likewise, emission time and intensity were raised by 4–6 times with hydrogel in solution over water alone. Confinement within the hydrogel reduces diffusion and rotation, thereby minimizing radiationless decay to increase reaction efficiency. The biomimetic environment produced by the polymeric gel also increased sensitivity of a 10^6 diluted haemoglobin solution to match the response from a solution two orders of magnitude more concentrated.

10.3.3 Multi-step Reactions

Both photosynthesis and glucose metabolism depend on the proximity and separation of the cellular membrane. Synthetic analogues of these cellular processes can also benefit from compartmentalization across solid state nanostructures [21].

Photocatalytic water splitting is an attempt to mimic hydrogenases, chiefly those of photosystem II, that employ visible light to drive the separation of protons from a donor species, ideally water [22]. PSII is a complex of protein subunits, cofactors, and electron donor and mediator molecules all operating in concert to achieve near quantum efficiency of photon capture. Natural photosynthesis incorporates light harvesting, charge stabilization, cofactor reduction, and the accumulation of oxidation equivalents for use by the oxygen evolving complex (water oxidizing complex). It is sufficiently complicated that in spite of intense research efforts the exact structure and mechanism of key active areas remains hotly debated [23]. However, artificial systems may be able to model the critical aspects, as illustrated by Fig. 10.8.

The challenge of efficient water splitting lies in bridging single electron photochemistry with the four electron chemistry of water oxidation.

$$2H_2O \rightarrow O_2 + 4H^+ + 4e^- \tag{10.2}$$

While the majority of photocatalytic research has focused on inorganic films and metal particles, there are some examples of self-assembling soft materials

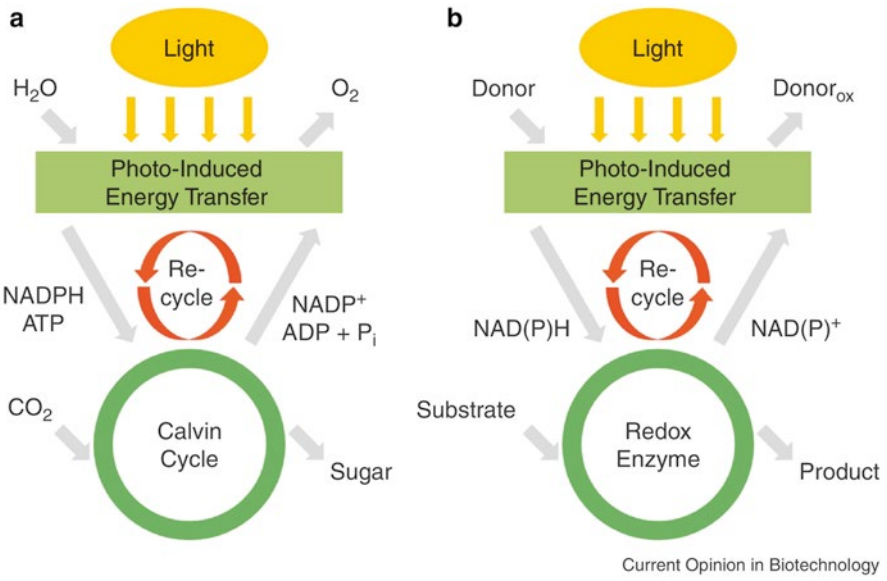

Fig. 10.8 Schematics of (**a**) natural and (**b**) artificial photocatalysis using electron mediating cofactors. (Reproduced from Kim et al. [24] with permission by Elsevier)

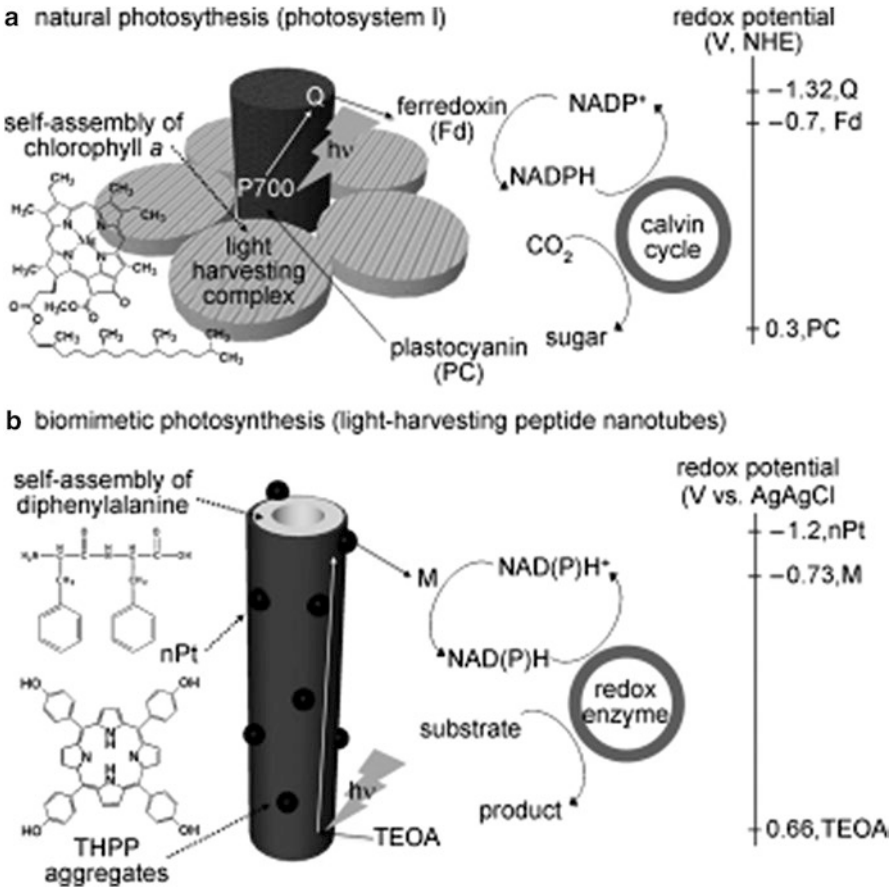

Fig. 10.9 Schematics of (**a**) natural photosynthesis in photosystem I and (**b**) biomimetic photosynthesis supported by light-harvesting and conductive peptide nanotubes. *White* and *black arrows* indicate electron photoexcitation and transfer, respectively. (Reproduced from Kim et al. [25] with permission by Wiley)

playing a functional role in photon capture and storage. Kim et al. describe a PSI mimic composed of a self-assembled diphenylalanine and tetra(p-hydroxyphenyl) porphyrin (THPP), shown in Fig. 10.9. Exciton coupling between THPP monomers accelerated light collection while platinum nanoparticles on the structure's surface accelerated charge separation between donor and mediator. On the platinum-porphyrin structure, a greater level of coordination between subunits leads to activity >40 times THPP alone.

Like their biological counterparts, the efficiency of biomimetic systems at this scale is highly dependent on the design of their subcomponents, which become a crucial element in the development of novel materials.

10.4 Structures from 1 to 10 nm

Reactions typically involve bulk organic solvents and metal catalysts; however, only the immediate chemical environment has any bearing on the reactants. Waste, toxic by-products, and inefficiencies could be significantly reduced by the development of water soluble reaction vessels just large enough for the reaction to occur within an interior surface matching the ideal solvent and containing precise, high surface area catalytic materials. Such a sustainable alternative sounds unlikely, yet enzymes operate in exactly this fashion. Enzymes are extremely efficient catalytic materials composed necessarily of organic macromolecules and the most common metals of the Earth's crust. Enzymes are not simply catalysts, or reaction vessels, or nanosensors, but all of these combined [26]. The active site is capable of bonding, catalyzing, and expelling substrates with phenomenal turnover.

They are not only able to recognize their specific precursors but in many cases they also sense and respond to the need for its reaction product and regulate its clearance rate accordingly. Enzymatic catalysis comprises substrate recognition and binding, geometric optimization, and catalytic binding of the transition state followed by efficient desolvation [27]. Broadly speaking, these phenomena fall into concerted thermodynamic and kinetic effects - confinement and catalysis. Putting a finer point on the effects either excludes too many enzymes to be general or includes properties too difficult to quantify to be of analytic use.

While there have been claims to the production of artificial enzymes, none match their biological counterparts for efficiency, specificity, and regulatory function [28]. That being said, the demands and constraints of natural and industrial products are very different. Enzymes in cytosol must separate their specific substrate from the variety of molecules present; synthetic reaction systems can be made to include only those molecules necessary for the desired product. Enzymes are also highly sensitive to environmental conditions and will lose conformation and effectiveness outside of tight boundaries of pH, radiation, temperature, ionic strength, and mechanical forces. An effective enzyme mimic should therefore incorporate the mechanisms of enzyme catalysis, though perhaps not their specificity, in a stable, confinement enhancing superstructure.

As Koblenz et al. [29] note, the difference in reactivity in a confined nanospace or in the bulk will either alter ΔG of activation ($\Delta G^{\#}$) or not. A change indicates that the catalytic structure is able to stabilize the transition state. Enthalpic stabilization is achieved by the reduction in energy through covalent or non-covalent bonding of the transition state; entropic advantage is obtained by restricted rotational, vibrational, and translational motion in the confined nanodomain. A simplified profile of transition state stabilization within the nanoreactor is shown in Fig. 10.10a. If $\Delta G^{\#}$ under confinement is equal to that of the bulk then the increased reaction rate is due only to the rise in effective molarity within the reaction vessel.

A confined microenvironment can also dictate whether one or another possible reaction product is optimized by blocking the pathway to others either by steric or energetic means. A schematic of this effect is shown in Fig. 10.10b.

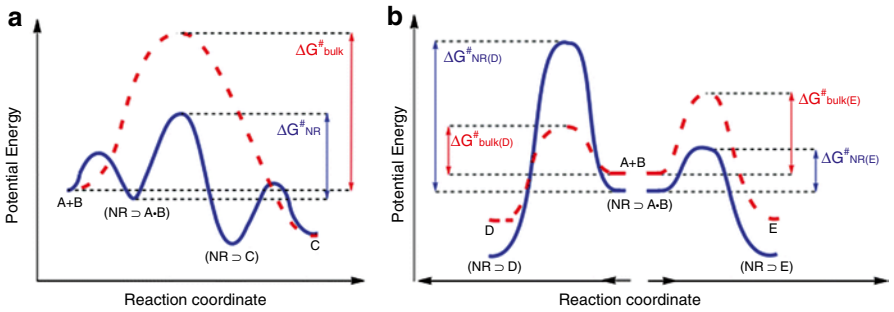

Fig. 10.10 (**a**) Simplified reaction profiles of a reaction in the bulk solution (*dashed line*) and within a nanoreactor (*solid line*). (**b**) Simplified reaction profiles of a reaction leading to product D which is unfavoured within a nanoreactor (*solid line*) compared to the bulk solution (*dashed line*), and of a reaction leading to product E which is stabilized by the nanoreactor (*solid line*) compared to the bulk solution (*dashed line*) (Reproduced from Koblenz et al. [29] with permission by the Royal Society of Chemistry)

10.4.1 Confined Catalysis

Enzymes in aqueous solution contain nanodomains lined by a combination of amino acid side groups that form a better solvation shell than the bulk solvent for substrate molecules but not for the reaction product. As described above, higher order confinement within vesicles or crowded cytosol contributes to the effectiveness of enzymes by increasing the probability of interaction with its substrate. Synthetic macromolecules can produce similar, though much less refined, nanodomains [30]. In seeking to minimize interfacial energy, certain amphiphilic molecules in water will take conformations which produce internal hydrophobic regions. Interfacial tension between component molecules and water is fundamental for supramolecular self-assembly [10]. As a component molecule moves within the solvent, its sections with relatively high interfacial tension will tend to remain in contact with each other while more soluble, low interfacial tension areas will tend to remain in contact with the solvent. This process of surface energy minimization supports or indeed makes possible weak (van der Waal's, electrostatic, hydrophobic, hydrogen) bonding between components. Self-assembly can be said to occur if these associations produce an ordered structure at either thermodynamic equilibrium (static) or while dissipating energy (dynamic) [31]. This process is well understood for surfactant micelles and for morphological transitions by amphiphilic diblock copolymers [32]. If the resulting structure contains cavities lined with non-polar moieties these areas act as hydrophobic nanodomains. Accordingly, small molecules that are insoluble in water will accumulate within these cavities by a process similar to that which drove structural self-assembly.

Loading of the nanodomains will continue until reaching equilibrium with counteracting forces, most notably the electronic repulsion that determines the intrinsic density of the small molecule solute. To the extent that compressive forces are greater

than repulsive forces, random movements by the solute molecules decrease and occupancy increases until reaching a stable packing conformation that minimizes global energy. In certain cases, the increased electronic excitation and lower entropy that result from the increased density and decreased degrees of freedom are sufficient to allow otherwise unfavourable reactions to be thermally initiated. It is the observation of molecular and reaction dynamics under nanoscale confinement which are inconsistent with bulk properties that define the confinement effect. The increase of reaction efficiency under confinement is often measured as effective molarity (EM), the ratio of the intermolecular versus intramolecular reaction rates [33].

10.4.2 Templated Nanoparticle Synthesis

An early biomimetic strategy for inorganic nanocrystal formation was to use the naturally occurring protein apoferritin as collector and cage for transition metal and metal oxides [34]. Because the cavity of apoferritin is 7 nm in diameter, monodisperse nanoparticles of iron, nickel, and chromium among others have been produced at that size [35].

As well as promoting thermodynamically unfavourable reactions, effective molarity under confinement may also allow for reactions which are kinetically unfavourable in ambient conditions. Lee et al. [36] observed that $GaCl_3$ in pH 10 solution with bolaamphiphile peptide could be hydrolyzed to β-Ga_2O_3 at room temperature (Fig. 10.11).

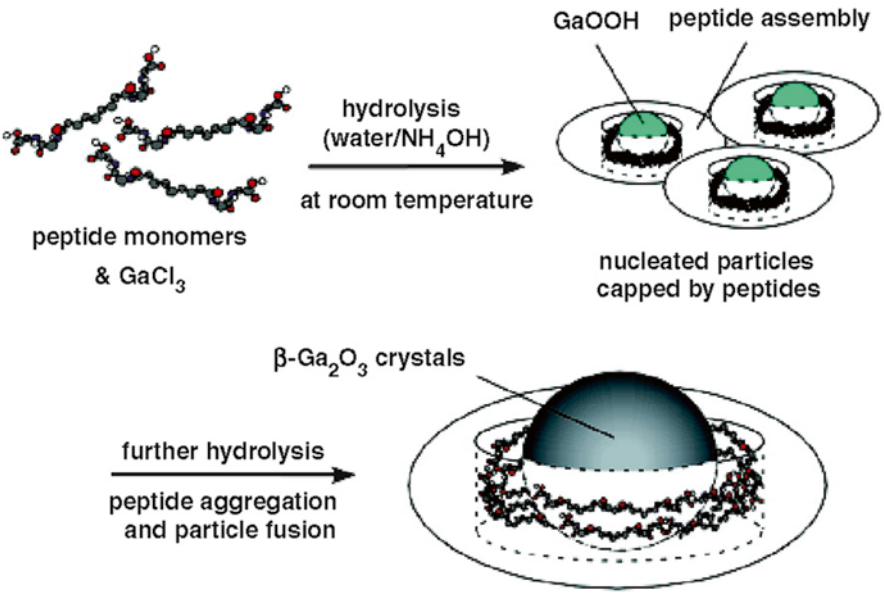

Fig. 10.11 Illustration of β-Ga_2O_3 growth mechanism via peptide capping and aggregation. (Reproduced from Lee et al. [36] with permission by Elsevier)

They observed that without the peptide in solution, the reaction conditions could produce GaO_2H but were too mild for further oxidation. Initial hydrolysis and size stabilization within the self-assembled peptide templates also produced GaO_2H in monodisperse 10 nm crystals. In the second stage of the synthesis, the peptide containers aggregated and their contents fused into 50 nm metal oxide crystals. It is in this step that the peptide is thought to play the critical catalytic role leading from mixed phase clusters to pure β-Ga_2O_3 nanocrystals.

10.4.3 Solar Fuel

Solar fuels refer to the end products of photocatalyzed or photoelectrically driven reactions that store the energy of collected solar radiation in chemical bonds. To be practical, the chemical products should be relatively easy to store, handle, and use; ideally no less so than current chemical fuels. Water splitting, as described above, produces a solar fuel in hydrogen gas. Its energy to mass ratio and clean combustion product, water, are excellent, but it becomes less attractive when considering the low energy to volume ratio and the accompanying difficulties in storage and distribution. Bearing in mind that nearly all of the energy humanity has ever used in our bodies and machines were sourced from plant-synthesized carbohydrates, and that the sun provides enough power in 1 h to power human civilization for a year, photocatalytic fuel production is a high-value research goal [37]. The steady rise in atmospheric CO_2 and its adverse effects since the industrial revolution makes the development of an industrial analogue to the Calvin cycle doubly attractive as it would provide a solution for energy and condensed carbon storage.

The simplicity of the concept belies the difficulty of the challenge: CO_2 is very stable and reducing it back to a useable fuel via light energy is a thus far intractable problem. Neither the enthalpic nor entropic components of reaction thermodynamics favour CO_2 reduction; reaction kinetics are likewise reduced by the need for multiple electron coordination. Kumar et al. [38] cite the thermodynamic potentials listed in Eqs. (10.3, 10.4, and 10.5) against a hydrogen electrode, pH 7, STP, 1 M for other solutes.

$$CO_2 + 2H^+ + 2e^- \rightarrow HCO_2HE^0 = -.61V \tag{10.3}$$

$$CO_2 + 6H^+ + 6e^- \rightarrow CH_2OH + H_2OE^0 = -.38V \tag{10.4}$$

$$CO_2 + 8H^+ + 8e^- \rightarrow CH_4 + 2H_2OE^0 = -.24V \tag{10.5}$$

Naturally, the biological solutions are a source of inspiration. The extant literature on photoelectric or photocatalytic energy capture largely focuses on inorganic chemistry and as such lie outside the scope of this chapter. However, the transfer mechanism of protons and excited electrons from the cathode or semiconductor junction is typically dependent on organo-hydride molecules. Natural photosynthesis

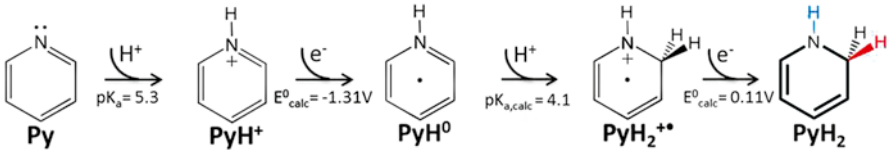

Fig. 10.12 Formation of 1,2-dihydropyridine from pyridine (Reproduced from Lim et al. [40] with permission by the American Chemical Society)

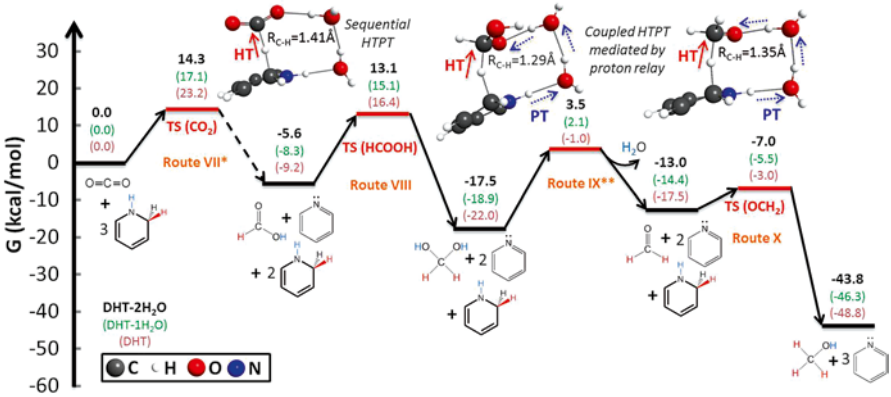

Fig. 10.13 Conversion of CO_2 to CH_3OH and H_2O by PyH_2 proceeds through three hydride and proton transfer steps. The reported free energies correspond to stationary points along the reaction potential energy surface models, catalyzed by the PyH_2/Py redox couple. (Reproduced from Lim et al. [40] with permission by the American Chemical Society)

and nanobiosynthetic model systems use the nicotinamide adenine dinucleotide phosphate (NADP+) and NADPH redox couple as an electron mediator for CO_2 reduction. Barton et al. [39] demonstrated 88–100 % faradaic efficiency of CO_2 reduction to CH_3OH using a p-GaP semiconductor electrode illuminated with light in the solar spectrum in pH 5.2 aqueous solution. The presence of pyridine allowed for the reaction to occur at significant undervoltages, but the catalytic mechanism was unknown.

Lim et al. [40] used quantum mechanical methods to investigate pyridine's role in the transfer of two photoexcited electrons to CO_2. The redox pathway from pyridine (Py) to 1,2,-dihydropyridine (PyH_2) and the reduction energies they found are shown in Fig. 10.12. Density functional theory M06/6-31G** was employed to map the reaction cycle and Møller–Plesset perturbation theory with aug-ccPVTZ basis sets were used to calculate point energies of the reaction and transition state energies to high precision. As Fig. 10.13 illustrates, that study revealed that the Py-PyH_2 redox couple coordinates the reduction of CO_2 to formic acid HCO_2H, methanediol $CH_2(OH)_2$, and finally to methanol CH_3OH by sequential hydride ($2e^- + H^+$) and proton (H^+) transfers (HTPT).

Pyridine's function as a recyclable two electron mediator through HTPT makes it a small, stable synthetic analogue to NADP(H) for catalyzing the reduction of CO_2 into a usable fuel. The original experimental work was performed in bulk solution with a macro-scale semiconductor electrode. In combination with metal or semiconductor nanocrystals and a macromolecular confinement structure, the results of this theoretical study could be incorporated into an efficient and fully artificial mimic of the biological carbon reduction process.

10.4.4 Biomimetic Nanoreactors

Polystyrene-alt-maleic anhydride is a particularly interesting polymer for the construction of soft nanoarchitectures that confine and support organic reactions in water (Fig. 10.14). It is an amphiphilic alternating copolymer which has been shown to produce supramolecular nanotubes (14 Å inner and 21 Å outer diameters) and nanosheet bilayers, a model of which is shown in Fig. 10.15, according to the average molecular weight of the polymer chains. The lighter, nanotube forming chains will lose their linear conformation in high or low pH and cause structural collapse, as with enzymes. Longer, nanosheet forming chains have proven to be stable over a broader pH range.

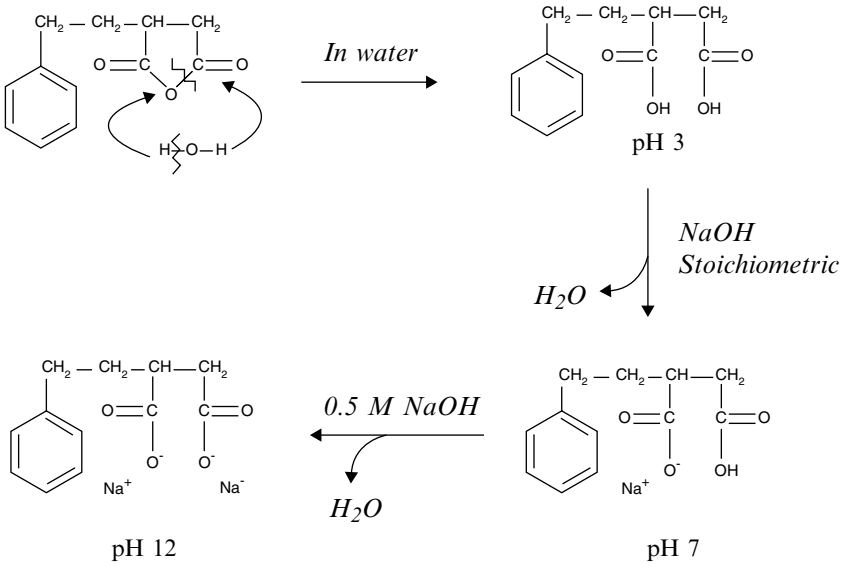

Fig. 10.14 The pH sensitivity of poly(styrene-alt-maleic acid) is produced by the successive deprotonation of its maleic acid moiety. Supramolecular association is optimized in the monodeprotonated state. (Reproduced from Malardier-Jugroot et al. [41] with permission by the American Chemical Society)

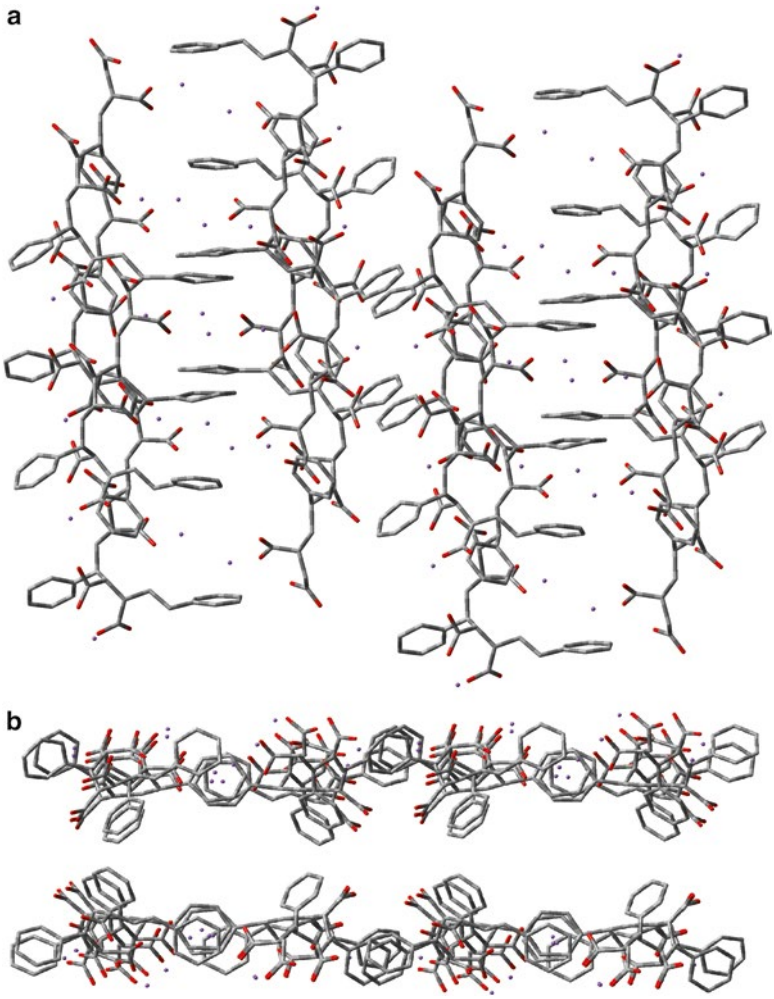

Fig. 10.15 DFT-B3LYP/6-31G optimized oligomers of SMA at pH 7 fit the interchain and π–π bond spacings as well as the bond progression angle observed under high-resolution TEM. (**a**) Shows the top view; (**b**) illustrates the concentration of hydrophobic groups in the bilayer interior (Reproduced from McTaggart et al. [42])

The self-assembly of either structure produces hydrophobic interior spaces that act as host to small hydrophobic molecules and exploit confinement to promote otherwise unfavourable reactions. This was shown by the spontaneous polymerization reaction of pyrrole in the SMA interior. When mixed into a 1 % wt/wt aqueous solution pyrrole is confined and polymerizes without additional chemical or physical inducement. The effective molarity is difficult to calculate in this case since the reaction rate of pyrrole outside of confinement is too slow to be practicably quantified.

Part of the reason for the lack of spontaneous polymerization in bulk solution is the fact that association only becomes an energetically favourable state for oligomers of six or more pyrrole molecules: where the bonding reaction of two is unlikely, the probability of six is effectively zero. The influence of confinement was proven by attempting pyrrole polymerization inside larger styrene-maleic acid micelles up to 50 nm in diameter. No reaction was observed in the larger volume. As mentioned previously, polypyrrole is an increasingly important conductive polymer for a wide range of technological fields whose polymerization generally requires specialized reaction agents and association with a degradable polymer superstructure. The polypyrrole synthesis method developed by Li and Malardier-Jugroot [43] both removes the need for chemical polymerization agents and incorporates the product into a biocompatible, biodegradable polymer nanoarchitecture.

The well-defined structure of the cavities of the SMA template provides a controlled environment for the growth of metal nanoclusters. Indeed the hydrophobic metal salt platinum(II) chloride was also added to SMA solution with $NaBH_4$ reducing agent to produce nanoparticles through a process analogous to biotemplated crystal growth. Given the interstitial spaces, metal crystals under 3 nm were expected. Monodisperse platinum crystals were observed to form with or, surprisingly, without an additional reducing agent. Figure 10.16 shows high-resolution transmission electron micrographs of the SMA nanosheet and platinum-SMA nanoreactor system. By reproducing the pyrrole polymerization experiment in the Pt-SMA nanoreactor the reaction rate was three times faster than in SMA alone (Fig. 10.17). By initiating and catalyzing an energetically unfavourable reaction through confinement and metal coordination the Pt-SMA nanoreactor mimics enzymatic action in an environmentally friendly synthetic process.

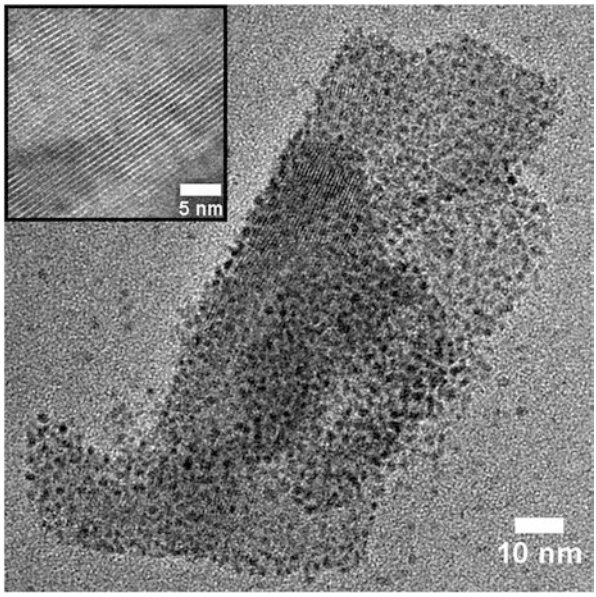

Fig. 10.16 HR-TEM image of the SMA-platinum nanoreactor. *Dark spots* are monodisperse platinum nanocrystals confined to the SMA interior. *Inset* is a magnified view of the SMA surface. (Reproduced from McTaggart et al. [42])

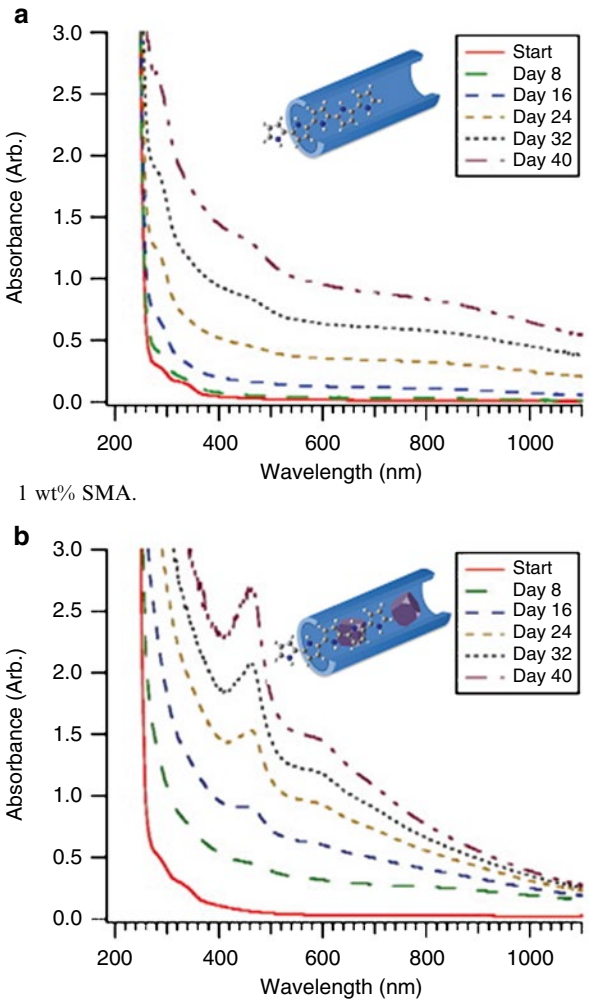

Fig. 10.17 UV/vis absorbance data taken every 8 days of the pyrrole polymerization reaction in (**a**) a 1 % wt/wt solution of SMA in water and (**b**) the same with platinum nanocrystals as formed in situ. (Reproduced from Groves et al. [44] with permission by Elsevier)

1 wt% SMA.

1 wt% SMA with embedded Pt nanoparticles.

The advantage of artificial materials to reproduce biologically inspired physical effects becomes apparent when considering stability across environmental conditions. Further experimentation showed that both the platinum nanocrystal synthetic method and the SMA-Pt nanoreactor are stable in pH ranging from 3.2 to 9, shown in Fig. 10.18, affording very high potential for application in proton exchange membrane fuel cells.

The synthetic method was also applied to gold(I) chloride but with very different results. Atomically thin and flat gold monolayers were observed to form on the exterior surface of the SMA bilayer (Fig. 10.19). Small angle neutron scattering models indicate that SMA and gold layers alternate into stacks in solution, potentially creating hydrophilic confined reaction spaces. The hexagonal close-packed

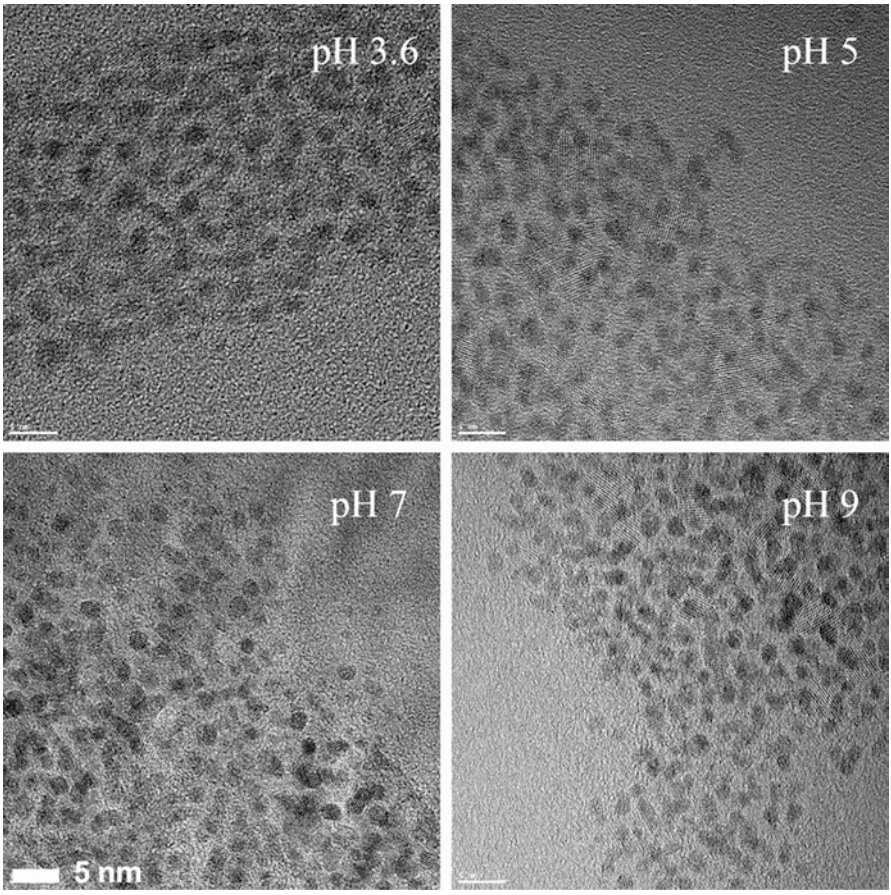

Fig. 10.18 The platinum nanocrystal synthetic method and resultant SMA-platinum nanoreactor are stable in between pH 3.6–9. (Reproduced from McTaggart et al. [42])

atomic arrangement of the gold monolayer is of interest as a synthetic or catabolic catalyst, as well as for applications in microelectronics, plasmonics, optics, and medicine [45].

As stated previously, true artificial enzymes incorporating the selectivity, reaction rate, and regulatory functions of the naturally produced variety remain out of reach, but advances in soft biomimetic nanomaterials are drawing closer to that ideal.

10.5 Conclusion

It is only recently that we have developed the tools needed to probe the structures and mechanisms of biological nanosystems tailored over millions of years of evolutionary optimization. Soft, responsive polymeric nanoarchitectures are well

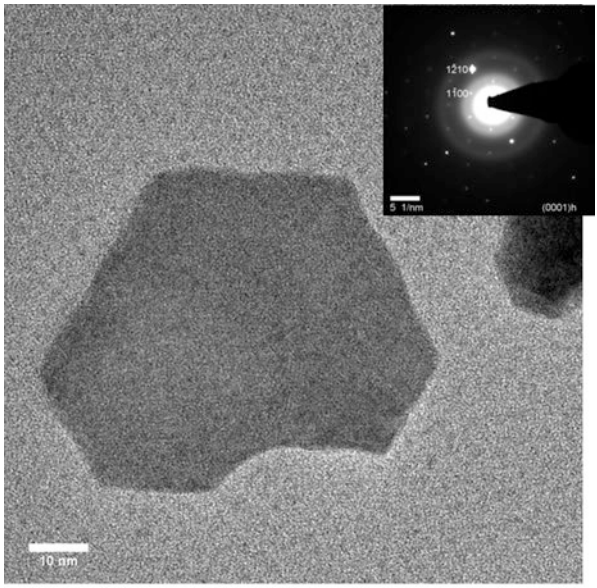

Fig. 10.19 HR-TEM image of a gold monolayer produced on an SMA template. Inset shows a selected area electron diffraction pattern revealing its hexagonal close-packing crystal structure. (Reproduced from McTaggart et al. [42])

suited to adapt the lessons of nature to improve processes in medicine, science, and technology. Inherently conductive polymer fibre networks and hydrogels are able to model the extracellular matrix and cytosol. Self-assembling systems can create confined environments that improve the catalytic efficiency of enzymes or indeed mimic confinement within enzymes themselves. The development of biomimetic polymer nanostructures is an important advance for sustainable energy collection, storage, and use that opens the possibility of closing the industrial carbon cycle for long-term energy security and climate management.

References

1. Whitesides GM, Mathias JP, Seto CT (1991) Molecular self-assembly and nanochemistry: a chemical strategy for the synthesis of nanostructures. Science 254:1312–1319
2. Wendell DW, Patti J, Montemagno CD (2006) Using biological inspiration to engineer functional nanostructured materials. Small 2:1324–1329
3. Raynal M, Ballester P, Vidal-Ferran A et al (2014) Supramolecular catalysis. Part 2: artificial enzyme mimics. Chem Soc Rev 43:1734–1787
4. Aida T, Meijer EW, Stupp SI (2012) Functional supramolecular polymers. Science 335:813–817
5. Kumar D, Sharma RC (1998) Advances in conductive polymers. Euro Polymer J 34:1053–1060
6. Guo B, Glavas L, Albertsson AC (2013) Biodegradable and electrically conducting polymers for biomedical applications. Progr Polymer Sci 38:1263–1286
7. McQuade DT, Pullen AE, Swager TM (2000) Conjugated polymer-based chemical sensors. Chem Rev 100:2537–2574
8. Tokarev I, Minko S (2009) Multiresponsive, hierarchically structured membranes: new, challenging, biomimetic materials for biosensors, controlled release, biochemical gates, and nanoreactors. Adv Mater 21:241–247

9. Lehn JM (2002) Toward self-organization and complex matter. Science 295:2400–2403
10. Isrealachvili JN, Mitchell DJ, Ninham BW (1976) Theory of self-assembly of hydrocarbon amphiphiles into micelles and bilayers. J Chem Soc Faraday Trans 2(72):1525–1568
11. Guimard NK, Gomez N, Schmidt CE (2007) Conducting polymers in biomedical engineering. Progr Polymer Sci 32:876–921
12. Fonner JM, Forciniti L, Nguyen H et al (2008) Biocompatibility implications of polypyrrole synthesis techniques. Biomed Mater 3:034124
13. Lee JY, Bashur CA, Goldstein AS et al (2009) Polypyrrole-coated electrospun PLGA nanofibres for neural tissue applications. Biomaterials 26:4325–4335
14. Lehn JM (2005) Dynamers: dynamic molecular and supramolecular polymers. Progr Polymer Sci 30:814–831
15. Jones DM, Smith JR, Huck WT et al (2002) Variable adhesion of micropatterned thermoresponsive polymer brushes: AFM investigations of poly (N-isopropylacrylamide) brushes prepared by surface-initiated polymerizations. Adv Mater 14:1130–1134
16. Gabai R, Sallacan N, Chegel V et al (2001) Characterization of the swelling of acrylamidophenylboronic acid-acrylamide hydrogels upon interaction with glucose by Faradaic impedance spectroscopy, chronopotentiometry, quartz-crystal microbalance (QCM), and surface plasmon resonance (SPR) experiments. J Phys Chem B 105:8196–8202
17. Discher DE, Eisenberg A (2002) Polymer vesicles. Science 297:967–973
18. Lin L, Yan J, Li J (2014) Small-molecule triggered cascade enzymatic catalysis in hour-glass shaped nanochannel reactor for glucose monitoring. Anal Chem 86:10546–10551. doi:10.1021/ac501983a
19. Minten IJ, Claessen VI, Blank K et al (2011) Catalytic capsids: the art of confinement. Chem Sci 2:358–362
20. Wang Q, Li L, Xu B (2009) Bioinspired supramolecular confinement of luminol and heme proteins to enhance the chemiluminescent quantum yield. Chem Eur J 15:3168–3172
21. Smitha B, Sridhar S, Khan AA (2005) Solid polymer electrolyte membranes for fuel cell applications—a review. J Membr Sci 259:10–26
22. Kudo A, Miseki Y (2009) Heterogeneous photocatalyst materials for water splitting. Chem Soc Rev 38:253–278
23. McEvoy JP, Brudvig GW (2006) Water-splitting chemistry of photosystem II. Chem Rev 106:4455–4483
24. Kim JH, Nam DH, Park CB (2014) Nanobiocatalytic assemblies for artificial photosynthesis. Curr Opin Biotechnol 28:1–9
25. Kim JH, Lee M, Lee JS et al (2012) Self-assembled light-harvesting peptide nanotubes for mimicking natural photosynthesis. Angew Chem Int Ed 51:517–520
26. Benkovic SJ, Hammes-Schiffer S (2003) A perspective on enzyme catalysis. Science 301:1196–1202
27. Eisenmesser EZ, Millet O, Labeikovsky W et al (2005) Intrinsic dynamics of an enzyme underlies catalysis. Nature 438:117–121
28. Dong Z, Luo Q, Liu J (2012) Artificial enzymes based on supramolecular scaffolds. Chem Soc Rev 41:7890–7908
29. Koblenz TS, Wassenaar J, Reek JNH (2008) Reactivity within a confined self-assembled nanospace. Chem Soc Rev 37:247–262
30. Conn MM, Rebek J (1997) Self-assembling capsules. Chem Rev 97:1647–1668
31. Whitesides GM, Grzybowski B (2002) Self-assembly at all scales. Science 29:2418–2421
32. Zhang S (2003) Fabrication of novel biomaterials through molecular self-assembly. Nat Chem 21:1171–1178
33. Kirby AJ (1996) Enzyme mechanisms, models, and mimics. Angew Chem Int Ed 35:706–724
34. Li M, Wong KK, Mann S (1999) Organization of inorganic nanoparticles using biotin-streptavidin connectors. Chem Mater 11:23–26
35. Okuda M, Iwahori K, Yamashita I et al (2003) Fabrication of nickel and chromium nanoparticles using the protein cage of apoferritin. Biotechnol Bioeng 84:187–194

36. Lee SY, Gao X, Matsui H (2007) Biomimetic and aggregation-driven crystallization route for room-temperature material synthesis: growth of β-Ga_2O_3 nanoparticles on peptide assemblies as nanoreactors. J Am Chem Soc 129:2954–2958
37. Izumi Y (2013) Recent advances in the photocatalytic conversion of carbon dioxide to fuels with water and/or hydrogen using solar energy and beyond. Coord Chem Rev 257:171–186
38. Kumar B, Llorente M, Froehlich J et al (2012) Photochemical and photoelectrochemical reduction of CO_2. Annu Rev Phys Chem 63:541–569
39. Barton EE, Rampulla DM, Bocarsly AB (2007) Selective solar-driven reduction of CO_2 to methanol using a catalyzed p-GaP based photoelectrochemical cell. J Am Chem Soc 130:6342–6344
40. Lim CH, Holder AM, Hynes JT et al (2014) Reduction of CO_2 to methanol catalyzed by a biomimetic organo-hydride produced from pyridine. J Am Chem Soc 136:16081–16095
41. Malardier-Jugroot C, van de Ven TGM, Whitehead MA (2005) Linear conformation of poly(styrene-alt-maleic anhydride) capable of self-assembly: a result of chain stiffening by internal hydrogen bonds. J Phys Chem B 109:7022–7032
42. McTaggart M, Malardier-Jugroot C, Jugroot M (2015) Self-assembled polymeric nanoreactors with precious metals as active centers. Macromolecules (submitted)
43. Li X, Malardier-Jugroot C (2013) Confinement effect in the synthesis of polypyrrole within polymeric templates in aqueous environments. Macromolecules 46:2256–2266
44. Groves MN, Malardier-Jugroot C, Jugroot M (2014) Environmentally friendly synthesis of supportless Pt based nanoreactors in aqueous solution. Chem Phys Lett 612:309–312
45. Huang X, Li S, Huang Y et al (2011) Synthesis of hexagonal close-packed gold nanostructures. Nat Commun 2:292

Chapter 11
Nanoarchitectonics Prepared by MAPLE for Biomedical Applications

Roxana Cristina Popescu and Alexandru Mihai Grumezescu

Abstract Thin film depositions by Matrix-Assisted Pulsed Laser Evaporation (MAPLE) technique have been intensively used in order to obtain nanoarchitectonics with different biomedical applications, like drug delivery systems, tissue engineering, implants with improved biocompatibility, improved adherent surfaces, antibacterial surfaces, etc. This chapter presents a description of the latest research regarding magnetite-based thin films and hybrid organic–inorganic thin films obtained by MAPLE. The most encountered preparation methods for magnetite-based thin films and several hybrid organic–inorganic systems are presented. Regarding the biomedical applications, our attention is directed to the antibacterial properties of differently modified surfaces for implants and medical devices.

Keywords Nanoarchitectonics • Thin film deposition • Matrix-assisted pulsed laser evaporation • Magnetite nanoparticles • Hybrid organic–inorganic

11.1 Matrix-Assisted Pulsed Laser Evaporation Technique: General Approach

Thin films are defined as layers of material with a thickness between nanometers to micrometers, while the thin film deposition is a term which refers to the technique of applying a film onto a substrate. The main techniques used for thin film deposition are classified as: (1) laser assisted deposition techniques and (2) non-laser assisted deposition techniques. Laser assisted techniques used for obtaining thin film depositions on different substrates have multiple advantages compared to other

R.C. Popescu • A.M. Grumezescu (✉)
Faculty of Applied Chemistry and Materials Science, Department of Science and Engineering of Oxide Materials and Nanomaterials, University Politehnica of Bucharest, Polizu Street No. 1-7, 011061 Bucharest, Romania
e-mail: grumezescu@yahoo.com

V.A. Basiuk, E.V. Basiuk (eds.), *Green Processes for Nanotechnology*,
DOI 10.1007/978-3-319-15461-9_11

techniques given the following facts: (1) control of the monolayer thickness; (2) strong adhesion of the thin film to the surface of the monolayer; (3) low substrate temperature; (4) ensuring the stoichiometry of precursors; (5) economical consumption of precursors [1]. The main laser-assisted techniques used for the deposition of thin films are: (1) pulsed laser deposition [2, 3]; (2) matrix-assisted pulsed laser evaporation technique [4–6]; (3) spin coating technique [7, 8]; (4) drop casting technique [9].

The interest for laser deposition techniques is given by the fact that the resulted thin films have a controlled topography, which can be manipulated at nanometric level [10]. These materials provide several important applications in the biological field, such as: (1) drug delivery systems [11–13], (2) tissue engineering [14], (3) implants with improved biocompatibility [4, 12], (4) improved adherent surfaces [15, 16], (5) antibacterial surfaces [17, 18], (6) gas sensors [19, 20], etc.

Matrix-assisted pulsed laser evaporation (MAPLE) technique is derived from pulsed laser deposition (PLD) technique, where the target is represented by a frozen homogenous solution of the material of interest, which is diluted in a volatile solvent (matrix solvent). The temperature at which the target solution is frozen is given by the liquid nitrogen temperature. The target is placed in a vacuum chamber and a high energy laser is directed trough it. The pulsed laser energy is absorbed by the solvent in the target and it is converted in thermal energy, which determines the evaporation of the solvent. The evaporating molecules of the solvent collide with the solute (material) molecules, which are transformed in a gas phase, because of the transferred kinetic energy. The advantages of MAPLE compared to PLD are given by the fact that this technique avoids the photochemical damage and the decomposition in PLD technique, which is determined by high energy of the laser pulses [10] (Fig. 11.1).

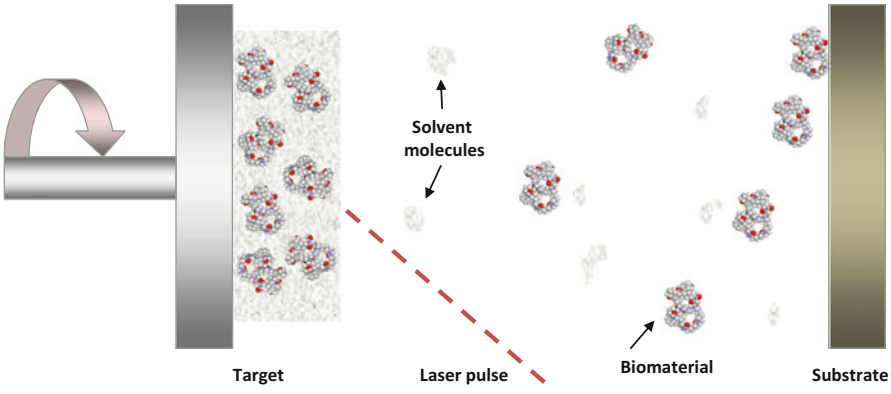

Fig. 11.1 Schematic representation of the principle of matrix-assisted pulsed laser evaporation technique (MAPLE)

11.2 The MAPLE Deposition Apparatus

The MAPLE technique was developed as an improvement for the PLD technique, in order to be used for thin film depositions of organic materials. It was implemented for the first time in the 1990s by the US Naval Research Laboratory to obtain functionalized polymer films [21].

The MAPLE apparatus, as shown in Fig. 11.2, consists of a sealed chamber which presents a cryogenically cooled rotating target holder and a substrate holder, also having a rotation movement. The target holder is connected to a liquid nitrogen tank. The chamber has an input for a background gas and for vacuum. It also presents the laser beam focusing system, which directs pulsating laser beam at a 45° angle, on the target surface [21].

Usually the technique uses an excimer laser such as KrF, with $\lambda = 248$ nm, or ArF, with $\lambda = 193$ nm, and a pulse width between 10 and 30 ns, focused on the target in a 1–10 mm^2 spot. The repetition rate is usually set between 1 and 20 Hz and the laser fluence is between 0.01 and 1.0 J/cm^2, being set according to the type of material (solute) and solvent used to make the target. The process can be held at different pressures, from vacuum, to 70 Pa, in the presence of an inert gas or a background gas [21].

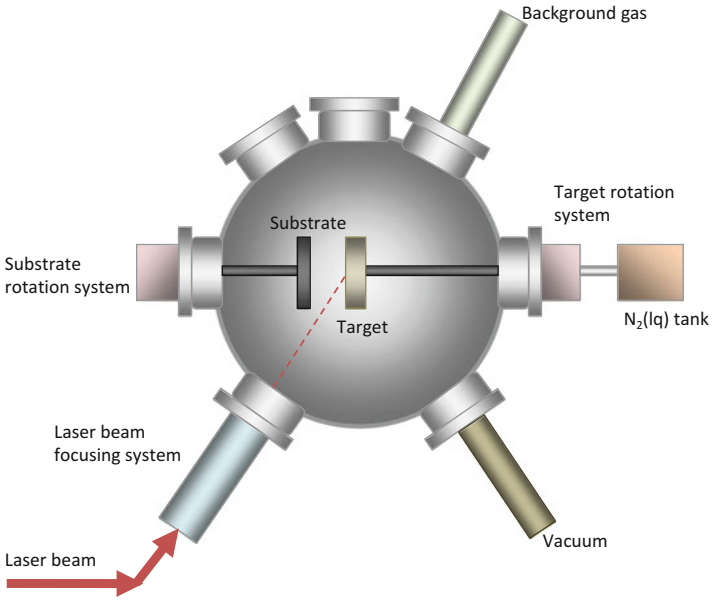

Fig. 11.2 Schematic representation of matrix-assisted pulsed laser evaporation (MAPLE) system; Important parameters in the technological process of MAPLE thin film deposition are the following: (1) the fluency of the laser, (2) the repetition rate, (3) the number of pulses, (4) the target rotation rate, (5) the angle at which the laser beam scans the target surface, (6) the background pressure, (7) the distance between substrate and target [22, 23]

11.3 Thin Films Based on Magnetite Nanostructures

Magnetite nanoparticles are intensively used in different biomedical applications especially due to their magnetic properties [24], biocompatibility [25], and easy obtaining methods [26–28]. Thus, Fe_3O_4 nanoparticle-based materials are used as: (1) drug delivery systems [29–31]; (2) antimicrobial materials [32–34]; (3) hyperthermia applications for cancer treatment [35, 36]; (4) contrast substance for magnetic resonance imaging techniques [35, 37]; etc.

11.3.1 Preparation

Magnetite can be found as a natural mineral, but it can also be artificially obtained using different chemical methods. Fe_3O_4 nanoparticles were obtained for the first time as a ferrofluid in 1981, by Massart [38] using a co-precipitation method, based on the combination of ferric and ferrous salts in an alkaline medium (sodium hydroxide).

Regarding the composition of magnetite, it is an iron oxide consisting of Fe^{3+} and Fe^{2+} ions, with a characteristic molar ratio of Fe^{3+}:Fe^{2+} = 2:1 [39].

The main preparation methods are presented in Table 11.1, where the methods' principle and the implied factors are briefly summarized.

11.3.2 Functionalized Magnetite Nanostructures

The functionalization of nanomaterials consists in modifying the surface of nanoparticles by means of attaching different type of molecules, in order to improve the properties of the inorganic structure: (1) the biocompatibility [50, 51], (2) stability [52, 53], (3) targeting properties [31, 35, 54, 55], (4) carrier properties [56–58] (Fig. 11.3).

Magnetite surface chemistry depends on the pH, acting like Lewis acids in aqueous systems: at low pH values the surface of Fe_3O_4 is positively charged, while at high pH values the magnetite surface is negatively charged [59–61]. The main classes of magnetite functionalization methods are: (1) covalent bonding and (2) non-covalent bonding. The non-covalent bonding between the functionalizing molecules and the magnetite nanoparticle surface is commonly encountered by means of hydrogen bonding with HO^- groups in Fe_3O_4.

The functionalizing agents which can interact with Fe_3O_4 nanoparticles are classified as follows: (1) organic functionalizations and (2) inorganic functionalizations. In the first class are included small molecules and surfactants (dehydroascorbic acid [37], silane compounds [62], folic acid [35], carboxyl [36]) generally applied to reduce the aggregation phenomena of magnetite nanoparticles in suspension;

Table 11.1 The main chemical methods for obtaining Fe_3O_4 nanoparticles

Obtaining method	Method principle	Factors influencing the obtaining process	Observations	References
Co-precipitation	The nucleation process of Fe^{3+} and Fe^{2+} ions takes place in an alkaline medium	Fe^{3+}–Fe^{2+} molar ratio (2:1)	Advantages: high yield synthesis, reproducibility, control of nanoparticle dimensions. Disadvantages: by means of traditional method, aggregation and oxidation of nanoparticles can take place	[26, 39–42]
		pH value (pH = 9-14)		
		Non-oxidant medium		
		Magnetic stirring, ultrasound assisting, mechanical stirring (favors the precursors interaction at molecular level)		
		Using surfactants to control the nanoparticles dimension		
		The crystallization temperature (influences the dimensions of nanoparticles)		
Hydrothermal	Obtaining singular magnetite crystals from water soluble minerals placed in an autoclave; this equipment assures maintaining exact parameters like pressure, temperature and reaction time.	Non-oxidant medium	Advantages: high yield synthesis; controlled technological process; narrow distribution of nanoparticles dimension Disadvantages: long reaction time	[27, 43–47]
		Temperature (influences the dimension of the nanoparticles)		
		Reaction time (influences the dimension of nanoparticles)		
		Pressure (high pressure)		
		Reduction agent (reduces the nanoparticles dimension)		
Solvothermal	Resembles the hydrothermal method, only the precursors are dissolved in organic solvents at a temperature higher that their boiling point.	Time of thermal treatment	Advantages: high control of nanoparticles dimension Disadvantages: The organic solvents used in the obtaining process can be toxic for biological usage	[24, 48, 49]
		Temperature		
		The stabilizer quantity (introduced as organic solvent)		

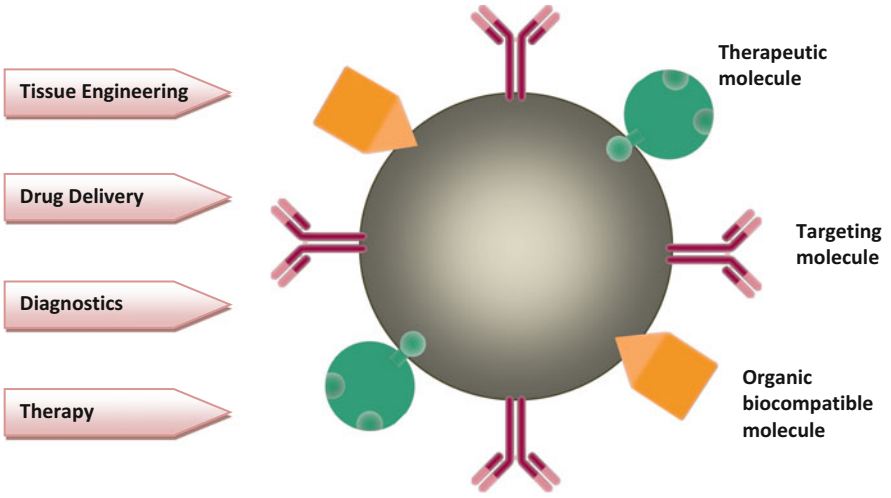

Fig. 11.3 Applications of functionalized magnetite nanoparticles

polymers (PEG [63], chitosan [64], PVA [65]), used to improve biocompatibility, stability, or to modify the character of the nanoparticle surface; enzymes (pullulanase [66], porphyrin [67], glucose oxidase [68]), with sensing properties; respectively, therapeutic molecules (docetaxel [31], usnic acid [32], danorubicin [69], umbelliprenin [70], rotavirus capsid surface protein [57]), used to obtain drug delivery systems. Magnetite functionalization with inorganic coatings is generally applied for different reasons, like: (1) enhancing the magnetic properties of the nanoparticles [71–73]; (2) enhancing the antioxidant properties of magnetite [74]; (3) inducing antibacterial properties [75]; (4) improving the biocompatibility of the system [76, 77].

11.3.3 Thin Films

Magnetite-based thin films can be obtained by several techniques, as follows: (1) pulsed laser deposition technique [78], (2) matrix-assisted laser evaporation technique [79], (3) ultrasound-enhanced ferrite plating [80], (4) chemical vapor deposition [81], (5) DC reactive magnetron sputtering [82] and reactive sputtering [83].

Previously obtained Fe_3O_4 functionalized nanoparticles are prepared as a diluted suspension in the matrix solvent (chloroform 1 % wt./vol.) [84] and then put into a precooled target holder and frozen in liquid nitrogen. For example, Cristescu et al. [84] used the following experimental parameters for all of the Fe_3O_4@oleic acid@ antibiotic MAPLE deposited thin film samples: a laser fluence between 65 and 300 mJ/cm^2, a repetition rate of 10 Hz, 7,200–20,000 laser pulses, a target rotation

rate of 0.4 Hz, an angle of 45° between the laser beam and the target surface, a distance of 4 cm between the substrate and target, and a background pressure of 30–100 Pa [84].

11.3.4 Biological Applications

Nosocomial infections, or hospital-acquired infections, are a current problem of the medical system, over 1.7 million hospital-associated infections contributing and causing over 99.000 deaths every year [85]. In Europe, gram-negative associated infections cause the most numerous untreatable infections [86], therefore combating the antibiotic resistance being an important subject of the latest scientific studies in the biomedical field. Biofilms are microbial communities included in a polysaccharide matrix, attached to a substrate. These are commonly encountered in unsterile prosthetic devices, contributing to a large number of infectious cases. Thus, there are several studies conducted in order to obtain anti-biofilm surface coatings for medical devices, and matrix-assisted pulsed laser evaporation technique offers great solutions; Table 11.2 gives a summary of the latest examples regarding this aspect.

Table 11.2 presents several examples of MAPLE deposited thin films based on modified magnetite nanoparticles, which exhibit antibacterial properties, which can be used as a growth support for cells. The Fe_3O_4@oleic acid/antibiotic thin films are excellent candidates which can be used as surface modification methods for medical devices and implants, with anti-adherence and antimicrobial properties [17]. However, the anti-adherence property refers only to the microbial colonies, as it was proved that human epithelial carcinoma HeLa cell monolayers can grow on these modified surfaces. The antimicrobial properties of the obtained samples were tested against both gram-negative (*Pseudomonas aeruginosa*, *Klebsiella pneumoniae*, *Escherichia coli*) and gram-positive (*Staphylococcus aureus*, *Bacillus subtilis*) bacteria, using the antimicrobial activity assay (API 20E biochemical tests, VITEK I automatic system), to compare the substrate effect with several antibiotic substrates and the microbiological assay investigation procedure to measure the percent of viable bacterial cells attached to the substrates (compared to a control, represented by glass substrate). The in vitro biocompatibility of the obtained samples was evaluated after the addition of the microbial suspensions over the HeLa cell monolayer cultivated on the MAPLE modified substrates. The samples were prepared by Giemsa staining and evaluated using an inverted microscope to conclude over the degree of cell confluency, the cytotoxic effect of nanoparticles, the number of adherent bacteria, and the adherence pattern (localized adherence, where bacteria form microcolonies, diffuse adherence, where bacteria adhere to the whole cell surface and aggregative adherence, where aggregates of bacteria attach to the cells, forming an overlapped arrangement. The cell morphology was not affected by the presence of the nanoparticles, neither was the adherence pattern or the adherence index, compared to control samples.

Table 11.2 Matrix-assisted pulsed laser evaporation technique for anti-biofilm surface coatings

No.	Description	Biological investigations	Reference
1	PLGA–PVA–Fe_3O_4@usnic acid thin film depositions obtained by MAPLE	*Staphylococcus aureus* anti-biofilm adherence surfaces	[87]
2	magnetite/salicylic acid/silica shell/antibiotics thin film depositions obtained by MAPLE	Anti-adherence of *Staphylococcus aureus* and *Pseudomonas aeruginosa* biofilms; biocompatibility proven for eukaryotic HEp-2 cells	[88]
3	Fe_3O_4@oleic acid@ceftriaxone/cefepime thin films deposited by MAPLE onto inert substrates	Microbial viability and microbial adherence tests using gram-negative and gram-positive bacteria proved the antibacterial activity of these films; proved biocompatibility for HeLa cells	[84]
4	Fe_3O_4@*Cinnamomum verum* MAPLE deposited thin films on gastrostomy tubes	Normal development of endothelial cells on the surface of the modified gastrostomy tubes; anti-adherent properties against gram-positive and gram-negative bacteria	[89]
5	PLA–CS–Fe_3O_4@eugenol thin film depositions using MAPLE	The obtained substrates have bioactive properties for human endothelial cells and anti-adherence properties against *Staphylococcus aureus* and *Pseudomonas aeruginosa* bacteria	[90]
6	Poly(3-hydroxybutyric acid-co-3-hydroxyvaleric acid)–polyvinyl alcohol–PVA–Fe_3O_4@eugenol MAPLE deposited thin films	Antibacterial and anti-biofilm characteristics of the obtained thin films proved by viable cell count method on *Staphylococcus aureus* and *Pseudomonas aeruginosa* cultures; biocompatibility proved by analyzing the thin films interaction with EAhy926 human endothelial cells	[79]

Our group obtained Fe_3O_4@eugenol nanoparticles by co-precipitation method, which were embedded in poly(3-hydroxybutyric acid-co-3-hydroxyvaleric acid)–polyvinyl alcohol (P(3HB-3HV)–PVA) microspheres by oil-in-water microemulsion method; these resulted microspheres were used as modifying material for inert substrates [79]. The P(3HB-3HV)–PVA–Fe_3O_4@eugenol thin films were obtained by MAPLE deposition from 1 % (w/v) microsphere suspension in DMSO using a KrF* laser source (248 nm, 25 ns laser pulses, 300–500 mJ/cm^2 laser fluence and a repetition rate of 15 Hz, with 45,000–160,000 laser pulses). The in vitro biocompatibility was evaluated using human endothelial cells EAhy929; the proliferation and viability of the cells was tested using commercial kits, resulting in high viability of

the endothelial cells, the cells' proliferation being increased at 24 h after incubation and being maintained at 48 and 72 h (compared to control). The obtained samples were also tested against biofilm formation for *Staphylococcus aureus* and *Pseudomonas aeruginosa* bacteria using the microbial biofilm assay, which demonstrated the anti-biofilm antibacterial growth effect of the resulted biomaterial.

The same experimental procedure was used by Holban et al. [90] to obtain polylactic acid (PLA)–chitosan (CS)–Fe_3O_4@eugenol microsphere thin films depositions. The in vitro biocompatibility was tested for human endothelial cells EAhy926, using a commercial cell proliferation assay and a fluorescence long term-tracking method. The tests showed that the obtained thin films offer biocompatible support for endothelial cells growth, their morphology and proliferation capability being normal [90]. For the anti-biofilm evaluation, *Staphylococcus aureus* and *Pseudomonas aeruginosa* strains were cultured in Luria Broth medium and put in contact with the resulted biomaterials. The biofilm formation is affected after 24 and 48 h of incubation compared to uncoated magnetite embedded in microspheres control.

Our research group also obtained polylactic-co-glycolic acid (PLGA)–polyvinyl alcohol (PVA)–Fe_3O_4@usnic acid thin film depositions by MAPLE using a KrF* laser source (248 nm, 25 ns laser pulses, 200–400 mJ/cm^2 laser fluence and a repetition rate of 10 Hz, with 10,000–20,000 laser pulses) [87]. The in vitro biocompatibility was evaluated for human mesenchymal stem cells from human bone marrow. The viability of the cultured cells was over 92 %, proving that the obtained thin films can support the normal development of the cells. Also, the normal morphology of the cells showed that the obtained materials have biocompatible properties. To evaluate the antibacterial effect, a minimal inhibitory assay and a microbial adherence and biofilm assay were employed for *S. aureus* bacteria. The obtained thin film inhibited the formation of bacterial strains for 3 days under static conditions, diminishing *S. aureus* adherence and biofilm formation.

Anghel et al. [89] obtained Fe_3O_4@*Cinnamomum verum* MAPLE thin film depositions on gastrostomy tubes, having antibacterial activity against gram-positive (*S. aureus*) and gram-negative (*E. coli*) bacteria [89]. *Cinnamomum verum* is a natural oil with anti-inflammatory, antiseptic, antifungal, and antiviral properties, which can stimulate the immune system and have antioxidant properties. The functionalized magnetite nanoparticles were obtained by co-precipitation method and dispersed in DMSO (1.5 % w/v solution) and frozen in liquid nitrogen. The MAPLE deposition was held using a KrF*laser (248 nm, 25 ns laser pulses, 300–500 mJ/cm^2 laser fluence and a repetition rate of 0.4 Hz, with 30,000–60,000 laser pulses). Regarding the antibacterial effect of the modified tubes, the most inhibitory effect was proved for *S. aureus* (compared to control). The in vitro biocompatibility effect, tested using the MTT assay on human endothelial cells, proved a normal development at 24 and 48 h after incubation, and an improved proliferation at 72 h, compared to control. The fluorescence microscopy images obtained at 5 days after incubation showed a normal growth and morphology of the cells.

11.4 Thin Films Based on Inorganic–Organic Hybrid Nanomaterials

Hybrid organic–inorganic nanomaterials have been intensively used in different biomedical applications due to the combination of properties from both organic and inorganic moieties [91]. Examples of such applications are: (1) tissue engineering [15], (2) antibacterial and anti-biofilm effect [92], (3) drug delivery systems [93].

There are several reasons for developing such materials, excelling in the improvement of properties like: (1) increased biocompatibility of the designed nanomaterials, by applying several organic functionalizing agents; (2) antibacterial properties of the organic material; (3) increased stability; (4) modifying the surface character; (5) drug loading.

11.4.1 Preparation

The preparation of hybrid nanomaterials can be done in several ways, which are grouped in two main classes, depending on the interactions that take place between the organic and inorganic phases: (1) methods where no covalent bond is formed between the two phases, (2) methods where covalent bonds are formed between the two phases. Table 11.3 [94] summarizes the main methods for obtaining organic–inorganic hybrid nanomaterials (Fig. 11.4).

11.4.2 Thin Films

Birjega et al. [119] obtained layered double hydroxide (LDH)–polyethylene glycol (PEG)/ethylene glycol (EG) thin films deposited by MAPLE technique [119]. The interest for LDH is given by the fact that it is an artificial clay, which consists of positively charged layers, arranged parallel one to another. It acts as a host material for anions located in the interlayer regions, which can be easily replaced by other negatively charged molecules of biological interest. The main application of these thin film coatings consists in modifying the surface character and controls its surface wetting. The Mg-Al LDH (Mg/Al = 3) was obtained using a co-precipitation method (at suprasaturation, pH = 10) from aqueous solutions of Mg and Al nitrates, sodium hydroxide and carbonate, resulting in a gel, which underwent a drying process (85 °C, 24 h), followed by a calcination process (460 °C, 18 h, nitrogen atmosphere). LDH-polymer (PEG/EG) composites were prepared by immersing Mg(Al)O mixed oxides powders immersed in aqueous polymer solutions (200 amu/1,450 amu, where Mg(Al)O/PEG and Mg(Al)O/EG = 1.76/1), separated by vacuum filtration and dried (vacuum, 30 °C, 24 h) [119]. For MAPLE deposition of the thin films, a Nd:YAG laser (266 nm, 5 ns pulses, with a repetition rate of 10Hz, a laser fluence of 1–2 J/cm^2) was used. Other important parameters are: (1) a

Table 11.3 Methods for obtaining organic–inorganic nanomaterials [94]

Class of methods	Method	Method description	Examples	Reference
Non covalent bond	Addition of pre-obtained nanoparticles in polymer solutions	Disadvantages: homogeneity of the resulted material; possible aggregation of nanoparticles	Psyllium-aspirin-TiO_2 for controlled delivery	[95]
			Bio-based phase change materials (fatty acids)-exfoliated graphite nanoplatelets/carbon nanotubes	[96]
			Polyacrylic acid- TiO_2	[97]
	In situ formation of nanoparticles		Polyamide-SiO_2	[98]
			Melamine- Ag	[99]
			Poly (vinylidene fluoride)- Ag	[100]
	Monomer polymerization in the inorganic material pores	Disadvantages: the polymerization process needs an initiator which can be toxic (usually this method has a phase of radical polymerization)	Poly L-lactide- layered double hydroxide	[101]
			Polyacrylamide-layered double hydroxide	[102]
			poly(methyl methacrylate)-layered double hydroxide	[103]
	Small molecules encapsulation	Advantages: this is a common method used to obtain drug delivery systems	$CaCO_3$–Lysozyme	[104]
			SiO_2–hemoglobin	[105]
			$CaCO_3$–Vaterite	[106]
	Interpenetrating networks	Advantages: both organic and inorganic parts grow simultaneously Disadvantages: the growing process of both phases must take place at similar rates; the process has little reproducibility	ZrO_2/PEG	[107]
			Polypropylene-silica	[108]
	Self-assembly	Advantages: High strength and stability	Gelatin-CaP	[109]

(continued)

Table 11.3 (continued)

Class of methods	Method	Method description	Examples		Reference
Covalent bond	Covalent linking at molecular level	Advantages: Improved dispersion of the modified nanoparticles	Surface polymerization	Poly(methyl methacrylate)- carbon doped TiO_2	[110]
				Poly(methyl methacrylate-(3-mercaptopropyl) trimethoxysilane–Fe_3O_4	[111]
				Poly(hydroethyl acrylate–bromo-acetamide–ZnO	[112]
	Covalent linking between a pre-obtained polymer and an inorganic nanoparticle	The method can be applied easily for polymers having a carboxyl group which can react with metal oxide nanoparticles	3-aminopropyltrimethoxysilane/3-Isocyanatopropyl trimethoxysilane- TiO_2 (condensation reaction)		[113]
			Poly(vinyl alcohol)–γ-aminopropyltriethoxy silane–TiO_2		[114]
			Amino propyl trimethoxy silane- TiO_2 (condensation reaction)		[115]
	Templating	Advantages: high precision and reproducible properties	Polyvinylidene fluoride- TiO_2- 1H,1H,2H,2H-perfluorododecyltrichlorosilane		[116]
			TiO_2–polyethylene glycol–SiO_2		[117]
			TiO_2–palygorskite		[118]

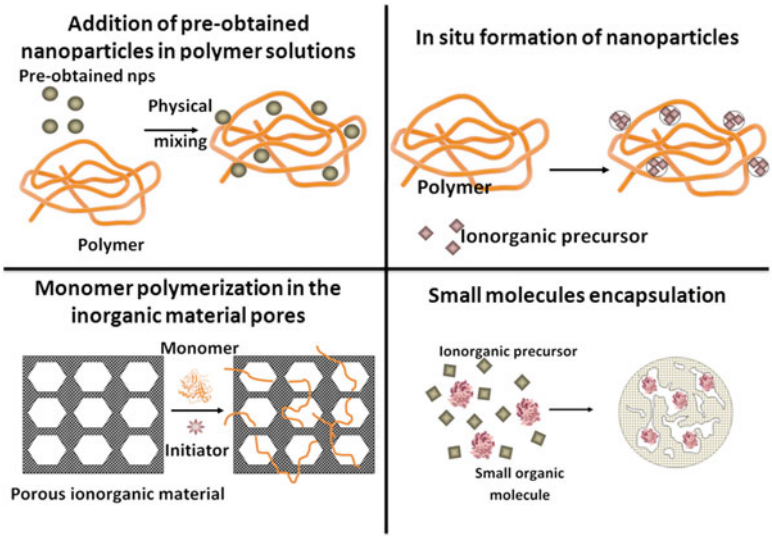

Fig. 11.4 Schematic representations of non-covalent bonding methods for obtaining hybrid nanomaterials

45° angle between the laser and the target; (2) a laser spot size between 0.6 and 0.8 mm^2; (3) 40,000–60,000 laser pulses.

Predoi et al. obtained γ-Fe_2O_3@dextran thin films deposited by MAPLE technique using a UV KrF* excimer laser (248 nm), with 25 ns pulses and a repetition rate of 10 Hz. 25×10^3 laser pulses were applied and a fluence of 0.5 J/cm^2 was assured [120]. The target was prepared using a solution of 0–25 wt.% iron oxide nanoparticles obtained by co-precipitation method, 10 wt.% dextran (2,500 Da) and distillated, frozen in liquid nitrogen solution. The surface morphology of the obtained samples was investigated by scanning electron microscopy technique, which proved an aggregated aspect of the films, consisting of micrometer sized grains. Also, by other investigations, the authors concluded that the resulted thin films have a crystallinity, chemical composition, and molecular structure identical to the materials used for target preparation.

In the experiment described by Miroiu et al. [15], hydroxyapatite–silk fibroin thin films were obtained by MAPLE deposition. The target was prepared using polymer solutions (2 wt.% and 4 wt.%, respectively) and adding hydroxyapatite (HA) in order to obtain a HA–fibroin weight ratio of about 3:2 and 3:4 respectively. The HA–fibroin solutions were mechanically stirred and several drops of NaOH or NaCl were added in order to adjust the pH to 7.4 (physiological value). Then, the solutions were frozen in liquid nitrogen to obtain the targets. For the deposition process, a KrF* excimer laser (248 nm, with 25 ns pulses, a repetition rate of 10–15 Hz and a laser fluence of 0.4–0.5 J/cm^2) was used; 20,000–50,000 pulses were applied for each film [15].

11.4.3 Biological Applications

Miroiu et al. obtained hydroxyapatite–silk fibroin thin films deposited by MAPLE on the surface of metallic prosthesis. The aim of the study was given by the fact that the biomimetic modifies surface display enhanced properties like bioaffinity and osteoconductivity. The in vitro biocompatibility test using SaOs2 osteosarcoma cells cultured for 72 h on the surface of the modified implants showed an improved viability and spreading of the cells. The elongated morphology of the cells proved that the resulted hydroxyapatite–silk fibroin coatings have good performances as bone implants, assuring an optimal interface between the living tissue and the metallic surface of the prosthesis. The best results were given by the HA3-FIB4 sample (3 wt% hydroxyapatite–4 wt% fibroin) [15].

The γ-Fe_2O_3@dextran thin film depositions obtained using MAPLE technique by Predoi et al. [120] were investigated as biocompatible structures used for implant modification coatings in locoregional cancer treatment by hyperthermia after a surgical intervention. Thus, human hepatocarcinoma cells HepG2 were cultivated on the obtained thin films, the viability investigated by MTT colorimetric assay, resulting in a good biocompatibility of the materials. Regarding the morphological aspect of the cells, the cells cultured on the 5 wt.% iron oxide samples grew into larger multicellular aggregates [120] (Table 11.4).

11.5 Conclusions and Perspectives

Matrix-assisted pulsed laser evaporation is the most frequently used method to obtain thin film nanoarchitectonics for biomedical applications, because of its numerous advantages, like assuring control of the monolayer thickness, a strong adhesion of the thin film to the surface of the monolayer, low substrate temperature, ensuring the stoichiometry of precursors, and economical consumption of precursors. This technique has been applied to obtain magnetite modified surfaces with antibacterial properties, used for implants and medical devices, in order to prevent the nosocomial infections, frequently associated with improper sterilization or surgical procedures. However, these systems do not affect the adherence and biocompatibility of tissue cells. Hybrid organic–inorganic nanomaterials are preferred because they combine properties from both components, resulting in an increased biocompatibility of the designed nanomaterials, by applying several organic functionalizing agents, antibacterial properties of the organic material, increased stability, a modified surface character, drug loading. Such thin films have been applied for modified surface prosthesis with antibacterial properties and improved biocompatibility and cellular adherence. Some systems have been designed for delivery action, in order to improve some properties, or for therapeutic effects.

Table 11.4 Classes of organic–inorganic thin film depositions using MAPLE

Class of inorganic material	Description of the system	Biological application	Biological evaluation	Reference
Silver-based	PEG–PLGA–AgNPs thin film depositions by MAPLE	Antibacterial properties	In vitro antibacterial activity against *Escherichia coli*	[121]
Calcium-based	Alendronate–hydroxyapatite deposited thin films by MAPLE	Tissue engineering (enhanced bioactivity)	In vitro interaction with osteoblast-like MG-63 cells and human osteoclasts; normal morphology, increased proliferation, high differentiation parameters for osteoblast cells; reduced proliferation of osteoclasts	[122]
	Hydroxyapatite@ maleate-vinyl acetate thin film deposition by MAPLE	Bone implantology	In vitro biocompatibility evaluation using human primary osteoblasts (OBs); specific and controlled proliferation (indicated by the measurements of collagen and non-collagenous proteins); normal cytoskeleton and vinculin dynamics indicating the adherence of OBs at the substrate	[123]
Silica-based	Fe_3O_4@salicylic acid@ SiO_2@ antibiotic MAPLE thin films	Antibacterial properties	In vitro biocompatibility evaluation using HEp-2 cells; in vitro anti-biofilm evaluation against *Staphylococcus aureus* and *Pseudomonas aeruginosa* strains	[88]
Iron oxide-based	γ-Fe_2O_3@dextran thin films obtained by MAPLE depositions	Biocompatible substrates	In vitro biocompatibility evaluation using Hep G2 cells (human liver cells); fluorescence visualization proved a normal development of actin cytoskeleton and a normal cell cycle	[124]

Acknowledgements This work was financially supported by Sectoral Operational Programme Human Resources Development, financed from the European Social Fund and by the Romanian Government under the contract number POSDRU/156/1.2/G/135764 "Improvement and implementation of university master programs in the field of Applied Chemistry and Materials Science–ChimMaster".

References

1. Wu PK, Ringeisen BR, Callahan J, Brooks M, Bubb DM, Wu HD, Pique A, Spargo B, McGill RA, Chrisey DB (2001) The deposition, structure, pattern deposition, and activity of biomaterial thin-films by matrix-assisted pulsed-laser evaporation (MAPLE) and MAPLE direct write. Thin Solid Films 398:607–614
2. Erakovic S, Jankovic A, Ristoscu C, Duta L, Serban N, Visan A, Mihailescu IN, Stan GE, Socol M, Iordache O, Dumitrescu I, Luculescu CR, Janackovic D, Miskovic-Stankovic V (2014) Antifungal activity of Ag:hydroxyapatite thin films synthesized by pulsed laser deposition on Ti and Ti modified by TiO_2 nanotubes substrates. Appl Surf Sci 293:37–45
3. Duta L, Oktar FN, Stan GE, Popescu-Pelin G, Serban N, Luculescu C, Mihailescu IN (2013) Novel doped hydroxyapatite thin films obtained by pulsed laser deposition. Appl Surf Sci 265:41–49
4. Visan A, Grossin D, Stefan N, Duta L, Miroiu FM, Stan GE, Sopronyi M, Luculescu C, Freche M, Marsan O, Charvilat C, Ciuca S, Mihailescu IN (2014) Biomimetic nanocrystalline apatite coatings synthesized by Matrix Assisted Pulsed Laser Evaporation for medical applications. Mater Sci Eng B-Adv 181:56–63
5. Iordache S, Cristescu R, Popescu AC, Popescu CE, Dorcioman G, Mihailescu IN, Ciucu AA, Balan A, Stamatin I, Fagadar-Cosma E, Chrisey DB (2013) Functionalized porphyrin conjugate thin films deposited by matrix assisted pulsed laser evaporation. Appl Surf Sci 278:207–210
6. Palla-Papavlu A, Rusen L, Dinca V, Filipescu M, Lippert T, Dinescu M (2014) Characterization of ethylcellulose and hydroxypropyl methylcellulose thin films deposited by matrix-assisted pulsed laser evaporation. Appl Surf Sci 302:87–91
7. Heredia E, Bojorge C, Casanova J, Cánepa H, Craievich A, Kellermann G (2014) Nanostructured ZnO thin films prepared by sol–gel spin-coating. Appl Surf Sci 317:19–25, http://dx.doi.org/10.1016/j.apsusc.2014.08.046
8. Carradò A, Viart N (2010) Nanocrystalline spin coated sol–gel hydroxyapatite thin films on Ti substrate: Towards potential applications for implants. Solid State Sci 12(7):1047–1050, http://dx.doi.org/10.1016/j.solidstatesciences.2010.04.014
9. Farag AAM, Yahia IS (2010) Structural, absorption and optical dispersion characteristics of rhodamine B thin films prepared by drop casting technique. Opt Commun 283(21): 4310–4317
10. Caricato AP, Luches A, Leggieri G, Martino M, Rella R (2012) Matrix-assisted pulsed laser deposition of polymer and nanoparticle films. Vacuum 86(6):661–666
11. Paun IA, Moldovan A, Luculescu CR, Dinescu M (2011) Biocompatible polymeric implants for controlled drug delivery produced by MAPLE. Appl Surf Sci 257(24):10780–10788
12. Sima F, Axente E, Iordache I, Luculescu C, Gallet O, Anselme K, Mihailescu N (2014) Combinatorial matrix assisted pulsed laser evaporation of a biodegradable polymer and fibronectin for protein immobilization and controlled release. Appl Surf Sci 306:75–79
13. Paun IA, Moldovan A, Luculescu CR, Staicu A, Dinescu M (2012) MAPLE deposition of PLGA:PEG films for controlled drug delivery: Influence of PEG molecular weight. Appl Surf Sci 258(23):9302–9308
14. Mihailescu M, Popescu RC, Matei A, Acasandrei A, Paun IA, Dinescu M (2014) Investigation of osteoblast cells behavior in polymeric 3D micropatterned scaffolds using digital holographic microscopy. Appl Optics 53(22):4850–4858

15. Miroiu FM, Socol G, Visan A, Stefan N, Craciun D, Craciun V, Dorcioman G, Mihailescu IN, Sima LE, Petrescu SM, Andronie A, Stamatin I, Moga S, Ducu C (2010) Composite biocompatible hydroxyapatite–silk fibroin coatings for medical implants obtained by Matrix Assisted Pulsed Laser Evaporation. Mater Sci Eng B 169(1–3):151–158, http://dx.doi.org/10.1016/j.mseb.2009.10.004
16. Rusen L, Dinca V, Mitu B, Mustaciosu C, Dinescu M (2014) Temperature responsive functional polymeric thin films obtained by matrix assisted pulsed laser evaporation for cells attachment–detachment study. Appl Surf Sci 302:134–140, http://dx.doi.org/10.1016/j.apsusc.2013.09.122
17. Cristescu R, Popescu C, Dorcioman G, Miroiu FM, Socol G, Mihailescu IN, Gittard SD, Miller PR, Narayan RJ, Enculescu M, Chrisey DB (2013) Antimicrobial activity of biopolymer–antibiotic thin films fabricated by advanced pulsed laser methods. Appl Surf Sci 278:211–213, http://dx.doi.org/10.1016/j.apsusc.2013.01.062
18. Grumezescu V, Socol G, Grumezescu AM, Holban AM, Ficai A, Truşcă R, Bleotu C, Balaure PC, Cristescu R, Chifiriuc MC (2014) Functionalized antibiofilm thin coatings based on PLA–PVA microspheres loaded with usnic acid natural compounds fabricated by MAPLE. Appl Surf Sci 302:262–267, http://dx.doi.org/10.1016/j.apsusc.2013.09.081
19. Caricato AP, Luches A, Rella R (2009) Nanoparticle thin films for Gas sensors prepared by matrix assisted pulsed laser evaporation. Sensors (Basel) 9(4):2682–2696
20. Kopecky D, Vrnata M, Vyslouzil F, Myslik V, Fitl P, Ekrt O, Matejka P, Jelinek M, Kocourek T (2009) Polypyrrole thin films for gas sensors prepared by matrix-assisted pulsed laser evaporation technology: effect of deposition parameters on material properties. Thin Solid Films 517(6):2083–2087
21. Pique A (2011) The matrix-assisted pulsed laser evaporation (MAPLE) process: origins and future directions. Appl Phys A-Mater 105(3):517–528
22. Itina TE, Zhigilei LV, Garrison BJ (2001) Matrix-assisted pulsed laser evaporation of polymeric materials: a molecular dynamics study. Nucl Instrum Meth B 180:238–244
23. Bubb DM, Papantonakis M, Collins B, Brookes E, Wood J, Gurudas U (2007) The influence of solvent parameters upon the surface roughness of matrix assisted laser deposited thin polymer films. Chem Phys Lett 448(4–6):194–197
24. Jia K, Zhang J, Huang X, Liu X (2014) Size dependent electromagnetic properties of Fe_3O_4 nanospheres. Chem Phys Lett 614:31–35, http://dx.doi.org/10.1016/j.cplett.2014.09.002
25. Xiao L, Li J, Brougham DF, Fox EK, Feliu N, Bushmelev A, Schmidt A, Mertens N, Kiessling F, Valldor M, Fadeel B, Mathur S (2011) Water-soluble superparamagnetic magnetite nanoparticles with biocompatible coating for enhanced magnetic resonance imaging. ACS Nano 5(8):6315–6324
26. Anbarasu M, Anandan M, Chinnasamy E, Gopinath V, Balamurugan K (2015) Synthesis and characterization of polyethylene glycol (PEG) coated Fe_3O_4 nanoparticles by chemical co-precipitation method for biomedical applications. Spectrochim Acta A Mol Biomol Spectrosc 135:536–539, http://dx.doi.org/10.1016/j.saa.2014.07.059
27. Ahmadi S, Chia CH, Zakaria S, Saeedfar K, Asim N (2012) Synthesis of Fe_3O_4 nanocrystals using hydrothermal approach. J Magn Magn Mater 324(24):4147–4150
28. Li YF, Jiang RL, Liu TY, Lv H, Zhou L, Zhang XY (2014) One-pot synthesis of grass-like Fe_3O_4 nanostructures by a novel microemulsion-assisted solvothermal method. Ceram Int 40(1):1059–1063
29. Gu L, He XM, Wu ZY (2014) Mesoporous Fe_3O_4/hydroxyapatite composite for targeted drug delivery. Mater Res Bull 59:65–68
30. Yan SF, Zhang X, Sun YY, Wang TT, Chen XS, Yin JB (2014) In situ preparation of magnetic Fe_3O_4 nanoparticles inside nanoporous poly(L-glutamic acid)/chitosan microcapsules for drug delivery. Colloid Surf B 113:302–311
31. Huang X, Yi C, Fan Y, Zhang Y, Zhao L, Liang Z, Pan J (2014) Magnetic Fe3O4 nanoparticles grafted with single-chain antibody (scFv) and docetaxel loaded β-cyclodextrin potential for ovarian cancer dual-targeting therapy. Mater Sci Eng C 42:325–332, http://dx.doi.org/10.1016/j.msec.2014.05.041

32. Grumezescu AM, Holban AM, Andronescu E, Mogosanu GD, Vasile BS, Chifiriuc MC, Lazar V, Andrei E, Constantinescu A, Maniu H (2014) Anionic polymers and 10 nm Fe_3O_4@ UA wound dressings support human foetal stem cells normal development and exhibit great antimicrobial properties. Int J Pharm 463(2):146–154
33. Amarjargal A, Tijing LD, Im I-T, Kim CS (2013) Simultaneous preparation of Ag/Fe_3O_4 core–shell nanocomposites with enhanced magnetic moment and strong antibacterial and catalytic properties. Chem Eng J 226:243–254, http://dx.doi.org/10.1016/j.cej.2013.04.054
34. Fang WJ, Zheng J, Chen C, Zhang HB, Lu YX, Ma L, Chen GJ (2014) One-pot synthesis of porous Fe_3O_4 shell/silver core nanocomposites used as recyclable magnetic antibacterial agents. J Magn Magn Mater 357:1–6
35. Jiang QL, Zheng SW, Hong RY, Deng SM, Guo L, Hu RL, Gao B, Huang M, Cheng LF, Liu GH, Wang YQ (2014) Folic acid-conjugated Fe_3O_4 magnetic nanoparticles for hyperthermia and MRI in vitro and in vivo. Appl Surf Sci 307:224–233
36. Barick KC, Singh S, Bahadur D, Lawande MA, Patkar DP, Hassan PA (2014) Carboxyl decorated Fe_3O_4 nanoparticles for MRI diagnosis and localized hyperthermia. J Colloid Interface Sci 418:120–125
37. Gupta H, Paul P, Kumar N, Baxi S, Das DP (2014) One pot synthesis of water-dispersible dehydroascorbic acid coated Fe_3O_4 nanoparticles under atmospheric air: Blood cell compatibility and enhanced magnetic resonance imaging. J Colloid Interface Sci 430:221–228, http://dx.doi.org/10.1016/j.jcis.2014.05.043
38. Massart R (1981) Preparation of aqueous magnetic liquids in alkaline and acidic media. IEEE T Magn 17(2):1247–1248
39. Faiyas APA, Vinod EM, Joseph J, Ganesan R, Pandey RK (2010) Dependence of pH and surfactant effect in the synthesis of magnetite (Fe_3O_4) nanoparticles and its properties. J Magn Magn Mater 322(4):400–404
40. Lin CC, Ho JM (2014) Structural analysis and catalytic activity of Fe_3O_4 nanoparticles prepared by a facile co-precipitation method in a rotating packed bed. Ceram Int 40(7): 10275–10282
41. Maier-Hauff K, Ulrich F, Nestler D, Niehoff H, Wust P, Thiesen B, Orawa H, Budach V, Jordan A (2011) Efficacy and safety of intratumoral thermotherapy using magnetic iron-oxide nanoparticles combined with external beam radiotherapy on patients with recurrent glioblastoma multiforme. J Neuro-Oncol 103(2):317–324
42. Meng HN, Zhang ZZ, Zhao FX, Qiu T, Yang JD (2013) Orthogonal optimization design for preparation of Fe_3O_4 nanoparticles via chemical coprecipitation. Appl Surf Sci 280:679–685
43. Ma FX, Sun XY, He K, Jiang JT, Zhen L, Xu CY (2014) Hydrothermal synthesis, magnetic and electromagnetic properties of hexagonal Fe_3O_4 microplates. J Magn Magn Mater 361:161–165
44. Yang XW, Jiang W, Liu L, Chen BH, Wu SX, Sun DP, Li FS (2012) One-step hydrothermal synthesis of highly water-soluble secondary structural Fe_3O_4 nanoparticles. J Magn Magn Mater 324(14):2249–2257
45. Yuan KF, Ni YH, Zhang L (2012) Facile hydrothermal synthesis of polyhedral Fe_3O_4 nanocrystals, influencing factors and application in the electrochemical detection of H_2O_2. J Alloy Compd 532:10–15
46. Wu R, Liu J-H, Zhao L, Zhang X, Xie J, Yu B, Ma X, Yang S-T, Wang H, Liu Y (2014) Hydrothermal preparation of magnetic Fe3O4@C nanoparticles for dye adsorption. J Environ Chem Eng 2(2):907–913, http://dx.doi.org/10.1016/j.jece.2014.02.005
47. Gao G, Qiu PY, Qian QR, Zhou N, Wang K, Song H, Fu HL, Cui DX (2013) PEG-200-assisted hydrothermal method for the controlled-synthesis of highly dispersed hollow Fe_3O_4 nanoparticles. J Alloy Compd 574:340–344
48. Chen FX, Liu R, Xiao SW, Zhang CT (2014) Solvothermal synthesis in ethylene glycol and adsorption property of magnetic Fe_3O_4 microspheres. Mater Res Bull 55:38–42
49. Liu J, Wang L, Wang J, Zhang LT (2013) Simple solvothermal synthesis of hydrophobic magnetic monodispersed Fe_3O_4 nanoparticles. Mater Res Bull 48(2):416–421

50. Patil RM, Shete PB, Thorat ND, Otari SV, Barick KC, Prasad A, Ningthoujam RS, Tiwale BM, Pawar SH (2014) Superparamagnetic iron oxide/chitosan core/shells for hyperthermia application: Improved colloidal stability and biocompatibility. J Magn Magn Mater 355:22–30
51. Wei Y, Yin GF, Ma CY, Huang ZB, Chen XC, Liao XM, Yao YD, Yin H (2013) Synthesis and cellular compatibility of biomineralized Fe_3O_4 nanoparticles in tumor cells targeting peptides. Colloid Surf B 107:180–188
52. Nigam S, Barick KC, Bahadur D (2011) Development of citrate-stabilized Fe_3O_4 nanoparticles: conjugation and release of doxorubicin for therapeutic applications. J Magn Magn Mater 323(2):237–243
53. Safari J, Masouleh SF, Zarnegar Z, Najafabadi AE (2014) Water-dispersible Fe_3O_4 nanoparticles stabilized with a biodegradable amphiphilic copolymer. C R Chim 17(2):151–155
54. Sohn C-H, Park SP, Choi SH, Park S-H, Kim S, Xu L, Kim S-H, Hur JA, Choi J, Choi TH (2015) MRI molecular imaging using GLUT1 antibody-Fe_3O_4 nanoparticles in the hemangioma animal model for differentiating infantile hemangioma from vascular malformation. Nanomedicine 11(1):127–135, http://dx.doi.org/10.1016/j.nano.2014.08.003
55. Tran LD, Hoang NMT, Mai TT, Tran HV, Nguyen NT, Tran TD, Do MH, Nguyen QT, Pham DG, Ha TP, Le HV, Nguyen PX (2010) Nanosized magnetofluorescent Fe_3O_4–curcumin conjugate for multimodal monitoring and drug targeting. Colloids Surf A Physicochem Eng Asp 371(1–3):104–112, http://dx.doi.org/10.1016/j.colsurfa.2010.09.011
56. Chen CY, Jiang XC, Kaneti YV, Yu AB (2013) Design and construction of polymerized-glucose coated Fe3O4 magnetic nanoparticles for delivery of aspirin. Powder Technol 236:157–163
57. Chen WH, Cao YH, Liu M, Zhao QH, Huang J, Zhang HL, Deng ZW, Dai JW, Williams DF, Zhang ZJ (2012) Rotavirus capsid surface protein VP4-coated Fe_3O_4 nanoparticles as a theranostic platform for cellular imaging and drug delivery. Biomaterials 33(31):7895–7902
58. Lu WS, Shen YH, Xie AJ, Zhang WQ (2013) Preparation and drug-loading properties of Fe_3O_4/Poly(styrene-co-acrylic acid) magnetic polymer nanocomposites. J Magn Magn Mater 345:142–146
59. Hajdu A, Illes E, Tombacz E, Borbath I (2009) Surface charging, polyanionic coating and colloid stability of magnetite nanoparticles. Colloid Surf A 347(1–3):104–108
60. Tombacz E, Toth IY, Nesztor D, Illes E, Hajdu A, Szekeres M, Vekas L (2013) Adsorption of organic acids on magnetite nanoparticles, pH-dependent colloidal stability and salt tolerance. Colloid Surf A 435:91–96
61. Salazar-Camacho C, Villalobos M, Rivas-Sanchez MD, Arenas-Alatorre J, Alcaraz-Cienfuegos J, Gutierrez-Ruiz ME (2013) Characterization and surface reactivity of natural and synthetic magnetites. Chem Geol 347:233–245
62. Atila Dinçer C, Yıldız N, Aydoğan N, Çalımlı A (2014) A comparative study of Fe_3O_4 nanoparticles modified with different silane compounds. Appl Surf Sci 318:297–304, http://dx.doi.org/10.1016/j.apsusc.2014.06.069
63. Yang JH, Zou P, Yang LL, Cao J, Sun YF, Han DL, Yang S, Wang Z, Chen G, Wang BJ, Kong XW (2014) A comprehensive study on the synthesis and paramagnetic properties of PEG-coated Fe_3O_4 nanoparticles. Appl Surf Sci 303:425–432
64. Shariatinia Z, Nikfar Z (2013) Synthesis and antibacterial activities of novel nanocomposite films of chitosan/phosphoramide/Fe_3O_4 NPs. Int J Biol Macromol 60:226–234
65. Ghanbari D, Salavati-Niasari M, Ghasemi-Kooch M (2014) A sonochemical method for synthesis of Fe_3O_4 nanoparticles and thermal stable PVA-based magnetic nanocomposite. J Ind Eng Chem 20(6):3970–3974, http://dx.doi.org/10.1016/j.jiec.2013.12.098
66. Long J, Jiao A, Wei B, Wu Z, Zhang Y, Xu X, Jin Z (2014) A novel method for pullulanase immobilized onto magnetic chitosan/Fe_3O_4 composite nanoparticles by in situ preparation and evaluation of the enzyme stability. J Mol Catal B Enzym 109:53–61, http://dx.doi.org/10.1016/j.molcatb.2014.08.007

67. Liu Q, Li H, Zhao Q, Zhu R, Yang Y, Jia Q, Bian B, Zhuo L (2014) Glucose-sensitive colorimetric sensor based on peroxidase mimics activity of porphyrin-Fe_3O_4 nanocomposites. Mater Sci Eng C 41:142–151, http://dx.doi.org/10.1016/j.msec.2014.04.038
68. Yang Z, Zhang C, Zhang J, Bai W (2014) Potentiometric glucose biosensor based on core–shell Fe_3O_4–enzyme–polypyrrole nanoparticles. Biosens Bioelectron 51:268–273, http://dx.doi.org/10.1016/j.bios.2013.07.054
69. Zhang G, Lai BB, Zhou YY, Chen BA, Wang XM, Lu Q, Chen YH (2011) Fe3O4 nanoparticles with daunorubicin induce apoptosis through caspase 8-PARP pathway and inhibit K562 leukemia cell-induced tumor growth in vivo. Nanomedicine 7(5):595–603
70. Khorramizadeh MR, Esmail-Nazari Z, Zarei-Ghaane Z, Shakibaie M, Mollazadeh-Moghaddam K, Iranshahi M, Shahverdi AR (2010) Umbelliprenin-coated Fe_3O_4 magnetite nanoparticles: antiproliferation evaluation on human fibrosarcoma cell line (HT-1080). Mat Sci Eng C-Mater 30(7):1038–1042
71. Tie SL, Lee HC, Bae YS, Kim MB, Lee K, Lee CH (2007) Monodisperse Fe_3O_4/Fe@SiO_2 core/shell nanoparticles with enhanced magnetic property. Colloid Surf A 293(1–3): 278–285
72. Larumbe S, Gomez-Polo C, Perez-Landazabal JI, Pastor JM (2012) Effect of a SiO_2 coating on the magnetic properties of Fe_3O_4 nanoparticles. J Phys-Condens Matter 24(26)
73. Abbas M, Rao BP, Islam MN, Naga SM, Takahashi M, Kim C (2014) Highly stable- silica encapsulating magnetite nanoparticles (Fe_3O_4/SiO_2) synthesized using single surfactantless-polyol process. Ceram Int 40(1):1379–1385
74. Mesarosova M, Kozics K, Babelova A, Regendova E, Pastorek M, Vnukova D, Buliakova B, Razga F, Gabelova A (2014) The role of reactive oxygen species in the genotoxicity of surface-modified magnetite nanoparticles. Toxicol Lett 226(3):303–313
75. Xia HQ, Cui B, Zhou JH, Zhang LL, Zhang J, Guo XH, Guo HL (2011) Synthesis and characterization of Fe_3O_4@C@Ag nanocomposites and their antibacterial performance. Appl Surf Sci 257(22):9397–9402
76. Arsianti M, Lim M, Lou SN, Goon IY, Marquis CP, Amal R (2011) Bi-functional gold-coated magnetite composites with improved biocompatibility. J Colloid Interface Sci 354(2): 536–545
77. Muzquiz-Ramos EM, Cortes-Hernandez DA, Escobedo-Bocardo JC, Zugasti-Cruz A (2012) In vitro bonelike apatite formation on magnetite nanoparticles after a calcium silicate treatment: Preparation, characterization and hemolysis studies. Ceram Int 38(8):6849–6856
78. Yun J-G, Lee Y-M, Lee W-J, Kim C-S, Yoon S-G (2013) Selective growth of pure magnetite thin films and/or nanowires grown in situ at a low temperature by pulsed laser deposition. J Mater Chem C 1(10):1977–1982. doi:10.1039/C2TC00672C
79. Grumezescu V, Holban AM, Iordache F, Socol G, Mogoşanu GD, Grumezescu AM, Ficai A, Vasile BŞ, Truşcă R, Chifiriuc MC, Maniu H (2014) MAPLE fabricated magnetite@eugenol and (3-hidroxybutyric acid-co-3-hidroxyvaleric acid)–polyvinyl alcohol microspheres coated surfaces with anti-microbial properties. Appl Surf Sci 306:16–22, http://dx.doi.org/10.1016/j.apsusc.2014.01.126
80. Oh CY, Oh JH, Ko T (2002) The microstructure and characteristics of magnetite thin films prepared by ultrasound-enhanced ferrite plating. IEEE T Magn 38(5):3018–3020
81. Mantovan R, Lamperti A, Georgieva M, Tallarida G, Fanciulli M (2010) CVD synthesis of polycrystalline magnetite thin films: structural, magnetic and magnetotransport properties. J Phys D Appl Phys 43(6)
82. Zhang GM, Fan CF, Pan LQ, Wang FP, Wu P, Qiu H, Gu YS, Zhang Y (2005) Magnetic and transport properties of magnetite thin films. J Magn Magn Mater 293(2):737–745
83. Qiu HM, Pan LQ, Li LW, Zhu H, Zhao XD, Xu M, Qin LQ, Xiao JQ (2007) Microstructure and magnetic properties of magnetite thin films prepared by reactive sputtering. J Appl Phys 102(11)
84. Cristescu R, Popescu C, Socol G, Iordache I, Mihailescu IN, Mihaiescu DE, Grumezescu AM, Balan A, Stamatin I, Chifiriuc C, Bleotu C, Saviuc C, Popa M, Chrisey DB (2012) Magnetic core/shell nanoparticle thin films deposited by MAPLE: investigation by chemical, morphological and in vitro biological assays. Appl Surf Sci 258(23):9250–9255

85. Andrew P (2010) Rising threat of infections unfazed by antibiotics. New York Times
86. Breathnach AS (2013) Nosocomial infections and infection control. Medicine 41(11): 649–653, http://dx.doi.org/10.1016/j.mpmed.2013.08.010
87. Grumezescu V, Holban AM, Grumezescu AM, Socol G, Ficai A, Vasile BS, Trusca R, Bleotu C, Lazar V, Chifiriuc CM, Mogosanu GD (2014) Usnic acid-loaded biocompatible magnetic PLGA-PVA microsphere thin films fabricated by MAPLE with increased resistance to staphylococcal colonization. Biofabrication 6(3)
88. Mihaiescu DE, Cristescu R, Dorcioman G, Popescu CE, Nita C, Socol G, Mihailescu IN, Grumezescu AM, Tamas D, Enculescu M, Negrea RF, Ghica C, Chifiriuc C, Bleotu C, Chrisey DB (2013) Functionalized magnetite silica thin films fabricated by MAPLE with antibiofilm properties. Biofabrication 5(1)
89. Anghel AG, Grumezescu AM, Chirea M, Grumezescu V, Socol G, Iordache F, Oprea AE, Anghel I, Holban AM (2014) MAPLE fabricated Fe_3O_4@*cinnamomum verum* antimicrobial surfaces for improved gastrostomy tubes. Molecules 19(7):8981–8994
90. Holban AM, Grumezescu V, Grumezescu AM, Vasile BS, Trusca R, Cristescu R, Socol G, Iordache F (2014) Antimicrobial nanospheres thin coatings prepared by advanced pulsed laser technique. Beilstein J Nanotechnol 5:872–880
91. Vivero-Escoto JL, Huang YT (2011) Inorganic-organic hybrid nanomaterials for therapeutic and diagnostic imaging applications. Int J Mol Sci 12(6):3888–3927
92. Simchi A, Tamjid E, Pishbin F, Boccaccini AR (2011) Recent progress in inorganic and composite coatings with bactericidal capability for orthopaedic applications. Nanomedicine 7(1):22–39
93. Guo R, Du X, Zhang R, Deng L, Dong A, Zhang J (2011) Bioadhesive film formed from a novel organic–inorganic hybrid gel for transdermal drug delivery system. Eur J Pharm Biopharm 79(3):574–583, http://dx.doi.org/10.1016/j.ejpb.2011.06.006
94. Nguyen TD (2013) Portraits of colloidal hybrid nanostructures: controlled synthesis and potential applications. Colloid Surf B 103:326–344
95. Rosu MC, Bratu I (2014) Promising psyllium-based composite containing TiO_2 nanoparticles as aspirin-carrier matrix. Prog Nat Sci-Mater 24(3):205–209
96. Yu S, Jeong SG, Chung O, Kim S (2014) Bio-based PCM/carbon nanomaterials composites with enhanced thermal conductivity. Sol Energ Mat Sol C 120:549–554
97. Yoshioka T, Chávez-Valdez A, Roether JA, Schubert DW, Boccaccini AR (2013) AC electrophoretic deposition of organic–inorganic composite coatings. J Colloid Interface Sci 392:167–171, http://dx.doi.org/10.1016/j.jcis.2012.09.087
98. Bounor-Legaré V, Cassagnau P (2014) In situ synthesis of organic–inorganic hybrids or nanocomposites from sol–gel chemistry in molten polymers. Prog Polym Sci 39(8): 1473–1497, http://dx.doi.org/10.1016/j.progpolymsci.2014.04.003
99. Wang H, Chen D, Yu L, Chang M, Ci L (2015) One-step, room temperature, colorimetric melamine sensing using an in-situ formation of silver nanoparticles through modified Tollens process. Spectrochim Acta A Mol Biomol Spectrosc 137:281–285, http://dx.doi.org/10.1016/j.saa.2014.08.041
100. Li X, Pang RZ, Li JS, Sun XY, Shen JY, Han WQ, Wang LJ (2013) In situ formation of Ag nanoparticles in PVDF ultrafiltration membrane to mitigate organic and bacterial fouling. Desalination 324:48–56
101. Katiyar V, Gerds N, Koch CB, Risbo J, Hansen HCB, Plackett D (2010) Poly L-lactide-layered double hydroxide nanocomposites via in situ polymerization of L-lactide. Polym Degrad Stabil 95(12):2563–2573
102. Fu PJ, Chen GM, Liu J, Yang JP (2009) An intercalated hybrid of polyacrylamide/layered double hydroxide prepared via in situ intercalative polymerization. Mater Lett 63(20): 1725–1728
103. Nogueira T, Botan R, Wypych F, Lona L (2011) Study of thermal and mechanical properties of PMMA/LDHs nanocomposites obtained by in situ bulk polymerization. Compos Part A-Appl S 42(8):1025–1030

104. Tran MK, Hassani LN, Calvignac B, Beuvier T, Hindre F, Boury F (2013) Lysozyme encapsulation within PLGA and $CaCO_3$ microparticles using supercritical CO_2 medium. J Supercrit Fluid 79:159–169
105. Ma F, Zhou L, Tang J, Wei SH, Zhou YH, Zhou JH, Wang FB, Shen J (2012) A facile method for hemoglobin encapsulation in silica nanoparticles and application in biosensors. Micropor Mesopor Mat 160:106–113
106. Fujiwara M, Shiokawa K, Kubota T, Morigaki K (2014) Preparation of calcium carbonate microparticles containing organic fluorescent molecules from vaterite. Adv Powder Technol 25(3):1147–1154
107. Catauro M, Papale F, Bollino F, Gallicchio M, Pacifico S (2014) Biological evaluation of zirconia/PEG hybrid materials synthesized via sol–gel technique. Mater Sci Eng C 40: 253–259, http://dx.doi.org/10.1016/j.msec.2014.04.001
108. Zu L, Li R, Jin L, Lian H, Liu Y, Cui X (2014) Preparation and characterization of polypropylene/silica composite particle with interpenetrating network via hot emulsion sol–gel approach. Prog Nat Sci 24(1):42–49, http://dx.doi.org/10.1016/j.pnsc.2014.01.001
109. Wang HA, Bongio M, Farbod K, Nijhuis AWG, van den Beucken J, Boerman OC, van Hest JCM, Li YB, Jansen JA, Leeuwenburgh SCG (2014) Development of injectable organic/inorganic colloidal composite gels made of self-assembling gelatin nanospheres and calcium phosphate nanocrystals. Acta Biomater 10(1):508–519
110. Wang XX, Song XM, Lin M, Wang HT, Zhao YL, Zhong W, Du QG (2007) Surface initiated graft polymerization from carbon-doped TiO2 nanoparticles under sunlight illumination. Polymer 48(20):5834–5838
111. Bach LG, Islam MR, Kim JT, Seo S, Lim KT (2012) Encapsulation of Fe_3O_4 magnetic nanoparticles with poly(methyl methacrylate) via surface functionalized thiol-lactam initiated radical polymerization. Appl Surf Sci 258(7):2959–2966
112. Liu P, Wang TM (2008) Poly(hydroethyl acrylate) grafted from ZnO nanoparticles via surface-initiated atom transfer radical polymerization. Curr Appl Phys 8(1):66–70
113. Zhao J, Milanova M, Warmoeskerken MMCG, Dutschk V (2012) Surface modification of TiO_2 nanoparticles with silane coupling agents. Colloid Surf A 413:273–279
114. Mallakpour S, Barati A (2011) Efficient preparation of hybrid nanocomposite coatings based on poly(vinyl alcohol) and silane coupling agent modified TiO_2 nanoparticles. Prog Org Coat 71(4):391–398
115. Sabzi M, Mirabedini SM, Zohuriaan-Mehr J, Atai M (2009) Surface modification of TiO_2 nano-particles with silane coupling agent and investigation of its effect on the properties of polyurethane composite coating. Prog Org Coat 65(2):222–228
116. Meng SW, Mansouri J, Ye Y, Chen V (2014) Effect of templating agents on the properties and membrane distillation performance of TiO_2-coated PVDF membranes. J Membrane Sci 450:48–59
117. Crippa M, Callone E, D'Arienzo M, Müller K, Polizzi S, Wahba L, Morazzoni F, Scotti R (2011) TiO_2 nanocrystals grafted on macroporous silica: a novel hybrid organic–inorganic sol–gel approach for the synthesis of highly photoactive composite material. Appl Catal B Environ 104(3–4):282–290, http://dx.doi.org/10.1016/j.apcatb.2011.03.018
118. Stathatos E, Papoulis D, Aggelopoulos CA, Panagiotaras D, Nikolopoulou A (2012) TiO_2/palygorskite composite nanocrystalline films prepared by surfactant templating route: Synergistic effect to the photocatalytic degradation of an azo-dye in water. J Hazard Mater 211:68–76
119. Birjega R, Matei A, Mitu B, Ionita MD, Filipescu M, Stokker-Cheregi F, Luculescu C, Dinescu M, Zavoianu R, Pavel OD, Corobea MC (2013) Layered double hydroxides/polymer thin films grown by matrix assisted pulsed laser evaporation. Thin Solid Films 543:63–68
120. Predoi D, Ciobanu CS, Radu M, Costache M, Dinischiotu A, Popescu C, Axente E, Mihailescu IN, Gyorgy E (2012) Hybrid dextran-iron oxide thin films deposited by laser techniques for biomedical applications. Mat Sci Eng C-Mater 32(2):296–302
121. Paun IA, Moldovan A, Luculescu CR, Dinescu M (2013) Antibacterial polymeric coatings grown by matrix assisted pulsed laser evaporation. Appl Phys A-Mater 110(4):895–902

122. Bigi A, Boanini E, Capuccini C, Fini M, Mihailescu IN, Ristoscu C, Sima F, Torricelli P (2009) Biofunctional alendronate–hydroxyapatite thin films deposited by matrix assisted pulsed laser evaporation. Biomaterials 30(31):6168–6177, http://dx.doi.org/10.1016/j.biomaterials.2009.07.066
123. Sima LE, Filimon A, Piticescu RM, Chitanu GC, Suflet DM, Miroiu M, Socol G, Mihailescu IN, Neamtu J, Negroiu G (2009) Specific biofunctional performances of the hydroxyapatite–sodium maleate copolymer hybrid coating nanostructures evaluated by in vitro studies. J Mater Sci Mater Med 20(11):2305–2316. doi:10.1007/s10856-009-3800-7
124. Ciobanu C, Iconaru S, Gyorgy E, Radu M, Costache M, Dinischiotu A, Le Coustumer P, Lafdi K, Predoi D (2012) Biomedical properties and preparation of iron oxide-dextran nanostructures by MAPLE technique. Chem Cent J 6(1):17

Chapter 12
Safer Nanoformulation for the Next Decade

Debjani Nath

Abstract Nanotechnology is one of the exciting, albeit infrequent, technological change that can influence all industries. It holds the potential for pervasive and revolutionary changes. These changes can either follow a path leading to waste, pollution and energy inefficiency or follow a path of green nanotechnology to a more sustainable future. It is our choice while the window of opportunity still remains open. Green nanotechnology offers the opportunity to head off adverse effects before they occur. It can proactively influence the design of nanomaterials or products by eliminating or minimizing pollution from the production of the nanomaterials, taking a life cycle approach to nanoproducts to estimate and mitigate where environmental impact might occur in the product chain, designing toxicity out of nanomaterials and using nanomaterial to remediate existing environmental problem.

Keywords Green synthesis • Engineered nanoparticles • Nanotoxicity • Formulation

Abbreviations

AgNP	Silver nanoparticle
AuNP	Gold nanoparticle
DRAM	Dynamic random access memory
ENM	Engineered nanomaterial
HF	Hydrogen fluoride
HTS	High throughput screening
IGC	Inert gas condensation
LDH	Lactate dehydrogenase
MNP	Magnetic nanoparticle
MTS	3-(4,5 Dimethylthiazol-2yl)-5-(3-carbonymethyl-2-(4sulphonyl)-2H-tetrazolium salt
MTT	3-(4,5 Dimethylthiazol-2yl)-2,5 diphenyltetrazolium bromide

D. Nath (✉)
Department of Zoology, University of Kalyani,
Kalyani, Kolkata, West Bengal 741245, India
e-mail: nath_debjani@yahoo.co.in

V.A. Basiuk, E.V. Basiuk (eds.), *Green Processes for Nanotechnology*,
DOI 10.1007/978-3-319-15461-9_12

QNTR	Quantitative nanostructure toxicity relationship
QSAR	Quantitative structure-activity relationship
REACH	Registration evaluation and authorization of chemicals
Sb_2O_3	Antimony trioxide
SRAM	Selective random access memory
SRM	Standard reference nanomaterials
TiO_2	Titanium dioxide

12.1 Introduction

Nanomaterials and nanotechnology have attracted a lot of attention both in the scientific field and in media communication. But up to now nanoproducts still target future possibilities in support of the concept of sustainability. The term sustainable development was coined in the paper "*Our Common Future*," released by the Brundtland Commission as "Sustainable development is the kind of development that meets the need of the present without compromising the ability of future generations to meet their own needs". The two key concepts of sustainable development were indicated as: (1) the concept of "needs" in particular the essential needs of the world's poorest people, to which they should be given overriding priority; and (2) the idea of limitations which is imposed by the state of technology and social organization on the environment's ability to meet both present and future needs [1]. The development goes well beyond manufacturing to encompass all human production and consumption activities, such as agriculture, land, air and water resource management, human habitat management, biodiversity, etc. [2].

Sustainable energy too has long been a dream of nanotechnologies and it has been seen as a technology with the potential to reduce green house emissions, but to date this has not been quantified. Many of the initial ideas were based around replacing current manufacturing techniques with bottom up technologies, whether assembling items atom by atom as proposed by Eric Drexler [3] "*Coal and diamonds, sand and computer chips, cancer and healthy tissue: throughout history, variations in the arrangement of atoms have distinguished the cheap from the cherished, the diseased from the healthy. Arranged one way, atoms make up soil, air, and water; arranged another, they make up ripe strawberries. Arranged one way, they make up homes and fresh air; arranged another, they make up ash and smoke*." or by attempting to understand how nature assembles useful devices from the bottom up and mimic or control these techniques. While bottom up nanomaterial engineering remains a topic of much interest,many of these applications of nanotechnology are still at the stage of infancy and there is general agreement that a breakthrough is still 10–15 years in the future.

Green nanotechnology maintains a commitment to rigor with application related to sustainability as well as alerts the prevention of harmful consequences from its successful implementations. In terms of nanofabrication process it is less energy and resource intense and as the principles of Green Chemistry green nanotechnology involve (a) the use of cost-effective, nontoxic precursors; (b) minimization of

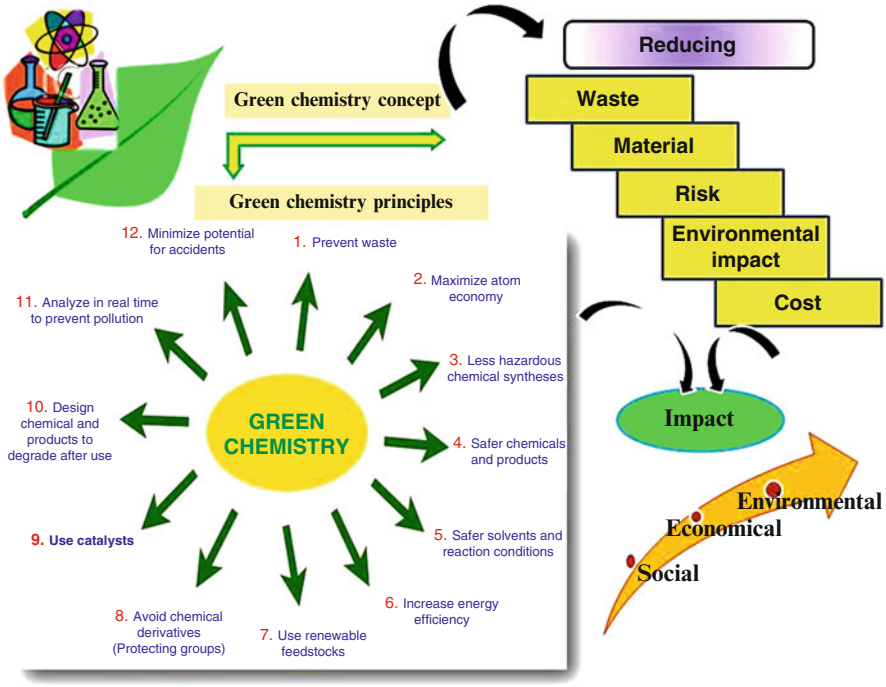

Fig. 12.1 Schematic representation of green chemistry integration in reduction of metal nanomaterials

carcinogenic reagents and solvents (if possible, through utilization of aqueous solvents in order to bypass potentially toxic, acidic, or basic analogues); (c) reduction of experiments carried out with either pyrophoric compounds or unstable precursors to avoid risk; (d) the use of relatively few numbers of reagents, i.e., atom economy, coupled with a conscious effort to circumvent the generation of greenhouse gases; (e) minimization of reaction steps leading to a reduction in waste, reagent use, and power consumption; (f) development of reactions to generate high-purity materials with little if any byproducts through high-yield processes; (g) ambient temperature and pressure synthesis, if at all possible, so as to preclude the need for either vacuum or high temperature processes; and (h) efficiency of scale-up (Fig. 12.1) [4].

12.2 Challenges of Nanosafety

12.2.1 Definition of Nanomaterial from the Viewpoint of Nanosafety

ENMs (engineered nano materials) are characterized by their complexity. This complexity is evident not only in their physico-chemical characteristics but also in their interactions with living systems. Due to the diverse nature of

nanomaterials, they have contributed to the birth of several subfields of nanosciences such as optoelectronics and printed electronics, innovative construction materials, novel surfaces and packaging. They have been the impetus for the creation of the discipline of safety-related nanotoxicology. Nanosciences and nanotechnologies deal with the manipulation of matter in a size-range from 1 to 100 nm in at least one dimension. Some of the recognized engineered nonmaterials have dimensions even smaller than 1 nm (e.g., fullerenes). This was truly not followed by the definition of EU in its true nature in the line of nanoformulation and designing. The European Commission has recently adopted a recommendation on the definition of nanomaterial (COM (2011) 696), according to which "nanomaterial means a natural, or manufactured material containing particles, in an unbound state or as an aggregate or as an agglomerate and where, for 50 % or more of the particles in the number size distribution, one or more external dimensions is in the size range of 1–100 nm. In specific cases and where warranted by concerns for the environment, health, safety or competitiveness the number size distribution threshold of 50 % may be replaced by a threshold between 1 and 50 %". Even though this definition has been currently incorporated into some pieces of EU legislation, it has also recently been challenged because it has been considered to be an obstacle for research in addition to being a reflection of relatively a static, not a dynamic, understanding of the nature of nanosized materials for the purpose of regulations [5]. The definition has indeed been defended by the regulatory requirements of engineered nanomaterials [6]. A number of engineered nanodevices of nanomaterials include functionalized carbon/organic/metal nanotubes, nanowires, metal, metal oxide and organics nanoparticles, and graphene. They also include bioactive and biodegradable ceramics and polymers, active gels, piezoelectrics, electrostrictives, ferroelectrics, multiferroics, nonlinear/tunable metamaterials, shape memory materials, supramolecular polymers, stimuli sensitive polymers, and possible combinations of these materials. Sometimes they are present in organized arrays, and sometimes as simple mixtures. They can express characteristics that enable self-assembly of nanosized materials into chemically similar but microsized structure. However, it is the flexibility for physical manipulation that endows all these materials with an amazing color of micro designs (Fig. 12.2). This is why products with nanomaterials can be so creative and innovative. However, this plethora of different types of materials at nanoscale not only confers almost unlimited technological benefits, but it also holds the possibilities for unexpected interactions between these materials and biological systems at the molecular, cellular, organ and organismic levels [7–9]. Furthermore, according to a recent evaluation by the European Commission (2nd Regulatory Review of REACH (EC (2012) 572), it is unlikely that the size of nanomaterials per se causes hazards or harm to the human health or the environment. Small size does enable easy access to living organisms and hence may lead to increased risks to various living systems. This leads directly to scientific uncertainty about the general safety of these materials, stressing the need for safety assessment of the nanosized substances.

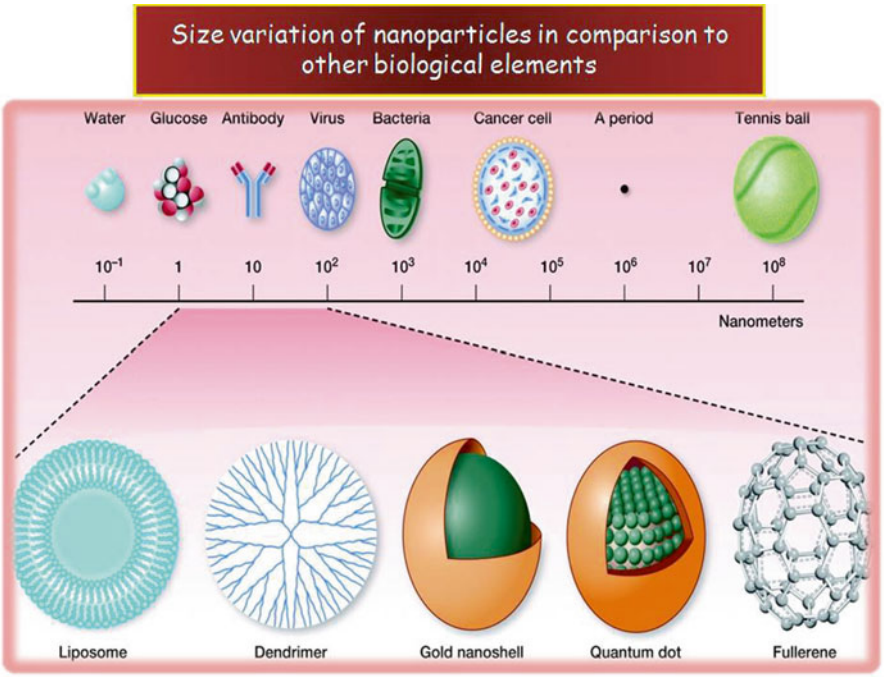

Fig. 12.2 Size variation of different nanoparticles in relation to biological elements

12.2.2 Challenges of Nanosafety: Pre-assessment of Nanotoxicity

Nanotechnology has rapidly encouraged the development a new generation of smart and innovative products and processes, and has created a tremendous growth potential for a large number of industry sectors. It is important that this development continues so that all the useful properties of engineered nanomaterials (ENM) can be safely utilized in a number of nanotechnology applications. However, there is a strong debate about the potential risks of ENM and nanotechnologies. In this regard, it is important to consider that research and innovation and application are the key drivers of social and economic prosperity. Policies on nanosafety are in a key-position to solve any challenges related to the concerns of ENM health or environmental effects and causing challenges to the promotion of these technologies. Without nanosafety research, widespread use of nanotechnologies in many sectors of society may well be slowed down and could even come to a complete stand still.

It is important to understand that we are still dealing with the first generation of nano-enabled products (i.e., passive nanostructures), but it is likely that we will

soon be achieving the second generation products containing active nanostructures and then to the third generation systems of integrated nano-systems and finally, by the year 2020, according to some prior predictions, to the fourth generation products or heterogeneous molecular nano-systems that allow the manufacture of molecular devices "*by design*." This indicates that methods for assessment of the safety of next generation nano-enabled products also must be evolved to confirm the safe existence of the systems in the next decade.

Challenges that we are facing in the science of nanosafety are the testing program of hazards in biological system. In this aspect, we need urgently a "new" programmed approach of toxicology for the validation of safer nanomaterials for the twenty-first century [10]. The central part of this novel toxicology is to describe toxicity pathways that lead to understanding the molecular fundamentals using toxicity testing primarily in animal models to in vitro assays and in vivo assays using lower model organisms, along with computational modeling, thus enabling the evolution of toxicology from being an observational science into a predictive science showing identification of the main modes of actions of toxicity for ENMs, understanding the transformation of ENMs during their life cycle and how this may influence their hazard potential and identification of the key physicochemical determinants that modulate ENM interactions and toxicity in biological systems. Currently, most of the existing in vitro or in vivo toxicity studies allow one at best, to make some kind of comparison in terms of the relative hazard potential provided that the batch-to-batch variability has been considered; the materials adequately characterized; the appropriate number of graded doses has been used and predictive endpoints have been measured (Fig. 12.3). In addition to the shortcomings described above, very little is known of the true internal dose of the materials to which living organisms are being exposed. In most cases, we do not have adequate methods to assess many crucial parameters, e.g., the dose received by liver or other organs, because we do not possess the required knowledge of the translocation of the materials in the body and across biological barriers, or the means to assess the dose in a given organ or type of cell in vivo [11].

12.2.3 Towards a New Toxicology for the Twenty-First Century: A Possible Move to Face Challenges

So the key challenge for nanomaterial safety assessment is the ability to handle the large number of newly engineered nanomaterials (ENMs), including developing cost-effective methods that can be used for hazard screening [12]. In order to develop an appropriate screening platform, it is necessary to assemble and synthesize nanomaterial libraries that can be used to screen for specific material compositions and properties that may lead to the generation of a biological hazard [12–15]. The acquisition and characterization of standard reference nanomaterial (SRM) libraries forms the basic infrastructure requirement that is necessary to screen for toxicity and to elucidate the material properties that are most likely to result in

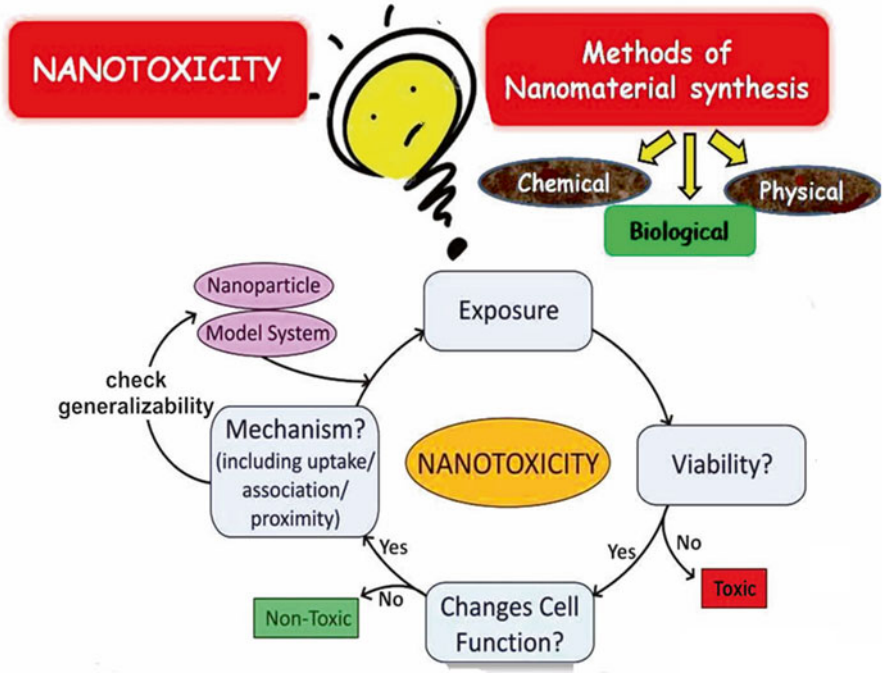

Fig. 12.3 Schematic representation on challenges of safety related nanotoxicity determination

biological injury [16]. The selection of the library materials should take into consideration the commercial production volumes of the different nanomaterials, incorporating the major current ENM classes of materials (metals, metal oxides, silica, and carbon-based nanomaterials). The choice of materials should also consider the exposure potential, route of exposure and delivery pathway (Fig. 12.4). For example, free nanoparticles or powders are more likely to become airborne with the potential to generate pulmonary toxicity after inhalation. Thus, it is appropriate to investigate this scenario using lung cells (in vitro) and pulmonary exposure (in vivo) that ideally should be linked in terms of mechanisms of potential injury. Ideal ENM libraries should also include positive and negative control ENMs to provide a reference point for the evaluation of material toxicity.

12.2.3.1 Development of In Vitro Screening Assays

Much of the knowledge about ENM cellular toxicity has been generated using fairly straightforward cellular viability assays such as the lactate dehydrogenase (LDH) and the colorimetric MTT/MTS assays or propidium iodide (PI) staining. The major drawback is that these assays are often not informative of a specific toxicological pathway because multiple stimuli can result in the same assay outcome, establishing

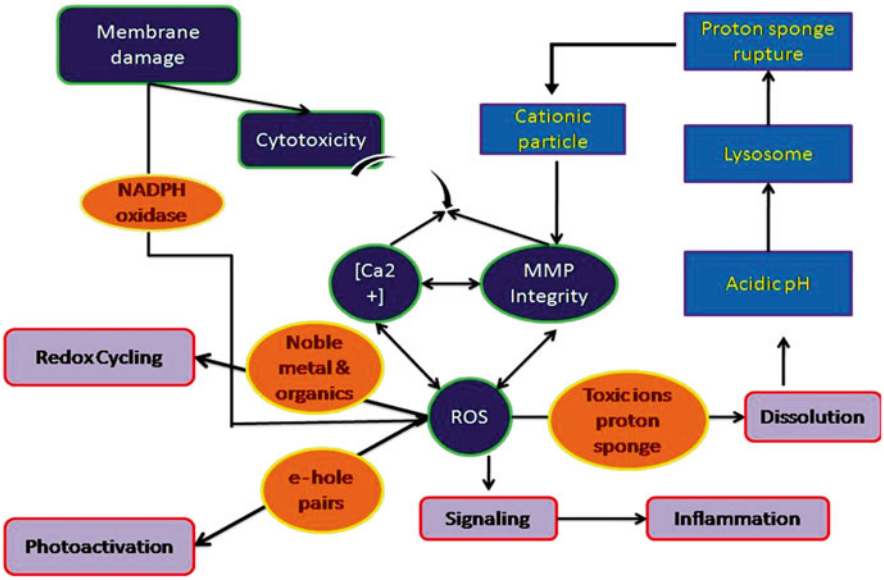

Fig. 12.4 Roadmap of nanotoxicity assessment

Table 12.1 Toxicological pathways related to different sized nanomaterials

Toxicological pathways	Nanomaterials
1. Membrane damage/leakage/thinning	Cationic NPs
2. Protein binding/unfolded responses/loss of functions/ fibrillation	Metal oxide NPs, polystyrene, dendrimers, carbon nanomaterials
3. DNA cleavage/mutation	Nano-Ag
4. Mitochondrial damage: e-transfer/ATP/apoptosis	UFPs, cationic NPs
5. Lysosomal damage: proton pump activity/lysis/frustrated phagocytosis	UFRs, cationic NPs, CNTs
6. Inflammation: signaling cascades/cytokines/chemokines/ adhesion	Metal oxide NPs, CNTs
7. Fibrogenesis and tissue modeling injury	CNTs
8. Vascular, endothelial and clotting abnormalities	SiO_2
9. Oxidative stress injury, radical production, GSH depletion, lipid peroxidation, membrane oxidation, protein oxidation	UFPs, CNTs, metal oxide NPs, cationic NPs

little connectivity between the biological outcome and specific ENM properties. Moreover, cellular viability assays also do not reflect sublethal toxicity effects. For these reasons there is a need of a mechanism-based in vitro assays because this is conceptually the easiest way to link in vitro toxicity screening with pathological effects in vivo. Currently, there are approximately ten major mechanistic pathways of toxicity that have been linked to ENMs (Table 12.1). These include injury paradigms such as the generation of reactive oxygen species and oxidative stress,

frustrated phagocytosis (e.g., in mesothelial surfaces), changes in protein structure and function (e.g., loss of enzymatic activity), protein unfolding response, immune response activation (e.g., through exposure of cryptic epitopes or immunostimulatory effects), fibrogenesis and tissue remodeling, blood clotting, vascular injury, neurotoxicity (e.g., oxidative stress and protein fibrillation), and genotoxicity.

12.2.3.2 Development of Rapid Screening for In Vitro Pathway Assessment

Particle-induced oxidative stress invokes three tiers of cellular responses including cellular antioxidant defense, activation of pro-inflammatory signaling pathways leading to the production of cytokines/chemokines, and mitochondria-mediated cell death [15, 17–19]. However, performing the entire panel of tests necessary to study the three tiers of oxidative stress requires at least 2–3 weeks of labor-intensive effort. A rapid throughput screening approach could offer several advantages over conventional assays. First, this approach speeds up the pace of knowledge generation that is possible with compositional and combinatorial ENM libraries. High-throughput screening (HTS) provides a rapid readout because of the standardization of the procedure, automation (e.g., cell seeding, liquid handling, imaging, and image analysis), and miniaturization (requiring smaller amounts of reagents and lowering the cost per assay) (Fig. 12.5). Not only is HTS capable of screening large libraries, but it can also accommodate multiple cell lines, time points and doses of exposure within the same experiment. Coupled with good bioinformatics and decision-making tools, this approach can significantly improve the reliability of toxicological screening as well as establishment of property–activity relationships [19].

In vivo screening is time consuming and expensive. A complete set of toxicological assays for a single chemical, including assessment of carcinogenicity, reproduction, and developmental effects could involve hundreds of animals and costs in the range of $1–3 million per test. As a result, less than 2 % of industrial chemicals have undergone toxicity testing in rodents. But the in vivo results are important to validate the in vitro screening as "predictive," thereby allowing the in vitro platform to be used as the primary screening procedure.

12.2.3.3 Quantitative Nanostructure–Toxicity Relationship (QNTR)

Quantitative structure–activity relationship (QSAR) has been widely used in pharmacology and related fields to predict the toxicity of drugs without the need for tedious, time-consuming, and expensive animal testing. An analogue of the model, QNTR, has been extended to nanomaterials. In this context, Winkler et al. [20] recently noted that structural properties of nanomaterials, which influence toxicity, may include size, shape, surface area, and degree of electrostatic interaction between nanomaterials and their cellular environments as well as other physicochemical properties of nanomaterials. These properties have been used as descriptors [20–22] for the prediction of the

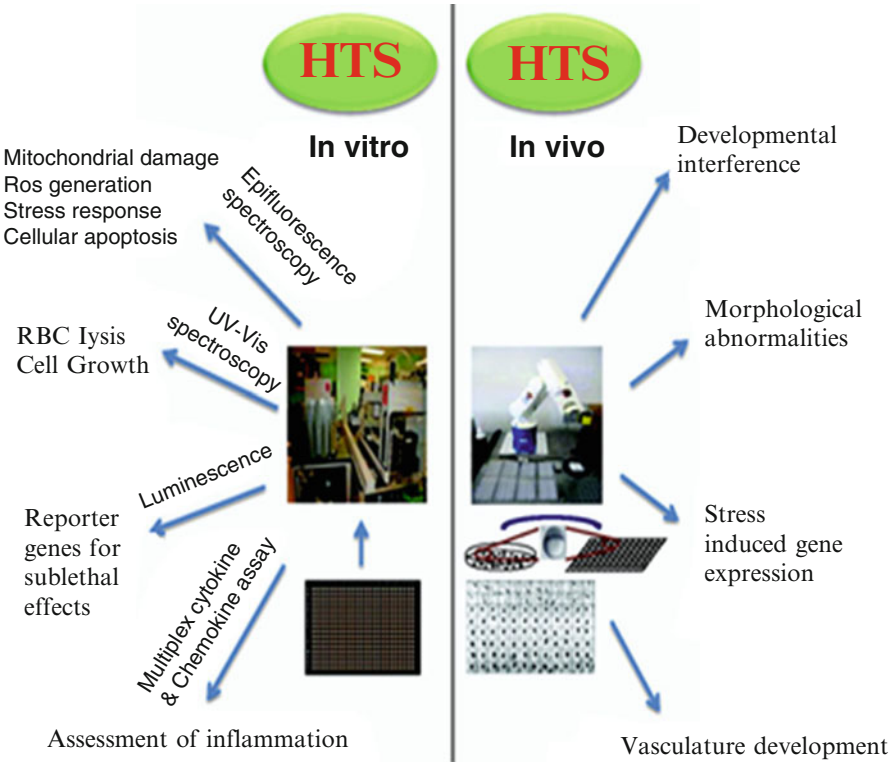

Fig. 12.5 In vitro and in vivo methods of nanotoxicity assessment for next decade

properties of new materials or for the explaining of their biological effects. In many instances, such predictions are facilitated by the use of multivariate data analysis techniques including regression models and artificial neural networks and verified by cross-validation, using training and validation data sets [23].

Emerging results from these types of studies indicate that the structural properties, which influence the toxicity of nanomaterials, can reside both in the core and on the surface of the materials [20, 24]. However, to extend QSAR to QNTR effectively, a number of challenges need to be addressed. Winkler et al. [20] have mentioned some of these challenges as (1) lack of adequate definition and understanding of the biologically important entities that moderate the adverse effects of nanomaterials, (2) need to choose the right assays that can be used to model and correlate the toxic effects of nanomaterials in vitro and in vivo, (3) accurate modeling of the complex interactions between nanomaterials and biological systems, (4) understanding of the relationship between QNTR methods and other computational approaches such as quantum chemistry and molecular dynamics.

These challenges arise due to following data gaps: (1) lack of sufficient empirical data on the composition of biocorona on the surfaces of nanomaterials; (2) lack

of in vitro data that can be used to predict in vivo effects of nanomaterials, and (3) the paucity of descriptors that can specifically be used for nanomaterials [20]. Despite these challenges and data gaps, progress has been made in probing and understanding the interactions of nanomaterials with their biological environments. However, the gaps in knowledge must be fully identified and understood before an internationally acceptable approach to QNTR is proposed, which can appeal to all stakeholders.

12.3 Why Green Synthesis?

The microelectronics industry once was considered "clean" when compared with heavy industries of the past, but we now know that its environmental impact is far greater than it first appeared. A single dynamic random access memory (DRAM) microchip that weighs a mere 2 g and goes inside a computer requires 1.7 kg of raw material inputs, including chemicals, water and fossil fuels [25]. So, the race is on to develop a memory chip that is faster and cheaper, requires less energy and material inputs and generates less waste than conventional DRAM, selective random access memory (SRAM) and flash memory. Since 2000, the semiconductor industry has been engaged in nanoscale manufacturing [25, 26]. And now, though very small in volume, nanomaterials are becoming a part of the waste stream from that factories [27]. This is only an example of a large number of companies that are engaged in the manufacturing nano-based products from computer chips to automobile parts and from clothing to cosmetics and dietary supplements At this early stage of nanotechnology commercialization, little is known about the transport and fate of these nanomaterials in the environment or about their risks to wildlife and people [27].

Today, a cadre of research scientists and engineers is working to develop cutting-edge methods for green manufacturing of nanoelectronics and other nanoproducts that are more people- and planet-friendly. A growing number of researchers are merging green chemistry and green engineering with nanotechnology, and they see a bright future for a new topic known as "*Green Nano*." Green chemistry is the utilization of a set of principle that reduces or eliminates the use or generations of hazardous substances in the designing, manufacturing and application of chemical products [28]. The 12 principles of green chemistry have now been applied to the design of a variety of chemical products and processes with the aim of minimizing chemical hazards to health and environment, reducing waste materials and preventing pollution. If green chemistry principles can be employed successfully in the production of highly functionalized nanomaterials like pharmaceuticals, a successful application of these materials could be expected. The development of high precision and low waste materials is also added with high quality for commercialization. So, green chemistry can provide best opportunities to add new vigor to this product with maximum benefits to the society and to the environment.

12.4 Application of Green Chemistry in Greenanomics

Green nanoscience/nanotechnology/greenanomics involves the application of green chemistry principles in designing and studying the nanoscale products, the development of production methods, and the application of nanomaterials [29]. It strives to discover synthesis/production methods that eliminate the need for harmful reagents and enhance the efficiency of these methods, while providing the necessary volume of pure material in an economically viable manner. It also provides proactive design schemes for assuring their inherent safety by assessing the biological and ecological hazards in tandem with design. In addition, a growing number of applications of nanotechnology are being developed that promise environmental benefit, including new catalysts for environmental remediation [28], cheap and efficient photovoltaics [30], thermoelectric materials for cooling without refrigerants [31], lightweight (and thus energy-conserving) nanocomposite materials for vehicles [32], miniaturized devices that reduce material consumption, and sensors that eliminate the need for (often) wasteful wet-chemical analyses. Nanoscale sensors [33] can also offer faster response times and lower detection limits, making on-site, real-time detection possible [34].

To realize new nanotechnologies that pose little harm to human health or the environment and to develop technologies that can be used to improve or protect the environment, it is desirable to design and use greener nanomaterials and to develop greener nanoproduction methods. Nearly all of the principles of green chemistry can be readily applied to the design of nanoscale products, the development of nanosynthesis methods, and the application of nanomaterials. Three of the 12 principles relate directly to nanomaterial design and the application of these materials toward nanodevices. These are principle 4 (Designing Safer Chemicals), principle 10 (Design for Degradation/Design for End of Life), and principle 12 (Inherent Safety). In some cases, self-assembled nanoscale systems might be disassembled for reuse in new devices. Application of principle 4 to product design involves considering the structural features of the nanomaterial (i.e., the size, shape, composition, and surface chemistry) that dictate its health hazards (e.g., toxicity) as well as its physical properties. In order to routinely implement this design approach, improved understanding of the structure—activity relationships for nanomaterials is needed. The rich structural diversity of nanomaterials provides significant opportunities to tune and optimize the physical and toxicological properties.

Ultrafine particle data show that materials such as silicates, asbestos fibers, and, to a lesser extent, carbon black and titanium dioxide can cause oxidative stress, induce pulmonary inflammation, trigger the release of cytokines, and induce signal transduction pathways [12]. “Nanoparticles” represent intentionally engineered products below 100 nm in diameter with carefully controlled sizes, shapes, and surface chemistries. The unusual properties of nanoparticles (e.g., chemical, optical, or electronic) could lead to adverse biological effects that may be unique compared to larger compositions of the same material. Variations in particle size [35–37] and surface chemistry [12, 37] can affect the degree of toxicity. For instance, smaller nanoparticles are more likely to enter the circulatory system and travel throughout the body, lodging in

distal organs [12, 38]. Methods developed to analyze the toxicity of ultrafine particles may provide a starting point for determining the toxicity of engineered nanoparticles, and comparisons can be made in terms of methods of injury (e.g., oxidative stress, inflammatory responses, signal transduction pathways, etc.). Traditional testing and screening strategies may be employed initially, leading to novel detection methods that account for the unique properties of nanoparticles. These include in vitro cellular assays [35, 39, 40] and biochemical analyses which probe the generation of reactive oxygen species and effects on enzymatic pathways. Using in vitro assays, the route of nanoparticle entry can be determined with its biochemical effects (protein interactions, DNA damage, gene expression changes, or generation of reactive oxygen species). Genomics and proteomics can track oxidative stress, induction of signal transduction pathways, and apoptosis. Since susceptibility factors vary across a given population based on individual genetic makeup, risk assessment evaluation should accompany information provided by various assays and screens. In vivo studies are essential for identifying potential target organs, travel routes of nanoparticles within the body, or other phenotypic changes. Such studies could lead to reliable methods for tracking and quantifying nanoparticles in cells and whole animals [41]. In addition, dose–response relationships, calculated using a variety of metrics including mass, number of nanoparticles, and surface area, provide a means of normalizing information gathered from individual toxicology studies. Thus, engineered nanoparticles should be well characterized, with known size and/or distribution, surface area, shape, solubility, purity, surface chemistry, and physical (e.g., crystal structure), electronic, or optical properties [34].

Principle 10 focuses on design related to the environmental impacts of nanomaterials. Here the design criteria aim to reduce harm to the environment from materials that may be released through their application or at the end of their product life. The approach is to design materials that rapidly degrade in the environment, producing innocuous degradation products. In order to implement principle 10, advanced understanding of the fate of designed nanomaterials in the environment will be needed. Long-term effects of nanoparticles in the air, soil, and water are also important considering its relation to human health because persistence in the environment is directly proportional to the amount of nanoparticles in use [36, 42]. Environmental impacts of nanoparticles are usually considered in terms of toxicity or exposure [36], but information gathered from the biological studies described above would complement our understanding of the corresponding environmental implications because bioaccumulation in aquatic and terrestrial organisms will aid in developing models for environmental impact. Taxonomic and genetic susceptibilities are also of important considerations. Since chronic exposures often mimic false picture to depict ecological risk so that, as precautionary measures long-term studies analyzing a range of sublethal doses should be included [13, 14, 43, 44]. However, very little is known yet to date concerning the detailed analytical data on ecotoxicity or chronic effects of nanomaterials.

Principle 12 addresses the inherent safety of the material being used. For example, nanomaterials that are incorporated into macroscale structures are less likely to be released into the workplace or environment. The high surface area of

nanoparticles may lead to higher reactivities, explosions, or fires in large-scale production. Taken together, principles 4, 10, and 12 provide a robust framework for designing nanomaterials with safety concerns on reduced biological and environmental toxicological impact.

12.5 Green Synthesis of Metal Nanoparticles

Many syntheses of nanoparticles have been developed in recent years, in an effort to produce structures that have a specific form and function relevant to a given application. The preparation of functionalized nanoparticles within a green context poses interrelated challenges in terms of maintaining product integrity (such as structure, shape and size dispersity, functionality, purity, and stability) while employing greener methods whenever possible. For example, control over particle size and dispersity may reduce purification requirements by eliminating the need for extensive separations, while the ability to control surface functionalization, intended to enhance particle stability and dictate surface chemistry, solubility, and the degree of particle interactions, helps to better define the safety.

Direct synthesis involves nanoparticle preparation under conditions where the nanoparticles nucleate and grow, usually by the reduction of metal ions. Nanoparticles are often synthesized in the presence of a ligand or a stabilizer that can bind to the surface of the newly formed particle, offering stability, modifying surface reactivity and possibly arrest of further particle growth, thus offering increased control over nanoparticle size and polydispersity. It is critical that the ligand does not interfere with particle development in an undesirable manner (i.e., by preventing reduction of the metal ion precursor, or inducing the formation of misshaped particles). Typical ligands include phosphines, thiol, and amines, which may be organic or water soluble, depending on the pendant functionality.

Synthesis of MNPs is carried out by several physical and chemical methods that include laser ablation [45], ion sputtering [46], solvothermal synthesis [47], chemical reduction [48], and sol–gel [49] method. All these methods are conventional either physical or chemical methods which should address the fundamental principles of "green chemistry" by using environmentally benign solvents and nontoxic chemicals. Basically, there are two approaches for nanoparticle synthesis, the top-down and bottom-up. *Laser ablation* [45] enables to obtain colloidal nanoparticles solutions in a variety of solvents. Nanoparticles are formed during the condensation of a plasma plume produced by the laser ablation of a bulk metal plate dipped in a liquid solution. This technique is considered as a "green technique" alternative to the chemical reduction method for obtaining noble MNPs. However, the main drawbacks of this methodology are the high energy required per unit of MNPs produced and the little control over the growth rate of the MNPs. *Inert gas condensation* (IGC) is the most widely used methods for MNPs synthesis at laboratory-scale. Gleiter [50] introduced the IGC technique in nanotechnology by synthesizing iron nanoparticles. In IGC, metals are evaporated in ultra high vacuum chamber filled with helium or argon gas at typical pressure of few hundreds Pascal's.

The evaporated metal atoms lose their kinetic energy by collisions with the gas, and condense into small particles. These particles then grow by Brownian coagulation and coalescence and finally form nano-crystals. Recent application of this technique includes size-controlled synthesis of Au/Pd NPs [51] and hetero-sized Au nanoclusters for non-volatile memory cell applications [52]. The *sol–gel process* is a wet-chemical technique developed recently in nanomaterial synthesis. The inorganic nanostructures are formed by the sol–gel process through formation of colloidal suspension (sol) and gelation of the sol to integrated network in continuous liquid phase (gel). Size and stability control quantum-confined semiconductor, metal, and metal oxide nanoparticles have been achieved by inverted micelles [53], polymer blends [54], block copolymers [55] and ex situ particle-capping techniques [56]. However, the fundamental problem of aqueous sol–gel chemistry is the complexity of process and the fact that the synthesized precipitates are generally amorphous. The *hydrothermal and solvothermal* synthesis of inorganic materials is an important methodology in nanomaterial synthesis. In hydrothermal method, the synthetic process occurs in aqueous solution above the boiling point of water, whereas in solvothermal method the reaction is carried out in organic solvents at temperatures (200–300 °C) higher than their boiling points. Though the development of hydrothermal and solvothermal synthesis has a history of 100 years, recently this technique has been applied in material synthesis process. Normally, hydrothermal and solvothermal reactions are conducted in a specially sealed container or high pressure autoclave under subcritical or supercritical solvent conditions. Under such conditions, the solubility of reactants increases significantly, enabling reaction to take place at lower temperature. Among numerous examples, TiO_2 photocatalysts were synthesized through hydrothermal process [57]. Because low cost and energy consumption, hydrothermal process can be scaled-up for industrial production. Solvothermal process enables to choose among numerous solvents or mixture thereof, thus increasing the versatility of the synthesis. For example, well-faceted nanocrystals of TiO_2 with high reactivity were synthesized in a mixture of the solvents hydrogen fluoride (HF) and 2-propanol [58]. The crystallographic control over the nucleation and growth of noble-metal nanoparticles has most widely been achieved using colloidal methods [59–62]. In general, metal nanoparticles are synthesized by reducing metal salt with chemical reducing agents like borodride, hydrazine, citrate, etc., followed by surface modification with suitable capping ligands to prevent aggregation and confer additional surface properties. Occasional use of organic solvents in this synthetic process often raises environmental questions. At the same time, these approaches produce multi-shaped nanoparticles requiring purification by differential centrifugation and consequently have low yield. Thus, the development of reliable experimental protocols for the synthesis of nanomaterials over a range of chemical compositions, sizes, and high monodispersity is one of the challenging issues in current nanotechnology. In this context, current drive focused on the development of green and biosynthetic technologies in for the production of nanocrystals with desired size and shape.

One of the key tenets of biology is the ability of biomolecules to self-assemble into supramolecular structures. This intrinsic ability has picked the interest of scientists and engineers to develop a bottom-up approach to nanofabrication. Biological

self-assembly occurs at the molecular scale and is often reversible, self-correcting, and self-healing. The shape and size of self-assembled structures are intricately controlled on the nanoscale. Understanding how biology self-assembled structures can also lead to synthetic methods for creating supramolecular structures, using nature's blueprints to create synthetic nanomaterials. Some organisms have the capability to take up minerals from their surrounding environment and create intricate inorganic–organic hybrid structures that possess remarkable nanoscale properties. Extracellular nanoparticle production could provide highly pure nanoparticles, thus eliminating the need to extract nanoparticles from intracellular biomass. This would expand the capability of nanoparticles for use in such systems as nonlinear optics, optoelectronic devices, or thin films. Most of these biogenic nanoparticles have not been tested in device applications. One potential problem with using whole organisms to produce nanoparticles might reside in the methods needed to purify the nanoparticles after synthesis. Extraction and purification methods might be critical, involve organic solvents, or cause destabilization of the nanoparticle. Though biological contaminants may not be toxic or environmentally harmful, they could interfere with device applications. Nevertheless, using whole organisms as putative bioreactors could be a poignant environmentally friendly method to produce nanoparticles, particularly semiconductor nanoparticles that are often made under harsh conditions. Biologically produced nanoparticles tend to be stable in solution, perhaps due to protein interactions, further suggesting that purification may not be an issue in some cases.

12.6 Biological Synthesis: By Whole Organisms

The use of microbial cells for the synthesis of nanosized materials has emerged as a novel approach for the synthesis of metal nanoparticles. *Bacteria* play a crucial role in metal biogeochemical cycling and mineral formation in surface and subsurface environments [63, 64]. Although the efforts directed towards the biosynthesis of nanomaterials are recent, the interactions between microorganisms and metals have been well documented, and the ability of microorganisms to extract and/or accumulate metals is employed in commercial biotechnological processes such as bioleaching and bioremediation [65]. Bacteria are known to produce inorganic materials either intra cellularly or extra cellularly. Microorganisms are considered as a potential biofactory for the synthesis of nanoparticles like gold, silver, zinc and cadmium sulphide. The formation of extracellular and intracellular metal nanoparticles by bacteria like *Escherichia coli*, *Pseudomonas stutzeri*, *Pseudomonas aeruginosa*, *Plectonema boryanum, Salmonells typlus*, *Staphylococcus currens, Vibrio cholerae*, etc., has been reported [66–69]. Many microorganisms are known to produce nanostructured mineral crystals and metallic nanoparticles with properties similar to chemically synthesized materials, while exercising strict control over size, shape and composition of the particles. Examples include the formation of magnetic nanoparticles by magnetotactic bacteria, the production of silver nanoparticles

within the periplasmic space of *Pseudomonas stutzeri* and the formation of palladium nanoparticles using sulphate reducing bacteria in the presence of an exogenous electron donor [65]. The supernatant of gram positive, thermophilic bacterium *Bacillus licheniformis* synthesized AgNPs in the range of 50 nm [70]. Formation of nanoscale elemental silver particles through enzymatic reduction was reported in *Geobacter sulfurreducens* [71]. Kalimuthu and co-workers [72] studied AgNPs synthesis using bacteria *B. licheniformis*, isolated from sewage collected from municipal wastes, and ultrasonically lysed bacterial cell. The synthesized AgNPs had average particle size of around 50 nm. Recently, a rapid method for synthesizing small (1–7 nm) monodiperse AgNPs has been described by electrochemically active biofilm (EAB) using sodium acetate as an electron donor [73]. Biofilm formation of gram-negative β-proteobacterium *Cupriavidus metallidurans* is very common on Au grains. The isolated *C. metallidurans* from soils and sediments from temperate and tropical Australian sites interacted with Au^{+3} ions and form AuNPs distributed homogenously throughout cell wall [74]. The AuNPs were also synthesized on the surface of *Rhodopseudomans capsulate* by interaction bacterial cells with $HAuCl_4$ solution [75]. The aqueous chloroaurate ions were reduced after 48 h of incubation and transformed to AuNPs. The pH value of the solution controlled the shape of AuNPs. In the case of bacteria, most metal ions are toxic and therefore the reduction of ions or the formation of water insoluble complexes is a defense mechanism developed by the bacteria to overcome such toxicity [76].

Actinomycetes are microorganisms that share important characteristics of fungi and prokaryotes such as bacteria. Even though they are classified as prokaryotes, they were originally designated as ray fungi. It has been observed that a novel alkalothermophilic actinomycete *Thermomonospora sp.* synthesized gold nanoparticles extracellularly when exposed to gold ions under alkaline conditions [76]. In an effort to elucidate the mechanism or the processes favouring the formation of nanoparticles with desired features, Ahmad and co-workers [77], studied the formation of monodisperse gold nanoparticles by *Thermomonospora sp.* and concluded that extreme biological conditions such as alkaline and slightly elevated temperature conditions were favourable for the formation of monodisperse particles. Based on this hypothesis, alkalotolerant actinomycete *Rhodococcus sp.* has been used for the intracellular synthesis of monodisperse gold nanoparticle [77]. In this study it was observed that the concentration of nanoparticles was more on the cytoplasmic membrane. This could have been due to the reduction of metal ions by the enzymes present in the cell wall and on the cytoplasmic membrane but not in the cytosol. The metal ions were also found to be nontoxic to the cells which continued to multiply even after the formation of the nanoparticles.

The *fungal*-mediated MNP synthesis is a relatively recent research area. Fungi have been widely used for the biosynthesis of nanoparticles and the mechanistic aspects governing the nanoparticle formation have also been documented for a few of them. In addition to monodispersity, nanoparticles with well-defined dimensions can be obtained using fungi. Yeast, belonging to the class ascomycetes of fungi, has shown to have good potential for the synthesis of nanoparticles. Gold nanoparticles have been synthesized intracellularly using the fungi *V. luteoalbum*. The rate of

particle formation and the size of the nanoparticles could be manipulated to an extent by controlling physical parameters such as pH, temperature, concentration of metal (gold) and exposure time. A biological process with this ability to strictly control the shape of the particles would be a considerable advantage [65]. Yeast, belonging to the class ascomycetes, has shown to have good potential for the synthesis of nanoparticles. Cells *of Schizosaccharomyces pombe* were found to synthesize semiconductor CdS nanocrystals and the productivity was maximum during the mid log phase of growth. Addition of Cd in the initial exponential phase of yeast growth affected the metabolism of the organism [78]. Baker's yeast (*Saccharomyces cerevisiae*) has been reported to be a potential candidate for the transformation of Sb_2O_3 nanoparticles and the tolerance of the organism towards Sb_2O_3 has also been assessed. Particles with a size range of 2–10 nm were obtained in this condition. Extracellular secretion of the microorganisms offers the advantage of obtaining large quantities of materials in a relatively pure state, free from other cellular proteins associated with the organism with relatively simpler downstream processing. Mycelia free spent medium of the fungus, *Cladosporium cladosporioides* was used to synthesize silver nanoparticles extracellularly. It was hypothesized that proteins, polysaccharides and organic acids released by the fungus were able to differentiate different crystal shapes and were able to direct their growth into extended spherical crystals [79]. The extracellular synthesis of AgNPs by a marine fungus *Penicillium fellutanum,* isolated from costal mangrove sediment, has been described by Kathiresan and co-workers [80]. *Fusarium oxysporum* has been reported to synthesize silver nanoparticles extracellularly. Studies indicate that a nitrate reductase was responsible for the reduction of silver ions and the corresponding formation of silver nanoparticles. However *Fusarium moniliformae* did not produce nanoparticles either intracellularly or extracellularly even though they had intracellular and extracellular reductases in the same fashion as *Fusarium oxysporum*. This indicates that probably the reductases in *F.moniliformae* were necessary for the reduction of Fe (III) to Fe (II) and not for Ag (I) to Ag (0) [81]. *Aspergillus flavus* has been found to accumulate silver nanoparticles on the surface of its cell wall when challenged with silver nitrate solution. Monodisperse silver nanoparticles with a size range of 8.92 ± 1.61 nm were obtained and it was also found that a protein from the fungi acted as a capping agent on the nanoparticles [82]. In addition to the synthesis of silver nanoparticles, *Fusarium oxysporum* has also been used to synthesize zirconia nanoparticles. It has been reported that cationic proteins with a molecular weight of 24–28 kDa (similar in nature to silicatein) were responsible for the synthesis of the nanoparticles [83]. The exposure of *Verticillium* sp. to silver ions resulted in a similar intracellular growth of silver nanoparticles (AgNPs) [84]. The intracellular formation mechanism of AuNPs and AgNPs has not been understood. However, it has been postulated that the gold and silver ions initially bind on the fungal cell surface through electrostatic interaction. The adsorbed metal ions are then reduced by enzymes present in the cell wall, leading to the formation of the metal nuclei, which subsequently grow through further reduction of metal ions. Absar et al. [85] reported the extra- and intracellular biosynthesis of AuNPs by fungus *Trichothecium* sp. They observed that *Trichothecium* sp. reacted with gold ions during stationary phase

and forms extracellular AuNPs of various morphologies, such as spherical, rod-like and triangular. However, under shaking conditions, the same fungal biomass forms intracellular AuNPs under shaking conditions. It was postulated that under shaking condition fungi secretes enzymes and proteins into the medium, however in shaking conditions these enzymes and proteins are not being released, thus resulting in the formation of extracellular or intracellular AuNP, respectively. Fungal templates have been used for noble-MNP synthesis [86]. Fungal cells were grown in the presence of AuNP. Growth of a variety of fungi, such as *Penicillium citreonigrum*, *Trametes versicolor*, *Fusarium sp.*, *Phanaerochaete crysosporium*, *Trichoderma viride*, *Neurospora crassa*, *Nematolona frowardii*, and *Bjerkandera adusta* was tested in citrate-stabilized colloidal medium containing different noble-metal nanoparticles. *Thermomonos* Sp. reduced the gold ions extracellularly, yielding ANPs [76]. Even the edible mushroom *Volvariella volvacea* can produce Au and Ag NPs through metal reducing compounds. The mushroom was boiled initially in water and then filtered. The filtrate was cooled to room temperature and used as a reducing agent for AuNPs synthesis. Following reduction, purple-colored AuNPs was formed. The mushroom biomass also prevents NPs aggregation after their formation [87]. Microbiological methods generate nanoparticles at a much slower rate than that observed when plant extracts are used. This is one of the major drawbacks of biological synthesis of nanoparticles using microorganisms and must be corrected if it must compete with other methods.

The advantage of using *plants* for the synthesis of nanoparticles is that they are easily available, safe to handle and possess a broad variability of metabolites that may aid in reduction. Gold nanoparticles with a size range of 2–20 nm have been synthesized using the live alfa alfa plants [88]. Nanoparticles of silver, nickel, cobalt, zinc and copper have also been synthesized inside the live plants of *Brassica juncea* (Indian mustard), *Medicago sativa* (Alfa alfa) and *Heliantus annus* (Sunflower). Certain plants are known to accumulate higher concentrations of metals compared to others and such plants are termed as hyperaccumulators. Of the plants investigated, *Brassica juncea* had better metal accumulating ability and later assimilating it as nanoparticles [89]. Recently much work has been done with regard to plant-assisted reduction of metal nanoparticles and the respective role of phytochemicals. The main phytochemicals responsible have been identified as terpenoids, flavones, ketones, aldehydes, amides and carboxylic acids in the light of IR spectroscopic studies. The main water soluble phytochemicals are flavones, organic acids and quinones which are responsible for immediate reduction. The phytochemicals present in *Bryophyllum sp*. (Xerophytes), *Cyprus sp.* (Mesophytes) and *Hydrilla sp.* (Hydrophytes) were studied for their role in the synthesis of silver nanoparticles. The Xerophytes were found to contain emodin, an anthraquinone which could undergo redial tautomerization leading to the formation of silver nanoparticles.

While fungi and bacteria require a comparatively longer incubation time for the reduction of metal ions, water soluble phytochemicals do it in a much lesser time. Therefore, compared to bacteria and fungi, plants are better candidates for the synthesis of nanoparticles. Recently, Fahmy et al. introduced fully green nanotechnology as a gateway to beneficiation of natural cellulose fibers [90, 91]. Taking use of

plant tissue culture techniques and downstream processing procedures, it is possible to synthesize metallic as well as oxide nanoparticles on an industrial scale once issues like the metabolic status of the plant, etc. are properly addressed. Recently, scientists in India have reported the green synthesis of silver nanoparticles using the leaves of the obnoxious weed, *Parthenium hysterophorus*. Particles in the size range of 30–80 nm were obtained after 10 min of reaction. The use of this noxious weed has an added advantage in that it can be used by nanotechnology processing industries [92]. *Mentha piperita* leaf extract has also been used recently for the synthesis of silver nanoparticles. Nanoparticles in the size range of 10–25 nm were obtained within 15 min of the reaction [92]. *Azadirachta indica* leaf extract has also been used for the synthesis of silver, gold and bimetallic (silver and gold) nanoparticles. Studies indicated that the reducing phytochemicals in the neem leaf consisted mainly of terpenoids. It was found that these reducing components also served as capping and stabilizing agents in addition to reduction as revealed from FTIR studies. The major advantage of using the neem leaves is that it is a commonly available medicinal plant and the antibacterial activity of the biosynthesized silver nanoparticle might have been enhanced as it was capped with the neem leaf extract. The major chemical constituents in the extract were identified as nimbin and quercetin [93, 94].

12.7 Conclusion

Nanotechnologies belong to emerging technologies which hold the promise of bringing significant economic and technological benefits but there is only limited knowledge on their possible hazard potential; for example, exposure to these materials either in the environment or via consumer products. Assessing true workplace exposure may be challenging in some cases because of lack of understanding of the predictive value of different metrics in predicting human hazard and risk. Today, the most urgent challenge related to ENM and nanotechnologies is how can we gather the essential knowledge that could be utilized for reliable risk assessment and adequate risk management and governance. Even though there is an increasing amount of information of the hazard potential on several ENM, there is a dramatic lack of systematic, and especially relevant, information on the potential hazards associated with these materials. What is lacking is the kind of scientific knowledge which would be suitable for regulatory decision making, i.e., reliable risk assessment data. As valuable as mechanistic studies are for our understanding of the potential hazard mechanisms of these materials, using their results in regulatory risk assessment is challenging unless they are associated with acceptable experimental animal studies serving risk assessment and management purposes. To be able to respond to the societal needs for safe nanomaterials and nanotechnologies, it is necessary to complement valuable mechanistic studies with systematic short-term and long-term animal experiments that would allow a reliable estimation of the possible risks of ENM. Currently, studies on nanomaterials cannot be used for risk assessment unless they have been adequately validated against appropriate animal studies as this is the

only way to demonstrate that they have any predictive power. At present, these kinds of validated in vitro studies simply do not exist, and this has hindered the development of novel intelligent testing strategies of these materials. The current situation is especially challenging, as testing abilities and resources do not allow investigators to make an adequate assessment of safety and risks of ENM. As long as there is no clear evidence of the predictive power of these approaches for in vivo systems, their acceptance as a part of the regulatory framework of nanomaterials or other chemicals is highly unlikely; there are simply too many uncertainties and safety is not an area where we can afford to take risks with untested technologies and techniques. Currently, most of the existing in vitro or in vivo toxicity studies of ENM allow—at best—one to make some kind of comparison in terms of the relative hazard potential provided that the batch-to-batch variability has been considered, the materials adequately characterized, the appropriate number of graded doses have been used, and predictive endpoints have been measured. Often the data are interesting but not suitable for quantitative or even qualitative risk assessment.

One of the major challenges is that, in many cases, technologies that would deliver the required piece of information do not exist, or even if theoretically the techniques are available, they would require such exhaustive resources to negate their implantation. There is enough information to question whether all the assessments are necessary—or, in the worst case scenario—enough. The majority of ENM may be harmless or only modestly harmful, but there is a plethora of evidence revealing many of the materials may be highly harmful. Hence, the crucial challenge in all cases is to identify the harmful agents and to differentiate them from their innocent counterparts so that the appropriate regulatory decisions can be made to protect human health and the environment. Thus, it is very important to gather reliable data on the toxicity of ENM to be used for risk assessment. It is equally important to gather all available data on exposure levels in workplaces, in the environment and through consumer products so that the state-of-the-art in terms of hazard and exposure can be evaluated. Hence in the coming years the most remarkable challenge for the nanotechnology industry, the academia and the regulators will be the exploitation of the novel safety culture in nanomaterial research and engineering. Incorporating the safety-by-design as a part of the core research activities of nanomaterial sciences and the production of ENM would be a major step forward in assuring nanosafety. This strategy will not be inexpensive, but the benefits that it will confer will be undeniable. In order to incorporate nanosafety as part of the creative process and in the final formulation of the devices or materials themselves, some steps must be taken. As mentioned above, it is the first necessity to gather knowledge on the safety issues of ENM, e.g., relating toxicity of the materials with material characteristics, to learn about the toxicity of the different generations of materials, their stability and degradability. Such information is available for a small number of ENM, but for most materials this information is lacking. Then, a proper risk assessment throughout the Life Cycle of the materials from their generation to disposal becomes an unavoidable issue. The Life Cycle Analysis needs to become a key tool for safety assessment. It will be necessary to know when and where the product throughout its lifetime could be viewed as hazardous. The potential for exposure must

be assessed separately for each of the generations of nanomaterial to the end of their life cycle. In the risk analysis, the integration of a nanomaterial into some material, and the use and possible degradation of the materials must be taken into account. This knowledge must be then integrated in the fabrication process but the success of this approach will only become apparent when scientists, government, and industry are convinced that this is the way to proceed. A strong dissemination and exploitation of this new approach is therefore required to create the awareness-consciousness of the various benefits and risks and ways that risk can be mitigated in the context of nanotechnologies. In addition, tools must be provided to ensure the transfer of knowledge acquired in the nanosafety studies done in research institutes to the companies manufacturing nanomaterials. Finally, the expected massive production of ENM may lead to new issues related to their disposal and the treatment of ENM waste. This is an aspect which is too easily over-looked but it has to be recognized that it may have important long-term consequences for the human health and the environment.

Acknowledgements We acknowledge the Vice Chancellor, Prof. R.L. Hangloo for his interest in this work and PURSE programme, Department of Science and Technology, Govt. of India, for their support.

References

1. Brundtland G (1987) Our common future: report of the world commission on environment and development. Oxford University Press, Oxford
2. Gallopoulos NE (2006) Industrial ecology: an overview. Progr Ind Ecol 3(1–2):10–27
3. Eric Drexler K (1986) Engines of creation. Random House Inc, New York
4. Binnig G, Rohrer H, Gerber C, Weibel E (1983) 7 × 7 reconstruction on Si(111) resolved in real space. Phys Rev Lett 50:120–123
5. Maynard AD, Warheit DB, Philbert MA (2011) The new toxicology of sophisticated materials: nanotoxicology and beyond. Toxicol Sci 120:109–129
6. Stamm H (2011) Risk factors: nanomaterials should be defined. Nature 476:399
7. Monopoli MP, Aberg C, Salvati A, Dawson KA (2012) Biomolecular coronas provide the biological identity of nanosized materials. Nat Nanotechnol 7:779–786
8. Nel A, Xia T, Meng H, Wang X, Lin S, Ji Z, Zhang H (2012) Nanomaterial toxicity testing in the 21st century: use of a predictive toxicological approach and high-throughput screening. Acc Chem Res doi:10.1021.ar300022
9. Shvedova AA, Kagan VE, Fadeel B (2010) Close encounters of the small kind: adverse effects of man-made materials interfacing with the nano-cosmos of biological systems. Annu Rev Pharmacol Toxicol 50:63–88
10. Hartung T (2009) Lessons learned from alternative methods and their validation for a new toxicology in the 21st century. J Toxicol Environ Health B Crit Rev 13(2–4):277–290
11. Oberdörster G, Maynard A, Donaldson K, Castranova V, Fitzpatrick J, Ausman K, Carter J, Karn B, Kreyling W, Lai D, Olin S, Monteiro-Riviere N, Warheit D, Yang H, ILSI Research Foundation/Risk Science Institute Nanomaterial Toxicity Screening Working Group (2005) Principles for characterizing the potential human health effects from exposure to nanomaterials: elements of a screening strategy. Part Fibre Toxicol 6:2–8

12. Nel A, Xia T, Madler L, Li N (2006) Toxic potential of materials at the nanolevel. Science 311:622–627
13. Oberdorster G, Maynard A, Donaldson K, Castranova V, Fitzpatrick J, Ausman K, Carter J, Karn B, Kreyling W, Lai D, Olin S, Monteiro-Riviere N, Warheit D, Yang H (2005) Part fibre. Toxicology 2:8
14. Oberdorster G, Oberdorster E, Oberdorster J (2005) Nanotoxicology: an emerging discipline evolving from studies of ultrafine particles. Environ Health Perspect 113:823–839
15. Xia T, Li N, Nel AE (2009) Annu Rev Public Health
16. Nel AE, Madler L, Velegol D, Xia T, Hoek EM, Somasundaran P, Klaessi F, Castranova V, Thompson M (2009) Nat Mater 8:543–557
17. Xia T, Kovochich M, Brant J, Hotze M, Sempf J, Oberley T, Sioutas C, Yeh JI, Wiesner MR, Nel AE (2006) Nano Lett 6:1794–1807
18. George S, Pokhrel S, Xia T, Gilbert B, Ji Z, Schowalter M, Rosenauer A, Damoiseaux R, Bradley KA, Madler L, Nel AE (2010) ACS Nano 4:15–29
19. Li N, Xia T, Nel AE (2008) Free Radic Biol Med 44:1689–1699
20. Winkler DA, Mombelli E, Pietroiusti A (2013) Applying quantitative structure-activity relationship approaches to nanotoxicology: current status and future potential. Toxicol 313:15–23
21. Puzyn T, Rasulev B, Gajewicz A (2011) Using nano-QSAR to predict the cytotoxicity of metal oxide nanoparticles. Nat Nanotechnol 6(3):175–178
22. Epa VC, Burden FR, Tassa C, Weissleder R, Shaw S, Winkler DA (2012) Modelling biological activities of nanoparticles. Nano Lett 12:5808–5812
23. Le TC, Epa VC, Burden FR, Winkler DA (2012) Quantitative structure-property relationship modelling of diverse materials properties. Chem Rev 112:2889–2919
24. Fourches D, Pu D, Tassa C (2010) Quantitative nanostructure—activity relationship modeling. ACS Nano 4(10):5703–5712
25. Eric W, Ayers R, Heller M (2002) The 1.7 kilogram microchip: energy and material use in the production of semiconductor devices. Environ Sci Technol 36:5504–5510
26. Reuters (2007) HP claims advance in semiconductor nanotechnology reuters
27. Shadman F (2006) Environmental challenges and opportunities in nano-manufacturing. Paper presented at the green nanotechnology event hosted by the project on emerging nanotechnologies at the Woodrow Wilson International Center for Scholars 26 Apr 2006
28. Anastas P, Warner J (1998) Green chemistry theory and practice. Oxford University Press, New York
29. McKenzie LC, Hutchison JE (2004) Green nanoscience: an integrated approach to greener products, processes, and applications. Chem Today 22:30–32
30. Hasobe T, Imahori H, Fukuzumi S, Kamat PV (2003) Light energy conversion using mixed molecular nanoclusters. Porphyrin and C60 cluster films for efficient photocurrent generation. J Phys Chem B 107:12105–12112
31. Venkatasubramanian R, Siivola E, Colpitts T, O'Quinn R (2001) Thin-film thermoelectric devices with high room-temperature figures of merit. Nature 413:597–602
32. Lloyd SM, Lave LR (2003) Life cycle economic and environmental implications of using nanocomposites in automobiles. Environ Sci Tech 37:3458–3466
33. Hahm JL, Lieber CM (2004) Direct ultrasensitive electrical detection of DNA and DNA sequence variations using nanowire nanosensors. Nano Lett 4:5154
34. Dahl JA, Maddux BLS, Hutchinson JE (2007) Towards greener nanosynthesis. Chem Rev 107:2228–2269
35. Chithrani RD, Ghazani AA, Chan WC (2006) Determining the size and shape dependence of gold nanoparticle uptake into mammalian cells. Nano Lett 6:662–668
36. Colvin VL (2003) The potential environmental impact of engineered nanomaterials. Nat Biotechnol 21:1166–1170
37. Magrez A, Kasas S, Salicio V, Pasquier N, Seo JW, Celio M, Catsicas S, Schwaller B, Forro L (2006) Cellular toxicity of carbon-based nanomaterials. Nano Lett 6:1121–1125
38. Albrecht MA, Evans CW, Raston CL (2006) Green chemistry and the health implications of nanoparticles. Green Chem 8:417–432

39. Pernodet N, Fang X, Sun Y, Bakhtina A, Ramakrishnan A, Sokolov J, Ulman A, Rafailovich M (2006) Adverse effects of citrate/gold nanoparticles on human dermal fibroblasts. Small 2:766–773
40. Derfus AM, Chan WCW, Bhatia SN (2004) Probing the cytotoxicity of semiconductor quantum dots. Nano Lett 4:11–18
41. Hurt RH, Monthioux M, Kane A (2006) Toxicology of carbon nanomaterials: status, trends, and perspectives on the special issue. Carbon 44:1028–1033
42. Wiesner MR, Charackli GW (1998) Metals and colloids in urban runoff. In: Brejchova D (eds) Ann Arbor Press, Chelsea, MI
43. Weare WW, Reed SM, Hutchison JE, Warner MG (2000) Improved synthesis of small (dCORE″, 1.5 nm) phosphine-stabilized gold nanoparticles. J Am Chem Soc 122:12890–12891
44. Oberdorster E (2004) Manufactured nanomaterials (fullerenes, C60) induce oxidative stress in the brain of juvenile largemouth bass. Environ Health Perspect 112:1058–1062
45. Mafuné F, Kohno J, Takeda Y, Kondow T (2001) Formation of gold nanoparticles by laser ablation in aqueous solution of surfactant. J Phys Chem B 105:225114–225120
46. Raffi M, Rumaiz AK, Hasan MM, Shah SI (2007) Studies of the growth parameters for silver nanoparticle synthesis by inert gas condensation. J Mater Res 22:3378–3384
47. Rosemary MJ, Pradeep T (2003) Solvothermal synthesis of silver nanoparticles from thiolates. J Colloid Interface Sci 268:81–84
48. Chaki NK, Sundrik SG, Sonawane HR, Vijayamohanan KJ (2002) Chem Soc Chem Commun 76
49. Shukla S, Seal S (1999) Cluster size effect observed for gold nanoparticles synthesized by sol-gel technique as studied by X-ray photoelectron spectroscopy. Nano Struct Mater 11:1181–1193
50. Gleiter H (1989) Nan crystalline materials. Progr Mater Sci 33:223–315
51. Pérez-Tijerina E, Gracia-Pinilla MA, Mejía-Rosales S, Ortiz-Méndez U, Torres A, José-Yacamán M (2008) Highly size-controlled synthesis of Au/Pd nanoparticles by inert-gas condensation. Faraday Discuss 138:353–362
52. Kang S, Kang MH, Lee E, Seo S, AhnFacile CWH (2011) Hetero-sized nanocluster array fabrication for investigating the nanostructure-dependence of nonvolatile memory characteristics. Nanotechnology 22:254018. doi:10.1088/0957-4484/22/25/254018
53. Gacoin T, Malier L, Boilot JP (1997) Sol–gel transition in CdS colloids. Chem Mater 9:1502
54. Yuan Y, Fendler J, Cabasso I (1992) Preparation and characterization of stable aqueous higher-order fullerenes. Chem Mater 4:312
55. Sankaran V, Yue J, Cahen RE, Schrock RR, Silbey RJ (1993) Advanced drug delivery advices. Chem Mater 5:1133
56. Olshavsky MA, Allcock HR (1997) Small scale system for in-vivo drug delivery. Chem Mater 9:1367
57. Ren W, Ai Z, Jia F, Zhang L, Fan X, Zou Z (2007) Low temperature preparation and visible light photocatalytic activity of mesoporous carbon-doped crystalline TiO_2. Appl Catal B 69:138–144
58. Yang HG, Sun CH, Qiao SH, Zou J, Liu G, Smith SC, Cheng HM, Lu GQ (2008) Anatase TiO_2 single crystals with a large percentage of reactive facets. Nature 453:638–641
59. Tao AR, Habas Yang SP (2008) Shape control of colloidal metal nanocrystals. Small 4:310–325
60. Turkevitch J, Stevenson PC, Hillier J (1951) Nucleation and growth process in the synthesis of colloidal gold. Discuss Faraday Soc 11:55–75
61. Frens G (1972) Particle size an d sol stability in metal colloids. Colloid Polym Sci 250:736–741
62. Brust M, Kiely CJ (2002) Some recent advances in nanostructure preparation from gold and silver: a short topical review. Colloids Surf A Physicochem Eng Asp 202:175–186
63. Lowenstam HA (1981) Minerals formed by organisms. Science 211:1126–1131
64. Southam G, Saunders JA (2005) The geomicrobiology of ore deposits. Econ Geol 100:1067–1084

65. Gericke M, Pinches A (2006) Biological synthesis of metal nanoparticles. Hydrometallurgy 83:132–140
66. Klaus T, Joerger R, Olsson E, Granqvist CG (1999) Silver-based crystalline nanoparticles, microbially fabricated. Proc Natl Acad Sci U S A 96(24):13611–13614
67. Konishi Y, Yoshida S, Asai S (1995) Bioleaching of pyrite by acidophilic thermophile Acidianus brierleyi. Biotechnol Bioeng 48(6):592–600
68. Beveridge TJ, Murray RGJ (1976) Uptake and retention of metals by cell walls of Bacillus subtilis. J Bacteriol 127(3):1502–1518
69. Southam G, Beveridge TJ (1994) The in vitro formation of placer gold by bacteria. Geochim Cosmochim Acta 58:4527–4530
70. Kalishwaralal K, Deepak V, Ram Kumar Pandian S, Gurunathan S (2009) Biosynthesis of gold nanocubes from Bacillus lichemiformis. Bioresour Technol 100:5356–5358
71. Law N, Ansari S, Livens FR, Renshaw JC, Lloyd JR (2008) Formation of nanoscale elemental silver particles via enzymatic reduction by Geobacter sulfurreducens. Appl Environ Microbiol 74:7090–7093
72. Kalimuthu K, Babu SR, Venkataraman D, Bilal M, Gurunathan S (2008) Biosynthes is of silver nanoparticles by Bacillus licheniformis. Colloids Surf B Biointerfaces 65:150–151
73. Kalathil S, Lee J, Cho MH (2011) Electrochemically active biofilm-mediated synthesis of silver nanoparticles in water. Green Chem. doi:10.1039/c1gc15309a
74. Reith F, Etschmann B, Grosse C, Moors H, Benotmane MA, Monsieurs P, Grass G, Doonan C, Vogt S, Lai B, Martinez-Criado G, George GN, Nies DH, Mergeay M, Pring A, Southam G, Brugger J (2009) Mechanisms of gold biomineralization in the bacterium Cupriavidus metallidurans. Proc Natl Acad Sci U S A 106:17757–17762
75. He S, Guo Z, Zhang Y, Zhang S, Wang J, Gu N (2007) Biosynthesis of gold nanoparticles using the bacteria Rhodopseudomonas capsulate. Mater Lett 61:3984–3987
76. Sastry M, Ahmad A, Khan IM, Kumar R (2003) Biosynthesis of metal nanoparticles using fungi and actinomycete. Curr Sci 85(2):162–170
77. Ahmad A, Mukherjee P, Senapati S, Mandal D, Khan MI, Kumar R, Sastry M (2003) Extracellular biosynthesis of silver nanoparticles using the fungus Fusarium oxysporum. Colloids Surf B Biointerfaces 28:313–318
78. Kaushik, P, Dhiman AK (2002) Medicinal plants and raw drugs of India, P.XII+623. Retrieved from http://www.vedicbooks.net/medicinal-plants-and-raw-drugs-of-india-p-886.html
79. Balaji DS, Basavaraja S, Deshpande R, Mahesh DB, Prabhakar BK, Venkataraman A (2009) Extracellular biosynthesis of functionalized silver nanoparticles by strains of Cladosporium cladosporioides fungus. Colloids Surf B Biointerfaces 68:88–92
80. Kathiresan K, Manivannan S, Nabeel AM, Dhivya B (2009) Studies on silver nanoparticles synthesized by a marine fungus Penicillum fellutanum isolated from coastal mangrove sediment. Colloids Surf B Biointerfaces 71:133–137
81. Duran N, Marcato DP, Alves LO, De Souza G, Esposito E (2005) Mechanical aspect of biosynthesis of silver nanoparticles by several Fusarium oxysporum strains. J Nanobiotechnol 117
82. Vigneshwaran N, Kathe AA, Varadarajan PV, Nachane RP, Balasubramanya RH (2007) Silver-protein (core-shell) nanoparticle production using spent mushroom substrate. Langmuir 23(13):7113–7117
83. Bansal V, Rautaray D, Ahmad A, Sastry M (2004) Biosynthesis of zirconia nanoparticles using the fungus Fusarium oxysporum. J Mater Chem 14:3303–3305
84. Mukherjee P, Ahmad A, Mandal D, Senapati S, Sainkar SR, Khan MI, Parischa R, Ajayakumar PV, Alam M, Kumar R, Sastry M (2001) Fungus mediated synthesis of silver nanoparticles and their immobilization in the mycelia matrix: a novel biological approach to nanoparticle synthesis. Nano Lett 1:515–519
85. Absar A, Satyajyoti S, Khan MI, Rajiv K, Sastry M (2005) Extra-/intracellular biosynthesis of gold nanoparticles by an alkalotolerant fungus, Trichothecium sp. J Biomed Nanotechnnol 1:147–153
86. Bigall NC, Reitzig M, Naumann W, Simon P, van Pée KH, Eychmüller A (2008) Fungal templates for noble metal nanoparticles and their application in catalysis. Chem Int 47:7876–7879

87. Philip D (2009) Biosynthesis of Au, Ag and Au-Ag nanoparticles using edible mushroom extract. Spectrochem Acta Part A 73:374–381
88. Torresday JLG, Parsons JG, Gomez Videa EJP, Troian HE, Santiago IP, Yacaman MJ (2002) Formation and growth of Au nanoparticles inside live alfa alfa plants. Nanolett 2(4):397–401
89. Bali R, Razak N, Lumb A, Harris AT (2006) The synthesis of metal nanoparticles inside live plants. IEEE Xplore. doi:10.1109/ICONN.2006.340592
90. Fahmy TYA, Mobarak F (2008) Vaccination of biological cellulose fibers with glucose: a gateway to novel nanocomposites. Int J Biol Macromol 42(1):52
91. Fahmy TYA, Mobarak F (2011) Green nanotechnology: a short cut to beneficiation of natural fibers. Int J Biol Macromol 48(1):134
92. Parasar UK, Saxena PS, Srivastava A (2009) Bioinspired synthesis of silver nanoparticles. Dig J Nanomater Biostruct 4(1):159–166
93. Shankar SS, Rai A, Ahmad A, Sastry M (2004) Rapid synthesis of Au, Ag and bimetallic Au core- Ag shell nanoparticles using neem (Azadirachta indica) leaf broth. J Colloid Interface Sci 275:496–502
94. Tripathi A, Chandrasekaran NA, Raichur M, Mukherjee A (2009) Antibacterial applications of silver nanoparticles synthesized by aqueous extract of Azadirachta indica (Neem) leaves. J Biomed Nanotechnol 5:93–98

Chapter 13
Time-Domain Ab Initio Modeling of Charge and Exciton Dynamics in Nanomaterials

Linjun Wang, Run Long, Dhara Trivedi, and Oleg V. Prezhdo

Abstract Nonequilibrium dynamical processes in nanoscale materials involving electrons, excitons, and vibrations are under active experimental investigation. Corresponding theoretical studies, however, are much scarcer. This chapter starts with the basics of time-dependent density functional theory, recent developments in nonadiabatic molecular dynamics methods, and the fusion of the two techniques. Ab initio simulations of this kind allow us to directly mimic a great variety of time-resolved experiments performed with pump-probe laser spectroscopies. We systematically investigate two important building blocks of modern nanotechnology, namely, quantum dots (QDs) and titanium dioxide (TiO_2). The focus is on the ultrafast photoinduced charge and exciton dynamics at interfaces formed by two complementary materials, including QD-TiO_2 hybrids, organic-QD and organic-TiO_2 interfaces, and all organic systems. These interfaces involve bulk semiconductors, metallic and semiconducting nanoclusters, graphene, carbon nanotubes, fullerenes, polymers, molecules and molecular crystals. The detailed atomistic insights available from time-domain ab initio studies provide a unique description and a comprehensive understanding of the competition between various dynamical processes (e.g., electron transfer, thermal relaxation, energy transfer, and charge recombination). These advances now make it possible to directly guide the development of organic and hybrid solar cells, as well as photocatalytic, electronic, spintronic, and other devices relying on complex interfacial dynamics.

Keywords Charge and exciton dynamics • Nanoscale materials • Nonadiabatic molecular dynamics • Quantum dot and titanium dioxide interfaces • Time-dependent density-functional theory

L. Wang (✉) • O.V. Prezhdo
Department of Chemistry, University of Southern California, Los Angeles, CA 90089, USA
e-mail: linjun.wang@usc.edu

Department of Chemistry, University of Rochester, Rochester, NY 14627, USA

R. Long
School of Physics and Complex & Adaptive Systems Laboratory,
University College Dublin, Belfield, Dublin 4, Ireland

D. Trivedi
Department of Physics and Astronomy, University of Rochester, Rochester, NY 14627, USA

V.A. Basiuk, E.V. Basiuk (eds.), *Green Processes for Nanotechnology*,
DOI 10.1007/978-3-319-15461-9_13

13.1 Introduction

Electron transfer (ET) at nano interfaces [1] is at the heart of many research fields, including photovoltaics [2, 3], photocatalysis [4, 5], photosynthesis [6, 7], photochemistry [8, 9], electrolysis [10, 11], as well as molecular electronics [12, 13] and spintronics [14, 15]. As shown in Fig. 13.1, efficient ET needs to compete with many other charge or exciton dynamical processes, e.g., thermal relaxation, energy transfer, and charge recombination. As a whole, they ultimately determine the overall device performance and have attracted numerous efforts to explore the underlying mechanisms and nonequilibrium nature. Time-resolved experiments, such as transient absorption spectroscopy [16, 17] and optical second harmonic generation techniques [18–20], have been widely used to obtain the time scales for all of these dynamical channels. On the theoretical side, nonadiabatic molecular dynamics (NAMD) provides the most popular and reliable solution to catch the essence of the experimental observations [21, 22]. Over the last two decades, a suite of NAMD approaches have been developed and implemented atomistically to model the dynamics in the time domain and at the ab initio level [23–29]. This chapter presents the current perspective on theory basics of various NAMD strategies and summaries the applications at different kinds of nano interfaces carried out by the Prezhdo group in recent years.

We present the standard approaches, including mean field (MF) [30–32], fewest switches surface hopping (FSSH) [21, 33], and quantized Hamiltonian dynamics (QHD) [34, 35]. Especially, Tully's FSSH has retained its popularity because of its

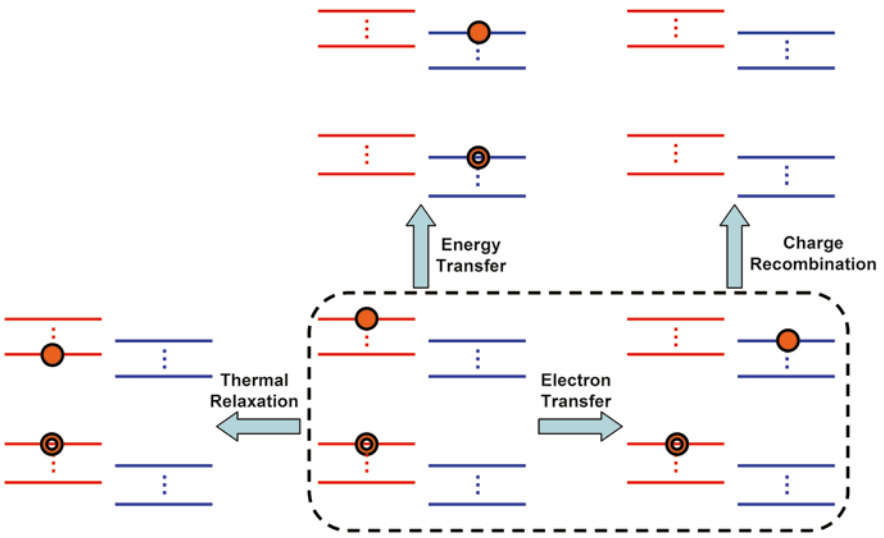

Fig. 13.1 Photoinduced electron transfer from a donor to an acceptor (highlighted with the *dashed square frame*), competing with thermal relaxation, energy transfer, and charge recombination processes. The energy levels of the donor and acceptor are shown as *red* and *blue solid horizontal lines*, respectively. Electron and hole are represented by *solid* and *open orange circles*

general reliability and ease of implementation, namely, we do not require explicit propagation of the nuclear wave function, and key quantities like forces and nonadiabatic (NA) couplings can be computed on-the-fly by efficient analytical derivate methods [22, 36, 37]. Due to its great success, FSSH has attracted intense attention, and a variety of situations requiring improvements have been identified. When high density of states (DOS) comes into play, in particular, in nanoscale materials, standard FSSH encounters the so-called trivial, or unavoided, crossing problem [38–41]. It can be overcome with several modern developments, including self-consistent fewest switches surface hopping (SC-FSSH) [42] and adaptive flexible surface hopping (FSH) [43, 44]. In addition, FSSH lacks the capability to describe the superexchange mechanism of population transfer, which can be well captured by global flux surface hopping (GFSH) developed very recently [45]. Decoherence is another issue that needs for proper descriptions when we encounter slow transitions between states separated by significant energy gaps [46–48]. Decoherence can be realized through the stochastic mean field (SMF) [49], decoherence-induced surface hopping (DISH) [50], and coherence penalty functional (CPF) [51] methods.

Ab initio density functional theory (DFT) provides a rigorous and efficient method to obtain the electronic structure of systems ranging from organic and inorganic materials to hybrids. In recent years, time-dependent density functional theory (TDDFT) has been extensively applied to a broad range of inorganic and organic systems undergoing energy relaxation, energy transfer, charge separation, charge recombination, charge transport, and chemical reactions [23–29]. Inorganic materials generally exhibit strong chemical bonding and high electrical conductivity. Their large dielectric constants result in strong electric field screening and reduced Coulomb binding between electrons and holes [52]. In contrast, organic systems are generally loosely packed with small charge mobility due to the weak electron–electron coupling and strong electron–phonon interaction [53–56]. Small dielectric constants lead to strong Coulombic binding of electron–hole pairs, and excitons tend to be localized [57–59]. The fundamentally different properties of inorganic and organic materials are described by either physics or chemistry, which differ in concepts and language: compare—band structure, excitons, phonons—employed by physicists with—orbitals, electron correlation, vibrations—used by chemists. Thus, significant challenges arise when trying to develop a unified description of inorganic and organic components and their hybrids. In this aspect, the state-of-the-art simulation approach combining NAMD and TDDFT provides a general time-domain atomistic solution to the various nonequilibrium charge and exciton dynamics in different kinds of materials that are fundamental to a wide variety of nanoscale applications.

Quantum dots (QDs) and titanium dioxide (TiO_2) are the important building blocks of modern nanotechnology due to their unique electronic properties. This chapter firstly covers the ab initio studies on the electronic structure of QDs and TiO_2 and then discusses charge and exciton dynamics at interfaces formed by two complementary materials, including QD–TiO_2 hybrids, organic–QD and organic–TiO_2 interfaces, and all organic systems (see Fig. 13.2). For QD–TiO_2 hybrids, the time-domain simulation has shown that hot electrons can be extracted from PbSe QDs prior to relaxation inside the QD [60]; electron–hole recombination rate can be minimized

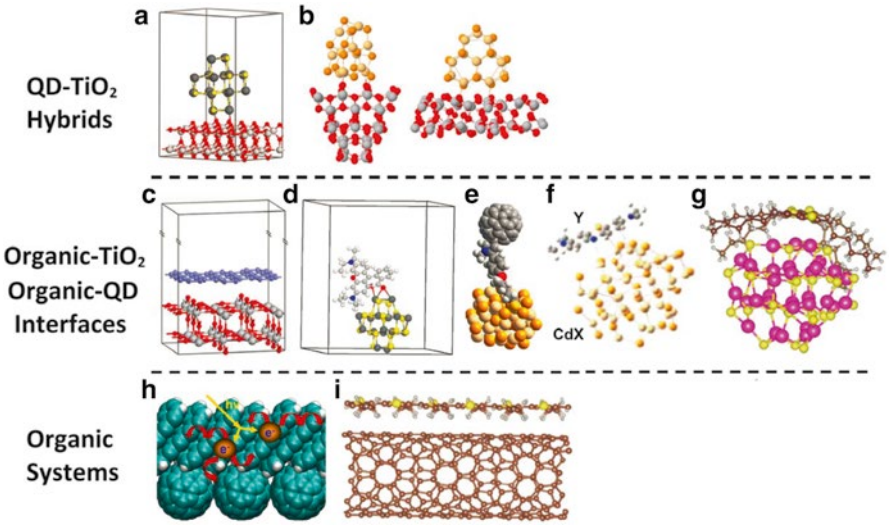

Fig. 13.2 Illustration of the applications discussed in the chapter: QD–TiO_2 hybrids (*top panel*), organic–TiO_2 and organic–QD interfaces (*middle panel*), and organic systems (*bottom panel*). (**a**) PbSe QD on TiO_2 surface, (**b**) CdSe QD connecting to either TiO_2 QD or TiO_2 nanobelt, (**c**) graphene interfaced on TiO_2 surface, (**d**) RhB molecule interacting with PbS QD, (**e**) C_{60} bound to CdSe QD, (**f**) CdX QD interacting with Y molecule (X = S, Se, and Te; Y = AQ, MV^{2+}, and MB^{+}), (**g**) P3HT on CdS QD, (**h**) pentacene–C_{60} composite, and (**i**) P3HT–CNT heterojunction

via tuning QD size and bridge length [61]; and the mechanism of electron injection from a CdSe QD donor into nanoscale TiO_2 acceptor depends on the acceptor dimensionality [62]. To exemplify organic–TiO_2 interfaces, we investigate graphene on TiO_2 and explain why metallic graphene can be used as a photosensitizer for the generation of high photocurrent [63]. Considering organic–QD interfaces, we reveal that atomic defects can be beneficial for charge separation at RhB–QD interface [64]; why a long, insulating bridge can accelerate ET in C_{60}–QD system [65]; nanoscale materials exhibit a new, Auger-assisted type of ET [66]; and dimensionality is inverted at a QD and conjugated polymer heterojunction [67]. Finally, for all organic systems, we demonstrate that optically dark states govern the rates and quantum yields of singlet fission and charge transfer at a pentacene/C_{60} interface [68]; and how the asymmetry in the electron and hole transfer at a polymer/nanotube heterojunction can be used to optimize solar cell performance [69].

In brief, we establish the mechanisms of all relevant photo-initiated dynamical processes, characterize the key electronic states and phonon modes involved, and describe the interplay between productive and unfavorable channels of photoinduced electron and energy flow. The summarized time-domain ab initio simulations provide valuable insights into the nature of the charge and energy transfer together with other related dynamical processes on the nanoscale, and generate important guidelines for designing and improvement of photovoltaic and photocatalytic devices for nanotechnologies.

13.2 Theoretical Approaches

13.2.1 Density Functional Theory

Wavefunction is the heart and soul of quantum mechanics and determines all observable properties through the calculation of expectation values [70]. However, it is still a forbidden task to find out the true many-electron wavefunction for large systems. The Hohenberg-Kohn theorems have demonstrated that the ground state properties of any system under the influence of a static external potential can be obtained directly from the electron density, which relies only on three spatial coordinates [71]. The many-electron problem can be further reduced by approximating it to a tractable picture of noninteracting electrons moving in an effective potential, resulting in the Kohn-Sham (KS) framework of DFT [72]. With proper choices of exchange-correlation (XC) functionals, DFT finds an increasingly broad application in physics, chemistry, biology, and material sciences for the atomistic interpretation and prediction of complex behavior [73].

13.2.2 Time-Domain Density Functional Theory

When the external perturbations, e.g., electro-magnetic field and vibrational motions, evolve in time, the Runge-Gross (RG) theorem has shown that the three-dimensional electron density is also sufficient to describe the time-dependent response of the system [74]. The obtained theory is known as TDDFT [75]. Within the KS representation, the electron density at time t, $\rho(\mathrm{r},t)$, is given as a summation over all occupied single-electron KS orbitals, $\{\varphi_i(\mathrm{r},t)\}$ [75],

$$\rho\left(\mathrm{r},t\right)=\sum_{i=1}^{N_e}\left|\varphi_i\left(\mathrm{r},t\right)\right|^2, \tag{13.1}$$

where N_e is the number of electrons and r represents the coordinates of the assemble of $3N_e$ electrons. The time-dependent variational principle can be applied to the KS energy [75],

$$E=\sum_{i=1}^{N_e}\left\langle\varphi_i\middle|K\left(\mathrm{r}\right)\middle|\varphi_i\right\rangle+\sum_{i=1}^{N_e}\left\langle\varphi_i\middle|V\left(\mathrm{r};\mathrm{R}\right)\middle|\varphi_i\right\rangle+\frac{e^2}{2}\iint\frac{\rho\left(\mathrm{r}\right)\rho\left(\mathrm{r}'\right)}{\left|\mathrm{r}-\mathrm{r}\right|}d^3\mathrm{r}d^3\mathrm{r}'+E_{xc}\left\{\rho\left(\mathrm{r}'\right)\right\}, \tag{13.2}$$

where $K(\mathrm{r})$ is the kinetic energy operator of noninteracting electrons, $V(\mathrm{r};\mathrm{R})$ is the electron-nuclear attraction potential energy that relies on both electronic coordinates r and nuclear coordinates R, the third term describes electron–electron Coulomb repulsion, and $E_{xc}\{\rho\}$ is the XC functional taking into account the many-body interactions. The time-dependent variational principle gives a set of coupled single-particle KS equations of motion (EOM) [75–77],

$$i\hbar \frac{\partial \varphi_i(\mathrm{r},t)}{\partial t} = H(\mathrm{r};\mathrm{R})\{\varphi(\mathrm{r},t)\}\varphi_i(\mathrm{r},t), \tag{13.3}$$

where the Hamiltonian $H(\mathrm{r};\mathrm{R})$ is a functional of the overall electron density, and therefore all occupied KS orbitals.

The adiabatic KS basis can be viewed as a numerical tool for solving the time-dependent Kohn-Sham (TDKS) equations given in Eq. (13.3) [78]. Expansion of the TDKS orbitals in the adiabatic KS basis, $\{\tilde{\varphi}_j(\mathrm{r};\mathrm{R})\}$,

$$\varphi_i(\mathrm{r},t) = \sum_{j=1}^{N_e} c_{ij}(t)\left|\tilde{\varphi}_j(\mathrm{r};\mathrm{R})\right., \tag{13.4}$$

yields a set of EOM for the expansion coefficients [21],

$$i\hbar \frac{\partial}{\partial t} c_{ij}(t) = \sum_{k}^{N_e} c_{ik}(t)(\tilde{\varepsilon}_k \delta_{jk} + \mathrm{d}_{jk}\cdot\dot{\mathrm{R}}), \tag{13.5}$$

where $\tilde{\varepsilon}_k$ is the corresponding energy of adiabatic KS state, $\tilde{\varphi}_k(\mathrm{r};\mathrm{R})$. The last term of Eq. (13.5) is the nonadiabatic coupling (NAC) constant [79–83],

$$\mathrm{d}_{jk}\cdot\dot{\mathrm{R}} = -i\hbar\left\langle \tilde{\varphi}_j(\mathrm{r};\mathrm{R})\middle|\nabla_{\mathrm{R}}\middle|\tilde{\varphi}_k(\mathrm{r};\mathrm{R})\right\rangle\cdot\dot{\mathrm{R}} = -i\hbar\left\langle \tilde{\varphi}_j(\mathrm{r};\mathrm{R})\middle|\frac{\partial}{\partial t}\middle|\tilde{\varphi}_k(\mathrm{r};\mathrm{R})\right\rangle, \tag{13.6}$$

which arises from the dependence of the adiabatic KS orbitals on the nuclear coordinates R [84]. Solving the TDKS equations in the adiabatic KS basis reduces the computational difficulty to the TDDFT problem [85].

Slater determinants formed from the single-electron KS orbitals can be viewed as an approximation to the many-electron adiabatic states [85]. A state basis is needed to perform NAMD, as discussed in the next subsection. The NACs between the Slater determinants are nonzero only if the determinants differ by only one orbital. As a result, the propagation involves very sparse matrices, allowing us to adopt large many-electron basis sets. At the level of TDKS equations, the adiabatic KS representation makes no approximations and can be regarded as a particular choice of basis set for NAMD. It also carries a number of other advantages associated with the fact that adiabatic KS orbitals are routinely computed by most DFT codes. The KS representation of excited states assumes that the error made in the calculation of the potential energy surface (PES) due to the missing TDDFT correction is constant in time, and therefore, it is independent of the structural evolution. As a result, the adiabatic KS states can be viewed as the zeroth-order adiabatic states in the linear response time-dependent density functional theory (LR-TDDFT) [86]. In practice, the KS excitation is generally the leading term in the expression of LR-TDDFT [87]. The agreement with LR-TDDFT is better for pure DFT functionals than for hybrid functionals. Larger systems with a greater number of electrons exhibit better agreement as well. The errors introduced with the KS description of electronic excitations should be compared with other approximations, such as those involved in the choice

of the DFT functional and in the classical description of vibrational motions, neglecting zero-point energy contributions to the NAC and decoherence in the electronic subsystem induced by quantum vibrations [78].

13.2.3 Nonadiabatic Molecular Dynamics

NAMD is a mixed quantum-classical molecular dynamical approach, which includes transitions between electronic states. It can describe excited state dynamics involving strong interstate couplings when Born-Oppenheimer approximation is broken down. This is achieved in a self-consistent way: the nuclear motions drive the electronic evolution, for instance, by TDDFT, and the electronic evolution influences the classical nuclear dynamics [33]. The latter can be carried out in a MF manner, leading to the Ehrenfest approximation [30]. Correlations between the dynamics of nuclei and electrons can be included by surface hopping (SH) techniques [21]. Typically, SH approaches are better performed in the adiabatic basis [88, 89], which is readily available from electronic structure calculations.

13.2.3.1 Classical Path and Ehrenfest Approximations, Quantized Hamilton Dynamics

The classical path approximation (CPA) [90] provides a very simple solution to the quantum back-reaction problem, that is, the influence of the electronic evolution on the classical nuclei. CPA assumes that the classical trajectory is independent of electronic dynamics, while the electronic dynamics still depends on the classical coordinates. CPA is appropriate if electron–electron interactions are much stronger than electron–phonon couplings [91], or the energy of the electrons is sufficiently smaller than that of the nuclei, such that the electron-nuclear energy exchange does not affect the nuclear evolution apparently. CPA is also valid if the PESs that are associated with different electronic states differ only slightly, in comparison for instance, with the amplitude of nuclear fluctuations due to thermal or zero-point energy.

The Ehrenfest approximation is another attractive choice for NAMD simulations due to its straightforward and rigorous foundations [30–32]. There, the force applied on any classical degree of freedom is obtained through the gradient of the expectation value of the Hamiltonian acting on the time-evolving wavefunction. If the energy flow between electronic and nuclear subsystems is insignificant, Ehrenfest is sufficient. At the Ehrenfest level, NAMD is independent of the chosen electronic basis, and thus the adiabatic representation is equivalent to spatial and plane-wave grids [76, 92] or a localized atomic basis [93]. When electron-nuclear correlations are important and nuclear trajectories branch depending on the electronic state, a trajectory SH needs to be adopted [21, 33, 88].

Instead of the Schrödinger representation, correlated electron-nuclear dynamics can be also studied within the Heisenberg representation. By treating quantum mechanically, not only the electron creation and annihilation operators, but also the nuclear position and momentum variables, the time derivative of the expectation value for any system observable of interest can be achieved from the Heisenberg equation. In this QHD method, there exists an interesting phenomenon: the original operators become coupled to higher order operators, resulting in a hierarchy of equations [34, 35, 94–96]. Different level of approximations to the quantum dynamics are achieved through the termination of the chain with a closure that expresses the expectation values of the higher order operators in terms of products of the expectations of the lower order operators. In particular, it was found that the first-order QHD coincides with the Ehrenfest theory [35]. Simple extensions to higher order QHDs can efficiently represent quantum nuclear effects, such as phonon zero-point energy, tunneling, and loss of coherence in the electronic subsystem caused by phonons.

13.2.3.2 Fewest Switches Surface Hopping, Self-Consistent Fewest Switches Surface Hopping, and Adaptive Flexible Surface Hopping

Among all SH strategies, Tully's FSSH [21] is the most widely used approach. It minimizes the number of surface hops by prescribing a SH probability based on population fluxes, rather than populations themselves. The NACs are used, along with the wavefunction amplitudes, to determine the SH probabilities. The time dependent probability of hopping between state i and state j within a time step Δt reads [21],

$$g_{ij}\left(t,\Delta t\right)=\max\left\{0,-\frac{b_{ij}\Delta t}{a_{ii}\left(t\right)}\right\}, \tag{13.7}$$

where

$$b_{ij}=-2\mathrm{Re}\left(a_{ij}^{*}\mathrm{d}_{ij}\cdot\dot{\mathrm{R}}\right), \tag{13.8}$$

$$a_{ij}=c_{i}c_{j}^{*}, \tag{13.9}$$

A ground state nuclear trajectory can be used to sample initial conditions to create ensemble averages for the excited state dynamics.

SH studies on weakly interacting or large-scale systems suffer severely from the trivial crossing problem, arising due to the high density of adiabatic PESs [38–41]. Around the trivial crossing point, the NAC becomes a delta function, FSSH probabilities cannot be computed accurately in numerical calculations using a finite time step. The SC-FSSH technique [42] offers a straightforward solution to the problem by introducing a self-consistency test into the standard FSSH procedure. The total FSSH probability hopping out of the active state i satisfies [42],

$$g_{tot} = \frac{a_{ii}(t) - a_{ii}(t + \Delta t)}{a_{ii}(t)}. \tag{13.10}$$

After calculating the energy differences between state i and all other adiabatic states, we find out the adiabatic state k, which gives the smallest value, and identify it as the main source of the trivial crossing. Then, we can correct the error by computing the SH probability corresponding to the trivial crossing, g_{ik}, using the simple expression,

$$g_{ik} = g_{tot} - \sum_{j \neq k} g_{ij}, \tag{13.11}$$

Using the Holstein Hamiltonian as an example, SC-FSSH allows us to reduce the simulation time 10,000-fold while retaining the FSSH accuracy already in a five-state system [42].

Because an electron is delocalized over a finite space and electron–phonon interactions are generally quite local [97–99], only a limited number of nuclear degrees of freedom (DOF) are strongly coupled to the electron dynamics. Thereby, one can treat only a small portion of the nuclei surrounding the electron in a SH manner, and the rest of the nuclei simply at the molecular dynamics (MD) level [43]. As both the central position and extension of the electron may change in time, this should be done in a flexible way through adding and/or removing neighboring nuclear DOF to/from the SH subsystem at each time step. In this aspect, the problematic trivial crossing problem is avoided because all adiabatic states are spatially close. Also, the computational cost is largely reduced because only a much smaller Hamiltonian matrix is diagonalized to obtain all important PESs. A flexible time step technique, which ensures the smoothness of all time-dependent adiabatic states, enables us to describe SH accurately with a relative large time step. This FSH algorithm [43, 44] based on a minimum subsystem implementing SH and a maximum time step for SH dynamics can recover all charge transport regimes described by existing theories [100–102] and can be easily extended to more complex Hamiltonians.

13.2.3.3 Global Flux Surface Hopping

Superexchange is a class of dynamical processes [103], where two electronic states are coupled indirectly through an intermediate state, typically with a higher energy. Common to nanoscale systems, Auger-type electron–hole energy exchange, multi-exciton generation and annihilation [104–106], are multiparticle reactions, which also involve intermediate states with high energy. Transitions into such intermediate states violate energy conservation and are forbidden in FSSH. Besides, FSSH only allows transitions between directly coupled states, and thus it mistreats quantum processes involving the superexchange mechanism. GFSH solves this problem while remaining identical to FSSH in other instances. Instead of using the FSSH state-to-state flux given by Eq. (13.7), the GFSH method [45] considers the gross population flow between states. The SH probabilities are expressed as

$$g_{ij} = \frac{\Delta a_{jj}}{a_{ii}} \frac{\Delta a_{ii}}{\sum_k \Delta a_{kk}} \left(\text{if } \Delta a_{ii} < 0,\ \Delta a_{jj} > 0, \text{ and } \Delta a_{kk} < 0 \right), \tag{13.12}$$

No other types of state switches are allowed. Similar to FSSH, GFSH uses a flux of populations rather than their absolute values, and therefore, it also minimizes the number of hops. Analogous to FSSH, GFSH fulfills the internal consistency: the changes in the state populations according to the SH rules, Eqs. (13.7) and (13.12), agree with the changes produced by solving the Schrödinger equation. Numerical calculation shows that GFSH captures the superexchange mechanism and Auger-type population transfer. GFSH can replace FSSH despite that further tests are needed [45].

13.2.3.4 Stochastic Mean Field, Decoherence Induced Surface Hopping, and Coherence Penalty Functional Theories

The SMF method [49] bridges the gap between mixed quantum-classical and full quantum descriptions. With the presence of additional terms in the Schrödinger equation to represent the system–environment interaction, SMF accounts for the quantum features of the environment with the Lindblad approach [107]. In the simplest form, the quantum environment, such as a set of harmonic oscillators linearly coupled to the system, is described by Markovian diffusion terms in the Schrödinger equation [49]. The SMF method simultaneously resolves the two major drawbacks of NAMD: decoherence effects within the quantum subsystem due to interactions with the environment are rigorously included, and the physical mechanism for trajectory branching is provided by decoherence. Besides, hop rejection due to violation of energy conservation disappears in SMF.

The quantum mechanical wave packet of the whole system, including both electrons and nuclei, splits into uncorrelated branches and loses coherence over time. The resulting decoherence can be viewed as an environment-induced destruction of the superposition between quantum states in the microscopic system [108, 109]. Inspired from the above SMF [49], stochastic Schrödinger and master equation methods [110–112], the DISH method [50] was proposed. By combining the computational simplicity of quantum-classical NAMD with a formal treatment of quantum decoherence, DISH provides a straightforward and physically justified SH scheme, in which quantum transitions between surfaces only occur during decoherence events. The transition probabilities are computed according to the standard quantum mechanical rules. On one hand, DISH can be regarded as a SH approach to quantum dynamics in dissipative environments. On the other hand, DISH unifies decoherence and NA transitions, providing a nonphenomenological account of quantum transitions in condensed-phase systems. DISH largely extends the feasibility of quantum-classical simulations to quantum systems in macroscopic environments.

The CPF method [51] is another approach to incorporate decoherence into NAMD. The method originates from a simple idea to dynamically penalize development of coherences during evolution of quantum DOF. The methodology is formulated on the grounds of the Ehrenfest method for semiclassical dynamics. Decoherence effects are introduced via an additional term in the classically mapped Hamiltonian, thus hold the overall Hamiltonian structure of the EOM. The CPF is analogous to XC functionals in DFT. It provides an effective way for introducing dynamical correlation effects, such as decoherence, on top of the Ehrenfest approach. The CPF methodology has a certain relation to QHD, and the method can be enhanced by allowing some of the variables entering the penalty functional to depend on time. A simple form for penalty functional has been proposed, and good results have been demonstrated [51]. The dependence of the penalty functional on coherences can be rather arbitrary, in principle, and other functional forms may prove more accurate, more general, or both. It is straightforward to combine the CPF scheme with FSSH and related approaches discussed above, where SH probabilities can include decoherence effects through the modified time-dependent Schrödinger equation.

13.2.4 User-Friendly Implementation: The PYXAID Program

The PYXAID (PYthon eXtension for Ab Initio Dynamics) simulation package has been developed as an open-source, flexible, and computationally efficient implementation of the NAMD methodology in the framework of KS DFT for large-scale condensed-phase systems [90, 113]. It carries out a great deal of basic and more advanced functionalities, including standard FSSH, DISH to consider decoherence corrections, the use of multiexciton basis configurations of the TDKS equations, and the direct simulation of photoexcitation via explicit light-mater interaction. Advanced integration techniques with Trotter factorization [114] of the evolution operator for solving the TD Schrödinger equation significantly speed up and stabilize the calculations. In addition, the CPA approximation [90] achieves considerable computational savings, and makes it possible to study photoinduced dynamics at the ab initio level in systems composed of hundreds of atoms and involving thousands of electronic states. The software is interfaced with Quantum Espresso [115], which is used as an efficient driver for ab initio electronic structure and MD simulations. The key features of the PYXAID program have been demonstrated by studying the electron-nuclear dynamics in a variety of systems. PYXAID is organized as a Python extension module and can be easily combined with other Python-driven modules, enhancing user-friendliness and flexibility of the software. In addition to Quantum Espresso, PYXAID has been interfaced with VASP and semiempirical electronic structure codes. The source and additional information are available on the web at http://gdriv.es/pyxaid. The program is released under the GNU General Public License.

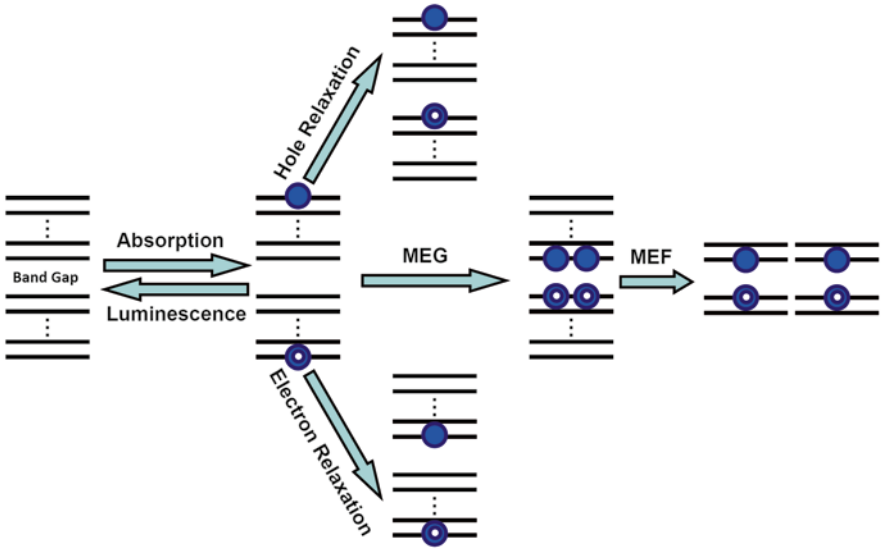

Fig. 13.3 Diagram showing pairs of electronic states involved in light absorption/luminescence, electron/hole relaxation, MEG, and MEF. The energy levels are shown as *black solid horizontal lines*. Electron and hole are represented by *solid* and *open blue circles*

13.3 Quantum Dots

Nanoscale clusters of bulk materials, known as QDs, exhibit unique electronic properties due to quantum confinement [116, 117]. Unlike either bulk or molecular materials, the optical spectra of QDs can be continuously modulated over the whole spectrum by changes in shape and size. The high absorption cross sections, decreased electron–phonon relaxation rates [118, 119], and multiple exciton generation (MEG) [120–122] make QDs excellent paradigms for modern nanotechnology, especially photovoltaic [117] and photocatalytic [4] applications.

As shown in Fig. 13.3, electronic excitations in QDs lead to complex dynamical processes. One photon normally excites one electron when the energy of incident photon matches or exceeds the band gap, producing one correlated electron–hole pair called exciton. Both electron and hole can exchange energy with phonons, and relax to the band edge. If the photon energy is not less than twice the energy of the band gap, the MEG phenomenon may occur, and more than one exciton can be created [123–125]. This effect is also known as impact ionization, which is the inverse of the Auger recombination. The multiple exciton states (MEs) are formed by coherent superpositions of single excitons (SEs). Elastic electron–phonon scattering induces dephasing, destroys this superposition, and breaks MEs into incoherent combinations of SEs, which, for instance, can emit independently. This process is named multiple exciton fission (MEF) [125]. In all of these dynamical processes, electronic structure, electron–hole and charge–phonon interactions carry both fundamental and practical importance.

Based on the state-of-the-art approaches described in the previous subsection for both the energy and time domains, we present below a comprehensive discussion of the dynamical processes in QDs, ranging from the initial light absorption to the final photon emission. The atomistic description of QDs complements phenomenological models, provides important details and creates new scientific paradigms. The ab initio approaches are particularly useful for studying geometric and electronic structure of QDs because they treat bulk, surface, ligands, and defects on equal footing and incorporate electronic correlation effects. NAMD simulations most closely mimic the complex coupled evolutions of charges, phonons, and spins as they occur in nature.

13.3.1 Symmetry Breaking in the Band Structure

The DOS for $Cd_{33}Se_{33}$ and $Pb_{68}Se_{68}$ QDs, obtained using DFT, are shown in Fig. 13.4 [26]. In the CdSe QD, there is an evident peak at the bottom of the conductive band (CB). This state, which is mainly contributed by the s electrons, is roughly spherically symmetric and is delocalized over the whole QD. Higher energy peaks can be attributed to *p*, *d*, etc. electronic orbitals, but state symmetries become harder to discern from electron densities [126, 127]. Relatively speaking, the valence band (VB) structure is less pronounced. Although DOS of VB still shows distinct peaks, they are separated only at the top of VB. In contrast, the band structures of PbSe QDs are significantly more symmetric. This behavior can be seen particularly well from peak heights of the DOS. Due to the asymmetric electron and hole band structures, CdSe QDs show a complex spectrum with more allowed transitions.

Both ab initio and atomistic pseudopotential calculations [128, 129] have demonstrated that atomic structure, surface effects, core/shell coupling, thermal fluctuations, spin-orbit and Coulomb interactions can further break degeneracies and create

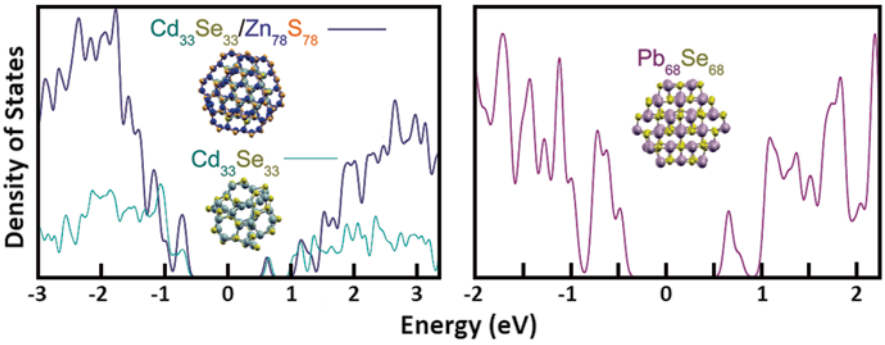

Fig. 13.4 DFT calculated DOS of core/shell $Cd_{33}Se_{33}/Zn_{78}S_{78}$ and core $Cd_{33}Se_{33}$ QDs (*left panel*) and $Pb_{68}Se_{68}$ QD (*right panel*). Adapted from Acc. Chem. Res. 42, 2005 (2009). Copyright 2009 American Chemical Society

complicated multilevel electronic structure near band edge. This observation is supported by experimental measurements with single PbS QDs [130], where fluorescence spectra show homogeneous broadening and complex structure. Photoluminescence blinking in single QDs also indicates that the photo-generated exciton is distributed over multiple on/off states. In Fig. 13.4, the DOS of core/shell $Cd_{33}Se_{33}/Zn_{78}S_{78}$ QD is also shown [26]. In comparison with bare CdSe QDs, surface passivation by ZnS shells dramatically changes the DOS. Because the VB edge of ZnS aligns with that of CdSe and ZnS has a much larger bandgap than CdSe, the DOS of CdSe and CdSe/ZnS QDs differ significantly only at higher energies. Low-energy CB states are localized entirely on the core, while low-energy VB states have notable contributions from both core and shell.

13.3.2 Ultrafast Relaxation at High Energies and Phonon Bottleneck at Low Energies

In Fig. 13.5, we use $Pb_{68}Se_{68}$ QD as an illustration to show the thermal fluctuations in the electronic DOS induced by nuclear vibrations. Although the strength of the fluctuations is minor, e.g., CB and VB edges change by less than 0.1 eV, phonon motions mix states of different symmetries and reduce gaps between states. NAMD is performed to simulate electron and hole relaxation due to coupling to phonons [126, 127, 131]. We can find that charge carriers spread first, visit multiple states during relaxation, and finally reappear near the band gap. Relaxation is nearly complete within a picosecond, in agreement with experiment [132, 133]. Due to small electronic energy gaps at high energies, transitions involve small amounts of energy that are close to phonon energies of 12–25 meV. Transitions involving larger amounts of energy using multiple phonon quanta also occur. Occasionally, up to 0.3–0.6 eV of electronic energy can be lost to phonons in a single event [126, 127, 131]. Such resonant electron–phonon energy exchange is efficient, particularly at higher energies.

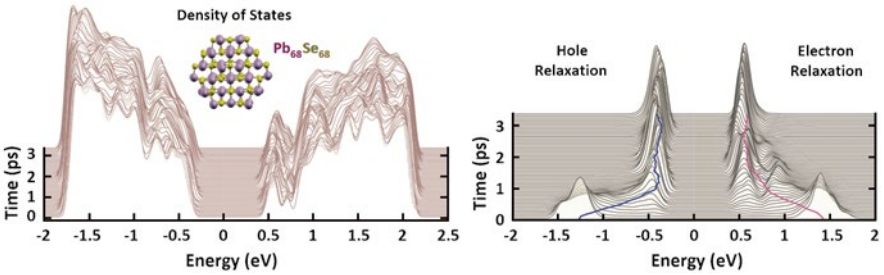

Fig. 13.5 Time-dependent DOS (*left panel*), electron and hole relaxation (*right panel*) in $Pb_{68}Se_{68}$ QD at room temperature. Adapted from Acc. Chem. Res. 42, 2005 (2009). Copyright 2009 American Chemical Society

For QDs like Cd33Se33, the DOS indicates that only s-electron state is separated from the rest (see Fig. 13.4). As a result, partial phonon bottleneck is associated with only final stages of electron relaxation [127], agreeing with observed slowing of charge relaxation as carriers approached band edge. Recent experiments detected nanosecond relaxation between p- and s-states of electrons injected into carefully designed multilayer CdSe QDs [119]. As this transition occurs slower than decoherence, NAMD must be augmented to properly include the decoherence. Theoretical analysis suggests that decoherence significantly decelerates the relaxation [134]. This expectation is closely related to quantum Zeno effect [135]. Note that the relaxation involving dense electronic state manifolds is not affected by coherence loss due to the large transition rate.

13.3.3 Optical Linewidths and Pure Dephasing

The optical linewidths of QDs have two major contributors, that is, inhomogeneous and homogeneous broadenings. The former is associated with distributions of optically active species, while the latter is an intrinsic property of optical transitions that is inversely proportional to the dephasing time, $\Gamma = 1/T_2$ [136]. To be more precise, we have the expression $\Gamma = 1/(2T_1) + 1/T_2^*$, where T_1 is the excited-state lifetime and T_2^* is the pure dephasing time [26]. In general, the first excited-state lifetimes in semiconducting QDs are very long, and thus both luminescence and lowest energy absorption linewidths are determined by pure dephasing.

Essentially speaking, pure dephasing is a result of the fluctuations of electronic levels due to coupling to phonons. The dephasing function describing the dephasing process between a pair of entangled states in a coherent superposition can be obtained directly by

$$D(t) = \exp(i\omega t)\left\langle \exp\left(-\frac{i}{\hbar}\int_0^t \Delta E(\tau)\, d\tau \right) \right\rangle, \tag{13.13}$$

where ω is the thermally averaged transition energy $<\Delta E>$ divided by $\hbar$. Note that the dephasing function can be also easily obtained using the second-order cumulant approximation [137]. The pure dephasing time is determined by the timescale of decay of the dephasing functions. Numerical calculations have found that phonon-induced pure dephasing between the ground and lowest energy excited states in light absorption/luminescence takes about 10 fs, and lowering temperature from 300 to 100 K can double the time [26]. The corresponding linewidths are calculated to be around 100 meV, in good agreement with experiment [130]. Note that Debye-type relaxation attributed to reorientation of surface ligands may produce additional dephasing and increase in optical linewidths [138]. Normally, electron–phonon coupling grows with decreasing system size, and thus dephasing is faster in smaller QDs [134].

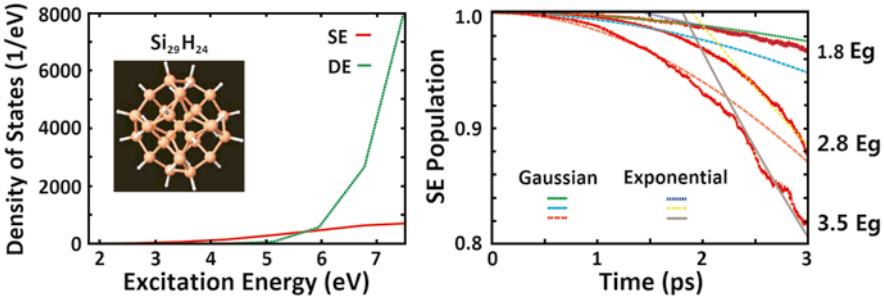

Fig. 13.6 DOS of SE and DE states (*left panel*) and decay of the total SE population starting from the initially excited SE with the displayed energy in the $Si_{29}H_{24}$ QD. Adapted from ACS Nano. 6, 1239 (2012). Copyright 2012 American Chemical Society

13.3.4 Multiple Exciton Generation

MEG of QDs has significant advantages in solar cells: it can potentially enhance the photoinduced current and increase the solar energy conversion efficiency [120–122, 126, 139]. The $Si_{29}H_{24}$ QD has been investigated to explore the mechanism of MEG [140]. The hydrogen passivation not only heals the dangling bonds on the bare Si QD surface, but also provides high-frequency vibrational modes due to the light hydrogen atoms. Figure 13.6 shows the DOS of SE and double exciton (DE) states. The bandgap, E_g, is calculated to be 2.1 eV, and thus the excitations with energies up to twice the bandgap, 4.2 eV, are all SEs. The DE DOS comes out at higher energies and increases significantly faster with energy compared to the SE DOS, due to the increasing combinatorial number of DEs with energy. If the photoexcitation energy can be exchanged freely between SE and ME states, most of the initial population will flow into DEs at high energy, and SEs appear only at low energies. However, actual transitions are also influenced by dynamics in SE states.

The right panel of Fig. 13.6 shows the decay of the total SE population, started from an initially excited SE state of different energies. As the SE population flows solely into DE states, this plot directly exhibits how the MEG appears in the Si29H24 QD. This strong energy dependence of MEG dynamics agrees well with the previous experimental observations and theoretical predictions [129, 139, 141, 142]. The NAMD simulation produces a transformation from an initial Gaussian decay to the later exponential decay, which is generic for all quantum dynamical process and appears only when sufficiently many quantum states are involved in the dynamics. Surprisingly, the MEG is observed even with the initial energy lower than the electronic threshold, 2 E_g, as seen in the 1.8 E_g case. The lack of the electronic energy, about 0.2 E_g, is compensated by the high-frequency Si-H surface vibrational modes, which are around 2,000/cm (0.25 eV) in the Si29H24 QD. It is expected that the surface ligands should become less important in larger QDs due to the decreased surface-to-volume ratio.

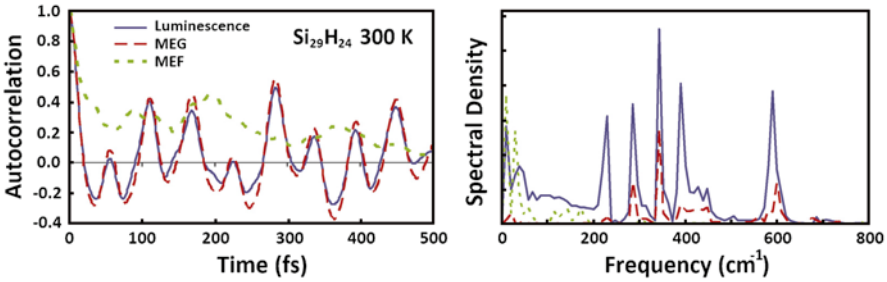

Fig. 13.7 Autocorrelation functions (*left panel*) describing phonon-induced pure dephasing involved in luminescence, MEG, and MEF processes for the $Si_{29}H_{24}$ QD at room temperature, and the corresponding Fourier transform (*right panel*). Adapted from ACS Nano. 3, 2487 (2009). Copyright 2009 American Chemical Society

13.3.5 Multiple Exciton Fission

For luminescence, MEG, and MEF dynamics, the pure dephasing time is related to fluctuations and uncertainties in the energy levels that arise from the coupling between electrons and phonons in the system. The fluctuations in the energy levels are best described in terms of correlation functions. The normalized autocorrelation function (ACF) for a transition of energy E is defined as $C(t) = <\Delta E(t)\Delta E(0)>/<\Delta E(0)\Delta E(0)>$, where $\Delta E = E - <E>$, and the angular brackets denote the statistical average over a canonical ensemble. The Fourier transform of the ACF is known as the influence spectrum or spectral density. It identifies which phonon mode frequencies are efficiently coupled to the electronic subsystem.

Based on the ACF shown in Fig. 13.7, the phonon-induced dephasing time for MEF is found to be an order of magnitude longer than the dephasing times for the luminescence and MEG [125]. This significantly slower MEF can be rationalized by the long-lived coherence between the two SE states that have similar energy and orbitals. Luminescence and MEG involve both acoustic and optical phonon modes up to high frequencies, while MEF only involves low-frequency acoustic modes. The dephasing between two coherent SE states of similar energy and orbitals during MEF involves only low-frequency phonon modes of the semiconductor core, with frequencies up to 200 cm^{-1}. The temperature dependence of the MEF dephasing related to low-frequency acoustic phonon modes is stronger than in the luminescence and MEG, whose electron–phonon couplings involve more modes, up to the high-frequency optical phonons [125]. The MEF exhibits four times faster decoherence at 300 K than at 80 K, where the dephasing is only twice faster for the luminescence and MEG at the higher temperature. The difference in the temperature dependence appears because the low-frequency phonons require small amounts of thermal energy and are more susceptible to temperature change.

13.4 Titanium Dioxide

TiO_2 is a semiconductor with a long history in photoelectrochemistry [143, 144]. It has a lot of striking features, e.g., high stability, efficient photoactivity, white color, reliable safety, and low cost. Among many candidates for photocatalysts, TiO_2 is no doubt the most widely used material at present and also probably in the future. For instance, TiO_2 has great potential to be used for hydrolysis, that is, break water into oxygen and hydrogen [145], which can be collected as a fuel for energy production. TiO_2 is also extensively used in dye-sensitized solar cells (DSSCs) [146] to convert sunlight to electricity. A modern DSSC device is typically composed of a porous layer of TiO_2 nanoparticles covered with organic dyes. Sunlight passes through a transparent electrode into the dye molecules where they are excited and rapidly inject electrons into TiO_2 network. TiO_2 thus serves double duty: it is used as a scaffold to hold a large number of dye molecules in a three dimensional matrix and also as a material for charge transport.

For a complete theoretical description of TiO_2-related photocatalytic and photovoltaic systems, one needs to reveal the role of oxygen vacancies and other relevant surface defects. This section is focused on the distribution of the electrons when they are first injected and the subsequent electron relaxation dynamics inside TiO_2 (see Fig. 13.8). The interfacial ET from dye molecules to TiO_2 will be systemically discussed in Sect. 13.6. Initially, the electrons are transferred from the chromophore to a localized surface state, and the injection typically occurs over a range of energies somewhere in the middle of the TiO_2 CB. Thus, the surface electron can simultaneously relax down in energy to the bottom of the CB or delocalize into the TiO_2 bulk.

13.4.1 Various TiO_2 Surfaces

TiO_2 nanoparticles exist as a mixture of rutile and anatase crystal forms with a variety of exposed surfaces [147–149] as shown in Fig. 13.9. Bare TiO_2 is highly chemically reactive and will interact with the substances that are present in solution and air. Under high vacuum, the surface will reconstruct in order to saturate the dangling bonds as much as possible. Variations in the structure can significantly influence the chemistry of surface reactions. Rutile (110) is one of the most stable and best studied surfaces. It has a well-described ideal structure, but several different kinds of defects can complicate the depiction. These include step edges, oxygen vacancies, line defects, and impurities. Rutile (100) has been less subjected to investigation, but it has several advantages when used in theoretical calculations. The (100) surface allows for a smaller cell, and the interaction of water with rutile (100) is straightforward [149], and a general form of the stable surface termination can be easily established. Compared with rutile (110) surface, it was found that both oxygen and other relevant point defects on anatase (101) are energetically more stable at bulk and subsurface sites than on the surface [28]. Besides, the energy barrier for the defects

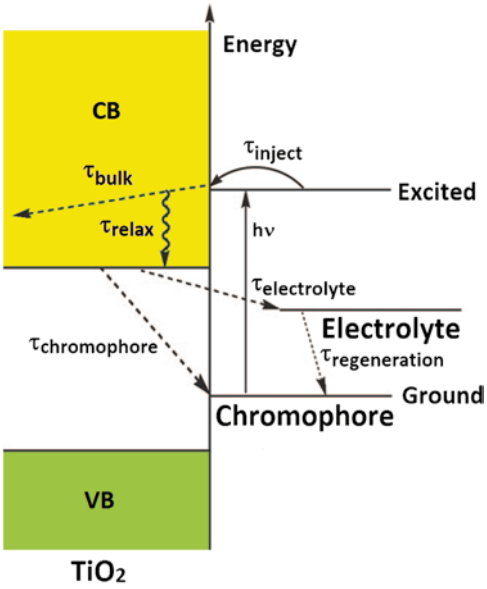

Fig. 13.8 Energy diagram of the electronic states participating in the electron dynamics at the chromophore–TiO_2 interface in DSSCs. The chromophore is excited from its ground state to an excited state. Following a rapid injection into the TiO_2 CB, the electron delocalizes to the bulk and relaxes down in energy to the CB edge. The delocalized electron can return to the TiO_2 surface, particularly in the presence of surface defects, which create trap states. A photoexcited electron at interface can be lost by recombination with the positive charge created on the chromophore by the photoexcitation, or by transfer to an electrolyte molecule. The electrolyte is present in the DSSC in order to regenerate the neutral chromophore by a separate ET event from the electrolyte to the chromophore ground state. Adapted from Acc. Chem. Res. 41, 339 (2008). Copyright 2008 American Chemical Society

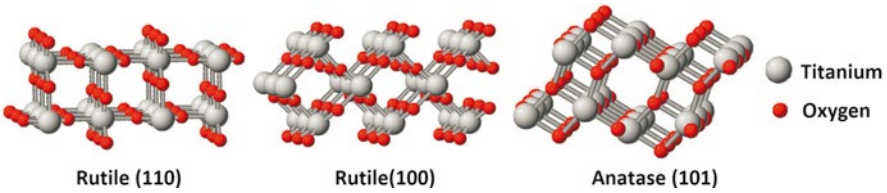

Fig. 13.9 Most commonly used TiO_2 semiconductor surfaces based on two existed crystalline forms: rutile and anatase. Adapted from Prog. Surf. Sci. 84, 30 (2009). Copyright 2009 Elsevier

to diffuse from surface to bulk is much lower than the opposite process from bulk to surface. Surface terminating oxygens interact with chromophores and water. Two types of oxygens are seen: (1) those that protrude from the surface have unsaturated bonds and are chemically reactive, and (2) the bridging oxygens located between surface titaniums have no dangling bonds and can interact with the adsorbed species

via hydrogen bonding. In any case, the presence of oxygen vacancies, dopants, and other point defects has a direct impact on the electronic structure of TiO_2 and, hence, on the photocatalytic properties of the resulting material.

13.4.2 Energy Distribution of the Injected Electrons

Thermal fluctuations in the atomic coordinates create an inhomogeneous ensemble of initial conditions for photoexcitation [150, 151]. Since the ET occurs faster than relaxation, the distribution of the injected electrons inside either chromophore or TiO_2 is determined by the photoexcited states. As a result, the injected electrons occupy multiple surface states with a distribution of localizations over a broad energy range, as exemplified with the alizarin-TiO_2 system in Fig. 13.10. Below the CB edge, the TiO_2 DOS is low, and there is very little mixing between the chromophore and TiO_2 states. The photoexcited state is therefore well localized on the chromophore (filled circles). As the energy increases progressively, more semiconductor states mix with the chromophore state. Under these circumstances, the localization decreases (empty circles), and a significant fraction of the photoexcited electron spreads onto TiO_2. In some instances, the photoexcited state is well localized on the chromophore. In other cases, over half of the photoexcited state density is on TiO_2. This depends on several factors even in a perfect system, including the energy match between the chromophore and surface states and the strength of the chromophore-TiO_2 coupling. The large variation in the localization strength within the CB band is somewhat unexpected and indicates that even in a perfect system, with no defects and well-defined bulk and surface structures, the ET process is very inhomogeneous and changes from sample to sample.

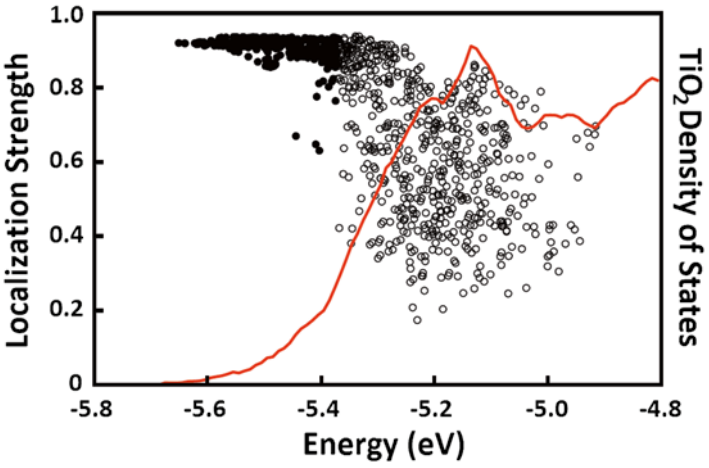

Fig. 13.10 Localization strength of the photoexcited states in the alizarin-TiO_2 system as a function of state energy (*filled* and *empty circles*) superimposed on the TiO_2 DOS (*solid red line*). Adapted from Prog. Surf. Sci. 84, 30 (2009). Copyright 2009 Elsevier

Chromophore-TiO_2 interface cannot be viewed as a single homogeneous object. At a finite temperature, nuclear coordinates fluctuate around the equilibrium geometry, and the number of TiO_2 states that can couple to the chromophore at a particular energy vary over time. In a given sample, the density of TiO_2 surface states at the chromophore state energy can be greater or less than the average. The spatial overlap between them and the chromophore excited state also varies substantially between the configurations. When the semiconductor produces an instantaneous nuclear fluctuation that makes the surface states energetically and spatially close to the molecular state, the chromophore excited state becomes strongly coupled and mixed with the states of the semiconductor. Using the alizarin-TiO_2 system as an example, the ab initio trajectories at 50 and 350 K have been obtained. It is found that the TiO_2 structure changes very little at the elevated temperature. However, the small fluctuations in the TiO_2 coordinates generate disorder in the crystal structure and lower the CB edge. The alizarin molecule and the hydrogens that terminate the interface move significant distances, making the distribution of the excited state energy significantly broader. As a result, the photoexcited electron is able to interact with a higher density of TiO_2 states, and a larger fraction of the state is delocalized on TiO_2. These both effects are favorable for the electron injection at higher temperatures.

13.4.3 Electron Delocalization and Relaxation

The photoexcited electron on the chromophore is difficult to relax in energy, because the ground molecular state is much lower in energy, while triplet states have different spin symmetry, and spin-orbit coupling is quite weak in purely organic chromophores [152–154]. The situation changes drastically once the electron is injected to TiO_2. The continuum of CB states facilitates rapid relaxation of the electron energy, which is released in the form of heat by exciting semiconductor vibrations.

The photoexcited electrons diffuse from the surface into the bulk, experiencing a sequence of NA electronic transitions [155]. Initially, the injected electron occupies a fairly localized surface state. The simulation shows that this state resides within the first few layers of the semiconductor [156, 157], and a single Ti atom can contribute up to 20 % of the state density [150, 158]. In detail, the chromophore distorts the TiO_2 surface geometry and carries a positive electrostatic charge after the photoinduced electron injection. Both effects can create well-defined localized surface defect states, which involves the chromophore itself. Infrared measurements [159, 160] show that the Fermi level of defective surfaces is quite close to the CB minimum. Occasionally, deep traps lie below the CB edge by much more than k_BT. In either case, and especially in the latter situation, the photoexcited electron trapped near the surface has a chance to interact with both the chromophore and the electrolyte, and to be annihilated by recombination with the positive charge without any further contribution.

The injected electron leaves the semiconductor surface and escapes into the bulk. The efficiency of electron delocalization into TiO_2 bulk is critical for many applica-

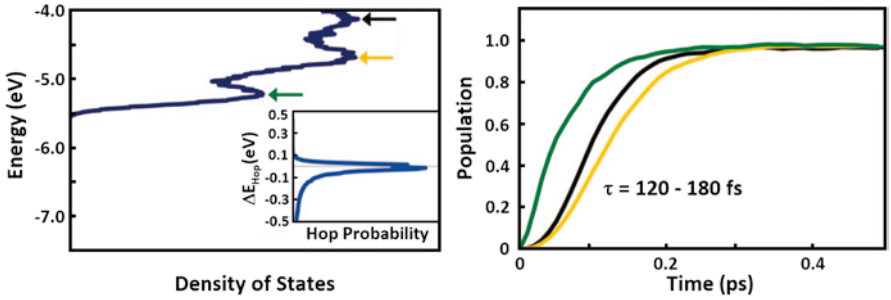

Fig. 13.11 (*Left panel*) CB DOS of the alizarin-TiO_2 system. The three *arrows* indicate injection energies corresponding to the DOS local maxima. The *inset* gives the probability distribution of the hop energy. (*Right panel*) time-dependent population of the indicated states characterizing the relaxation of the electron injected into the TiO_2 CB. Adapted from Acc. Chem. Res. 41, 339 (2008). Copyright 2008 American Chemical Society

tions. Simulations [157] indicate that the electron leaves the surface region and delocalizes into the semiconductor bulk on a 100 fs time scale, in agreement with the available experimental data [161]. The electron evolves inside TiO_2 both spatially and energetically by the NA mechanism, since it involves quantum transitions between different electronic states. Generally, the delocalization process is not uniform in space but rather exhibits preferential directions, which depend on the symmetry of the photoexcited state.

Simultaneously with the energy delocalization, the injected electron loses its energy to phonons and relaxes to the bottom of the CB. As shown in Fig. 13.11, the relaxation time scale is essentially independent of the injection energy, indicating that the transfers between energetically separated states make a strong contribution to the movement of the electron downward through the band. As much as half an electron volt of energy can be lost in a single hop (see inset in Fig. 13.11). Still, the majority of the hops induce only small energy changes, as emphasized by the exponential decay of the probability distribution. The probability of a gain in the electron energy is, however, significantly smaller than the possibility of an energy loss, especially for large energy hops. The relaxation creates a quasi-equilibrium distribution of state populations near the bottom of the CB.

13.5 QD–TiO_2 Hybrids

Inorganic materials, e.g., colloidal QDs and TiO_2, exhibit high charge carrier conductivity and excellent photostability. Photoinduced ET across their interfaces is essential for various photovoltaic and photocatalytic applications. Transfer of the photoexcited electron localized on the donor into the acceptor can proceed by either an adiabatic or a NA mechanism [60]. Adiabatic ET is induced by a vibrational motion driving the electronic subsystem over a transition state, and NA ET occurs by a

quantum transition between electron donor and acceptor states. Adiabatic ET relies on strong donor–acceptor coupling, while NA ET operates in the weak-coupling regime. The NA ET rate is enhanced by high density of acceptor states. The adiabatic and NA mechanisms are described by different mathematical expressions, e.g., an Arrhenius expression and Fermi's golden rule [54], respectively. The complex interplay of donor–acceptor and electron–phonon interactions creates a broad spectrum of electron injection scenarios. This section describes recent atomistic simulations on real time photoinduced ET at interfaces of bulk and nanoscale TiO_2 sensitized with semiconducting and metallic nanoparticles. We analyze in detail why hot electrons can be efficiently extracted from PbSe QDs into TiO_2, how modulation of QDs size and bridge length minimize electron–hole recombination on TiO_2 sensitized with PbSe QDs, and how TiO_2 dimensionality determines the mechanism of ET from CdSe QDs.

13.5.1 Extraction of Hot Electrons from a PbSe QD into a TiO_2 Slab

QD is an appealing alternative to organic dyes and has been extensively employed as chromophores for TiO_2 sensitization producing quantum dot-sensitized solar cells (QDSCs) [162]. Advantages of QDs include the tunability of optical properties with size, better heterojunction with the solid conductors, large intrinsic dipole moments, high extinction coefficients, and good photostability. Particularly, QDSCs have the unique potential to produce photon-to-electron quantum yields greater than one because of MEG. QDs provide great opportunities for increasing solar cell voltage by rapid extraction of hot charge carriers and enhancing current by using the additional energy available at the blue end of the solar spectrum [163]. In order to achieve high currents and voltages, the separation and transport of photogenerated carriers as well as interfacial ET across the contact to the semiconductor must be fast compared to the carrier cooling.

Among all processes, photoinduced ET is the key for QDSC performance because it determines the charge separation efficiency and quantum yields of free charge carriers. As a representative, the photogenerated ET from a PbSe QD into a rutile TiO_2 (110) surface has been investigated [60]. A good agreement between the theoretical simulations and the recent time-resolved experiments is obtained [19, 20]. The calculated result directly demonstrates that the ultrafast interfacial ET in the PbSe-TiO_2 system successfully competes with energy losses due to electron–phonon relaxation inside the PbSe QD. The ET proceeds primarily by the adiabatic mechanism because of the strong coupling between the two parts of the hybrid systems, while the NA transfer component is nearly an order of magnitude slower. Due to the large size and high rigidity of QDs, the electron donor density is spread over the whole QD, while the acceptor density is distributed nearly uniformly across the TiO_2 slab. The optical phonons available in the PbSe-TiO_2 system are of the same order of magnitude of thermal energies because QDs are composed of heavy elements. These vibrations, in particular polar Pb-Se and Ti-O stretches, promote

the ET, because they can rapidly shift the electronic density between the donor and acceptor species. Low frequency modes of TiO_2 and PbSe create an inhomogeneous distribution of initial conditions for ET.

13.5.2 Minimizing Electron–Hole Recombination on TiO_2 Sensitized with PbSe QDs

Despite the rapid interfacial charge separation, electron–hole recombination occurring at the interface limits the quantum yields of the light-induced processes in QDSCs. Minimizing charge recombination can highly enhance the photon-to-electron conversion efficiency and maintain high solar cells voltage.

We have investigated the charge recombination at the PbSe QD-TiO_2 interface by a unique ab initio NAMD combined with analytic theory [61]. The time-domain atomistic simulation directly mimics the laser experiment [20]. The studies generate important details of the recombination mechanism, indicating that the recombination is promoted largely by a high-frequency optical Raman-active mode of TiO_2, while lower frequency optical modes contribute to a lesser extent. The elastic electron–phonon scattering occurs within 40 fs, which is an order of magnitude shorter than the picosecond time scale of inelastic scattering. A good agreement for the electron–hole recombination time scale is achieved between simulation and experiment [20]. In contrast to the photoinduced charge separation process occurring from a QD state with a bit delocalization onto TiO_2 into a full TiO_2 state, the donor and acceptor states are strongly localized on the corresponding materials for charge recombination, which is significantly slower than the charge separation. Unexpectedly, the PbSe-TiO_2 bonding becomes stronger at an elevated temperature, because thermal fluctuations disrupt the optimized geometry and create additional bonding opportunities.

An analytic theory extends the simulation results to larger QDs and longer QD-TiO_2 bridges. It shows that the electron–hole recombination rate can be suppressed exponentially by increasing either the bridge length or the QD size. Changes in both donor–acceptor coupling and energy gap give rise to the exponential dependence, with the coupling providing a more significant contribution. By varying QD size and/or ligand length, one can reduce charge losses while still maintaining efficient charge separation, providing design principles for optimizing solar cells.

13.5.3 Dimensionality of TiO_2 Determines Photoinduced ET Mechanism from CdSe QDs

Recently, highly ordered one-dimensional (1D) nanostructures, e.g., nanotubes, nanowires, and nanorods, have received considerable attention as a solar material [164–166]. They provide significant improvement in the charge transport and photoconversion efficiency compared to zero-dimensional (0D) QDs. The photoinjection mechanism of electron across QD–TiO_2 interfaces may vary with the shape of the

semiconductor nanostructure. As shown in Sect. 13.3, the decrease in dimensionality from bulks to QDs results in a dramatic transformation of the electronic structure from energy bands to atomic-like discrete levels. Further reduction of acceptor TiO_2 dimensionality can alter the interaction between the QDs and TiO_2 and affect the ET mechanism. The dependence of ET efficiency on system properties is very different for the adiabatic and NA ET mechanisms. The adiabatic mechanism requires strong donor–acceptor coupling, and therefore, it is very sensitive to the binding mode, and presence and length of a bridge. In contrast, the NA mechanism operates in the weak donor–acceptor coupling regime, and requires a high density of acceptor states and available phonon modes to accommodate the electronic energy losses during NA transitions. As a result, the efficiency of NA ET relies on the photoexcitation energy and acceptor size.

In order to explore the impact of dimensionality of nanoscale TiO_2 on the photoinduced ET, a CdSe QD interfaced with quasi-0D TiO_2 QD and 1D TiO_2 nanobelt has been studied [62]. As shown in Fig. 13.12, the adiabatic mechanism dominates in the TiO_2-QD system due to the strong chemical binding between the two components of the system, arising from unsaturated chemical bonds on the QD surface. The density of acceptor states in TiO_2 QD is low, inhibiting the NA mechanism. In contrast, the NA mechanism operates in the TiO_2 nanobelt system, because the donor–acceptor coupling is weak, the acceptor state density is high, and multiple phonons can accommodate changes in the electronic energy. The CdSe adsorbent

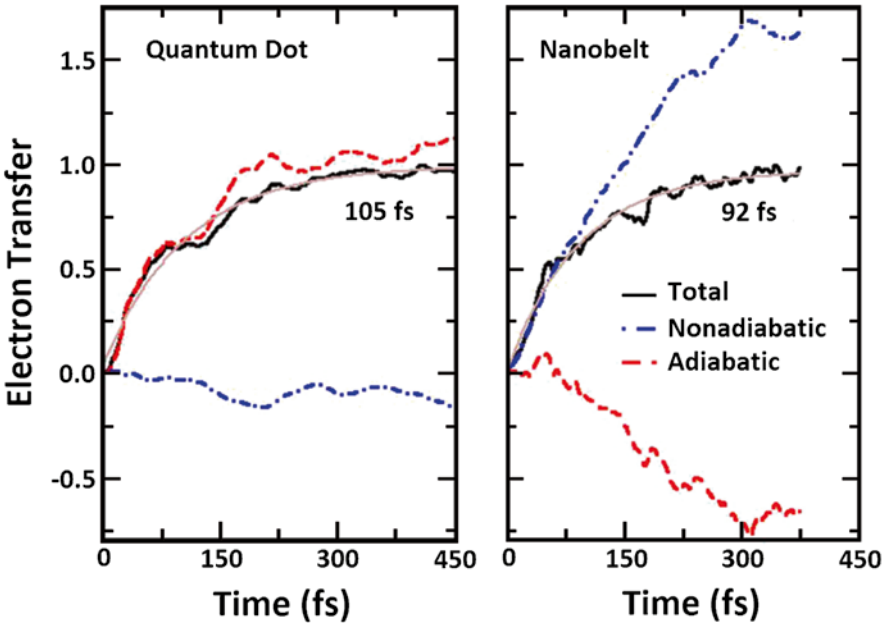

Fig. 13.12 Photoinduced ET dynamics from a CdSe QD into either a TiO_2 QD (*left*) or a TiO_2 nanobelt (*right*). The *solid black*, *dash-dotted blue*, and *dashed red lines* represent the total, nonadiabatic, and adiabatic ET, respectively. The *brown lines* show the exponential fits of the total ET data. Adapted from Nano Lett. 14, 1790 (2014). Copyright 2014 American Chemical Society

breaks the symmetry of delocalized band-type states of the TiO_2 nanobelt, creating localized acceptor states. It also relaxes donor–acceptor and NA coupling selection rules, and creates more ET channels. Although both mechanisms generate efficient and ultrafast injection, the fundamental principles leading to efficient charge separation depend strongly on the nanoscale materials themselves.

13.6 Organic–TiO_2 and Organic–QD Interfaces

Organic/inorganic nanocomposites are not simple mixtures of two types of materials. They possess advantageous properties over each of them and have a broad of applications in photovoltaic, photocatalytic, and transport devices. Metallic graphene exhibits ultrahigh charge mobility and extremely excellent mechanical property [167, 168]. Efficient photoinduced charge separation needs to compete successfully with energy losses due to rapid geminate electron–hole annihilation in graphene. In contrast, bulk semiconductors, QDs, molecules, and polymers possess band gaps, thus charge recombination can be restrained. In this section, we describe recent work focusing on graphene–TiO_2, QD–molecule, and QD–polymer interfaces. We show that both electron and energy transfer from graphene to the TiO_2 surface are consistently faster than energy relaxation. We find that defects are essential rather than detrimental for fast ET from QDs to molecules. We rationalize a counter-intuitive result that along insulating bridge can enhance photoinduced charge separation. We introduce a new type of ET mechanism—Auger-assisted ET—which eliminates the ET rate reduction in the Marcus inverted regime. Since Auger-type processes are generic to nanoscale materials, Auger-assisted ET should be very common in these systems. Finally, we reveal that inverted dimensionality gives rise to a symmetric electron and hole transfer dynamics in QD-polymer hybrid systems.

13.6.1 Efficient Photoinduced Charge Separation Across the Graphene–TiO_2 Interface

Recently, a number of experimental efforts are focusing on synthesis of hybrid graphene-TiO2 nanocomposites for photovoltaic and photocatalytic applications [169, 170]. The advantages of graphene include high surface area for interfacial contact, excellent charge conductivity, and outstanding mechanical properties. Graphene can harvest a larger fraction of the solar spectrum than many other nanostructured materials. It has been found that photovoltaic cells using graphene hybridized with TiO_2 achieve efficient photocurrent conversion [171]. However, graphene is a metal, and thus the photogenerated electrons and holes may rapidly relax through the continuous manifold of states and annihilate, providing strong motivation to explore the electron and energy transfer as well as energy relaxation dynamics in this system.

A representative hybrid graphene-TiO_2 system has been constructed [63]. At ambient temperatures, the interfacial oxygen atoms disrupt the π-electron system

of graphene. This makes graphene locally semiconducting, and strengthens graphene–TiO_2 bonding. The electron and energy transfer in graphene–TiO_2 composites can proceed in both directions, depending on the energy of the excited electron. Once the electron relaxes to the bottom of the TiO_2 CB, it can move back onto graphene because graphene has energy levels within the TiO_2 band gap. The back-transfer process competes with electron delocalization into bulk TiO_2 that is driven by entropy, related to the TiO_2 DOS.

NAMD simulations have been adapted to obtain the photoinduced electron and energy transfer as well as electron–phonon energy relaxation time scales. The ultrafast electron injection takes place due to the strong donor–acceptor coupling, favoring photoexcitation of states that are delocalized significantly between the two subsystems. Injection is promoted by both out-of-plane graphene motions and high-frequency bond stretching and bending vibrations. The former modulates the graphene–TiO_2 distance and interaction, while the latter creates large NA coupling. NA mechanism dominates over adiabatic mechanism primarily because of the high density of donor and acceptor states and the weak donor–acceptor coupling due to the absence of covalent bonding between graphene and TiO_2 [60]. The subsequent evolution occurs by rapid NA transitions down the manifold of delocalized states, resulting in simultaneous ET, energy transfer and electron-vibrational energy relaxation. The simulation shows that both ET and energy transfer from graphene to the TiO_2 surface are consistently faster than the relaxation, regardless of the excitation energy. This finding rationalizes the experimental observation that graphene–TiO_2 solar cells display high direct light-to-current conversion efficiencies [171]. Consequently, graphene–TiO_2 composites can form the basis for photovoltaic and photocatalytic devices.

13.6.2 Defects Are Needed for Fast Photoinduced ET from a QD to a Molecule

Surfaces of most optically active QDs are metal rich because metal atoms can reconstruct nanocrystal surfaces to eliminate unsaturated chemical bonds and other defects [172]. As a result, QD surfaces miss the complementary elements, for instance, S atoms in CdS QDs, creating defect states below the edge of CB [173]. In many applications, defects are detrimental, e.g., QD blinking happens due to charge trapping and rapid electron–phonon energy losses arising from decreased electronic energy gaps and increased electron–phonon coupling. Surface defects, however, have a positive effect on the photoinduced charge separation at QD–molecule interface, thereby holding the promise for improving solar energy conversion efficiencies [64].

Experiment reported an interesting result in a hybrid system formed by PbS QD and the rhodamine B (RhB) molecule that charge separation is faster than charge recombination despite the donor–acceptor energy gap in the former process is about twice larger than the latter. To clarify this divarication, we have systemically investigated the ET from a PbS QD to the RhB molecule and subsequent electron return from RhB to the QD, referring to charge separation and recombination pro-

cesses, respectively [64]. Both charge separation and recombination are NA processes, driven by atomic motions. The NA electron–phonon coupling is created primarily by the molecular motions, because it is composed of lighter atoms and is more labile than the QD. In contrast, the donor–acceptor coupling arises because the wavefunction of QD is more delocalized and leaks onto the adsorbed molecular species, generating the required overlap between the donor and the acceptor wavefunctions. Although the donor–acceptor energy gap is smaller for the recombination, the NAMD simulation supports the experimental observation [174] that charge recombination is slower than separation, rationalizing this fact by a twice-weaker averaged NA coupling absolute value for the backward than the forward ET reaction. The computed electron–hole recombination time scale obtained for the system without defects agreed very well with experiment [174]. The charge separation time scale, however, is significantly overestimated. Repeating the simulation by including a sulfur vacancy has improved agreement between theory and experiment. Missing sulfur creates unsaturated chemical bonds on Pb atoms, which gives rise to defect states below the CB edge of the PbS. As a result, the QD lowest unoccupied molecular orbital (LUMO) is lowered in energy, decreasing the donor–acceptor energy gap. Mostly importantly, the unsaturated bonds extend the LUMO density onto the adsorbed molecule, increasing the donor–acceptor coupling. The combination of a decreased energy gap and an increased NA coupling accelerates the charge separation (see Fig. 13.13). The counterintuitive conclusion that defects are helpful rather than harmful to charge separation brings a novel perspective on QD synthesis for photovoltaic and photocatalytic applications.

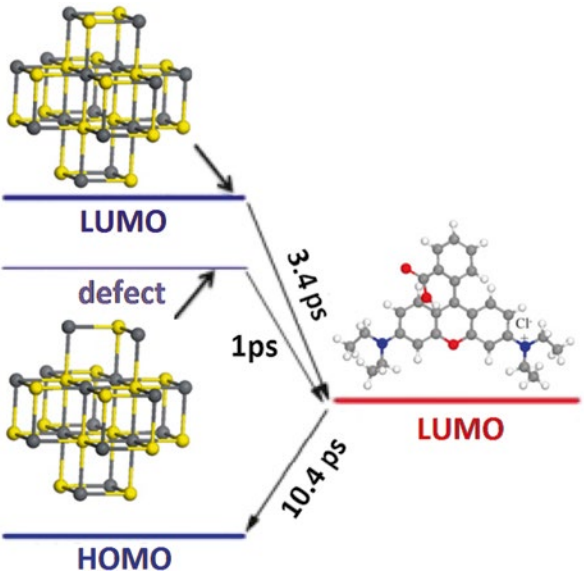

Fig. 13.13 Energy levels and time scales involved in the charge separation and recombination processes in the PbS QD-RhB system. The geometries of the QD and RhB are shown next to their corresponding levels. Adapted from J. Am. Chem. Soc. 135, 18892 (2013). Copyright 2013 American Chemical Society

13.6.3 An Insulating Bridge Greatly Enhances Photoinduced ET in QD-Fullerene Nanocomposites

Fullerene-QD solar cells have attracted great attention because QDs possess unique electronic properties and fullerene serves as an excellent electron-accepting material. To effectively harvest solar energy, a key strategy is to construct the heterojunction with a type II band alignment, which facilitates charge separation at the interface. Generally, the electron donor and acceptor parts are chemically linked to enhance the interaction between them and stabilize the architecture. As shown in the experiment [175], C_{60} can be functionalized with a thiol compound and covalently linked to the CdSe QD. The photoinduced ET from the QD to C_{60} has been investigated using time-resolved transient absorption spectroscopy. Interestingly, the covalent linking provided a significant improvement in the charge separation and photoconversion efficiency compared with the previous work utilizing a mechanical blend.

In order to rationalize the experimental findings, we have investigated the photoinduced ET from a CdSe QD into a C_{60} with and without covalent binding in between [65], using the state-of-the-art approach combing TDDFT with NAMD. We have shown that a covalent bridge connecting the QD to C_{60} significantly accelerates the ET from the QD photon-harvester to the C_{60} electron acceptor. In contrast, the ET dynamics is decelerated in the mechanical mixtures of QD and C_{60} because van der Waals interaction provides a notably weaker donor–acceptor coupling than a molecular bridge despite of its length and insulation. We have also demonstrated that the ET rate in a nonbonded mixture can be enhanced by C_{60} doping with Li. The calculated ET times are in good agreement with experiment [175]. The following three factors are responsible for the enhanced ET rate in the QD-C_{60} system involving chemical bonds. (1) The NA coupling is enhanced by the bridge because of its high-frequency vibrational modes. The electron–photon coupling is vital to the ET, because significant amounts of the electronic energy have to be deposited into vibrational modes. At the same time, the bridge improves the donor–acceptor interaction. (2) The QD wavefunction is allowed to extend onto the bridge. Consequently, the QD size is effectively increased, the QD band gap is lowered, and then the donor–acceptor energy gap is reduced. (3) The bridge provides long-range correlations between the atomic motions of the donor and acceptor species. As a result, the phonon-induced pure-dephasing rate is decreased and quantum coherence during the NA transition is protracted. This study generates valuable insights into design principle for enhancing photoinduced charge separation in nanoscale light harvesting materials.

13.6.4 Auger-Assisted ET from Photoexcited QDs to Molecular Acceptors

In chemistry, ET processes are traditionally described in terms of the Marcus theory, which has gained considerable success [176]. Because of strong electron–phonon interaction in molecules, intermolecular ET is accompanied by large rearrangement of nuclear configuration. The dependence of the ET rate on the driving force, ranging

from the normal, barrier-less, to inverted regimes, can be described by the Marcus theory. In bulk inorganic semiconductors, ET requires negligible change in nuclear geometry because of weak electron–nuclear interaction [177], and charge carriers are regarded as quasi-free particles. Both electron–hole and electron–phonon interactions in nanoscale materials fall between those in molecules and bulk. The most appropriate model and method for describing photoinduced ET on the nanoscale interfaces containing two different materials remain unclear and are under rapid development.

Because of quantum confinement, semiconductor QDs exhibit atomic-like discrete electronic levels and corresponding excitonic transitions that can be broadly modulated by QD size [178], providing an ideal platform for testing theoretical models for describing ET. Bearing this in mind, the photoinduced ET from CdS, CdSe, and CdTe QDs to three molecular acceptors, anthraquinone (AQ), methyl viologen (MV^{2+}), and methylene blue (MB^{+}) has been experimentally studied combing with a model analysis in detail [66]. The reported ET rates increase with decreasing QD size, regardless of QD compositions and acceptor redox potentials, showing a lack of the Marcus inverted regime over a broad range of driving force from 0 to 1.3 eV. The unexpected driving force dependence can be explained by the recently proposed Auger-assisted ET model [66], in which the transfer of the electron is coupled to excitation of the hole, circumventing the unfavorable Franck-Condon overlap in the Marcus inverted regime. This model is supported by time-domain NAMD computational studies on a realistic CdSe QD-MB^{+} complex.

The study illustrates that the photoinduced ET from QDs is fundamentally different from those in molecular chromophores and bulk semiconductors. Based on the time-resolved energies of various parts of the system along a representative trajectory, we proposed the Auger-assisted ET mechanism, which accounts for experimental observations. During ET, the energy lost by the electron during the transfer is gained at the initial stage exclusively by the hole rather than by phonons. Because Auger-type processes are common in most nanomaterials exhibiting quantum confinement, the Auger-assisted ET model proposed for CdX (X = S, Se, Te) QDs can be generally applied to exciton dissociation in other nanomaterials, including nanotubes, nanowires, quantum wells, graphene, and so on.

13.6.5 Inverted Dimensionality Restores Electron–Hole Symmetry in a QD-Polymer Hybrid

Compared to small molecules, polymers can tune their electronic properties by changing their morphology. Other advantages include solution processability and straightforward chemical synthesis. Combing inorganic QDs and polymers shows great promise for fabrication of hybrid heterojunction photovoltaic cells for

low-cost and scalable solar power conversion. However, Coulomb interactions between charge carriers are strong due to low dielectric constants, giving rise to strongly bound electron–hole pairs [179]. This drawback significantly reduces the power conversion efficiency of polymer-based solar cells.

Compared to fullerenes, used as electron acceptors in traditional organic solar cells, colloidal QDs exhibit better environmental stability and higher electron mobilities. In addition, QDs improve light harvesting due to large absorption cross sections, easily tunable over the entire solar spectrum. Hot-carrier generation and carrier multiplication provide opportunities to improve conversion efficiencies of QDSCs by reducing the loss of high-energy carriers. Using the advantageous of both organic polymer and inorganic QD materials opens new ways of enhancing solar cell performance. There, charge separation, nongeminate recombination across the interface, and geminate recombination inside the same material compete with each other and significantly affect the final conversion efficiencies.

We chose a heterojunction formed by a poly(3-hexylthiophene) (P3HT) and a CdS QD, and investigated the photoinduced electron and hole dynamics, as well as nongeminate and geminate recombination using the approach combining NAMD with TDDFT. In conventional view, QDs are viewed as quasi-0D materials with discrete energy levels, while polymers are 1D possessing continuous bands. However, the DFT calculations give a different picture. Generally, QDs exhibit discrete levels only close to the band gap. Indeed, Fig. 13.14 shows that CdS QD LUMO is separated from LUMO + 1 by about 0.5 eV. At higher energies relevant for the charge separation dynamics, the QD spectrum is continuous. The polymer indeed exhibits band-like electronic structure. At the same time, the DOS of the polymer is much lower than that of the QD. In the local interaction QD-P3HT region involved in the photoinduced charge separation, and at the relevant energy range, P3HT behaves as a molecule, while QD is nearly bulk-like. The inversion of the dimensionally, relative to the common expectation, helps to balance the electron and hole injection rates. Such balance is essential for a solar device, since otherwise one of the charges will present a bottleneck to the photoinduced dynamics. The driving force for the hole transfer from QD to P3HT is larger, but the density of P3HT acceptor states is small (Fig. 13.14). In comparison, the driving force for the ET from P3HT to QD is small, but the density of QD acceptor states is large. The leveling of the two factors produce electron and hole injection times on a time scale of several hundred femtoseconds, in agreement with experiment [180]. The phonon-induced nongeminate recombination across the QD/polymer interface is slower than the geminate recombination across the band gap of each species, in particular on the QDs, indicating that hole transfer following by excitation of QD could lead to high solar cells performance, as reported by experiment [180]. Our simulations suggest novel design principles such as selective photoexcitation materials for developing photovoltaic and photocatalytic devices.

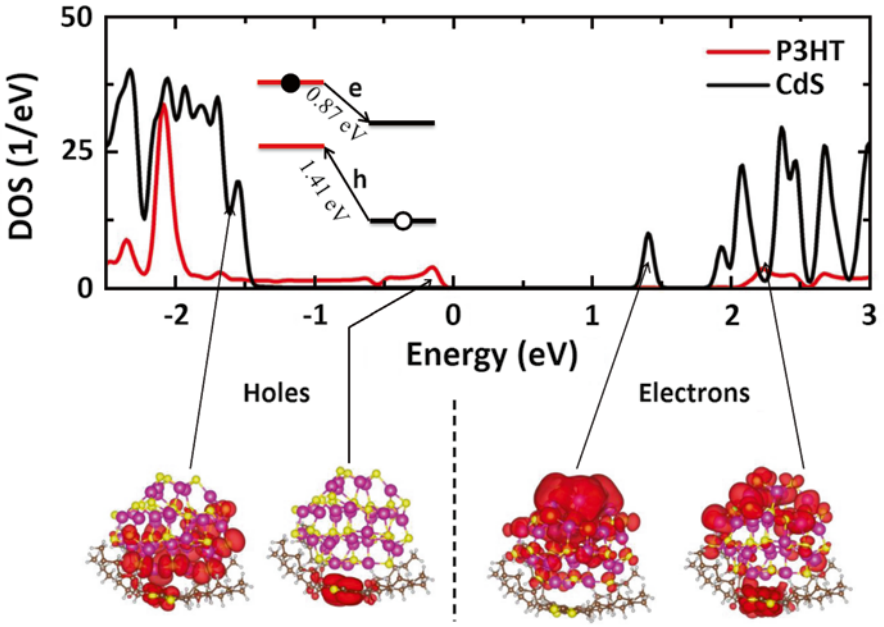

Fig. 13.14 Projected DOS of the P3HT-CdSe QD system and charge densities of the corresponding donor and acceptor orbitals for the electron and hole transfer, where the energy offsets between the donor and acceptor orbitals are shown in the *inset*. The electron donor state is delocalized significantly between P3HT and QD. Similarity, the hole donor state is also shared by QD and P3HT. The acceptor states are localized in both cases. The *vertical arrows* relate the donor and acceptor orbital densities to the energies

13.7 Organic Nanosystems

Organic systems, including small molecules and polymers, exhibit both advantages and disadvantages compared to inorganic compounds. They are extremely diverse, mechanically flexible, and light-weight, providing an essentially unlimited availability of raw materials for mass production at low cost. However, they contain strong bounded electron–hole pairs inside, which challenge photoinduced charge separation. The opposite process—radiative recombination of injected charges—occurs more readily, giving rise to light-emitting diodes. At the same time, electron–phonon interaction is strong in organic materials, generating polarons with large effective masses and low mobilities. Due to these demerits, knowledge of charge and exciton dynamics at organic interfaces are essential for solar energy and electronics applications. In this section, we present a comprehensive kinetics at a pentacene–C_{60} interface, exhibiting a fundamentally interesting and practically important phenomenon known as singlet fission (SF). SF allows one to convert one photon into two electron–hole pairs, thereby greatly increasing photon-to-electron yields. We also explore the origin of significant asymmetric dynamics in electron and hole transfer at a

polymer–carbon nanotube (CNT) interface, and propose how this asymmetry can be utilized to tune photovoltaic performance.

13.7.1 Singlet Fission and Charge Transfer at the Pentacene–C_{60} Interface

SF characterizes the phenomenon in organic systems that a single absorbed photon generates two electron–hole pairs [181–183]. On one hand, SF is interesting from the fundamental point of view, because simple selection rules forbid excitation of two electrons by one photon. On the other hand, SF is important because it provides the possibility that a low-cost photovoltaic cell could achieve a high power conversion efficiency, which is determined by complex dynamics involving key electronic states coupled to particular nuclear motions. Extensive experimental and theoretical studies are dedicated to this topic, generating multiple opinions on the nature of such states and motions, their properties, and mechanisms of the competing processes, including electron–phonon relaxation, SF, and charge separation [181, 182]. Time-domain NAMD simulations can identify the most important steps involved in SF and subsequent charge separation, and build a comprehensive kinetic scheme that agrees with the available experimental and theoretical results. The model reveals the importance of intermediate charge transfer states and the nature of energy level alignment, SF mechanism, and time scales of quantum dynamics.

A minimalistic atomistic model has been constructed to describe SF at the pentacene/C_{60} interface [68]. The simulation has demonstrated that SF competes with the traditional photoinduced ET between pentacene and C_{60} layers. Efficient SF relies on the presence of intermediate dark states. These configurations can be viewed as either independent states, or components of the multiexciton (ME) and triplet pair (TT) states arising due to electron correlation. Several pentacene–pentacene and pentacene–fullerene charge transfer (CT) states should be taken into account, including the lowest energy CT state (CT_0) and excited CT states (CT_1 and CT_2). Having ME and CT character, these states play critical roles in the dynamics and should be considered explicitly when explaining the entire process from the photoexcitation to the final charge separation.

The relative energies of the states involved in the photoinduced dynamics should be carefully aligned with respect to each other. Assigning the energy of the CT_0 state around 0.5 eV according to the experiment [184], produces a consistent quantum dynamical scheme. Energy alignment provides an interesting way to control the SF efficiency. If CT_2 is designed to have the energy larger than that of TT, triplet production can be maximized. After dissociation of TT, each triplet can access states of the CT_0 type, provided that their energy is lower than the energy of TT. Then, the generation of two electron–hole pairs will be maximized. The S_1 (the lowest singlet state) and ME states involved in the SF process are coupled weakly. Direct NA transitions between these states are suppressed, although not forbidden. Because S_1 and TT are also weakly coupled, the triplet production originates only from the ME state, which is populated during photoexcitation (see Fig. 13.15). Generally, photo-

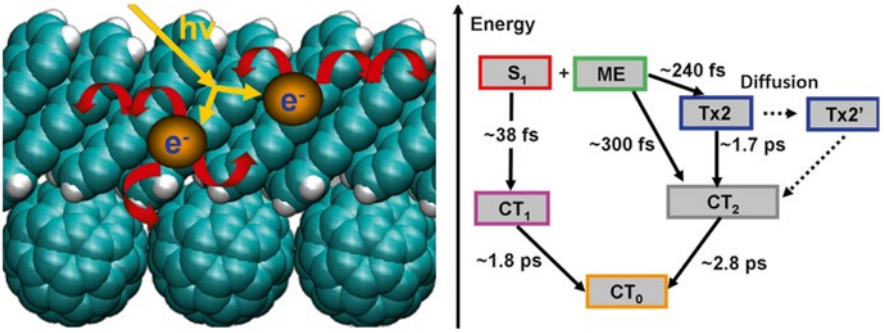

Fig. 13.15 (*Left panel*) Simulated pentacene–C_{60} interface, and (*right panel*) comprehensive kinetic scheme of the singlet fission and charge transfer processes at the interface. Adapted from J. Am. Chem. Soc. 136, 1599 (2014). Copyright 2014 American Chemical Society

excitation creates a superposition of the S_1 and ME configurations. To maximize the SF yield, one should design systems and utilize photoexcitation conditions, under which the contribution of the ME configurations is maximized. One can also consider designing electromagnetic fields to directionally pump S_1 into ME or TT. The reported analysis enhances the understanding of the complex quantum dynamics in nanoscale materials capable of the SF and charge transfer processes.

13.7.2 Asymmetric Electron and Hole Transfer at a P3HT-CNT Heterojunction

Bulk-heterojunction organic photovoltaics have been demonstrated as low-cost alternatives to silicon-based solar cells, offering a long-term solution for clean and renewable energy [185]. To achieve high photon-to-charge conversion efficiency, the electron–hole pair generated by photon absorption in organic photovoltaic systems must overcome the Coulomb attraction, which often results in voltage loss. Efficient charge separation at the all organic interfaces requires a type II band alignment with large driving forces for both electrons and holes in order to break the strongly bound electron–hole pairs into free charge carriers. Often, the electron and hole transfer has diversity and is determined by driving force, donor–acceptor coupling, NA coupling, and the involved phonon modes.

As a representative, the photoinduced electron and hole transfer dynamics as well as energy relaxation across a P3HT–CNT interface have been investigated, using the unique methodologies combining TDDFT and NAMD [69]. The simulations establish that the electron and hole dynamics are highly asymmetric. Particularly, photoexcitation of the polymer results in a 100 fs ET, in agreement with experiment [186], followed by a loss of 0.6 eV of energy within 0.5 ps. Photoexcitation of the CNT leads to hole transfer, which requires nearly 2 ps, but loses only 0.3 eV of energy. The strong disparity arises due to the differences in the

localization of the photoexcited donor states, the densities of the acceptor states, the strength of donor–acceptor interaction, and the phonon modes involved. The transfer of both electrons and holes is promoted primarily by the high-frequency C–C stretching modes of both materials, while the electron relaxation additionally involves low-frequency radial breathing modes of CNT and P3HT torsional motions. Used as a chromophore, P3HT induces fast charge separation but results in large energy losses, and cannot harvest light in the red region of the solar spectrum. In contrast, CNT can absorb a broader range of photons and reduce energy losses but gives less efficient charge separation.

The complementary properties of P3HT and CNT can be utilized to improve the performance of solar cells by optimizing simultaneously light harvesting, charge separation, and energy relaxation, which affect photovoltaic yields, current, and voltage. By increasing the CNT concentration, one can harvest a broader range of solar spectrum and reduce energy and voltage losses. By increasing the P3HT concentration, one achieves better charge separation and higher currents. The simulations provide a comprehensive description of the charge transfer and energy relaxation dynamics in the hybrid nanoscale materials, and produce novel design principles for photovoltaic and photocatalytic devices with photoexcitation of selective component in a type-II heterojunction.

13.8 Conclusions and Outlook

The amount of solar energy reaching the Earth's surface is about 7,000 times more than the current human energy consumption. It carries an enormous potential to resolve the current energy and environmental pollution problems. Development of efficient tools for conversion of sunlight to electrical and chemical energy is critical for promoting the renewable energy economy. A diversity of materials have been designed, synthesized, and applied in photovoltaic and photocatalytic devices, and some of them show great promise for commercialization. Due to substantial difference in the origin and nature of the investigated inorganics and organics, ab initio atomistic simulations hold great advantages of exploring the charge and exciton dynamics in photovoltaic and photocatalytic devices.

In combination with TDDFT, NAMD has been applied to a broad spectrum of systems to study various nonequilibrium processes, and it has obtained a series of success. This chapter has summarized recent efforts in both methodological developments and realistic applications. The time scales for various processes, such as electron and energy transfer, thermal relaxation, and charge recombination, have been obtained in many systems consisting of two complementary inorganic and/or organic materials and have been compared extensively with available experiments. The competition among the various dynamical processes governs the global efficiency of photovoltaic and photocatalytic devices and determines efficiency bottlenecks. A comprehensive understanding of the mechanisms underlying each dynamical channel generates critical insights and useful guidelines for improving solar cells performance. The obtained knowledge can be used in electronic, spintronic, and other types of transport devices, where the above-addressed issues are widely encountered.

An atomistic simulation of nonequilibrium processes in molecular, nanoscale, and condensed-phase systems relies on an accurate description of the electronic structure and a reliable representation of the electron–phonon dynamics. These require development of more robust and efficient XC DFT functionals for proper description of long-range interaction, bond breaking, multiply excited states, and other situations that take the system far from the ground state equilibrium. At the same time, the computational cost for electronic structure in large-scale systems has to be reduced. The density-functional tight-binding (DFTB) method [187], which parameterizes the key DFT quantities, such as pseudo-atomic orbitals, matrix elements, and short-range repulsions, affords promising solution and has received significant attention. DFTB can reduce significantly the computational complexity, while maintaining reasonable accuracy [188]. Implementing time-dependent DFTB can greatly extend the NAMD applications from inorganic and/or organic composites to large-scale biological systems. To date, most NAMD applications still neglect decoherence [46–48] and other quantum nuclear effects, which play important roles in many dynamical processes and deserve serious considerations. With rare exceptions, semiclassical NAMD algorithms are capable of capturing these effects but only apply to model or small systems. Further simplifying approximations and implementations of such schemes are definitely needed. NAMD simulations can explore longer dynamics in the time domain, and thus hold great power to handle a wide range of issues arising in systems perturbed far from equilibrium, satisfying the impending demand of mechanism exploration and material design for more efficient nanotechnological devices.

Acknowledgments The authors are indebted to many experimentalist and theoretician colleagues for fruitful and illuminating discussions. Many thanks go to the past and current group members, including Alexey Akimov, Amanda Neukirch, Vitaly Chaban, Heather Jaeger, and Hyeon-Deuk Kim. R. L. is grateful to the SIRG Program 11/SIRG/E2172 of the Science Foundation Ireland. The research was supported by the U.S. National Science Foundation, Grant No. CHE-1300118 and the U. S. Department of Energy, Grant No. DE-SC0006527.

References

1. Akimov AV, Neukirch AJ, Prezhdo OV (2013) Chem Rev 113:4496
2. Hagfeldt A, Grätzel M (2000) Acc Chem Res 33:269
3. Anderson NA, Lian T (2005) Annu Rev Phys Chem 56:491
4. Zhao W, Ma W, Chen C, Zhao J, Shuai Z (2004) J Am Chem Soc 126:4782
5. Anfuso CL, Snoeberger RC, Ricks AM, Liu W, Xiao D, Batista VS, Lian T (2011) J Am Chem Soc 133:6922
6. Tang J, Durrant JR, Klug DR (2008) J Am Chem Soc 130:13885
7. Roy P, Das C, Lee K, Hahn R, Ruff T, Moll M, Schmuki P (2011) J Am Chem Soc 133:5629
8. Kamat PV (1993) Chem Rev 93:267
9. Zhu X (1994) Annu Rev Phys Chem 45:113
10. Jiang D, Zhao H, Zhang S, John R (2004) J Catal 223:212
11. Cracknell JA, Vincent KA, Armstrong FA (2008) Chem Rev 108:2439
12. Nitzan A, Ratner MA (2003) Science 300:1384
13. Fan F-RF, Yao Y, Cai L, Cheng L, Tour JM, Bard AJ (2004) J Am Chem Soc 126:4035

14. Naber WJM, Faez S, Wiel WGvd (2007) J Phys D Appl Phys 40:R205
15. Wolf SA, Awschalom DD, Buhrman RA, Daughton JM, von Molnár S, Roukes ML, Chtchelkanova AY, Treger DM (2001) Science 294:1488
16. Furube A, Katoh R, Yoshihara T, Hara K, Murata S, Arakawa H, Tachiya M (2004) J Phys Chem B 108:12583
17. Furube A, Du L, Hara K, Katoh R, Tachiya M (2007) J Am Chem Soc 129:14852
18. Shen YR (1989) Nature 337:519
19. Tisdale WA, Williams KJ, Timp BA, Norris DJ, Aydil ES, Zhu X-Y (2010) Science 328:1543
20. Tisdale WA, Zhu X-Y (2011) Proc Natl Acad Sci U S A 108:965
21. Tully JC (1990) J Chem Phys 93:1061
22. Tully JC (2012) J Chem Phys 137:22A301
23. Duncan WR, Prezhdo OV (2007) Annu Rev Phys Chem 58:143
24. Prezhdo OV, Duncan WR, Prezhdo VV (2008) Acc Chem Res 41:339
25. Prezhdo OV, Duncan WR, Prezhdo VV (2009) Prog Surf Sci 84:30
26. Prezhdo OV (2009) Acc Chem Res 42:2005
27. Hyeon-Deuk K, Prezhdo OV (2012) J Phys Condens Matter 24:363201
28. Sousa C, Tosoni S, Illas F (2012) Chem Rev 113:4456
29. Neukirch AJ, Hyeon-Deuk K, Prezhdo OV (2014) Coord Chem Rev 263–264:161
30. Ehrenfest P (1927) Z Physik 45:455
31. Prezhdo OV, Kisil VV (1997) Phys Rev A 56:162
32. Bornemann FA, Nettesheim P, Schütte C (1996) J Chem Phys 105:1074
33. Parandekar PV, Tully JC (2005) J Chem Phys 122:094102
34. Prezhdo O (2006) Theor Chem Acc 116:206
35. Wang L, Akimov AV, Chen L, Prezhdo OV (2013) J Chem Phys 139:174109
36. Drukker K (1999) J Comput Phys 153:225
37. Barbatti M (2011) WIREs Comput Mol Sci 1:620
38. Fabiano E, Keal TW, Thiel W (2008) Chem Phys 349:334
39. Evenhuis C, Martínez TJ (2011) J Chem Phys 135:224110
40. Granucci G, Persico M, Toniolo A (2001) J Chem Phys 114:10608
41. Fernandez-Alberti S, Roitberg AE, Nelson T, Tretiak S (2012) J Chem Phys 137:014512
42. Wang L, Prezhdo OV (2014) J Phys Chem Lett 5:713
43. Wang L, Beljonne D (2013) J Phys Chem Lett 4:1888
44. Wang L, Beljonne D (2013) J Chem Phys 139:064316
45. Wang L, Trivedi D, Prezhdo OV (2014) J Chem Theory Comput 10:3598
46. Bittner ER, Rossky PJ (1995) J Chem Phys 103:8130
47. Hack MD, Truhlar DG (2001) J Chem Phys 114:9305
48. Bedard-Hearn MJ, Larsen RE, Schwartz BJ (2005) J Chem Phys 123:234106
49. Prezhdo OV (1999) J Chem Phys 111:8366
50. Jaeger HM, Fischer S, Prezhdo OV (2012) J Chem Phys 137:22A545
51. Akimov AV, Long R, Prezhdo OV (2014) J Chem Phys 140:194107
52. Young KF, Frederikse HPR (1973) J Phys Chem Ref Data 2:313
53. Coropceanu V, Cornil J, da Silva Filho DA, Olivier Y, Silbey R, Brédas J-L (2007) Chem Rev 107:926
54. Wang L, Nan G, Yang X, Peng Q, Li Q, Shuai Z (2010) Chem Soc Rev 39:423
55. Shuai Z, Wang L, Li Q (2011) Adv Mater 23:1145
56. Troisi A (2011) Chem Soc Rev 40:2347
57. Knupfer M (2003) Appl Phys A 77:623
58. Nayak PK (2013) Synt Met 174:42
59. Engel M, Kunze F, Lupascu DC, Benson N, Schmechel R (2012) Phys Status Solidi RRL 6:68
60. Long R, Prezhdo OV (2011) J Am Chem Soc 133:19240
61. Long R, English NJ, Prezhdo OV(2014) J Phys Chem Lett 5:2941
62. Tafen DN, Long R, Prezhdo OV (2014) Nano Lett 14:1790
63. Long R, English NJ, Prezhdo OV (2012) J Am Chem Soc 134:14238
64. Long R, English NJ, Prezhdo OV (2013) J Am Chem Soc 135:18892
65. Chaban VV, Prezhdo VV, Prezhdo OV (2013) J Phys Chem Lett 4:1

66. Zhu H, Yang Y, Hyeon-Deuk K, Califano M, Song N, Wang Y, Zhang W, Prezhdo OV, Lian T (2013) Nano Lett 14:1263
67. Long R, Prezhdo OV (2014) (in preparation)
68. Akimov AV, Prezhdo OV (2014) J Am Chem Soc 136:1599
69. Long R, Prezhdo OV (2014) Nano Lett 14:3335
70. Feynman RP (1948) Rev Mod Phys 20:367
71. Hohenberg P, Kohn W (1964) Phys Rev 136:B864
72. Kohn W, Sham LJ (1965) Phys Rev 140:A1133
73. Ziegler T (1991) Chem Rev 91:651
74. Runge E, Gross EKU (1984) Phys Rev Lett 52:997
75. Marques MAL, Gross EKU (2004) Annu Rev Phys Chem 55:427
76. Baer R, Neuhauser D (2004) J Chem Phys 121:9803
77. Tretiak S, Igumenshchev K, Chernyak V (2005) Phys Rev B 71:033201
78. Fischer SA, Habenicht BF, Madrid AB, Duncan WR, Prezhdo OV (2011) J Chem Phys 134:024102
79. Chernyak V, Mukamel S (2000) J Chem Phys 112:3572
80. Baer R (2002) Chem Phys Lett 364:75
81. Hu C, Hirai H, Sugino O (2007) J Chem Phys 127:064103
82. Tavernelli I, Tapavicza E, Rothlisberger U (2009) J Chem Phys 130:124107
83. Send R, Furche F (2010) J Chem Phys 132:044107
84. Hammes-Schiffer S, Tully JC (1994) J Chem Phys 101:4657
85. Craig CF, Duncan WR, Prezhdo OV (2005) Phys Rev Lett 95:163001
86. Petersilka M, Gossmann UJ, Gross EKU (1996) Phys Rev Lett 76:1212
87. Appel H, Gross EKU, Burke K (2003) Phys Rev Lett 90:043005
88. Prezhdo OV, Rossky PJ (1997) J Chem Phys 107:825
89. Neria E, Nitzan A (1993) J Chem Phys 99:1109
90. Akimov AV, Prezhdo OV (2013) J Chem Theory Comput 9:4959
91. Wang L, Beljonne D, Chen L, Shi Q (2011) J Chem Phys 134:244116
92. Neuhauser D, Lopata K (2008) J Chem Phys 129:134106
93. Meng S, Kaxiras E (2008) J Chem Phys 129:054110
94. Prezhdo OV, Pereverzev YV (2000) J Chem Phys 113:6557
95. Kilin DS, Pereversev YV, Prezhdo OV (2004) J Chem Phys 120:11209
96. Akimov AV, Prezhdo OV (2012) J Chem Phys 137:224115
97. Wang LJ, Peng Q, Li QK, Shuai Z (2007) J Chem Phys 127:044506
98. Wang LJ, Li QK, Shuai Z (2008) J Chem Phys 128:194706
99. Wang L, Li Q, Shuai Z, Chen L, Shi Q (2010) Phys Chem Chem Phys 12:3309
100. Cheng Y-C, Silbey RJ (2008) J Chem Phys 128:114713
101. Hannewald K, Bobbert PA (2004) Phys Rev B 69:075212
102. Fratini S, Ciuchi S (2003) Phys Rev Lett 91:256403
103. Berkelbach TC, Hybertsen MS, Reichman DR (2013) J Chem Phys 138:114102
104. Seidel W, Titkov A, André JP, Voisin P, Voos M (1994) Phys Rev Lett 73:2356
105. Hartmann T, Reineker P, Yudson VI (2011) Phys Rev B 84:245317
106. Sippel P, Albrecht W, Mitoraj D, Eichberger R, Hannappel T, Vanmaekelbergh D (2013) Nano Lett 13:1655
107. Lindblad G (1976) Commun Math Phys 48:119
108. Zurek WH (2003) Rev Mod Phys 75:715
109. Leggett AJ, Chakravarty S, Dorsey AT, Fisher MPA, Garg A, Zwerger W (1987) Rev Mod Phys 59:1
110. Plenio MB, Knight PL (1998) Rev Mod Phys 70:101
111. Strunz WT (2001) Chem Phys 268:237
112. Diósi L, Strunz WT (1997) Phys Lett A 235:569
113. Akimov AV, Prezhdo OV (2014) J Chem Theory Comput 10:789
114. Trotter HF (1959) Proc Amer Math Soc 10:545
115. Paolo G et al (2009) J Phys Condens Matter 21:395502

116. Zhu H, Yang Y, Lian T (2012) Acc Chem Res 46:1270
117. Beard MC, Luther JM, Semonin OE, Nozik AJ (2012) Acc Chem Res 46:1252
118. Nozik AJ (2001) Annu Rev Phys Chem 52:193
119. Pandey A, Guyot-Sionnest P (2008) Science 322:929
120. Schaller RD, Klimov VI (2004) Phys Rev Lett 92:186601
121. Ellingson RJ, Beard MC, Johnson JC, Yu P, Micic OI, Nozik AJ, Shabaev A, Efros AL (2005) Nano Lett 5:865
122. McGuire JA, Joo J, Pietryga JM, Schaller RD, Klimov VI (2008) Acc Chem Res 41:1810
123. Shabaev A, Efros AL, Nozik AJ (2006) Nano Lett 6:2856
124. Murphy JE, Beard MC, Norman AG, Ahrenkiel SP, Johnson JC, Yu P, Mićić OI, Ellingson RJ, Nozik AJ (2006) J Am Chem Soc 128:3241
125. Madrid AB, Hyeon-Deuk K, Habenicht BF, Prezhdo OV (2009) ACS Nano 3:2487
126. Prezhdo OV (2008) Chem Phys Lett 460:1
127. Kilina SV, Kilin DS, Prezhdo OV (2008) ACS Nano 3:93
128. Wang L-W, Califano M, Zunger A, Franceschetti A (2003) Phys Rev Lett 91:056404
129. Franceschetti A, An JM, Zunger A (2006) Nano Lett 6:2191
130. Peterson JJ, Krauss TD (2006) Nano Lett 6:510
131. Kilina SV, Craig CF, Kilin DS, Prezhdo OV (2007) J Phys Chem C 111:4871
132. Schaller RD, Pietryga JM, Goupalov SV, Petruska MA, Ivanov SA, Klimov VI (2005) Phys Rev Lett 95:196401
133. Cooney RR, Sewall SL, Anderson KEH, Dias EA, Kambhampati P (2007) Phys Rev Lett 98:177403
134. Habenicht BF, Prezhdo OV (2008) Phys Rev Lett 100:197402
135. Prezhdo OV, Rossky PJ (1998) Phys Rev Lett 81:5294
136. Skinner JL (1988) Annu Rev Phys Chem 39:463
137. Mukamel S (1995) Principles of Nonlinear Optical Spectroscopy, Oxford University Press
138. Salvador MR, Hines MA, Scholes GD (2003) J Chem Phys 118:9380
139. Isborn CM, Kilina SV, Li X, Prezhdo OV (2008) J Phys Chem C 112:18291
140. Hyeon-Deuk K, Prezhdo OV (2012) ACS Nano 6:1239
141. Luo J-W, Franceschetti A, Zunger A (2008) Nano Lett 8:3174
142. Rabani E, Baer R (2008) Nano Lett 8:4488
143. Linsebigler AL, Lu G, Yates JT (1995) Chem Rev 95:735
144. Thompson TL, Yates JT (2006) Chem Rev 106:4428
145. Moser J, Graetzel M (1983) J Am Chem Soc 105:6547
146. O'Regan B, Gratzel M (1991) Nature 353:737
147. Bonnell DA (1998) Prog Surf Sci 57:187
148. Henrich VE (1995) Prog Surf Sci 50:77
149. Diebold U (2003) Surf Sci Rep 48:53
150. Stier W, Prezhdo OV (2002) Israel J Chem 42:213
151. Duncan WR, Prezhdo OV (2008) J Am Chem Soc 130:9756
152. Asbury JB, Anderson NA, Hao E, Ai X, Lian T (2003) J Phys Chem B 107:7376
153. McCusker JK (2003) Acc Chem Res 36:876
154. Henry W et al (2008) J Phys Chem A 112:4537
155. Duncan WR, Craig CF, Prezhdo OV (2007) J Am Chem Soc 129:8528
156. Stier W, Duncan WR, Prezhdo OV (2004) Adv Mater 16:240
157. Duncan WR, Stier WM, Prezhdo OV (2005) J Am Chem Soc 127:7941
158. Stier W, Prezhdo OV (2002) J Phys Chem B 106:8047
159. Warren DS, McQuillan AJ (2004) J Phys Chem B 108:19373
160. Panayotov DA, Yates JT Jr (2007) Chem Phys Lett 436:204
161. Ramakrishna S, Willig F, Knorr A (2004) Surf Sci 558:159
162. Prakash T (2012) Electron Mater Lett 8:231
163. Kohler A, dos Santos DA, Beljonne D, Shuai Z, Bredas JL, Holmes AB, Kraus A, Mullen K, Friend RH (1998) Nature 392:903
164. Salant A, Shalom M, Tachan Z, Buhbut S, Zaban A, Banin U (2012) Nano Lett 12:2095

165. Moon GD, Ko S, Xia Y, Jeong U (2010) ACS Nano 4:2307
166. Kim JY, Noh JH, Zhu K, Halverson AF, Neale NR, Park S, Hong KS, Frank AJ (2011) ACS Nano 5:2647
167. Morozov SV, Novoselov KS, Katsnelson MI, Schedin F, Elias DC, Jaszczak JA, Geim AK (2008) Phys Rev Lett 100:016602
168. Chen L, Wang L, Shuai Z, Beljonne D (2013) J Phys Chem Lett 4:2158
169. Williams G, Seger B, Kamat PV (2008) ACS Nano 2:1487
170. Zhang H, Lv X, Li Y, Wang Y, Li J (2009) ACS Nano 4:380
171. Manga KK, Zhou Y, Yan Y, Loh KP (2009) Adv Funct Mater 19:3638
172. Wei HH-Y, Evans CM, Swartz BD, Neukirch AJ, Young J, Prezhdo OV, Krauss TD (2012) Nano Lett 12:4465
173. Inerbaev TM, Masunov AE, Khondaker SI, Dobrinescu A, Plamadă A-V, Kawazoe Y (2009) J Chem Phys 131:044106
174. Yang Y, Rodríguez-Córdoba W, Lian T (2011) J Am Chem Soc 133:9246
175. Bang JH, Kamat PV (2011) ACS Nano 5:9421
176. Marcus RA (1956) J Chem Phys 24:966
177. Marcus RA (1965) J Chem Phys 43:679
178. Brus LE (1983) J Chem Phys 79:5566. http://dx.doi.org/10.1063/1.445676
179. Caruso D, Troisi A (2012) PNAS
180. Cappel UB, Dowland SA, Reynolds LX, Dimitrov S, Haque SA (2013) J Phys Chem Lett 4:4253
181. Smith MB, Michl J (2010) Chem Rev 110:6891
182. Smith MB, Michl J (2013) Annu Rev Phys Chem 64:361
183. Beljonne D, Yamagata H, Brédas JL, Spano FC, Olivier Y (2013) Phys Rev Lett 110:226402
184. Rao A, Wilson MWB, Hodgkiss JM, Albert-Seifried S, Bässler H, Friend RH (2010) J Am Chem Soc 132:12698
185. Anthony JE (2010) Chem Mater 23:583
186. Stranks SD, Weisspfennig C, Parkinson P, Johnston MB, Herz LM, Nicholas RJ (2010) Nano Lett 11:66
187. Porezag D, Frauenheim T, Köhler T, Seifert G, Kaschner R (1995) Phys Rev B 51:12947
188. Koskinen P, Mäkinen V (2009) Comput Mater Sci 47:237

Chapter 14
Life Cycle Assessment of Nanomaterials

Girish Upreti, Rajive Dhingra, Sasikumar Naidu, Isaac Atuahene, and Rapinder Sawhney

Abstract Nanotechnology has wide range of applications. This paper emphasizes the need to conduct "life cycle"-based assessments as early in the new product development process as possible, for a better understanding of the potential environmental and human health consequences of nanomaterials over the entire life cycle of a nano-enabled product. This is further supported through an illustrative case study on automotive exterior body panels, which shows that the perceived environmental benefits of nano-based products in the Use stage may not adequately represent the complete picture, without examining the impacts in the other life cycle stages, particularly Materials Processing and Manufacturing. Nanomanufacturing methods often have associated environmental and human health impacts, which must be kept in perspective when evaluating nanoproducts for their "greenness." Incorporating life cycle thinking for making informed decisions at the product design stage, combining life cycle and risk analysis, using sustainable manufacturing practices, and employing green chemistry alternatives are seen as possible solutions.

Keywords Nanomaterials • Life cycle assessment • Risk analysis

14.1 Nanomaterials

A nanometer is one-billionth of a meter. According to the National Nanotechnology Initiative, a program established in 2001 to coordinate federal nanotechnology research and development, nanotechnology is the "the understanding and control of matter at dimensions between approximately 1 and 100 nm, where unique phenomena enable novel applications. Encompassing nanoscale science, engineering, and technology, nanotechnology involves imaging, measuring, modeling, and

G. Upreti (✉) • R. Dhingra • I. Atuahene • R. Sawhney
Department of Industrial and Systems Engineering, University of Tennessee, Knoxville, TN 37996-2315, USA
e-mail: gupreti@vols.utk.edu

S. Naidu
Axcess Financial, Avenida Felipe Pardo y Aliaga 675, San Isidro 15073, Peru

V.A. Basiuk, E.V. Basiuk (eds.), *Green Processes for Nanotechnology*,
DOI 10.1007/978-3-319-15461-9_14

manipulating matter at this length scale" [1]. Nanotechnology is considered an all-pervasive "enabling" technology [2] that transcends sectoral boundaries, resulting in novel applications of nanomaterials that promise radical improvements in various spheres of life. Examples include paper-thin, high-energy, nanoengineered batteries. Capable of being folded and cut like paper and infused with carbon nanotubes, these sheets of nanocomposite paper serve as ultra-thin, flexible batteries and energy storage devices for next-generation electronics and implantable medical equipment [3]. Nano-enabled miniaturized diagnostic devices can be implanted in the human body for early diagnosis of illnesses, and the use of nanotechnology for in vivo drug delivery and imaging systems is expanding rapidly [4]. Nano-based coatings can improve the bioactivity and biocompatibility of implants [5], while nanocoatings are also finding use in corrosion-resistance, dirt repellency, water repellency, thermal insulation, and anti-microbial applications.

Applications of nanotechnology that directly benefit the environment are nanotechnologies for site remediation and wastewater treatment [6], nanomaterial-based solar cells for improved energy efficiency, the use of nanocatalysts for air purification [7], and nanostructured filters or nanoreactive membranes for water purification [8].

Despite the seemingly obvious benefits of nanotechnology, there could be unintended health and environmental risks associated with the widespread use of nanomaterials which might not have yet been fully understood. As discussed in the following sections, there is a need to use a life cycle-based approach, possibly combined with risk assessment, in order to better understand the potential problems, and to adopt green nanomanufacturing methods that are less burdensome to the environment and human health.

Hischier proposes the identification of advantages and disadvantages of nanomaterials from a sustainability perspective which comprise: inventory modeling; collection of comprehensive, transparently documented and quality ensured data of the most important engineered nanomaterials and making them available in a widely accepted format; and Identification of physical characteristics for toxicity assessment of nanoparticles [9]. The study concludes that 7 out of the 17 studies identified are based on a functional unit of 1 weight unit of produced nanomaterial which is acceptable when analyzing the production process of the respective engineered nanomaterial, but not when comparing the functionality of nanomaterials with traditional materials. Finally, a reiteration on a complete lack of characterization factors for release of nanoparticles indoors and outdoors with respect to impact assessment is presented.

The burgeoning field of nanotech applications has left us with no doubt that nano-enabled products will play a dominant role in global manufacturing in the not-so-distant future. With new applications being discovered every day in areas as diverse as medicine, automotive, energy, agriculture, and entertainment, we are becoming increasingly aware of the benefits of nanotechnology in terms of cost and energy savings, increased productivity, increased efficiency, as well as reduced environmental impacts. According to Lux Research, the total revenue from products incorporating nanotechnology is expected to be $2.5 trillion in 2015, even though this estimate is down 21 % from their previous projections [10], the downward

revision being made considering the global economic downturn, as a result of which the rate of nanotech adoption was expected to be somewhat slower than originally anticipated.

14.2 Nanomanufacturing Technique and Environmental Effect

Nanoscale manufacturing involves one of two approaches: top-down or bottom-up. The top-down approach starts with micro-systems and miniaturizes them, through carving or grinding methods, such as lithography, etching, or milling. Bottom-up methods mimic nature by starting at the atomic or molecular level and building-up through nucleation and/or growth from liquid, solid, or gas precursors by chemical reactions or physical processes. Examples of techniques include sol-gel or epitaxy [5, 11]. It is generally believed that top-down methods generate a lot more waste. Though the bottom-up approach is in its early development phase, it promises sweeping changes to current methods of production.

Nanostructured materials can be classified as one-dimensional (1D), two-dimensional (2D), or three-dimensional (3D). Examples of 1-D nanoproducts are thin films and coatings, while 2-D include nanotubes and nanorods, and 3-D nanoproducts include fullerenes and nanoparticles. The production of 2-D and 3-D nanoproducts, generally, has stricter purity requirements. Many of the processes required to manufacture them have low process yields and, therefore, low material efficiencies, resulting in excessive waste. Moreover, these processes usually consume large quantities of energy, water, and solvents. In addition to being excessively resource and energy intensive, some of these processes have the potential to cause unintended acute and chronic human health impacts, from accidental exposure to nanomaterials.

Sengül et al. [11] have discussed various nanomanufacturing methods and have summarized the characteristics of nanomanufacturing processes that make them energy and resource intensive as follows:

- Stricter purity requirements
- Lower process yields
- Repeated processing, postprocessing, or reprocessing steps of a single process or batch
- Use of toxic, acidic, or basic chemicals and organic solvents
- Need for moderate to high vacuum
- Use of or generation of greenhouse gases

Sengul et al. article [11] provides an in-depth analysis of the issues pertaining to nanomanufacturing methods for 1-D, 2-D, and 3-D nanostructured materials. The manufactured quantities of nanomaterials are expected to increase as the technology becomes pervasive and starts displacing conventional materials in products. The starting materials used in manufacturing processes are usually rare and involve

resource intensive extraction or processing that puts additional strain on natural resources and increases the overall life cycle environmental impact of the product they are ultimately used in, as demonstrated in a case study that follows. This raises the issue of finding suitable starting materials for nanomanufacturing methods.

14.3 Industrial Ecology and LCA

Industrial Ecology is a systems approach that provides a holistic view of environmental problems, and helps us understand the way humans use natural resources in the production of goods and services. It emphasizes the need to study the interactions of industrial systems with the environment, and to design products and manufacturing processes in a way that optimizes the use of by-products, maximizes recycling, and minimizes waste [12]. This approach strives to ensure that industrial growth in the future is sustainable and in harmony with the environment. The foregoing discussion leads us right to the definition of Sustainable Development which, according to a World Commission on Environment and Development (WCED) report of 1987, is "Development that meets the needs of the present without compromising the ability of future generations to meet their own needs" [13].

The wide-ranging applications of nanotechnology have an equally widespread potential to adversely affect human health and the environment, through various exposure routes of nanoparticles [14], including occupational exposure [15]. Despite early calls to adopt measures that would ensure the sustained growth of nanotechnology, little has been done so far, in the unrelenting quest to rapidly introduce more and more novel nano-applications [16].

Life Cycle Assessment (LCA) is an invaluable tool for assessing the environmental impacts associated with the entire life cycle of a product. In fact, it would be premature to make any claims on the environmental benefits of a product or manufacturing process without first considering its environmental consequences in a "life cycle" context.

The steps typically involved in an LCA are (1) defining the goals and scope of the assessment, (2) quantifying the material and energy inputs, as well as the environmental releases for each unit process that forms part of the assessment (known as Life-Cycle Inventory or LCI), (3) evaluating the potential human health and environmental impacts associated with the inputs and outputs identified in the LCI data collection step, and (4) interpreting the results, highlighting significant issues, drawing conclusions, and making recommendations [17]. The life cycle stages usually considered are Material Extraction, Processing, Manufacturing, Use, Transportation, and End-of-Life (Recycling/Disposal).

Conducting a life cycle assessment of conventional products is in itself a daunting task, with boundaries often having to be drawn to limit the scope of the assessment, in order to complete it within a reasonable amount of time, with the finite resources available. Some of the methods available for curtailing the scope of the assessment (also known as LCA streamlining) include (1) restricting it to certain life cycle stages of interest, for example, the Use stage, (2) identifying certain

environmental impact categories of particular relevance, such as Global Warming, or (3) just conducting a comparative study of two different manufacturing processes that result in the creation of otherwise identical products.

With nanomaterials, the task of conducting a life cycle assessment becomes even more difficult because of lack of available inventory data on these materials, since their manufacturing processes are new and often subject to confidentiality constraints [18]. Another reason for not being able to use inventory data the same way as in the case of conventional materials is that cutoffs based on mass alone do not make sense for nanoparticles [14]. Also, current impact assessment methodologies do not incorporate formulas for computing the health and environmental effects of nanomaterials, simply because these effects are not yet fully known. Moreover, manufacturing processes for the production of nanomaterials are not yet standardized, but are in an evolutionary stage, changing constantly. For this reason, the environmental impacts associated with Production Method A for a given product could vary considerably from those associated with Production Method B. In the case of new technologies such as these, which are in their developmental phase, it might be beneficial to conduct scenario analyses when performing LCAs, for addressing uncertainties in possible future outcomes.

Hischier study's the inventory modeling rules and presents an application example of LCA of manufactured nanomaterials [19]. This study identify and tackle weak points in LCA studies, which includes the lack of inventory data and missing characterization factors, partly due to a lack of clear modeling rules for a LCA of MNM. The study provides a foundation for a clear guidance for coherent and comprehensive inventory modeling of nanomaterials along their complete life cycle. Most importantly, four main objectives are addressed which have been published in separately in three different journals; (1) A general set-up that allows the application of life cycle thinking principles (being the driving force behind the LCA tool) to the whole spectrum of applications of MNM; (2) An up-to-date and comprehensive overview of current published work in the area of 'LCA and nanotechnology' in order to clearly identify weaknesses and missing elements that have so far prevented a coherent and comprehensive application of the LCA process along the complete life cycle of MNM; (3) A framework on the level of inventory modeling that eliminates the weaknesses and missing elements identified beforehand, by keeping in mind the requirements from (the subsequent) impact assessment step; and finally (4) A first application example of the methodological developments by applying the framework on a display technology (the field emission display technology) using carbon nanotubes.

Miseljic presents a literature review of assessment status on LCA of engineered nanomaterials [20]. This study analyzes the 29 case studies of published literature on LCA of engineered nano materials. An investigation of the sensitivity of case studies with respect to ecotoxicity impacts through a quantification of the potential ecotoxicity impacts to algae, daphnia, and fish as a result of direct release of Ag and TiO_2 ENPs (mainly <200 nm in nominal diameter size) from various ENM products to the freshwater compartment is presented. The study finds a linear regression between Ag ENM content in the considered products and the potential ecotoxicity impacts to the freshwater species, according to release of total Ag during use (mainly washing).

In spite of the challenges faced in conducting LCAs of nanomaterials, a number of LCAs have been attempted [21–26], and even if complete LCAs cannot be performed, it is important to take a life cycle view of new technologies such as these, to help bring to light any issues or concerns in any of the upstream or downstream stages that may be elusive at first. This "life cycle thinking" approach needs to be applied at an early stage in the product development process, in order to better understand the environmental implications of new technologies and to be able to make informed decisions on the benefits or drawbacks of one alternative over another. There have been several suggestions to apply the life cycle thinking approach to nanotechnology development [15, 27–29].

Recognizing the drawbacks of LCA in being inadequate for analyzing the health effects and exposure routes of nanoparticles, this paper later describes more appropriate frameworks that combine the LCA approach with Risk Assessment (RA). The two frameworks discussed are nanoLCRA (Life Cycle Risk Assessment) and Comprehensive Environmental Assessment (CEA). Likely environmental impacts during each life cycle stage of nano-enabled products are shown in Fig. 14.1.

The apparent benefits of nano-enabled products, usually in the "Use" stage, often take center stage, while the environmental problems associated with the remaining

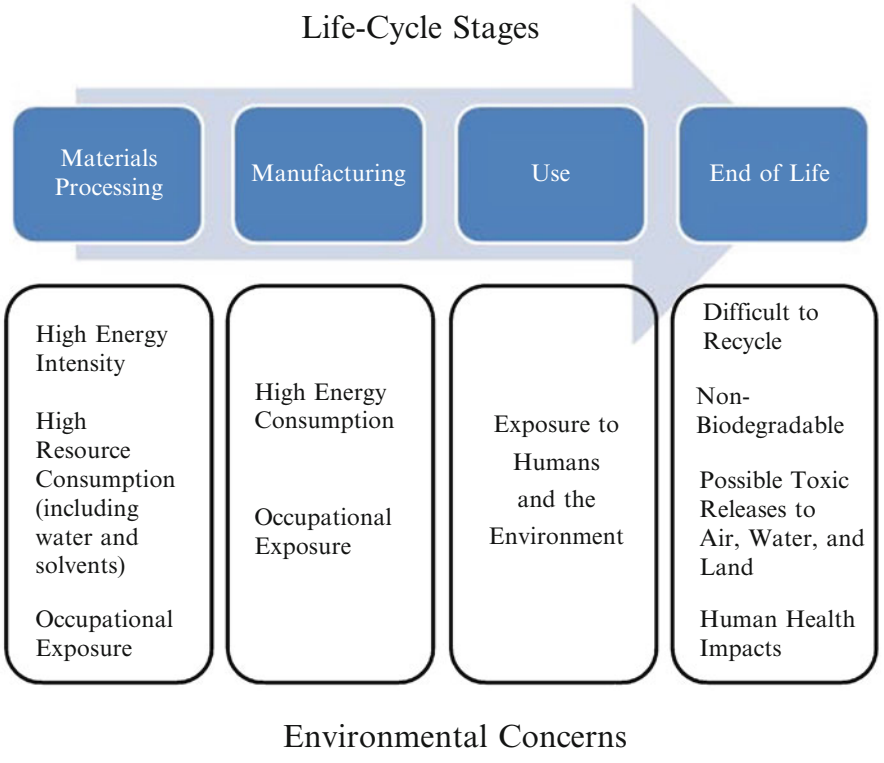

Fig. 14.1 Life cycle of nanomaterials (simplified). Reprinted from [37] with permission by the Molecular Diversity Preservation International AG

upstream and downstream life cycle stages tend to get overlooked [28]. Of particular concern are the Materials Processing and End-of-Life (Recycling/Disposal) stages. The creation of nanomaterials can often be highly energy and resource intensive, as discussed earlier in Sect. 14.2. At the End-of-Life stage, we are confronted with the problem of disposing of the nano-enabled product, if it is not fully recyclable and/or reusable. Manufactured nanomaterials have the potential to be released to the environment at each stage of the product life cycle [30].

14.4 Energy Intensity of Carbon Nanofibers and Nanoparticles

Although aluminum is thought to be one of the most energy intensive materials to produce, it has highly desirable properties, namely, light weight and higher strength as compared to steel, the material it usually competes with. Another drawback of aluminum is its higher price, but both the price and higher energy intensity do not usually come in the way of its use in certain critical aerospace, automotive and other applications. Because of its high energy intensity, aluminum has become a kind of yardstick by which some other, newer, materials are evaluated for their energy intensities.

Carbon nanoparticles and nanofibers are examples of such materials that are much more energy intensive to produce than aluminum. Two recent studies, one on nanofibers and the other on nanoparticles, show that carbon nanofibers produced from a range of feedstock materials require 13–50 times the energy required for the production of primary aluminum on an equal mass basis [31], while the carbon nanoparticles study finds their energy intensity to be 2–100 times that of aluminum [32].

When selecting conventional (non-nano) materials for use in a new product or application, product designers have traditionally been confronted with issues like strength, performance, cost, and esthetics. More recently, keeping the principles of Design for the Environment (DfE) in mind, additional environmental considerations like energy intensity, toxicity, recyclability, and ease of disassembly have made their way into their list of design criteria. The advent of nanomaterials, however, has necessitated a change in the traditional material selection process, because now product designers will not only have to keep the above issues in consideration but will also have to think about the health and safety of those who might be exposed to these nanoscale materials that have the potential to be inhaled or to penetrate the skin, and possibly affect vital organs.

14.5 Automotive Body Panels: A Case Study

The results from one of the author's previous studies have been used to show how nano-based products that seem environmentally preferable over other alternatives in the Use stage may not actually turn out to be so when the whole life cycle is considered. The original study compared lightweight alternatives to exterior body panels in

Table 14.1 Exterior body panels study: Major assumptions

Mass of the baseline (1994 Taurus class) vehicle	3,248 lb
Useful life of vehicle	120,000 miles
Life of body panels	Equal to life of vehicle
Baseline vehicle fuel efficiency	26.6 mpg
Mass of steel closure panels	220 lb
Material substitution factor for CFRP	0.4
CFRP composition	30 % CF in epoxy resin
Secondary weight savings factor	1.5
Fuel efficiency improvement factor	0.7[a]
Gasoline density	6.154 lb/gal
Gasoline heat content	115,400 BTUs/gal

[a]Vehicle fuel efficiency improves by 7 % for each 10 % reduction in vehicle weight [22]

vehicles of the future [33, 34]. Aluminum, carbon fiber reinforced polymer (CFRP) composite, and glass fiber reinforced polymer (GFRP) composite were considered as alternatives to steel closure panels (consisting of the four doors, hood, and deck lid) in a baseline vehicle [35]. The data for that study (which we will refer to as the "exterior body panels" study) were based on carbon fiber produced from polyacrylonitrile (PAN) precursor fiber, which is oxidized and carbonized into carbon fiber by exposing it to progressively higher temperatures in the presence of nitrogen.

The energy required to produce the PAN-based carbon fiber is substituted with the energy required to produce carbon nanofiber, the data for which have been taken from a recent study on carbon nanofiber production [31], performed by Khanna et al., based on vapor grown fibers synthesized from three different hydrocarbon feedstocks—methane, ethylene, and benzene, using the average energy of the range provided in the study (2,872–10,925 MJ/kg). Thus, the carbon fiber reinforced polymer (CFRP) composite in the exterior body panels study has been replaced with carbon nanofiber reinforced polymer (CNFRP) composite material, focusing only on the life cycle energy requirements.

The major assumptions of the previous study are stated in Table 14.1.

Based on the above assumptions, using a material substitution factor of 0.4 for CFRP [36], it was estimated that the weight of CFRP panels would be 88 lb if they were to replace 220 lb of steel, resulting in overall weight savings of 132 lb. However, any major weight reduction in vehicle weight provides opportunities for additional weight reductions in other components (known as secondary weight savings). Taking the secondary weight savings into account, the overall weight savings go up to 198 lb, bringing the CFRP vehicle weight down to 3,050 lb. Applying the fuel efficiency improvement factor of 0.7 to the baseline vehicle fuel efficiency of 26.6 mpg, the fuel efficiency of the CFRP vehicle was calculated to be 27.74 mpg. This works out to 4,327 gal of gasoline used by the CFRP vehicle over its lifetime, as against 4,511 gal by the baseline vehicle. Since the functional unit for the exterior body panels study was not the whole vehicle, but only the closure panels driven over the lifetime of the vehicle, the quantity of gasoline consumed on account of the

Table 14.2 Energy use for exterior body panels by life cycle stages

Energy use (MMBTUs)	E&MP	Use—fuel use	Use—fuel prod.	EOL	Total
Steel	1.19	35.25	7.78	0.01	44.24
Aluminum	12.97	19.69	4.35	0.02	37.02
GFRP	2.00	24.58	5.43	0.01	32.02
CFRP	4.53	14.40	3.18	0.00	22.11
CNFRP	**43.67**	**14.40**	**3.18**	**0.00**	**61.26**

body panels alone is the fractional ratio of the mass of CFRP closure panels to the whole car, or 124.8 gal. This translates to 768 lb, embodying an energy content of 14.40 million BTUs (MMBTUs).

The Energy use results from the exterior body panels study, as well as the modifications incorporating carbon nanofibers in place of bulk carbon fibers, are presented in Table 14.2. It has been assumed that the CNFRP composite will require only half the mass of carbon fibers, as compared to the CFRP composite material in the original study, because of the much higher strength of nanofibers. The 70/30 epoxy/carbon fiber mix in the original study, therefore, has been replaced with an 85/15 epoxy/carbon nanofiber mix, requiring only 13.2 lb of nanofiber in 88 lb of CNFRP panels. In estimating the energy requirements of CNFRP panels, the additional energy required to produce nanofibers has been taken into account, based on an average value of 6,899 MJ/kg (taken from the study by Khanna et al., as described above), as well as the energy required to produce the additional quantity of epoxy resin in the mix. Their study revealed that the production of nanofibres and polymer nanocomposites is more energy demanding than a steel product.

Table 14.2 shows the results of the previous study, along with an additional row representing the new CNFRP analysis (in bold). It is observed that the only change in energy numbers for CNFRP over CFRP is in the Extraction & Materials Processing (E&MP) stage, on account of the additional energy required to produce carbon nanofibers, with everything else remaining the same. In the previous study, CFRP turned out to be the material of choice, not only on account of its lowest total life cycle energy requirement, but also because it was less environmentally burdensome in 8 other environmental impact categories (not shown here), out of a total of 14 impact categories evaluated [33, 34].

It is noteworthy that, while the Use (driving) stage typically dominates the environmental life cycle of the automobile, accounting for about 80 % of the environmental impacts, substituting the body panels with nanofiber-based material, albeit in a small quantity, makes the Use stage seem insignificant compared to the Extraction and Materials Processing stage [37]. In the previous assessment, aluminum was the most energy intensive material to produce, with its E&MP stage accounting for 35 % of the life cycle energy impacts. However, the introduction of CNFRP makes the E&MP stage for this material the biggest contributor to total life cycle energy, as depicted in Fig. 14.2. In fact, the use of nanofibers totally turns the results of the study around, to make this choice of material the worst, at least on the energy front.

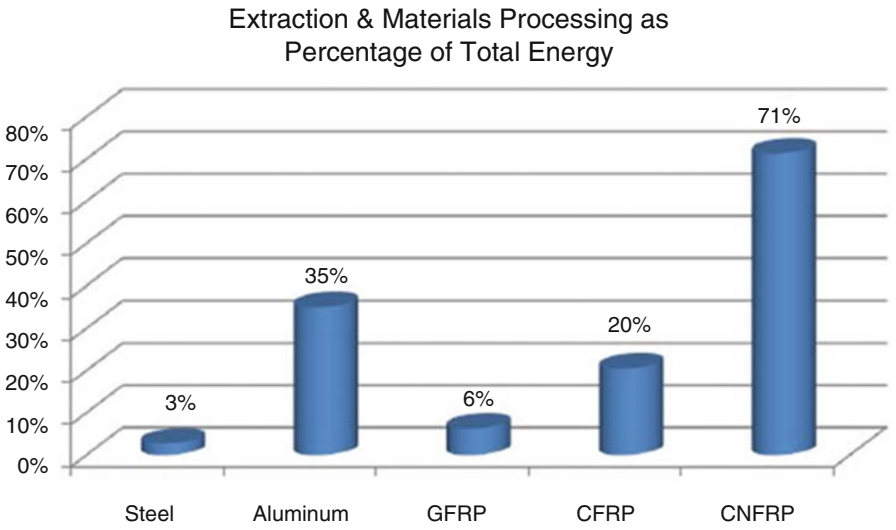

Fig. 14.2 Contribution of the extraction and materials processing stage to total life-cycle energy. Reprinted from [37] with permission by the Molecular Diversity Preservation International AG

The above study clearly indicates that newer materials that are being chosen have numerous advantages, by way of their high strength, light weight, etc., but are also likely to have a relatively higher energy and material resource intensity in the upstream processing stages. In order to derive maximum benefit from the use of these materials in an environmentally responsible manner, we need to look at ways in which we can reduce their environmental burden in the life cycle stages prior to the Use stage.

Since the above results are based on the assumption that half the quantity of carbon nanofibers will be needed in the CNFRP composite as compared to the CFRP material, a sensitivity analysis was conducted using higher and lower percentages of carbon nanofiber in the epoxy resin mix. Values of 10 and 20 % by mass of carbon nanofibers were utilized to calculate the changes in the energy consumption. The energy required by the three different compositions of CNFRP in the Extraction and Materials Processing stage is graphically depicted in Figure 14.3, which also shows comparisons with the energy requirements of the other competing materials.

It is observed that in spite of varying the quantity of carbon nanofibers in the epoxy composite mix, the E&MP energy of the nanocomposites is still much higher than that of the other materials, with the nanofibers continuing to play a dominant role in the total energy requirement. Noting that the purpose of vehicle weight reduction is to maximize fuel economy, with a corresponding decrease in fuel use, it is seen that in the case of all three CNFRP compositions, the benefit of reduced fuel use is negated by the high energy required for the production of these materials. This is clearly understood by taking a look at the total energy results for the various CNFRP compositions compared to the four competing materials, steel, aluminum, GFRP, and CFRP, as shown in Table 14.3.

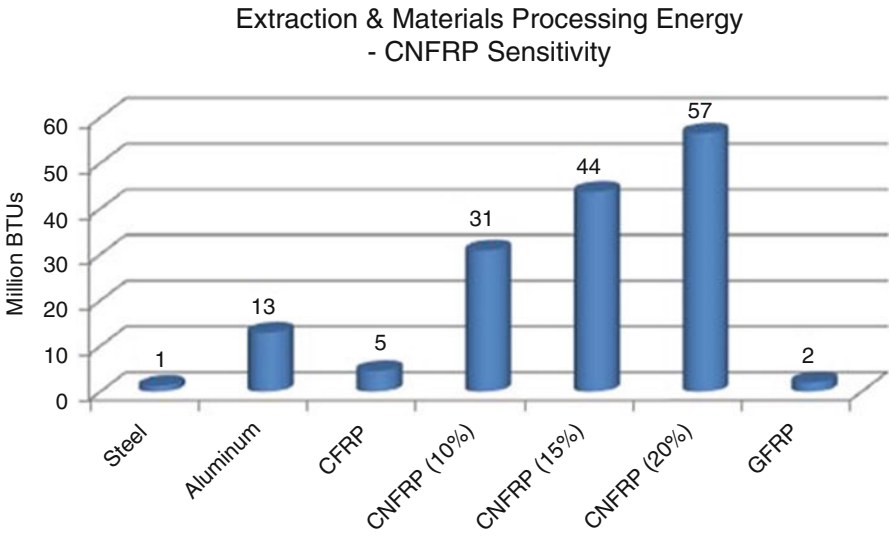

Fig. 14.3 Comparison of extraction and materials processing energy. Reprinted from [37] with permission by the Molecular Diversity Preservation International AG

Table 14.3 Energy Use Sensitivity to CNFRP Composition

Energy use (MMBTUs)	E&MP	Total
Steel	1.19	44.24
Aluminum	12.97	37.02
GFRP	2.00	32.02
CFRP	4.53	22.11
CNFRP (10 %)	**30.78**	**48.36**
CNFRP (15 %)	**43.67**	**61.26**
CNFRP (20 %)	**56.57**	**74.15**

In the case of the 10 % CNFRP material, the total energy approaches the baseline vehicle energy of 44 MMBTUs. However, it is the strength of carbon nanofibers and the mechanics of the nanofiber-matrix interface that ultimately determine the quantity of nanofibers in the epoxy resin mix. For comparison, aluminum has a tensile strength of 110 MegaPascals (MPa), with carbon nanofiber being approximately 50 times stronger, having a tensile strength of 5,000 MPa, or 5 GigaPascals (GPa). Carbon nanofiber is also about 10–15 times stronger than the grade of steel used for automotive body panels (which has a tensile strength of about 400 MPa) [38, 39]. A study conducted on the strength of carbon nanofiber-epoxy composites estimates the minimum interfacial strength of the nanofiber-epoxy composite system to be 170 MPa [39]. Carbon Nanotubes (CNTs), on the other hand, are much stronger than even carbon nanofiber, with a tensile strength in the range of 30–200 GPa [40].

In addition to being highly energy-intensive, nanomanufacturing processes can be highly resource-intensive, too. Certain nanomaterials require a practically contaminant-free environment, such as clean rooms and ultrapure water. Nanomanufacturing methods and the environmental concerns associated with them are discussed earlier in Sect. 14.2.

14.6 Proposed Solutions

Considering that the production of nanomaterials could be environmentally burdensome, and that there are potential health and safety concerns associated with their production, it is important for us to study the tradeoffs involved by weighing the prospective benefits of nano-based products against their unintended negative impacts. Compounding the problem is the fact that existing policies regulate only conventional chemical substances, and there is no obligation on the part of manufacturing companies to label nanomaterials on their products [41]. Potential solutions are seen in the form of greener nanosynthesis methods, which we call "Green Alternatives," and assessment frameworks that combine life cycle and risk assessment, such as Comprehensive Environmental Assessment (CEA) and Life Cycle Risk Assessment (LCRA). These are discussed in the following sub-sections.

14.6.1 Green Alternatives

Michael Berger of Nanowerk LLC [42] has suggested a potential solution by applying the following principles of green chemistry, as outlined by the US Environmental Protection Agency (EPA) on their "Green Chemistry" website, to nanomanufacturing processes.

1. Design chemical syntheses to prevent waste
2. Design safer chemicals and products
3. Design less-hazardous chemical syntheses
4. Use raw materials and feedstocks that are renewable
5. Minimize waste by using catalytic reactions
6. Avoid chemical derivatives
7. Maximize atom economy
8. Use safer solvents and reaction conditions
9. Increase energy efficiency
10. Design chemicals and products to degrade after use
11. Analyze in real time to prevent pollution
12. Minimize the potential for accidents

The application and acceptance of such methods in manufacturing can only be achieved if all the stakeholders are involved in the decision-making process, and the benefits and drawbacks of manufacturing alternatives are evaluated both from process metrics and green chemistry metrics [43]. James Hutchison, director of the Safer Nanomaterials and Nanomanufacturing Initiative (SNNI), which is the leading green nanotechnology effort in the world, suggests an evolving approach towards nanotechnology Environmental Health and Safety (EHS) research in three phases [44].

1. Studies of nanomaterial implications.
2. Coordinated applications and implications research.
3. A green nanoscience approach to material and process design to eliminate hazards throughout the material's life cycle.

While research activities are presently being carried out in each of the above three phases, the bulk of the research currently being done is transitioning from Phase 1 to Phase 2, with activities in Phases 2 and 3 each just beginning. The maximum benefit can be achieved by focusing on the development of Phase 3, which is a more proactive approach, as it attacks the problem at the source. This leads to reduced potential environmental and human health impacts from the manufacturing process itself and helps us focus on the environmental impacts of nanomaterials and nanoenabled products because most of the syntheses of nanomaterials begin with known toxic materials as raw materials or solvents, which impose additional environmental burdens associated with nanomaterials and nanoenabled products. If there are health and/or safety concerns in handling materials used in the production of nanomaterials, we should study the tradeoffs involved and then see if alternative methods of production can be used to manufacture them. Examples of alternative processes based on green chemistry [45] are:

1. Electrochemical methods and Microcapillary and Integrated Microchannel reactors that minimize the use of solvents, reactants, and process times.
2. Sonochemistry and Microwave-based techniques as sources of energy which shorten process times and energy consumption.
3. Alternate solvents like Supercritical Fluids (SCF), Ionic Liquids, mixture of SCF and organic solvents that are environmentally benign.
4. Bio-based approaches using biomimetic synthesis or biosynthetic approaches that use microorganisms to grow nanomaterials.

Though efforts to make nanomanufacturing processes greener are currently underway, they need to be coordinated with the efforts of LCA practitioners and product designers who are actually concerned with studying the impact of the use of these materials in nano-enabled products.

14.6.2 Combining Life Cycle and Risk Assessment

There is definitely a need for adequately addressing the human health consequences of the use of nanomaterials. However, current LCA methodology does have its limitations, as pointed out earlier. For instance, current LCA methodology has no means of distinguishing nanoparticles from bulk materials. Moreover in Step 3 of LCA methodology (Impact Assessment), the effects on human health and the environment are characterized based on environmental loadings. In other words, human health and environmental impacts are calculated using formulas based upon quantities of pollutants discharged to air, water, and land. Life-Cycle Assessment, therefore, can essentially only conclude that less is better but not whether one particular impact is more significant than another, when tradeoffs are involved [46]. Risk Assessment addresses that issue, by helping us better understand the nature and probability of adverse human health effects from exposure to toxic substances and other contaminants [47]. Risk Assessment goes from quantities of pollutants discharged to analyzing their effects under ambient conditions, through various

exposure pathways. In the case of nanomaterials where, in addition to quantity, additional parameters such as particle size and surface area play a significant role in affecting human health, an approach that combines LCA and Risk Assessment is likely to work well; even though they are faced with similar challenges in terms of data gaps for nanomaterials, they complement each other [48, 49]. One such approach that combines LCA and Risk Assessment is the ten-step Nano LCRA (Life Cycle Risk Assessment) framework for nanomaterials, an iterative process that involves the following [50]:

1. Describe the life cycle of the product.
2. Identify the materials and assess potential hazards in each life cycle stage.
3. Conduct a qualitative exposure assessment for materials at each life cycle stage.
4. Identify stages of life cycle when exposure may occur.
5. Evaluate potential human and nonhuman toxicity at key life cycle stages.
6. Analyze risk potential for selected life cycle stages.
7. Identify key uncertainties and data gaps.
8. Develop mitigation/risk management strategies and next steps.
9. Gather additional information.
10. Iterate process, revisit assumptions, adjust evaluation and management steps.

Another approach that combines the "environmental impact" focus of LCA with the "exposure" focus of Risk Assessment (RA) and includes toxicological effects of nanomaterials is Comprehensive Risk Assessment (CEA). A basic structure to summarize the CEA approach is proposed by Davis [51]. It begins with a qualitative description of the life cycle of the product, thus providing a framework for systematically characterizing the potential multimedia impacts associated with the nanomaterials. Primary and secondary contaminants are then identified as entering various exposure pathways. The process ends with the evaluation of their effects on human health and ecosystems.

No instances could be found from studies that have been conducted using any of the above "combined approach" frameworks. This is because of lack of inventory data and the fact that impact and risk characterization methods have not yet been developed for nanomaterials. In the future, when more data become available on these materials, using a combined LCA-RA approach would be immensely useful in evaluating the environmental and human health consequences of nanomaterials. This process can be speeded up if practitioners in the areas of LCA and RA work more closely together in the future, specifically in the area of nanomaterials.

References

1. National Nanotechnology Intiative. Nanotech facts: what is nanotechnology? http://www.nano.gov. Accessed 13 Jun 2013
2. Fleischer T, Grunwald A (2008) Making nanotechnology developments sustainable. A role for technology assessment? J Clean Prod 16:889–898
3. Mullaney M (2007) Beyond batteries: storing power in a sheet of paper. Rensselaer Polytechnic Institute, Troy, NY, http://www.eurekalert.org/pub_releases/2007-08/rpi-bbs080907.php. Accessed 16 June 2013

4. Koo OM, Rubinstein I, Onyuksel H (2005) Role of nanotechnology in targeted drug delivery and imaging: a concise review. Nanomedicine 1:193–212
5. Commission of European Communities (2004) Communication from the commission—towards a European strategy for nanotechnology. Brussels, Belgium, European Communities
6. Watlington K (2005) Emerging nanotechnologies for site remediation and wastewater treatment. EPA, Washington, DC
7. Sinha A, Suzuki K, Takahara M et al (2007) Mesostructured manganese oxide/gold nanoparticle composites for extensive air purification. Angew Chem Int Ed Engl 46:2891–2894
8. Theron J, Walker JA, Cloete TE (2008) Nanotechnology and water treatment: applications and emerging opportunities. Crit Rev Microbiol 34:43–69
9. Hischier R, Walser T (2012) Life cycle assessment of engineered nanomaterials: state of the art and strategies to overcome existing gaps. Sci Total Environ 425:271–282
10. Lux Research: Nanotech in the Recession (2013) http://www.luxresearchinc.com/blog/2009/07/nanotech-in-the-recession. Accessed 14 Jun 2013
11. Sengul H, Theis TL, Ghosh S (2008) Toward sustainable nanoproducts: an overview of nanomanufacturing methods. J Ind Ecol 12:329–359
12. Garner A, Keoleian GA (1995) Industrial ecology: an introduction. National Pollution Prevention Center for Higher Education, Ann Arbor, MI
13. World Commission on Environment and Development (1987) Our common future. Oxford University Press, Oxford
14. Curran MA, Frankl P, Heijungs R et al (2007) Nanotechnology and life cycle assessment—a systems approach to nanotechnology and the environment. Woodrow Wilson Center for Scholars, Washington, DC
15. Boccuni F, Rondinone B, Petyx C et al (2008) Potential occupational exposure to manufactured nanoparticles in Italy. J Clean Prod 16:949–956
16. Allenby BR, Rejeski D (2008) The industrial ecology of emerging technologies. J Ind Ecol 12:267–269
17. National Risk Management Research Laboratory (2006) Life cycle assessment: principles and practice. US EPA, Cincinnati, OH, EPA/600/R-06/060
18. Meyer DE, Curran MA, Gonzalez MA (2009) An examination of existing data for the industrial manufacture and use of nanocomponents and their role in the life cycle impact of nanoproducts. Environ Sci Technol 43:1256–1263
19. Hischier R (2014) Life cycle assessment of manufactured nanomaterials: inventory modelling rules and application example. Int J Life Cycle Assess 19:941–943
20. Miseljic M, Olsen SI (2014) Life-cycle assessment of engineered nanomaterials: a literature review of assessment status. J Nanopart Res 16:2427
21. Khanna V, Bhavik B, Lee LJ (2007) Life cycle energy analysis and environmental life cycle assessment of carbon nanofibers production. IEEE international symposium on electronics & the environment, Orlando, FL
22. Krishnan N, Boyd S, Somani A et al (2008) A hybrid life cycle inventory of nano-scale semiconductor manufacturing. Environ Sci Technol 42:3069–3075
23. Lloyd SM, Lave LB (2003) Life cycle economic and environmental implications of using nanocomposites in automobiles. Environ Sci Technol 37:3458–3466
24. Lloyd SM, Lave LB, Matthews HS (2005) Life cycle benefits of using nanotechnology to stabilize platinum-group metal particles in automotive catalysts. Environ Sci Technol 39:1384–1392
25. Osterwalder N, Capello C, Hungerbühler K et al (2006) Energy consumption during nanoparticle production: how economic is dry synthesis? J Nanopart Res 8:1–9
26. Roes A, Marsili E, Nieuwlaar E, Patel M (2007) Environmental and cost assessment of a polypropylene nanocomposite. J Polym Environ 15:212–226
27. Gleich AV, Steinfeldt M, Petschow U (2008) A suggested three-tiered approach to assessing the implications of nanotechnology and influencing its development. J Clean Prod 16:899–909
28. Bauer C, Buchgeister J, Hischier R et al (2008) Towards a framework for life cycle thinking in the assessment of nanotechnology. J Clean Prod 16:910–926

29. Köhler AR, Som C, Helland A et al (2008) Studying the potential release of carbon nanotubes throughout the application life cycle. J Clean Prod 16:927–937
30. Oberdörster G, Oberdörster E, Oberdörster J (2005) Nanotoxicology: an emerging discipline evolving from studies of ultrafine particles. Environ Health Perspect 113:823–839
31. Khanna V, Bakshi BR, Lee LJ (2008) Carbon nanofiber production: life cycle energy consumption and environmental impact. J Ind Ecol 12:394–410
32. Kushnir D, Sanden BA (2008) Energy requirements of carbon nanoparticle production. J Ind Ecol 12:360–375
33. Das S, Overly JG, Dhingra R et al (2002) Environmental evaluation of lightweight exterior body panels in new-generation vehicles. In Proceedings of the 2002 Future Car Congress, Arlington, VA, 3–5 June 2002, SAE Technical Paper Series. Society of Automotive Engineers, Warrendale, PA
34. Schexnayder SM, Das S, Dhingra R, Overly JG, Tonn BE, Peretz JH, Waidley G, Davis GA (2001) Environmental evaluation of new generation vehicles and vehicle components. Oak Ridge National Laboratory, Oak Ridge, TN
35. National Research Council (2000) Review of the research program of the partnership for a new generation of vehicles: sixth report. National Academy Press, Washington, DC
36. Sullivan J, Hu J (1995) Life cycle energy analysis for automobiles. In Proceedings of the 1995 total life cycle conference and exposition, Vienna, Austria, 16–19 October 2010. Society of Automotive Engineers, Detroit, MI
37. Dhingra R, Naidu S, Upreti G et al (2010) Sustainable nanotechnology: through green methods and life-cycle thinking. Sustainability 2:3323–3338
38. Engineering toolbox. Elastic properties and Young modulus for some materials; Available online: http://www.engineeringtoolbox.com/young-modulus-d_417.html. Accessed 16 Sep 2013
39. Manoharan MP, Sharma A, Desai AV et al (2009) The interfacial strength of carbon nanofiber epoxy composite using single fiber pullout experiments. Nanotechnology 20:295701
40. Sun Y, Sun J, Liu M et al (2007) Mechanical strength of carbon nanotube-nickel nanocomposites. Nanotechnology 18:505704
41. Som C, Berges M, Chaudhry Q et al (2010) The importance of life cycle concepts for the development of safe nanoproducts. Toxicology 269:160–169
42. Berger M (2008) Nanotechnology—not that Green? Nanowerk LLC, Berlin, Available online: http://www.nanowerk.com/spotlight/spotid=7853.php. Accessed 16 Jun 2013
43. Naidu S, Sawhney R, Li X (2008) A methodology for evaluation and selection of nanoparticle manufacturing processes based on sustainability metrics. Environ Sci Technol 42:6697–6702
44. Hutchison JE (2008) Greener nanoscience: a proactive approach to advancing applications and reducing implications of nanotechnology. ACS Nano 2:395–402
45. Dahl JA, Maddux BLS, Hutchison JE (2007) Toward greener nanosynthesis. Chem Rev 107:2228–2269
46. Matthews HS, Lave L, MacLean H (2002) Life cycle impact assessment: a challenge for risk analysts. Risk Anal 22:853–860
47. US EPA. Risk assessment portal: human health risk assessment. http://www.epa.gov/riskassessment/health-risk.htm. Accessed 16 Jun 2013
48. Savolainen K, Alenius H, Norppa H, Pylkkänen L, Tuomi T, Kasper G (2010) Risk assessment of engineered nanomaterials and nanotechnologies—a review. Toxicology 269:92–104
49. Olsen SI, Christensen FM, Hauschild M et al (2001) Life cycle impact assessment and risk assessment of chemicals—a methodological comparison. Environ Impact Assess Rev 21:385–404
50. Shatkin JA (2008) Nanotechnology: health and environmental risks. CRC Press, Boca Raton, FL, p 167
51. Davis JM (2007) How to assess the risks of nanotechnology: Learning from past experience. J Nanosci Nanotechnol 7:402–409

Chapter 15
The Economic Contributions of Nanotechnology to Green and Sustainable Growth

Philip Shapira and Jan Youtie

Abstract One of the impact promises associated with nanotechnology is that it will facilitate greener and more sustainable economic growth. We explore the extent to which nanotechnology development and commercialization is achieving this goal, drawing on secondary sources and available data. After defining the concepts of nanotechnology and green and sustainable development, we examine six nanotechnology application areas that are pertinent to green growth and sustainability. These application areas are assessed relative to their scale and scope through market forecasts, green benefits and potential issues and limitations. These six application areas are: nano-enabled solar cells, energy storage, nanogenerators, thermal energy, fuel catalysis, and water treatment. Nanotechnology-enabled applications in these areas offer potential benefits, such as reduced costs, less toxicity, greater efficiency, operating frequency, voltage, reduced complexity, and reliability. However, many sales forecasts associated with these applications have been adjusted downwards not only as a result of the economic downturn in the first decade of the 2000s but also due to the limited value offered by these nanotechnology-enabled application compared to what is already on the market (the incumbent technology). We find that while green nanotechnologies have the potential to make contributions both to addressing green challenges and to fostering sustainable economic development, development and diffusion is taking longer than previously anticipated, and in some cases the promised scale of benefits is unlikely to be realized. Additionally, the potential life cycle environmental overheads of some complex engineered nanomaterials must be taken more fully into account in assessing net contributions to green growth.

Keywords Nanotechnology • Green growth • Sustainability • Life cycle assessment

P. Shapira (✉)
Manchester Institute of Innovation Research, Manchester Business School, University of Manchester, Manchester M13 9PL, UK

School of Public Policy, Georgia Institute of Technology, Atlanta, GA 30332-0345, USA
e-mail: pshapira@mbs.ac.uk

J. Youtie
Enterprise Innovation Institute, Georgia Institute of Technology, Atlanta, GA 30308, USA
e-mail: jan.youtie@innovate.gatech.edu

V.A. Basiuk, E.V. Basiuk (eds.), *Green Processes for Nanotechnology*,
DOI 10.1007/978-3-319-15461-9_15

15.1 Introduction

Green nanotechnologies have attracted recent attention in discussions about how nanotechnology can address societal grand challenges. This paper identifies and discusses a range of specific applications of nanotechnology to green and sustainable growth, focusing especially on the use of nanotechnology in sustainable energy production and use, water provision, and other environmental applications.[1] The global demand for energy is estimated to increase by more than 30 % from 2010 to 2035 [1], while more than 800 million people worldwide currently are without access to safe drinking water [2]. The development of affordable and safe ways of meeting these needs has never been more pressing, further bolstered by fluctuations and uncertainties in markets and the reliability of supplies and by demands to reduce carbon emissions and other environmental impacts. While requirements for new energy sources and clean water are particularly pressing in non-OECD countries, developed countries also need to find ways to sustainably fuel and support their people and economies. These challenges drive interest in the applications of nanotechnology both to improve existing technologies and to offer new alternatives.

The paper considers examples of the possible scale and scope of contributions of nanotechnology to energy production and use, water provision, and other environmental applications. It provides some insight into how the economic contribution of nanotechnology to green and sustainable growth might be conceptualized and valued. Questions about potential issues and risks are also raised. The paper begins with a review of how nanotechnology in general, and green nanotechnology in particular, have been defined. This is followed by discussion of green nanotechnology applications, market forecast examples, and indicators of economic impact. Our concluding remarks stress the importance of assessing the economic impact of nanotechnology from a life-cycle perspective that considers the full range of economic, environmental, and societal implications.

15.2 Definitions

It has been suggested that green nanotechnology will allow us to make and use products "with the environment in mind" [3]. This could include using nanotechnology to make solar cells more efficient in generating renewable electricity or more

[1] This chapter is reprinted (with permission) from P. Shapira and J. Youtie, The Economic Contributions of Nanotechnology to Green and Sustainable Growth, Background Paper 3, *OCED/NNI International Symposium on Assessing the Economic Impact of Nanotechnology*, DSTI/STP/NANO(2012)14, Organisation for Economic and Cooperation, March 2012. While a few details are corrected in the version printed in this book, the data and forecasts contained in this chapter are as available at the time of original preparation (late 2011/early 2012). The opinions expressed and arguments employed herein should not be taken as representing the views or positions of the OECD or its member countries.

effectively cleaning polluted water. But what is nanotechnology? And, what makes a particular application of nanotechnology green?

To consider the first question, the US National Nanotechnology Initiative (NNI) highlights size, novelty, and human manipulation in its definition of nanotechnology.

> Nanotechnology is the creation and utilization of materials, devices, and systems through the control of matter on the nanometer-length scale, that is at the level of atoms, molecules, and supramolecular structures. The essence of nanotechnology is the ability to work at these levels to generate structures with fundamentally new molecular organization. These "nanostructures" … exhibit novel physical, chemical, and biological properties and phenomena ([4], p. iii).

Other official organizations have proposed similar types of definitions of nanotechnology, with some variations by nanoscale dimensional lengths (see, for example, [5], pp. 5–6; also [6]). Nanotechnology is frequently characterized at the length scale of 1–100 nm (with 1 nm equivalent to one billionth of a meter). Several bibliometric definitions have arisen to delineate scientific research in nanotechnology. Based on academic journal articles, researchers have used a range of methods to portray nanotechnology research. For example, Porter and colleagues use a two-stage Boolean search strategy comprised of keyword based search terms for nanomaterials, nano-processes, and instruments heavily used in nanotechnology; a second stage follows in which articles defining nanotechnology based on size alone are excluded [7]. In contrast, Zitt and Bassecoulard [8] use a citation-based approach for field definition. Across most of these definitions, the studies have found nanotechnology to be highly multidisciplinary, centered on materials science, physics, and chemistry, with biomedical fields comprising a growing share of research publications [9, 10]. In addition, there is evidence that nanotechnology has early characteristics of a general purpose technology, which suggests that nanotechnology has the potential to enable future waves of technological and economic innovation [11].

These scientific definitions fit less easily into commercialization characterizations, however. While nanotechnology has applications across multiple industries, there are no standard classifications of nanotechnology developing or using sectors. This has given rise to the use of various patent classes (including nanotechnology "cross-classes" such as International Patent Class B82, the Japanese Patent and Trade Office Class ZNM, the US Patent and Trademark Office (USPTO) Class 977, and the European Patent Office Class Y01N), product inventories, and case studies to determine the extent to which companies and products are indeed engaged in nanotechnology [12]. Companies and countries vary in practices to indicate whether products and processes are nano-enabled. With limited requirements to declare the use of nanotechnology through labeling or other disclosures, much remains unknown about the scale and scope of nanotechnology in commercial sectors.

The second question, about the nature of green nanotechnology, adds a further level of complexity. There is much diversity about what a green application is and green growth is arguably an even harder concept to measure and track than nanotechnology per se. One approach to understanding greenness is by focusing on outcomes and identifying how nanotechnology is contributing to sustainability targets. The OECD Green Growth Strategy, for example, promotes economic growth and development alongside the preservation of natural assets and the environment [13].

Yet there is diversity in targets and strategies among member countries. For example, Korea has set an emission reduction target of 30 % reduction in greenhouse gas emissions by 2020 over base year 2005 estimates and is seeking to meet this target through voluntary commitments and measures to allocate 2 % of GDP to green growth in the country's 5-year plan. Ireland's National Development Plan [14] addresses waste management, transportation, sustainable energy, and climate change and environmental research through investment plans amounting to a €25 billion (2007–2013). China's Twelfth Five Year Plan includes six green pillars: resource management, closed-loop economics, environmental and ecosystem protection, water conservation, disaster recovery, and climate change. The plan includes several emission reduction targets, for example a 17 % reduction of carbon per GDP unit by 2017 [15].

The OECD has itself promulgated indicators for measuring green growth milestones. These indicators recognize innovation as a key to green growth but it requires multidisciplinary involvement from fields outside energy and environmental domains, absorptive capacity through human capital and trade and foreign direct investment, and collaborative intellectual property mechanisms to scale-up diffusion in developing countries. Monitoring green growth strategies involves the development of indicators of the environment and resource productivity of the economy, natural asset base, environment health risks as well as services and amenities, economic opportunities and policies in regulation and other areas, and socioeconomic context [16]. Measuring the contribution of nanotechnology to the achievement of these indicators across these broad categories would be a major undertaking, with information requirements that would be problematic to satisfy particularly if multicountry or global benchmarks are sought.

Another approach to assessing nanotechnology's contribution to green growth and development is by looking at the production system—the means and processes of green growth rather than the ends. For instance, there have been attempts to define green industries and sectors. The US Bureau of Labor Statistics [17] proposed two approaches to measuring green industries and occupations. The narrower output approach identifies establishments that produce green goods and services. These are goods or activities which have favorable impacts on the environment. The broader process approach identifies establishments that utilize environmentally friendly production processes based on worker responsibilities. These definitions result in five broad groupings: (1) energy from renewable sources, including wind, biomass, geothermal, solar, ocean, hydropower, and landfill gas and municipal solid waste, (2) energy efficiency, including energy-efficient equipment, appliances, buildings, and vehicles, as well as products and services that improve the energy efficiency of buildings and the efficiency of energy storage and distribution, such as Smart Grid technologies, (3) pollution reduction and removal, greenhouse gas reduction, and recycling and reuse, (4) natural resources conservation, including organic agriculture and sustainable forestry; land management; soil, water, or wildlife conservation; and storm water management, and (5) environmental compliance, education and training, and public awareness. The former four comprise businesses with a more technological orientation.

This approach is consistent with the definitions promulgated by the United Nations and OECD. The United Nations Environment Program defines green jobs as "positions in agriculture, manufacturing, construction, installation, and maintenance, as well as scientific and technical, administrative, and service-related activities, which contribute substantially to preserving or restoring environmental quality. Specifically, but not exclusively, this includes jobs that help to protect and restore ecosystems and biodiversity; reduce energy, materials, and water consumption through high-efficiency and avoidance strategies; de-carbonize the economy; and minimize or altogether avoid generation of all forms of waste and pollution" ([18], pp. 35–36). OECD research concludes that "green jobs span a wide array of skills, educational backgrounds, occupational models, and can be found at any point on the supply chain of what are considered to be green firms or business" ([19], p. 21).

A complementary approach to identifying potential green nanotechnology applications is offered through patent records. Patent filings indicate inventions that promise novelty and utility. While only a subset of granted patents subsequently have innovation value, trends in patent applications and grants can help in signifying technological trajectories and corporate intellectual property strategies in emerging domains. As already noted, patent offices in the USA, Europe, and Japan have developed cross-classes for defining nanotechnology. Technometric search strategies have also been used to identify nanotechnology patents [7]. Additionally, patent offices and databases have developed green patent classes that address many of the areas already specified. The USPTO's definition of green patent classes in its Green Technology Pilot Program (to provide accelerated review of patents related to green technologies) encompasses alternative and renewable energy production, energy storage (batteries and fuel cells), energy distribution (including "smart grid"), energy conservation and efficiency improvements, greenhouse gas reduction, carbon sequestration, environmental purification, protection or remediation, and environmentally friendly farming [20]. The World Intellectual Property Office has a definition of green patent classes that encompasses similar categories of "environmentally sound technologies": alternative energy production, transportation, energy conservation, waste management, agriculture and forestry, administrative, regulatory or design aspects, and nuclear power generation [21]. Derwent World Patents Index also codes green patents based on a set of technology manual codes [22].

Several studies have addressed the overlap between nanotechnology and green applications. Strumsky and Lobo [23] examine the subset of USPTO that fall in nanotechnology cross-class 977. Nine percent of nanotechnology patents are classified as green technologies, based on this definition. The authors find that green nanotechnology patents have the same number of inventors as the average green patent but more claims, more citations received, and more technology codes, suggesting that these patents are substantially more inventively novel than the average green patent. Lux Research [24] reported that nanotechnology comprises 5 % of government investment in green technology, 24 % of publications related to green science and technology research, 15 % of green patents, 19 % of cleantech startups, and 15 % of venture capital devoted to green technology.

15.3 Green Applications of Nanotechnology

Consideration of the overlap between green and nanotechnology application has attracted increasing attention and investment. In the USA, nanotechnology for solar energy collection and conversion was one of three signature initiatives in the NNI's 2011 strategic plan. This area was comprised of research investments in seven different areas: (1) conversion efficiency (photovoltaic, thermophotovoltaic), (2) solar thermal, thermal conductivity, (3) nanoparticle fluid, heat transfer, (4) thermoelectric, (5) solar fuel, (6) solar characterization, and (7) energy storage [25]. This initiative received 3.7 % (US$68.8 million) of the overall NNI budget and the proposed budget for fiscal year 2012 called for the budget to nearly double and account for 5.9 % of the NNI budget.

Green nanotechnology also plays a central role in future roadmaps for the larger nanotechnology field. A recent example is Nanotechnology Research Directions for Societal Needs in 2020 ("Nano 2")—which included a prospective outlook component engaging a wide range of US researchers, companies, analysts, and other stakeholders along with expert workshops in Europe and Asia [26]. A central element of this future vision concerned green nanotechnology, with particular attention given to several areas for nanotechnology emergence: (1) nanostructured photovoltaics (organic, inorganic), (2) artificial photosynthesis for fuel production, (3) nanostructures for energy storage (batteries), (4) solid state lighting, (5) thermoelectrics, and (6) water treatment, desalination, reuse.

These green nanotechnology areas can be better seen through a presentation of illustrative applications and research areas. Nano-enabled solar cells use lower cost organic materials (as opposed to current photovoltaic technologies which use rare materials such as platinum) to convert solar energy. In addition, nano-enabled solar cells can be less expensive to produce. Examples include die sensitized solar cells, which use dye molecules, which take in sunlight, over a scaffold of titanium oxide nanoparticles. Copper zinc tin sulfide based solar cells represent another approach that uses less rare and toxic materials for photovoltaic solar electricity generation. The biggest limiting factor in current nano-enabled solar cells is the need for efficiency and lifetime (i.e., stability of materials) to be on par with conventional inorganic-based photovoltaics [27]. For inorganic photovoltaics, nanostructures have been used through colloidal synthesis to increase photovoltaic performance. In addition, nanostructuring can reduce charge travel distances, allowing the use of less costly materials.

Nanogenerators use piezoelectric material such as zinc oxide nanowires to transfer human movement to energy. By stacking of deposits of millions of nanogenerators on polymer chips, it could be possible to generate the energy equivalent of AA batteries. Self-powered sensors, wearable devices, and implantable energy receivers are examples of nanogenerators applications [28].

Energy storage can be viewed in terms of the use of nanotechnology for improvements to existing batteries and nano-enabled fuel cells. Many current batteries use lithium-ion technologies. Nanoparticles offer improvements such as quicker recharging capability and greater shelf life. Research into printed batteries suggests that electrolyte

components of a battery can be thinly layered with nanotube ink, eventually producing a battery that can be used with disposable products such as Radio-frequency identification (RFID) tags and certain applications that require greater power [29]. Fuel cells face a barrier in their use of rare platinum materials to act as catalysts for generating electrical currents. Nanotechnology plays a near-term and longer-term role concerning these catalysts. In the nearer term, nanomaterials are used to improve the performance of platinum-based electrocatalysts. Longer term directions point toward non-platinum electrocatalysts composed of nanocomposites that are less expensive, more stable and durable, and have greater efficiency [30].

Thermal energy applications of nanotechnology include not only improvements in energy sources but also insulation. Nanoparticle coatings are widely used on glass to provide UV protection, self-cleaning capabilities, and water resistance and are also available in paints. Vacuum insulation panels are expected to be among the major uses of nanoporous aerogel and nanoparticulate fumed silica [31].

In fuel catalysis, nanoparticles are used in production, refining, fuels, and automobile emission reduction. Dewaxing compounds for lubricants and low sulfur fuels are provided through shape selectivity features of certain molecules. High silica, porous zeolites are used for support for catalytic converters. Molybdenum disulfide and copper–zinc oxide particles have application in removal of sulfur and hydrogen in mixed fuel stocks from diesel or methanol sources. Future platforms for energy conversion and biofuel processing are long-term applications of nanotechnology in fuel catalysis [32, 33].

The provision of safe drinking water has been a major area for nanotechnology research. Nanotechnology-based solutions to water shortage issues involve treatment, desalination, and reuse [34]. Nanoabsorbents (such as nanoclays, zeolites, metal oxide nanoparticles, nanoporous carbon fibers, and polymeric adsorbents) can eliminate particulates from contaminated water. Toxic organic solutions can be converted into nontoxic by-products through nanocatalysts and redox active nanoparticles. Bacteria can be deactivated without creating by-products through the use of nanobiocides. Carbon nanotube filters, reverse osmosis membranes using zeolite nanocomposites and carbon nanotube membranes, and polymeric nanofibrous membranes have been used for water treatment and desalination. Dendrimer-based ultrafiltration systems and nanofluidic systems have used low-pressure membrane systems to remove ions from water solutions [35]. Photocatalytic methods using UV-light to irradiate pollutants is another example of the use of nanotechnology in this area, with nanoparticles such as titanium dioxide and zinc oxide used as the photocatalyst [36].

15.4 Market Forecasts: Examples

There are four main issues with forecasts of green nanotechnologies. Green industries and nanotechnology have been characterized as platform technologies which to date have exhibited evolutionary patterns of development while, many early forecasts suggested steeper growth trajectories. Some of these growth trajectories now appear

aggressive because large shares of the sectors in which nanotechnology is deployed are attributed to the estimate. For example, the 2001 forecast of nanotechnology's global market size of US$1 trillion by 2015 was first introduced in Roco and Bainbridge [37]. This estimate is based on the total anticipated manufacturing, electronics, health care, pharmaceuticals, chemical processing, transportation, and sustainability improvements arising from nanotechnology. Sustainability improvements were estimated at a savings of US$100 billion a year for 10–15 years based on nanotechnology-enabled lighting. This estimate also indicated a 200 billion ton reduction in carbon emissions from nanotechnology-enabled lighting. Lux Research's 2007 estimates of the size of the nanotechnology market also assumed a steep growth trajectory to US$2.6 trillion by 2014. This estimate was more than 70 % higher than Lux's earlier 2005 report estimate [38, 39].

Overly optimistic forecasts may also be possible in that the full sales of products with a small nanotechnology contribution may be attributed in a green nanotechnology forecast rather than apportioning out the true nanotechnology part of the product, which indeed may be very difficult for some products that use nanomaterials and processes. Nanotechnology's contribution may emerge from incorporation of nanomaterials, processes or instruments used to develop nanomaterials, and even the science itself that has developed around nanotechnology. These potential contributions may be over-estimated or even under-reported (in that there is difficulty in linking advances in a field of science to an application). In looking at the size of the nanomaterials market relative to the size of the overall estimates for nanotechnology, one can see that the former is much smaller than the latter. Lux Research's estimates of nanomaterials versus products from these materials (through nanointermediaries and nano-enabled products) published in 2005 suggested that nanomaterials would comprise only 0.5 % of product sales or US$3.6 billion (by 2010) out of a total global nanotechnology market estimate of US$1.5 trillion [38].

The economic downturn since 2008 has caused some downward adjustment in these market forecasts. Lux Research's 2009 global nanotechnology market forecast was decreased to $2.5 trillion by 2015, 4 % less than the 2007 estimates. Declines in the automobile and construction industries were also estimated to affect market demand for nanomaterials and composites [40].

Finally, the viability of forecasts relates to the extent to which the technology will be able to produce significant benefits over and above what is already on the market. These benefits include not only lower costs but other factors as well, such as efficiency, operating frequency, voltage, reduced complexity, and reliability and lifetime.

A summary of available forecasts for selected green nanotechnology products generally presents a picture of moderate estimates of potential market size on a global basis (see Fig. 15.1). It should be noted that some of these forecasts are for specific and targeted green nanotechnologies. We have examined a number of selected green nanotechnology applications in more detail. For each technology, we consider benefits relative to green growth and potential market size forecasts. Issues in estimating application market size are noted as are barriers to achieving nanotechnology contributions to green growth. (See also Table 15.1 for a summary of these

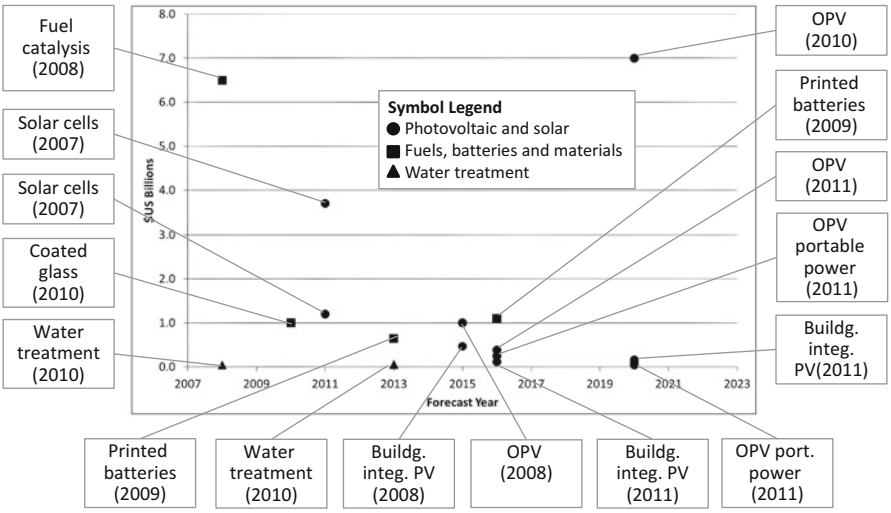

Fig. 15.1 Global sales forecasts—selected green nanotechnologies. *Sources*: Cientifica [41]; Lux Research [24, 40]; BCC Research [42]; Global Industry Analytics [43]. Year of estimate in parentheses. PV = Photovoltaic; OPV = Organic Photovoltaic

Table 15.1 Selected nano-enabled green applications: benefits, global market estimates, and issues

Application	Green benefits	Market estimate (worldwide)	Issues and challenges
Nano-enabled solar cells	Lower cost, less toxic, more abundant materials	US$1.2 billion for 2011 (2007 estimate)	Nano-enabled solar cells must be able to reach performance and cost levels of existing non-organic PVs
Energy storage	Improved performance of existing materials (e.g., quicker recharge, greater shelf life) and long-term use of new less expensive, more stable and durable, and efficient new materials	US$3.7 billion in 2011 (2007 estimate)	Substitutes for rare materials not yet technologically available.
Nanogenerators	Self-powering of small electronic devices	See energy storage estimates.	Application of nanogenerators awaits market commercialization
Thermal energy	Integration into existing materials for greater insulation, UV protection, water resistance.	Aerogels: US$140 million (2012 estimate)	Cost of these materials compared to traditional building materials is an issue. The strong integration of nanotechnology into the existing product makes it difficult to separate the contribution of nanotechnology

(continued)

Table 15.1 (continued)

Application	Green benefits	Market estimate (worldwide)	Issues and challenges
Fuel catalysis	Greater efficiency and performance in fuel use	US$5–US$8 billion a year as of 2008	Assumes that nanotechnology derived synthetic methods can be applied to the full fuel catalysis market
Water treatment, desalination, reuse	New clean, safe water sources	US$6.6 billion in 2015	Market is in developing countries while technological leadership is in developed countries plus China. Potential environmental, health and safety concerns may limit commercialization.

Note: See text for sources and further discussion

selected nanotechnology applications and their benefits relative to green growth.) The selected green nanotechnology applications are broadly in energy, water, and related environmental domains and are discussed below.

Solar cells and photovoltaics. Nanotechnology-enabled solar cells and photovoltaic applications are frequently highlighted as potential growth markets. Lux Research's [24] estimate of the global market for nano-enabled solar cells for 2011 was US$1.2 billion. However, promised performance relative to cost advantages have yet to fully materialize. Additionally, the price of conventional silicon solar cell panels has continued to fall in recent years as manufacturers (particularly those based in China) have expanded increasingly efficient production facilities [44]. The segment of this market concerning organic photovoltaics (OPV) is illustrative. Earlier reports from 2007 and 2008 projected significant growth for the OPV market. These reports acknowledged the underlying technological challenges of OPV, but they believed market growth would result from substantial technological improvements and the low comparative costs for OPV compared to conventional PV. According to these reports, these advances, at least partially, would be supported by dramatic increases in venture capital investments and policy initiatives from the US Department of Energy's Solar Technology Energies Program. NanoMarkets [45] projected the 2015 worldwide market for organic photovoltaics to grow to US$1 billion, driven by a projected US$470 million building-integrated photovoltaics (BIPV) market. However, these technologies have not advanced in the marketplace by as much as earlier reports had anticipated. Technology challenges present significant obstacles to commercialization and future market growth. Conversion efficiency for OPV cells is expected to continue to increase, but the technology will not be able to compete with conventional silicon-based photovoltaics for some time. Additionally, costs—the widely cited advantage of OPV versus traditional PV technologies—continue to be a challenge. As conventional PV technologies have seen rapid decreases in costs, some reports find that OPV is losing its cost advantage [46].

To successfully commercialize, OPV technology must overcome significant conversion efficiency, lifetime, and cost barriers. Given these continued challenges, by 2011 market researchers were taking a much more conservative outlook for OPV. Recent market reports believed future growth of OPV applications would be limited to specific product segments, such as portable power, where flexibility and low costs are necessary and efficiency and lifetime are less important. Until efficiency, lifetimes, and costs can compare with conventional PV technologies, OPV will not compete with other PV product segments. NanoMarkets, which in early 2008 expected the OPV market to grow to $1 billion by 2015, revised its forecast to $387 million by 2016 [47]. Rather than building-integrated photovoltaics, portable power is now expected to drive more modest OPV growth. OPV portable power, for which the technology's challenges of efficiency and lifetime are not major concerns, is projected to grow to $250 million by 2016. Potential growth for BIPV, however, remains limited by the technology challenges, as well as an overall decline in construction with the most recent recession. Nanomarkets subsequently projected BIPV to be much slower to grow in popularity, with only $113 million in revenue by 2016 [47]. Lux Research shares a similar, but less-optimistic view about OPV growth. Citing that conventional PV manufacturing costs continue to decrease, the report forecasts the entire OPV market to grow to only $159 million by 2020. Like NanoMarkets, Lux Research (in Energy Weekly News [48]) believes this growth will be driven by portable power, primarily used in the defense industry, and by BIPV applications. With this forecast, these two segments will account for approximately $80 million and $44 million of the entire market, respectively.

Energy storage. Nanotechnology in energy storage in 2007 was estimated to be a US$3.7 billion market by 2011 according to Lux Research. Printed batteries for energy storage are an enabling component for other organic electronic applications, including RFID tags, smart cards, and sensors. With the growth of these applications, industry analysts project revenue from printed batteries to exceed US$1 billion by 2016 [49]. Despite printed battery's potential for widespread commercialization, analysts note that the cluster faces significant funding and investment hurdles before the technology can fully develop and be used in these other applications [50]. *Nanogenerators* have yet to reach the market in a significant commercial way. Limited commercial activity for this technology makes it difficult to estimate the size of the market. Estimates associated with the energy storage market are likely to be most applicable.

Thermal energy. Nanotechnology in the thermal energy domain has diverse applications that are lighter and reduce the porosity of building materials and make them more energy efficient. Aerogels, a nano-structured solid foam that substitutes for denser foam-based insulation, was projected to increase in global market size from about $140 million in 2012 to more than $330 million by 2017 [51]. The primary uses are for insulation in gas and oil pipes, medical devices, and aerospace rather than insulation in building construction. Other applications, such as nanocoating of flat glass for thermal control, are penetrating high-performance construction market sectors [52]. Yet the relatively high cost of these materials, relative

to conventional building materials for insulation and coated glass, is a barrier to entry. Similarly constraints to the adoption and penetration of nano-coated glass in the automotive industry include cost and the ability to incorporate machines and skills into production lines.

Fuel catalysis. Fuel catalysis is a major area for nanotechnology application. Nanotechnology derived synthetic methods have been estimated to be used in 30–40 % of global fuel catalysis products representing US$18–20 billion a year. However, the extent to which this share of the fuel catalysis market that can be claimed as a direct effect of nanotechnology is debatable [33].

Water and water treatment. There is significant need in developing countries for clean, safe water, especially in rural areas, as well as in rapidly expanding mega-cities, and this is a significant potential market. Worldwide, more than 0.8 billion people are without access to safe drinking water, with 2.6 billion people lacking improved sanitation facilities [2]. This imposes high human, environmental, and economic costs. Nano-engineered structures, membranes and crystals have been put forward for water disinfection and cleaning as well as for desalination [53]. The market for nano-enabled water and wastewater applications is predicted to reach $6.6 billion by 2015, up from $1.6 billion in 2007. Nano-enabled applications are said to have energy-saving advantages over conventional approaches. For example, current desalination techniques (such as reverse osmosis) require significant amounts of energy. Less energy-intensive nanotechnology-enabled applications have been proposed, including using desalination batteries with sodium manganese oxide nanorods and silver electrodes to generate drinking water from seawater by extracting sodium and chloride ions [54]. Developed countries (such as the USA, Germany, and Japan) are considered to be developing the most advanced nano-enabled water treatment technologies, although China also is developing capabilities. The greatest needs are in rural Asia, Africa, and Central and South America. The disjuncture between the location of capabilities and areas of greatest need could limit opportunities for the commercialization of nano-enabled water treatment technologies. This is not only because of knowledge and market demand gaps but also because of potential concerns (validated or not) in the sending (developed) as well as receiving (developing) countries related to the environmental, health, and safety implications of nano-enabled water treatments.

15.5 Indicators of Economic Impact

There are several ways of approaching the question of the economic impact of green nanotechnologies and indicators to assess those impacts. This section considers how direct and indirect economic impacts can be conceptualized. We also highlight potential indicators of impact and discuss issues and cautions associated with the application of those indicators.

The market studies discussed in the previous section suggest that there are major potential markets for green nanotechnologies. However, investment, including in

research, technological development, production, testing, marketing, standards setting, regulation, user adoption, and monitoring needs to occur before these markets can be realized. The range of public and private capital and ongoing costs associated with the application of green nanotechnologies needs to be offset against benefits, taking into account such factors as the timing and distribution of various benefits and costs, interest rates and opportunity costs, and the relative advantages of green nanotechnologies compared with conventional applications. In the process of producing and using green nanotechnology products, there are likely to be a series of indirect effects, including on supply chains and other spillovers to third parties and the environment. Not all of these benefits and costs will be measurable, and some impacts (including health, safety and environmental impacts) may not be apparent (or known not to be an issue) until years after initial use.

Simple analyses of the economic contribution of green nanotechnologies would give consideration to the net costs of technological development and market entry relative to the value of the outputs and outcomes achieved, taking into account considerations of time and perspective (or standing). The net costs include such inputs as public R&D, knowledge development, and facilities costs, private industry R&D costs, and prototyping, testing, commercialization, production start-up, and marketing costs. The outputs of such expenditures can include contributions to science and knowledge, generic or specific technologies developed, intellectual property development (including patents and licenses), standards development, and new company start-ups. These outputs can have intermediate economic value, but the greatest economic potential is through outcomes such as profitable sales from new products, increased productivity and other process improvements, savings of costs that would otherwise be incurred, employment and wage generation, and benefits to consumers and users. These outcomes can lead to developmental and public benefits including contributions to national and regional gross domestic product, improved competitiveness and balance of trade, and environmental and other societal benefits. There can also be strategic benefits in the use of nanomaterials, for example to reduce reliance on rare metals and materials sourced from overseas locations. However, standing is critical: the relative weight of benefits and costs of a new technology may vary according to whether the perspective is that of a producer, competitor, customer, worker, industry, region, or country.

Policymakers are often especially interested in the economic development effects of new technologies, such as green nanotechnologies, including impacts on jobs and wages. Employment will be generated through research, manufacturing, delivery, use, and maintenance related to green nanotechnology products and processes, and associated industries and services, although predicting the number of new jobs is difficult. Existing workers may shift into green nanotechnology activities as conventional products are replaced. It is also difficult to define what is a nanotechnology job or a green job, let alone what is a green nanotechnology job. Nanotechnology is a broad platform technology, it cuts across multiple industrial sectors, and frequently represents a small proportion of other downstream products, raising issues of the unit of analysis. Hence wide ranges are seen in estimates of nanotechnology jobs. US estimates of nanotechnology jobs have varied from tens of thousands today

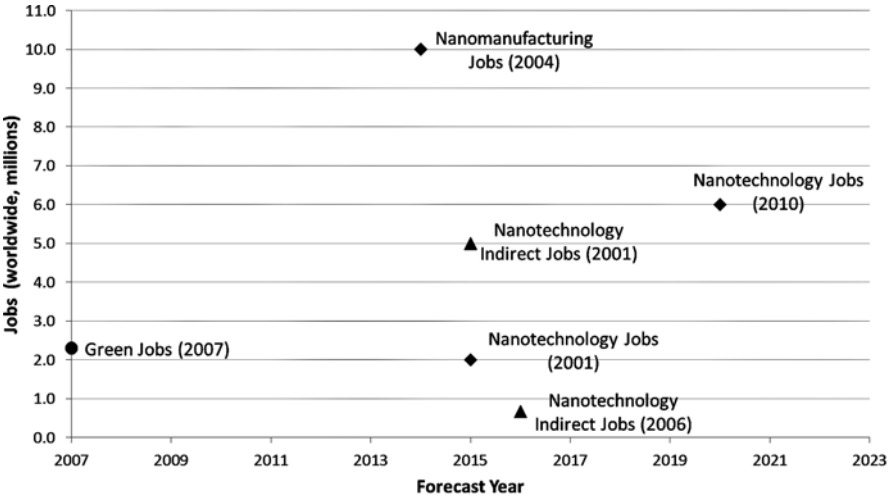

Fig. 15.2 Nanotechnology and green jobs—selected worldwide forecasts. *Sources*: Invernizzi [55]; UNEP [18]. Year of estimate in parentheses

to close to one million by 2015, with worldwide estimates of nanotechnology jobs (see Fig. 15.2) apparently diminishing from earlier estimates of ten million (in manufacturing) in 2014 to six million by 2020 (see also discussion in [55]). Green nanotechnology jobs will employ a significant share of the nanotechnology workforce, depending on the share designated as green, with potentially a share of other green sector jobs again depending on the definitions used (for recent attempts to define and measure green jobs, see [17, 18, 56]). Not all nanotechnology jobs will be well-paid, and there will likely to be some offset in employment as certain conventional products and skills are replaced [55].

A further reason why it is difficult to predict jobs related to nanotechnology, including green nanotechnology, lies in the often lengthy time scale for the economic development benefits of emerging technologies to materialize. Different kinds of cost and benefits usually occur differentially over time. For example, R&D costs typically occur early in the cycle of a new technology, although there may well be ongoing R&D costs as the technology is continuously improved and adapted. Similarly, as Tassey [57] notes, various benefits can occur at different time scales. In the short-term, intermediate outcomes such as patents, R&D partnering, prototyping, and the attraction of venture capital may occur; in the medium-term, new products and processes and company growth may be seen; while it is in the longer term that broad industry, economic and societal benefits appear. The definition of these terms (by years) varies by the technology and market acceptability. Nanotechnology R&D began to take off in the mid-1990s, with big boosts in public R&D from the 2000s onwards [58]. After more than a decade of significant worldwide public and private R&D, and many scientific and technological achievements [26], most nanotechnologies are arguably still at early stages of development. Cost–benefit analyses conventionally discount future costs and benefits to today's values, using the current interest rate or alternate (often higher) hurdle rates of return.

A well-elaborated example of a comparative method for assessing the economic value of nanotechnologies is provided by Walsh et al. [59] in a study for the UK Department for Environment, Food and Rural Affairs (DEFRA). This study delineates a methodology for estimating the net value-added of a nanotechnology innovation, which is defined as the difference between the value-added of the nano-enabled product and that of the comparable incumbent product. It assumes that that there are conventional incumbent products against which new nanotechnology products can be matched. The net value added is comprised of three elements: producer surplus (sales less costs) plus consumer surplus (consumer value less price); plus other externalities (net benefits to third parties). A multistep process is employed which involves defining the nano-enabled product, identifying its use and function, identifying a comparable incumbent product, determining the production costs of the nano product and its comparator, determining sales prices, identifying the nano-product's effect on the market, determining externalities (including net environmental benefits and R&D spillovers), and calculating producer surplus, consumer surplus, and externalities. Market scenarios are identified where the incumbent product is replaced with the new product but with variations as to whether the market size is unchanged or increased and whether functionality is increased, with consumer surplus a function of price declines and improved performance for the nano product relative to the incumbent. The approach further allows geographic allocation of producer surplus and externalities (where location of production differs from location of consumption). The model considers the "phase-in" time of the product (diffusion time) using an S-curve model. Discount rates are applied to adjust future expected cash flows to present values. The rate is comprised of two parts: a normal (or risk free) component accounting for expected inflation; and a premium that discounts the probability that the product may not successfully reach the market. Walsh and colleagues apply their approach to several green nanotechnology cases studies, including nano-enabled food packaging, thin-film photovoltaics, fuel catalysts, amperometric electrochemical gas sensors, nano-enabled antifouling paints, and nZVI technology [59]. The case studies illustrate that net economic benefits are relatively small where the nano-enabled product has limited advantages over incumbent products and market size is unchanged; larger benefits accrue where the nano product reduces costs compared with the incumbent, markets are expanded, and diffusion is relatively rapid (Table 15.2). The cases studies take a national perspective. For the UK, economic externalities are reduced for some technologies because R&D, materials production, or manufacturing are overseas. In the main, net benefits are estimated for UK markets (which are a relatively small share of potential global markets). Environmental benefits and costs outside of the UK are not included in the analyses (although they are mentioned). The authors recognize that there are significant uncertainties in the forecasts of markets and nanotechnology penetration. It is also noted that environmental impacts often cannot be reliably monetized, and that current evidence is inconclusive on some potential environmental impacts. Subsequent findings of health or environmental harm would negatively change the calculated benefit–cost ratios.

This kind of approach to estimating economic value is instructive, but it is sensitive to the assumptions and discount rates used and there are a series of caveats. The comparative approach assumes that nanotechnology innovations do not offer

Table 15.2 Summary of DEFRA case studies of economic value of innovation in green nanotechnologies in the UK

	Gas-impermeable nano-clay film	Thin film photovoltaics	Fuel-enhancement catalysts	Gas sensors	Antifouling paints	Nano zero-valent iron
Application	Food packaging	Energy production	Fuel additive	CO gas detection	Ship building	Remediation of contaminated sites
Incumbent product	Plastic film	Crystalline silicon photovoltaics	Diesel fuel	Electrochemical sensor	Foul release paints	Pump and treat
Market scale	80.32 m (10 g) units/year (UK)	250 MW/year (UK)	25 b liters/year (UK)	823,000 households/year (UK)	£2.3 m (UK). Possible export sales of £143 m over 20 years	40 sites/year (UK)
Market characteristics	Fixed (no unit growth)	Fixed (no unit growth)	Total sales of diesel (UK)	6 year replacement	5 % of merchant ships	10 % of contaminated sites
Nanotechnology product advantage	Reduced household food waste by 2 % annually	Reduced CO_2 by half over silicon based PV	Improves fuel efficiency by 5 %	Increases performance per unit mass, or reduces the mass required	1 % improvement in fuel efficiency	25–30 times faster reaction rates
Price differential	+10 % for nano product	+36 % higher than the incumbent	14–20 % higher for nano product	5–10 % below incumbent price	Initially 24 % higher, then matching incumbent over time	90 % lower for nano product
Benefits (surplus) to producers	£11.41 m/year	£1.75 m/year	£50.82 m/year	£1.24 m/year to £0 m/year	£0.34 m to −£0.074 m/year	−£0.365 m/year

Benefits (surplus) to consumers	£0.60 m/year	£7.89 m/year	£1,142.5 m/year	£0.1 m/year to £0.35 m/year	0–£398,000/year	£136 m/year
Economic Externalities	£122.85 m/year household savings	No R&D externalities to UK	£1.44 m/year	No R&D or other externalities anticipated for UK	£0.6 m to £0.7 m/year	No additional externalities identified.
Environmental Externalities	Reduction of 243,000 tonnes of CO_2 e/year (=£5.36 m at DECC carbon price)	Reduced CO_2, NOX, SOX emissions; fewer heavy metals then conventional PV	0.111 kg of CO_2 per liter of fuel consumed	None in UK. Reduction in platinum mining overseas.	8,640 tonnes of CO_2/year (UK)	No conclusive evidences. Impacts of nanoparticle release not known.
Diffusion rate	50 % UK market share = 8 years	100 % UK market (full replacement of silicon PV)	50 % UK market share = 8 years	66 % UK market = 8 years	50 % UK market share = 8 years	50 % UK market share = 8 years
Net present value to UK economy	£4.941 b (20 years)	£205 m (20 years); negative £1.1 b 20-year value with tariff subsidies	£15.3 b (20 years)	£12.4 m (20 years)	£2.3 m (20 years)	£2.4 b (20 years)

Source: Walsh et al. [59] (cases in main report and in supplemental working guide) in report for the UK Department for Environment, Food and Rural Affairs (DEFRA)
Note: m = million; b = billion

completely new functionalities and that matching conventional products can be found. The approach also works best with one nanotechnology innovation and one function at a time. Indirect effects, for example on suppliers, are not included. Nanotechnology product prices are assumed to decline over time (although this assumption can be modified). Where data is not available, proxies are used, which may or may not be accurate. Environmental impacts can be included as externalities but only where they can be foreseen and monetized (for example, valuing reduced carbon emissions based on traded carbon prices).

The approach described above also assumes that societal benefit will be maximized when producers and consumers maximize their own benefits. This may or may not be the case. End users, when analyzing from their own specific economic perspectives, will typically consider the price-performance parameters of a new technology such as nanotechnology when compared with other alternatives. Direct purchasing, capital and operational costs will surely be of concern. Depending on the user and application, the societal impacts of the product or process may or may not be of particular interest compared with specific factors of performance and functionality. For example, a medical device could be made smaller with increased operating life by incorporating a nano-enabled printed battery sheet; a user needing this medical device is likely to focus on those improved performance characteristics, including reliability and accuracy, and may well pay a premium for them. How this device is made and how it can be disposed of or recycled after use may or may not be of concern at the point of purchase. Similarly, for a novel nano-enabled insulating window glass, a customer will likely be interested in the cost of purchase and installation and in the savings in energy costs over multiple years compared with conventional window units. Considerations of the energy required to manufacture and recycle the new nano units again may, or may not, be influential in the adoption decision. Such spillovers are typically not in the control of the producer or consumer, and assessment of them may not be prominent in the purchasing or adoption decision. The extent to which these externalities are considered by individual purchasers in the valuations they make of the relative advantages or disadvantages of green nanotechnologies will vary, although they may be influenced by the availability of information, regulatory provisions, standards, and the adoption of codes of practice related to sustainability.

However, from a broader economic and societal perspective, as well as from the view of responsible and sustainable innovation, these life cycle considerations are of fundamental importance in considering the potential and applications of green nanotechnologies. Life cycle assessment (LCA) considers a "product's full life cycle: from the extraction of resources, through production, use, and recycling, up to the disposal of remaining waste" ([60], p. iv). There are a variety of approaches and tools within the rubric of LCA, including methods focusing on economic inputs and outputs and associated environmental impacts and on direct and indirect energy requirements over the life of a product (for reviews of LCA, see: [61, 62]). An LCA perspective raises a series of important issues for the evaluation of green nanotechnologies:

- While green nanotechnology applications may save energy costs and reduce carbon emissions in use, significant amounts of energy can be involved in the upstream production of component nanomaterials. Early estimates of the amount

of energy required to produce single-walled carbon nanotubes (SWCNT) were relatively high [63]; another study concludes that two of the most economically viable methods of carbon nanotube production were energy intensive (due to the high temperatures and pressures required) and would thus add significant carbon dioxide emissions [64]. More recent estimates [65] continue to suggest wide disparities in energy requirements for SWNT manufacture, depending on the method used although large variations are reported for what seem to be similar processes. Using a prospective LCA approach, Wender and Seager [66] argue that the intensive energy requirements for the large-scale manufacture of SWCNT-enabled lithium-ion batteries currently make them impracticable. Energy and manufacturing costs for nanomaterial production are likely to reduce over time as process technologies are improved and new materials emerge. Nonetheless, it remains important to track and consider energy and other resource extraction costs associated with the production of materials used in green nanotechnology applications.

- Some green nanotechnology applications have raised concerns about environmental, health and safety (EHS) implications. There has been attention to potential exposure risks to workers in laboratories and factories involved in the development and manufacturing of various forms of nanostructures [67, 68]. Reviews of standards and guidance to minimize occupational and other exposure risks from nanostructures indicate a range of actions and activities under way (mainly in developed countries and by international bodies) but also limited and inconsistent evidence on longer-term implications [69]. Concerns are also extended to potential EHS risks through the use and disposal of nanostructures employed in green nanotechnology applications. For example, nanomaterials such as nZVI (nano metallic iron) are effective in absorbing and remove groundwater pollutants [70, 71]. nZVI has been used in a series of remediation projects in the USA and in several European countries including Germany, Italy, and the Czech Republic [72]. Yet apprehension has been raised about potential EHS impacts, including the toxicity of partially remediated compounds and downstream entry into water sources and plant and food chains [72–74]. Similarly, quantum dots—extremely small particles of semiconductor materials with customizable electrical and optical features—have potential green applications in low energy lighting and more efficient solar cells. Quantum dots are often comprised from cadmium and selenium and they may, under certain conditions, release toxic compounds in use or on disposal [75, 76]. There are many permutations and varied applications of quantum dots and the toxicology is not yet definitive. Additionally, at least one company (UK-based Nanoco) now offers cadmium-free quantum dots, now under development for LED lighting [77]. These examples highlight the uncertainties, particularly over the long run, associated with the EHS profiles of an unknown number of green nanotechnology applications. Risk concerns may or may not be justified, and more biocompatible alternatives may be found. Many recent and current nanotechnology EHS studies contain calls for further research and monitoring. Studies in the insurance industry have suggested that, potentially, there may be major economic consequences related to the production and use of nanotechnology [78, 79].

- Nanotechnology development and production is geographically widespread, with more than 60 countries pursuing national nanotechnology research and innovation programs [58], with the use and application of nanotechnology occurring globally. Regulation and oversight is primarily national, with some growth in nanotechnology information exchange, harmonization, and standards setting at supranational and international levels [69], including activity by the OECD through its Working Parties on Nanotechnology [80] and on Manufactured Nanomaterials [81]. Arguably, some best practices are emerging [82], but there remain significant differences by countries in the governance and regulation of nanotechnology. There are variations in the overall approaches to, and investment in, the assessment of environmental, health, safety, ethical, legal, and societal implications of nanotechnology; differences in legislative and regulatory actions, including the role of formal requirements and voluntary codes; and contrasts in the infrastructures of governance, including the roles of agencies, industry, consumer groups, think tanks, and other organizations in deliberations on nanotechnology research, commercialization, labeling, education, and regulation [83]. There are also significant differences between and among developed and developing countries in their activities and capabilities in nanotechnology and in its regulation and governance (see, for example, [84]). As global production and consumption chains emerge in nanotechnology, including green nanotechnology applications, there are anticipated opportunities for developing countries to benefit from applications pioneered in other countries. Yet there is also the potential for an inequitable distribution of risks and benefits. Intellectual property rights (including patents) in nanotechnology are assigned mainly to developed countries and a few emerging economies, potentially limiting access or increasing application costs in developing countries. Some green nanotechnology applications, for example in selectively enhancing agricultural productivity, may negatively affect countries that rely on conventional methods [85]. Nanotechnology applications may be marketed in, and nanomaterials production outsourced to, countries with less-developed capabilities for risk monitoring and regulatory control. Over the life cycle of nanotechnology products, costs and benefits may thus accrue asymmetrically.

The potential risks of new green nanotechnologies need to be compared against those of current technologies (which may also be energy intensive and present various risks) and against the human and environmental costs of not effectively addressing key global challenges (such as reducing carbon emissions or providing potable water). Yet it is apparent that labeling or promoting a nanotechnology as green does not, in and of itself, mean that this technology or its applications are sustainable or risk-free. Nor does it mean that the technology is without possible economic costs as well as economic benefits. This reinforces the point that, in considering indicators of the impact of green nanotechnology, it is appropriate to ask how that indicator contributes to the appreciation of the range of potential economic, environmental, and societal implications over time and space.

Ideally, from a broader societal perspective, LCA needs to be situated in the context of an anticipatory and socially responsible approach to governing innovation.

Anticipatory governance is the capacity to model, deliberate upon, and prepare for future developments with the involvement of key stakeholders and public engagement [86]. The methods of anticipatory governance can include foresight, scenarios, technology assessment, and other analytical techniques (such as LCA) as well as connecting research and innovation agendas and integrating the natural and social sciences. A socially responsible approach to innovation (also known as responsible research and innovation) considers social and environmental benefits in the design of research and innovation, engages societal groups, takes account of social, ethical, and environmental impacts, and incorporates openness and transparency [87].

15.6 Concluding Remarks

Landmark studies of the long-term economic impacts of major technological accomplishments are typically retrospective in nature. Martin and Tang [88] offered a review of multiple studies that have examined the consequences of public R&D investments. These studies fall into three groups: econometric studies, surveys, and case studies. Martin and Tang also note the variety of channels through which economic and societal impacts are generated, including through growth in the stock of knowledge, human capital enhancement, new instruments and methods, networks and social interaction, problem solving, new firms, and social knowledge.

A key point about such studies is that they are retrospective. The innovations are known, and a sufficient time has elapsed since their introduction for them to be recognized and for their economic and societal impacts to be assessed. Such studies are always difficult to do well, but there are methods and sources that can be tapped. When we seek to prospectively assess and measure the impacts of new technologies, there are available methods including technological foresight and forecasting methods. However, particularly if we seek to go out many years, a great deal of uncertainty is inevitable not only in the trajectory of technological development but also in predicting economic and societal conditions which will influence take-up and use. In the nanotechnology domain, prospective economic assessment is further complicated by uncertainty about the environmental, health and safety implications of some nanotechnologies.

That said, the complications and uncertainties of predicting future technology trajectories should motivate rather than discourage efforts to evaluate the likely economic implications of green nanotechnology. There are a range of methodological options that are available to probe these potential implications including the use of multi-criteria and dynamic assessment techniques, anticipatory life-cycle approaches, and scenarios and modeling. Interdisciplinary opportunities (engaging natural and social scientists) to advance these and other methodologies should be pursued.

Although development and diffusion may take longer than previously anticipated, green nanotechnologies have the potential to make significant contributions both to addressing green challenges and to fostering sustainable economic development. There appears to be substantial promise particularly in nano-enabled applications in solar cells, photovoltaics, batteries, fuel catalysts, and water filtration.

Other nano-enabled applications have the potential to reduce operational energy needs through offering comparable or better performance yet with less weight, more durability or greater efficiency. Yet attention has to be given over the life cycle to the energy and resource requirements to initially produce nano-scale materials, to the sources of energy (renewable or nonrenewable) required for their large-scale manufacture, to the fate and disposition of nanomaterials during and after use and associated environmental, health, safety and societal implications, and to broader societal values and considerations. We have suggested that such considerations can be incorporated through an anticipatory approach which models, deliberates upon, and prepares for future developments. An anticipatory approach is likely to be facilitated through a mix of measures and methods, with the ability to model and probe different scenarios and to prompt "what if" and "what about" questions.

Acknowledgements The authors acknowledge the support of the National Science Foundation under Grant No. 0937591 (Center for Nanotechnology in Society at Arizona State University).

References

1. International Energy Agency (2011) World energy outlook 2011. International Energy Agency, Paris
2. WHO (2010) Progress on sanitation and drinking water. 2010 Update. World Health Organization and UNICEF, Geneva
3. Schmidt KF (2007) Green nanotechnology: it's easier than you think. Project on emerging nanotechnologies. Woodrow Wilson Center, Washington, DC
4. NSTC (1999) Nanotechnology research directions: vision for nanotechnology in the next decade. National Science and Technology Council, Committee on Technology, and the Interagency Working Group on Nanoscience, Engineering and Technology. Washington, DC. http://www.wtec.org/loyola/nano/IWGN.Research.Directions/. Accessed August 17, 2014
5. ICCR (2010) Report of the ICCR Joint Ad Hoc Working Group on Nanotechnology in cosmetic products: criteria and methods of detection. International Cooperation on Cosmetic Regulation initiative (ICCR-4), Toronto, ON
6. Klaessig F, Marrapese M, Abe S (2011) Current perspectives in nanotechnology terminology and nomenclature. In: Murashov V, Howard J (eds) Nanotechnology standards. Springer, New York, NY, pp 21–52
7. Porter AL, Youtie J, Shapira P, Schoeneck D (2008) Refining search terms for nanotechnology. J Nanopart Res 10(5):715–728
8. Zitt M, Bassecoulard E (2006) Delineating complex scientific fields by a hybrid lexical-citation method: an application to nanosciences. Inform Process Manag 42(3):1513–1531
9. Porter AL, Youtie J (2009) How interdisciplinary is nanotechnology? J Nanopart Res 11(5):1023–1041
10. Porter AL, Youtie J (2009) Where does nanotechnology belong in the map of science? Nat Nanotechnol 4:534–536, September
11. Youtie J, Iacopetta M, Graham S (2008) Assessing the nature of nanotechnology: can we uncover an emerging general purpose technology? J Tech Transfer 33(3):315–329
12. Shapira P, Youtie J (2011) Nanotechnology innovation and policy: current strategies and future trajectories. J Tech Transfer 36(6):581–586
13. OECD (2011a) Towards green growth. Organisation for Economic Cooperation and Development, Paris. http://www.oecd.org/dataoecd/37/34/48224539.pdf. Accessed August 17, 2014

14. National Development Plan (2007) Transforming Ireland: a better quality of life for all. Pn. A7/0004. The Stationary Office, Dublin
15. Jones RS, Yoo B (2011) Korea's green growth strategy: mitigating climate change and developing new growth engines. OECD Economics Department Working Papers, No. 798, DOI: 10.1787/5kmbhk4gh1ns-en
16. OECD (2011b) Towards green growth: monitoring progress. OECD indicators. Organisation for Economic Cooperation and Development, Paris. http://www.oecd.org/dataoecd/37/33/48224574.pdf. Accessed February 12, 2012
17. BLS (2011) The BLS green jobs definition. US Bureau of Labor Statistics, Washington, DC. http://www.bls.gov/green/green_definition.pdf. Accessed December 10, 2011
18. UNEP (2008) Green jobs: towards decent work in a sustainable, low-carbon world. UNEP, ILO, IOE, and ITUC http://www.unep.org/PDF/UNEPGreenjobs_report08.pdf. Accessed November 28, 2014
19. Martinez-Fernandez C, Hinojosa C, Miranda G (2010) Green jobs and skills: the local labour market implications of addressing climate change. Working document, CFE/LEED, OECD http://www.oecd.org/cfe/leed/44683169.pdf. Accessed November 28, 2014
20. USPTO (2009) Pilot program for green technologies including greenhouse gas reduction. Fed Reg 74(234): pp 64666–64699, December 8. www.uspto.gov/patents/law/notices/74fr64666.pdf. Accessed November 28, 2014
21. WIPO (2012) IPC Green Inventory. World Intellectual Property Office. http://www.wipo.int/classifications/ipc/en/est/index.html. Accessed August 17, 2014
22. Thomson Reuters (2012) Green technology manual codes. Derwent World Patents Index. http://ip.thomsonreuters.com/dwpi_greencodes. Accessed August 17, 2014
23. Strumsky D, Lobo J (2011) How green is my nano? Evidence from USPTO patents. Conference presentation at S. Net Conference, Tempe, AR, November
24. Lux Research (2007) The Nanotech Report 2006: investment overview and market research for nanotechnology. Lux Research, New York, NY
25. NSET (2011) National nanotechnology initiative strategic plan, 2011. Nanoscale Science, Engineering and Technology Subcommittee, Committee on Technology, National Science and Technology Council, Washington, DC. http://www.nano.gov/sites/default/files/pub_resource/2011_strategic_plan.pdf. Accessed August 17, 2014
26. Roco MC, Mirkin CA, Hersam MC (2011) Nanotechnology research directions for societal needs in 2020: retrospective and outlook. Springer, Berlin
27. Organic electronics association (2009) OE - a roadmap for organic and printed electronics, 3rd edn. Organic Electronics Association, Frankfurt, Germany
28. Wang ZL (2008) Towards self-powered nanosystems: from nanogenerators to nanopiezotronic. Adv Funct Mater 18:3553–3567
29. Simonite T (2007) Nanotube tangles power printable batteries. New Scientist. November 16
30. Berger M (2008) Nanotechnology is key to improving fuel cell performance. Nanowerk, October 31
31. Brinker J, Ginger D (2011) Nanotechnology for sustainability: energy conversion, storage, and conservation. In: Roco MC, Mirkin CA, Hersam MC (eds) Nanotechnology research directions for societal needs in 2020: retrospective and outlook. Springer, Berlin
32. Davis M (2010) Nanotechnology in catalysis: a decade of progress and into the future. NSF Grantees Conference 2010, Arlington VA, December 6–8
33. Hu E, Davis M, David R, Scher E (2011) Applications: catalysis by nanostructured materials. In: Roco MC, Mirkin CA, Hersam MC (eds) Nanotechnology research directions for societal needs in 2020: retrospective and outlook. Springer, Berlin
34. OECD (2011c) Fostering nanotechnology to address global challenges: water. Organisation for economic cooperation and development, Paris. http://www.oecd.org/dataoecd/22/58/47601818.pdf. Accessed February 19, 2012
35. Diallo M, Brinker J (2011) Nanotechnology for sustainability: environment, water, food, minerals, and climate. In: Roco MC, Mirkin CA, Hersam MC (eds) Nanotechnology research directions for societal needs in 2020: retrospective and outlook. Springer, Berlin

36. Müller N, Nowack B, Oy S, Saari D (2010) Briefing No. 2: Environment – photocatalysis for water. ObservatoryNANO August 2010. Available at: http://www.sswm.info/sites/default/files/reference_attachments/MULLER%20et%20al%202010%20Photocatalysis%20for%20Water%20Treatment.pdf. Accessed November 28, 2014
37. Roco M, Bainbridge W (2001) Societal implications of nanoscience and nanotechnology. Springer, Berlin
38. Berger M (2007) Debunking the trillion dollar nanotechnology market size hype. Nanowerk, April 18
39. Lux Research (2005) Sizing nanotechnology's value chain. Lux Research Inc., Boston, MA
40. Lux Research (2010) The recession's impact on nanotechnology. Lux Research Inc., Boston, MA
41. Cientifica (2007) Half way to the trillion dollar market. In: Berger M (ed.), Debunking the trillion dollar nanotechnology market size hype, Nanowerk, April 18, 2007. http://www.nanowerk.com/spotlight/spotid=1792.php. Accessed March 7, 2012
42. BCC Research (2009) Nanotechnology: a realistic market assessment. BCC Research, Wellesley, MA
43. Global Industry Analysts (2012) Nanotechnology: a global industry outlook. Global Industry Analysts, San Jose, CA
44. Bullis K (2012) The Chinese solar machine. Technol Rev 115(1):46–49
45. Nanomarkets (2008) NanoMarkets issues new report on organic photovoltaic markets, PR Newswire, May 7
46. Nanomarkets (2010a) Organic and dye-sensitized cell photovoltaics: materials, applications and opportunities 2010, Nanomarkets, Glen Allen, VA, May 13. Summary available at http://www.reportlinker.com/p0397475-summary/Organic-and-Dye-Sensitized-Cell-Photovoltaics-Materials-Applications-and-Opportunities.html. Accessed November 28, 2014
47. Solar Novus Today (2011) Organic photovoltaics market to increase six-fold. April 27. http://www.solarnovus.com/index.php?option=com_content&view=article&id=2699:organic-photovoltaics-market-to-increase-six-fold&catid=37:business-news&Itemid=241. Accessed February 12, 2012
48. Energy Weekly News (2011) Lux Research; Organic photovoltaic markets fall short of expectations, May 6, 176
49. Nanomarkets (2009) NanoMarkets report shows where thin-film batteries will generate revenues, PR Newswire, May 7
50. Nanomarkets (2010b) Thin-film and printable batteries: strategies for the future. Summary available at: http://nanomarkets.net/blog/article/thin-film_and_printable_batteries_strategies_for_the_future. Accessed November 28, 2014
51. BCC Research (2013) Aerogels. AVM052C. BCC Research, Wellesley, MA
52. Bax L (2010) Construction – nano-enabled insulation materials, Briefing No. 3 ObservatoryNANO August 2010 http://bwcv.es/assets/2011/1/12/ObservatoryNANO_Briefing_No.3_Nano-Enabled_Insulation_Materials.pdf. Accessed November 28, 2014
53. Shannon MA, Bohn PW, Elimelech M, Georgiadis JG, Mariñas BJ, Mayes AM (2008) Science and technology for water purification in the coming decades. Nature 252(20):301–310
54. Pasta M, Wessells CD, Cui Y, La Mantia F (2012) A desalination battery. Nano Lett 12(2):839–843
55. Invernizzi N (2011) Nanotechnology between the lab and the shop floor: what are the effects on labor? J Nanopart Res 13:2249–2268
56. Chapple K (2008) Defining the green economy: a primer on green economic development. Center for Community Innovation, University of California, Berkeley, CA. http://community-innovation.berkeley.edu/reports/Chapple%20-%20Defining%20the%20Green%20Economy.pdf. Accessed March 7, 2012
57. Tassey G (2003) Methods for assessing the economic impacts of government R&D, planning report 03-1. National Institute of Standards and Technology, Gaithersburg, MD
58. Shapira P, Wang J (2010) Follow the money. What was the impact of the nanotechnology funding boom of the past ten years? Nature 469:627–628

59. Walsh B, Willis P, MacGregor A (2010) A comparative methodology for estimating the economic value of innovation in nanotechnologies. A report for DEFRA. Oakdene Hollins, Aylesbury, UK
60. European Commission (2010) International Reference Life Cycle Data System (ILCD) handbook, General guide for life cycle assessment – detailed guidance. Joint Research Centre, Institute of Environment and Sustainability, Publications Office of the European Union, Luxembourg
61. Rebitzer G, Ekvall T, Frischknecht R, Hunkeler D, Norris G, Rydberg T, Schmidt WP, Suh S, Weidema BP, Pennington DW (2004) Life cycle assessment - Part 1: framework, goal and scope definition, inventory analysis, and applications. Environ Int 30(5):701–720
62. Finnveden G, Hauschild MZ, Ekvall T, Guinee J, Heijungs R, Hellweg S, Koehler A, Pennington D, Suh S (2009) Recent developments in life cycle assessment. J Environ Manage 91(1):1–21
63. Isaacs JA, Tanwani A, Healy ML (2006) Environmental assessment of SWNT production. Electronics and the environment, 2006. Proceedings of the 2006 IEEE international symposium on electronics and the environment, Scottsdale, AZ, May 8–11, pp 38–41. DOI: 10.1109/ISEE.2006.1650028
64. Agboola AE, Pike RW, Hertwig TA, Lou HH (2007) Conceptual design of carbon nanotube processes. Clean Tech Environ Policy 9(4):289–311
65. Gutowski TG, Liow JYH, Sekulic DP (2010) Minimum exergy requirements for the manufacturing of carbon nanotubes. IEEE International Symposium on Sustainable Systems and Technologies, Washington, DC, May 16–19
66. Wender BA, Seager TP (2011) Towards prospective life cycle assessment: single carbon nanotubes for lithium-ion batteries. 2011 IEEE International Symposium on Sustainable Systems and Technology (ISSST), Chicago, IL, May 16–18. DOI: 10.1109/ISSST.2011.5936889
67. Aitken RJ, Creely KS, Tran CL (2004) Nanoparticles: an occupational hygiene review, research report 274. Institute of Occupational Medicine, Edinburgh
68. Schulte PA, Trout D, Zumwalde RD, Kuempel E, Geraci CL, Castranova V, Mundt DJ, Mundt KA, Halperin WE (2008) Options for occupational health surveillance of workers potentially exposed to engineered nanoparticles: state of the science. J Occup Environ Med 50(5):517–526
69. Murashov V, Howard J (2011) Health and safety standards. In: Murashov V, Howard J (eds) Nanotechnology standards. Springer, New York, NY, pp 209–238
70. Kanel SR, Manning B, Charlet L, Choi H (2005) Removal of arsenic(III) from groundwater by nanoscale zero-valent iron. Environ Sci Tech 39(5):1291–1298
71. Li XQ, Elliott DW, Zhang WX (2006) Zero-valent iron nanoparticles for abatement of environmental pollutants: materials and engineering aspects. Crit Rev Sol State Mater Sci 31(4):111–122
72. Müller N, Nowack B (2010) Nano zero valent iron – the solution for water and soil remediation? ObservatoryNANO Focus report 2010. Available at: https://www.yumpu.com/en/document/view/6104945/nano-zero-valent-iron-the-solution-for-water-and-soil-remediation. Accessed November 28, 2014
73. Royal Society (2004) Nanoscience and nanotechnologies: opportunities and uncertainties. Royal Society and the Royal Academy of Engineering, London
74. Grieger KD, Fjordbøge A, Hartmann NB, Eriksson E, Bjerg PL, Baun A (2010) Environmental benefits and risks of zero-valent iron nanoparticles (nZVI) for in situ remediation: risk mitigation or trade-off? J Contam Hydrol 118(3–4):165–183
75. Mahendra S, Zhu H, Colvin VL, Alvarez PJ (2008) Quantum dot weathering results in microbial toxicity. Environ Sci Tech 42(24):9424–9430
76. Botrill M, Green M (2011) Some aspects of quantum dot toxicity. Chem Commun 47(25):7039–7050
77. Williams A (2011) Cadmium-free quantum dot firm wins major LED lighting deal. ElectronicsWeekly.com, December 14. http://www.electronicsweekly.com/blogs/led-lights/2011/12/cadmium-free-quantum-dot-firm-wins-major-led-lighting-deal.html. Accessed August 17, 2014

78. Lloyd's Emerging Risks Team (2007) Nanotechnology: recent developments, risks, and opportunities. Lloyd's, London
79. Kingdollar C (2011) Nanotechnology – the smallest and biggest emerging issue facing casualty insurers? Gen Re. Research, Stamford, CT
80. OECD (2011a) OECD Working Party on Nanotechnology. http://www.oecd.org/science/sci-tech/oecdworkingpartyonnanotechnology.htm. Accessed November 28, 2014
81. OECD (2011b) OECD Working Party on Manufactured Nanomaterials. http://www.oecd.org/env/ehs/nanosafety. Accessed November 28, 2014
82. IRGC (2007) Nanotechnology risk governance. Policy brief. International Risk Governance Council, Geneva
83. Pelley J, Saner M (2009) International approaches to the regulatory governance of nanotechnology. Carleton University, School of Public Policy and Administration, Ottawa, ON
84. Jayanthi AP, Beumer K, Bhattacharya S (2012) Nanotechnology: "Risk Governance" in India. Economic and Political Weekly, XLVII, 4, January 28, 34–40
85. Gruère G, Narrod C, Abbott L (2011) Agriculture, food and water nanotechnologies for the poor: opportunities and constraints. IFPRI policy brief 19. International Food Policy Research Institute, Washington, DC
86. Karinen R, Guston DH (2010) Toward anticipatory governance: the experience with nanotechnology. In: Kaiser M, Kurath M, Maasen S, Rehmann-Sutter C (eds) Governing future technologies: nanotechnology and the rise of an assessment regime. Springer, Dordrecht, The Netherlands, pp 217–232
87. Suttcliffe H (2012) A report on responsible research & innovation. Matter, London. Available at: http://ec.europa.eu/research/science-society/document_library/pdf_06/rri-report-hilary-sutcliffe_en.pdf. Accessed March 28, 2014
88. Martin BR, Tang P (2007) The benefits from publicly-funded research. SPRU Electronic Working Paper Series, No. 161. http://www.sussex.ac.uk/spru/documents/sewp161.pdf. Accessed November 28, 2014

Index

V.A. Basiuk, E.V. Basiuk (eds.), *Green Processes for Nanotechnology*,
DOI 10.1007/978-3-319-15461-9